

LAGRANGE INTERPOLATION AND QUASI-INTERPOLATION USING TRIVARIATE SPLINES ON A UNIFORM PARTITION

Inauguraldissertation
zur Erlangung des akademischen Grades
eines Doktors der Naturwissenschaften
der Universität Mannheim

vorgelegt von
Diplom-Mathematiker Georg Hubert Schneider
aus Merzig

Mannheim, 2013

Dekan: Professor Dr. Heinz Jürgen Müller, Universität Mannheim
Referent: Professor Dr. Andreas Neuenkirch, Universität Mannheim
Korreferent: Professor Dr. Jürgen Hesser, Universität Heidelberg

Tag der mündlichen Prüfung: 21. November 2013

Abstract

We develop quasi-interpolation methods and a Lagrange interpolation method for trivariate splines on a regular tetrahedral partition, based on the Bernstein-Bézier representation of polynomials. The partition is based on the body-centered cubic grid.

Our quasi-interpolation operators use quintic C^2 splines and are defined by giving explicit formulae for each coefficient. One operator satisfies a certain convexity condition, but has sub-optimal approximation order. A second operator has optimal approximation order, while a third operator interpolates the provided data values. The first two operators are defined by a small set of computation rules which can be applied independently to all tetrahedra of the underlying partition. The interpolating operator is more complex while maintaining the best-possible approximation order for the spline space. It relies on a decomposition of the partition into four classes, for each of which a set of computation rules is provided.

Moreover, we develop algorithms that construct blending operators which are based on two quasi-interpolation operators defined for the same spline space, one of which is convex. The resulting blending operator satisfies the convexity condition for a given data set.

The local Lagrange interpolation method is based on cubic C^1 splines and focuses on low locality. Our method is 2-local, while comparable methods are at least 4-local.

We provide numerical tests which confirm the results, and high-quality visualizations of both artificial and real-world data sets.

Zusammenfassung

Wir entwickeln Quasi-Interpolationsmethoden und eine Methode zur lokalen Lagrange-Interpolation mit trivariaten Splines, definiert über einer regelmäßigen Tetraederpartition. Die Splines basieren auf der Bernstein-Bézier Darstellung trivariater Polynome. Die Tetraederpartition basiert auf dem kubisch innenzentrierten Gitter (body-centered cubic grid).

Die Quasi-Interpolationsoperatoren verwenden quintische C^2 Splines und sind durch explizite Formeln für die Koeffizienten definiert. Der erste Operator genügt einer gewissen Konvexitätsbedingung, besitzt aber sub-optimale Approximationsordnung. Der zweite Operator besitzt die für den Spline-raum bestmögliche Approximationsordnung, während der dritte Operator die bereitgestellten Daten interpoliert. Zur Definition der ersten beiden Operatoren genügt ein einzelner Satz an Berechnungsformeln für die Koeffizienten, der auf alle Tetraeder der Partition unabhängig voneinander angewendet werden kann. Der interpolierende Operator ist komplexer, besitzt aber ebenfalls die bestmögliche Approximationsordnung. Dem liegt eine Zerlegung der Partition in vier Tetraederklassen zugrunde, für die jeweils ein Formelsatz zur Berechnung der Koeffizienten vorliegt.

Darüber hinaus entwickeln wir Algorithmen, die, basierend auf zwei Quasi-Interpolationsoperatoren, von denen einer konvex ist, einen Hybrid-Operator konstruieren. Der Hybrid-Operator erfüllt das Konvexitätskriterium für den gegebenen Datensatz.

Die lokale Lagrange-Interpolationsmethode verwendet kubische C^1 Splines und wurde mit Hinblick auf eine möglichst geringe Lokalität entwickelt. Die Methode ist 2-lokal, während vergleichbare Methoden eine Lokalität von mindestens 4 besitzen.

Unsere numerischen Tests bestätigen die Ergebnisse. Wir erzeugen Visualisierungen, sowohl von synthetischen Funktionen, als auch von Datensätzen aus Computertomographen, die die Qualität der Rekonstruktionen aufzeigen.

Contents

1	Introduction	1
2	Preliminaries	7
2.1	Tetrahedral partitions	8
2.2	A tetrahedral partition based on the body-centered cubic grid	13
2.3	Bernstein-Bézier techniques	21
2.4	Trivariate splines on tetrahedral partitions	38
3	Quasi-interpolation using quintic C^2 splines on the BCC partition	43
3.1	A convex quasi-interpolation operator	53
3.2	An optimal quasi-interpolation operator	62
3.3	An interpolating quasi-interpolation operator	70
3.4	Error bounds for the quasi-interpolation operators	88
4	Enforcing convexity with parametric quasi-interpolation	95
4.1	Improving the algorithm	101
5	Lagrange interpolation using splines of low locality on the BCC partition	105
5.1	Cubic C^1 -splines	107
5.2	Error bounds	131
6	Numerical tests and visualizations	135
6.1	Error tables	135
6.2	Isosurface extraction	138
6.3	Volume ray casting	147
Appendices		147
A	B-coefficient computation rules for the convex quasi-interpolation operator	155
B	B-coefficient computation rules for the optimal quasi-interpolation operator	169

C	B-coefficient computation rules for the interpolating quasi-interpolation operator	191
D	A program used in the proofs of several theorems for the quasi-interpolation operators	311
Bibliography		331

Chapter 1

Introduction

Polynomial splines are fundamental tools in the field of approximation theory. They are widely used in various forms in many areas such as computer-aided geometric design, image processing, and engineering, where they find many practical applications. Hence, it is no surprise that the term ‘spline’ is borrowed from the shipbuilding industry where, in times before digital computers where commonly used, it described a thin strip of wood that was bent around a number of lead weights to form a smooth curve. These strips behave like piecewise cubic polynomials, minimizing the tension along the curve. It is generally agreed upon that it was the Romanian-born mathematician Isaac Jacob Schoenberg who introduced the term into mathematics, when he used it in his 1946 paper “Contributions to the problem of approximation of equidistant data by analytic functions” [75] to describe smooth approximations by piecewise polynomials.

Thus, even the theory of univariate splines is comparatively young. The theory developed rapidly, however, especially between the 1960’s and 1980’s. Splines can be defined by only a few parameters. They can be stably evaluated by efficient algorithms, like the de Casteljau algorithm for splines in B-form [19, 20], or the algorithms by de Boor [11] and Cox [27] for B-splines. They also possess excellent approximation properties. These features make them an ideal tool to use in conjunction with modern digital computers, which became increasingly common during these years. There are many outstanding publications on the subject of univariate splines, among them the monographs by de Boor [12], Nürnberger [57], and Schumaker [77].

It was also during that time that the French engineer Pierre Étienne Bézier developed a representation of polynomial curves for his work at the vehicle manufacturer Renault, an account of which can be found in chapter 1 of [37]. This representation is based on the well-known Bernstein basis polynomials, which were introduced in 1912 by the Russian mathematician Sergei Natanovich Bernstein, who used them for his elegant constructive proof of

the Weierstrass approximation theorem [8]. To recognize the contributions of both Bernstein and Bézier, the representation is known as the *Bernstein-Bézier representation* (see [10]) or, following a suggestion by de Boor [13], the *B-form*. The B-form, though originally developed for univariate polynomials, can be readily extended to the multivariate setting. The splines developed in this thesis are based on the trivariate equivalent of this representation.

Early steps towards the development of bivariate splines based on the B-form began as early as the 1950's when Lorentz [49] and Stancu [83] studied bivariate Bernstein basis polynomials on a triangle. With the increasing possibilities of computer graphics and the development of computer-aided geometric design came the use of such polynomials as a representation of surfaces in the 1970's, for example in the works of Farin [33, 34] and Sabin [73]. The latter contained the characterization of C^1 smoothness for two polynomial pieces defined on neighboring triangles, while the generalization for the C^r case were introduced by Farin in [35]. This characterization proved to be central to the development of bivariate spline theory, as it combined the advantages of the B-form with the straightforward description of smoothness as linear conditions for the coefficients of the polynomials. It was also Farin [34] who first suggested the B-Form as a representation for bivariate splines on triangulations. Since then, a vast literature on the subject has accumulated. The works of Chui [21] and Lai and Schumaker [46] give comprehensive insight into the theory and are among the standard literature in this area of research.

First results for trivariate splines, defined on tetrahedral partitions and based on Bernstein-Bézier techniques, were not long in coming. Among them were the research papers on trivariate macro-elements by Alfeld [1, 2], Worsey and Farin [89], and Worsey and Piper [90], and several articles investigating the dimension of trivariate spline spaces (see [3, 5–7]). The latter problem has still not been completely solved for arbitrary tetrahedral partitions, or even in the bivariate case for arbitrary triangulations, although several upper and lower bounds for the dimension are known (see [4, 46]). Today, the theory of trivariate splines still is an area of ongoing research, to which this thesis is a contribution.

There exist a huge number of trivariate spline interpolation methods, which can be classified into three categories. Macro-element methods are widely used to construct Hermite-type interpolants, which use function values as well as derivatives to construct a spline. The earlier mentioned articles by Alfeld, Worsey, Farin and Piper (see [1, 2, 89, 90]) are classic examples for this kind of method. Recent contributions to this area are the book of Lai and Schumaker [46], the works of Matt [52, 53], and also the references in these. An important tool in the construction of such methods is the *minimal determining set*, which is a subset of certain points related to a spline

space such that fixing all coefficients associated with these points uniquely determines a spline. Usually, it is also necessary to know the dimension of the spline space.

The second category consists of local Lagrange interpolation methods. The classic Lagrange interpolation problem is completely solved for univariate B-splines, but it is much more complex in the multivariate setting. This is largely due to the fact that there exist no Haar spaces of dimension greater than two in two or more variables (see [28, 50]). There are many such methods using bivariate splines (see [22, 43, 58, 63, 64, 66], the survey [65], and the references in [46]), and recent years have seen an increasing number of local Lagrange interpolation methods in the trivariate setting (see [41, 42, 44, 54, 55, 59, 61, 62, 78]). In many of these, the locality is achieved by a decomposition of the underlying triangulation or tetrahedral partition into several classes, and by the subdivision of some of all of the simplices using a macro-element method. One of the methods using this technique, which we co-authored with Nürnberger [61], is the subject of chapter 5 of this thesis. Our goal was the construction of a Lagrange interpolant with low locality. The key to the low locality is our use of a regular partition which allows an efficient decomposition into very few classes of tetrahedra. This partition is based on the well-known body-centered cubic grid and unifies the approximation methods developed in this thesis. Our method uses cubic C^1 -splines and is 2-local, while the comparable methods developed in [55] and [41] are 4- and 5-local, respectively. For arbitrary partitions, the locality can be as high as 10 (see [42]). Similarly to macro-element methods, the Lagrange interpolation methods also rely on the construction of a minimal determining set, and the knowledge of the dimension of the underlying spline space.

The third category comprises quasi-interpolation methods. These methods usually define a linear operator mapping the space of continuous functions onto a spline space, and thus the other two categories can be interpreted as a subset of this class. In contrast to macro-element methods and Lagrange interpolation methods, however, a quasi-interpolation operator does not necessarily rely on a minimal determining set, or even on the knowledge of the dimension of the spline space. The interpolation sets used in macro-element methods and Lagrange interpolation methods are often not equidistantly distributed, and thus an intermediate step is necessary when gridded data is to be approximated. Quasi-interpolation methods, on the other hand, can be specifically designed to approximate regularly spaced data directly, as we show in chapter 3. Some methods work with *box splines*, which can be interpreted as the multivariate equivalent to the univariate B-splines. These methods define quasi-interpolation operators as linear combinations of translates of basic functions, without using Bernstein-Bézier techniques. Examples

for such methods can be found in [14, 21, 30, 31, 38, 69]. Related to these are also the so-called simplex splines of [74]. In contrast to those methods are the quasi-interpolation operators based on the B-form of multivariate polynomials. These methods construct a spline by giving explicit computation rules for each coefficient. This approach has many advantages. It is not necessary to construct and evaluate basic functions. The spline is rather evaluated using the efficient de Casteljau algorithm. Since the rules are given as linear combinations of the surrounding data values, the methods are implicitly local and stable. Any symmetries inherent in the underlying partition can be mirrored by the rules, thus greatly reducing the number of distinct rules needed to define the operator. Hence, such methods are usually based on regular partitions which exhibit many symmetries. Moreover, the coefficients can be computed independently of each other, which can be exploited by the parallelization capabilities of modern computer hardware. Examples for this kind of quasi-interpolation operator are the bivariate and trivariate C^1 -methods in [60, 71, 72, 80–82]. It is operators of this type that we develop in chapter 3 of this thesis. Our quasi-interpolation operators, however, use quintic C^2 -splines defined on a tetrahedral partition based on the body-centered cubic grid. To our knowledge, these are the first C^2 operators defined in this fashion.

This thesis is structured as follows. Chapter 2 gives a comprehensive overview of the theory which our work is based on. We begin the chapter with some fundamental facts about tetrahedra and tetrahedral partitions before we introduce the body-centered cubic grid. Based on this grid, we define a regular tetrahedral partition, called the *BCC partition*, which is common to all spline spaces used in this thesis. We also develop some related lemmas that are used in our main results. We continue with basic facts about trivariate polynomial approximation and introduce the B-form and related Bernstein-Bézier techniques. These include the central theorem concerning the characterization of smoothness conditions between neighboring tetrahedra, and the de Casteljau algorithm. We conclude the chapter with the basic theory of trivariate splines defined over tetrahedral partitions, the introduction of minimal determining sets, and the concepts of locality and stability.

We start chapter 3 by establishing some notation and terminology about quasi-interpolation using Bernstein-Bézier techniques. We introduce the B-coefficient computation rules which our operators are based on, and develop related concepts such as symmetry, locality and stability. Moreover, we introduce a new convexity condition which is motivated by the convexity of the B-form. This concept of convexity is the basis for the algorithms we develop in chapter 4. Building on these fundamentals, we develop three quasi-interpolation operators with different properties, using quintic C^2 -splines on the BCC partition. The operators are defined by giving explicit computation

rules for the coefficients of the splines. These definitions can be found in the appendix. The first operator, which we call the *convex operator*, fulfills our convexity condition. This comes at the expense of the approximation order, which is sub-optimal for this operator. Our second operator, on the other hand, is constructed to achieve the best-possible approximation order for the underlying spline space, and we call it the *optimal operator*. Both operators use only a small set of coefficient computation rules that can be applied to all tetrahedra of the partition. The number of distinct rules is further reduced by exploiting the symmetries of the BCC partition. Most quasi-interpolation methods interpolate none or only some of the provided data values. Our goal in the development of the third operator was to construct a quasi-interpolation method that does interpolate the provided data values while maintaining the best-possible order of approximation. While the operator achieves this, it is more complex than the other two operators and relies on a decomposition of the BCC partition into four classes of tetrahedra, for each of which a separate set of rules is given. This technique is similar to many local Lagrange interpolation methods (see [54, 59, 61], among others), in that these methods also use a decomposition of the underlying partition. In contrast to those methods, however, our splines can be constructed independently on each tetrahedron in an arbitrary order. This makes the parallelization of many algorithms straightforward and was another criterion in designing the operators. The three quasi-interpolation operators were developed to approximate gridded data, such as is acquired in computed tomography. The final section in this chapter establishes local and global error bounds for the three quasi-interpolation operators. Some of the main results in this chapter are proved with the help of a computer program which we wrote using the Mathematica® software package by Wolfram Research. We give a listing of this program and a detailed description in the appendix.

The convexity condition introduced in chapter 3 is the basis for the algorithms developed in chapter 4. The motivation for these algorithms actually came from observations on bivariate spline surfaces, where surfaces produced by non-convex operators tend to oscillate in regions where the approximated data jumps from one level to another. We observed a similar behavior in non-convex trivariate operators. Here, the splines can take values outside of the original data range. The convexity condition was developed to suppress such behavior. Since a convex operator usually has only sub-optimal approximation order, we devised algorithms to construct a *blending operator* from two quasi-interpolation operators, one of which is convex. The main idea behind these algorithms is to produce an operator that satisfies the convexity condition in critical areas, while maintaining the better approximation properties of the second operator in regions where the condition is already fulfilled.

Chapter 5 is dedicated to our local Lagrange interpolation method [61]. Here, we define the Lagrange interpolation operator as a specialization of the quasi-interpolation operators from chapter 3. This allows us to use a consistent terminology throughout the thesis. We start the chapter with lemmas and theorems concerning Lagrange interpolation on single edges, faces, and tetrahedra of a partition. In particular, we give a theorem about partial Worsey-Farin splits which play an important role for the locality of the method. We define the partition used in the interpolation process and its decomposition into several classes of tetrahedra. Based on this decomposition we introduce algorithms that construct a Lagrange interpolation set for cubic C^1 splines. Our main results show the improved locality and the stability of the method. We conclude the chapter with local and global error bounds.

In the final chapter we present numerical tests and visualizations. Using the programming language C++, we wrote computer programs that implement the operators and algorithms developed in this thesis. We conducted numerical tests with the quasi-interpolation operators and the Lagrange interpolation operator and measured the approximation error of their reconstructions of the test function proposed by Marschner and Lobb [51]. These tests confirm the approximation order of the respective operators. Moreover, we wrote software to extract and visualize isosurfaces of our reconstructions. These visualizations are also presented here. Finally, we used our quasi-interpolation operators to reconstruct data sets acquired by computed tomography. To visualize these reconstructions, we wrote a computer program which implements our adaption of the ray-casting-based volume visualization algorithm introduced by Levoy [48], using two-dimensional transfer functions as proposed in [45] to classify the data.

We thank Professor Dr. Günther Nürnberger for his encouragement, his valuable advice, and his constant willingness to discuss our results, throughout the creation of this thesis.

Chapter 2

Preliminaries

This chapter encompasses the fundamentals which this thesis is based on. The first section introduces the geometric concept of tetrahedral partitions which is integral to the field of trivariate spline theory. We then define a specific tetrahedral partition, based on the body-centered cubic (BCC) grid. This partition, which we call the *BCC partition*, is the geometric basis for our approximation methods. The main part of this chapter is a comprehensive overview of the Bernstein-Bézier techniques, which are a fundamental tool in the field of multivariate approximation theory. These techniques are essential for the methods developed in the following chapters. We conclude this chapter with a section concerning the theory of trivariate splines on tetrahedral partitions.

We begin with some notation and definitions which we frequently use throughout this thesis. As usual, we denote the set of non-negative integers by $\mathbb{N}_0 := \mathbb{N} \cup \{0\}$, and the set of continuous real-valued functions defined on $\Omega \subseteq \mathbb{R}^m$ by $C(\Omega)$. For an arbitrary set A , we denote its cardinality by $\#A$. We use the symbol by $\text{Conv}(X)$ to denote the convex hull of the set $X \subset \mathbb{R}^n$. Given a real-valued function $f \in C^1(\Omega)$, $\Omega \subseteq \mathbb{R}^n$ and a vector $u \in \mathbb{R}^n \setminus \{0\}$, we call

$$D_u f(v) := \frac{d}{dt} f(v + tu) \Big|_{t=0}, \quad v \in \Omega,$$

the *directional derivative of f along u at v* . We denote Kronecker's delta by

$$\delta_{i,j} := \begin{cases} 1, & i = j, \\ 0 & \text{otherwise.} \end{cases}$$

Usually, i and j will be integers. Throughout this thesis, we frequently use the expression “ $i + j + k + l = m$ ”, or variants thereof, to indicate which values i, j, k and l can take. Unless stated otherwise, we assume that i, j, k and l are non-negative integers, implying that $0 \leq i, j, k, l \leq m$.

Definition 2.1. Let Ω be a convex compact subset of \mathbb{R}^n . We call

$$|\Omega| := \max_{u,v \in \Omega} \|u - v\|_2,$$

where $\|\cdot\|_2$ is the Euclidean norm, the size of Ω .

It sometimes is convenient to use the following multi-index notation.

Definition 2.2. We call a k -tuple $\alpha := (\alpha_1, \dots, \alpha_k) \in \mathbb{N}^k$ of non-negative integers a multi-index. The length of the multi-index is defined as $|\alpha| := \alpha_1 + \dots + \alpha_k$. For a function $f \in C^{|\alpha|}(\Omega)$, $\Omega \subseteq \mathbb{R}^k$, we define

$$D^\alpha f := D_{x_1}^{\alpha_1} \cdots D_{x_k}^{\alpha_k} f.$$

Here, D_{x_i} is the partial derivative with respect to the i -th variable of f . Moreover, the factorial of α is defined as $\alpha! := \alpha_1! \cdots \alpha_k!$, while $x^\alpha := x_1^{\alpha_1} \cdots x_k^{\alpha_k}$.

When measuring the size of functions and their derivatives, we use the standard L_∞ -norm and seminorm.

Definition 2.3. Let f be a measurable function on a domain $\Omega \subset \mathbb{R}^n$. Then

$$\|f\|_\Omega := \operatorname{ess\,sup}_{v \in \Omega} |f(v)|.$$

For a sufficiently smooth function f , we define

$$|f|_{k,\Omega} := \max_{|\alpha|=k} \|D^\alpha f\|_\Omega.$$

2.1 Tetrahedral partitions

In the univariate setting, polynomial splines are defined by subdividing an interval $[a, b] \subset \mathbb{R}$ into sub-intervals and constructing a polynomial on each sub-interval. Analogously, trivariate polynomial splines are piecewise defined polynomials. Instead of intervals, which are 1-simplices, the trivariate polynomials are defined relative to 3-simplices, or tetrahedra.

Tetrahedral partitions are well known in crystallography and the finite element literature. We briefly discuss some facts of general tetrahedral partitions and tetrahedral subdivision schemes before we introduce the uniform BCC partition, which the approximation methods in this thesis are based on (see [17, 18]), in the next section. Many uniform tetrahedral partitions are constructed by subdividing each cell of a uniform cube partition into five or more tetrahedra, see [18]. This is not the case for the BCC partition, although its vertices form two interleaved cubic grids.

Definition 2.4. Let $v_0, \dots, v_3 \in \mathbb{R}^3$ be four non-coplanar points. The convex hull of these points is called a non-degenerate tetrahedron T . We denote tetrahedra by $T := \langle v_0, v_1, v_2, v_3 \rangle$. The points v_i , $i = 0, \dots, 3$, are called the vertices of T . The convex hull of any three of the vertices forms a triangle in 3-space and is called a face of T . Similarly, the convex hull of any two vertices forms a line in 3-space and is called an edge of T .

A tetrahedron has four distinct faces and six distinct edges. We denote faces and edges by $\langle v_0, v_1, v_2 \rangle$ and $\langle v_0, v_1 \rangle$, respectively, with similar notation for the other faces and edges of T . We say $\langle v_0, v_1, v_2 \rangle$ lies opposite the vertex v_3 and vice versa, and the edge $\langle v_0, v_1 \rangle$ is opposite to $\langle v_2, v_3 \rangle$.

The volume of any non-degenerate tetrahedron is positive and given by the following formula.

Lemma 2.5. The volume of a non-degenerate tetrahedron $T := \langle v_0, v_1, v_2, v_3 \rangle$ is given by

$$\text{vol}(T) := \frac{1}{6} \left| \det \begin{pmatrix} v_0 & v_1 & v_2 & v_3 \\ 1 & 1 & 1 & 1 \end{pmatrix} \right|.$$

The entry v_m in this matrix is a shorthand for the three coordinates of the vertex v_m , and thus the matrix is square.

Definition 2.6. Let $T := \langle v_0, v_1, v_2, v_3 \rangle$ be a non-degenerate tetrahedron. By $|T|$ we denote the length of the longest edge of T . Let ρ_T be the radius of the largest ball B such that $B \subset T$. We call B the insphere of T , ρ_T the inradius of T and the center of B the incenter of T . We define

$$\kappa_T := \frac{|T|}{\rho_T}$$

and call it the shape parameter of T .

The shape parameter of a regular tetrahedron, where all six edges are of the same length, is $12/\sqrt{6}$. For any other tetrahedron the shape parameter is larger. The shape parameter indicates how flat a tetrahedron is. Hence, it is related to certain angles inside the tetrahedron.

Definition 2.7. Let T be a non-degenerate tetrahedron. For each face F of T , we call the angles between the edges of F the face angles. We denote the smallest of the face angles by ϕ_T . For any two faces F_1, F_2 of T , we call the angle formed by these faces the dihedral angle of F_1 and F_2 . For a vertex v , let $B(v)$ be the ball around v that touches the plane defined by the opposite face, and r its radius. Let A be the area of the spherical triangle defined by the intersection of $B(v)$ with T . We call A/r the solid angle of T at v , and denote the smallest of all solid angles of T by θ_T .

Spline spaces are defined over a collections of tetrahedra. The following definition specifies how the tetrahedra in such a collection are interconnected.

Definition 2.8. *A system $\Delta = \{T_1, \dots, T_N\}$ of $N \in \mathbb{N}$ tetrahedra, where the intersection of any two tetrahedra $T_i \neq T_j \in \Delta$ is either empty, or a common vertex, or a common edge, or a common face, is called a tetrahedral partition of the region $\Omega := \bigcup_{i=1}^N T_i \subset \mathbb{R}^3$. We call*

$$|\Delta| := \max_{T \in \Delta} |T|$$

the mesh size of Δ . The unions of the vertices, edges, and faces of the tetrahedra of Δ are called the vertices, edges, and faces of Δ , respectively. The vertices of Δ sitting on the boundary of Ω are called the boundary vertices, and all other vertices are interior vertices. An edge is called a boundary edge if both its vertices are boundary vertices, while a face is called a boundary face if all three vertices are boundary vertices. The other edges and faces are called interior edges and interior faces, respectively. A tetrahedron which has at least one boundary face is called a boundary tetrahedron, while the other tetrahedra are interior tetrahedra. Two tetrahedra that share a common face are called neighbors.

We denote the smallest face angle of all tetrahedra in Δ by

$$\phi_\Delta := \min_{T \in \Delta} \phi_T$$

and the smallest solid angle by

$$\theta_\Delta := \min_{T \in \Delta} \theta_T.$$

Even though a tetrahedral partition Δ is a set of tetrahedra, it can also be interpreted as a set of points in 3-space. For the sake of convenience, we use the same notation for both aspects of a partition. Let x be a point and Ω a subset of \mathbb{R}^3 . Then we say $x \in \Delta$ if and only if there exists a tetrahedron $T \in \Delta$ with $x \in T$. Moreover, we define

$$\Omega \cap \Delta := \bigcup_{T \in \Delta} (\Omega \cap T).$$

We define certain sub-partitions of a tetrahedral partition, relative to a vertex or tetrahedron.

Definition 2.9. *Let Δ be a tetrahedral partition and V the set of its vertices. For a vertex $v \in V$, we define*

$$\text{star}(v) := \text{star}^1(v) := \{T \in \Delta; v \in T\},$$

and for $\ell > 1$,

$$\text{star}^\ell(v) := \{T \in \Delta; T \cap \text{star}^{\ell-1}(v) \neq \emptyset\}.$$

For a tetrahedron $T \in \Delta$, we define

$$\text{star}(T) := \text{star}^0(T) := \{T\},$$

and for $\ell > 0$,

$$\text{star}^\ell(T) := \{T \in \Delta; T \cap \text{star}^{\ell-1}(T) \neq \emptyset\}.$$

The diameter of a star can be estimated in terms of the longest edge of a tetrahedral partition. We develop the following lemma as a variant of lemma 16.19 in [46], where stars relative to a vertex are considered. Our version concerns stars relative to a tetrahedron.

Lemma 2.10. *Let Δ be a tetrahedral partition and $T \in \Delta$ a tetrahedron. Then*

$$|\Omega_T^\ell| \leq 2(\ell + 1)|\Delta|,$$

where

$$\Omega_T^\ell := \text{Conv} \left(\bigcup_{\tilde{T} \in \text{star}^\ell(T)} \tilde{T} \right).$$

Proof. We show by induction that Ω_T^ℓ is contained in a ball with radius $(\ell + 1)|\Delta|$. Let v_T be the barycenter of T and B_r the closed ball with center v_T and radius r . For $\ell = 0$, $\Omega_T^0 = T$. Since $|T| \leq |\Delta|$, $\|v_T - v\|_2 \leq |\Delta|$ for all $v \in T$ and thus $\Omega_T^0 \subset B_{|\Delta|}$. Now suppose that $\Omega_T^k \subset B_{(k+1)|\Delta|}$ for some $k \in \mathbb{N}_0$. Let $\tilde{T} \in \text{star}^{k+1}(T)$ and $v \in \tilde{T}$. By definition there exists a vertex $u \in \text{star}^k(T) \cap \tilde{T}$. But then

$$\|v_T - v\|_2 \leq \|v_T - u\|_2 + \|u - v\|_2 \leq (k + 1)|\Delta| + |\Delta|.$$

Thus, $\Omega_{k+1}^T \subset B_{(k+2)|\Delta|}$, which concludes the induction. \square

The definition of a tetrahedral partition allows for very general partitions which can contain holes or cavities, or can even consist of unconnected regions. For the remainder of this thesis, we restrict our study to tetrahedral partitions of contractible regions unless stated otherwise. The next theorem gives relationships between the number of vertices, edges, and faces of such partitions. These results can be found in [32]. These are known as the *Euler relations*.

Theorem 2.11 (Euler relations). *Let Δ be a tetrahedral partition of a simply connected region, and V_I, V_B, E_I, E_B, F_I and F_B be the sets of interior and boundary vertices, interior and boundary edges, and interior and boundary faces of Δ , respectively. Let $V = V_I \cup V_B$, $E = E_I \cup E_B$ and $F = F_I \cup F_B$. Then*

- (i) $\#\Delta = \#E_I + \#V_B - \#V_I - 3$,
- (ii) $\#\Delta = \#F_I/2 + \#F_B/4$,
- (iii) $\#E_B = 3\#V_B - 6$,
- (iv) $\#F_B = 2\#E_B/3$.

It often is necessary to refine a tetrahedron by splitting it into a number of subtetrahedra. Many macro-element methods make use of such refinements.

Definition 2.12. Let T be a tetrahedron. A tetrahedral partition Δ_T of T is called a refinement of T . The tetrahedra of Δ_T are called the subtetrahedra of T .

Refining each tetrahedron of a partition Δ results in a refinement of Δ , provided that the refinement is still a tetrahedral partition.

Definition 2.13. Let Δ be a tetrahedral partition of Ω , and for each $T \in \Delta$, let Δ_T be a refinement of T . The union

$$\Delta_R = \bigcup_{T \in \Delta} \Delta_T,$$

is called a refinement of Δ , if Δ_R is a tetrahedral partition of Ω .

This definition assures that the refinements of the individual tetrahedra are such that faces shared by two tetrahedra are split in the same fashion.

Common examples of refinements of a tetrahedron are the Alfeld split (or trivariate Clough-Tocher split, see [2]), the Worsey-Farin split (see [89]), and the partial Worsey-Farin split (see [41]). The Alfeld split results from introducing a new vertex in the interior of a tetrahedron, and connecting it with the four original vertices. It can be interpreted as the trivariate analogon to the well known bivariate Cough-Tocher split introduced in [25].

Definition 2.14. Let $T := \langle v_0, v_1, v_2, v_3 \rangle$ be a non-degenerate tetrahedron and v_T a point in the interior of T . The refinement

$$\Delta_{Alfeld}(T) := \{ \langle v_T, v_1, v_2, v_3 \rangle, \langle v_0, v_T, v_2, v_3 \rangle, \langle v_0, v_1, v_T, v_3 \rangle, \langle v_0, v_1, v_2, v_T \rangle \}$$

is called the Alfeld split of T .

Since the Alfeld split introduces no new vertices on the boundary of T , it can be applied to all tetrahedra in a tetrahedral partition without any restrictions.

The Worsey-Farin split can be interpreted as a refinement of the Alfeld split of a tetrahedron T . Each subtetrahedron of the Alfeld split is subdivided into three subtetrahedra by introducing a new vertex in the interior of each of the original faces of T .

Definition 2.15. Let $T := \langle v_0, v_1, v_2, v_3 \rangle$ be a non-degenerate tetrahedron, $v_4 := v_0$, $v_5 := v_1$, and v_T a point in the interior of T . For $i = 1, \dots, 4$, let $F_i := \langle v_{i-1}, v_i, v_{i+1} \rangle$ be the faces of T , and v_{F_i} a point in the interior of F_i . The tetrahedral partition

$$\Delta_{WF}(T) := \bigcup_{i=1}^4 \{ \langle v_{i-1}, v_i, v_{F_i}, v_T \rangle, \langle v_i, v_{i+1}, v_{F_i}, v_T \rangle, \langle v_{i+1}, v_{i-1}, v_{F_i}, v_T \rangle \}$$

is called the Worsey-Farin split of T .

When applying the Worsey-Farin split to each tetrahedron of a partition, it has to be made sure that the new vertices introduced to common faces of two neighboring tetrahedra match. Figure 2.1 shows The Alfeld split and the Worsey-Farin split of a tetrahedron.

The partial Worsey-Farin split is constructed in the same way as the Worsey-Farin split, but not necessarily all of the faces of the original tetrahedron are subdivided.

Definition 2.16. Let $T := \langle v_0, v_1, v_2, v_3 \rangle$ be a non-degenerate tetrahedron, $v_4 := v_0$, $v_5 := v_1$, and v_T a point in the interior of T . For $i = 1, \dots, 4$, let $F_i := \langle v_{i-1}, v_i, v_{i+1} \rangle$ be the faces of T . Given an integer $0 \leq m \leq 4$, let v_{F_i} be a point in the interior of F_i , $i = 1, \dots, m$, and

$$\tilde{\Delta}_i := \begin{cases} \{ \langle v_{i-1}, v_i, v_{F_i}, v_T \rangle, \langle v_i, v_{i+1}, v_{F_i}, v_T \rangle, \langle v_{i+1}, v_{i-1}, v_{F_i}, v_T \rangle \}, & 1 \leq i \leq m, \\ \{ \langle v_{i-1}, v_i, v_{i+1}, v_T \rangle \}, & m < i \leq 4. \end{cases}$$

Then we call

$$\Delta_{WF}^m(T) := \bigcup_{i=1}^4 \tilde{\Delta}_i$$

the m -th degree partial Worsey-Farin split of T .

Note that the partial Worsey-Farin split of degree 0 is identical to the Alfeld split, while the 4-th degree partial Worsey-Farin split is identical to the Worsey-Farin split, when applied with the same split points.

2.2 A tetrahedral partition based on the body-centered cubic grid

In this section we describe a tetrahedral partition which is the basis for the methods developed in chapters 3 and 5. The vertices of the partition are those of the well-known body-centered cubic grid. Given a regular cube partition of 3-space, the body-centered cubic grid is the union of the vertices

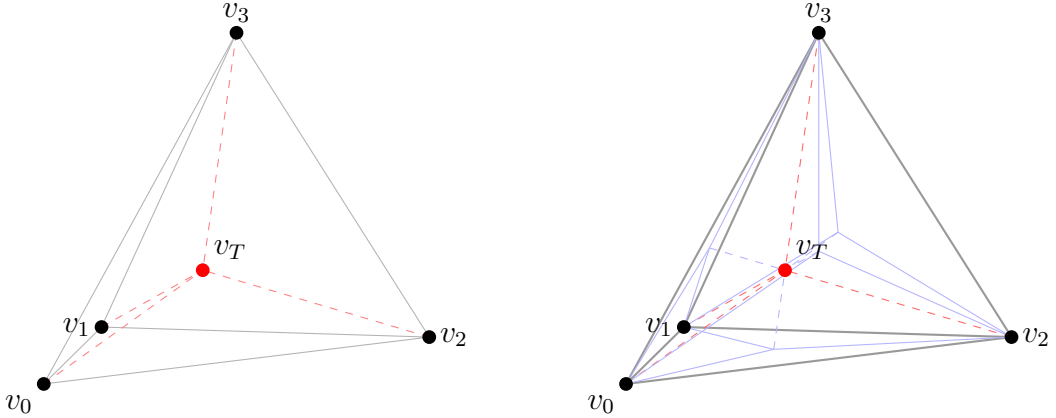


Figure 2.1: On the left side, the Alfeld split of a tetrahedron T is shown. The right side shows the Worsey-Farin split T . Dashed lines run in the interior of T . The blue solid lines split the faces of T .

of the cubes and their centers. Definitions of a uniform tetrahedral partition using these vertices can be found in [17, 18]. For our purposes we choose a slightly modified definition where we not only consider cubes, but also cuboids whose edges have not necessarily the same length. This allows us to use our methods on data sets which are generated by either computed tomography or magnetic resonance tomography. These data sets commonly sit on a cuboid grid, which may use different scales for each axis.

Definition 2.17. *Given a triple $H := (h_1, h_2, h_3) \in \mathbb{R}_+^3$ of positive real numbers, we define*

$$\mathcal{V}_H := \{v_{ijk} := (ih_1, jh_2, kh_3); i, j, k \in \mathbb{Z}\} \subset \mathbb{R}^3$$

and

$$\mathcal{W}_H := \{w_{ijk} := (h_1(i + \frac{1}{2}), h_2(j + \frac{1}{2}), h_3(k + \frac{1}{2})); i, j, k \in \mathbb{Z}\} \subset \mathbb{R}^3.$$

We call \mathcal{V}_H the set of cube vertices, and \mathcal{W}_H the set of cube centers. Both sets form uniform cubic grids. The union $\mathcal{V}_{BCC} := \mathcal{V}_H \cup \mathcal{W}_H$ of these two sets is called the body-centered cubic grid with spacing H .

Note that for each i, j, k , the vertices $\{v_{i+i',j+j',k+k'}; 0 \leq i', j', k' \leq 1\}$ form a rectangular cuboid with center w_{ijk} (cf. Figure 2.2). Likewise, a cuboid of the same size with center v_{ijk} is formed by the vertices $\{w_{i-i',j-j',k-k'}; 0 \leq i', j', k' \leq 1\}$. For the special case $h_1 = h_2 = h_3$, they form a cube.

We use the following notation to address the vertices relative to each other. A combination of letters is used to define the position of one vertex relative to another vertex. These letters L, R, U, D, F and B are mnemonics for the directions left, right, up, down, front and back, respectively.

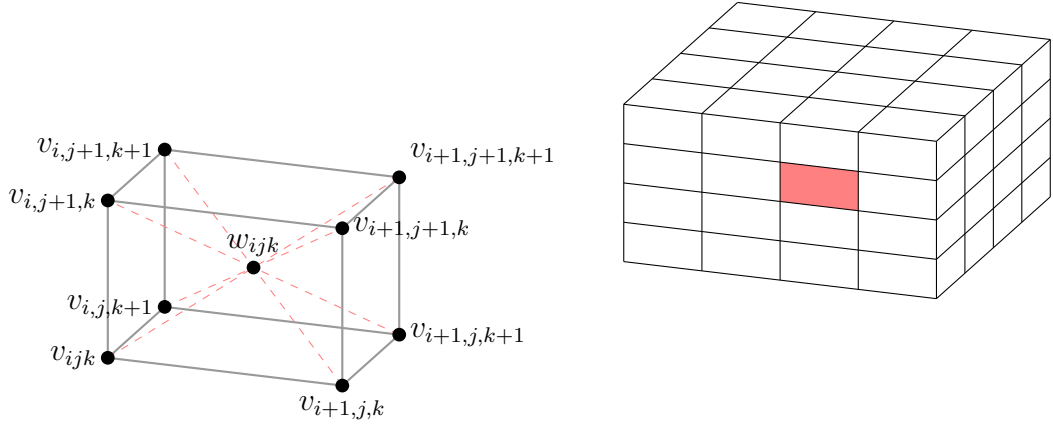


Figure 2.2: A portion of the cubic grid formed by the vertices in \mathcal{V}_H is shown on the right. On the left, the red cuboid with center w_{ijk} is shown.

Definition 2.18. Given a vertex $v \in \mathcal{V}_{BCC}$, with indices i, j, k . We define

$$\begin{aligned}
v_L &:= \begin{cases} v_{i-1,j,k}, & v \in \mathcal{V}_H, \\ w_{i-1,j,k}, & v \in \mathcal{W}_H. \end{cases} & v_R &:= \begin{cases} v_{i+1,j,k}, & v \in \mathcal{V}_H, \\ w_{i+1,j,k}, & v \in \mathcal{W}_H. \end{cases} \\
v_D &:= \begin{cases} v_{i,j-1,k}, & v \in \mathcal{V}_H, \\ w_{i,j-1,k}, & v \in \mathcal{W}_H. \end{cases} & v_U &:= \begin{cases} v_{i,j+1,k}, & v \in \mathcal{V}_H, \\ w_{i,j+1,k}, & v \in \mathcal{W}_H. \end{cases} \\
v_F &:= \begin{cases} v_{i,j,k-1}, & v \in \mathcal{V}_H, \\ w_{i,j,k-1}, & v \in \mathcal{W}_H. \end{cases} & v_B &:= \begin{cases} v_{i,j,k+1}, & v \in \mathcal{V}_H, \\ w_{i,j,k+1}, & v \in \mathcal{W}_H. \end{cases} \\
v_{LDF} &:= \begin{cases} w_{i-1,j-1,k-1}, & v \in \mathcal{V}_H, \\ v_{i,j,k}, & v \in \mathcal{W}_H. \end{cases} & v_{RDF} &:= \begin{cases} w_{i,j-1,k-1}, & v \in \mathcal{V}_H, \\ v_{i+1,j,k}, & v \in \mathcal{W}_H. \end{cases} \\
v_{LUF} &:= \begin{cases} w_{i-1,j,k-1}, & v \in \mathcal{V}_H, \\ v_{i,j+1,k}, & v \in \mathcal{W}_H. \end{cases} & v_{RUF} &:= \begin{cases} w_{i,j,k-1}, & v \in \mathcal{V}_H, \\ v_{i+1,j+1,k}, & v \in \mathcal{W}_H. \end{cases} \\
v_{LDB} &:= \begin{cases} w_{i-1,j-1,k}, & v \in \mathcal{V}_H, \\ v_{i,j,k+1}, & v \in \mathcal{W}_H. \end{cases} & v_{RDB} &:= \begin{cases} w_{i,j-1,k}, & v \in \mathcal{V}_H, \\ v_{i+1,j,k+1}, & v \in \mathcal{W}_H. \end{cases} \\
v_{LUB} &:= \begin{cases} w_{i-1,j,k}, & v \in \mathcal{V}_H, \\ v_{i,j+1,k+1}, & v \in \mathcal{W}_H. \end{cases} & v_{RUB} &:= \begin{cases} w_{i,j,k}, & v \in \mathcal{V}_H, \\ v_{i+1,j+1,k+1}, & v \in \mathcal{W}_H. \end{cases}
\end{aligned}$$

These vertices are shown in figure 2.3.

We obtain a tessellation consisting of tetrahedra and octahedra by connecting the vertices defined in (2.17). Each $v \in \mathcal{V}_{BCC}$ is connected to the four

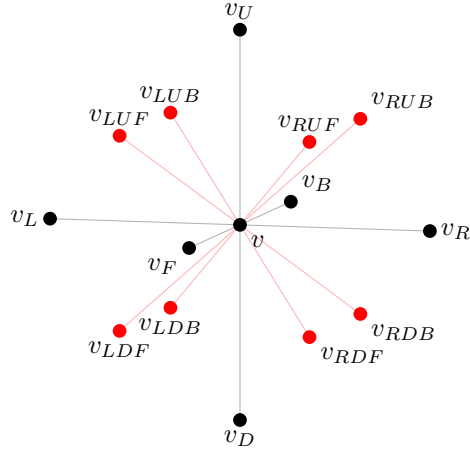


Figure 2.3: The vertices relative to v defined in 2.18. Black vertices are in the same set as v , while red vertices are in the other set.

vertices v_L, v_R, v_F and v_B . This results in a uniform rectangular tiling of each of the equidistant planes $y = j h_2 / 2$, $j \in \mathbb{Z}$. We continue by connecting v to the eight vertices $v_{LDF}, v_{RDF}, v_{LUF}, v_{RUF}, v_{LDB}, v_{RDB}, v_{LUB}$ and v_{RUB} . The result is a wireframe mesh which can be interpreted as a decomposition of 3-space into tetrahedra and octahedra. We use a similar notation to specify these relative to a vertex.

Definition 2.19. For each vertex $v \in \mathcal{V}_{BCC}$, we call

$$\begin{aligned} O_D(v) &:= \langle v, v_D, v_{LDF}, v_{RDF}, v_{LDB}, v_{RDB} \rangle, \\ O_U(v) &:= \langle v, v_U, v_{LUF}, v_{RUF}, v_{LUB}, v_{RUB} \rangle. \end{aligned}$$

the octahedra originating at v . Similar to the definition of tetrahedra, the angle brackets denote the convex hull of the enclosed vertices.

Connecting its first two vertices subdivides each tetrahedron into four tetrahedra. The resulting tetrahedral partition is the basis for all methods developed in this thesis.

Definition 2.20. For each vertex $v \in \mathcal{V}_{BCC}$, we call

$$\begin{aligned} T_{LD}(v) &:= \langle v, v_L, v_{LDF}, v_{LDB} \rangle, & T_{LU}(v) &:= \langle v, v_L, v_{LUF}, v_{LUB} \rangle, \\ T_{LF}(v) &:= \langle v, v_L, v_{LDF}, v_{LUF} \rangle, & T_{LB}(v) &:= \langle v, v_L, v_{LDB}, v_{LUB} \rangle, \\ T_{RD}(v) &:= \langle v, v_R, v_{RDF}, v_{RDB} \rangle, & T_{RU}(v) &:= \langle v, v_R, v_{RUF}, v_{RUB} \rangle, \\ T_{RF}(v) &:= \langle v, v_R, v_{RDF}, v_{RUF} \rangle, & T_{RB}(v) &:= \langle v, v_R, v_{RDB}, v_{RUB} \rangle, \\ T_{DL}(v) &:= \langle v, v_D, v_{LDF}, v_{LDB} \rangle, & T_{DR}(v) &:= \langle v, v_D, v_{RDF}, v_{RDB} \rangle, \\ T_{DF}(v) &:= \langle v, v_D, v_{LDF}, v_{RDF} \rangle, & T_{DB}(v) &:= \langle v, v_D, v_{LDB}, v_{RDB} \rangle, \\ T_{UL}(v) &:= \langle v, v_U, v_{LUF}, v_{LUB} \rangle, & T_{UR}(v) &:= \langle v, v_U, v_{RUF}, v_{RUB} \rangle, \\ T_{UF}(v) &:= \langle v, v_U, v_{LUF}, v_{RUF} \rangle, & T_{UB}(v) &:= \langle v, v_U, v_{LUB}, v_{RUB} \rangle, \\ T_{FL}(v) &:= \langle v, v_F, v_{LDF}, v_{LUF} \rangle, & T_{FR}(v) &:= \langle v, v_F, v_{RDF}, v_{RUF} \rangle, \\ T_{FD}(v) &:= \langle v, v_F, v_{LDF}, v_{RDF} \rangle, & T_{FU}(v) &:= \langle v, v_F, v_{LUF}, v_{RUF} \rangle, \\ T_{BL}(v) &:= \langle v, v_B, v_{LDB}, v_{LUB} \rangle, & T_{BR}(v) &:= \langle v, v_B, v_{RDB}, v_{RUB} \rangle, \\ T_{BD}(v) &:= \langle v, v_B, v_{LDB}, v_{RDB} \rangle, & T_{BU}(v) &:= \langle v, v_B, v_{LUB}, v_{RUB} \rangle. \end{aligned}$$

the tetrahedra originating at v . We denote the union of the tetrahedra originating at v by $\mathcal{T}(v)$, and call

$$\Delta_{BCC} := \bigcup_{v \in \mathcal{V}_{BCC}} \mathcal{T}(v)$$

the BCC partition with spacing H .

For each pair of index letters, there are two distinct tetrahedra with these letters. The tetrahedra $T_{DL}(v)$ and $T_{LD}(v)$, for example, do not define the same tetrahedron.

Remark 2.21. Two of the vertices of each tetrahedron T in the resulting tetrahedral partition are in the set \mathcal{V}_H , while the other two vertices are in \mathcal{W}_H . Hence, of the six edges of T , one connects vertices in \mathcal{V}_H , one connects vertices in \mathcal{W}_H , while the remaining four share one vertex each of \mathcal{V}_H and \mathcal{W}_H . These four edges have the same length, which is half the length of the space diagonal of a cuboid. This results in three different types of tetrahedra, identified by the lengths of their edges. They are shown in figure 2.4.

Our next lemma concerns the mesh size of the BCC partition, which is closely related to the spacing parameters.

Lemma 2.22. Let Δ_{BCC} be the BCC partition with spacing $H := (h_1, h_2, h_3)$. Then

$$|\Delta_{BCC}| = \max_{i=1,2,3} h_i.$$

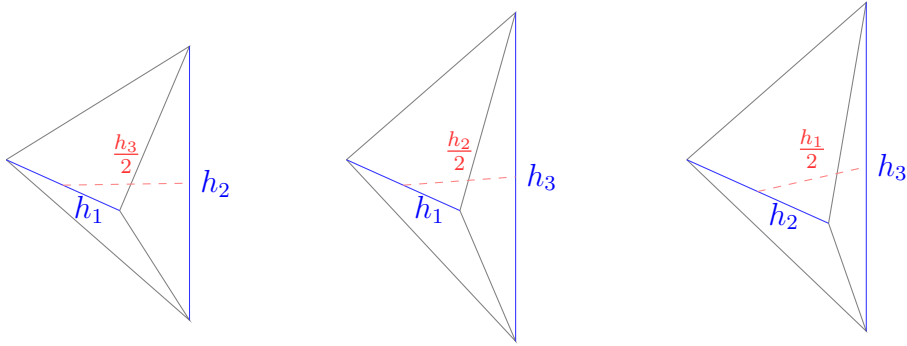


Figure 2.4: The three different types of tetrahedra of Δ_{BCC} . They gray edges all have the same length, $\sqrt{h_1^2 + h_2^2 + h_3^2}/2$.

Proof. Let $Q := [v_{ijk}, v_{i+1,j,k}] \times [v_{ijk}, v_{i,j+1,k}] \times [v_{ijk}, v_{i,j,k+1}]$. The length of the space diagonal of the cuboid Q is $h_s := \sqrt{h_1^2 + h_2^2 + h_3^2}$. Looking at the edges e_i of a tetrahedron $T \in \Delta_{BCC}$ and remark 2.21, we see that $|e_i| \in \{h_1, h_2, h_3, h_s/2\}$. Let $h_{max} := \max_{j=1,2,3} h_j$, then

$$\frac{h_s}{2} = \frac{1}{2}\sqrt{h_1^2 + h_2^2 + h_3^2} \leq \frac{1}{2}\sqrt{3h_{max}^2} \leq \frac{1}{2}h_{max}\sqrt{3} < h_{max}.$$

Thus, $|\Delta_{BCC}| = \max_{i=1,2,3} h_i$. □

The shape and the angles of the tetrahedra of Δ_{BCC} are determined by the ratio of the smallest and largest spacing parameters. Our following lemma estimates the lengths of the edges of Δ_{BCC} in terms of that ratio.

Lemma 2.23. *Let Δ_{BCC} be the BCC partition with spacing $H := (h_1, h_2, h_3)$, $h_{min} := \min\{h_1, h_2, h_3\}$ and $h_{max} := \max\{h_1, h_2, h_3\}$. We call*

$$K_H := \frac{h_{min}}{h_{max}}$$

the shape parameter of Δ_{BCC} . For any $T \in \Delta_{BCC}$,

$$(i) \quad K_H |\Delta_{BCC}| \leq |T| \leq |\Delta_{BCC}|,$$

$$(ii) \quad \rho_T \geq \frac{\sqrt{2}K_H^2}{8} |T|.$$

Proof. Fix $T \in \Delta_{BCC}$. By the construction of Δ_{BCC} , one of the edges of T connects two vertices $v_0, v_1 \in \mathcal{V}_H$, and the opposite edge of T connects two vertices $v_2, v_3 \in \mathcal{W}_H$. Let $e_1 := \langle v_0, v_1 \rangle$ and $e_2 := \langle v_2, v_3 \rangle$ be these edges.

(i). By lemma 2.22, $|\Delta_{BCC}| = h_{max}$. Thus, $K_H |\Delta_{BCC}| = h_{min}$. Since $|e_1|, |e_2| \in \{h_1, h_2, h_3\}$, the first inequality follows. The second inequality of (i) follows from the definition of the mesh size.

(ii). We calculate the inradius of T . Suppose T is a tetrahedron with edge lengths $|e_1| = h_1$, $|e_2| = h_2$, as depicted in figure 2.5 on the left. Due to the symmetry of the partition, the incenter v_ρ is located on the line connecting the midpoints of e_1 and e_2 which we call u_1 and u_2 , respectively. The line segment $\langle u_1, u_2 \rangle$ is perpendicular to both edges e_1 and e_2 and has the length $\frac{h_3}{2}$. Let w_1 and w_2 be the point of intersection of the insphere with the faces $\langle v_1, v_2, v_3 \rangle$ and $\langle v_0, v_1, v_2 \rangle$, respectively. The points v_0, v_1, u_1, u_2, w_1 and v_ρ are coplanar and sit on a isosceles triangle with vertices v_0, v_1, u_2 . The edges of this triangle have the lengths h_1 , h'_1 and h'_1 , where

$$h'_1 := \sqrt{\left(\frac{h_3}{2}\right)^2 + \left(\frac{h_1}{2}\right)^2}.$$

Likewise, the points v_2, v_3, u_1, u_2, w_2 and v_ρ are coplanar and sit on a isosceles triangle with vertices v_2, v_3, u_1 and edges with lengths h_2 , h'_2 and h'_2 , where

$$h'_2 := \sqrt{\left(\frac{h_3}{2}\right)^2 + \left(\frac{h_2}{2}\right)^2}.$$

Both triangles are shown in figure 2.5.

The triangles $\langle u_2, v_\rho, w_1 \rangle$ and $\langle u_2, v_0, u_1 \rangle$ are similar, and we use the intercept theorem to calculate ρ_T . Let $d := \|u_2, v_\rho\|_2$, then

$$\frac{\rho_T}{d} = \frac{h_1/2}{h'_1}.$$

The triangles $\langle v_\rho, w_2, u_1 \rangle$ and $\langle v_3, u_2, u_1 \rangle$ are also similar. Note that $\|u_1, v_\rho\|_2 = \frac{h_3}{2} - d$. We use the intercept theorem again and obtain

$$\frac{\rho_T}{\frac{h_3}{2} - d} = \frac{h_2/2}{h'_2}.$$

We solve for d and combine the equations, then solve for ρ_T which yields

$$\rho_T = \frac{h_1 h_2 h_3}{4(h_1 h'_2 + h_2 h'_1)} = \frac{h_1 h_2 h_3}{2 \left(h_1 \sqrt{h_2^2 + h_3^2} + h_2 \sqrt{h_1^2 + h_3^2} \right)}.$$

The length of the longest edge of T is either h_1 or h_2 , since the other edges have the lengths

$$\frac{1}{2} \sqrt{h_1^2 + h_2^2 + h_3^2} \leq \frac{1}{2} \sqrt{3h_{min}^2} \leq h_{min}.$$

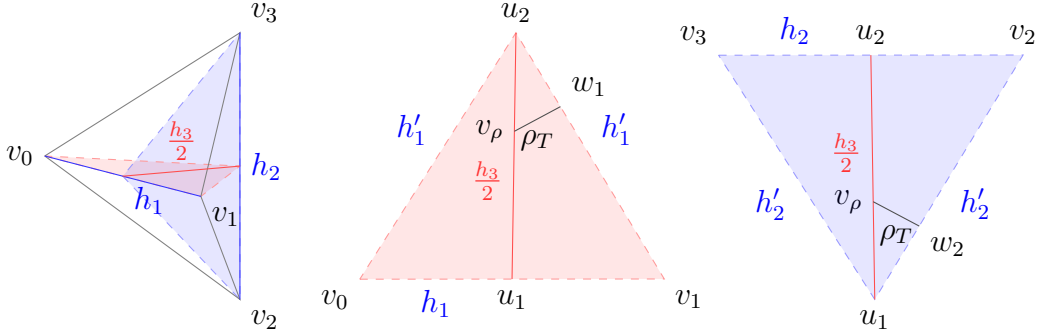


Figure 2.5: Calculation of the inradius. Due to the symmetry of the tetrahedra, the incenter is located on the line connecting the midpoints of two opposite edges.

Then we estimate

$$\begin{aligned} \rho_T &\geq \frac{|T| h_{min}^2}{2 \left(h_{max} \sqrt{h_{max}^2 + h_{max}^2} + h_{max} \sqrt{h_{max}^2 + h_{max}^2} \right)} \\ &\geq \frac{|T| h_{min}^2}{2 \left(\sqrt{2} h_{max}^2 + \sqrt{2} h_{max}^2 \right)} = \frac{|T| h_{min}^2}{4\sqrt{2} h_{max}^2} = \frac{|T| K_H^2}{4\sqrt{2}}. \end{aligned}$$

The proof is analogous for the other types of tetrahedra. \square

Our following lemma shows how the distance between two vertices of the BCC partition can be expressed in terms of vertex stars.

Lemma 2.24. *Let $v, w \in \mathcal{V}_{BCC}$ with $w = v + (xh_1, yh_2, zh_3)$. Then*

$$w \in \text{star}^N(v),$$

where

$$N := |x| + |y| + |z| - \min\{|x|, |y|, |z|\}.$$

Proof. We show that there exists a sequence of N edges that connect v to w . Note that x, y and z are multiples of $\frac{1}{2}$, since both v and w are vertices of Δ_{BCC} . Thus, there exist integers i, j, k with $i = 2x, j = 2y$ and $k = 2z$. Since $\mathcal{W}_H = \mathcal{V}_H + (h_1, h_2, h_3)/2$, i, j and k are either all even, or all odd. Let $r := \min\{|x|, |y|, |z|\}$. Then $2r$ is also an integer and has the same parity as i, j and k , and the numbers $|i| - 2r, |j| - 2r$ and $|k| - 2r$ are even. It follows that the numbers $|x| - r, |y| - r$ and $|z| - r$ are non-negative integers. Let

$$\begin{aligned} e_x &:= (\text{sgn}(x)h_1, 0, 0), & e_y &:= (0, \text{sgn}(y)h_2, 0), \\ e_z &:= (0, 0, \text{sgn}(z)h_3), & e_s &:= \frac{1}{2}(e_x + e_y + e_z). \end{aligned}$$

Then if u is a vertex of Δ_{BCC} , so are $u + e_x$, $u + e_y$, $u + e_z$ and $u + e_s$. Let $v_0 := v$ and

$$v_\ell := \begin{cases} v_{\ell-1} + e_x, & 0 < \ell \leq |x| - r, \\ v_{\ell-1} + e_y, & |x| - r < \ell \leq |x| - r + |y| - r, \\ v_{\ell-1} + e_z, & |x| - r + |y| - r < \ell \leq |x| - r + |y| - r + |z| - r, \\ v_{\ell-1} + e_s, & \ell > |x| - r + |y| - r + |z| - r. \end{cases}$$

But then, since

$$N = |x| + |y| + |z| - r = (|x| - r) + (|y| - r) + (|z| - r) + 2r,$$

$$\begin{aligned} v_N &= v + (|x| - r)e_x + (|y| - r)e_y + (|z| - r)e_z + 2re_s \\ &= v + |x|e_x + |y|e_y + |z|e_z + 2re_s - r(e_x + e_y + e_z) \\ &= v + (xh_1, yh_2, zh_3) = w, \end{aligned}$$

and it follows that there exists a sequence of N edges $e_\ell := \langle v_{\ell-1}, v_\ell \rangle$, $\ell = 1, \dots, N$, that connect v to w . \square

The following corollary shows how this result can be applied to tetrahedra.

Corollary 2.25. *Let $T := \langle v_0, v_1, v_2, v_3 \rangle \in \Delta_{BCC}$ be a tetrahedron and $w \in \mathcal{V}_{BCC}$ a vertex of the BCC partition. For $m = 0, \dots, 3$, let N_m be the number from lemma 2.24 such that $w \in \text{star}^{N_m}(v_m)$. Then*

$$w \in \text{star}^N(T),$$

where

$$N := \min_{m=0,\dots,3} N_m.$$

2.3 Bernstein-Bézier techniques

The splines considered in this thesis are trivariate piecewise polynomial functions defined on tetrahedral partitions. We begin this section with some general results about polynomial approximation, before we introduce the Bernstein basis for trivariate polynomials.

Definition 2.26. *The space of trivariate polynomials of total degree d is defined as*

$$\mathcal{P}_d := \text{span} \{x^i y^j z^k; i, j, k \in \mathbb{N}_0, 0 \leq i + j + k \leq d\}.$$

The dimension of that space is well-known.

Lemma 2.27 (Lemma 15.1 in [46]). *The dimension of the space \mathcal{P}_d is $\binom{d+3}{3}$.*

Polynomials are an important tool in the field of approximation theory. There exist a number of results on the approximation power of polynomials. We will use a few of these results to provide error bounds for the splines constructed in this thesis.

The following result is the multivariate equivalent of the well-known Markov inequality. It has been formulated and proven in [26] and [87]. We use the specialized version of the inequality for the maximum norm on a tetrahedron that can be found in [46] (Theorem 15.28).

Theorem 2.28. *Let T be a non-degenerate tetrahedron and $p \in \mathcal{P}_d$ a polynomial. Then there exists a constant $K > 0$ depending only on d , such that*

$$\|D^\alpha p\|_T \leq \frac{K}{\rho_T^{|\alpha|}} \|p\|_T, \quad (2.1)$$

where ρ_T is the inradius of T .

Another important result concerns the approximation power of polynomials, using the multivariate Taylor polynomial.

Theorem 2.29 (Theorem 15.32 in [46]). *Let $\Omega \subseteq \mathbb{R}^3$ be convex and compact and fix $d \in \mathbb{N}_0$. Then for each $f \in C^{d+1}(\Omega)$ there exists a polynomial $p_f \in \mathcal{P}_d$, such that*

$$\|D^\alpha(f - p_f)\|_\Omega \leq K |\Omega|^{d+1-|\alpha|} |f|_{d+1,\Omega}, \quad 0 \leq |\alpha| \leq d, \quad (2.2)$$

where K is a positive constant depending only on d . This polynomial is called the Taylor polynomial of degree d associated with f and has the form

$$p_f(v) := \sum_{|\alpha| \leq d} \frac{D^\alpha f(u)}{\alpha!} (v - u)^\alpha,$$

with u being the center of the largest ball B such that $B \subseteq \Omega$.

The inequality (2.2) also holds for non-convex domains Ω with a Lipschitz smooth boundary. In these cases, we use a theorem by Stein (see [84], p.181) to extend $D^\alpha(f - p_f)$ to $\text{Conv}(\Omega)$. The constant K then also depends on the Lipschitz constant of the boundary of Ω .

We will now introduce an alternative basis for the space of trivariate polynomials, which is far more suitable than the monomial basis when working with splines on tetrahedral partitions. This basis uses the Bernstein basis polynomials, which were introduced for the univariate case in 1912 by S. Bernstein, when he used them for an elegant proof of the Weierstrass theorem in [8]. French engineer P. Bézier used this basis in the early 1960's to

represent curves in CAGD. Some details on his work can be found in [37], while [9] is a translation of his book from French. The generalization to the trivariate setting has been extensively studied in the literature, see [36, 37, 39] for details. The properties of the B-form and related theorems given in this section can be found in [13, 39, 40, 46, 47].

The fundamental building blocks of the Bernstein basis polynomials are certain linear polynomials which are symmetric to a tetrahedron T . The earliest reference to these barycentric coordinates we have found is in [56].

Definition 2.30. Let $T := \langle v_0, v_1, v_2, v_3 \rangle$ be some non-degenerate tetrahedron. The unique linear polynomials $\varphi_m^T : \mathbb{R}^3 \rightarrow \mathbb{R}$, $m = 0, \dots, 3$, defined by

$$\begin{aligned}\varphi_0^T(v) &:= \frac{\det \begin{pmatrix} v & v_1 & v_2 & v_3 \\ 1 & 1 & 1 & 1 \end{pmatrix}}{\det \begin{pmatrix} v_0 & v_1 & v_2 & v_3 \\ 1 & 1 & 1 & 1 \end{pmatrix}}, & \varphi_1^T(v) &:= \frac{\det \begin{pmatrix} v_0 & v & v_2 & v_3 \\ 1 & 1 & 1 & 1 \end{pmatrix}}{\det \begin{pmatrix} v_0 & v_1 & v_2 & v_3 \\ 1 & 1 & 1 & 1 \end{pmatrix}}, \\ \varphi_2^T(v) &:= \frac{\det \begin{pmatrix} v_0 & v_1 & v & v_3 \\ 1 & 1 & 1 & 1 \end{pmatrix}}{\det \begin{pmatrix} v_0 & v_1 & v_2 & v_3 \\ 1 & 1 & 1 & 1 \end{pmatrix}}, & \varphi_3^T(v) &:= \frac{\det \begin{pmatrix} v_0 & v_1 & v_2 & v \\ 1 & 1 & 1 & 1 \end{pmatrix}}{\det \begin{pmatrix} v_0 & v_1 & v_2 & v_3 \\ 1 & 1 & 1 & 1 \end{pmatrix}},\end{aligned}$$

are the barycentric coordinates relative to T . Note that the barycentric coordinates are well-defined, since the determinant in the denominator is non-zero for non-degenerate tetrahedra. For a fixed $v \in \mathbb{R}^3$, the 4-tuple $(\varphi_0^T(v), \varphi_1^T(v), \varphi_2^T(v), \varphi_3^T(v))$ is called the barycentric coordinates of v relative to T .

It often will be clear from context which tetrahedron we are referring to. In those cases we sometimes write φ_m instead of φ_m^T .

We now state some properties of the barycentric coordinates.

Lemma 2.31. Let $T := \langle v_0, v_1, v_2, v_3 \rangle$ be some non-degenerate tetrahedron and φ_i , $i = 0, \dots, 3$, the barycentric coordinates relative to T .

(i) For $i, j \in \{0, \dots, 3\}$,

$$\varphi_i(v_j) = \delta_{ij}. \quad (2.3)$$

(ii) (Partition of unity)

$$\sum_{m=0}^3 \varphi_m(v) = 1 \quad (2.4)$$

for all $v \in \mathbb{R}^3$.

(iii) (*Non-negativity on T*)

For $m = 0, \dots, 3$ and $v \in T$,

$$\varphi_m(v) \geq 0. \quad (2.5)$$

Moreover, the barycentric coordinates of v are simultaneously non-negative if and only if $v \in T$:

$$\varphi_m(v) \geq 0 \text{ for all } m = 0, \dots, 3 \quad \Leftrightarrow \quad v \in T.$$

(iv) (*Reproduction of the identity*)

Every $v \in \mathbb{R}^3$ has the unique representation

$$v = \sum_{m=0}^3 \varphi_m(v) v_m. \quad (2.6)$$

Proof. Part (i) follows immediately from the definition. If $i = j$, the determinants in the numerator and denominator are equal, and if $i \neq j$, the matrix in the numerator is singular.

To show that (ii) and (iv) hold, we consider the linear system

$$\begin{pmatrix} v_0 & v_1 & v_2 & v_3 \\ 1 & 1 & 1 & 1 \end{pmatrix} \phi = \begin{pmatrix} v \\ 1 \end{pmatrix}.$$

The matrix is nonsingular, and the solution is $\phi = (\varphi_0(v), \varphi_1(v), \varphi_2(v), \varphi_3(v))$ by Cramer's rule.

The functions φ_m are linear polynomials. It follows from (i) that $\varphi_m(v) = 0$ for all $v \in \pi_m$, where π_m is the plane containing the face of T which lies opposite of v_m . This plane divides \mathbb{R}^3 into two regions, $\pi_m^+ := \{v \in \mathbb{R}^3; \varphi_m(v) \geq 0\}$ and $\pi_m^- := \{v \in \mathbb{R}^3; \varphi_m(v) \leq 0\}$. Since $\varphi_m(v_m) = 1$, $T \subset \pi_m^+$. Thus $T = \cap_{m=0}^3 \pi_m^+$, and (iii) follows. \square

Our following lemma reveals the relationship between the barycentric coordinates relative to two neighboring tetrahedra.

Lemma 2.32. *Let $T := \langle v_0, v_1, v_2, v_3 \rangle$ and $\tilde{T} := \langle v_0, v_1, v_2, \tilde{v}_3 \rangle$ be two non-degenerate tetrahedra that share a common face, and let v be some point in 3-space. Let $\psi_i := \varphi_i^T(\tilde{v}_3)$ and $\varphi_i := \varphi_i^T(v)$, $i = 0, \dots, 3$, be the barycentric coordinates of \tilde{v}_3 and v relative to T , respectively. Then the barycentric coordinates of v relative to \tilde{T} are*

$$\varphi_i^{\tilde{T}}(v) = \varphi_i - \psi_i \frac{\varphi_3}{\psi_3}, \quad i = 0, 1, 2, \quad \text{and} \quad \varphi_3^{\tilde{T}}(v) = \frac{\varphi_3}{\psi_3}.$$

Proof. Since \tilde{T} is non-degenerate, \tilde{v}_3 is not in the plane passing through v_0, v_1, v_2 . Thus, $\psi_3 \neq 0$. Using (2.6), we get

$$v = \varphi_0 v_0 + \varphi_1 v_1 + \varphi_2 v_2 + \varphi_3 v_3 \quad \text{and} \quad \tilde{v}_3 = \psi_0 v_0 + \psi_1 v_1 + \psi_2 v_2 + \psi_3 v_3. \quad (2.7)$$

Let $\tilde{\varphi}_i$, $i = 0, \dots, 3$, be the barycentric coordinates of v relative to \tilde{T} . Then

$$v = \tilde{\varphi}_0 v_0 + \tilde{\varphi}_1 v_1 + \tilde{\varphi}_2 v_2 + \tilde{\varphi}_3 \tilde{v}_3.$$

We substitute v and \tilde{v}_3 in the equation above with (2.7).

$$\varphi_0 v_0 + \varphi_1 v_1 + \varphi_2 v_2 + \varphi_3 v_3 = \tilde{\varphi}_0 v_0 + \tilde{\varphi}_1 v_1 + \tilde{\varphi}_2 v_2 + \tilde{\varphi}_3 (\psi_0 v_0 + \psi_1 v_1 + \psi_2 v_2 + \psi_3 v_3).$$

Collecting the terms yields

$$0 = (\tilde{\varphi}_0 + \tilde{\varphi}_3 \psi_0 - \varphi_0) v_0 + (\tilde{\varphi}_1 + \tilde{\varphi}_3 \psi_1 - \varphi_1) v_1 + (\tilde{\varphi}_2 + \tilde{\varphi}_3 \psi_2 - \varphi_2) v_2 + (\tilde{\varphi}_3 \psi_3 - \varphi_3) v_3.$$

Since T is non-degenerate, the coefficients of the vertices must be zero, and solving for $\tilde{\varphi}_i$ concludes the proof. \square

The barycentric coordinates are the fundamental building blocks of the well-known Bernstein basis polynomials. These polynomials form an alternative basis of \mathcal{P}_d , which is highly suitable for the representation of piecewise polynomials defined on tetrahedra. Bernstein basis polynomials are defined relative to some tetrahedron T .

Definition 2.33. Let $T := \langle v_0, v_1, v_2, v_3 \rangle$ be some non-degenerate tetrahedron and $d \in \mathbb{N}_0$. For all non-negative integers i, j, k, l with $i + j + k + l = d$, the trivariate Bernstein basis polynomials of degree d are defined as

$$B_{ijkl}^T(v) := \frac{d!}{i!j!k!l!} \varphi_0^i(v) \varphi_1^j(v) \varphi_2^k(v) \varphi_3^l(v), \quad v \in \mathbb{R}^3,$$

where φ_m , $m = 0, \dots, 3$, are the barycentric coordinates relative to T . For simplicity's sake, we define $0^0 := 1$ in this context.

If at least one of the indices i, j, k, l is negative, we define $B_{ijkl} := 0$.

Note that for the Bernstein basis polynomials of degree 1 are the barycentric coordinates:

$$B_{1000}^T = \varphi_0^T, \quad B_{0100}^T = \varphi_1^T, \quad B_{0010}^T = \varphi_2^T, \quad B_{0001}^T = \varphi_3^T.$$

When dealing with Bernstein basis polynomials, it often is clear which tetrahedron we are referring to. In those cases we may omit the superscript T , writing B_{ijkl} instead of B_{ijkl}^T .

The following theorem states that the Bernstein basis polynomials form a basis of the space of trivariate polynomials.

Theorem 2.34 (Theorem 15.8 in [46]). *Let T be some non-degenerate tetrahedron and $d \in \mathbb{N}_0$, then*

$$\mathcal{P}_d = \text{span} \{ B_{ijkl}^T; i + j + k + l = d \}.$$

We give some important properties of the Bernstein basis polynomials. Some of those properties are inherited from the barycentric coordinates.

Lemma 2.35. *Let $T := \langle v_0, v_1, v_2, v_3 \rangle$ be some non-degenerate tetrahedron, B_{ijkl} , $i + j + k + l = d \in \mathbb{N}_0$, the Bernstein basis polynomials of degree d relative to T , and φ_m , $m = 0, \dots, 3$, the barycentric coordinates relative to T .*

(i) *(Recursion formula)*

The Bernstein basis polynomials comply with the recursion

$$B_{ijkl} := \begin{cases} 0, & i < 0, j < 0, k < 0 \text{ or } l < 0, \\ 1, & i = j = k = l = 0, \\ \varphi_0 B_{i-1,j,k,l} + \varphi_1 B_{i,j-1,k,l} \\ + \varphi_2 B_{i,j,k-1,l} + \varphi_3 B_{i,j,k,l-1} & \text{otherwise.} \end{cases}$$

(ii) *(Partition of unity)*

For all $d \in \mathbb{N}_0$ and $v \in \mathbb{R}^3$,

$$\sum_{i+j+k+l=d} B_{ijkl}(v) = 1, \quad (2.8)$$

(iii) *(Non-negativity on T)*

$$B_{ijkl}(v) \geq 0 \text{ for all } i + j + k + l = d \quad \Leftrightarrow \quad v \in T. \quad (2.9)$$

(iv) *(Symmetry)*

The Bernstein basis polynomials relative to T are symmetric in the following sense. For all $v \in \mathbb{R}^3$, Then

$$B_{ijkl}(v) = B_{jikl}(\tilde{v}), \quad i + j + k + l = d,$$

with $\tilde{v} := \varphi_1(v)v_0 + \varphi_0(v)v_1 + \varphi_2(v)v_2 + \varphi_3(v)v_3$. This follows immediately from the definition of the Bernstein basis polynomials. The Bernstein basis polynomials exhibit other symmetries analogously.

Proof. The recursion formula in (i) follows immediately from the definition of the Bernstein basis polynomials.

To show that (ii) holds, we use the binomial expansion and (2.4) to obtain

$$1 = 1^d = \left(\sum_{m=0}^3 \varphi_m(v) \right)^d = \sum_{i+j+k+l=d} B_{ijkl}(v).$$

Part (iii) is an immediate consequence of 2.31 (iii), and (iv) again follows from the definition of the Bernstein basis polynomials. \square

In view of theorem 2.34 it is clear that every trivariate polynomial of total degree d can be written as a linear combination of the Bernstein basis polynomials of degree d relative to some non-degenerate tetrahedron T . This representation of polynomials is known as the B-form to recognize the works of both Bernstein and Bézier (see [13]). Polynomials in B-form are also known as *Bernstein polynomials* in the literature.

Definition 2.36. Let T be a non-degenerate tetrahedron, $d \in \mathbb{N}$, and $p \in \mathcal{P}_d$. The representation

$$p \equiv \sum_{i+j+k+l=d} c_{ijkl} B_{ijkl}, \quad (2.10)$$

is called the B-form (relative to T) of p . The coefficients c_{ijkl} are called the B-coefficients of p .

Remark 2.37. Note that most Bernstein basis polynomials associated with a tetrahedron T vanish on the planes containing the faces of T . For example, let $F := \langle v_0, v_1, v_2 \rangle$ and P_F the plane containing F , then the barycentric coordinate φ_3 relative to T is zero for each $v \in P_F$. It follows from definition 2.33 that

$$B_{ijkl}(v) = 0 \quad \text{for all } v \in P_F \text{ and } l \neq 0,$$

since in these cases $\varphi_3^l(v) = 0$. Thus, the B-form of p restricted to this plane can be written as

$$p|_{P_F} \equiv \sum_{i+j+k+l=d} c_{ijkl} B_{ijkl} \equiv \sum_{i+j+k=d} c_{ijk0} B_{ijk0},$$

which essentially is a bivariate polynomial.

Similarly, p becomes a univariate polynomial when restricted to a line containing one of the edges of T .

Associated with the B-coefficient are certain equally spaced points on T .

Definition 2.38. Let T be a non-degenerate tetrahedron and $d \in \mathbb{N}$. The points

$$\xi_{ijkl}^T := \frac{i}{d} v_0 + \frac{j}{d} v_1 + \frac{k}{d} v_2 + \frac{l}{d} v_3, \quad i + j + k + l = d$$

are called the domain points of degree d relative to T . We denote the set of domain points relative to T by

$$\mathcal{D}_d(T) := \{\xi_{ijkl}; i + j + k + l = d\}.$$

Certain subsets of the domain points are frequently used. We denote

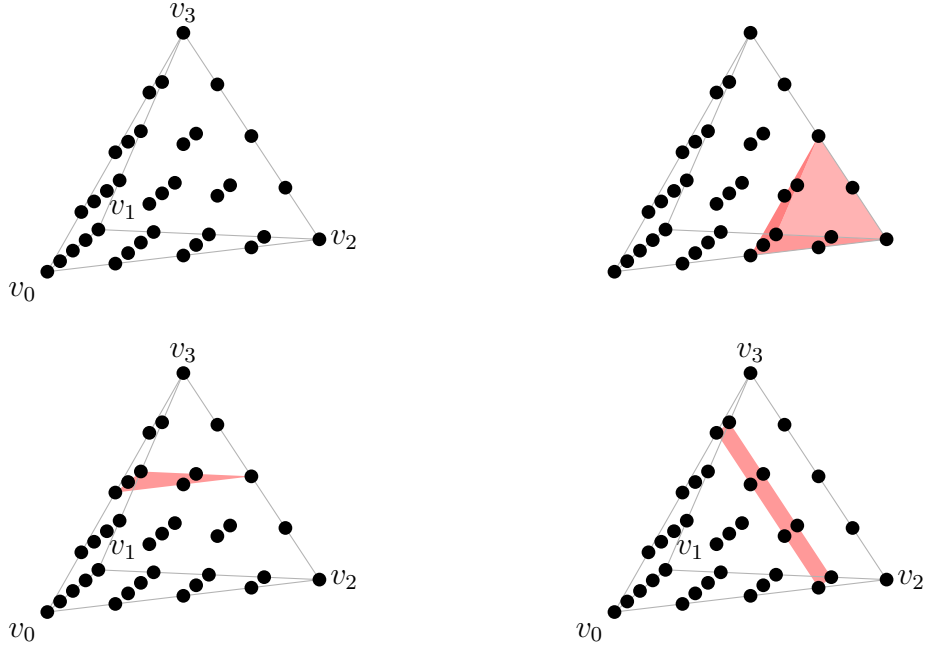


Figure 2.6: The domain points of degree 4 are shown in the upper left. In the upper right, the C^2 ball around v_2 ($D_2^T(v_2)$) is shown. The figures in the lower left and lower right show the C^2 shell around v_3 ($R_2^T(v_3)$) and the C^1 tube around the edge $\langle v_2, v_3 \rangle$ ($t_1^T(\langle v_2, v_3 \rangle)$), respectively.

- the ball of radius r around v_0 by

$$D_r^T(v_0) := \{\xi_{ijkl}^T; i \geq d - r\}.$$

- the shell of radius r around v_0 by

$$R_r^T(v_0) := \{\xi_{ijkl}^T; i = d - r\}.$$

- the tube of radius r around the edge $e := \langle v_0, v_1 \rangle$ by

$$t_r^T(e) := \{\xi_{ijkl}^T; i + j = d - r\}.$$

For the other vertices and edges, as use the analogous definitions.

Figure 2.6 shows the domain points of degree 4 and various subsets thereof.

Note that for each B-coefficient c_{ijkl} of a trivariate polynomial p in B-form relative to T , there exists a domain point $\xi_{ijkl} \in \mathcal{D}_d(T)$. Let $\xi = \xi_{ijkl}$, then

we call $c_\xi := c_{ijkl}$ the *associated B-coefficient* and $B_\xi := B_{ijkl}$ the *associated Bernstein basis polynomial*. Using this notation, we can write

$$p \equiv \sum_{\xi \in \mathcal{D}_d(T)} c_\xi B_\xi$$

for (2.10). The four-dimensional vector consisting of the coordinates of a domain point and the associated B-coefficient is called a *control point* of p . The following theorem shows that the graph of p runs inside the convex hull of its control points.

Theorem 2.39. *Let $p := \sum_{\xi \in \mathcal{D}_d(T)} c_\xi B_\xi$ be the B-form of a trivariate polynomial of degree d . For all $v \in T$,*

$$\begin{pmatrix} v \\ p(v) \end{pmatrix} \in \text{Conv} \left(\left\{ \begin{pmatrix} \xi \\ c_\xi \end{pmatrix} \right\}_{\xi \in \mathcal{D}_d(T)} \right) \subset \mathbb{R}^4.$$

In particular,

$$\min_{\xi \in \mathcal{D}_d(T)} c_\xi \leq p(v) \leq \max_{\xi \in \mathcal{D}_d(T)} c_\xi.$$

Proof. First we show that

$$\sum_{i+j+k+l=d} \xi_{ijkl} B_{ijkl}(v) = v. \quad (2.11)$$

By 2.31 (iv) and 2.35 (ii),

$$v = (\varphi_0(v)v_0 + \varphi_1(v)v_1 + \varphi_2(v)v_2 + \varphi_3(v)v_3) \sum_{i+j+k+l=d-1} B_{ijkl}(v).$$

We expand the sum and use the definition of the Bernstein basis polynomials, then consider the first term of the result.

$$\begin{aligned} & \varphi_0(v)v_0 \frac{(d-1)!}{i!j!k!l!} \varphi_0^i(v)\varphi_1^j(v)\varphi_2^k(v)\varphi_3^l(v) \\ &= \frac{(i+1)}{d} v_0 \frac{d!}{(i+1)!j!k!l!} \varphi_0^{i+1}(v)\varphi_1^j(v)\varphi_2^k(v)\varphi_3^l(v) = \frac{(i+1)}{d} v_0 B_{i+1,j,k,l}. \end{aligned}$$

Thus, we obtain

$$v = \sum_{i+j+k+l=d-1} \frac{(i+1)}{d} v_0 B_{i+1,j,k,l} + \dots + \sum_{i+j+k+l=d-1} \frac{(l+1)}{d} v_3 B_{i,j,k,l+1}.$$

We shift the indices and obtain

$$v = \sum_{i+j+k+l=d} \left(\frac{i}{d} v_0 + \frac{j}{d} v_1 + \frac{k}{d} v_2 + \frac{l}{d} v_3 \right) B_{ijkl},$$

which gives (2.11). Let $v \in T$. Then

$$\begin{pmatrix} v \\ p(v) \end{pmatrix} = \begin{pmatrix} \xi_{ijkl} \\ c_{ijk} \end{pmatrix} B_{ijkl}(v).$$

This is a convex combination, since by 2.35 (ii) and (iii), $0 \leq B_{ijkl}(v) \leq 1$. This concludes the proof. \square

The B-form of a polynomial relative to a tetrahedron T depends on the order in which the vertices of T are given, since each of the indices is associated with a barycentric coordinate, which in turn is associated with a vertex. Our following lemma shows how to obtain the B-form of a polynomial relative to a tetrahedron whose vertices have been rearranged.

Lemma 2.40. *Let $T := \langle v_0, v_1, v_2, v_3 \rangle$ be a non-degenerate tetrahedron and σ a permutation of the set $\{0, 1, 2, 3\}$. Let $\tilde{T} := \langle v_{\sigma(0)}, v_{\sigma(1)}, v_{\sigma(2)}, v_{\sigma(3)} \rangle$, and*

$$p := \sum_{i_0+i_1+i_2+i_3=d} c_{i_0,i_1,i_2,i_3} B_{i_0,i_1,i_2,i_3}^T$$

a polynomial of degree d in B-form relative to T . Then

$$p := \sum_{i_0+i_1+i_2+i_3=d} c_{i_{\tau(0)},i_{\tau(1)},i_{\tau(2)},i_{\tau(3)}} B_{i_0,i_1,i_2,i_3}^{\tilde{T}}$$

is the B-form of p relative to \tilde{T} , with $\tau = \sigma^{-1}$. Moreover, the relationship between the barycentric coordinates relative to T and \tilde{T} is

$$\varphi_m^{\tilde{T}} = \varphi_{\sigma(m)}^T, \quad m = 0, \dots, 3.$$

Proof. The indices of the B-coefficients correspond to the indices of their associated domain points. We establish the relationship between domain points relative to T and domain points relative to \tilde{T} . Let $\tilde{v}_m := v_{\sigma(m)}$, $m = 0, \dots, 3$. Then $\varphi_m^{\tilde{T}} = \varphi_{\sigma(m)}^T$, and

$$\xi_{i_0,i_1,i_2,i_3}^{\tilde{T}} = \frac{1}{d} \sum_{m=0}^3 i_m \tilde{v}_m = \frac{1}{d} \sum_{m=0}^3 i_m v_{\sigma(m)} = \frac{1}{d} \sum_{m=0}^3 i_{\tau(m)} v_m = \xi_{i_{\tau(0)},i_{\tau(1)},i_{\tau(2)},i_{\tau(3)}}^T.$$

\square

A polynomial of degree d can be written as a polynomial of higher degree. The following lemma shows how the B-coefficients of the new representation are calculated.

Lemma 2.41 (Theorem 15.37 in [46]). *Let $p \in \mathcal{P}_d$ be a polynomial of degree d in B-form relative to some non-degenerate tetrahedron T , and let c_{ijkl} , $i + j + k + l = d$ be the B-coefficients of p . Then the B-form of p as a polynomial of degree $d + 1$ is*

$$p \equiv \sum_{i+j+k+l=d+1} \frac{1}{d+1} (ic_{i-1,j,k,l} + jc_{i,j-1,k,l} + kc_{i,j,k-1,l} + lc_{i,j,k,l-1}) B_{ijkl},$$

where the B-coefficients with negative indices are zero.

This lemma can be used repeatedly to raise p to any degree.

The following theorem shows that the B-form is stable.

Theorem 2.42 (Theorem 15.9 in [46]). *Let p be a polynomial of degree d in B-form relative to a non-degenerate tetrahedron T with B-coefficients c_ξ . There exists a constant K depending only on d such that*

$$\frac{1}{K} \max_{\xi \in \mathcal{D}_d(T)} |c_\xi| \leq \|p\|_T \leq \max_{\xi \in \mathcal{D}_d(T)} |c_\xi|. \quad (2.12)$$

The Russian mathematician S. Bernstein introduced the following operator in 1912 and famously used it for a constructive proof of the Weierstrass theorem (see [8]).

Definition 2.43. *Let T be a non-degenerate tetrahedron and B_ξ the Bernstein basis polynomials relative to T . For continuous function $f \in C(T)$, the Bernstein operator is defined as $\mathcal{B}_d : C(T) \rightarrow \mathcal{P}_d$ with*

$$\mathcal{B}_d f := \sum_{\xi \in \mathcal{D}_d(T)} f(\xi) B_\xi.$$

We will use the following result on the approximation properties of the Bernstein operator:

Theorem 2.44. *Suppose $f \in C^2(T)$, then*

$$\|f - \mathcal{B}_d f\|_T \leq \frac{1}{d} |T|^2 \|f\|_{2,T}.$$

Proof. We closely follow the proof of theorem 2.45 in [46], where the bivariate setting is covered. Using 2.35 (ii), we have

$$\mathcal{B}_d f(v) - f(v) = \sum_{i+j+k+l=d} (f(\xi_{ijkl}) - f(v)) B_{ijkl}(v).$$

Let $u_{ijkl} := \xi_{ijkl} - v$. By Taylor's theorem, there exists an $h_{ijkl} \in [0, 1]$ such that

$$f(\xi_{ijkl}) - f(v) = D_{u_{ijkl}} f(v) + \frac{1}{2} D_{u_{ijkl}}^2 f(v + h_{ijkl}(\xi_{ijkl} - v)).$$

Then

$$\begin{aligned}\mathcal{B}_d f(v) - f(v) &= \sum_{i+j+k+l=d} D_{ijkl} f(v) B_{ijkl}(v) \\ &\quad + \frac{1}{2} \sum_{i+j+k+l=d} D_{ijkl}^2 f(v + h_{ijkl}(\xi_{ijkl} - v)) B_{ijkl}(v).\end{aligned}$$

Let $v := (x, y, z)$ and $v_m := (x_m, y_m, z_m)$. Then

$$D_{ijkl} f(v) = (\xi_{ijkl}^x - x) D_x f(v) + (\xi_{ijkl}^y - y) D_y f(v) + (\xi_{ijkl}^z - z) D_z f(v),$$

where the coordinates of the domain points are

$$\xi_{ijkl}^x = \frac{i}{d} x_0 + \frac{j}{d} x_1 + \frac{k}{d} x_2 + \frac{l}{d} x_3,$$

with similar expressions for ξ_{ijkl}^y and ξ_{ijkl}^z . Therefore,

$$\begin{aligned}\sum_{i+j+k+l=d} D_{ijkl} f(v) B_{ijkl}(v) &= D_x f(v) \sum_{i+j+k+l=d} (\xi_{ijkl}^x - x) B_{ijkl}(v) \\ &\quad + D_y f(v) \sum_{i+j+k+l=d} (\xi_{ijkl}^y - y) B_{ijkl}(v) + D_z f(v) \sum_{i+j+k+l=d} (\xi_{ijkl}^z - z) B_{ijkl}(v).\end{aligned}$$

It follows from (2.11) that these sums vanish. We now estimate

$$|D_{ijkl}^2 f(v + h_{ijkl}(\xi_{ijkl} - v))| \leq 2\|v - \xi_{ijkl}\|_2^2 |f|_{2,T}.$$

Combining the above yields

$$|f(v) - \mathcal{B}_d f(v)| \leq |f|_{2,T} \sum_{i+j+k+l=d} \|v - \xi_{ijkl}\|_2^2 B_{ijkl}(v). \quad (2.13)$$

To estimate this further, we observe that

$$\begin{aligned}\sum_{i+j+k+l=d} ij B_{ijkl}(v) &= \sum_{i+j+k+l=d} ij \frac{d!}{i!j!k!l!} \varphi_0^i(v) \varphi_1^j(v) \varphi_2^k(v) \varphi_3^l(v) \\ &= \sum_{(i-1)+(j-1)+k+l=d-2} d(d-1) \varphi_0(v) \varphi_1(v) B_{i-1,j-1,k,l}(v) \\ &= d(d-1) \varphi_0(v) \varphi_1(v),\end{aligned}$$

due to 2.35 (ii). A similar calculation leads to

$$\sum_{i+j+k+l=d} i^2 B_{ijkl}(v) = d(d-1) \varphi_0^2(v) + d \varphi_0(v),$$

with analogous identities for the other index combinations. Then we obtain

$$\begin{aligned}
& \sum_{i+j+k+l=d} \|v - \xi_{ijkl}\|_2^2 B_{ijkl}(v) \\
&= \sum_{i+j+k+l=d} ((\xi_{ijkl}^x - x)^2 + (\xi_{ijkl}^y - y)^2 + (\xi_{ijkl}^z - z)^2) B_{ijkl}(v) \\
&= \sum_{i+j+k+l=d} \left(\frac{i}{d}(x_0 - x) + \dots + \frac{l}{d}(x_3 - x) \right)^2 B_{ijkl}(v) \\
&+ \sum_{i+j+k+l=d} \left(\frac{i}{d}(y_0 - y) + \dots + \frac{l}{d}(y_3 - y) \right)^2 B_{ijkl}(v) \\
&+ \sum_{i+j+k+l=d} \left(\frac{i}{d}(z_0 - z) + \dots + \frac{l}{d}(z_3 - z) \right)^2 B_{ijkl}(v)
\end{aligned}$$

Now we use the identities from above together with (2.11) and 2.31 (ii). Then

$$\begin{aligned}
& \sum_{i+j+k+l=d} \left(\frac{i}{d}(x_0 - x) + \dots + \frac{l}{d}(x_3 - x) \right)^2 B_{ijkl}(v) \\
&= \frac{d(d-1)}{d^2} \left(\underbrace{\varphi_0(v)(x_0 - x) + \dots + \varphi_3(v)(x_3 - x)}_{=0} \right)^2 \\
&+ \frac{1}{d} (\varphi_0(v)(x_0 - x)^2 + \dots + \varphi_3(v)(x_3 - x)^2),
\end{aligned}$$

with analogous results for the other two sums. Thus,

$$\begin{aligned}
& \sum_{i+j+k+l=d} \|v - \xi_{ijkl}\|_2^2 B_{ijkl}(v) \\
&= \frac{1}{d} \left(\varphi_0(v)((x_0 - x)^2 + (y_0 - y)^2 + (z_0 - z)^2) \right. \\
&\quad \left. + \dots + \varphi_3(v)((x_3 - x)^2 + (y_3 - y)^2 + (z_3 - z)^2) \right) \\
&= \frac{1}{d} \left(\varphi_0(v) \|v_0 - v\|_2^2 + \dots + \varphi_3(v) \|v_3 - v\|_2^2 \right) \\
&\leq \frac{1}{d} |T|^2.
\end{aligned}$$

This completes the proof. \square

We also present a result on the relationship between p and its B-coefficients.

Theorem 2.45. *Let p be a polynomial of degree d in B-form relative to a non-degenerate tetrahedron T with B-coefficients c_ξ . Then there exists a constant K depending only on d such that*

$$\max_{\xi \in \mathcal{D}_d(T)} |c_\xi - p(\xi)| \leq K |p|_{2,T} |T|^2. \quad (2.14)$$

Proof. Consider the polynomial

$$\tilde{p} := \sum_{\xi \in \mathcal{D}_d(T)} (c_\xi - p(\xi)) B_\xi.$$

By (2.12), there exists a constant depending only on d such that

$$\max_{\xi \in \mathcal{D}_d(T)} |c_\xi - p(\xi)| \leq K \|\tilde{p}\|_T = K \left\| \sum_{\xi \in \mathcal{D}_d(T)} (c_\xi - p(\xi)) B_\xi \right\|_T = K \|p - \mathcal{B}_d p\|_T.$$

Then (2.14) follows from theorem 2.44. \square

The following algorithm provides an efficient way to compute the values of a polynomial in B-form. The univariate and bivariate versions of this algorithm have been developed by French engineer Paul de Casteljau in 1959 and 1963, respectively (cf. [19, 20]). A trivariate versions of this algorithm can be found in [39].

In addition to calculating the values of a polynomial, the intermediate values generated by the algorithm can be used for a number of other tasks, such as determine the representation of the polynomial relative to a different tetrahedron or calculating derivatives of the polynomial.

Algorithm 2.46 (de Casteljau). Let $T := \langle v_0, v_1, v_2, v_3 \rangle$ be a non-degenerate tetrahedron and φ_m , $m = 0, \dots, 3$, the barycentric coordinates relative to T . Let

$$p := \sum_{i+j+k+l=d} c_{ijkl} B_{ijkl}$$

be a polynomial of degree d in B-form relative to T , and fix $v \in \mathbb{R}^3$.

- 1) For $i + j + k + l = d$, set $c_{ijkl}^{[0]} := c_{ijkl}$.
- 2) For $m = 1, \dots, d$, do:
 - 2.1) For $i + j + k + l = d - m$, set
 $c_{ijkl}^{[m]} := \varphi_0(v)c_{i+1,j,k,l}^{[m-1]} + \varphi_1(v)c_{i,j+1,k,l}^{[m-1]} + \varphi_2(v)c_{i,j,k+1,l}^{[m-1]} + \varphi_3(v)c_{i,j,k,l+1}^{[m-1]}$

The real numbers $c_{ijkl}^{[m]}$ are called the *de Casteljau coefficients* of $p(v)$.

Theorem 2.47 (Theorem 15.10 in [46]). *Given a polynomial p of degree d in B-form and $v \in \mathbb{R}^3$, let $c_{ijkl}^{[m]}$ be the de Casteljau coefficients of $p(v)$. Then*

$$p(v) = \sum_{i+j+k+l=d-m} c_{ijkl}^{[m]} B_{ijkl}(v)$$

for all $m = 0, \dots, d$. In particular, $p(v) = c_{0000}^{[d]}$. Moreover, the de Casteljau coefficients can be computed directly by

$$c_{ijkl}^{[m]} = \sum_{i_0+j_0+k_0+l_0=m} c_{i+i_0,j+j_0,k+k_0,l+l_0} B_{i_0,j_0,k_0,l_0}(v), \quad i + j + k + l = d - m.$$

Note that the B_{ijkl} in the theorem above are the Bernstein basis polynomials of degree $d - m$ relative to T .

Corollary 2.48. *Let $T := \langle v_0, v_1, v_2, v_3 \rangle$ be a non-degenerate tetrahedron and*

$$p := \sum_{i+j+k+l=d} c_{ijkl} B_{ijkl}$$

a polynomial of degree d in B-form relative to T . Then

- $p(v_0) = c_{d,0,0,0}$,
- $p(v_1) = c_{0,d,0,0}$,
- $p(v_2) = c_{0,0,d,0}$,
- $p(v_3) = c_{0,0,0,d}$.

Proof. The barycentric coordinates of v_0 relative to T are $(1, 0, 0, 0)$. Following de Casteljau's algorithm and theorem 2.47, we have

$$p(v_0) = c_{0000}^{[d]} = c_{1000}^{[d-1]} = \dots = c_{d-1,0,0,0}^{[1]} = c_{d,0,0,0}^{[0]} = c_{d,0,0,0}.$$

Analogous calculations for the other cases conclude the proof. \square

The intermediate values produced by the algorithm are the B-coefficients of the B-form relative to the subtetrahedra.

Theorem 2.49 (Theorem 15.36 in [46]). *Given a polynomial p in B-form and $v \in \mathbb{R}^3$, let $c_{ijkl}^{[m]}$ be the de Casteljau coefficients of $p(v)$. Let*

$$\begin{aligned} p_0 &:= \sum_{i+j+k+l=d} c_{0jkl}^{[i]} B_{ijkl}^{T_0}, & p_1 &:= \sum_{i+j+k+l=d} c_{i0kl}^{[j]} B_{ijkl}^{T_1}, \\ p_2 &:= \sum_{i+j+k+l=d} c_{ij0l}^{[k]} B_{ijkl}^{T_2}, & p_3 &:= \sum_{i+j+k+l=d} c_{ijk0}^{[l]} B_{ijkl}^{T_3}, \end{aligned}$$

where $T_0 := \langle v, v_1, v_2, v_3 \rangle$, $T_1 := \langle v_0, v, v_2, v_3 \rangle$, $T_2 := \langle v_0, v_1, v, v_3 \rangle$ and $T_3 := \langle v_0, v_1, v_2, v \rangle$. Then for each $m = 0, \dots, 3$, where T_m is non-degenerate,

$$p \equiv p_m.$$

This means that the de Casteljau coefficients can be interpreted as the B-coefficients of the B-form of p relative to certain tetrahedra which share a face with T . Notice that the vertex v may sit in the interior of T . In this case, the resulting subtetrahedra form an Alfeld split of the original tetrahedron, and the polynomials p_0, \dots, p_3 are the B-form of p relative to these subtetrahedra.

With theorem 2.49, the B-form of p relative to an arbitrary tetrahedron can be calculated.

Corollary 2.50. Let $T := \langle v_0, v_1, v_2, v_3 \rangle$ and $\tilde{T} := \langle \tilde{v}_0, \tilde{v}_1, \tilde{v}_2, \tilde{v}_3 \rangle$ be non-degenerate tetrahedra, and p a polynomial in B-form relative to T . Then the B-form of p relative to \tilde{T} can be computed by applying de Casteljau's algorithm at most four times.

The de Casteljau algorithm can be modified to calculate directional derivatives of polynomials in B-form.

Algorithm 2.51 (de Casteljau for directional derivatives). Let $T := \langle v_0, v_1, v_2, v_3 \rangle$ be a non-degenerate tetrahedron and φ_m , $m = 0, \dots, 3$, the barycentric coordinates relative to T . Let $c_{ijkl}^{[m]}$, $m = 0, \dots, d$, be the de Casteljau coefficients of $p(v)$ and u_1, \dots, u_r non-trivial vectors.

- 1) For $i + j + k + l = d - r$, set $\hat{c}_{ijkl}^{[0]} := c_{ijkl}^{[d-r]}$.
- 2) For $m = 1, \dots, r$:
 - 2.1) For $i = 0, \dots, 3$, set $\psi_i(u_m) := \varphi_i(u_m) - \varphi_i(0)$.
 - 2.2) For $i + j + k + l = d - r - m$, set

$$\hat{c}_{ijkl}^{[m]} := \psi_0(u_m)\hat{c}_{i+1,j,k,l}^{[m-1]} + \psi_1(u_m)\hat{c}_{i,j+1,k,l}^{[m-1]} + \psi_2(u_m)\hat{c}_{i,j,k+1,l}^{[m-1]} + \psi_3(u_m)\hat{c}_{i,j,k,l+1}^{[m-1]}$$

We call the real numbers $\hat{c}_{ijkl}^{[m]}$ the *de Casteljau coefficients of $D_{u_1} \cdots D_{u_r} p(v)$* .

Thus, the calculation of a directional derivative $D^\alpha p(v)$ involves $d - |\alpha|$ steps of the de Casteljau algorithm 2.46, followed by $|\alpha|$ steps of the modified de Casteljau algorithm above.

Theorem 2.52 (Theorem 15.14 in [46]). Given a polynomial p in B-form, $v \in \mathbb{R}^3$, and u_1, \dots, u_r non-trivial vectors. Let $\hat{c}_{ijkl}^{[m]}$ be the de Casteljau coefficients of $D_{u_1} \cdots D_{u_r} p(v)$ produced by algorithm 2.51. Then

$$D_{u_1} \cdots D_{u_r} p(v) = \frac{d!}{(d-r)!} \hat{c}_{0000}^{[r]}.$$

One of the advantages of the B-form is the simple description of conditions for the differentiability of two polynomial pieces defined on neighboring tetrahedra. These conditions are given as relations between the B-coefficient of the two polynomials. For the C^1 case, these conditions have been formulated in [2]. The C^r conditions can be found in [13, 37, 47].

The following theorem is central to the theory of splines in B-form.

Theorem 2.53 (Theorem 15.31 in [46]). Let $T := \langle v_0, v_1, v_2, v_3 \rangle$ and $\tilde{T} := \langle v_0, v_1, v_2, \tilde{v}_3 \rangle$ be two non-degenerate neighboring tetrahedra with the common face $F := \langle v_0, v_1, v_2 \rangle$. Let

$$p := \sum_{i+j+k+l=d} c_{ijkl}^T B_{ijkl}^T \quad \text{and} \quad \tilde{p} := \sum_{i+j+k+l=d} \tilde{c}_{ijkl}^{\tilde{T}} \tilde{B}_{ijkl}^{\tilde{T}}.$$

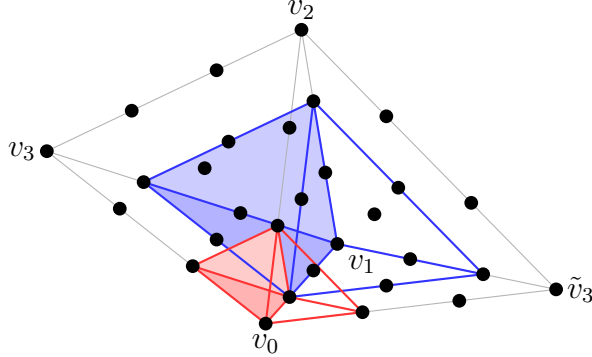


Figure 2.7: Visualization of the smoothness conditions between two polynomials defined on neighboring tetrahedra. For a C^1 -condition (red), four B-coefficients in the left tetrahedron determine one B-coefficient in the right tetrahedron. For a C^2 -condition (blue), six B-coefficients in the left tetrahedron determine one B-coefficient in the right tetrahedron.

be two polynomials of degree d in B-form relative to T and \tilde{T} , respectively. Let $f \in C^{-1}(\{T, \tilde{T}\})$ be defined by

$$f(v) := \begin{cases} p(v), & v \in T, \\ \tilde{p}(v) & \text{otherwise.} \end{cases}$$

Then $f \in C^r(\{T, \tilde{T}\})$ if and only if for all $\rho = 0, \dots, r$,

$$c_{ijk\rho}^{\tilde{T}} = \sum_{i_0+j_0+k_0+l_0=\rho} c_{i+i_0,j+j_0,k+k_0,l_0}^T B_{i_0,j_0,k_0,l_0}^T(\tilde{v}_3), \quad \text{for all } i+j+k = d-\rho. \quad (2.15)$$

The equations 2.15 are called C^r smoothness conditions. In particular, the theorem says that two polynomial pieces are joined continuously at the common face F if and only if their B-coefficients associated with F match:

$$c_{ijk0}^{\tilde{T}} = c_{ijk0}^T \quad \text{for all } i+j+k = d. \quad (2.16)$$

Their first derivatives are continuous if and only if in addition to (2.16),

$$c_{ijk1}^{\tilde{T}} = c_{i+1,j,k,0}^T \varphi_0^T(\tilde{v}_3) + c_{i,j+1,k,0}^T \varphi_1^T(\tilde{v}_3) + c_{i,j,k+1,0}^T \varphi_2^T(\tilde{v}_3) + c_{i,j,k,1}^T \varphi_3^T(\tilde{v}_3) \quad (2.17)$$

for all $i+j+k = d-1$. The convex hull of the domain points associated with the B-coefficients in the sum of (2.15) form a smaller version of the tetrahedron T . Figure 2.7 shows which B-coefficients are relevant for a typical C^1 and C^2 -condition between cubic polynomials.

The smoothness conditions are simplified when \tilde{v}_3 sits in a plane containing one of the faces of T . Similarly to the situation discussed in remark 2.37, p and \tilde{p} degenerate to bivariate polynomials when restricted to this plane, and thus the smoothness conditions also degenerate to bivariate smoothness conditions. Moreover, they degenerate to univariate smoothness conditions when \tilde{v}_3 and two of the vertices of T are collinear.

2.4 Trivariate splines on tetrahedral partitions

Piecewise polynomials defined on tetrahedral partitions have been studied in the finite-element literature without using Bernstein-Bézier methods (see [15, 86] and references therein). Two of the first methods to use the B-form for this purpose were developed by Alfeld [2] and Worsey and Farin [89], who studied certain macro-element spaces to solve Hermite interpolation problems.

Definition 2.54. Let Δ be a tetrahedral partition of a simply connected region $\Omega \subseteq \mathbb{R}^3$. Given two integers $d \in \mathbb{N}_0$ and $0 \leq r \leq d$, the space of continuous trivariate polynomial splines of degree d and smoothness r over Δ is defined by

$$\mathcal{S}_d^r(\Delta) := \{s \in C^r(\Delta); s|_T \in \mathcal{P}_d \text{ for all } T \in \Delta\}.$$

Spline spaced can be characterized by the C^ρ smoothness conditions, $\rho = 0, \dots, r$, in theorem 2.53, as the following theorem shows.

Theorem 2.55. Let Δ be a tetrahedral partition of a polygonally bounded domain $\Omega \in \mathbb{R}^3$, $\mathcal{S} := \mathcal{S}_d^r(\Delta)$ a trivariate spline space over Δ , and $s \in \mathcal{S}^{-1}(\Delta)$. Then $s \in \mathcal{S}$ if and only if for every pair $T := \langle v_0, v_1, v_2, v_3 \rangle$, $\tilde{T} := \langle v_0, v_1, v_2, \tilde{v}_3 \rangle$ of neighboring tetrahedra in Δ , (2.15) is satisfied for $\rho = 0, \dots, r$.

Proof. This follows immediately from the definition of the spline space, and from theorem 2.53. \square

Often certain subspaces of $\mathcal{S}_d^r(\Delta)$ are used, where the order of smoothness is increased at the vertices, edges and faces of the underlying partition.

Definition 2.56. Let Δ, r, d be defined as in 2.54. Let V and E denote the sets of vertices and edges of Δ , respectively. For integers $r \leq \nu \leq \mu \leq d$, the subspace

$$\begin{aligned} \mathcal{S}_d^{r,\mu,\nu}(\Delta) := & \{s \in \mathcal{S}_d^r(\Delta); s \in C^\mu(v) \text{ for all } v \in V, \\ & s \in C^\nu(e) \text{ for all } e \in E\} \end{aligned}$$

is called the superspline space of degree d and smoothness (r, μ, ν) .

By $s \in C^\mu(v)$ we indicate that the partial derivatives of all polynomial pieces of s meeting at the vertex v match up to the order μ . Likewise, $s \in C^\nu(e)$ means that all polynomial pieces defined on tetrahedra sharing the edge e have matching partial derivatives up to the order ν .

Superspline spaces can also be characterized by smoothness conditions.

Theorem 2.57. *Let Δ be a tetrahedral partition of a polygonally bounded domain $\Omega \in \mathbb{R}^3$, $\mathcal{S} \subseteq \mathcal{S}_d^0(\Delta)$ a trivariate spline space over Δ , and $s \in \mathcal{S}_d^{-1}(\Delta)$.*

- (i) *Let v be a vertex of Δ and $0 \leq r \leq d$. Then $s \in C^r(v)$ if and only if for every pair $T := \langle v, v_1, v_2, v_3 \rangle$, $\tilde{T} := \langle v, v_1, v_2, \tilde{v}_3 \rangle$ of neighboring tetrahedra in Δ which share the vertex v , and for all $\rho = 0, \dots, r$, the smoothness condition*

$$c_{ijk\rho}^{\tilde{T}} = \sum_{i_0+j_0+k_0+l_0=\rho} c_{i+i_0,j+j_0,k+k_0,l_0}^T B_{i_0,j_0,k_0,l_0}^T(\tilde{v}_3)$$

is satisfied for all $i + j + k = d - \rho$ with $i \geq r$.

- (ii) *Let $e := \langle v_0, v_1 \rangle$ be an edge of Δ and $r \leq 0$. Then $s \in C^r(e)$ if and only if for every pair $T := \langle v_0, v_1, v_2, v_3 \rangle$, $\tilde{T} := \langle v_1, v_1, v_2, \tilde{v}_3 \rangle$ of neighboring tetrahedra in Δ which share the edge e , and for all $\rho = 0, \dots, r$, the smoothness condition*

$$c_{ijk\rho}^{\tilde{T}} = \sum_{i_0+j_0+k_0+l_0=\rho} c_{i+i_0,j+j_0,k+k_0,l_0}^T B_{i_0,j_0,k_0,l_0}^T(\tilde{v}_3)$$

is satisfied for all $i + j + k = d - \rho$ with $i + j \geq r$.

Notice that the domain points associated with the B-coefficients in 2.57, (i) and (ii), are those in the balls $D_r^T(v)$, $D_r^{\tilde{T}}(v)$, and in the tubes $t_r^T(e)$, $t_r^{\tilde{T}}(e)$, respectively.

Proof. We follow the proof of lemma 5.9 in [46]. The B-coefficients of s associated with the ball $D_r(v)$ can be regarded as the B-coefficients of a spline $s_v \in \mathcal{S}_r^{-1}(\text{star}^1(v))$. Then $s \in C^r(v)$ only if s_v reduces to a polynomial, in which case $s_v \in \mathcal{S}_r^r(\text{star}^1(v))$. Then (i) follows from theorem 2.55. Likewise, for the edge $e := \langle u_1, u_2 \rangle$, the B-coefficients of s associated with the tube $t_r(e)$ can be regarded as the B-coefficients of a spline $s_e \in \mathcal{S}_r^{-1}(\text{star}^1(u_1) \cup \text{star}^1(u_2))$. Again, $s \in C^r(e)$ only if $s_e \in \mathcal{S}_r^r(\text{star}^1(u_1) \cup \text{star}^1(u_2))$, and (ii) follows from theorem 2.55. \square

We extend definition 2.38 to spline spaces.

Definition 2.58. For a spline space $\mathcal{S} \subseteq \mathcal{S}_d^0(\Delta)$ defined over a tetrahedral partition Δ , we denote the set of domain points of degree d of Δ by

$$\mathcal{D}_d(\Delta) := \bigcup_{T \in \Delta} \mathcal{D}_d(T).$$

Let V and E be the sets of vertices and edges of Δ , respectively. For $0 \leq m \leq d$ we call

$$D_m(v) := \bigcup_{T \in \text{star}(v)} D_m^T(v)$$

the ball of radius m around v and

$$R_m(v) := \bigcup_{T \in \text{star}(v)} R_m^T(v)$$

the shell of radius m around v , where $v \in V$. For an edge $e := \langle v_0, v_1 \rangle \in E$, we call

$$t_m(e) := \bigcup_{T \in \text{star}(v_1) \cap \text{star}(v_2)} t_m^T(e)$$

the tube with radius m around e .

A space of continuous splines can be parametrized by the union of the B-coefficients of all polynomial pieces. It follows from (2.16) that for any two such polynomials defined relative to neighboring tetrahedra, the B-coefficients associated with domain points on the common face match, and thus only one parameter is needed to define both coefficients. Hence, the total number of domain points is an upper bound for the dimension of any continuous spline space.

Lemma 2.59. Let $\mathcal{S} \subseteq \mathcal{S}_d^0(\Delta)$ be a spline space, then

$$\dim \mathcal{S} \leq \#\mathcal{D}_d(\Delta).$$

For $\mathcal{S} = \mathcal{S}_d^0(\Delta)$, the numbers are equal.

Proof. By theorem 2.53, $s \in \mathcal{S}_d^0(\Delta)$ if and only if those B-coefficients of neighboring polynomial pieces which are associated with the common face match. Hence, fixing such a B-coefficient determines all B-coefficients associated with the respective domain point. Therefore, the number of independent B-coefficients is equal to the number of distinct domain points. \square

The next corollary shows how the smoothness conditions in theorem 2.57 can be used to determine B-coefficients associated with balls and tubes. This is an integral part of many Lagrange interpolation methods.

Corollary 2.60. *Let Δ be a tetrahedral partition and $\mathcal{S} := \mathcal{S}_d^{r,\mu,\nu}(\Delta)$ a trivariate spline space over Δ . Let T be a tetrahedron of Δ , and v and e a vertex and an edge of T , respectively. Suppose the B-coefficients associated with $D_\mu^T(v)$ of a spline $s \in \mathcal{S}$ are known. Then the B-coefficients associated with $D_\mu(v)$ are uniquely determined by smoothness conditions from theorem 2.57 (i). Likewise, if the B-coefficients associated with $t_\nu^T(e)$ are known, then the B-coefficients associated with $t_\nu(e)$ are uniquely determined by smoothness conditions from theorem 2.57 (ii).*

The B-coefficients associated with the ball $D_\mu(v)$ are determined by first applying the smoothness conditions to determine the B-coefficients associated with $D_{\tilde{T}}^T(v)$ for all neighbors \tilde{T} of T . This process is repeated for all \tilde{T} to determine B-coefficients of their neighbors, and so on. The process for the B-coefficients associated with the tube $t_\nu(e)$ is similar.

An important tool in the study of spline spaces is the *minimal determining set*. This is a subset of the domain points such that fixing the B-coefficients associated with the set determines all other B-coefficients as well.

Definition 2.61. *Let $\mathcal{S} \subseteq \mathcal{S}_d^r(\Delta)$ be a spline space. Let $\Gamma \subseteq \mathcal{D}_d(\Delta)$ be a subset of the domain points of degree d . Γ is called a determining set for \mathcal{S} , if*

$$c_\eta = 0 \text{ for all } \eta \in \Gamma \quad \Rightarrow \quad s \equiv 0.$$

A determining set is called minimal if no determining set with fewer elements exists. It is called consistent, if by fixing all C-coefficients associated with Γ of a spline s , all remaining B-coefficients of s are determined, and all smoothness conditions are satisfied.

We usually denote minimal determining sets by the letter \mathcal{M} .

There is a relation between determining sets and the dimension of spline spaces.

Theorem 2.62. *Let Γ be a determining set for a spline space $\mathcal{S} \subseteq \mathcal{S}_d^0(\Delta)$. Then*

- (i) $\dim \mathcal{S} \leq \#\Gamma$.
- (ii) *If Γ is consistent, then $\#\Gamma = \dim \mathcal{S}$.*
- (iii) *If $\#\Gamma = \dim \mathcal{S}$, then Γ is minimal.*

Proof. Parts (i) and (iii) are covered by theorems 17.8 and 17.10 in [46]. To show part (ii), we refer to the proof of theorem 5.15 therein. \square

We conclude this section by defining two important properties of minimal determining sets.

Definition 2.63. Let \mathcal{M} be a minimal determining set for a spline space $\mathcal{S} \subseteq \mathcal{S}_d^r(\Delta)$. For domain points $\xi \in \mathcal{M}$ and $\eta \in \mathcal{D}_d(\Delta)$, we say the B -coefficient c_η of a spline $s \in \mathcal{S}$ depends on c_ξ , if changing the value of c_ξ also changes the value of c_η . For each $\eta \in \mathcal{D}_d(\Delta)$, we define

$$\Gamma_\eta := \{\xi \in \mathcal{M}; c_\eta \text{ depends on } c_\xi\}.$$

\mathcal{M} is called local if there exists an integer $\ell \in \mathbb{N}_0$ which does not depend on Δ , such that for all domain points $\eta \in \mathcal{D}_d(\Delta)$ there exists a tetrahedron T_η containing η with

$$\Gamma_\eta \subseteq \text{star}^\ell(T_\eta).$$

Moreover, \mathcal{M} is called stable if there exists a constant K which depends only on ℓ, θ_Δ and ϕ_Δ , such that for each domain point $\eta \in \mathcal{D}_d(\Delta)$,

$$|c_\eta| \leq K \max_{\xi \in \Gamma_\eta} |c_\xi|.$$

Here, θ_Δ and ϕ_Δ are the smallest face and solid angles of Δ defined in 2.8.

Chapter 3

Quasi-interpolation using quintic C^2 splines on the BCC partition

In this chapter we investigate the problem of constructing quasi-interpolation operators based on quintic C^2 -splines on the BCC partition which approximate a given set of discrete data values located on a regular cuboid grid. The space of such splines has been investigated by Strang and Fix in [85], and it is known that the best possible approximation order of this space is four.

There exist some quasi-interpolation methods for this spline space using box splines (see [30, 31, 38]). These methods rely on samples on the BCC grid and the evaluation of translated basic functions to generate a reconstruction. Our methods, in contrast, give an explicit representation of the polynomial pieces by providing formulas for each B-coefficient. Thus, our method is similar to the bivariate operators by Sorokina and Zeilfelder (see [80, 82]), and the trivariate operators in [60, 72, 81]. This approach to approximation has several advantages. One does not need to determine the dimension of the underlying spline space, which is a highly non-trivial problem. Nor is it necessary to explicitly construct a local and stable basis, or even a minimal determining set, to achieve a certain approximation order. From the point of view of an application programmer, this technique has the additional advantage that a spline can be constructed independently on each tetrahedron of the partition from only a small portion of the data set. This allows the application of our methods to huge data sets, as there is no need to retain the B-coefficients associated with an individual tetrahedron, once all computations regarding the related polynomial piece are completed. It also means that many algorithms using these operators can be readily parallelized. This was one of the main design criteria for the operators. Another criterion was the use of only to gridded data, which is available in many real-world applications, such as computed tomography.

We construct three quasi-interpolation operators with different properties. The first operator satisfies a certain convexity condition, but has a less than optimal approximation order. The second operator has the best possible approximation order for the underlying spline space. While it is more complex than the convex operator, it can still be defined by giving a single set of B-coefficient computation rules which is applied to all tetrahedra of the underlying partition. The third operator interpolates all of the data values located on the unit cube while maintaining the best possible approximation order. To achieve this, the tetrahedra of the underlying partition are decomposed into four classes, and a separate set of computation rules is provided for each class.

We begin this chapter by establishing some terminology regarding quasi-interpolation with polynomial spline spaces. Although all definitions and statements are given explicitly for trivariate splines, it should be noted that most can be easily adapted to the n -variate setting.

Definition 3.1. *Given a set $X \subset \mathbb{R}^3$ of discrete points, we call the space*

$$\mathcal{F}_X := \{f : X \rightarrow \mathbb{R}\}$$

of discrete real-valued functions the sample space for the set of sample points X . For $f \in \mathcal{F}_X$, we call $f(x)$ the data value of the sample point $x \in X$. Given a space $\mathcal{S} \subseteq \mathcal{S}_d^r(\Delta)$ of trivariate polynomial splines of degree d and smoothness r over a tetrahedral partition Δ , we call a linear operator

$$Q : \mathcal{F}_X \rightarrow \mathcal{S},$$

where each B-coefficient of $Q(f)$ is a linear combination of the data values $\{f(x)\}_{x \in X}$, a trivariate quasi-interpolation operator for (X, \mathcal{S}) of degree d and smoothness r .

When dealing with a continuous function $f \in C(\Omega)$, with $\text{Conv}(X) \subseteq \Omega$, we implicitly mean the restriction of f to X when writing $Q(f)$.

The quasi-interpolation operators developed in this chapter are defined by giving explicit computation rules for all B-coefficients of the spline. These rules can be written as linear combinations of data values.

Definition 3.2. *Let Q be a quasi-interpolation operator for (X, \mathcal{S}) of degree d and Δ the underlying tetrahedral partition of \mathcal{S} . Let $f \in \mathcal{F}_X$, $T \in \Delta$, $\eta \in \mathcal{D}_d(T)$ and c_η^T the associated B-coefficient of $Q(f)|_T$. The linear combination*

$$c_\eta^T = \sum_{x \in X} w_{\eta, x}^T f(x)$$

is called a B-coefficient computation rule of Q for c_η^T . The real numbers $w_{\eta,x}^T$ are called weights. The set

$$X_\eta^T := \{x \in X; w_{\eta,x}^T \neq 0\}$$

is called the support of the rule for c_η^T . We denote the union of the supports of the rules for all B-coefficients of T by

$$X_T := \bigcup_{\eta \in \mathcal{D}_d(T)} X_\eta^T.$$

As usual, we may omit the superscript T whenever it is clear which tetrahedron we are referring to.

Explicitly giving a rule for each B-coefficient defines a quasi-interpolation operator. It obviously would be highly impractical if all of these rules used different sets of weights. Thus, for the quasi-interpolation operators in this chapter, we take advantage of the regular nature of the BCC partition and define the rules relative to a tetrahedron. For the first two operators, this results in a small set of rules which can be applied to each tetrahedron of the BCC partition. The third operator is more complex, and the tetrahedra are decomposed into four classes, for each of which a set of rules is given.

Remark 3.3. Let $\eta \in \mathcal{D}_d(\Delta)$ and $T \neq \tilde{T} \in \Delta$ with $\eta \in T \cap \tilde{T}$. If \mathcal{S} is a space of continuous splines, then the rules for c_η^T and $c_\eta^{\tilde{T}}$ are identical, which means that they share the same support and use the same weights. This is a consequence of the C^0 condition (2.16). In such a case, it suffices to give one rule for each $\eta \in \mathcal{D}_d(\Delta)$ to define a quasi-interpolation operator.

The following definition allows us to address the data values relative to a tetrahedron.

Definition 3.4. Let $T := \langle v_0, v_1, v_2, v_3 \rangle$ be some non-degenerate tetrahedron, $f \in \mathcal{F}_X$, and $x \in X$ a sample point. Let $\phi := (\varphi_0, \dots, \varphi_3)$ be the barycentric coordinates of x relative to T . Then we write

$$f_\phi^T = f_{\varphi_0, \varphi_1, \varphi_2, \varphi_3}^T := f(\varphi_0 v_0 + \dots + \varphi_3 v_3) = f(x).$$

A collection of sample points can also be written relative to T . For $Y \subseteq X$, we write

$$\Phi_Y^T := \{(\varphi_0^T(x), \dots, \varphi_3^T(x)); x \in Y\}.$$

We may omit the superscript T when it is clear which tetrahedron we are referring to.

Using the definition above, the B-coefficient computation rules of a quasi-interpolation operator Q can be written as

$$c_\eta^T = \sum_{\phi \in \Phi_{X_\eta}^T} w_{\eta,\phi}^T f_\phi^T, \quad (3.1)$$

where the c_η^T are the B-coefficients of $Q(f)|_T$. Here, we write X_η instead of X_η^T , since it is clear which tetrahedron the rule is associated with.

Example 3.5. The following rule defines the computation of the B-coefficient c_{5000} associated with the domain point ξ_{5000} of some tetrahedron T . The data values are given relative to T .

$$\begin{aligned} c_{5000} := & \frac{1}{480} \left(216 f_{1,0,0,0} \right. \\ & + 28(f_{0,1,-1,1} + f_{2,-1,1,-1} + f_{2,0,-1,0} + f_{1,-1,0,1} + f_{1,1,0,-1} + f_{0,0,1,0}) \\ & + 6(f_{1,-1,2,-1} + f_{3,-1,0,-1} + f_{2,-2,1,0} + f_{2,1,-1,-1} + f_{2,-1,-1,1} + f_{2,0,1,-2} \\ & \quad + f_{1,1,-2,1} + f_{-1,1,0,1} + f_{0,2,-1,0} + f_{0,1,1,-1} + f_{0,-1,1,1} + f_{0,0,-1,2}) \\ & + 3(f_{-1,2,0,0} + f_{1,-2,2,0} + f_{1,2,-2,0} + f_{1,0,2,-2} + f_{1,0,-2,2} + f_{-1,0,0,2} \\ & \quad \left. + f_{3,0,0,-2} + f_{3,-2,0,0} \right) \end{aligned}$$

In addition to this description of B-coefficient computation rules, we provide graphical representations, where the support of each rule is shown in a three dimensional grid, with the weights written at the associated sample points. We call such a representation a *weight mask*. Figure 3.1 shows the weight mask for the rule given in the example above. Note that only the numerators of the weights are shown at the grid points, and the common denominator is given separately. The tetrahedron T is shown both in the grid, where its relative location to the sample points can be seen, and in a bigger version on the right, where the arrangement of the vertices, and the domain point associated with the B-coefficient are shown.

The relative notation of definition 3.4 allows us to define certain symmetries for B-coefficient computation rules.

Definition 3.6. Let η, ξ be two domain points of a tetrahedron $T \in \Delta$. We say, the rules

$$c_\eta^T = \sum_{\phi \in \Phi_{X_\eta}^T} w_{\eta,\phi}^T f_\phi^T \quad \text{and} \quad c_\xi^T = \sum_{\phi \in \Phi_{X_\xi}^T} w_{\xi,\phi}^T f_\phi^T$$

of a quasi-interpolation operator Q for (X, \mathcal{S}) are $(0, 1)$ -symmetric to each other if and only if

All weights multiplied by $\frac{1}{480}$

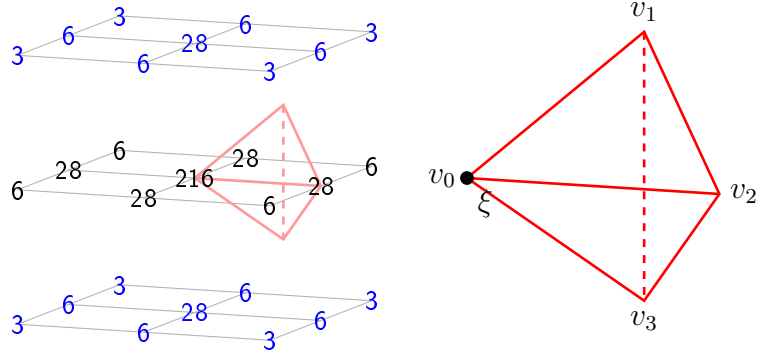


Figure 3.1: Weight mask for the rule for c_{5000} defined in example 3.5. The associated domain point is shown in the tetrahedron on the right.

- (i) $(\varphi_0, \varphi_1, \varphi_2, \varphi_3) \in \Phi_{X_\eta}^T \Leftrightarrow (\varphi_1, \varphi_0, \varphi_2, \varphi_3) \in \Phi_{X_\xi}^T$, and
- (ii) for each $(\varphi_0, \varphi_1, \varphi_2, \varphi_3) \in \Phi_{X_\eta}^T$,

$$w_{\eta,(\varphi_0,\varphi_1,\varphi_2,\varphi_3)}^T = w_{\xi,(\varphi_1,\varphi_0,\varphi_2,\varphi_3)}^T.$$

The other cases of (i, j) -symmetry with $i, j \in \{0, 1, 2, 3\}$ are defined analogously, with i and j referring to the indices of the tuples in Φ_X^T .

Two rules that are symmetric to each other share the same set of weights. Thus, symmetries between two B-coefficient computation rules can also be expressed by swapping the barycentric coordinates of the sample points.

Lemma 3.7. Fix $T \in \Delta$ and suppose the rules for two B-coefficients c_η^T and c_ξ^T of a quasi-interpolation operator Q are $(0, 1)$ -symmetric to each other, then

$$c_\xi^T = \sum_{(\varphi_0, \varphi_1, \varphi_2, \varphi_3) \in \Phi_{X_\eta}^T} w_{\eta,(\varphi_0,\varphi_1,\varphi_2,\varphi_3)}^T f_{\varphi_1, \varphi_0, \varphi_2, \varphi_3}^T.$$

For the other cases of symmetry, analogous statements hold.

Proof. Using 3.6 (ii), we write the rule for c_ξ^T with the weights $w_{\eta, \phi}^T$.

$$c_\xi^T = \sum_{(\varphi_0, \varphi_1, \varphi_2, \varphi_3) \in \Phi_{X_\xi}^T} w_{\eta,(\varphi_1,\varphi_0,\varphi_2,\varphi_3)}^T f_{\varphi_0, \varphi_1, \varphi_2, \varphi_3}^T.$$

We then swap φ_0 and φ_1 to obtain

$$c_\xi^T = \sum_{(\varphi_1, \varphi_0, \varphi_2, \varphi_3) \in \Phi_{X_\xi}^T} w_{\eta,(\varphi_0,\varphi_1,\varphi_2,\varphi_3)}^T f_{\varphi_1, \varphi_0, \varphi_2, \varphi_3}^T.$$

Using 3.6 (i) completes the proof. \square

We use lemma 3.7 to simplify the definition of quasi-interpolation operators. For example, in definition 3.17 (A.2), the rules for the B-coefficients c_{0140} , c_{4001} and c_{0041} can be derived from the rule for c_{4100} by using both $(0, 2)$ - and $(1, 3)$ -symmetry.

The following lemma is used to prove certain reproduction properties of the operators defined later in this chapter.

Lemma 3.8. *Fix $T \in \Delta$ and suppose the rules for two B-coefficients c_η^T and c_ξ^T of a quasi-interpolation operator Q are $(0, 1)$ -symmetric to each other. Let f and \tilde{f} be functions such that $f_{\varphi_0, \varphi_1, \varphi_2, \varphi_3}^T = \tilde{f}_{\varphi_1, \varphi_0, \varphi_2, \varphi_3}^T$ for all $(\varphi_0, \varphi_1, \varphi_2, \varphi_3) \in \Phi_{X_T}^T$. Then $c_\eta^T = \tilde{c}_\xi^T$, where c_η^T and \tilde{c}_ξ^T are B-coefficients of $Q(f)|_T$ and $Q(\tilde{f})|_T$, respectively. Similar statements hold for the other symmetries.*

Proof. Using lemma 3.7, we write

$$\tilde{c}_\xi^T = \sum_{(\varphi_0, \varphi_1, \varphi_2, \varphi_3) \in \Phi_{X_\eta}^T} w_{\eta, (\varphi_0, \varphi_1, \varphi_2, \varphi_3)}^T \tilde{f}_{\varphi_1, \varphi_0, \varphi_2, \varphi_3}^T$$

and use the symmetry of the functions to complete the proof. \square

Note that the Bernstein basis polynomials relative to T exhibit such symmetries.

The next definition is motivated by the convex hull property of the B-form and defines a concept of convexity for quasi-interpolation operators.

Definition 3.9. *Let Q be a trivariate spline quasi-interpolation operator for (X, \mathcal{S}) . Q is called convex, if for all $f \in \mathcal{F}_X$ the condition*

$$f_{min}^T \leq Q(f)(v) \leq f_{max}^T \text{ for all } v \in T, \quad (3.2)$$

holds for each $T \in \Delta$, where

$$f_{min}^T := \min_{x \in X_T} f(x) \quad \text{and} \quad f_{max}^T := \max_{x \in X_T} f(x).$$

In other words, each polynomial piece p of a convex quasi-interpolation operator is bounded by the least and greatest data values that were used in the construction of p . It should be noted that f_{min}^T and f_{max}^T are not the minimum and maximum values of $f|_T$, but the minimum and maximum values of f that are relevant for the construction of $Q(f)|_T$.

The convexity of a quasi-interpolation operator Q can be expressed by a similar condition for the rules for Q .

Lemma 3.10. Let Q be a trivariate spline quasi-interpolation operator for (X, \mathcal{S}) which is defined by the rules

$$c_\eta^T = \sum_{x \in X} w_{\eta,x}^T f(x), \quad \eta \in \mathcal{D}_d(T), \quad T \in \Delta.$$

For each $\eta \in \mathcal{D}_d(T)$, let

$$f_{\eta,\min} := \min_{x \in X_\eta^T} f(x) \quad \text{and} \quad f_{\eta,\max} := \max_{x \in X_\eta^T} f(x).$$

If for all $f \in \mathcal{F}_X$,

$$f_{\eta,\min} \leq c_\eta^T \leq f_{\eta,\max} \tag{3.3}$$

for each $T \in \Delta$ and each $\eta \in \mathcal{D}_d(T)$, then Q is convex.

Proof. Since $X_\eta^T \subseteq X_T$, $f_{\min}^T \leq f_{\eta,\min}$ and $f_{\eta,\max} \leq f_{\max}^T$. Let (3.3) hold for each $T \in \Delta$. Then

$$f_{\min}^T \leq f_{\eta,\min} \leq c_\eta^T \leq f_{\eta,\max} \leq f_{\max}^T \quad \text{for each } \eta \in \mathcal{D}_d(T).$$

Since $Q(f)|_T$ is a polynomial in B-form, it follows from lemma 2.39 that

$$f_{\min}^T \leq Q(f)|_T(v) \leq f_{\max}^T \quad \text{for all } v \in T.$$

□

The next lemma shows that an operator is convex if each B-coefficient is a convex combination of the sample values.

Lemma 3.11. Let Q be a trivariate spline quasi-interpolation operator for (X, \mathcal{S}) which is defined by the rules

$$c_\eta^T = \sum_{x \in X} w_{\eta,x}^T f(x), \quad \eta \in \mathcal{D}_d(T) \quad T \in \Delta,$$

where $w_{\eta,x}^T \geq 0$ for all $x \in X$ and all $\eta \in \mathcal{D}_d(\Delta)$, and $\sum_{x \in X} w_{\eta,x}^T = 1$ for all $\eta \in \mathcal{D}_d(T)$ and all $T \in \Delta$. Then Q is convex.

Proof. We show that (3.3) holds for each $\eta \in \mathcal{D}_d(T)$ and each $T \in \Delta$. Fix $f \in \mathcal{F}_X$. First we observe that for each $\eta \in \mathcal{D}_d(T)$,

$$c_\eta^T = \sum_{x \in X} w_{\eta,x}^T f(x) = \sum_{x \in X_\eta^T} w_{\eta,x}^T f(x).$$

Since all weights are non-negative, it follows that

$$f_{\eta,\min} = \underbrace{\left(\sum_{x \in X_\eta^T} w_{\eta,x}^T \right)}_{=1} f_{\eta,\min} \leq \sum_{x \in X_\eta^T} w_{\eta,x}^T f(x) = c_\eta^T.$$

and

$$c_\eta^T = \sum_{x \in X_\eta^T} w_{\eta,x}^T f(x) \leq \sum_{x \in X_\eta^T} w_{\eta,x}^T f_{\eta,\max} = f_{\eta,\max}.$$

The convexity of Q follows from lemma 3.10. \square

The following definition introduces the concepts of locality and stability, which are known for minimal determining sets from definition 2.63, to quasi-interpolation operators.

Definition 3.12. *Let Q be a trivariate spline quasi-interpolation operator for (X, \mathcal{S}) which is defined by the rules*

$$c_\eta^T = \sum_{x \in X} w_{\eta,x}^T f(x), \quad \eta \in \mathcal{D}_d(T), \quad T \in \Delta.$$

We say Q is ℓ -local if there exists a constant $\ell \in \mathbb{N}$ such that for all $f \in \mathcal{F}_X$

$$X_T \subset \text{star}^\ell(T) \text{ for all } T \in \Delta.$$

The operator Q is called stable, if there exists a constant K , depending only on ℓ and the smallest face and solid angles of Δ , such that for each $\eta \in \mathcal{D}_d(T)$ and $T \in \Delta$,

$$|c_\eta^T| \leq K \max_{x \in X_T} |f(x)|.$$

Most quasi-interpolation operators are designed to take advantage of the uniform structure of the underlying partition. In the ideal case, such an operator is defined by a single set of rules which can be applied to all tetrahedra. Two of the operators developed in this chapter belong to this class, while the third operator uses four sets of rules.

The operators are designed to approximate data sitting on a uniform cuboid grid on the unit cube. Given the fact that the locality of all operators is greater than zero, additional data values have to be supplied outside the boundary of the unit cube. This is taken into account by the following definition of a set of sample points which our operators will use.

Definition 3.13. *Given a set of $N_1 \times N_2 \times N_3$ data values, where $N_i > 2P + 1$, $i = 1, 2, 3$, for some small $P \in \mathbb{N}_0$, we assume that these values are located at the vertices of the regular cuboid grid*

$$\begin{aligned} \mathcal{X} := \{x_{i,j,k} &:= (ih_1, jh_2, kh_3); i = -P, \dots, n_1 - 1 + P, \\ &j = -P, \dots, n_2 - 1 + P, \\ &k = -P, \dots, n_3 - 1 + P\} \subset \mathbb{R}^3, \end{aligned}$$

with $n_i := N_i - 2P$ and $h_i := \frac{1}{n_i - 1}$, $i = 1, 2, 3$. We call \mathcal{X} the set of uniform cuboid sample points. We call P the padding parameter.

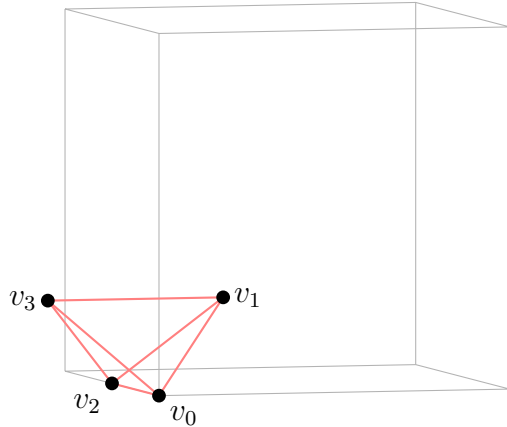


Figure 3.2: A tetrahedron in the boundary region of a small partition Δ_1 . The vertices v_0 and v_2 sit on the boundary of the black unit cube. Vertex v_1 is inside the unit cube, while v_3 is outside.

The padding parameter P can be interpreted as the number of layers of cuboids outside the unit cube. Based on \mathcal{X} , we construct a partition $\Delta_1 \subset \Delta_{BCC}$ covering the unit cube, and develop quasi-interpolation operators for $\mathcal{S}_5^2(\Delta_1)$.

Definition 3.14. Let $H := (h_1, h_2, h_3)$ be the positive real numbers defined in 3.13, Δ_{BCC} the BCC partition with spacing H , and $\Omega_1 := [0, 1]^3$ the unit cube. Then

$$\Delta_1 := \{T \in \Delta_{BCC}; \text{vol}(T \cap \Omega_1) > 0\}.$$

The partition Δ_1 is constructed such that the vertices of \mathcal{X} coincide with those in \mathcal{V}_1 . Of the tetrahedra in the boundary region of the unit cube, at most one vertex lies outside of Ω_1 . Figure 3.2 shows such a tetrahedron.

From a structural point of view, all tetrahedra in Δ_{BCC} are the same. To be more precise, the relationship between any two neighboring tetrahedra can be described by the same 4-tuple of barycentric coordinates.

Lemma 3.15. Let $T := \langle v_0, v_1, v_2, v_3 \rangle$ and $\tilde{T} := \langle v_0, v_1, v_2, \tilde{v}_3 \rangle$ be two neighboring tetrahedra of Δ_{BCC} . Then the vertices of T and \tilde{T} can be arranged such that $v_0, v_2 \in \mathcal{V}_H$ and $v_1, v_3, \tilde{v}_3 \in \mathcal{W}_H$, or vice versa. Moreover, the barycentric coordinates of \tilde{v}_3 relative to T are $(1, 0, 1, -1)$.

Proof. The vertices of \mathcal{V}_H form a uniform cuboid grid with cube centers \mathcal{W}_H . Suppose $\langle v_0, v_2 \rangle$ is an edge of this grid, and $v_1, v_3, \tilde{v}_3 \in \mathcal{W}_H$ are cube centers, as shown in figure 3.3. Then the midpoint of this edge is $(v_0 + v_2)/2 = (v_3 + \tilde{v}_3)/2$, and thus $\tilde{v}_3 = v_0 + v_2 - v_3$.

Now suppose $v_0, v_2 \in \mathcal{W}$. The vertices \mathcal{W}_H also form a uniform cuboid grid, which is translated by $(h_1/2, h_2/2, h_3/2)$ and has cube centers \mathcal{V}_H .

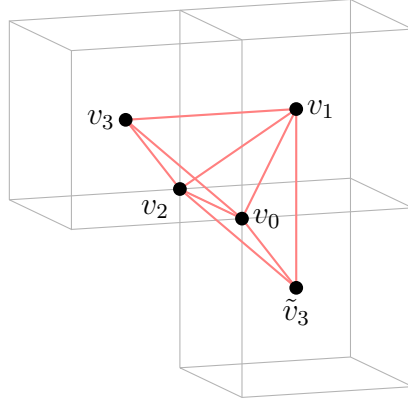


Figure 3.3: Two neighboring tetrahedra of Δ_{BCC} . The cubes indicate the cuboid grid defined by either \mathcal{V}_H or \mathcal{W}_H .

We use the same arguments as before to obtain the barycentric coordinates $(1, 0, 1, -1)$. \square

This means that the smoothness conditions of spline spaces defined over Δ_{BCC} can be characterized by a small number of conditions. The next corollary follows immediately from theorem 2.53 and lemma 3.15, and gives these conditions explicitly for the Space $\mathcal{S}_5^2(\Delta_{BCC})$.

Theorem 3.16. *The smoothness condition of $\mathcal{S}_5^2(\Delta_{BCC})$ between neighboring tetrahedra $T, \tilde{T} \in \Delta_{BCC}$ are be completely characterized by the equations*

$$c_{ijk0}^{\tilde{T}} = c_{ijk0}^T, \quad i + j + k = 5, \quad (3.4)$$

$$c_{ijk1}^{\tilde{T}} + c_{ijk1}^T = c_{i+1,j,k,0}^T + c_{i,j,k+1,0}^T, \quad i + j + k = 4, \quad (3.5)$$

$$c_{ijk2}^{\tilde{T}} + c_{i+1,j,k,1}^T + c_{i,j,k+1,1}^T = c_{i+1,j,k,1}^{\tilde{T}} + c_{i,j,k+1,1}^{\tilde{T}} + c_{i,j,k,2}^T, \quad i + j + k = 3. \quad (3.6)$$

Proof. We arrange the vertices of T and \tilde{T} according to lemma 3.15 and use theorem 2.53, obtaining

$$\begin{aligned} c_{ijk0}^{\tilde{T}} &= c_{ijk0}^T, & i + j + k &= 5, \\ c_{ijk1}^{\tilde{T}} &= c_{i+1,j,k,0}^T + c_{i,j,k+1,0}^T - c_{ijk1}^T, & i + j + k &= 4, \\ c_{ijk2}^{\tilde{T}} &= c_{i+2,j,k,0}^T + 2c_{i+1,j,k+1,0}^T + c_{i,j,k+2,0}^T \\ &\quad - 2c_{i+1,j,k,1}^T - 2c_{i,j,k+1,1}^T + c_{i,j,k,2}^T, & i + j + k &= 3. \end{aligned}$$

We rearrange the terms in the third equation and substitute using the second equation.

$$\begin{aligned} c_{ijk2}^T &= \underbrace{c_{i+2,j,k,0}^T + c_{i+1,j,k+1,0}^T - c_{i+1,j,k,1}^T}_{c_{i+1,j,k,1}^T} \\ &\quad + \underbrace{c_{i+1,j,k+1,0}^T + c_{i,j,k+2,0}^T - c_{i,j,k+1,1}^T}_{c_{i,j,k+1,1}^T} \\ &\quad - c_{i+1,j,k,1}^T - c_{i,j,k+1,1}^T + c_{i,j,k,2}^T, \end{aligned} \quad i+j+k = 3.$$

□

3.1 A convex quasi-interpolation operator

In this section we develop a convex quintic C^2 quasi-interpolation operator that approximates data located on a cuboid grid. For the remainder of this section, we assume that \mathcal{X} is constructed with a padding parameter $P \geq 2$, and that Δ_1 is the BCC partition associated with \mathcal{X} as defined in 3.14. We define $\mathcal{S} := \mathcal{S}_5^2(\Delta_1)$.

Definition 3.17. *For each $T := \langle v_0, v_1, v_2, v_3 \rangle \in \Delta_1$, we assume that the vertices of T are arranged such that $v_0, v_2 \in \mathcal{V}_H$ and $v_1, v_3 \in \mathcal{W}_H$. Then Q_{conv} is the quasi-interpolation operator defined by the B-coefficient computation rules (A.1)-(A.20), which are given relative to T , and the following symmetries. For each $i + j + k + l = 5$, the rule for c_{ijkl} is $(0, 2)$ -symmetric to the rule for c_{kjl} and $(1, 3)$ -symmetric to the rule for c_{ilkj} .*

The main result of this section shows that a spline constructed by these rules satisfies all smoothness conditions of \mathcal{S} and uses only data values located at the sample points in \mathcal{X} .

Theorem 3.18. *The operator Q_{conv} , defined by the B-coefficient computation rules (A.1)-(A.20), is a quasi-interpolation operator for $(\mathcal{X}, \mathcal{S})$.*

Proof. First we show that all sample points used by the rules are indeed in the set \mathcal{X} . Fix $T := \langle v_0, v_1, v_2, v_3 \rangle \in \Delta_1$. The sample points used by the rules for Q_{conv} are depicted in figure 3.5 as blue and black barycentric coordinates. Looking at definitions 2.17 and 3.13, it is clear that $\mathcal{X} \cap \mathcal{V}_H = \mathcal{X}$. Since both v_0 and v_2 belong to \mathcal{V}_H , the vertices $v_0 + i(v_2 - v_0)$, $i \in \mathbb{Z}$, are also in \mathcal{V}_H . These vertices have the barycentric coordinates $(1-i, 0, i, 0)$ relative to T . Likewise, the vertices $v_0 + j(v_3 - v_1)$, $j \in \mathbb{Z}$, belong to \mathcal{V}_H , since $v_1, v_3 \in \mathcal{W}_H$ and $\mathcal{W}_H = \mathcal{V}_H + (1/2, 1/2, 1/2)$. The barycentric coordinates of these vertices relative to T are $(1, -j, 0, j)$. By a similar argument, the vertices $v_0 + k(v_3 - v_0 + v_1 - v_2)$,

$k \in \mathbb{Z}$, with barycentric coordinates $(1-k, k, -k, k)$ relative to T are also in the set \mathcal{V}_H . Hence, the vertices in \mathcal{V}_H can be represented by the barycentric coordinates $(1-i-k, k-j, i-k, j+k)$ relative to T . This introduces a local orthogonal coordinate system with origin v_0 and units h_1, h_2, h_3 , where the vertices of \mathcal{V}_H are identified by integer coordinates. The axes of this coordinate system are parallel to the edges of the cuboid grid defined by \mathcal{V}_H . Figure 3.4 shows a tetrahedron and the associated axes together with a small portion of this grid. Table 3.1 shows selected values of (i, j, k) , the associated barycentric coordinates relative to T , and the smallest star which contains the sample point. All sample points used in the rules for Q_{conv} can be found in this table, and thus all data values sit on the grid defined by \mathcal{V}_H .

It remains to show that no sample point outside of \mathcal{X} is referenced by the rules. The definition of Δ_1 assures that at least three of the four vertices of T are contained in the unit cube. The padding parameter $P \geq 2$ guarantees that all sample points with local coordinates in the range of $-2, \dots, 2$ are in \mathcal{X} . The only sample point we need to take a closer look at is $(3, 0, 0)$. The barycentric coordinates relative to T of this point are $(-2, 0, 3, 0)$. Thus, it sits at a distance of two units from v_2 and is also contained in \mathcal{X} .

We now show that the smoothness conditions (3.4) - (3.6) are fulfilled. We distinguish between two cases. In the first case, the vertex arrangement of the neighboring tetrahedra reflects the situation of theorem 2.53. In the second case, the vertices of the neighboring tetrahedra are arranged in a different way than in theorem 2.53, and thus the indices of the B-coefficients in (3.4)-(3.6) have to be adjusted.

Case 1. Let $T := \langle v_0, v_1, v_2, v_3 \rangle, \tilde{T} := \langle v_0, v_1, v_2, \tilde{v}_3 \rangle \in \Delta_1$ be two neighboring tetrahedra with $v_0, v_2 \in \mathcal{V}_H$ and $v_1, v_3, \tilde{v}_3 \in \mathcal{W}_H$ as shown in figure 3.3. According to lemma 3.15, the barycentric coordinates of v_3 relative to \tilde{T} are $(1, 0, 1, -1)$. We use lemma 2.32 to rewrite the rules for $c_{\xi}^{\tilde{T}}$ relative to T . Let $(\varphi_0, \dots, \varphi_3)$ be the barycentric coordinates of an arbitrary point v relative to \tilde{T} , then the barycentric coordinates of v relative to T are $(\varphi_0 + \varphi_3, \varphi_1, \varphi_2 + \varphi_3, -\varphi_3)$. Thus, a sample value relative to \tilde{T} can be written as

$$f_{\varphi_0, \varphi_1, \varphi_2, \varphi_3}^{\tilde{T}} = f_{\varphi_0 + \varphi_3, \varphi_1, \varphi_2 + \varphi_3, -\varphi_3}^T. \quad (3.7)$$

To show that (3.4) is satisfied, we use the equation above on each sample point in the rule for $c_{ijk0}^{\tilde{T}}$. This reveals that the rules for $c_{ijk0}^{\tilde{T}}$ and c_{ijk0}^T use the same set of sample points with the same weights, and thus the rules are identical. We use the same technique with the equations (3.5) and (3.6). These calculations were performed by a computer program that we wrote using the Mathematica® software package by Wolfram Research. We refer to appendix D for a detailed description of our program and its source code.

Case 2. Let $T := \langle v_0, v_1, v_2, v_3 \rangle, \tilde{T} := \langle \tilde{v}_0, v_1, v_2, v_3 \rangle \in \Delta_1$ be two neighboring tetrahedra with $\tilde{v}_0, v_0, v_2 \in \mathcal{V}_H$ and $v_1, v_3 \in \mathcal{W}_H$. In this case, the

common face of T and \tilde{T} is $\langle v_1, v_2, v_3 \rangle$ rather than $\langle v_0, v_1, v_2 \rangle$. We rearrange the vertices of T and \tilde{T} with the permutation

$$\sigma := \begin{pmatrix} 0 & 1 & 2 & 3 \\ 1 & 2 & 3 & 0 \end{pmatrix},$$

resulting in the situation described in case 1. Then we use lemma 2.40 to adjust the indices of the B-coefficients in the smoothness conditions (3.4) - (3.6) and obtain

$$\begin{aligned} c_{0ijk}^{\tilde{T}} &= c_{0ijk}^T, & i+j+k &= 5, \\ c_{1ijk}^{\tilde{T}} + c_{1ijk}^T &= c_{0,i+1,j,k}^T + c_{0,i,j,k+1}^T, & i+j+k &= 4, \\ c_{2ijk}^{\tilde{T}} + c_{1,i+1,j,k}^T + c_{1,i,j,k+1}^T &= c_{1,i+1,j,k}^{\tilde{T}} - c_{1,i,j,k+1}^{\tilde{T}} + c_{2,i,j,k}^T, & i+j+k &= 3. \end{aligned}$$

We also adjust (3.7), using the relationship between the barycentric coordinates described in lemma 2.40. Let $U := \langle u_0, u_1, u_2, u_3 \rangle$ and $\tilde{U} := \langle u_0, u_1, u_2, \tilde{u}_3 \rangle$ be the tetrahedra resulting from rearranging T and \tilde{T} , respectively. Then $u_m = v_{\sigma(m)}$, $m = 0, \dots, 3$, and $\tilde{u}_3 = \tilde{v}_0$. Thus, $\varphi_m^U(v) = \varphi_{\sigma(m)}^T(v)$ and, using the inverse permutation,

$$\varphi_m^T(v) = \varphi_{\sigma^{-1}(m)}^U(v). \quad (\text{I})$$

Furthermore,

$$\varphi_m^{\tilde{U}}(v) = \varphi_{\sigma(m)}^{\tilde{T}}(v). \quad (\text{II})$$

for an arbitrary point v . Let x be a sample point with barycentric coordinates $\varphi_m^{\tilde{U}}(x)$ relative to \tilde{U} . It follows from (3.7) that the barycentric coordinates of x relative to U are

$$(\varphi_0^U(x), \varphi_1^U(x), \varphi_2^U(x), \varphi_3^U(x)) = (\varphi_0^{\tilde{U}}(x) + \varphi_3^{\tilde{U}}(x), \varphi_1^{\tilde{U}}(x), \varphi_2^{\tilde{U}}(x) + \varphi_3^{\tilde{U}}(x), -\varphi_3^{\tilde{U}}(x)). \quad (\text{III})$$

To obtain the barycentric coordinates of x relative to T , we then write

$$\begin{aligned} &(\varphi_0^T(x), \varphi_1^T(x), \varphi_2^T(x), \varphi_3^T(x)) \\ &\stackrel{(\text{I})}{=} (\varphi_3^U(x), \varphi_0^U(x), \varphi_1^U(x), \varphi_2^U(x)) \\ &\stackrel{(\text{III})}{=} (-\varphi_3^{\tilde{U}}(x), \varphi_0^{\tilde{U}}(x) + \varphi_3^{\tilde{U}}(x), \varphi_1^{\tilde{U}}(x), \varphi_2^{\tilde{U}}(x) + \varphi_3^{\tilde{U}}(x)) \\ &\stackrel{(\text{II})}{=} (-\varphi_0^{\tilde{T}}(x), \varphi_1^{\tilde{T}}(x) + \varphi_0^{\tilde{T}}(x), \varphi_2^{\tilde{T}}(x), \varphi_3^{\tilde{T}}(x) + \varphi_0^{\tilde{T}}(x)). \end{aligned}$$

Thus, we obtain

$$f_{\varphi_0, \varphi_1, \varphi_2, \varphi_3}^{\tilde{T}} = f_{-\varphi_0, \varphi_0 + \varphi_1, \varphi_2, \varphi_0 + \varphi_3}^T. \quad (3.8)$$

We conclude the proof by using the same method as in case 1 to verify that all smoothness conditions are fulfilled. The calculations were also performed by our computer program, see appendix D. \square

(i, j, k)	bary. coords.	star	(i, j, k)	bary. coords.	star
(0, 0, 0)	(1, 0, 0, 0)	0	(−1, 0, 1)	(1, 1, −2, 1)	2
(1, 0, 0)	(0, 0, 1, 0)	0	(1, −1, −1)	(1, 0, 2, −2)	2
(−1, 0, 0)	(2, 0, −1, 0)	1	(−1, 1, 1)	(1, 0, −2, 2)	2
(0, 0, −1)	(2, −1, 1, −1)	1	(1, 1, −1)	(1, −2, 2, 0)	2
(0, −1, 0)	(1, 1, 0, −1)	1	(0, 2, 0)	(1, −2, 0, 2)	2
(1, 0, −1)	(1, −1, 2, −1)	1	(0, −2, 1)	(0, 3, −1, −1)	2
(0, 1, 0)	(1, −1, 0, 1)	1	(1, −2, 0)	(0, 2, 1, −2)	2
(0, −1, 1)	(0, 2, −1, 0)	1	(2, −1, −1)	(0, 0, 3, −2)	2
(1, −1, 0)	(0, 1, 1, −1)	1	(2, 0, −1)	(0, −1, 3, −1)	2
(0, 0, 1)	(0, 1, −1, 1)	1	(0, 2, 1)	(0, −1, −1, 3)	2
(0, 1, 1)	(0, 0, −1, 2)	1	(2, 1, −1)	(0, −2, 3, 0)	2
(1, 1, 0)	(0, −1, 1, 1)	1	(1, 2, 0)	(0, −2, 1, 2)	2
(1, −1, 1)	(−1, 2, 0, 0)	1	(1, −2, 1)	(−1, 3, 0, −1)	2
(1, 0, 1)	(−1, 1, 0, 1)	1	(0, −1, 2)	(−1, 3, −2, 1)	2
(2, 0, 0)	(−1, 0, 2, 0)	1	(0, 0, 2)	(−1, 2, −2, 2)	2
(1, 1, 1)	(−1, 0, 0, 2)	1	(2, −1, 0)	(−1, 1, 2, −1)	2
(−1, −1, −1)	(3, 0, 0, −2)	2	(0, 1, 2)	(−1, 1, −2, 3)	2
(−1, 0, −1)	(3, −1, 0, −1)	2	(2, 1, 0)	(−1, −1, 2, 1)	2
(−1, 1, −1)	(3, −2, 0, 0)	2	(1, 2, 1)	(−1, −1, 0, 3)	2
(−1, −1, 0)	(2, 1, −1, −1)	2	(1, −1, 2)	(−2, 3, −1, 1)	2
(0, −1, −1)	(2, 0, 1, −2)	2	(2, −1, 1)	(−2, 2, 1, 0)	2
(−1, 1, 0)	(2, −1, −1, 1)	2	(1, 0, 2)	(−2, 2, −1, 2)	2
(0, 1, −1)	(2, −2, 1, 0)	2	(2, 0, 1)	(−2, 1, 1, 1)	2
(0, −2, 0)	(1, 2, 0, −2)	2	(1, 1, 2)	(−2, 1, −1, 3)	2
(−1, −1, 1)	(1, 2, −2, 0)	2	(2, 1, 1)	(−2, 0, 1, 2)	2

Table 3.1: The sample points used by the rules for Q_{conv} relative to a tetrahedron $T \in \Delta_1$. The tuples (i, j, k) in the left column are the local coordinates introduced in the proof of theorem 3.18. The associated barycentric coordinates relative to T are shown in the middle column. In the right column, a number ℓ is given to indicate that the point is contained in $\text{star}^\ell(\tilde{T})$, where \tilde{T} is the tetrahedron in Δ_{BCC} which is analogous to T .

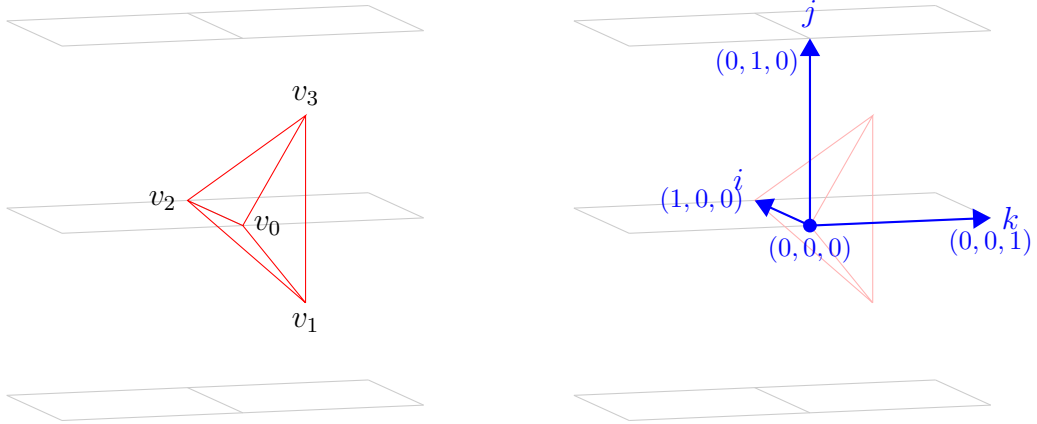


Figure 3.4: A tetrahedron T (left) and the local coordinate system relative to T which was introduced in the proof of theorem 3.18 (right). The grid lines show a portion of the cuboid grid defined by the vertices in \mathcal{V} .

The following theorem shows the convexity and locality of Q_{conv} . Since Q_{conv} uses sample values outside of Δ_1 , we have to adjust the concept of locality from definition 3.12 slightly. The partition Δ_1 is a subset of Δ_{BCC} , and hence there exists a tetrahedron $\tilde{T} \in \Delta_{BCC}$ for each $T \in \Delta_1$ with $T = \tilde{T}$. The locality is measured using $\text{star}^\ell(\tilde{T})$.

Theorem 3.19. *The operator Q_{conv} is convex. It is also 2-local in the following sense. For each $T \in \Delta_1$, let \tilde{T} be the analogous tetrahedron in Δ_{BCC} . Then*

$$\mathcal{X}_T \subset \text{star}^2(\tilde{T}).$$

Proof. For each of the B-coefficient computation rules for Q_{conv} , the sum of the weights is 1 and all weights are non-negative. The convexity follows from lemma 3.11.

To show the locality of the operator, we use the local coordinate system introduced in the proof of theorem 3.18. For each sample point, the local coordinates are given in table 3.1. The vertices of T have local coordinates $(0, 0, 0)$, $(1/2, -1/2, 1/2)$, $(1, 0, 0)$, and $(1/2, 1/2, 1/2)$. Using corollary 2.25, we directly calculate the number ℓ for each sample point x such that $x \in \text{star}^\ell(T)$. These numbers are given in the right column of table 3.1.

We demonstrate this process for the sample point x with barycentric coordinates $(-1, 3, 0, -1)$ relative to T . The local coordinates of x are $(1, -2, 1)$. Local coordinates are multiples of h_1, h_2 and h_3 , which are also used in lemma 2.24 to calculate stars relative to a vertex. Thus, we calculate the local coordinates of $x - v_m$ for each vertex, and use lemma 2.24 to calculate the number N_m with $x \in \text{star}^{N_m}(v_m)$. Then we use corollary 2.25 with these results.

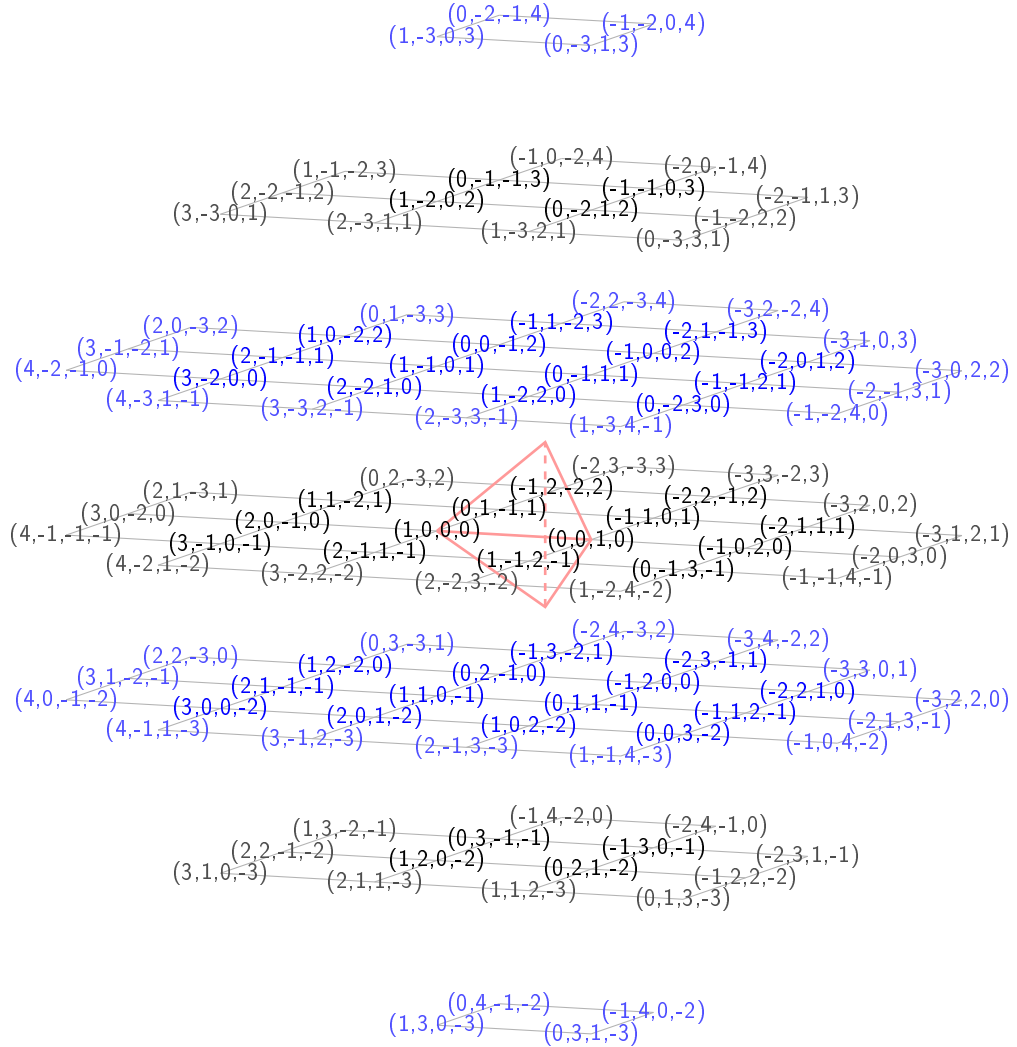


Figure 3.5: Union of the supports of all rules for Q_{conv} (blue and black) and Q_{opt} (light blue and gray). The barycentric coordinates relative to the red tetrahedron are written at each grid location.

The local coordinates of $x - v_0$ are $(1, -2, 1)$. By lemma 2.24, $x \in \text{star}^{N_0}(v_0)$, where $N_0 = |1| + |-2| + |1| - \min\{|1|, |-2|, |1|\} = 3$. The local coordinates of $x - v_1$, $x - v_2$, and $x - v_3$ are $(1/2, -3/2, 1/2)$, $(0, -2, 1)$, and $(1/2, -5/2, 1/2)$, respectively, and thus $x \in \text{star}^2(v_1)$, $x \in \text{star}^3(v_2)$, and $x \in \text{star}^3(v_3)$. By corollary 2.25, $x \in \text{star}^N(T)$ with $N = \min\{3, 2, 3, 3\} = 2$.

Repeating this process reveals that all sample points are contained at most in $\text{star}^2(T)$. To illustrate the stars, we show the support of all rules in figure 3.5, and two chains of tetrahedra, connecting selected sample points to T , in figure 3.6 \square

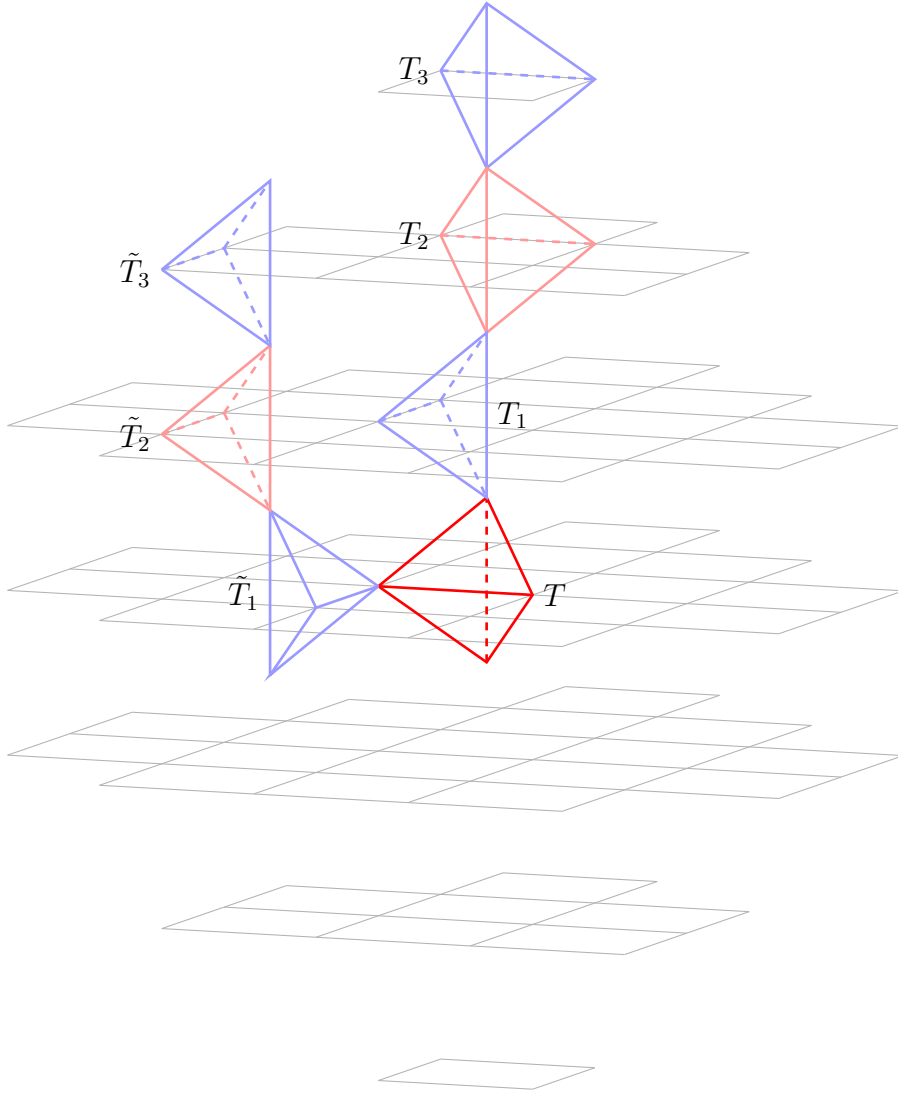


Figure 3.6: A subset of $\text{star}^3(T)$ for a tetrahedron $T \in \Delta_{BCC}$, showing two selected chains of tetrahedra with $T_\ell, \tilde{T}_\ell \subseteq \text{star}^\ell(T)$.

As a consequence of the convexity, Q_{conv} is also stable, as the following theorem shows.

Theorem 3.20. *Let $T \in \Delta_1$ and $f \in \mathcal{F}_{\mathcal{X}}$. Then*

$$\|Q_{conv}(f)\|_T \leq \max_{x \in \mathcal{X}_T} |f(x)|.$$

Proof. Let $\eta \in \mathcal{D}_5(T)$. Then the B-coefficient c_η is computed by one of the rules for Q_{conv} . Since the support of the rule is contained in \mathcal{X}_T , and since

$w_{\eta,x} = 0$ for $x \notin \mathcal{X}_\eta$, we have

$$c_\eta = \sum_{x \in \mathcal{X}_\eta} w_{\eta,x} f(x) = \sum_{x \in \mathcal{X}_T} w_{\eta,x} f(x).$$

But then, by the triangle inequality,

$$|c_\eta| \leq \sum_{x \in \mathcal{X}_T} |w_{\eta,x}| |f(x)| \leq \sum_{x \in \mathcal{X}_T} |w_{\eta,x}| \max_{x \in \mathcal{X}_T} |f(x)| \leq \max_{x \in \mathcal{X}_T} |f(x)| \sum_{x \in \mathcal{X}_T} |w_{\eta,x}|.$$

Since all weights are non-negative, and the sum of all weights used in any given rule is 1, we have

$$|c_\eta| \leq \max_{x \in \mathcal{X}_T} |f(x)|.$$

It follows from theorem 2.42 that

$$\|Q_{conv}(f)\|_T \leq \max_{\eta \in \mathcal{D}_5(T)} |c_\eta| \leq \max_{x \in \mathcal{X}_T} |f(x)|.$$

□

Finally, we show that linear polynomials are reproduced by the operator.

Theorem 3.21. *Q_{conv} reproduces linear polynomials. For each $p \in \mathcal{P}_1$, $Q_{conv}(p) \equiv p$.*

Proof. Since Q_{conv} is linear, it suffices to show that the Bernstein basis polynomials B_{ijkl} , $i + j + k + l = 1$, relative to a fixed tetrahedron $T \in \Delta_1$ are reproduced. We first compute the B-coefficients of B_{ijkl} , written as a polynomial of degree five, by repeatedly using lemma 2.41. These are then compared to the B-coefficients of $Q_{conv}(B_{ijkl})|_T$, computed with the rules (A.1)-(A.20).

Due to the symmetry of both the Bernstein basis polynomials and the B-coefficient computation rules of Q_{conv} , it suffices to proof the reproduction of B_{1000} and B_{0100} , since then the reproduction of the remaining Bernstein basis polynomials is implied by the symmetry, using lemmas 2.35 (iv) and 3.8.

The B-coefficients B_{1000} and B_{0100} , written as polynomials of degree five, are shown in figures 3.7 and 3.8, respectively. The complete calculations of the B-coefficients of $Q_{conv}(B_{1000})|_T$ and $Q_{conv}(B_{0100})|_T$ were too vast to be printed here, and were performed by a computer program that we wrote. The output of the program reveals that all B-coefficients match. The source code of this program, as well as a detailed description thereof, are included in appendix D of this thesis.

Since all B-coefficients of B_{ijkl} match their respective counterparts of $Q_{conv}(B_{ijkl})|_T$, the proof is concluded. □

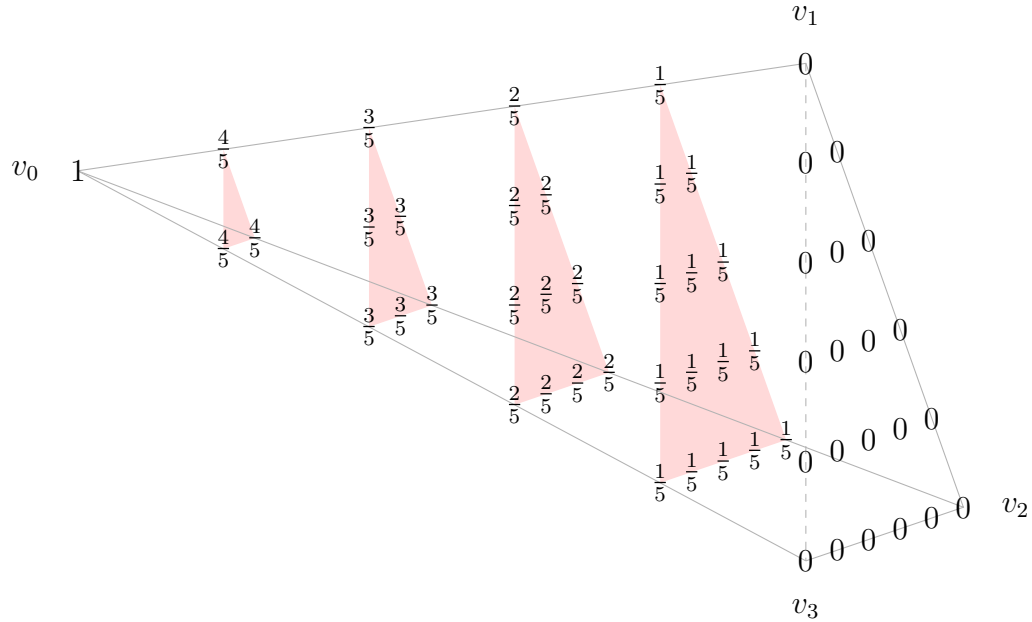


Figure 3.7: The B-coefficients of the B-form of B_{1000} , written as a polynomial of degree 5. The shells $R_m^T(v_0)$, $m = 1, \dots, 4$, are shown in red.

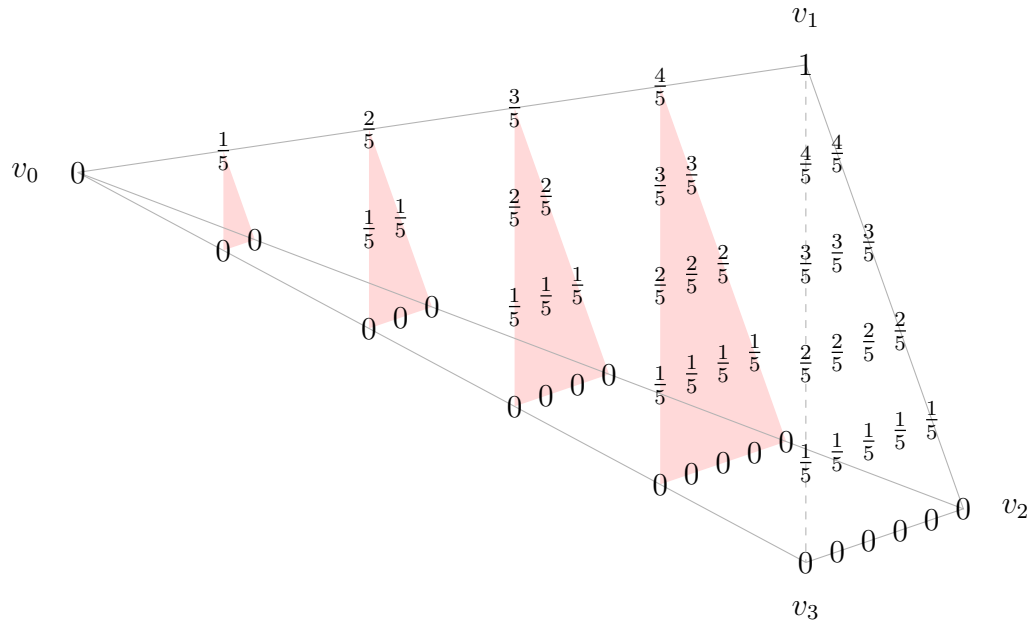


Figure 3.8: The B-coefficients of the B-form of B_{0100} , written as a polynomial of degree 5. The shells $R_m^T(v_0)$, $m = 1, \dots, 4$, are shown in red.

3.2 An optimal quasi-interpolation operator

Since the convex quasi-interpolation operator developed in the previous section only reproduces linear polynomials, it is clear that its approximation order is no higher than two. In this section, we develop a quasi-interpolation operator which reproduces polynomials up to degree three and thus has approximation order four, which is optimal for the underlying spline space. This operator is similar to the one developed in the previous section, albeit it is slightly more complex. Throughout this section, we assume that the sample points \mathcal{X} are constructed as in definition 3.13, with a padding parameter $P = 3$, and that Δ_1 is the associated BCC partition defined in 3.14. Moreover, let $\mathcal{S} := \mathcal{S}_5^2(\Delta_1)$ for the remainder of this section.

Definition 3.22. *For each $T = \langle v_0, v_1, v_2, v_3 \rangle \in \Delta_1$, let the vertices be arranged such that $v_0, v_2 \in \mathcal{V}_H$ and $v_1, v_3 \in \mathcal{W}_H$. Then Q_{opt} is the quasi-interpolation operator defined by the rules (B.1)-(B.20). These rules are given relative to T . Moreover, for each $i + j + k + l = 5$, the rule for c_{ijkl} is $(0, 2)$ -symmetric to the rule for c_{kjl} and $(1, 3)$ -symmetric to the rule for c_{ilkj} .*

Analogously to the convex operator constructed in the previous section, we first show that Q_{opt} satisfies all smoothness conditions of \mathcal{S} and uses only data values located at the points in \mathcal{X} .

Theorem 3.23. *The operator Q_{opt} , defined by the rules B.1-B.20, is a quasi-interpolation operator for $(\mathcal{X}, \mathcal{S})$.*

Proof. We follow the proof of theorem 3.18. First we show that only sample points located on the grid \mathcal{X} are used. Fix $T \in \Delta_1$. The sample points relevant for the construction of $Q_{opt}(f)|_T$, $f \in \mathcal{F}_{\mathcal{X}}$, are depicted in figure 3.5. We use the local coordinate system introduced in the proof of theorem 3.18 to show that the sample points sit on the grid \mathcal{V} . Tables 3.1 and 3.2 give a list of all sample points used by the rules for Q_{opt} , both in the local coordinate system and as barycentric coordinates relative to T . Since none of the local coordinates is greater than 3, and since \mathcal{X} is constructed with a padding parameter $P = 3$, all sample points are contained in \mathcal{X} .

To show that all smoothness conditions of \mathcal{S} are satisfied, we use the same method as is the proof of theorem 3.18, since Q_{opt} and Q_{conv} are defined on the same partition, and since the rules for both operators share the same symmetries. All calculations were performed by our computer program, a detailed description of which can be found in appendix D. The output of the program reveals that all smoothness conditions are satisfied. \square

We provide a theorem concerning the locality of Q_{opt} . Since the operator is designed to use sample values outside of Δ_1 , we adjust the concept of

(i, j, k)	bary. coords.	star	(i, j, k)	bary. coords.	star
(-2, -1, -1)	(4, 0, -1, -2)	3	(-1, -1, 2)	(0, 3, -3, 1)	3
(-1, -1, -2)	(4, -1, 1, -3)	3	(-1, 0, 2)	(0, 2, -3, 2)	3
(-2, 0, -1)	(4, -1, -1, -1)	3	(2, -2, -1)	(0, 1, 3, -3)	3
(-1, 0, -2)	(4, -2, 1, -2)	3	(-1, 1, 2)	(0, 1, -3, 3)	3
(-2, 1, -1)	(4, -2, -1, 0)	3	(0, 3, 1)	(0, -2, -1, 4)	3
(-1, 1, -2)	(4, -3, 1, -1)	3	(2, 2, -1)	(0, -3, 3, 1)	3
(-1, -2, -1)	(3, 1, 0, -3)	3	(1, 3, 0)	(0, -3, 1, 3)	3
(-2, -1, 0)	(3, 1, -2, -1)	3	(1, -3, 1)	(-1, 4, 0, -2)	3
(-2, 0, 0)	(3, 0, -2, 0)	2	(0, -2, 2)	(-1, 4, -2, 0)	3
(0, -1, -2)	(3, -1, 2, -3)	3	(2, -2, 0)	(-1, 2, 2, -2)	3
(-2, 1, 0)	(3, -1, -2, 1)	3	(3, -1, -1)	(-1, 0, 4, -2)	3
(0, 0, -2)	(3, -2, 2, -2)	2	(0, 2, 2)	(-1, 0, -2, 4)	3
(0, 1, -2)	(3, -3, 2, -1)	3	(3, 0, -1)	(-1, -1, 4, -1)	3
(-1, 2, -1)	(3, -3, 0, 1)	3	(3, 1, -1)	(-1, -2, 4, 0)	3
(-1, -2, 0)	(2, 2, -1, -2)	3	(2, 2, 0)	(-1, -2, 2, 2)	3
(-2, -1, 1)	(2, 2, -3, 0)	3	(1, 3, 1)	(-1, -2, 0, 4)	3
(0, -2, -1)	(2, 1, 1, -3)	3	(1, -2, 2)	(-2, 4, -1, 0)	3
(-2, 0, 1)	(2, 1, -3, 1)	3	(0, -1, 3)	(-2, 4, -3, 2)	3
(-2, 1, 1)	(2, 0, -3, 2)	3	(2, -2, 1)	(-2, 3, 1, -1)	3
(1, -1, -2)	(2, -1, 3, -3)	3	(0, 0, 3)	(-2, 3, -3, 3)	3
(1, 0, -2)	(2, -2, 3, -2)	2	(0, 1, 3)	(-2, 2, -3, 4)	3
(-1, 2, 0)	(2, -2, -1, 2)	3	(3, -1, 0)	(-2, 1, 3, -1)	3
(1, 1, -2)	(2, -3, 3, -1)	3	(3, 0, 0)	(-2, 0, 3, 0)	2
(0, 2, -1)	(2, -3, 1, 1)	3	(1, 2, 2)	(-2, 0, -1, 4)	3
(0, -3, 0)	(1, 3, 0, -3)	3	(3, 1, 0)	(-2, -1, 3, 1)	3
(-1, -2, 1)	(1, 3, -2, -1)	3	(2, 2, 1)	(-2, -1, 1, 3)	3
(1, -2, -1)	(1, 1, 2, -3)	3	(1, -1, 3)	(-3, 4, -2, 2)	3
(2, -1, -2)	(1, -1, 4, -3)	3	(2, -1, 2)	(-3, 3, 0, 1)	3
(-1, 2, 1)	(1, -1, -2, 3)	3	(1, 0, 3)	(-3, 3, -2, 3)	3
(2, 0, -2)	(1, -2, 4, -2)	3	(3, -1, 1)	(-3, 2, 2, 0)	3
(2, 1, -2)	(1, -3, 4, -1)	3	(2, 0, 2)	(-3, 2, 0, 2)	3
(1, 2, -1)	(1, -3, 2, 1)	3	(1, 1, 3)	(-3, 2, -2, 4)	3
(0, 3, 0)	(1, -3, 0, 3)	3	(3, 0, 1)	(-3, 1, 2, 1)	3
(0, -3, 1)	(0, 4, -1, -2)	3	(2, 1, 2)	(-3, 1, 0, 3)	3
(1, -3, 0)	(0, 3, 1, -3)	3	(3, 1, 1)	(-3, 0, 2, 2)	3

Table 3.2: The sample points used in the rules for Q_{opt} , in addition to those in table 3.1.

locality to reflect this fact. The partition Δ_1 is a subset of Δ_{BCC} , and thus each tetrahedron $T \in \Delta_1$ has a counterpart in Δ_{BCC} . We use this counterpart to measure the locality.

Theorem 3.24. *The operator Q_{opt} is 3-local in the following sense. For all $T \in \Delta_1$, let \tilde{T} be the analogous tetrahedron in Δ_{BCC} . Then*

$$\mathcal{X}_T \subset \text{star}^3(\tilde{T}).$$

Proof. We use the same method as in theorem 3.19 to compute the stars for each sample point. Tables 3.1 and 3.2 give the local coordinates for the sample points, and we use corollary 2.25 to obtain the stars. The numbers are shown in right column of the tables. All sample points are contained at most in $\text{star}^3(T)$. Figure 3.6 gives two examples of how outlying sample points are connected to T by a chain of at most three tetrahedra. \square

Even though Q_{opt} is not convex, there exists an estimate similar to theorem 3.20.

Theorem 3.25. *Let $T \in \Delta_1$ and $f \in \mathcal{F}_{\mathcal{X}}$. Then*

$$\|Q_{opt}(f)\|_T \leq \frac{19}{12} \max_{x \in \mathcal{X}_T} |f(x)|.$$

Proof. Let $\eta \in \mathcal{D}_5(T)$. We consider the rule for c_η ,

$$c_\eta = \sum_{x \in \mathcal{X}_\eta} w_{\eta,x} f(x).$$

Using the triangle inequality, we obtain

$$|c_\eta| \leq \sum_{x \in \mathcal{X}_\eta} |w_{\eta,x}| |f(x)| \leq \sum_{x \in \mathcal{X}_\eta} |w_{\eta,x}| \max_{x \in \mathcal{X}_\eta} |f(x)| \stackrel{\mathcal{X}_\eta \subseteq \mathcal{X}_T}{\leq} \max_{x \in \mathcal{X}_T} |f(x)| \underbrace{\sum_{x \in \mathcal{X}_\eta} |w_{\eta,x}|}_{=: \hat{w}_\eta}.$$

For each rule, we calculate \hat{w}_η , using B.1-B.20. Taking the maximum over all domain points yields

$$\max_{\eta \in \mathcal{D}_5(T)} \hat{w}_\eta = \frac{19}{12},$$

and thus

$$|c_\eta| \leq \frac{19}{12} \max_{x \in \mathcal{X}_T} |f(x)|.$$

This shows that Q_{opt} is stable. It follows from theorem 2.42 that

$$\|Q_{opt}(f)\|_T \leq \max_{\eta \in \mathcal{D}_5(T)} |c_\eta| \leq \frac{19}{12} \max_{x \in \mathcal{X}_T} |f(x)|.$$

\square

The next theorem states the reproduction properties of Q_{opt} .

Theorem 3.26. *Q_{opt} reproduces polynomials of total degree three. For each $p \in \mathcal{P}_3$, $Q_{opt}(p) \equiv p$.*

Proof. Analogously to theorem 3.21, we show that the basis polynomials B_{ijkl} , $i + j + k + l = 3$, relative to a fixed tetrahedron $T \in \Delta_1$ are reproduced. Due to the symmetries of the Bernstein basis polynomials and the B-coefficient computation rules of Q_{opt} , it suffices to show the reproduction of B_{3000} , B_{2100} , B_{2010} , B_{1110} , B_{1101} , B_{0300} , B_{0210} and B_{0201} . The reproduction of the remaining basis polynomials is then implied by lemmas 2.35 (iv) and 3.8.

The coefficients of these Bernstein basis polynomials, written in their B-forms as polynomials of degree five, are shown in figures 3.9 - 3.16. These coefficients are obtained by repeatedly using lemma 2.41. We use the rules B.1-B.20 to calculate the B-coefficients of $Q_{opt}(B_{ijkl})|_T$. The calculations were performed by our computer program, the source code of which is printed in appendix D. The output of the program shows that all B-coefficients match their respective counterparts, which implies the reproduction of cubic polynomials. \square

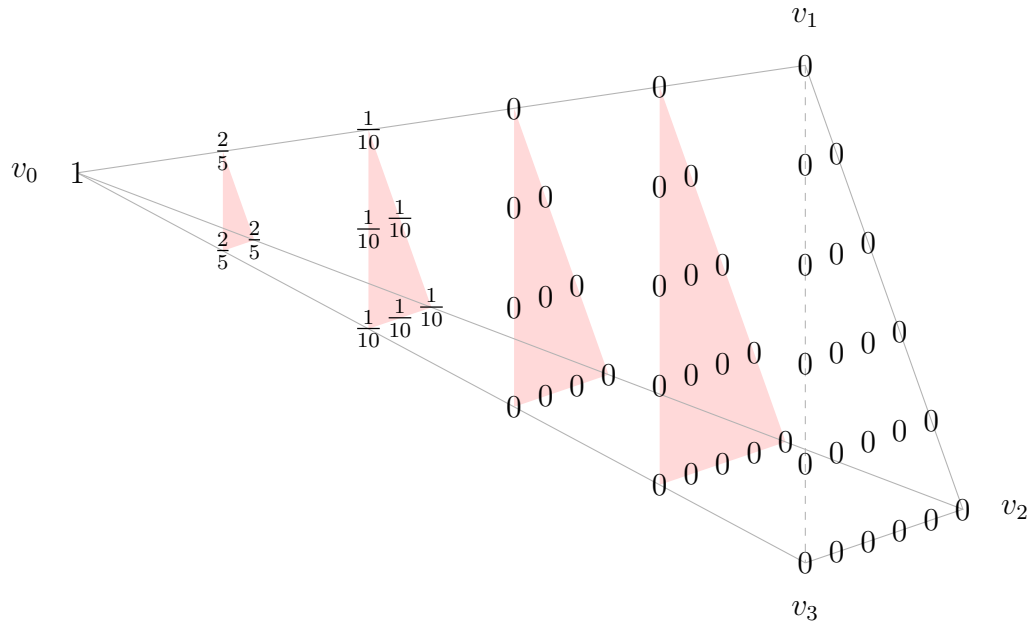


Figure 3.9: The B-coefficients of the B-form of B_{3000} , written as a polynomial of degree 5. The shells $R_m^T(v_0)$, $m = 1, \dots, 4$, are shown in red.

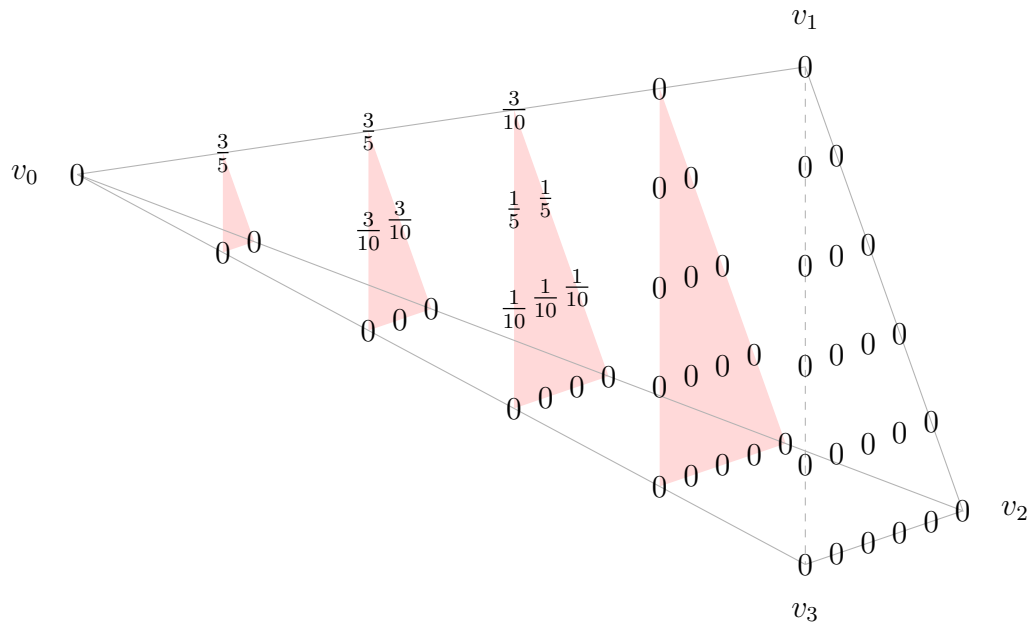


Figure 3.10: The B-coefficients of the B-form of B_{2100} , written as a polynomial of degree 5. The shells $R_m^T(v_0)$, $m = 1, \dots, 4$, are shown in red.

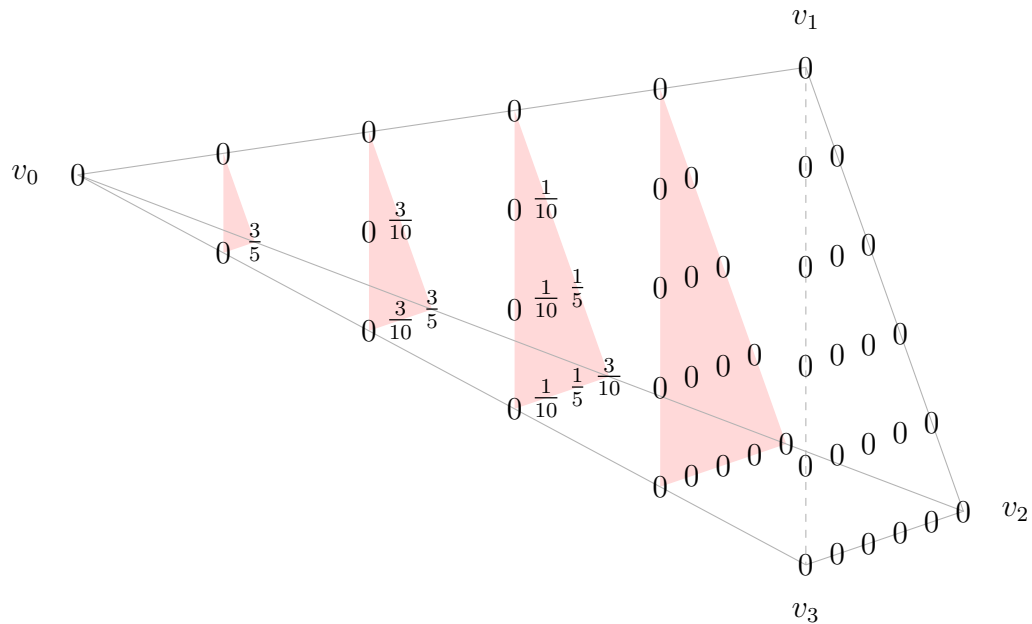


Figure 3.11: The B-coefficients of the B-form of B_{2010} , written as a polynomial of degree 5. The shells $R_m^T(v_0)$, $m = 1, \dots, 4$, are shown in red.

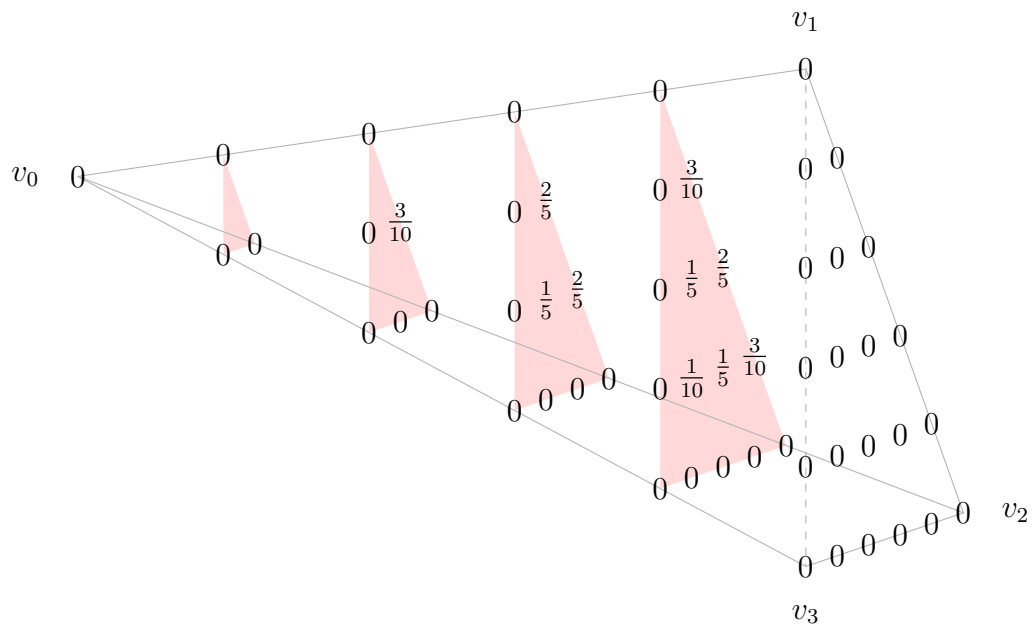


Figure 3.12: The B-coefficients of the B-form of B_{1110} , written as a polynomial of degree 5. The shells $R_m^T(v_0)$, $m = 1, \dots, 4$, are shown in red.

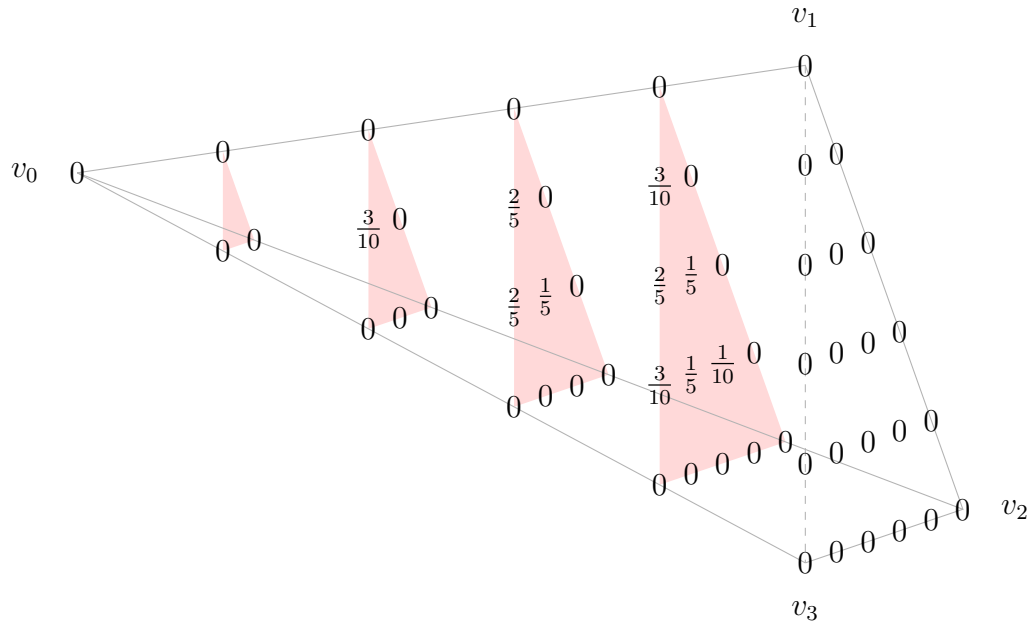


Figure 3.13: The B-coefficients of the B-form of B_{1101} , written as a polynomial of degree 5. The shells $R_m^T(v_0)$, $m = 1, \dots, 4$, are shown in red.

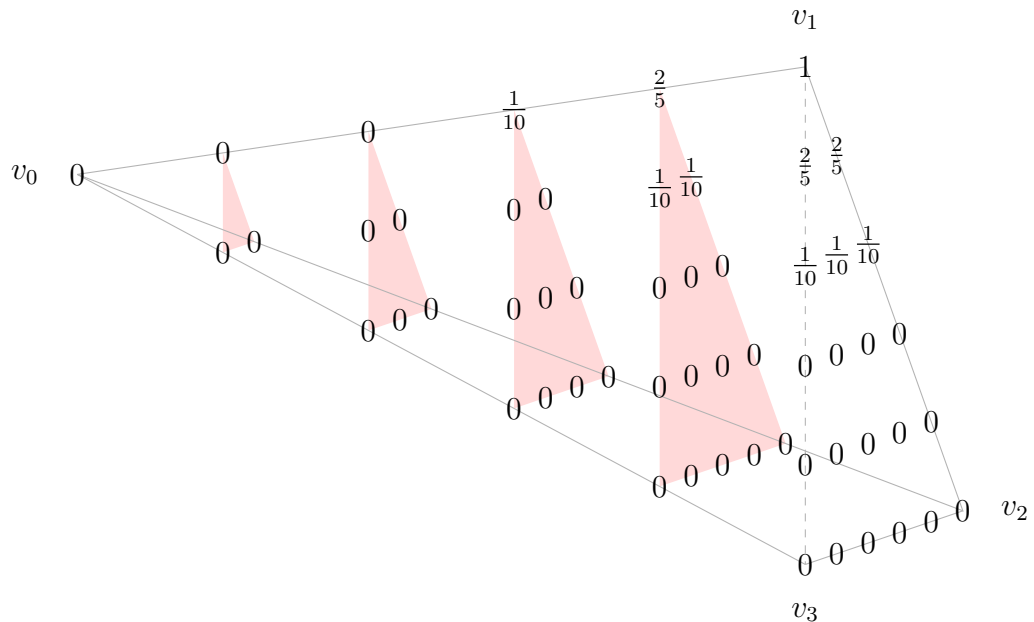


Figure 3.14: The B-coefficients of the B-form of B_{0300} , written as a polynomial of degree 5. The shells $R_m^T(v_0)$, $m = 1, \dots, 4$, are shown in red.

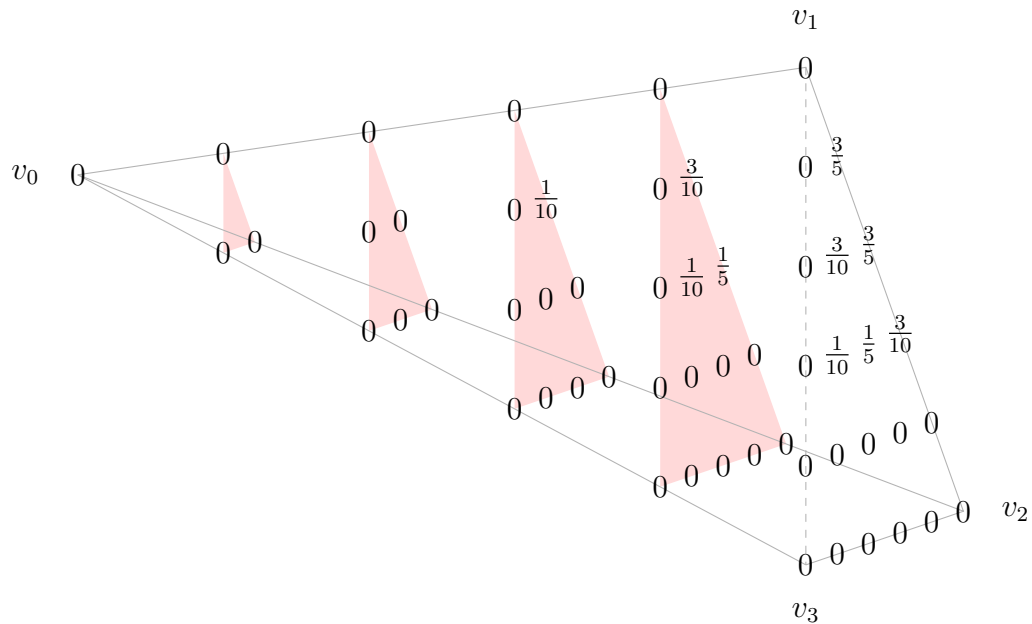


Figure 3.15: The B-coefficients of the B-form of B_{0210} , written as a polynomial of degree 5. The shells $R_m^T(v_0)$, $m = 1, \dots, 4$, are shown in red.

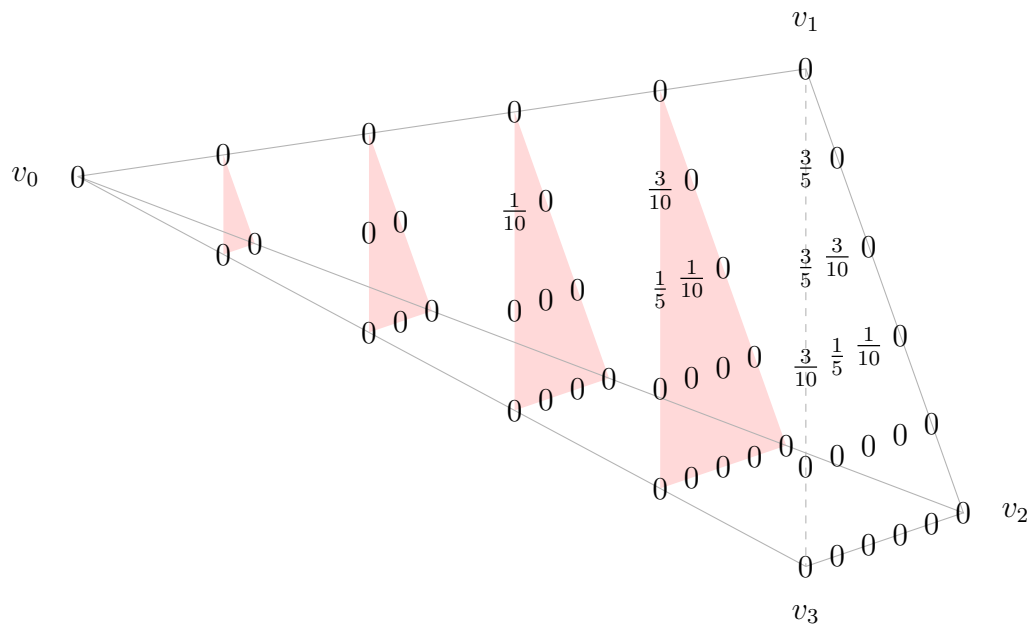


Figure 3.16: The B-coefficients of the B-form of B_{0201} , written as a polynomial of degree 5. The shells $R_m^T(v_0)$, $m = 1, \dots, 4$, are shown in red.

3.3 An interpolating quasi-interpolation operator

In this chapter we develop a quasi-interpolation operator for quintic C^2 -splines on the BCC partition which interpolates the provided data values while maintaining the optimal approximation order 4. To achieve this, we adjust the spacing of the underlying BCC partition to be half the spacing of the sample grid. This results in four different classes of tetrahedra, characterized by their relative position to the sample points. For each of these classes, we provide a set of coefficient computation rules. Throughout this section, we assume that \mathcal{X} is a sample set constructed as in 3.13 with a padding parameter $P = 2$. We begin by specifying the tetrahedral partition on which the operator is based.

Definition 3.27. Let h_1, h_2, h_3 be the positive real numbers defined in 3.13 and Δ_{BCC} the BCC partition with spacing $H = (h_1/2, h_2/2, h_3/2)$. Let $\Omega_1 := [0, 1]^3$ be the unit cube, then

$$\Delta_2 := \{T \in \Delta_{BCC}; \text{vol}(T \cap \Omega_1) > 0\}.$$

The difference between the spacing of the sample points \mathcal{X} and the spacing of Δ_2 results in the relationship

$$x_{ijk} = v_{2i,2j,2k}$$

between \mathcal{X} and \mathcal{V}_H .

The problem investigated here can be stated as follows.

Problem 3.28. Construct a quasi-interpolation operator Q_I for $(\mathcal{X}, \mathcal{S})$, where $\mathcal{S} := \mathcal{S}_5^2(\Delta_2)$, such that

$$Q_I(f)(x) = f(x) \quad \text{for all } x \in \mathcal{X} \cap \Omega_1 \text{ and } f \in \mathcal{F}_{\mathcal{X}}.$$

Even though this problem is related to the Lagrange interpolation problem stated in chapter 5, there is a major difference. Here, the number of interpolation points is not equal to the dimension of the spline space, and thus the operator developed here is not a Lagrange interpolation operator as defined in chapter 5.

Our construction begins with the classification of the vertices of Δ_2 . The decomposition of the tetrahedra into four different classes is based on this classification.

Definition 3.29. Let $\mathcal{V} := \mathcal{V}_H \cap \Delta_2$ and $\mathcal{W} := \mathcal{W}_H \cap \Delta_2$. For a vertex $v_{ijk} \in \mathcal{V}$, we set

$$\pi(v_{ijk}) := i \bmod 2 + j \bmod 2 + k \bmod 2.$$

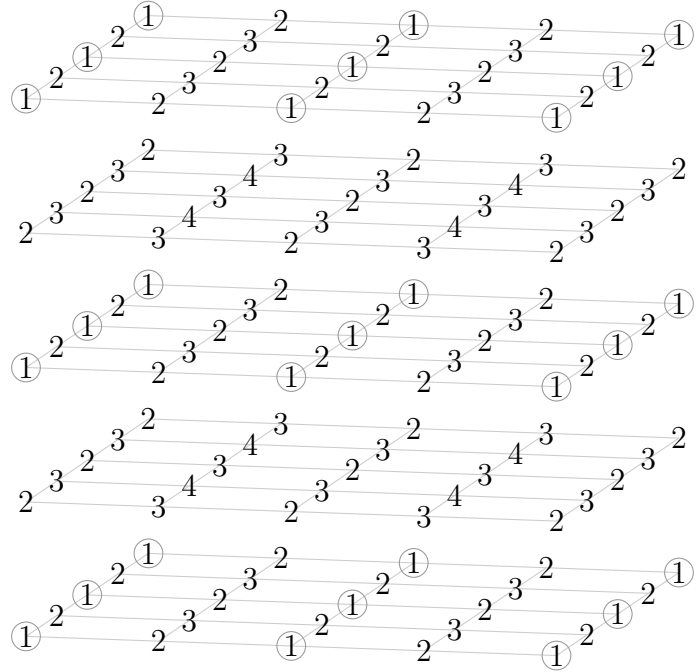


Figure 3.17: Distribution of the vertices in the first four classes. The sample points, which coincide with the vertices in class \mathcal{V}_1 , are circled.

Then

$$\begin{aligned}\mathcal{V}_1 &:= \{v_{ijk} \in \mathcal{V}; \pi(v_{ijk}) = 0\}, \\ \mathcal{V}_2 &:= \{v_{ijk} \in \mathcal{V}; \pi(v_{ijk}) = 1\}, \\ \mathcal{V}_3 &:= \{v_{ijk} \in \mathcal{V}; \pi(v_{ijk}) = 2\}, \\ \mathcal{V}_4 &:= \{v_{ijk} \in \mathcal{V}; \pi(v_{ijk}) = 3\}, \\ \mathcal{V}_5 &:= \mathcal{W}.\end{aligned}$$

Note that $\bigcup_{m=1}^4 \mathcal{V}_m = \mathcal{V}$ and $\mathcal{V}_1 \subseteq \mathcal{X}$. Figure 3.17 gives an impression of the distribution of the vertices belonging to the first four classes. The definition assures that of the four vertices of each tetrahedron in Δ_2 , exactly two belong to the class \mathcal{V}_5 . There are three possible class combinations for the remaining two vertices. They either belong to classes \mathcal{V}_1 and \mathcal{V}_2 , or they belong to classes \mathcal{V}_2 and \mathcal{V}_3 , or to classes \mathcal{V}_3 and \mathcal{V}_4 . Hence, the vertices of a tetrahedron $T = \langle v_0, v_1, v_2, v_3 \rangle \in \Delta_2$ can be arranged such that $v_0 \in \mathcal{V}_m, v_2 \in \mathcal{V}_{m+1}$, and $v_1, v_3 \in \mathcal{V}_5$, with an appropriate $m \in \{1, 2, 3\}$.

We recall that the vertices of $\mathcal{V}_1, \dots, \mathcal{V}_4$ form a cuboid grid as depicted in figures 2.2 and 3.17, with the vertices of \mathcal{V}_5 as centers. Of the eight corners of each cuboid, exactly one belongs to class \mathcal{V}_1 , representing a sample point. Therefore, each vertex $v \in \mathcal{V}_5$ is connected to exactly one sample point by an edge of the partition Δ_2 .

Definition 3.30. For each vertex $v \in \mathcal{V}_5$, we denote the unique sample point which is connected to v by an edge of Δ_2 by $SP(v)$.

We are now ready to classify the tetrahedra of Δ_2 .

Definition 3.31. For each $T := \langle v_0, v_1, v_2, v_3 \rangle \in \Delta_2$, let the vertices of T be arranged such that $v_0 \in \mathcal{V}_m$, $v_2 \in \mathcal{V}_{m+1}$, and $v_1, v_3 \in \mathcal{V}_5$, with $m \in \{1, 2, 3\}$. Then

$$\begin{aligned}\mathcal{K}_1 &:= \{T \in \Delta_2; v_0 \in \mathcal{V}_1, v_2 \in \mathcal{V}_2\}, \\ \mathcal{K}_2 &:= \{T \in \Delta_2; v_0 \in \mathcal{V}_2, v_2 \in \mathcal{V}_3, SP(v_1) = SP(v_3)\}, \\ \mathcal{K}_3 &:= \{T \in \Delta_2; v_0 \in \mathcal{V}_2, v_2 \in \mathcal{V}_3, SP(v_1) \neq SP(v_3)\}, \\ \mathcal{K}_4 &:= \{T \in \Delta_2; v_0 \in \mathcal{V}_3, v_2 \in \mathcal{V}_4\}.\end{aligned}$$

These classes are designed to reflect the different positions of the tetrahedra relative to the sample grid. For each of the classes, a tetrahedron is shown in figure 3.18 together with a small portion of the cuboid grid \mathcal{V} . The figure not only highlights the vertex configurations for each class, but also allows to examine the neighborhood relationship between tetrahedra of different classes. The following corollary is later used to study the smoothness conditions between neighboring tetrahedra.

Corollary 3.32. Let $T := \langle v_0, v_1, v_2, v_3 \rangle \in \Delta_2$, with the vertices arranged as in 3.31, and T_m , $m = 0, \dots, 3$, the neighbor tetrahedron sharing the face opposite of v_m with T . Then the following table shows the classes which T and its neighbors belong to.

T	T_0	T_1	T_2	T_3
\mathcal{K}_1	\mathcal{K}_2	\mathcal{K}_1	\mathcal{K}_1	\mathcal{K}_1
\mathcal{K}_2	\mathcal{K}_2	\mathcal{K}_3	\mathcal{K}_1	\mathcal{K}_3
\mathcal{K}_3	\mathcal{K}_4	\mathcal{K}_2	\mathcal{K}_3	\mathcal{K}_2
\mathcal{K}_4	\mathcal{K}_4	\mathcal{K}_4	\mathcal{K}_3	\mathcal{K}_4

We show two images in chapter 6 that might help to understand the arrangement of the tetrahedra in these four classes. Figure 6.3 (page 143) shows two isosurfaces extracted from reconstructions by the operator defined in this section. The colors in these images reflect the classes of the tetrahedra that the surface passes through and confirms the neighborhood relationships established in corollary 3.32

In contrast to the previously constructed quasi-interpolation operators defined sections 3.1 and 3.2, a single set of B-coefficient computation rules does not suffice to define the interpolating operator. Instead, we provide four sets of rules, one for each of the classes of tetrahedra. Our interpolating operator is defined as follows.

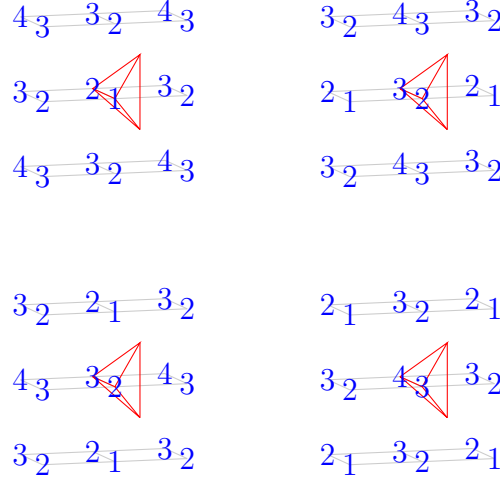


Figure 3.18: Tetrahedra belonging to the four classes. The figures in the upper left, upper right, lower left and lower right show a tetrahedron belonging to \mathcal{K}_1 , \mathcal{K}_2 , \mathcal{K}_3 and \mathcal{K}_4 , respectively. The numbers at the grid points represent the class \mathcal{V}_m which the associated vertex belongs to. The figures in the upper right and lower left highlight the difference between classes \mathcal{K}_2 and \mathcal{K}_3 : the location of the sample points, represented by the vertices of class \mathcal{V}_1 , relative to the tetrahedron is different.

Definition 3.33. For each $T := \langle v_0, v_1, v_2, v_3 \rangle \in \Delta_2$, let the vertices of T be arranged such that $v_0 \in \mathcal{V}_m$, $v_2 \in \mathcal{V}_{m+1}$, $m \in \{1, 2, 3\}$, and $v_1, v_3 \in \mathcal{V}_5$. Then Q_I is the quasi-interpolation operator defined by the B -coefficient computation rules

- (C.1)-(C.34) if $T \in \mathcal{K}_1$,
- (C.35)-(C.68) if $T \in \mathcal{K}_2$,
- (C.69)-(C.102) if $T \in \mathcal{K}_3$,
- (C.103)-(C.136) if $T \in \mathcal{K}_4$.

All B -coefficients and sample points in these rules are relative to T . In each of these sets of rules, the rules for c_{ijkl} and c_{ilkj} are $(1, 3)$ -symmetric to each other for all $i + j + k + l = 5$.

The following theorems are the main results of this section. We show that the Q_I is in quasi-interpolation operator for $(\mathcal{X}, \mathcal{S})$ which solves problem 3.28.

Theorem 3.34. The operator Q_I , defined in 3.33, is a quasi-interpolation operator for $(\mathcal{X}, \mathcal{S})$.

Proof. We follow the proof of theorem 3.18 and show first that all sample points addressed by the rules for Q_I are contained in \mathcal{X} . Let $T :=$

$\langle v_0, v_1, v_2, v_3 \rangle \in \Delta_2$. We recall the local coordinate system introduced in the proof of theorem 3.18, where (i, j, k) is defined as the point in 3-space with barycentric coordinates $(1 - i - k, k - j, i - k, j + k)$ relative to T . The origin of this coordinate system is the vertex v_0 , but here the units are $h_1/2, h_2/2$ and $h_3/2$, since Δ_2 was constructed with that spacing. Thus, the vertices of \mathcal{V}_H are represented by integer coordinates. The coordinate system relative to a tetrahedron is depicted in figure 3.4.

Let $\tilde{\mathcal{X}} := \{v_{ijk} \in \mathcal{V}_H; \pi(v_{ijk}) = 0\}$, where $\pi(v_{ijk})$ is defined as the sum of the parities of the indices as in 3.29. Then $\mathcal{X} \subset \tilde{\mathcal{X}}$. We now characterize the vertices of $\tilde{\mathcal{X}}$, depending on the class of T , using local coordinates. This characterization follows from the definitions 3.29 and 3.31 and can be verified by comparing figures 3.18 and 3.4.

- $T \in \mathcal{K}_1 : \tilde{\mathcal{X}} = \{(i, j, k); i, j, k \text{ even}\}$.
- $T \in \mathcal{K}_2 : \tilde{\mathcal{X}} = \{(i, j, k); i, j \text{ even}, k \text{ odd}\}$.
- $T \in \mathcal{K}_3 : \tilde{\mathcal{X}} = \{(i, j, k); i, k \text{ even}, j \text{ odd}\}$.
- $T \in \mathcal{K}_4 : \tilde{\mathcal{X}} = \{(i, j, k); i \text{ even}, j, k \text{ odd}\}$.

Analogously to the proof of theorems 3.18 and 3.23, we provide the tables 3.3-3.6, one for each class, containing the local coordinates of all sample points used in the B-coefficient computation rules for Q_I . All sample points comply with the characterization above. Figures 3.20-3.23 show the sample points relative to a tetrahedron of class $\mathcal{K}_1-\mathcal{K}_4$, respectively.

It remains to show that no sample points outside of \mathcal{X} are used in the rules for the B-coefficients of Q_I . $\tilde{\mathcal{X}}$ subdivides the unit cube Ω_1 into congruent cuboids. The size of these cuboids, measured in units of the local coordinate system, is $2 \times 2 \times 2$. By the construction of Δ_2 , there exists a cuboid C_T with

$$\text{vol}(C_T \cap T) > 0 \text{ and } C_T \cap \Omega_1 = C_T. \quad (3.9)$$

We show that all sample points used in the computation of the B-coefficients associated with T are no more than two cuboids, or four units, away from C_T . Since the padding parameter $P = 2$ can be interpreted as the number of layers of cuboids outside the unit cube where sample points are provided, and since $C_T \subseteq \Omega_1$, it then follows that all required sample points are contained in \mathcal{X} . Figure 3.19 is intended to visualize the following part of this proof. Let $T \in \mathcal{K}_1$. Then $C_T := [0, 2] \times [0, 2] \times [0, 2]$ is a cuboid satisfying (3.9). Thus, all sample points with local coordinates $i \in \{-4, 6\}, j \in \{-4, 6\}$ and $k \in \{-4, 6\}$ relative to T are contained in \mathcal{X} . Table 3.3 shows that all sample points satisfy this condition. Now suppose $T \in \mathcal{K}_2$. Then the cuboid $C_T := [0, 2] \times [0, 2] \times [-1, 1]$ fulfills (3.9). The sample points lying within a distance of 4 units from C_T have local coordinates in the range of $i \in$

$\{-4, 6\}, j \in \{-4, 6\}$ and $k \in \{-5, 5\}$ relative to T . All sample points in table 3.4 comply with this characterization. For $T \in \mathcal{K}_3$, the cuboid $C_T := [0, 2] \times [-1, 1] \times [0, 2]$ contains T , and all sample points with local coordinates $i \in \{-4, 6\}, j \in \{-5, 5\}$ and $k \in \{-4, 6\}$ are contained in \mathcal{X} . Again, the coordinates of all sample points in table 3.5 lie within this range. Finally, let $T \in \mathcal{K}_4$. Then $C_T := [0, 2] \times [-1, 1] \times [-1, 1]$ fulfills (3.9), resulting in a valid coordinate range of $i \in \{-4, 6\}, j \in \{-5, 5\}$ and $k \in \{-5, 5\}$, which is satisfied by all sample points in table 3.6.

In the next part of the proof, we show that the B-coefficient computation rules of Q_I satisfy the smoothness conditions (3.4) - (3.6) of \mathcal{S} . We use the same notation as in corollary 3.32 to denote the four neighbors of a tetrahedron T writing T_m , $m = 0, \dots, 3$, for the neighbor tetrahedron sharing the face opposite of v_m with T .

Case 1. Let $T := \langle v_0, v_1, v_2, v_3 \rangle \in \mathcal{K}_1$. The vertex configurations for T and its four neighbors are depicted in figure 3.24. Consider the neighbor $T_0 := \langle \tilde{v}_0, \tilde{v}_1, \tilde{v}_2, \tilde{v}_3 \rangle$, belonging to the class \mathcal{K}_2 . For both tetrahedra, let the vertices be arranged as in 3.33. This means that $\tilde{v}_0 = v_2$, $\tilde{v}_1 = v_1$, $\tilde{v}_2 = v_1 + v_3 - v_0$ and $\tilde{v}_3 = v_3$. We use the same method as in case 2 of the proof of theorem 3.18 to align the tetrahedra. The vertices of T and T_0 are rearranged using the permutations

$$\sigma := \begin{pmatrix} 0 & 1 & 2 & 3 \\ 1 & 2 & 3 & 0 \end{pmatrix} \quad \text{and} \quad \tau := \begin{pmatrix} 0 & 1 & 2 & 3 \\ 1 & 0 & 3 & 2 \end{pmatrix},$$

respectively, and the indices in the smoothness conditions (3.4)-(3.6) are adjusted according to lemma 2.40, resulting in

$$\begin{aligned} c_{jio_k}^{T_0} &= c_{0ijk}^T, & i + j + k &= 5, \\ c_{ji1k}^{T_0} + c_{1ijk}^T &= c_{0,i+1,j,k}^T + c_{0,i,j,k+1}^T, & i + j + k &= 4, \\ c_{ji2k}^{T_0} + c_{1,i+1,j,k}^T + c_{1,i,j,k+1}^T &= c_{2ijk}^T + c_{j,i+1,1,k}^{T_0} + c_{j,i,1,k+1}^{T_0}, & i + j + k &= 3. \end{aligned}$$

We also adjust the sample points with the same permutations and obtain

$$f_{\varphi_0, \varphi_1, \varphi_2, \varphi_3}^{T_0} = f_{-\varphi_2, \varphi_1 + \varphi_2, \varphi_0, \varphi_2 + \varphi_3}^T.$$

This process is discussed in detail in the proof of theorem 3.18. We verify the conditions in the usual way, by rewriting the sample points and comparing both sides, using the rules for class \mathcal{K}_1 and \mathcal{K}_2 to calculate the B-coefficients of T and T_0 , respectively. The actual calculations were performed by our computer program. A listing of this program can be found in appendix D. The output verifies the smoothness conditions.

Due to the $(1, 3)$ -symmetry, the smoothness conditions between T_1 and T have the same representation as the smoothness conditions between T_3 and

T . In the latter case, the vertices align as in case 1 of theorem 3.18, and no vertex permutations are necessary. Both T_1 and T_3 belong to the class \mathcal{K}_1 , and we use the corresponding set of rules for the verification.

For the neighbor T_2 , we use the permutation

$$\sigma := \begin{pmatrix} 0 & 1 & 2 & 3 \\ 1 & 0 & 3 & 2 \end{pmatrix}$$

on both T and T_2 and obtain

$$\begin{aligned} c_{ji0k}^{T_2} &= c_{ji0k}^T, & i+j+k &= 5, \\ c_{ji1k}^{T_2} + c_{ji1k}^T &= c_{j,i+1,0,k}^T + c_{j,i,0,k+1}^T, & i+j+k &= 4, \\ c_{ji2k}^{T_2} + c_{j,i+1,1,k}^T + c_{j,i,1,k+1}^T &= c_{ji2k}^T + c_{j,i+1,1,k}^{T_2} + c_{j,i,1,k+1}^{T_2}, & i+j+k &= 3. \end{aligned}$$

The sample points used in the rules for the B-coefficients of T_2 can be written as

$$f_{\varphi_0, \varphi_1, \varphi_2, \varphi_3}^{T_2} = f_{\varphi_0, \varphi_1 + \varphi_2, -\varphi_2, \varphi_2 + \varphi_3}^T.$$

Case 2. Now suppose $T \in \mathcal{K}_2$. Figure 3.25 shows how the vertices of T align with the vertices of its neighbors. As in case 1, we describe the permutations used to align the tetrahedra, and the resulting smoothness conditions. First we consider the neighbor T_0 which also belongs to class \mathcal{K}_2 . The vertex configuration of T and T_0 is the same as in case 2 of theorem 3.18, and we verify the smoothness conditions between the two tetrahedra using the formulae provided there.

As in case 1, the situation for T_1 and T_3 , which belong to class \mathcal{K}_3 , is symmetric. We show that all smoothness conditions are satisfied, using the same technique as in 3.18, case 1.

The relationship between T and T_2 has already been described in case 1.

Case 3. We consider the neighbors of a tetrahedron $T \in \mathcal{K}_3$, as depicted in figure 3.26. The vertex configurations of T and its neighbors are analogous to case 1, and thus we have the same smoothness conditions here.

Case 4. The final case, in which T belongs to $T \in \mathcal{K}_4$, mirrors the situation described in case 2. Figure 3.27 shows the vertex configurations of T and its four neighbors.

We used our computer program to perform all calculations that are necessary to verify the smoothness conditions described in cases 1-4. A detailed description of this program is contained in appendix D of this thesis.

□

We show that the operator is indeed a solution to the interpolation problem 3.28.

Theorem 3.35. Q_I solves problem 3.28. For all $f \in \mathcal{F}_{\mathcal{X}}$,

$$Q_I(f)(x) = f(x), \quad \text{for all } x \in \mathcal{X} \cap \Omega_1.$$

(i, j, k)	bary. coords.	star	(i, j, k)	bary. coords.	star
$(0, 0, 0)$	$(1, 0, 0, 0)$	0	$(-2, 0, 2)$	$(1, 2, -4, 2)$	4
$(2, 0, 0)$	$(-1, 0, 2, 0)$	1	$(2, -2, -2)$	$(1, 0, 4, -4)$	4
$(-2, 0, 0)$	$(3, 0, -2, 0)$	2	$(-2, 2, 2)$	$(1, 0, -4, 4)$	4
$(0, 0, -2)$	$(3, -2, 2, -2)$	2	$(2, 2, -2)$	$(1, -4, 4, 0)$	4
$(0, -2, 0)$	$(1, 2, 0, -2)$	2	$(0, 4, 0)$	$(1, -4, 0, 4)$	4
$(0, 2, 0)$	$(1, -2, 0, 2)$	2	$(0, 0, 4)$	$(-3, 4, -4, 4)$	4
$(0, 0, 2)$	$(-1, 2, -2, 2)$	2	$(2, 0, -4)$	$(3, -4, 6, -4)$	5
$(2, 0, -2)$	$(1, -2, 4, -2)$	3	$(0, -4, 2)$	$(-1, 6, -2, -2)$	5
$(0, -2, 2)$	$(-1, 4, -2, 0)$	3	$(2, -4, 0)$	$(-1, 4, 2, -4)$	5
$(2, -2, 0)$	$(-1, 2, 2, -2)$	3	$(4, -2, -2)$	$(-1, 0, 6, -4)$	5
$(0, 2, 2)$	$(-1, 0, -2, 4)$	3	$(4, 0, -2)$	$(-1, -2, 6, -2)$	5
$(2, 2, 0)$	$(-1, -2, 2, 2)$	3	$(0, 4, 2)$	$(-1, -2, -2, 6)$	5
$(2, -2, 2)$	$(-3, 4, 0, 0)$	3	$(4, 2, -2)$	$(-1, -4, 6, 0)$	5
$(2, 0, 2)$	$(-3, 2, 0, 2)$	3	$(2, 4, 0)$	$(-1, -4, 2, 4)$	5
$(4, 0, 0)$	$(-3, 0, 4, 0)$	3	$(2, -4, 2)$	$(-3, 6, 0, -2)$	5
$(2, 2, 2)$	$(-3, 0, 0, 4)$	3	$(0, -2, 4)$	$(-3, 6, -4, 2)$	5
$(-2, -2, -2)$	$(5, 0, 0, -4)$	4	$(4, -2, 0)$	$(-3, 2, 4, -2)$	5
$(-4, 0, 0)$	$(5, 0, -4, 0)$	4	$(0, 2, 4)$	$(-3, 2, -4, 6)$	5
$(-2, 0, -2)$	$(5, -2, 0, -2)$	4	$(4, 2, 0)$	$(-3, -2, 4, 2)$	5
$(0, 0, -4)$	$(5, -4, 4, -4)$	4	$(2, 4, 2)$	$(-3, -2, 0, 6)$	5
$(-2, 2, -2)$	$(5, -4, 0, 0)$	4	$(2, -2, 4)$	$(-5, 6, -2, 2)$	5
$(-2, -2, 0)$	$(3, 2, -2, -2)$	4	$(4, -2, 2)$	$(-5, 4, 2, 0)$	5
$(0, -2, -2)$	$(3, 0, 2, -4)$	4	$(2, 0, 4)$	$(-5, 4, -2, 4)$	5
$(-2, 2, 0)$	$(3, -2, -2, 2)$	4	$(4, 0, 2)$	$(-5, 2, 2, 2)$	5
$(0, 2, -2)$	$(3, -4, 2, 0)$	4	$(2, 2, 4)$	$(-5, 2, -2, 6)$	5
$(0, -4, 0)$	$(1, 4, 0, -4)$	4	$(6, 0, 0)$	$(-5, 0, 6, 0)$	5
$(-2, -2, 2)$	$(1, 4, -4, 0)$	4	$(4, 2, 2)$	$(-5, 0, 2, 4)$	5

Table 3.3: The sample points used by the rules (C.1)-(C.34) for the B-coefficients of Q_I , for a tetrahedron $T \in \mathcal{K}_1$. The left column shows the local coordinates of a sample point x relative to T , the middle column shows the barycentric coordinates of x , and the right column shows the minimal number ℓ such that $x \in \text{star}^\ell(T)$.

(i, j, k)	bary. coords.	star	(i, j, k)	bary. coords.	star
$(0, 0, -1)$	$(2, -1, 1, -1)$	1	$(2, 0, 3)$	$(-4, 3, -1, 3)$	4
$(0, 0, 1)$	$(0, 1, -1, 1)$	1	$(4, 0, 1)$	$(-4, 1, 3, 1)$	4
$(0, -2, 1)$	$(0, 3, -1, -1)$	2	$(2, 2, 3)$	$(-4, 1, -1, 5)$	4
$(2, 0, -1)$	$(0, -1, 3, -1)$	2	$(-2, -2, -3)$	$(6, -1, 1, -5)$	5
$(0, 2, 1)$	$(0, -1, -1, 3)$	2	$(-4, 0, -1)$	$(6, -1, -3, -1)$	5
$(2, 0, 1)$	$(-2, 1, 1, 1)$	2	$(-2, 0, -3)$	$(6, -3, 1, -3)$	5
$(-2, 0, -1)$	$(4, -1, -1, -1)$	3	$(0, 0, -5)$	$(6, -5, 5, -5)$	5
$(0, 0, -3)$	$(4, -3, 3, -3)$	3	$(-2, 2, -3)$	$(6, -5, 1, -1)$	5
$(0, -2, -1)$	$(2, 1, 1, -3)$	3	$(-4, 0, 1)$	$(4, 1, -5, 1)$	5
$(-2, 0, 1)$	$(2, 1, -3, 1)$	3	$(0, -2, -3)$	$(4, -1, 3, -5)$	5
$(0, 2, -1)$	$(2, -3, 1, 1)$	3	$(0, 2, -3)$	$(4, -5, 3, -1)$	5
$(2, -2, -1)$	$(0, 1, 3, -3)$	3	$(0, -4, -1)$	$(2, 3, 1, -5)$	5
$(2, 2, -1)$	$(0, -3, 3, 1)$	3	$(2, -2, -3)$	$(2, -1, 5, -5)$	5
$(2, -2, 1)$	$(-2, 3, 1, -1)$	3	$(2, 2, -3)$	$(2, -5, 5, -1)$	5
$(0, 0, 3)$	$(-2, 3, -3, 3)$	3	$(0, 4, -1)$	$(2, -5, 1, 3)$	5
$(2, 2, 1)$	$(-2, -1, 1, 3)$	3	$(-2, -2, 3)$	$(0, 5, -5, 1)$	5
$(-2, -2, -1)$	$(4, 1, -1, -3)$	4	$(2, -4, -1)$	$(0, 3, 3, -5)$	5
$(-2, 2, -1)$	$(4, -3, -1, 1)$	4	$(-2, 0, 3)$	$(0, 3, -5, 3)$	5
$(-2, -2, 1)$	$(2, 3, -3, -1)$	4	$(-2, 2, 3)$	$(0, 1, -5, 5)$	5
$(-2, 2, 1)$	$(2, -1, -3, 3)$	4	$(2, 4, -1)$	$(0, -5, 3, 3)$	5
$(2, 0, -3)$	$(2, -3, 5, -3)$	4	$(2, -4, 1)$	$(-2, 5, 1, -3)$	5
$(0, -4, 1)$	$(0, 5, -1, -3)$	4	$(4, -2, -1)$	$(-2, 1, 5, -3)$	5
$(0, 4, 1)$	$(0, -3, -1, 5)$	4	$(4, 2, -1)$	$(-2, -3, 5, 1)$	5
$(0, -2, 3)$	$(-2, 5, -3, 1)$	4	$(2, 4, 1)$	$(-2, -3, 1, 5)$	5
$(0, 2, 3)$	$(-2, 1, -3, 5)$	4	$(0, 0, 5)$	$(-4, 5, -5, 5)$	5
$(4, 0, -1)$	$(-2, -1, 5, -1)$	4	$(4, -2, 1)$	$(-4, 3, 3, -1)$	5
$(2, -2, 3)$	$(-4, 5, -1, 1)$	4	$(4, 2, 1)$	$(-4, -1, 3, 3)$	5

Table 3.4: The sample points used by the rules (C.35)-(C.68) for the B-coefficients of Q_I , for a tetrahedron $T \in \mathcal{K}_2$. The left column shows the local coordinates of a sample point x relative to T , the middle column shows the barycentric coordinates of x , and the right column shows the minimal number ℓ such that $x \in \text{star}^\ell(T)$.

(i, j, k)	bary. coords.	star	(i, j, k)	bary. coords.	star
$(0, -1, 0)$	$(1, 1, 0, -1)$	1	$(4, -1, 0)$	$(-3, 1, 4, -1)$	4
$(0, 1, 0)$	$(1, -1, 0, 1)$	1	$(4, 1, 0)$	$(-3, -1, 4, 1)$	4
$(0, -1, 2)$	$(-1, 3, -2, 1)$	2	$(2, 3, 2)$	$(-3, -1, 0, 5)$	4
$(2, -1, 0)$	$(-1, 1, 2, -1)$	2	$(-2, -3, -2)$	$(5, 1, 0, -5)$	5
$(0, 1, 2)$	$(-1, 1, -2, 3)$	2	$(-4, -1, 0)$	$(5, 1, -4, -1)$	5
$(2, 1, 0)$	$(-1, -1, 2, 1)$	2	$(-4, 1, 0)$	$(5, -1, -4, 1)$	5
$(-2, -1, 0)$	$(3, 1, -2, -1)$	3	$(0, -1, -4)$	$(5, -3, 4, -5)$	5
$(0, -1, -2)$	$(3, -1, 2, -3)$	3	$(0, 1, -4)$	$(5, -5, 4, -3)$	5
$(-2, 1, 0)$	$(3, -1, -2, 1)$	3	$(-2, 3, -2)$	$(5, -5, 0, 1)$	5
$(0, 1, -2)$	$(3, -3, 2, -1)$	3	$(-2, -3, 0)$	$(3, 3, -2, -3)$	5
$(0, -3, 0)$	$(1, 3, 0, -3)$	3	$(0, -3, -2)$	$(3, 1, 2, -5)$	5
$(2, -1, -2)$	$(1, -1, 4, -3)$	3	$(2, -1, -4)$	$(3, -3, 6, -5)$	5
$(2, 1, -2)$	$(1, -3, 4, -1)$	3	$(-2, 3, 0)$	$(3, -3, -2, 3)$	5
$(0, 3, 0)$	$(1, -3, 0, 3)$	3	$(2, 1, -4)$	$(3, -5, 6, -3)$	5
$(2, -1, 2)$	$(-3, 3, 0, 1)$	3	$(0, 3, -2)$	$(3, -5, 2, 1)$	5
$(2, 1, 2)$	$(-3, 1, 0, 3)$	3	$(0, -5, 0)$	$(1, 5, 0, -5)$	5
$(-2, -1, -2)$	$(5, -1, 0, -3)$	4	$(-2, -3, 2)$	$(1, 5, -4, -1)$	5
$(-2, 1, -2)$	$(5, -3, 0, -1)$	4	$(2, -3, -2)$	$(1, 1, 4, -5)$	5
$(-2, -1, 2)$	$(1, 3, -4, 1)$	4	$(-2, 3, 2)$	$(1, -1, -4, 5)$	5
$(-2, 1, 2)$	$(1, 1, -4, 3)$	4	$(2, 3, -2)$	$(1, -5, 4, 1)$	5
$(0, -3, 2)$	$(-1, 5, -2, -1)$	4	$(0, 5, 0)$	$(1, -5, 0, 5)$	5
$(2, -3, 0)$	$(-1, 3, 2, -3)$	4	$(4, -1, -2)$	$(-1, -1, 6, -3)$	5
$(0, 3, 2)$	$(-1, -1, -2, 5)$	4	$(4, 1, -2)$	$(-1, -3, 6, -1)$	5
$(2, 3, 0)$	$(-1, -3, 2, 3)$	4	$(2, -1, 4)$	$(-5, 5, -2, 3)$	5
$(2, -3, 2)$	$(-3, 5, 0, -1)$	4	$(4, -1, 2)$	$(-5, 3, 2, 1)$	5
$(0, -1, 4)$	$(-3, 5, -4, 3)$	4	$(2, 1, 4)$	$(-5, 3, -2, 5)$	5
$(0, 1, 4)$	$(-3, 3, -4, 5)$	4	$(4, 1, 2)$	$(-5, 1, 2, 3)$	5

Table 3.5: The sample points used by the rules (C.69)-(C.102) for the B-coefficients of Q_I , for a tetrahedron $T \in \mathcal{K}_3$. The left column shows the local coordinates of a sample point x relative to T , the middle column shows the barycentric coordinates of x , and the right column shows the minimal number ℓ such that $x \in \text{star}^\ell(T)$.

(i, j, k)	bary. coords.	star	(i, j, k)	bary. coords.	star
(0, -1, 1)	(0, 2, -1, 0)	1	(2, 3, 1)	(-2, -2, 1, 4)	4
(0, 1, 1)	(0, 0, -1, 2)	1	(2, -1, 3)	(-4, 4, -1, 2)	4
(0, -1, -1)	(2, 0, 1, -2)	2	(4, -1, 1)	(-4, 2, 3, 0)	4
(0, 1, -1)	(2, -2, 1, 0)	2	(2, 1, 3)	(-4, 2, -1, 4)	4
(2, -1, -1)	(0, 0, 3, -2)	2	(4, 1, 1)	(-4, 0, 3, 2)	4
(2, 1, -1)	(0, -2, 3, 0)	2	(-4, -1, -1)	(6, 0, -3, -2)	5
(2, -1, 1)	(-2, 2, 1, 0)	2	(-2, -1, -3)	(6, -2, 1, -4)	5
(2, 1, 1)	(-2, 0, 1, 2)	2	(-4, 1, -1)	(6, -2, -3, 0)	5
(-2, -1, -1)	(4, 0, -1, -2)	3	(-2, 1, -3)	(6, -4, 1, -2)	5
(-2, 1, -1)	(4, -2, -1, 0)	3	(-2, -3, -1)	(4, 2, -1, -4)	5
(-2, -1, 1)	(2, 2, -3, 0)	3	(-4, -1, 1)	(4, 2, -5, 0)	5
(-2, 1, 1)	(2, 0, -3, 2)	3	(-4, 1, 1)	(4, 0, -5, 2)	5
(0, -3, 1)	(0, 4, -1, -2)	3	(-2, 3, -1)	(4, -4, -1, 2)	5
(0, 3, 1)	(0, -2, -1, 4)	3	(-2, -3, 1)	(2, 4, -3, -2)	5
(0, -1, 3)	(-2, 4, -3, 2)	3	(-2, 3, 1)	(2, -2, -3, 4)	5
(0, 1, 3)	(-2, 2, -3, 4)	3	(0, -5, 1)	(0, 6, -1, -4)	5
(0, -1, -3)	(4, -2, 3, -4)	4	(-2, -3, 3)	(0, 6, -5, 0)	5
(0, 1, -3)	(4, -4, 3, -2)	4	(-2, -1, 3)	(0, 4, -5, 2)	5
(0, -3, -1)	(2, 2, 1, -4)	4	(-2, 1, 3)	(0, 2, -5, 4)	5
(2, -1, -3)	(2, -2, 5, -4)	4	(-2, 3, 3)	(0, 0, -5, 6)	5
(2, 1, -3)	(2, -4, 5, -2)	4	(0, 5, 1)	(0, -4, -1, 6)	5
(0, 3, -1)	(2, -4, 1, 2)	4	(0, -3, 3)	(-2, 6, -3, 0)	5
(2, -3, -1)	(0, 2, 3, -4)	4	(0, 3, 3)	(-2, 0, -3, 6)	5
(2, 3, -1)	(0, -4, 3, 2)	4	(2, -3, 3)	(-4, 6, -1, 0)	5
(2, -3, 1)	(-2, 4, 1, -2)	4	(0, -1, 5)	(-4, 6, -5, 4)	5
(4, -1, -1)	(-2, 0, 5, -2)	4	(0, 1, 5)	(-4, 4, -5, 6)	5
(4, 1, -1)	(-2, -2, 5, 0)	4	(2, 3, 3)	(-4, 0, -1, 6)	5

Table 3.6: The sample points used by the rules (C.103)-(C.136) for the B-coefficients of Q_I , for a tetrahedron $T \in \mathcal{K}_4$. The left column shows the local coordinates of a sample point x relative to T , the middle column shows the barycentric coordinates of x , and the right column shows the minimal number ℓ such that $x \in \text{star}^\ell(T)$.

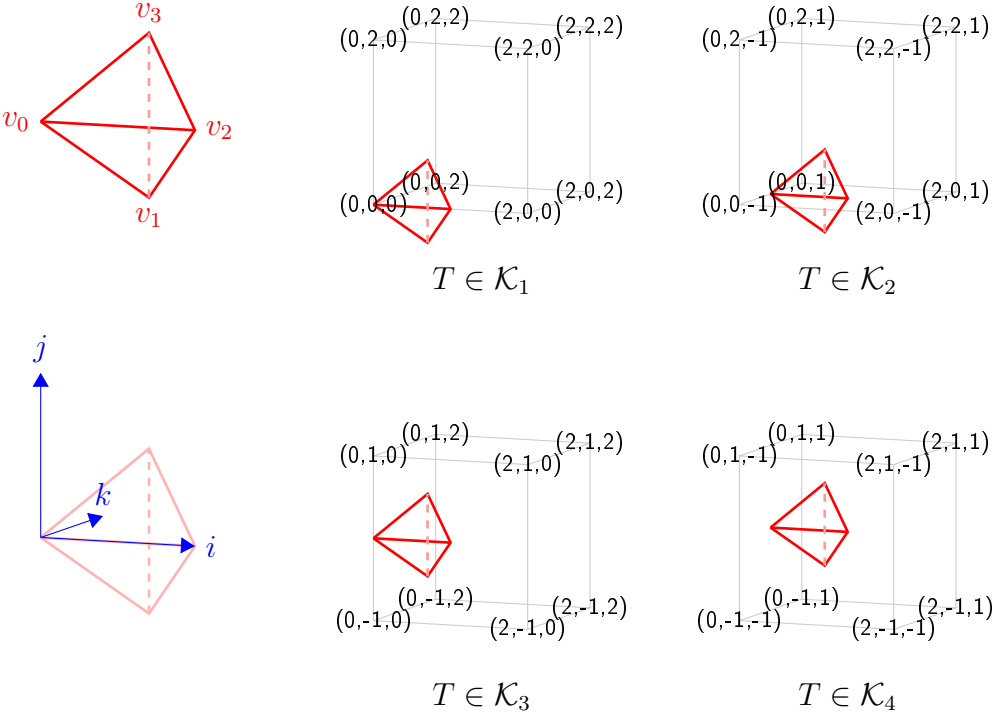


Figure 3.19: The four different cases of a tetrahedron T and an associated cuboid C_T as defined in the proof of theorem 3.34. In the upper left corner, the vertex arrangement of the tetrahedra is shown. The local coordinate system relative to the tetrahedra is shown in the lower left corner. The coordinates of the cuboid corners are given in the local coordinate system.

Proof. Let $x \in \mathcal{X} \cap \Omega_1$ and $T := \langle v_0, v_1, v_2, v_3 \rangle$ be a tetrahedron containing x . Definition 3.27 assures the existence of such a tetrahedron. By 3.31, T must be in class \mathcal{K}_1 , with $x = v_0$. Let $f \in \mathcal{F}_{\mathcal{X}}$ and c_{ijkl} be the B-coefficients of $Q_I(f)|_T$. According to the B-coefficient computation rule (C.1)

$$c_{5000} = f_{1,0,0,0} = f(v_0) = f(x).$$

Using corollary 2.48, we obtain

$$Q_I(f)(x) = Q_I(f)|_T(x) = c_{5000} = f(x).$$

□

We give a result about the locality of the operator. To account for the fact that Q_I uses sample values outside of Δ_2 , we measure the locality in terms of stars of the underlying BCC partition of which Δ_2 is a subset.

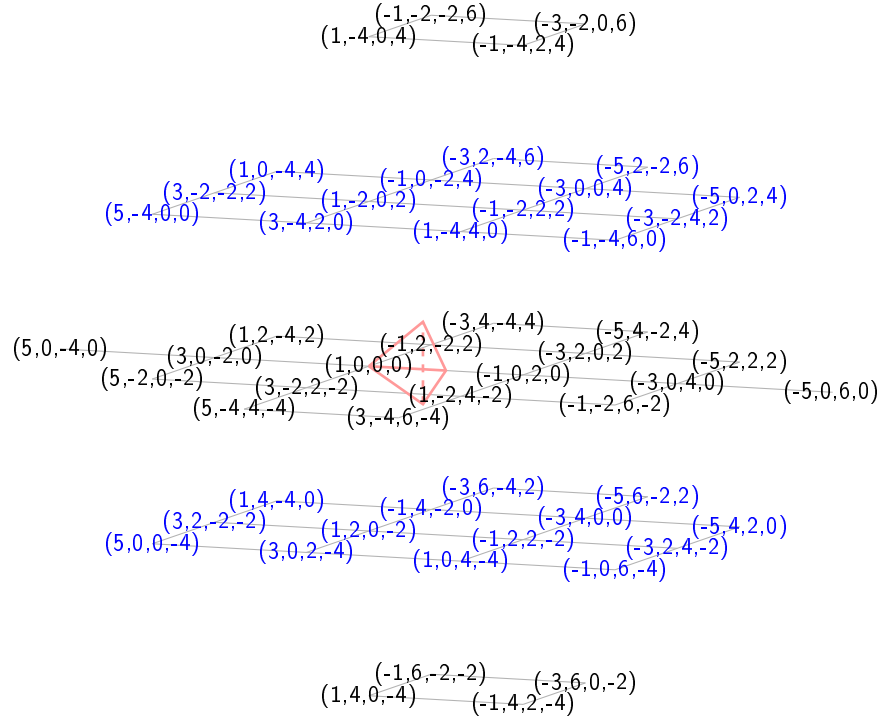


Figure 3.20: Support of the rules (C.1)-(C.34) for the B-coefficients of Q_I , for a tetrahedron $T \in \mathcal{K}_1$. The barycentric coordinates relative to T of each sample point are shown at the grid points.

Theorem 3.36. *The operator Q_I is 5-local in the following sense. For each $T \in \Delta_2$, let \tilde{T} be the analogous tetrahedron in Δ_{BCC} . Then*

$$\mathcal{X}_T \subset \text{star}^5(\tilde{T}).$$

Proof. We use the same technique as in the proof of theorem 3.19. The tables 3.3-3.6 provide a list of the local coordinates of the sample points for each of the four classes of tetrahedra. Using these local coordinates in conjunction with corollary 2.25, we calculate the star for each sample point. The numbers are given in the right column of the tables. All sample points are contained at most in $\text{star}^5(T)$. \square

We provide an estimate for the maximum norm of $Q_I(f)$ on a tetrahedron.

Theorem 3.37. *Let $T \in \Delta_2$ and $f \in \mathcal{F}_{\mathcal{X}}$. Then*

$$\|Q_I(f)\|_T \leq \frac{12703}{6912} \max_{x \in \mathcal{X}_T} |f(x)|.$$

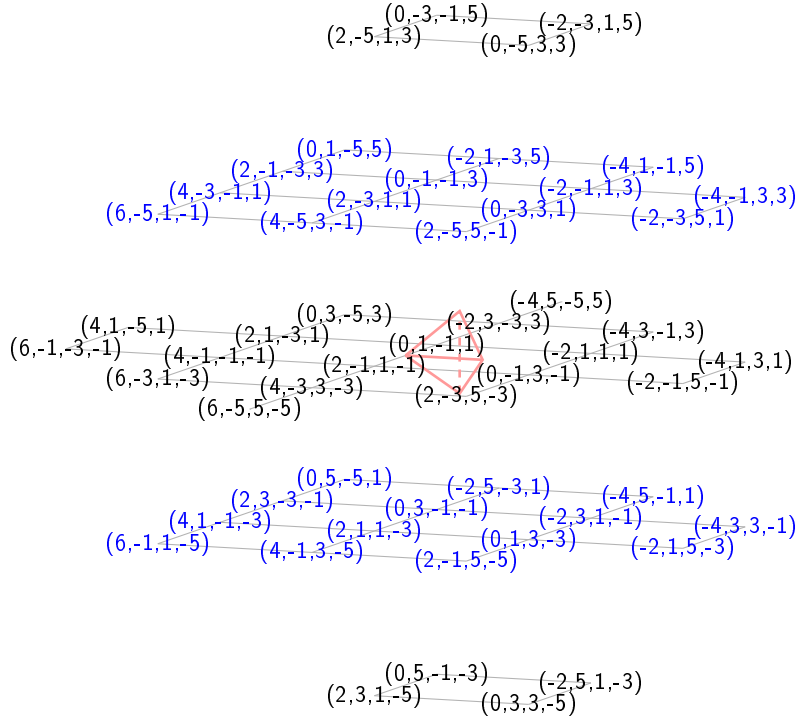


Figure 3.21: Support of the rules (C.35)-(C.68) for the B-coefficients of Q_I , for a tetrahedron $T \in \mathcal{K}_2$. The barycentric coordinates relative to T of each sample point are shown at the grid points.

Proof. Suppose \mathcal{K}_m is the class which T belongs to. We consider the B-coefficient computation rules associated with that class. Let $\eta \in \mathcal{D}_5(T)$ and

$$c_\eta = \sum_{x \in \mathcal{X}_\eta} w_{\eta,x} f(x)$$

be the rule for c_η . Analogously to the proof of theorem 3.25 we estimate

$$|c_\eta| \leq \max_{x \in \mathcal{X}_T} |f(x)| \sum_{x \in \mathcal{X}_\eta} |w_{\eta,x}|.$$

We then calculate

$$\hat{w}_T := \max_{\eta \in \mathcal{D}_5(T)} \sum_{x \in \mathcal{X}_\eta} |w_{\eta,x}|,$$

using the rules (C.1)-(C.136), and obtain

$$\hat{w}_T = \begin{cases} \frac{3175}{1728}, & T \in \mathcal{K}_1, \\ \frac{12703}{6912}, & T \in \mathcal{K}_2, \\ \frac{12703}{6912}, & T \in \mathcal{K}_3, \\ \frac{7}{4}, & T \in \mathcal{K}_4. \end{cases}$$

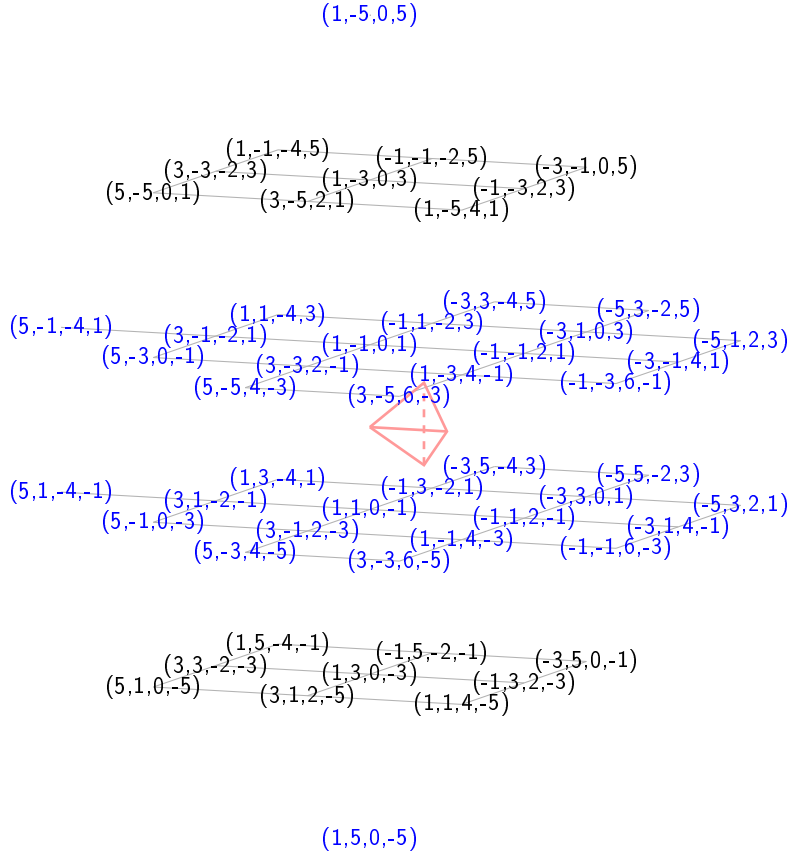


Figure 3.22: Support of the rules (C.69)-(C.102) for the B-coefficients of Q_I , for a tetrahedron $T \in \mathcal{K}_3$. The barycentric coordinates relative to T of each sample point are shown at the grid points.

Therefore,

$$\hat{w}_T \leq \frac{12703}{6912} \quad \text{and} \quad |c_\eta| \leq \frac{12703}{6912} \max_{x \in \mathcal{X}_T} |f(x)|.$$

Thus, Q_I is stable and it follows from theorem 2.42 that

$$\|Q_I(f)\|_T \leq \max_{\eta \in \mathcal{D}_5(T)} |c_\eta| \leq \frac{12703}{6912} \max_{x \in \mathcal{X}_T} |f(x)|.$$

□

The next theorem shows that the operator reproduces polynomials up to degree three.

Theorem 3.38. *The operator Q_I reproduces polynomials up to degree 3. For all $p \in \mathcal{P}_3$,*

$$Q_I(p) \equiv p.$$

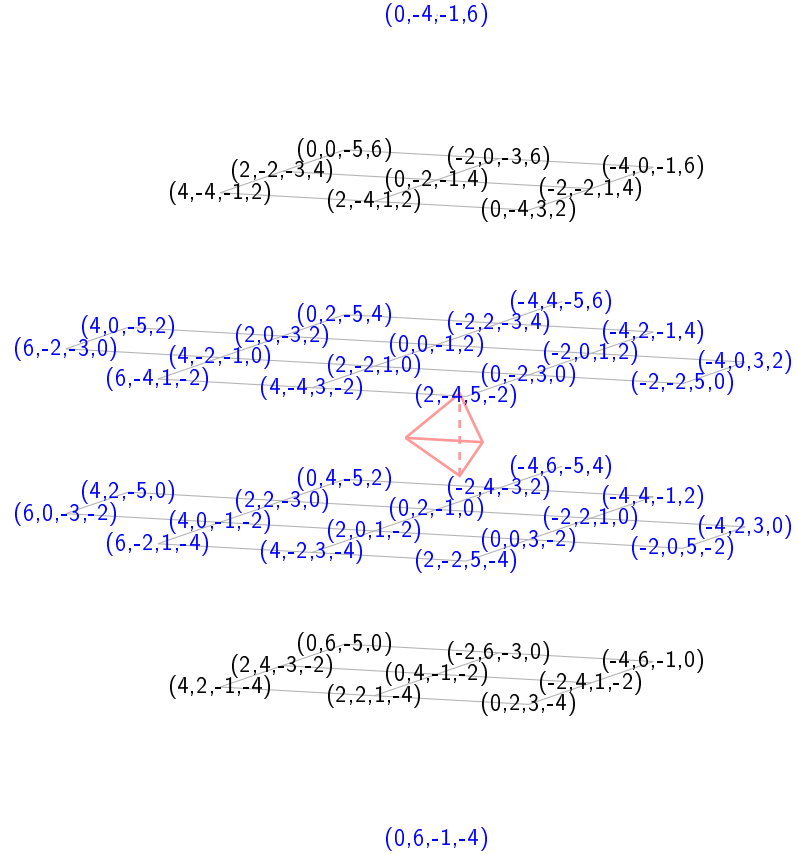


Figure 3.23: Support of the rules (C.103)-(C.136) for the B-coefficients of Q_I , for a tetrahedron $T \in \mathcal{K}_4$. The barycentric coordinates relative to T of each sample point are shown at the grid points.

Proof. This proof is essentially analogous to the proof of theorem 3.26. Due to the linearity of Q_I it suffices to show that the Bernstein basis relative to a tetrahedron $T \in \Delta_2$ is reproduced. The symmetry of the Bernstein basis polynomials and the rules simplifies the proof further. We show that the basis polynomials $B_{3000}, B_{2100}, B_{2010}, B_{1200}, B_{1110}, B_{1101}, B_{1021}, B_{0300}, B_{0210}, B_{0201}, B_{0120}$ and B_{0030} are reproduced. The reproduction of the remaining Bernstein basis polynomials follows then from the fact that the rules for c_{ijkl} and c_{ilkj} are $(1,3)$ -symmetric to each other, using lemmas 2.35 (iv) and 3.8. To verify that a Bernstein basis polynomial B_{ijkl} is reproduced, we first calculate its representation as a polynomial of degree five, using lemma 2.41 twice. Then the B-coefficients of $Q_I(B_{ijkl})$ are calculated using the rules for the operator. These calculations are performed for each of the four sets of rules. The resulting B-coefficients are compared to the B-coefficients which were obtained by raising the degree of the basis polynomial. We wrote a

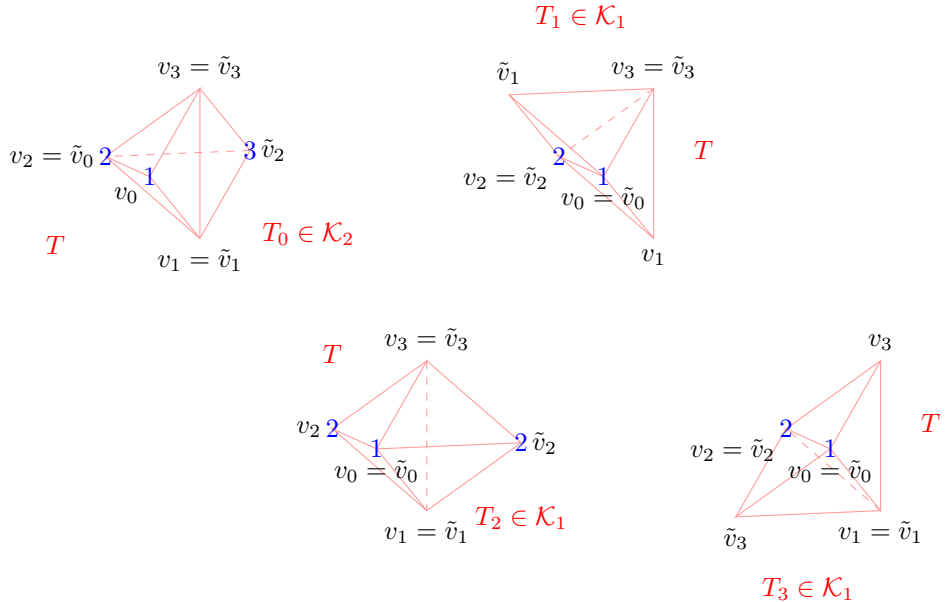


Figure 3.24: The relationship between the vertices v_0, \dots, v_3 of $T \in \mathcal{K}_1$ and the vertices $\tilde{v}_0, \dots, \tilde{v}_3$ of the neighbors of T . The blue numbers represent the vertex classes. The vertices without numbers belong to class \mathcal{V}_5 .

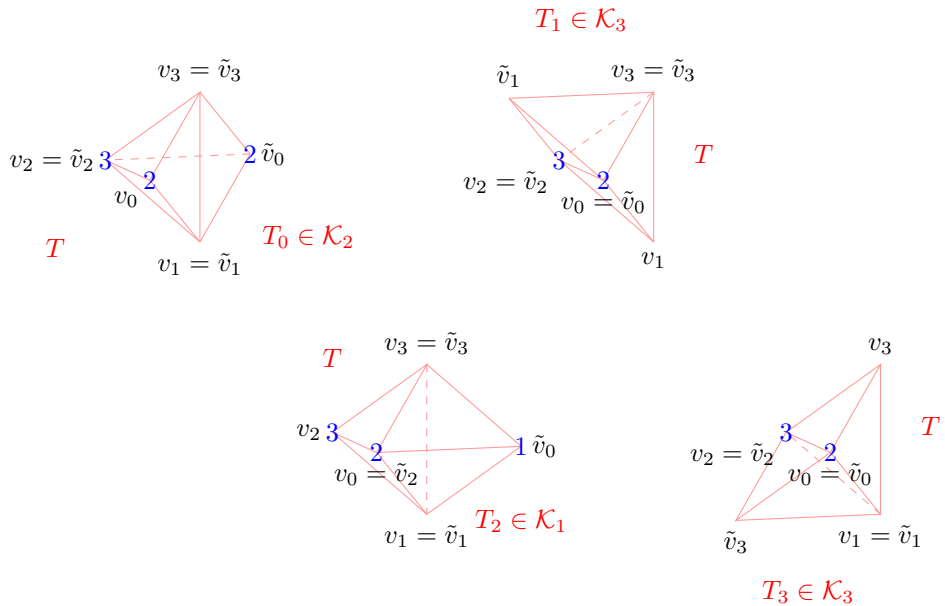


Figure 3.25: The relationship between the vertices v_0, \dots, v_3 of $T \in \mathcal{K}_2$ and the vertices $\tilde{v}_0, \dots, \tilde{v}_3$ of the neighbors of T . The blue numbers represent the vertex classes. The vertices without numbers belong to class \mathcal{V}_5 .

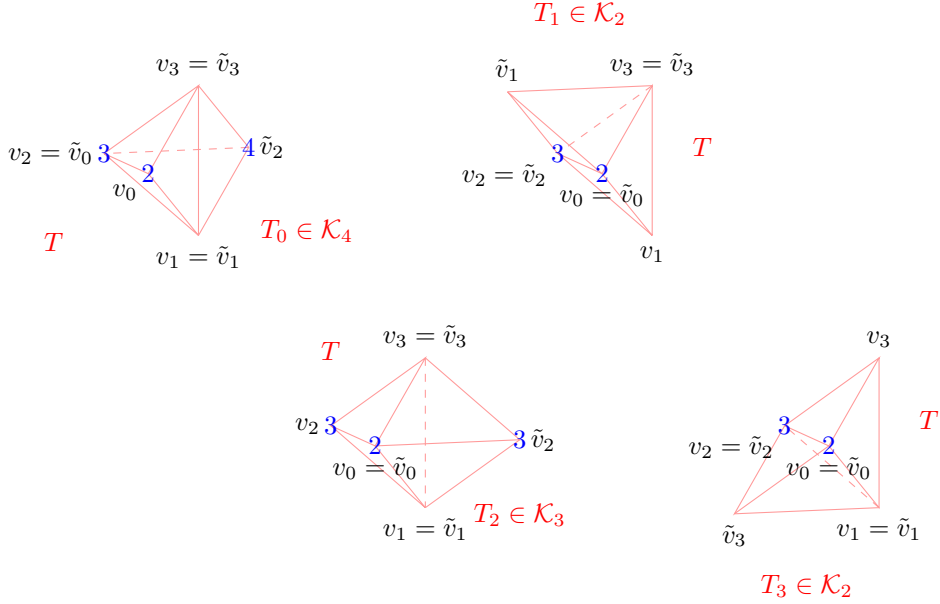


Figure 3.26: The relationship between the vertices v_0, \dots, v_3 of $T \in \mathcal{K}_3$ and the vertices $\tilde{v}_0, \dots, \tilde{v}_3$ of the neighbors of T . The blue numbers represent the vertex classes. The vertices without numbers belong to class \mathcal{V}_5 .

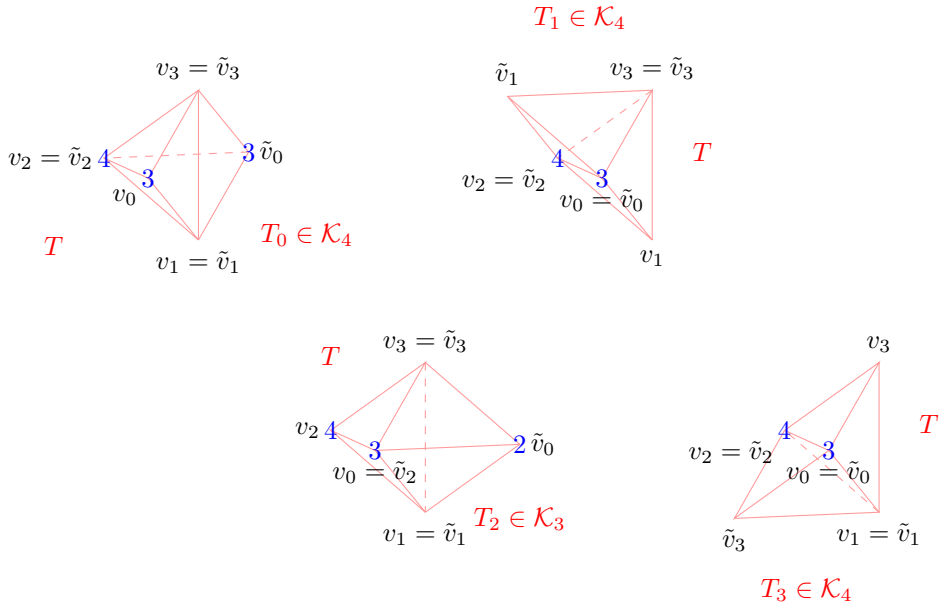


Figure 3.27: The relationship between the vertices v_0, \dots, v_3 of $T \in \mathcal{K}_4$ and the vertices $\tilde{v}_0, \dots, \tilde{v}_3$ of the neighbors of T . The blue numbers represent the vertex classes. The vertices without numbers belong to class \mathcal{V}_5 .

computer program to perform all necessary calculations. This program is described in detail in appendix D. The output of the program verifies the reproduction of cubic polynomials. \square

3.4 Error bounds for the quasi-interpolation operators

In this section, we provide estimates for the approximation error of the quasi-interpolation operators developed in this chapter. For each operator, there is a local result that gives a bound for the error on a single tetrahedron, and a global result for the error on the unit cube.

Theorem 3.39. *Let Q_{conv} be the operator defined in 3.17, and \mathcal{X} the sample set associated with this operator. Let Δ_1 be the tetrahedral partition defined in 3.14 with spacing H and associated with \mathcal{X} . Fix $T \in \Delta_1$ and let*

$$\Omega_T := \bigcup_{\hat{T} \in \text{star}^2(\tilde{T})} \hat{T},$$

where \tilde{T} is the tetrahedron in Δ_{BCC} with $T = \tilde{T}$. Then for every $f \in C^m(\Omega_T)$ with $0 \leq m \leq 1$,

$$\|D^\alpha(Q_{conv}(f) - f)\|_T \leq K|T|^{m+1-|\alpha|}|f|_{m+1,\Omega_T}, \quad 0 \leq |\alpha| \leq m, \quad (3.10)$$

where K is a constant depending only on the shape parameter K_H from lemma 2.23 and the Lipschitz constant of Ω_T .

Proof. Let p_f be the Taylor polynomial of degree m associated with f . Then by theorem 2.29 and the Stein extension theorem (see [84], p.181), there exists a constant $\tilde{K}_m > 0$, depending only on m and the Lipschitz constant of the boundary of Ω_T , such that

$$\|D^\beta(f - p_f)\|_{\Omega_T} \leq \tilde{K}_m |\Omega_T|^{m+1-|\beta|} |f|_{m+1,\Omega_T}, \quad 0 \leq \beta \leq m.$$

Let $K_0 := \max\{\tilde{K}_0, \tilde{K}_1\}$. By lemmas 2.10 and 2.23 (i), $|\Omega_T| \leq 6|\Delta_1| \leq 6|T|/K_H$, and since $K_H \leq 1$,

$$\|D^\beta(f - p_f)\|_{\Omega_T} \leq K_1 |T|^{m+1-|\beta|} |f|_{m+1,\Omega_T}, \quad 0 \leq \beta \leq m, \quad (3.11)$$

with $K_1 := 36K_0/K_H^2$. We use the triangle inequality and the linearity of the differential operator, obtaining

$$\begin{aligned} \|D^\alpha(Q_{conv}(f) - f)\|_T &\leq \|D^\alpha(Q_{conv}(f) - p_f + p_f - f)\|_T \\ &\leq \|D^\alpha(Q_{conv}(f) - p_f)\|_T + \|D^\alpha(p_f - f)\|_T. \end{aligned} \quad (3.12)$$

Since $T \subset \Omega_T$, we estimate the second term with (3.11). To further estimate the first term, we use the linearity of Q_{conv} and the reproduction of linear polynomials from theorem 3.21, resulting in

$$\|D^\alpha(Q_{conv}(f) - p_f)\|_T \leq \|D^\alpha(Q_{conv}(f - p_f))\|_T.$$

But then, since $Q_{conv}(f - p_f)|_T$ is a polynomial, we can use the Markov inequality (2.1) to obtain

$$\|D^\alpha(Q_{conv}(f - p_f))\|_T \leq \frac{K_2}{\rho_T^{|\alpha|}} \|Q_{conv}(f - p_f)\|_T,$$

where K_2 is the constant from theorem 2.28. Since this constant depends only on the degree of the polynomial, which is 5 in this case, it is an absolute constant. By lemma 2.23 (ii), there exists a constant $K_3 < 1$, depending only on K_H , such that $\rho_T \geq K_3|T|$. Since $0 \leq |\alpha| \leq 1$,

$$\frac{K_2}{\rho_T^{|\alpha|}} \|Q_{conv}(f - p_f)\|_T \leq \frac{K_2}{K_3|T|^{|\alpha|}} \|Q_{conv}(f - p_f)\|_T.$$

By theorem 3.20, we have

$$\|(Q_{conv}(f - p_f))\|_T \leq \max_{x \in \mathcal{X}_T} |f(x) - p_f(x)|.$$

By theorem 3.19, $\mathcal{X}_T \subset \Omega_T$, and it follows that

$$\max_{x \in \mathcal{X}_T} |f(x) - p_f(x)| \leq \|f - p_f\|_{\Omega_T}.$$

We use (3.11) with $|\beta| = 0$ and combine the results, which yields

$$\|D^\alpha(Q_{conv}(f - p_f))\|_T \leq \frac{K_1 K_2}{K_3} |T|^{m+1-|\alpha|} |f|_{m+1, \Omega_T}.$$

We estimate (3.12) using the inequality above and (3.11), which concludes the proof. \square

The global version of the previous theorem follows almost immediately.

Theorem 3.40. *Let Q_{conv} be the operator defined in 3.17, and Δ_1 the tetrahedral partition associated with this operator. Let Ω_T be defined as in theorem 3.39,*

$$\Omega := \bigcup_{T \in \Delta_1} \Omega_T,$$

and $\Omega_1 := [0, 1]^3$ the unit cube. Suppose $f \in C^{m+1}(\Omega)$ for some $0 \leq m \leq 1$, then

$$\|D^\alpha(Q_{conv}(f) - f)\|_{\Omega_1} \leq K |\Delta_1|^{m+1-|\alpha|} |f|_{m+1, \Omega}, \quad 0 \leq |\alpha| \leq 1,$$

where K is a constant depending only on shape parameter K_H defined in lemma 2.23, and the Lipschitz constant of the boundary of Ω .

Proof. By definition 3.14, $\Omega_1 \subset \Delta_1$. It follows from theorem 3.39 that there exists a constant K such that

$$\|D^\alpha(Q_{conv}(f) - f)\|_{\Omega_1} \leq \max_{T \in \Delta_1} \|D^\alpha(Q_{conv}(f) - f)\|_T \leq \max_{T \in \Delta_1} K|T|^{m+1-|\alpha|}|f|_{m+1,\Omega_T}.$$

Since $|T| \leq |\Delta_1|$,

$$\begin{aligned} \max_{T \in \Delta_1} K|T|^{m+1-|\alpha|}|f|_{m+1,\Omega_T} &\leq \max_{T \in \Delta_1} K|\Delta_1|^{m+1-|\alpha|}|f|_{m+1,\Omega_T} \\ &= K|\Delta_1|^{m+1-|\alpha|} \max_{T \in \Delta_1} |f|_{m+1,\Omega_T}. \end{aligned}$$

This concludes the proof since $\Omega_T \subset \Omega$. \square

The results for the other operators are quite similar. The reproduction of cubic polynomials is responsible for the better approximation order. We give a local estimate for the approximation error of Q_{opt} in the following theorem.

Theorem 3.41. *Let Q_{opt} be the quasi-interpolation operator for $(\mathcal{X}, \mathcal{S}_5^2(\Delta_1))$ defined in 3.22. For each $T \in \Delta_1$, let \tilde{T} be the corresponding tetrahedron in Δ_{BCC} , and*

$$\Omega_T := \bigcup_{\hat{T} \in \text{star}^3(\tilde{T})} \hat{T}.$$

Fix $T \in \Delta_1$. Then for each $f \in C^{m+1}(\Omega_T)$ with $0 \leq m \leq 3$,

$$\|D^\alpha(Q_{opt}(f) - f)\|_T \leq K|T|^{m+1-|\alpha|}|f|_{m+1,\Omega_T}, \quad 0 \leq |\alpha| \leq m, \quad (3.13)$$

where K is a constant depending only on the shape parameter K_H of Δ_{BCC} and the Lipschitz constant of the boundary of Ω_T .

Proof. The proof is analogous to the proof of theorem 3.39. By theorem 2.29 and the Stein extension theorem (see [84], p.181), there exists a polynomial p_f of degree m and a constant \tilde{K}_m such that

$$\|D^\beta(f - p_f)\|_{\Omega_T} \leq \tilde{K}_m|\Omega_T|^{m+1-|\beta|}|f|_{m+1,\Omega_T}, \quad 0 \leq |\beta| \leq m,$$

where \tilde{K}_m depends on the degree of p_f and the Lipschitz constant of the boundary of Ω_T . Let $K_0 := \max_{m=0}^3 \tilde{K}_m$. It follows from lemmas 2.10 and 2.23 (i) that $|\Omega_T| \leq 8|T|/K_H$. Using the fact that $K_H \leq 1$, we estimate

$$\|D^\beta(f - p_f)\|_{\Omega_T} \leq K_1|T|^{m+1-|\beta|}|f|_{m+1,\Omega_T}, \quad 0 \leq |\beta| \leq m, \quad (3.14)$$

with $K_1 := 8^4 K_0 / K_H^4$. By the triangle inequality and the linearity of the differential operator,

$$\|D^\alpha(Q_{opt}(f) - f)\|_T \leq \|D^\alpha(Q_{opt}(f) - p_f)\|_T + \|D^\alpha(p_f - f)\|_T. \quad (3.15)$$

Since Q_{opt} is linear and, by theorem 3.26, reproduces cubic polynomials,

$$\|D^\alpha(Q_{opt}(f) - p_f)\|_T \leq \|D^\alpha(Q_{opt}(f - p_f))\|_T.$$

The restriction of $Q_{opt}(f - p_f)$ to T is a polynomial of degree 5. Hence, we can use the Markov inequality (2.1) to estimate

$$\|D^\alpha(Q_{opt}(f - p_f))\|_T \leq \frac{K_2}{\rho_T^{|\alpha|}} \|Q_{opt}(f - p_f)\|_T,$$

with K_2 the constant from theorem 2.28. We use lemma 2.23 (ii) to obtain

$$\frac{K_2}{\rho_T^{|\alpha|}} \|Q_{opt}(f - p_f)\|_T \leq \frac{K_2}{K_3^4 |T|^{|\alpha|}} \|Q_{opt}(f - p_f)\|_T,$$

where K_3 depends only on K_H . It follows from theorem 3.25 and theorem 3.24 that

$$\|Q_{opt}(f - p_f)\|_T \leq \frac{19}{12} \max_{x \in \mathcal{X}_T} |f(x) - p_f(x)| \leq \frac{19}{12} \|f - p_f\|_{\Omega_T}.$$

We combine the results and use (3.14) with $|\beta| = 0$, obtaining

$$\|D^\alpha(Q_{opt}(f - p_f))\|_T \leq \frac{19}{12} \frac{K_1 K_2}{K_3^4} |T|^{m+1-|\alpha|} |f|_{m+1, \Omega_T}.$$

Using this inequality and (3.14) to estimate (3.15) concludes the proof. \square

The global result follows by taking the maximum local error over all tetrahedra.

Theorem 3.42. *Let Q_{opt} be the operator from 3.22. Then there exists a constant $K > 0$, depending only on the shape parameter K_H and the Lipschitz constant of the boundary of Ω , such that for every $f \in C^{m+1}(\Omega)$ with $0 \leq m \leq 3$,*

$$\|D^\alpha(Q_{opt}(f) - f)\|_{\Omega_1} \leq K |\Delta_1|^{m+1-|\alpha|} |f|_{m+1, \Omega}, \quad 0 \leq |\alpha| \leq m,$$

where

$$\Omega := \bigcup_{T \in \Delta_1} \Omega_T$$

and $\Omega_1 := [0, 1]^3$ is the unit cube.

Proof. By theorem 3.41, and since $\Omega_1 \subset \Delta_1$, there exists a constant K such that

$$\|D^\alpha(Q_{opt}(f) - f)\|_{\Omega_1} \leq \max_{T \in \Delta_1} \|D^\alpha(Q_{opt}(f) - f)\|_T \leq \max_{T \in \Delta_1} K |T|^{m+1-|\alpha|} |f|_{m+1, \Omega_T}.$$

Since $|T| \leq |\Delta_1|$ for all $T \in \Delta_1$,

$$\begin{aligned} \max_{T \in \Delta_1} K|T|^{m+1-|\alpha|}|f|_{m+1,\Omega_T} &\leq \max_{T \in \Delta_1} K|\Delta_1|^{m+1-|\alpha|}|f|_{m+1,\Omega_T} \\ &= K|\Delta_1|^{m+1-|\alpha|} \max_{T \in \Delta_1} |f|_{m+1,\Omega_T}. \end{aligned}$$

This concludes the proof, since $\Omega_T \subseteq \Omega$. \square

Finally, we provide the analogous error bounds for the interpolating operator.

Theorem 3.43. *Let Q_I be the operator defined in 3.33. Let Δ_2 be the tetrahedral partition defined in 3.27, \mathcal{X} the associated sample set, and K_H the shape parameter from lemma 2.23. Fix $T \in \Delta_2$ and let*

$$\Omega_T := \bigcup_{\hat{T} \in \text{star}^5(\tilde{T})} \hat{T},$$

where \tilde{T} is the tetrahedron in Δ_{BCC} with $T = \tilde{T}$. Then there exists a constant K depending only on K_H and the Lipschitz constant of the boundary of Ω_T , such that for all $f \in C^{m+1}(\Omega_T)$ with $0 \leq m \leq 3$,

$$\|D^\alpha(Q_I(f) - f)\|_T \leq K|T|^{m+1-|\alpha|}|f|_{m+1,\Omega_T}, \quad 0 \leq |\alpha| \leq m. \quad (3.16)$$

Proof. By theorem 2.29 and the Stein extension theorem (see [84], p.181), there exists a constant \tilde{K}_m such that

$$\|D^\beta(f - p_f)\|_{\Omega_T} \leq \tilde{K}_m|\Omega_T|^{m+1-|\beta|}|f|_{m+1,\Omega_T}, \quad 0 \leq |\beta| \leq m + 1,$$

where p_f is the Taylor polynomial of degree m associated with f . Let $K_0 := \max_{m=0}^3 \tilde{K}_m$. We use lemmas 2.10 and 2.23 (i) and obtain

$$\|D^\beta(f - p_f)\|_{\Omega_T} \leq K_1|T|^{m+1-|\beta|}|f|_{m+1,\Omega_T}, \quad 0 \leq |\beta| \leq m, \quad (3.17)$$

with $K_1 = 12^4 K_0 / K_H^4$. Using the triangle inequality and the linearity of the differential operator leads to

$$\|D^\alpha(Q_I(f) - f)\|_T \leq \|D^\alpha(Q_I(f) - p_f)\|_T + \|D^\alpha(p_f - f)\|_T. \quad (3.18)$$

The quasi-interpolation operator is linear and, by theorem 3.38, reproduces cubic polynomials. Thus,

$$\|D^\alpha(Q_I(f) - p_f)\|_T \leq \|D^\alpha(Q_I(f) - p_f)\|_T.$$

The restriction of Q_I to T is a polynomial, and we use the Markov inequality from theorem 2.28 to obtain

$$\|D^\alpha(Q_I(f) - p_f)\|_T \leq \frac{K_2}{\rho_T^{|\alpha|}} \|Q_I(f - p_f)\|_T,$$

with K_2 depending only on the degree of the polynomial which is 5. It follows from lemma 2.23 (ii) that $\rho_T \geq K_3|T|$ for some constant $K_3 < 1$ depending only on the shape parameter K_H . Together with the fact that $0 \leq |\alpha| \leq 4$ and the stability of Q_I from theorem 3.37 this yields

$$\|D^\alpha(Q_I(f - p_f))\|_T \leq \frac{K_2}{K_3^4|T|^{\alpha}} \frac{12703}{6912} \max_{x \in \mathcal{X}_T} |f(x) - p_f(x)|.$$

Then we use the locality from theorem 3.36 and (3.17) with $|\beta| = 0$ and obtain

$$\begin{aligned} \|D^\alpha(Q_I(f - p_f))\|_T &\leq \frac{K_2}{K_3^4|T|^{\alpha}} \frac{12703}{6912} \|f - p_f\|_{\Omega_T} \\ &\leq \frac{K_1 K_2}{K_3^4} \frac{12703}{6912} |T|^{m+1-|\alpha|} |f|_{m+1, \Omega_T}. \end{aligned}$$

To conclude the proof, we combine this inequality with (3.17) to obtain an estimate for (3.18). \square

We conclude this section with a global error bound for the interpolating operator.

Theorem 3.44. *Let Q_I be the quasi-interpolation operator defined in 3.33 and Δ_2 the associated tetrahedral partition. For each $T \in \Delta_2$, let Ω_T be defined as in theorem 3.43 and*

$$\Omega := \bigcup_{T \in \Delta_2} \Omega_T.$$

Let $\Omega_1 := [0, 1]^3$ be the unit cube. Suppose $f \in C^{m+1}(\Omega)$ for some $0 \leq m \leq 3$. Then there exists a constant K , depending only on the shape parameter K_H and the Lipschitz constant of the boundary of Ω , such that

$$\|D^\alpha(Q_I(f) - f)\|_{\Omega_1} \leq K |\Delta_2|^{m+1-|\alpha|} |f|_{m+1, \Omega}, \quad 0 \leq |\alpha| \leq m.$$

Proof. Since $\Omega_1 \subset \Delta_2$, we estimate

$$\|D^\alpha(Q_I(f) - f)\|_{\Omega_1} \leq \max_{T \in \Delta_2} \|D^\alpha(Q_I(f) - f)\|_T.$$

It follows from theorem 3.16 that there exists a constant K with

$$\max_{T \in \Delta_2} \|D^\alpha(Q_I(f) - f)\|_T \leq \max_{T \in \Delta_2} K |T|^{m+1-|\alpha|} |f|_{m+1, \Omega_T}.$$

But then, since $|T| \leq |\Delta_2|$ and $\Omega_T \subset \Omega$,

$$\begin{aligned} \max_{T \in \Delta_2} K |T|^{m+1-|\alpha|} |f|_{m+1, \Omega_T} &\leq K |\Delta_2|^{m+1-|\alpha|} \max_{T \in \Delta_2} |f|_{m+1, \Omega_T} \\ &\leq K |\Delta_2|^{m+1-|\alpha|} |f|_{m+1, \Omega}. \end{aligned}$$

\square

Chapter 4

Enforcing convexity with parametric quasi-interpolation

Non-convex quasi-interpolation operators tend to produce splines whose values lie outside the data range. This can be observed especially in regions where the data values jump from one level to another. One example for such a situation are data values acquired by computer tomography, where different types of material have distinct density value ranges. In the boundary regions where one material meets another, a non-convex operator might produce values that can fall into the range of a third material, resulting in features in the reconstruction which are not present in the data. This may lead to a misinterpretation of the reconstructed volume. We show this behavior in a reconstruction of an artificial data set, representing a solid cube, in figure 4.1. We reconstructed the data set using our convex and optimal quasi-interpolation operators developed in the previous chapter. Figure 4.2 shows 2D histograms (see [45]) of both reconstructions, where the horizontal axis displays the data values, while the vertical axis shows the magnitude of the gradients. Thus, each arch in the histogram represents a boundary between two materials. In the histogram of the convex reconstruction, only one such arch is present, while the histogram of the reconstruction by the optimal operator also shows several smaller arches. From these smaller arches, we extracted the ‘phantom features’ shown in figure 4.1, which are not present in the original data.

Using a convex operator would solve this problem, but these operators usually have a sub-optimal approximation order. Given a sample set $X := \{x_1, \dots, x_N\}$ and an associated spline space $\mathcal{S} \subseteq \mathcal{S}_d^r(\Delta)$ defined over a tetrahedral partition Δ , let Q and Q_{conv} be two linear local trivariate spline quasi-interpolation operators for (X, \mathcal{S}) , of which Q_{conv} is convex, while Q has a better approximation order. We present an algorithm that enforces the convexity condition (3.2) on Q by locally blending the weights of the

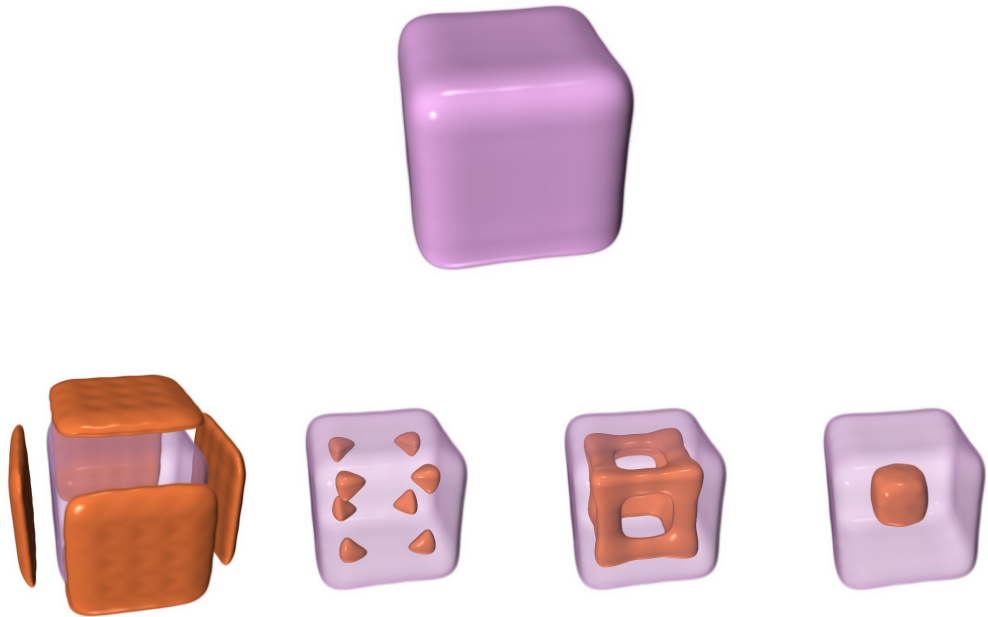


Figure 4.1: A reconstruction of a solid cube by a non-convex quasi-interpolation operator. The bottom images show phantom features, both inside and outside the cube, extracted from the reconstruction.

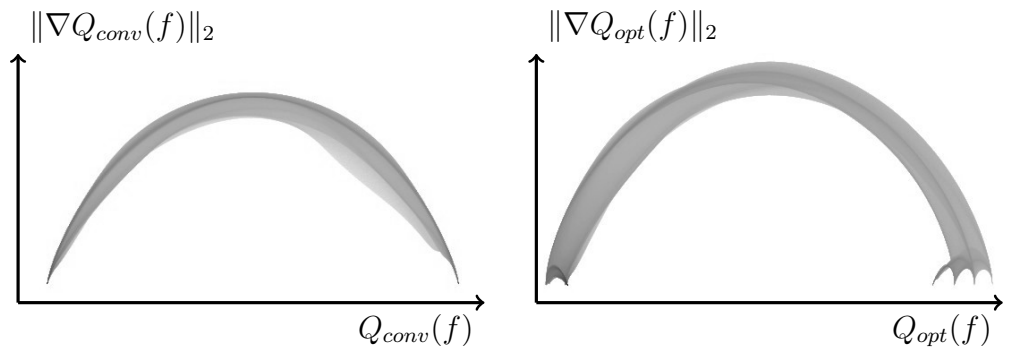


Figure 4.2: The 2D histograms of reconstructions by a convex operator (left) and a non-convex operator (right).

B-coefficient computation rules of Q with those of Q_{conv} where (3.2) is not satisfied by Q .

This is motivated by the fact that a linear combination of the two operators also is a quasi-interpolation operator for (X, \mathcal{S}) . In particular, we investigate the blending operator

$$Q_t := (1 - t)Q + tQ_{conv}.$$

Let Q and Q_{conv} be defined by the B-coefficient computation rules

$$c_\eta^T = \sum_{k=1}^N w_{\eta,x_k}^T f_k \quad \text{and} \quad \tilde{c}_\eta^T = \sum_{k=1}^N \tilde{w}_{\eta,x_k}^T f_k,$$

respectively. Then the rules of Q_t can be written as

$$\begin{aligned} c_\eta^T(t) &= (1 - t) \sum_{k=1}^N w_{\eta,x_k}^T f_k + t \sum_{k=1}^N \tilde{w}_{\eta,x_k}^T f_k \\ &= \sum_{k=1}^N ((1 - t)w_{\eta,x_k}^T + t\tilde{w}_{\eta,x_k}^T) f_k. \end{aligned} \tag{4.1}$$

Obviously Q_1 fulfills the convexity condition (3.2), while Q_0 has the characteristics and better approximation order of Q . But we would like to maintain the characteristics of Q in those regions where Q fulfills the convexity condition, and only blend to Q_{conv} where it does not satisfy (3.2). Therefore we need to find a way to blend the operators locally rather than globally. Since both Q and Q_{conv} are local, Q_t is also local. In fact, if Q is ℓ -local and Q_{conv} is $\tilde{\ell}$ -local, then Q_t is $\max\{\ell, \tilde{\ell}\}$ -local.

For the remainder of this chapter, we assume that both Q and Q_{conv} are at least continuous. To be more precise, we assume that if a domain $\eta \in \mathcal{D}_d(\Delta)$ is the domain point of two separate tetrahedra T and \tilde{T} , then the rules for c_η^T and $c_\eta^{\tilde{T}}$ are identical. The quasi-interpolation operators developed in the previous chapter are of that type. Thus, we omit the superscript T when denoting B-coefficients and weights (see remark 3.3).

Fix $f \in \mathcal{F}_X$. Note that since f is a discrete function, we can decompose f into the functions $f^{[k]} \in \mathcal{F}_X$ defined by

$$f^{[k]}(x_i) := \delta_{ki} f_i.$$

Then

$$f \equiv \sum_{k=1}^N f^{[k]}.$$

Using the linearity of Q_t , we have

$$Q_t(f) = Q_t \left(\sum_{k=1}^N f^{[k]} \right) = \sum_{k=1}^N Q_t(f^{[k]}).$$

Looking at the right side of the equation, we see that we can use a different parameter t for each term.

Definition 4.1. Let $\theta := (t_1, \dots, t_N) \in [0, 1]^N$, then we define

$$Q_\theta(f) := \sum_{k=1}^N Q_{t_k}(f^{[k]}).$$

We call θ the parameter set for the blending operator Q_θ .

The locality of Q_t assures that each of the t_k influences the spline $Q_\theta(f)$ only in the neighborhood of the sample point x_k .

We use (4.1) to obtain the B-coefficient computation rules of $Q_\theta(f)$.

$$c_\eta(\theta) = \sum_{k=1}^N c_\eta(t_k) = \sum_{k=1}^N \sum_{i=1}^N ((1-t_k)w_{\eta,x_i} + t_k \tilde{w}_{\eta,x_i}) f^{[k]}(x_i)$$

But since $f^{[k]}(x_i) = 0$ for $i \neq k$, all terms of the inner sum vanish except the term where $i = k$. Thus,

$$c_\eta(\theta) := \sum_{k=1}^N \underbrace{((1-t_k)w_{\eta,x_k} + t_k \tilde{w}_{\eta,x_k})}_{w_{\eta,x_k}(\theta)} f_k.$$

Since the weights $w_{\eta,x_k}(\theta)$ can be zero for certain values of θ , we need a modified definition for the support of these rules. We write

$$\hat{X}_\eta := \{x \in X; w_{\eta,x} \neq 0 \text{ or } \tilde{w}_{\eta,x} \neq 0\}$$

for the support of the rule for $c_\eta(\theta)$, and

$$\hat{X}_T := \bigcup_{\eta \in \mathcal{D}_d(T)} \hat{X}_\eta$$

for the union of all supports relevant for a tetrahedron $T \in \Delta$. Note that $c_\eta(\theta)$ depends only on those parameters t_k whose associated sample points x_k are in the support \hat{X}_η . For a fixed k , the set of domain points whose associated B-coefficients $c_\eta(\theta)$ depend on t_k are those whose support contains x_k , and we write

$$D_k := \left\{ \eta \in \mathcal{D}_d(\Delta); x_k \in \hat{X}_\eta \right\}.$$

We adapt definition 3.9 to the blending operator.

Definition 4.2. A parameter set θ for $Q_\theta(f)$ is called convex for f , if

$$f_{min}^T \leq Q_\theta(f)(v) \leq f_{max}^T \quad \text{for all } T \in \Delta, \quad (4.2)$$

where

$$f_{min}^T := \min_{x \in \hat{X}_T} f(x) \quad \text{and} \quad f_{max}^T := \max_{x \in \hat{X}_T} f(x)$$

Note that a parameter set which is convex for a fixed $f \in \mathcal{F}_X$ is not necessarily convex for another function $\tilde{f} \in \mathcal{F}_X$.

The following lemma adapts lemma 3.10 to the blending operator.

Lemma 4.3. Let θ be a parameter set for $Q_\theta(f)$. If

$$f_{\eta,min} \leq c_\eta(\theta) \leq f_{\eta,max} \quad \text{for all } \eta \in \mathcal{D}_d(\Delta), \quad (4.3)$$

where

$$f_{\eta,min} := \min_{x \in \hat{X}_\eta} f(x) \quad \text{and} \quad f_{\eta,max} := \max_{x \in \hat{X}_\eta} f(x),$$

then θ is convex for f .

The proof is analogous to the proof of lemma 3.10.

Our goal is it to construct a convex parameter set where the parameters t_k are close to zero to preserve the characteristics of Q . First we show that at least one convex character set exists.

Proposition 4.4. The parameter set $\theta_1 := (1, \dots, 1) \in [0, 1]^N$ is convex for all $f \in \mathcal{F}_X$.

Proof. This follows immediately from the fact that $Q_{\theta_1}(f) = Q_{conv}(f)$. \square

The idea of the following algorithm is to use (4.1) to compute a minimal t_η for each domain point, such that (3.3) holds. An initial parameter set $\theta = \{t_1, \dots, t_N\}$ is then generated, where t_k is set to the maximum of those t_η with $\eta \in D_k$. In the main loop of the algorithm, each coefficient $c_\eta(\theta)$ is tested against (4.3), and the parameters t_k with $x_k \in \hat{X}_\eta$ are increased until (4.3) holds. The existence of the convex parameter set θ_1 of proposition 4.4 assures the termination of this process. It follows from lemma 4.3 that the final parameter set is convex.

The following lemma shows that for each domain point, there exists an interval $[t_\eta, 1]$ such that $c_\eta(t)$ satisfies (3.3) for all $t \in [t_\eta, 1]$. This indicates that, once the convexity condition (4.3) is fulfilled for some $c_\eta(\theta)$, increasing some of the t_k will not result in a situation where (4.3) can no longer be achieved.

Lemma 4.5. Fix $\eta \in \mathcal{D}_d(\Delta)$. Let

$$t_\eta := \min \{t \in [0, 1]; f_{\eta, \min} \leq c_\eta(t) \leq f_{\eta, \max}\}. \quad (4.4)$$

Then

$$f_{\eta, \min} \leq c_\eta(t) \leq f_{\eta, \max} \quad \text{for all } t \in [t_\eta, 1].$$

Proof. The convexity of Q_{conv} assures that $1 \in \{t \in [0, 1]; f_{\eta, \min} \leq c_\eta(t) \leq f_{\eta, \max}\}$, and thus the minimum t_η exists. Let $c_{\min} := \min\{c_\eta(t_\eta), c_\eta(1)\}$ and $c_{\max} := \max\{c_\eta(t_\eta), c_\eta(1)\}$. Note that $c_\eta(t)$ is a linear univariate polynomial in t , and thus monotonic. Hence, for all $t \in [t_\eta, 1]$, $c_\eta(t) \in [c_{\min}, c_{\max}] \subseteq [f_{\eta, \min}, f_{\eta, \max}]$. \square

Remark 4.6. The minimum (4.4) can be computed quite easily. Using (4.1), we obtain

$$c_\eta(t) = (1-t)c_\eta + t\tilde{c}_\eta = c_\eta + t(\tilde{c}_\eta - c_\eta).$$

If $\tilde{c}_\eta = c_\eta$, the convexity of Q_{conv} assures that (3.3) holds for c_η , and the minimum is 0. Let $\tilde{c}_\eta \neq c_\eta$ and set

$$t_0 := \frac{f_{\eta, \min} - c_\eta}{\tilde{c}_\eta - c_\eta} \quad \text{and} \quad t_1 := \frac{f_{\eta, \max} - c_\eta}{\tilde{c}_\eta - c_\eta}.$$

Since $c_\eta(t)$ is a monotonic function and $c_\eta(1) = \tilde{c}_\eta \in [f_{\eta, \min}, f_{\eta, \max}]$,

$$\min\{t_0, t_1\} \leq 1 \leq \max\{t_0, t_1\}.$$

and

$$c_\eta(t) \in [f_{\eta, \min}, f_{\eta, \max}] \quad \text{for all } t \in [\min\{t_0, t_1\}, \max\{t_0, t_1\}].$$

Thus, the minimum is given by

$$t_\eta := \max \{0, \min\{t_0, t_1\}\}.$$

The initial parameter set is constructed such that for each domain point η , the parameters lie in the intervals $[t_\eta, 1]$. Since $c_\eta(\theta)$ is usually not equal to $c_\eta(t)$, this does not guarantee the convexity of the initial set. It shows, however, that increasing the parameters in each adjustment step will eventually result in a convex parameter set.

Algorithm 4.7. This algorithm constructs a convex parameter set $\theta = (t_1, \dots, t_N)$ for $Q_\theta(f)$.

- 1) Set $\theta := (0, \dots, 0) \in [0, 1]^N$.
 - 2) For each $\eta \in \mathcal{D}_d(\Delta)$:
- 2.1) Compute $t_\eta := \min \{t \in [0, 1]; f_{\eta, \min} \leq c_\eta(t) \leq f_{\eta, \max}\}$.

- 2.2) For each $x_k \in \hat{X}_\eta$, update $t_k \leftarrow \max\{t_k, t_\eta\}$.
- 3) Set $D := \mathcal{D}_d(\Delta)$.
- 4) While $D \neq \emptyset$:
 - 4.1) Get $\eta \in D$ and update $D \leftarrow D \setminus \{\eta\}$.
 - 4.2) While $c_\eta(\theta) < f_{\eta,\min}$ or $c_\eta(\theta) > f_{\eta,\max}$:
 - (a) Compute $t_{\eta,\min} := \min\{t_k; x_k \in \hat{X}_\eta\}$.
 - (b) Compute $t_\eta^* := \min\{t_k; t_k > t_{\eta,\min} \text{ and } x_k \in \hat{X}_\eta\}$.
 - (c) For each $x_k \in \hat{X}_\eta$ with $t_k = t_{\eta,\min}$ do
 - Update $t_k \leftarrow t_\eta^*$.
 - Update $D \leftarrow D \cup D_k \setminus \{\eta\}$.

Theorem 4.8. *Algorithm 4.7 terminates after a finite number of steps. The parameter set constructed by the algorithm is convex for f .*

Proof. First we show that the algorithm terminates. Let $\Theta := \{t_\eta; \eta \in \mathcal{D}_d(\Delta)\}$ be the set of all distinct initial parameters generated in step 2.1) of the algorithm. Note that there exist at most N such distinct values. Let $t_{\max} := \max \Theta$. By lemma 4.5, the set $(t_{\max}, \dots, t_{\max}) \in [0, 1]^N$ is a convex parameter set.

Each time step 4.2 (c) is reached, the value of at least one of the parameters t_k is replaced by the value of another parameter which is greater than t_k . Since there are only a finite number of parameters, and since each parameter can only be increased a finite number of times until it reaches t_{\max} , the algorithm terminates after a finite number of steps.

In the update step 4.2 (c), all domain points whose associated B-coefficients depend on at least one of the updated parameters, are reinserted into D . Thus, when the algorithm terminates, all B-coefficients have been tested against the final parameter set θ and passed the test. It follows from lemma 4.3 that this parameter set is convex for f . \square

4.1 Improving the algorithm

Revisiting definition 4.2, we notice that (4.3) only gives a rough estimate for (4.2). Thus, the parameters produced by algorithm 4.7 are not necessarily the least parameters for which (4.2) holds. To improve the algorithm, we change the computation in the loop in step 2), and the test in step 4.2), to produce potentially better parameters.

This is achieved by iterating over the tetrahedra of Δ rather than the domain points $\mathcal{D}_d(\Delta)$ and testing each polynomial piece of $Q_\theta(f)$ against (4.3).

To estimate the minimum and maximum values of these polynomial pieces, we create a local refinement $\Delta_T := \{\tilde{T}_1, \dots, \tilde{T}_m\}$ of each tetrahedron, such that

$$\max_{i=1, \dots, m} |\tilde{T}_i| < |T|.$$

It follows from theorem 2.45 that the B-coefficients of the refined polynomials are a better estimate for the values of $Q_\theta(f)|_T$ than the original B-coefficients. We then compute the B-form of $Q_\theta(f)$ relative to each subtetrahedron. Let $c_\eta^{\tilde{T}}(\theta)$ be the B-coefficients of $Q_\theta(f)|_{\tilde{T}}$. We define

$$c_{min}^T(\theta) := \min \bigcup_{\tilde{T} \in \Delta_T} \left\{ c_\eta^{\tilde{T}}(\theta); \eta \in \mathcal{D}_d(\tilde{T}) \right\}$$

and

$$c_{max}^T(\theta) := \max \bigcup_{\tilde{T} \in \Delta_T} \left\{ c_\eta^{\tilde{T}}(\theta); \eta \in \mathcal{D}_d(\tilde{T}) \right\}.$$

Then

$$c_{min}^T(\theta) \leq Q_\theta(f)(v) \leq c_{max}^T(\theta) \quad \text{for all } v \in T.$$

These values are then tested against f_{min}^T and f_{max}^T to see if (4.2) holds. If the test fails, the parameters t_k with $t_k \in \hat{X}_T$ are again gradually increased. Whenever a parameter t_k is changed, those tetrahedra whose associated polynomial pieces depend on t_k , have to be re-evaluated. We denote those tetrahedra by

$$\Delta_k := \{T \in \Delta; \mathcal{D}_d(T) \cap D_k \neq \emptyset\}.$$

The computation of the B-coefficients $c_\eta^{\tilde{T}}(\theta)$ is a two-step process. First, the B-coefficient computation rules are applied to compute the B-form of $Q_\theta(f)$. Then, de Casteljau's algorithm is used to compute the representation of $Q_\theta(f)$ relative to each subtetrahedron.

We use a similar approach to generate the initial parameter set. For each tetrahedron, the B-coefficient computation rules for Q and Q_{conv} are used to compute c_η and \tilde{c}_η for all $\eta \in \mathcal{D}_d(T)$. For each subtetrahedron of \tilde{T} , let $c_\eta^{\tilde{T}}$ and $\tilde{c}_\eta^{\tilde{T}}$ be the B-coefficients of $Q(f)|_{\tilde{T}}$ and $Q_{conv}(f)|_{\tilde{T}}$, respectively. These, again, are obtained by using de Casteljau's algorithm. Now we set

$$c_\eta^{\tilde{T}}(t) := (1-t)c_\eta^{\tilde{T}} + t\tilde{c}_\eta^{\tilde{T}}$$

and use remark 4.6 to compute the minimal initial parameters t_η . Taking the maximum over all t_η with $\eta \in \bigcup_{\tilde{T} \in \Delta_T} \mathcal{D}_d(\tilde{T})$ yields the initial parameter for T . We replace $f_{\eta,min}$ and $f_{\eta,max}$ with f_{min}^T and f_{max}^T , respectively, for these computations, since we test against (4.2) rather than (4.3).

We're now ready to give the improved algorithm.

Algorithm 4.9. This algorithm produces a convex parameter set $\theta := (t_1, \dots, t_N)$ for $Q_\theta(f)$.

- 1) Set $\theta := (0, \dots, 0) \in [0, 1]^N$.
- 2) For each $T \in \Delta$:
 - 2.1) Set $t_T := 0$.
 - 2.2) For each $\tilde{T} \in \Delta_T$:
 - (a) For each domain point $\eta \in \mathcal{D}_d(\tilde{T})$:
 - Compute $t_\eta := \min\{t \in [0, 1]; f_{min}^T \leq c_\eta^{\tilde{T}}(t) \leq f_{max}^T\}$.
 - Update $t_T \leftarrow \max\{t_T, t_\eta\}$.
 - (b) For each $x_k \in \hat{X}_T$, update $t_k \leftarrow \max\{t_k, t_T\}$.
 - 3) Set $\hat{\Delta} := \Delta$.
 - 4) While $\hat{\Delta} \neq \emptyset$:
 - 4.1) Get $T \in \hat{\Delta}$ and update $\hat{\Delta} \leftarrow \hat{\Delta} \setminus T$.
 - 4.2) While $c_{min}^T(\theta) < f_{min}^T$ or $c_{max}^T(\theta) > f_{max}^T$.
 - (a) Compute $t_{T,min} := \min\{t_k; x_k \in \hat{X}_T\}$.
 - (b) Compute $t_T^* := \min\{t_k; t_k > t_{T,min} \text{ and } x_k \in \hat{X}_T\}$.
 - (c) For each $x_k \in \hat{X}_T$ with $t_k = t_{T,min}$:
 - Update $t_k \leftarrow t_T^*$.
 - Update $\hat{\Delta} \leftarrow \hat{\Delta} \cup \Delta_k \setminus \{T\}$.

Theorem 4.10. Algorithm 4.9 terminates after a finite number of steps. The constructed parameter set is convex for f .

Proof. We follow the proof of theorem 4.8. The number of distinct initial parameter values generated in the loop 2) is at most N . Let $t_{max} \in [0, 1]$ be the maximum of these initial values. It follows from lemma 4.5 that $(t_{max}, \dots, t_{max}) \in [0, 1]^N$ is a convex parameter set for f . During the update step 4.2 (c), at least one of the parameters t_k is increased. Since t_k can only be increased a finite number of times until it reaches t_{max} , and since only a finite number of parameters exist, the algorithm terminates eventually.

By the time the algorithm terminates, each tetrahedron has passed the test in step 4.2), and thus the final parameter set is convex for f . \square

We conclude this chapter with the following remark. Even though we consider only trivariate operators in this chapter, the algorithms presented here can be easily adapted to the multivariate setting.

Chapter 5

Lagrange interpolation using splines of low locality on the BCC partition

Given an n -dimensional subspace G of $C(\Omega)$, where $\Omega \subseteq \mathbb{R}^m$ contains n distinct points x_i , the Lagrange interpolation problem is to determine a function $g \in G$ such that $g(x_i) = f_i$ for $i = 1, \dots, n$, and associated data values f_i . This problem has been thoroughly investigated for many types of functions. If G is a Haar space (or Chebyshev space), then the problem has a unique solution. A classic example for a Haar space is the space of univariate polynomials of degree $n - 1$. Unfortunately, for $m \geq 2$ there exist no Haar spaces of dimension $n \geq 2$. This is known as the Mairhuber-Curtis theorem and has been proved independently by Mairhuber [50] and Curtis [28] in 1956 and 1959, respectively. Thus, the existence of a solution to the problem depends on the position of the points x_i for these cases, which leads to the following definition

Definition 5.1. *Let G be an n -dimensional linear subspace of $C(\Omega)$, where $\Omega \subseteq \mathbb{R}^m$. A subset $X \subset \Omega$ of n distinct points is called a Lagrange interpolation set for G , if for every $f \in C(\Omega)$ there exists a unique $g \in G$ with*

$$g(x) = f(x) \quad \text{for all } x \in X.$$

The Lagrange interpolation problem has also been completely solved for univariate spline spaces by Schoenberg and Whitney in [76]. Here, the existence of a solution also depends on the distribution of the points x_i . Chung and Yao examined the problem for the spaces of multivariate polynomials and point sets on certain lattices in [24], while Chui and Lai provide results for more general point sets in [23]. Sommer and Strauss generalized the Schoenberg-Whitney condition to the multivariate setting for *almost interpolation*, where the points x_i may have to be moved slightly to produce a

unique solution for the interpolation problem. These results can be found in [79].

Local Lagrange interpolation by bivariate splines has been extensively studied, and it has been shown in [29] that spline spaces over arbitrary partitions do not always have a stable local basis. Thus, many local Lagrange interpolation methods rely on local refinements of the given partition. The vast literature on this subjects includes methods that work on certain classes of triangulations (see [63, 64]), as well as methods for arbitrary triangulations (see [22, 43, 58, 66]). This list is not complete by far, and we refer the interested reader to the survey [65] and the references in [46] for more information on the subject.

In recent years, a number of local Lagrange interpolation methods for the trivariate setting have appeared. As in the bivariate case, these methods usually decompose the underlying partition into disjoint classes of tetrahedra and construct the splines step by step on these classes. Most of these methods, like [41, 42, 44, 54, 55, 61, 62], also use a local refinement of some or all tetrahedra to avoid over-determined B-coefficients which may arise when multiple smoothness conditions from different neighboring tetrahedra affect the same B-coefficient. One of these methods, [61], which we co-authored with Nürnberger, is the subject of the following section. Notable examples to this technique are [59] and [78]. Here, a combination of a uniform partition, a high polynomial degree compared to the order of smoothness, and certain superspline conditions at some of the vertices, provide the locality while avoiding over-determined B-coefficients. Also of special interest is the method developed in [55], as it is the only one using C^2 splines.

We define our Lagrange interpolation operators as a specialization of the quasi-interpolation operators defined in 3.1.

Definition 5.2. *Let Δ be a tetrahedral partition of a polygonally bounded region $\Omega \subset \mathbb{R}^3$, and $\mathcal{S} \subseteq \mathcal{S}_d^r(\Delta)$ a spline space. A quasi-interpolation operator \mathcal{L} for (X, \mathcal{S}) is called a Lagrange interpolation operator, if X is a Lagrange interpolation set for \mathcal{S} , and if for every $f \in \mathcal{F}_X$,*

$$\mathcal{L}(f)(x) = f(x) \quad \text{for all } x \in X.$$

Thus, the quasi-interpolation operator Q_I from chapter 3, section 3.3, is not a Lagrange interpolation operator for two reasons. The number of sample points used by Q_I is not equal to the dimension of the associated spline space, and some sample points lie outside the tetrahedral partition.

In contrast to the quasi-interpolation operators defined in chapter 3, we do not give explicit B-coefficient computation rules for our Lagrange interpolation operators. We rather show that all B-coefficients can be computed from the data values by successively solving a number of small linear systems.

The main idea behind most of the local Lagrange interpolation methods cited in the introduction to this chapter is to decompose the partition into several classes of tetrahedra (or clusters of tetrahedra) in such a way that the spline can be constructed independently on the tetrahedra of the first class. Then the smoothness conditions are applied to determine some of the B-coefficients associated with the surrounding tetrahedra, and the spline is constructed on the tetrahedra of the second class. This process is repeated until all B-coefficients of the spline are determined. Typically, a tetrahedron belonging to a higher class is surrounded by more than one tetrahedron of lower classes, and has to be subdivided to avoid that B-coefficients are overdetermined.

5.1 Cubic C^1 -splines

We develop a local Lagrange interpolation method for cubic C^1 -splines on the BCC partition. The main focus of our method lies on constructing splines with low locality. Hecklin, Nürnberger, Schumaker and Zeilfelder developed a method in [42] for cubic C^1 splines on arbitrary partitions, where the locality depends on the structure of the partition and can be as high as 10 in the worst case. The locality can be improved by using regular partitions. The method by the same authors for Freudenthal partitions, developed in [41], achieves a locality of 5, while the splines constructed by Matt and Nürnberger in [55] on the Type-4 partition are 4-local. All three methods rely on a priority principle to achieve the locality of the splines, where the underlying partition is decomposed into classes of tetrahedra with an increasing number of common vertices and edges. The latter two methods make use of the cube structure of the respective partitions to simplify this process.

Our method follows the same basic principle, but focuses on a partition which allows a decomposition into only a few classes. This partition is a subset of the BCC partition. The method achieves a locality of two and has been published in [61].

In preparation of the main results of this section, we give some lemmas. The first lemma deals with Lagrange interpolation at the domain points associated with a single edge.

Lemma 5.3. *Let $e := \langle v_0, v_1 \rangle$ be an edge of a tetrahedron $T := \langle v_0, v_1, v_2, v_3 \rangle$. Let $\xi_{ij} := \xi_{ij00} \in \mathcal{D}_3(T)$, $i + j = 3$, be the domain points located on that edge, and c_{ij} the associated B-coefficients of a polynomial p in B-form relative to T . Fix values $f_{ij} \in \mathbb{R}$, $i + j = 3$. Then $p|_e$ is uniquely determined by*

$$p|_e(\xi_{ij}) = f_{ij}, \quad i + j = 3.$$

Proof. The restriction of p to e is essentially a univariate polynomial, see remark 2.37, and we write

$$p|_e := \sum_{i+j=3} c_{ij} B_{ij},$$

where $B_{ij} := B_{ij00}^T$. We show that all B-coefficients of $p|_e$ are uniquely determined by the interpolation conditions. From the Lagrange interpolation conditions $p|_e(\xi_{30}) = f_{30}$ and $p|_e(\xi_{03}) = f_{03}$, it follows with 2.48 that $c_{30} = f_{30}$ and $c_{03} = f_{03}$. The remaining two conditions lead to the linear system

$$\begin{aligned} f_{30}B_{30}(\xi_{21}) + c_{21}B_{21}(\xi_{21}) + c_{12}B_{12}(\xi_{21}) + f_{03}B_{03}(\xi_{21}) &= f_{21}, \\ f_{30}B_{30}(\xi_{12}) + c_{21}B_{21}(\xi_{12}) + c_{12}B_{12}(\xi_{12}) + f_{03}B_{03}(\xi_{12}) &= f_{12}. \end{aligned}$$

Written as a matrix equation, this becomes

$$\begin{pmatrix} \frac{4}{9} & \frac{2}{9} \\ \frac{2}{9} & \frac{4}{9} \end{pmatrix} \begin{pmatrix} c_{21} \\ c_{12} \end{pmatrix} = \begin{pmatrix} r_1 \\ r_2 \end{pmatrix}, \quad (5.1)$$

where the constants r_1 and r_2 are linear combinations of the interpolation values f_{ij} . The determinant of the matrix is $\frac{4}{27}$, and thus the system has a unique solution. \square

The situation in the following lemma is similar to the one considered in the previous lemma, but here two of the B-coefficients are already known.

Lemma 5.4. *Using the notation of lemma 5.3, suppose that the B-coefficients c_{30} and c_{21} of the polynomial p are already known. Then for all pairs $f_{12}, f_{03} \in \mathbb{R}$, $p|_e$ is uniquely determined by*

$$p(\xi_{12}) = f_{12}, \quad p(\xi_{03}) = f_{03}.$$

Proof. The cubic polynomial $p|_e$ is determined by the four B-coefficients c_{ij} , $i+j=3$, two of which are already known. Following the proof of lemma 5.3, $c_{30} = f_{30}$ and

$$c_{30}B_{30}(\xi_{12}) + c_{21}B_{21}(\xi_{12}) + c_{12}B_{12}(\xi_{12}) + f_{03}B_{03}(\xi_{12}) = f_{12}. \quad (5.2)$$

Since $B_{12}(\xi_{12}) = 4/9$, the equation can be uniquely solved for the remaining B-coefficient c_{12} . \square

The next lemma concerns Lagrange interpolation at the barycenter of a face, when all B-coefficients associated with the remaining domain points of that face are already known.

Lemma 5.5. Let $F := \langle v_0, v_1, v_2 \rangle$ be a face of a tetrahedron $T := \langle v_0, v_1, v_2, v_3 \rangle$. Analogously to lemma 5.3, we denote the domain points, B-coefficients and Bernstein basis polynomials associated with F by ξ_{ijk} , c_{ijk} and B_{ijk} , $i+j+k=3$, respectively. Suppose all B-coefficients associated with F of a polynomial p in B-form relative to T are known except c_{111} . Then for each value $f \in \mathbb{R}$, $p|_F$ is uniquely determined by

$$p|_F(\xi_{111}) = f.$$

Proof. Regarding remark 2.37, the restriction of p to F is a bivariate polynomial. We show that all B-coefficients of $p|_F$ are uniquely determined by the interpolation condition. In the equation

$$p|_F(\xi_{111}) = \sum_{i+j+k=3} c_{ijk} B_{ijk}(\xi_{111}) = f, \quad (5.3)$$

all values except c_{111} are known. Since $B_{111}(\xi_{111}) = \frac{2}{9}$, the problem has a unique solution. \square

The interpolation process involves subdividing selected tetrahedra with a partial Worsey-Farin split. This includes the splitting of some of the faces by a Clough-Tocher split. The following lemma deals with Lagrange interpolation on such a face. Figure 5.1 depicts the situation.

Lemma 5.6. Let $F := \langle v_0, v_1, v_2 \rangle$ be a face of a tetrahedron $T := \langle v_0, v_1, v_2, v_3 \rangle$. Let v_F be a point located in the interior of F and T_1, T_2, T_3 the subtetrahedra of T that result from splitting F at v_F , defined by

$$T_1 := \langle v_0, v_1, v_F, v_3 \rangle, \quad T_2 := \langle v_1, v_2, v_F, v_3 \rangle, \quad T_3 := \langle v_2, v_0, v_F, v_3 \rangle.$$

Suppose the B-coefficients associated with the edges of F , as well as those associated with the domain points $\xi_{1110}^{T_2}$ and $\xi_{1110}^{T_3}$, are known. Fix $f \in \mathbb{R}^3$ and let $s \in \mathcal{S}_3^1(\{T_1, T_2, T_3\})$. Then $s|_F$ is uniquely determined by

$$s|_F(v_F) = f.$$

Proof. We apply the smoothness conditions between the three subtetrahedra to calculate the unknown B-coefficients from the known B-coefficients. The domain points associated with F are $\xi_{ijk0}^{T_1}$, $\xi_{ijk0}^{T_2}$, $\xi_{ijk0}^{T_3}$, $i+j+k=3$. We show that all B-coefficients associated with these domain points are uniquely determined. By theorem 2.53, two domain points belonging to different polynomial pieces of s are equal if their associated domain points coincide, since s is continuous. We use the following notation for the distinct domain points and B-coefficients. Let

$$\xi_{ijkl} := \frac{i}{3}v_0 + \frac{i}{3}v_1 + \frac{i}{3}v_2 + \frac{i}{3}v_F.$$

Then $\xi_{ijk0} = \xi_{ijk0}^{T_1}$, $\xi_{0ijk} = \xi_{0ijk}^{T_2}$, and $\xi_{j0ik} = \xi_{j0ik}^{T_3}$, $i + j + k = 3$. We denote the B-coefficient associated with ξ_{ijkl} by c_{ijkl} . Notice that the known B-coefficients associated with the edges of F are those with $l = 0$. Let $(\varphi_0, \varphi_1, \varphi_2, \varphi_3)$ be the barycentric coordinates of v_F relative to T . Since v_F is located in the interior of F , $\varphi_3 = 0$ and $\varphi_m > 0$, $m = 0, 1, 2$. By lemma 2.32, the barycentric coordinates of v_2 relative to T_1 are

$$\left(-\frac{\varphi_0}{\varphi_2}, -\frac{\varphi_1}{\varphi_2}, \frac{1}{\varphi_2}, 0 \right).$$

Likewise, the barycentric coordinates of v_0 relative to T_2 are

$$\left(-\frac{\varphi_1}{\varphi_0}, -\frac{\varphi_2}{\varphi_0}, \frac{1}{\varphi_0}, 0 \right).$$

The domain points associated with known B-coefficients are shown as black squares in figure 5.1. First we show how the B-coefficients $c_{2001}, c_{0201}, c_{0021}$ are obtained from C^1 smoothness conditions. The associated domain points are represented by white squares in figure 5.1. Since the B-coefficients c_{3000}, c_{2100} and c_{2010} are known, we use the C^1 condition 2.17 between T_1 and T_3 to compute c_{2001} ,

$$c_{2010} = -\frac{\varphi_0}{\varphi_2}c_{3000} - \frac{\varphi_1}{\varphi_2}c_{2100} + \frac{1}{\varphi_2}c_{2001}$$

Solving for c_{2001} , we obtain

$$c_{2001} = \varphi_0c_{3000} + \varphi_1c_{2100} + \varphi_2c_{2010}.$$

Analogously, we calculate c_{0201} from the known B-coefficients $c_{1200}, c_{0300}, c_{0210}$ by applying the C^1 condition between T_1 and T_2 , resulting in

$$c_{0201} = \varphi_0c_{1200} + \varphi_1c_{0300} + \varphi_2c_{0210}.$$

The B-coefficient c_{0021} is obtained from the known B-coefficients $c_{1020}, c_{0030}, c_{0120}$ by using the smoothness condition between T_2 and T_3 , which yields

$$c_{0021} = \varphi_0c_{1020} + \varphi_1c_{0120} + \varphi_2c_{0030}.$$

Since the B-coefficients c_{1011} and c_{0111} are also known, we obtain c_{0012} in the same way, resulting in

$$c_{0012} = \varphi_0c_{1011} + \varphi_1c_{0111} + \varphi_2c_{0021}.$$

The associated domain points is shown as a white circle in figure 5.1. By corollary 2.48, the interpolation condition yields $c_{0003} = f$. A black diamond represents the associated domain point in figure 5.1. At this point,

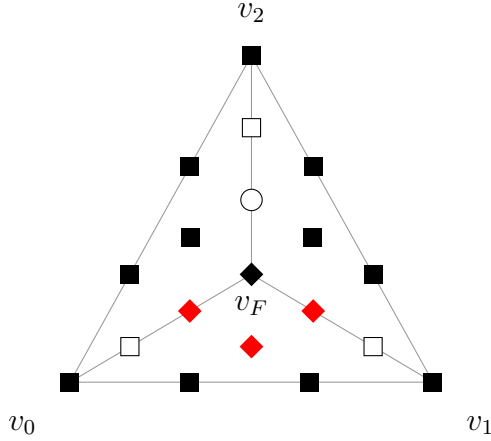


Figure 5.1: Lagrange interpolation on a subdivided face of a tetrahedron. The black squares represent the domain points where the associated B-coefficients are known. The white squares and circle represent domain points whose associated B-coefficients are computed by smoothness conditions. The B-coefficient associated with the black diamond is computed from the interpolation condition. The B-coefficients associated with the red diamonds are calculated from a small linear system of smoothness conditions.

all B-coefficients except c_{1101}, c_{1002} and c_{0102} are determined. Their associated domain points are shown as red diamonds. These are involved in the following C^1 conditions.

$$\begin{aligned} c_{1002} &= \varphi_0 c_{2001} + \varphi_1 c_{1101} + \varphi_2 c_{1011}, \\ c_{0102} &= \varphi_0 c_{1101} + \varphi_1 c_{0201} + \varphi_2 c_{0111}, \\ c_{0003} &= \varphi_0 c_{1002} + \varphi_1 c_{0102} + \varphi_2 c_{0012}. \end{aligned}$$

We rewrite the linear system as a matrix equation,

$$\begin{pmatrix} \varphi_1 & -1 & 0 \\ \varphi_0 & 0 & -1 \\ 0 & \varphi_0 & \varphi_1 \end{pmatrix} \begin{pmatrix} c_{1101} \\ c_{1002} \\ c_{0102} \end{pmatrix} = \begin{pmatrix} r_1 \\ r_2 \\ r_3 \end{pmatrix}, \quad (5.4)$$

where r_1, r_2, r_3 are combinations of known values. The determinant of the matrix is $2\varphi_0\varphi_1$, which is non-zero since v_F lies in the interior of F . \square

We immediately obtain a minimal determining set for the face F .

Corollary 5.7. *Given the situation from lemma 5.6, let \mathcal{M}_E be the domain points associated with the original edges of F , and*

$$\mathcal{M}_F := \mathcal{M}_E \cup \{v_F, \xi_{1110}^{T_2}, \xi_{1110}^{T_3}\}.$$

Then \mathcal{M}_F is a minimal determining set for $\mathcal{S}_3^1(\Delta_{CT}(F))$, where $\Delta_{CT}(F)$ is the triangulation obtained by applying a Clough-Tocher split to F .

Proof. The proof is essentially the same as the proof for 5.6. Suppose that all B-coefficients associated with \mathcal{M}_F are known, then by lemma 5.6 all remaining B-coefficients are uniquely determined. \square

An integral part of the interpolation method is the subdivision of some of the tetrahedra by using a partial Worsay-Farin split. The following theorem uses the same notation as definition 2.16 and gives a minimal determining set for cubic C^1 splines defined over such refinements.

Theorem 5.8. *Let T be a non-degenerate tetrahedron that has been subdivided by an m -th degree partial Worsey-Farin split as in definition 2.16. Let E be the union of the edges of the original tetrahedron T and*

$$\mathcal{M}_E := \mathcal{D}_3(T) \cap E.$$

For $1 \leq i \leq m$, we denote the subtetrahedra that touch the face F_i by $T_i^1 := \langle v_{i-1}, v_i, v_{F_i}, v_T \rangle$, $T_i^2 := \langle v_i, v_{i+1}, v_{F_i}, v_T \rangle$, $T_i^3 := \langle v_{i+1}, v_{i-1}, v_{F_i}, v_T \rangle$, and

$$\mathcal{M}_i := \{\xi_{1110}^{T_i^1}, \xi_{1110}^{T_i^2}, \xi_{1110}^{T_i^3}\}.$$

For $m < i \leq 4$, let $T_i := \langle v_{i-1}, v_i, v_{i+1}, v_T \rangle$ and

$$\mathcal{M}_i := \{\xi_{1110}^{T_i}\}.$$

Then

$$\mathcal{M} := \mathcal{M}_E \cup \mathcal{M}_1 \cup \mathcal{M}_2 \cup \mathcal{M}_3 \cup \mathcal{M}_4$$

is a minimal determining set for $\mathcal{S}_3^1(\Delta_{WF}^m(T))$.

Proof. We show how all B-coefficients of a spline $s \in \mathcal{S}_3^1(\Delta_{WF}^m(T))$ are uniquely determined from the B-coefficients associated with the set \mathcal{M} . First we consider the B-coefficients associated with domain points on the faces of T . Let $1 \leq i \leq m$, then the face F_i is subdivided by a Clough-Tocher split. Twelve of the domain points associated with F_i are contained in \mathcal{M} , and the remaining seven are determined directly by C^1 -conditions as shown in the proof of lemma 5.6. For $m < i \leq 4$, F_i is not split, and all B-coefficients associated with that face are contained in \mathcal{M} . At this point, all B-coefficients associated with domain points in the shell $R_3(v_T)$ are uniquely determined.

We now consider the B-coefficients associated with domain points contained in the ball $D_2(v_T)$. The convex hull of these domain points defines a tetrahedron \tilde{T} which is a smaller version of T , as shown in figure 5.2. These B-coefficients can be considered as the B-coefficients of a spline $\tilde{s} \in \mathcal{S}_2^1(\Delta_{WF}^m(\tilde{T}))$. Let $\tilde{\mathcal{M}}_E$ be the set of domain points associated

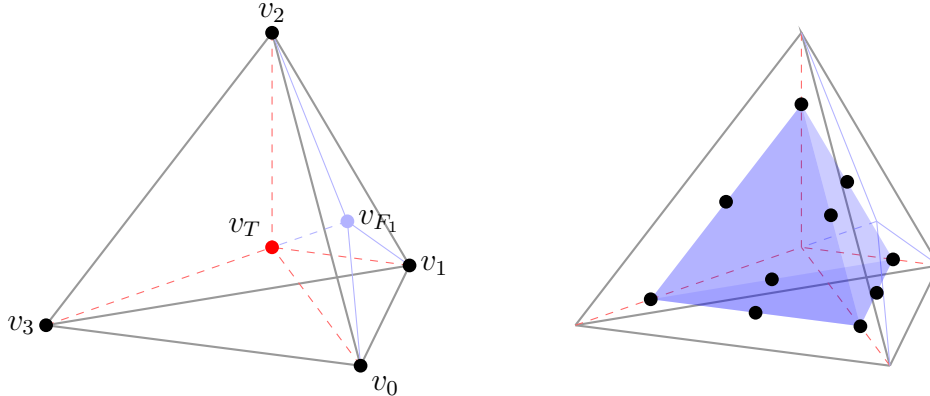


Figure 5.2: A tetrahedron that has been subdivided by a partial Worsey-Farin split of degree 1. The smaller blue tetrahedron on the right is the convex hull of $D_2(v_T)$, while the black circles represent domain points associated with the edges of that tetrahedron.

with the edges of \tilde{T} . Suppose that all B-coefficients associated with $\tilde{\mathcal{M}}_E$ are zero, then it is easy to see that the remaining B-coefficients of \tilde{s} are also zero, as they can be directly computed from known coefficients by (2.17). Then by definition 2.61, $\tilde{\mathcal{M}}_E$ is a determining set for $\mathcal{S}_2^1(\Delta_{WF}^m(\tilde{T}))$. Since there are 10 such domain points, $\dim \mathcal{S}_2^1(\Delta_{WF}^m(\tilde{T})) \leq 10$. But the 10-dimensional space of trivariate quadratic polynomials is a subspace of $\mathcal{S}_2^1(\Delta_{WF}^m(\tilde{T}))$, and hence $\dim \mathcal{S}_2^1(\Delta_{WF}^m(\tilde{T})) \geq 10$. Hence, $\tilde{\mathcal{M}}_E$ is a minimal determining set for $\mathcal{S}_2^1(\Delta_{WF}^m(\tilde{T}))$.

It remains to show that the B-coefficients associated with $\tilde{\mathcal{M}}_E$ are uniquely determined by the B-coefficients associated with $R_3(v_T)$. Let $\xi \in \tilde{\mathcal{M}}_E$, then c_ξ is determined by a C^1 smoothness condition (2.17). The other four B-coefficients in that equation are already determined, since they are associated with domain points in $R_3(v_T)$. Thus, c_ξ is uniquely determined, and the proof is complete. \square

The interpolation process developed in this chapter is based on a classification of the tetrahedra of Δ_{BCC} . The first two classes, defined below, are used to determine the B-coefficients associated with the edges of the partition. We use the relative notation introduced in 2.20 to specify the tetrahedra.

Definition 5.9. *Given the BCC partition, we define*

$$\begin{aligned} K_0 &:= \{T_{LD}(w_{ijk}) \in \Delta_{BCC}; i, j, k \in \mathbb{Z}, i + k \text{ even}\}, \\ K_1 &:= \Delta_{BCC} \setminus K_0. \end{aligned}$$

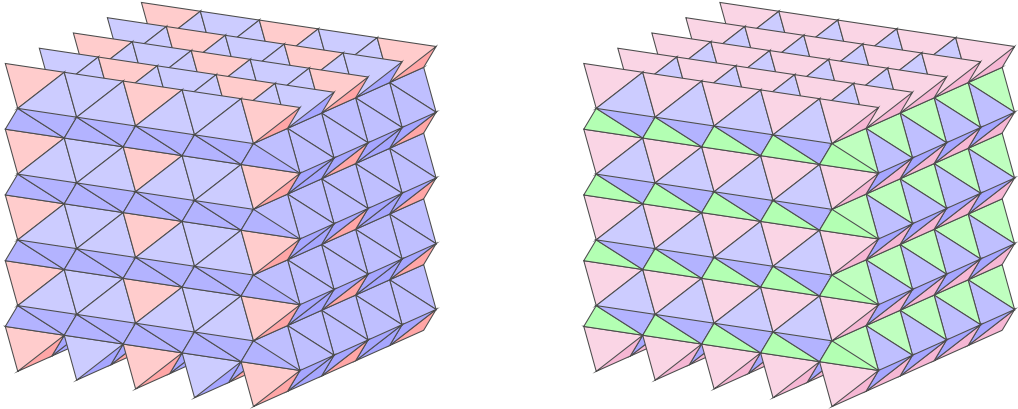


Figure 5.3: On the left: the tetrahedra in class K_0 (red), shown in a subset of the BCC partition. The remaining blue tetrahedra belong to class K_1 . On the right: the tetrahedra in classes K_2 and K_3 are shown in magenta and green, respectively. The remaining blue tetrahedra belong to class K_4 .

The class K_0 is chosen such that all tetrahedra belonging to that class are disjoint, and each vertex of Δ_{BCC} is the vertex of exactly one tetrahedron $T \in K_0$, as the following lemma shows. The tetrahedra belonging to this class are pictured in figure 5.3. The second class is the complement of K_0 .

Lemma 5.10. *Each vertex v of Δ_{BCC} is the vertex of exactly one tetrahedron $T \in K_0$.*

Proof. For each interior vertex v of Δ , there exist even indices i and k and an index j such that

$$v \in \{v_{ijk}, v_{i+1,j,k}, v_{i,j,k+1}, v_{i+1,j,k+1}, w_{ijk}, w_{i+1,j,k}, w_{i,j,k+1}, w_{i+1,j,k+1}\}.$$

By definitions 2.18 and 2.20, it is clear that each of these vertices is the vertex of one of the tetrahedra $T_{LD}(w_{ijk})$, $T_{LD}(w_{i+2,j,k})$, $T_{LD}(w_{i+1,j,k-1})$, $T_{LD}(w_{i+1,j,k+1})$, as shown in figure 5.4. But since i and j are even, these tetrahedra belong to the class K_0 . \square

Another classification of the tetrahedra of Δ_{BCC} is used to determine the B-coefficients associated with the faces of the partition.

Definition 5.11. *Given the BCC partition, we define*

$$\begin{aligned} K_2 &:= \{T_{LD}(v), T_{BU}(v); v \in \mathcal{W}_H\}, \\ K_3 &:= \{T_{BD}(v), T_{LU}(v); v \in \mathcal{W}_H\}, \\ K_4 &:= \bigcup_{v \in \mathcal{V}_{BCC}} \diamond(v), \end{aligned}$$

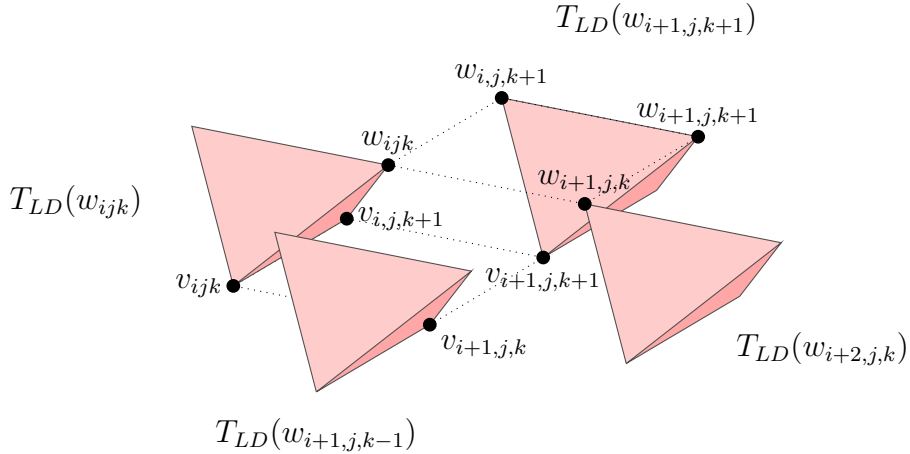


Figure 5.4: The situation described in the proof of lemma 5.10. The indices i and k are even.

where

$$\diamondsuit(v) := \{T_{UF}(v), T_{UL}(v), T_{UB}(v), T_{UR}(v)\},$$

The set $\diamondsuit(v)$ is a tetrahedral partition of the octahedron $O_U(v)$ defined in 2.19. Notice that the classes K_2 , K_3 and K_4 also form a decomposition of Δ_{BCC} , just like the classes K_0 and K_1 . The arrangement of the tetrahedra in these classes is shown in figure 5.3 on the right.

Lemma 5.10 showed that each vertex of Δ_{BCC} belongs to a unique tetrahedron in class K_0 . The tetrahedra of class K_2 have a similar property, regarding the edges of Δ_{BCC} , as the following two lemmas show.

Lemma 5.12. *Let T be a tetrahedron belonging to class K_3 . Then for each edge e of T , there exists a unique $T_e \in K_2$ with $T \cap T_e = e$.*

Proof. Fix $T \in K_3$.

Suppose $T = T_{BD}(w_{ijk})$. Then each interior edge of T is shared by one of the tetrahedra $T_{LD}(w_{ijk})$, $T_{LD}(w_{i+1,j,k})$, $T_{LD}(w_{i,j,k+1})$, $T_{LD}(w_{i+1,j,k+1})$, $T_{BU}(w_{ijk})$, or $T_{BU}(w_{i,j-1,k})$, which belong to K_2 .

Now suppose $T = T_{LU}(w_{ijk})$. Then each edge of T is shared either with a tetrahedron $T_{BU}(w_{ijk})$, $T_{BU}(w_{i-1,j,k})$, $T_{BU}(w_{i,j,k-1})$, $T_{BU}(w_{i-1,j,k-1})$, $T_{LD}(w_{ijk})$ or $T_{LD}(w_{i,j+1,k})$. These tetrahedra also belong to K_2 .

Figure 5.5 depicts the situation. □

Lemma 5.13. *Let $v \in \mathcal{V}_{BCC}$ and e a boundary edge of $\diamondsuit(v)$. Then there exists a unique $T_e \in K_2$ with $T \cap T_e = e$.*

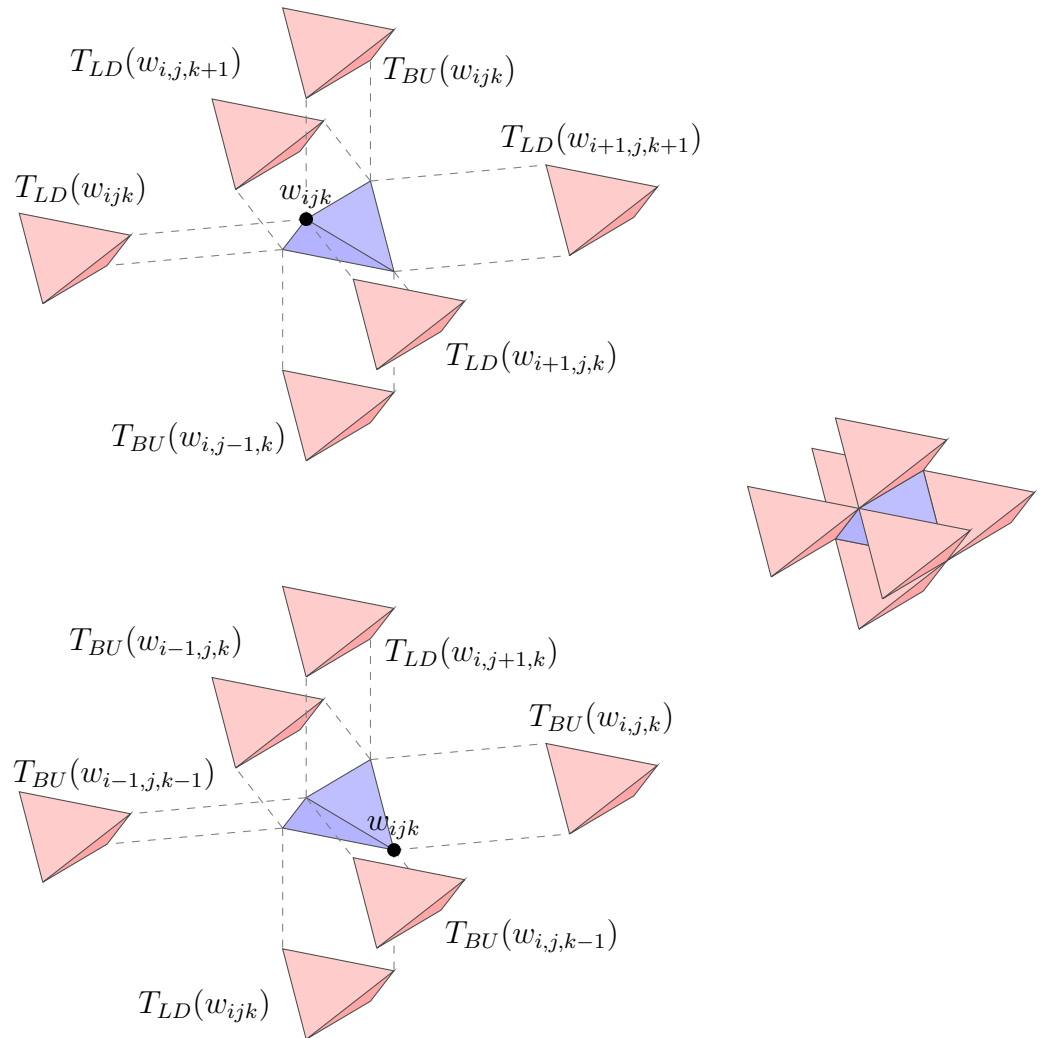


Figure 5.5: The situation described in lemma 5.12. All edges of a tetrahedron T belonging to class K_3 (blue), are shared with the tetrahedra belonging to class K_2 (red). The left side shows exploded views for the case $T = T_{BD}(w_{ijk}) \in L^2$ (top left), and for the case $T = T_{LU}(w_{ijk}) \in L^4$ (bottom left).

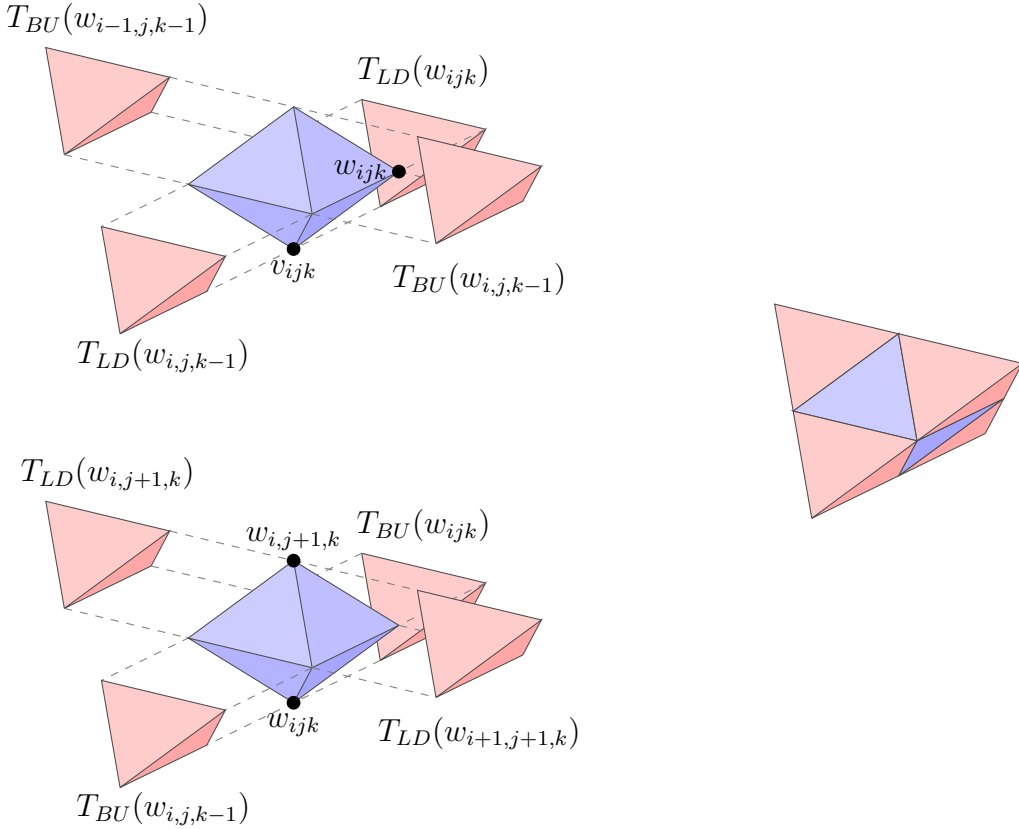


Figure 5.6: The situations described in lemma 5.13. All edges of a tetrahedron T belonging to class K_4 , except for the interior edge of the octahedron $\diamond(v)$ (blue) which T belongs to, are shared with the tetrahedra belonging to class K_2 (red). On the left, exploded views for both cases described in the lemma are shown.

Proof. As in lemma 5.12, there are two cases to consider.

Suppose $v = v_{ijk} \in \mathcal{V}_H$. Then the tetrahedra $T_{LD}(w_{ijk})$, $T_{LD}(w_{i,j,k-1})$, $T_{BU}(w_{i,j,k-1})$ and $T_{BU}(w_{i-1,j,k-1})$, which are in K_2 , share one face each with the tetrahedra in $\diamond(v)$, such that all boundary edges of $\diamond(v)$ are shared by these tetrahedra.

Likewise, if $v = w_{ijk} \in \mathcal{W}_H$, all boundary edges of $\diamond(v)$ are shared by the tetrahedra $T_{BU}(w_{ijk})$, $T_{BU}(w_{i,j,k-1})$, $T_{LD}(w_{i,j+1,k})$ and $T_{LD}(w_{i+1,j+1,k})$ which belong to K_2 .

Figure 5.6 shows how these tetrahedra surround $\diamond(v)$. \square

We now describe the finite subset of the BCC partition on which the interpolating splines are constructed. For the remainder of this section, let Δ_{BCC} be the BCC partition with spacing $H := (h_1, h_2, h_3)$, as defined in 2.20.

Definition 5.14. Given three odd integers $N_1, N_2, N_3 \geq 3$, we define the following sets of tetrahedra.

$$\begin{aligned} L_j^1 &:= \{T_{LD}(w_{ijk}); 0 \leq i < N_1, 0 \leq k < N_3\}, \\ L_j^2 &:= \{T_{BD}(w_{ijk}); 0 \leq i < N_1 - 1, 0 \leq k < N_3 - 1\}, \\ L_j^3 &:= \bigcup \diamond(v_{ijk}), \quad 0 \leq i < N_1, 1 \leq k < N_3, \\ L_j^4 &:= \{T_{LU}(w_{ijk}); 0 \leq i < N_1, 0 \leq k < N_3\}, \\ L_j^5 &:= \{T_{BU}(w_{ijk}); 0 \leq i < N_1 - 1, 0 \leq k < N_3 - 1\}, \\ L_j^6 &:= \bigcup \diamond(w_{ijk}), \quad 0 \leq i < N_1 - 1, 0 \leq k < N_3. \end{aligned}$$

Moreover, we define

$$\begin{aligned} L^1 &:= \bigcup_{j=0}^{N_2-1} L_j^1, & L^2 &:= \bigcup_{j=1}^{N_2-2} L_j^2, & L^3 &:= \bigcup_{j=0}^{N_2-2} L_j^3, \\ L^4 &:= \bigcup_{j=0}^{N_2-2} L_j^4, & L^5 &:= \bigcup_{j=0}^{N_2-2} L_j^5, & L^6 &:= \bigcup_{j=0}^{N_2-2} L_j^6. \end{aligned}$$

Then the tetrahedral partition Δ is defined by

$$\Delta := \bigcup_{k=1}^6 L^k.$$

The sets L_j^1, \dots, L_j^6 can be interpreted as layers of tetrahedra which are stacked to construct the partition Δ . Each layer is a subset of one of the classes K_2 - K_4 . More precisely, $L^1 \cup L^5 \subset K_2$, $L^2 \cup L^4 \subset K_3$, and $L^3 \cup L^6 \subset K_4$. These layers are shown in figure 5.7. A small partition Δ is depicted in figure 5.8.

During the interpolation process, we use lemmas 5.10, 5.12 and 5.13 to decide which B-coefficients are determined by smoothness conditions. However, Δ is a finite partition, and special situations arise at the boundary. In particular, for some boundary vertices, there exists no K_0 -tetrahedron in Δ which shares the vertex. Similarly, not all boundary edges are shared by a K_2 -tetrahedron in Δ . These missing K_0 and K_2 -tetrahedra are replaced by tetrahedra in Δ .

Definition 5.15. Given the tetrahedral partition Δ from 5.14, we define

$$\begin{aligned} K'_1 &:= \{T \in L^1; T \text{ shares exactly 3 vertices with the tetrahedra in } K_0\}, \\ K'_3 &:= \{T \in K_3 \cap \Delta; T \text{ shares exactly 4 edges with the tetrahedra in } K_2\}, \\ K''_3 &:= \{T \in K_3 \cap \Delta; T \text{ shares exactly 3 edges with the tetrahedra in } K_2\}. \end{aligned}$$

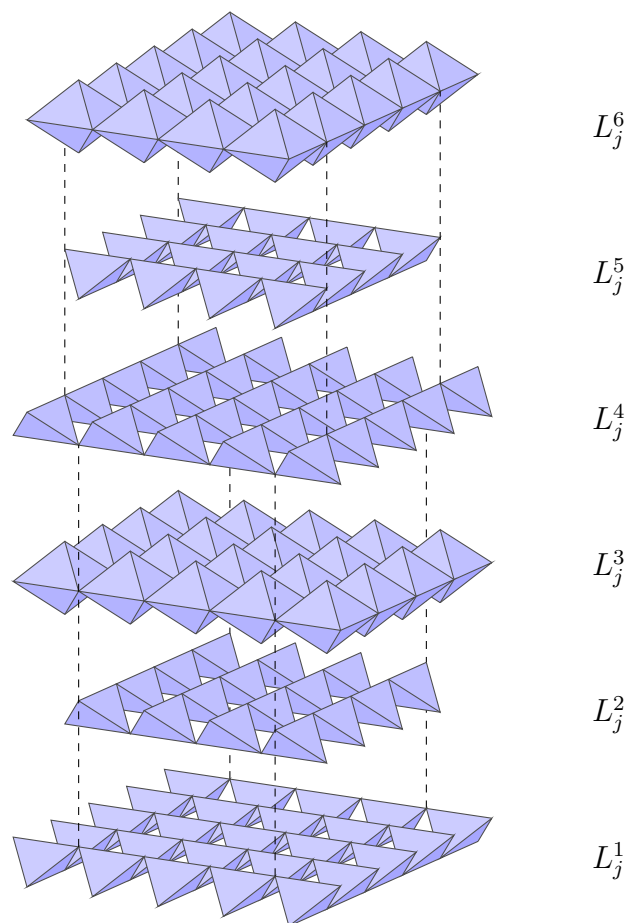


Figure 5.7: Exploded view of the layers L_j^1, \dots, L_j^6 of a partition Δ constructed with $N_1 = N_3 = 5$. The dashed lines indicate how the layers are stacked.

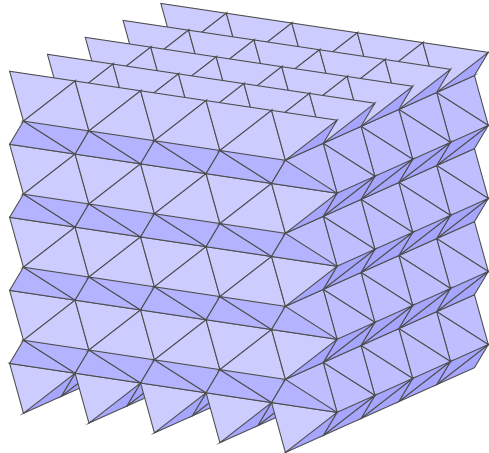


Figure 5.8: The subset Δ of the BCC partition which is used in the Lagrange interpolation method, with parameters $N_1 = N_2 = N_3 = 5$.

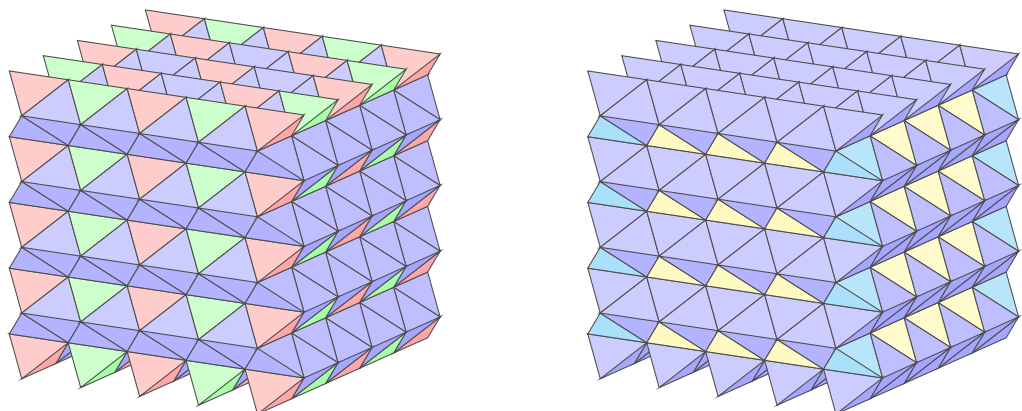


Figure 5.9: The additional classes of boundary tetrahedra defined in 5.15. On the left, the class K'_1 is shown in green, while the red tetrahedra represent the original class K_0 . On the right, the classes K'_3 and K''_3 are shown in yellow and cyan, respectively.

The additional classes are shown in figure 5.9.

We proceed to construct a refinement of the tetrahedral partition Δ by subdividing certain tetrahedra using a partial Worsey-Farin split. When applying the splits, we use the following principles to choose the split points. Whenever a partial Worsey-Farin split is applied to a tetrahedron T , we use the incenter of T as the inner split point. If a face F of T is split, and if F is a boundary face of Δ , we use the barycenter of F as the face split point. If F is an interior face of Δ , and \tilde{T} is the neighbor of T which shares F , then we use the intersection of F with the line connecting the incenters of T and \tilde{T} as the face split point. This choice of split points provides the C^1 -smoothness across the common face of T and \tilde{T} , as shown in theorems 4.1 and 4.2 of [89]. The splits are defined using the classes K_2 - K_4 .

Definition 5.16. Let Δ be the tetrahedral partition defined in 5.14. Then the tetrahedral partition Δ^* is obtained from Δ as follows.

- (i) Each tetrahedron $T \in \Delta \cap K_2$ is not subdivided.
- (ii) For each tetrahedron $T \in \Delta \cap K_3$, all faces of T which are interior faces of Δ are split using a Clough-Tocher split. A partial Worsey-Farin split is then applied accordingly.
- (iii) For each tetrahedron $T \in \Delta \cap K_4$, all faces of T which are not shared with some tetrahedron $\tilde{T} \in \Delta \cap K_2$ are split using a Clough-Tocher split. A partial Worsey-Farin split is then applied accordingly.

Each edge of Δ has a corresponding edge in Δ^* . We call these edges the primary edges of Δ^* . Likewise, each face of Δ has a corresponding face in Δ^* , which may be subdivided by a Clough-Tocher split. We call these faces the primary faces of Δ^* .

The partition Δ^* consists of the following partial Worsey-Farin splits. The tetrahedra in class K'_3 are subdivided by a 3-rd degree partial Worsey-Farin split. The boundary faces of these tetrahedra are not subdivided. A 2-nd degree partial Worsey-Farin split is applied to the tetrahedra in class K''_3 . Again, the boundary faces remain un-split. These two cases are depicted in figure 5.10. The remaining tetrahedra in class $K_3 \cap \Delta$ are subdivided by a full Worsey-Farin split. For all tetrahedra in class $K_4 \cap \Delta$ that have no boundary faces, a 3-rd degree partial Worsey-Farin split is used. These tetrahedra share one face with a K_2 -tetrahedron, which is the face that is not split. The remaining tetrahedra in class $K_4 \cap \Delta$ have two boundary faces. Those tetrahedra are subdivided using a full Worsey-Farin split.

We introduce two algorithms to construct a Lagrange interpolation set for $\mathcal{S}_3^1(\Delta^*)$. Notice that both algorithms operate on the tetrahedra of the

original triangulation Δ , while the output is a subset of the domain points of Δ^* . The first algorithm constructs an interpolation set for the primary edges of Δ^* .

Algorithm 5.17. For a tetrahedron $T := \langle v_0, v_1, v_2, v_3 \rangle$, let

$$\mathcal{M}_E(T) := \bigcup_{m=0}^3 D_1^T(v_m).$$

- 1) Set $\mathcal{X}_E := \emptyset$.
- 2) For each $T \in \Delta \cap K_0$, update $\mathcal{X}_E \leftarrow \mathcal{X}_E \cup \mathcal{M}_E(T)$.
- 3) For each $T \in \Delta \cap K'_1$, update $\mathcal{X}_E \leftarrow \mathcal{X}_E \cup D_1^T(v)$, where v is the vertex of T which is not shared by some tetrahedron $\tilde{T} \in K_0$.

The second algorithm constructs the interpolation points on the primary faces of Δ^* .

Algorithm 5.18. For a tetrahedron T , let

$$\mathcal{M}_F(T) := \{\xi_{1110}^T, \xi_{1011}^T, \xi_{1101}^T, \xi_{0111}^T\}.$$

- 1) Set $\mathcal{X}_F := \emptyset$.
- 2) For each $T \in \Delta \cap K_2$, update $\mathcal{X}_F \leftarrow \mathcal{X}_F \cup \mathcal{M}_F(T)$.
- 3) For each $T \in \Delta \cap (K'_3 \cup K''_3)$:
 - 3.1) For each face F of T :
 - a) If exactly two edges of F are shared by tetrahedra in class K_2 , then update $\mathcal{X}_F \leftarrow \mathcal{X}_F \cup \{v_F\}$.
- 4) For each octahedron $\diamondsuit(v) \subset \Delta$:
 - 4.1) If there exists a boundary tetrahedron $\tilde{T} \in \diamondsuit(v)$ then:
 - a) Set $T := \tilde{T}$.
 - b) For each boundary face F of T , update $\mathcal{X}_F \leftarrow \mathcal{X}_F \cup v_F$.
 - else
 - a) Set $T := T_{UB}(v)$.
- 4.2) For each face F of T which is an interior face of $\diamondsuit(v)$, update $\mathcal{X}_F \leftarrow \mathcal{X}_F \cup v_F$.

The domain points added by step 3) of the algorithm are shown in figure 5.10.

We proceed with the main results of this section.

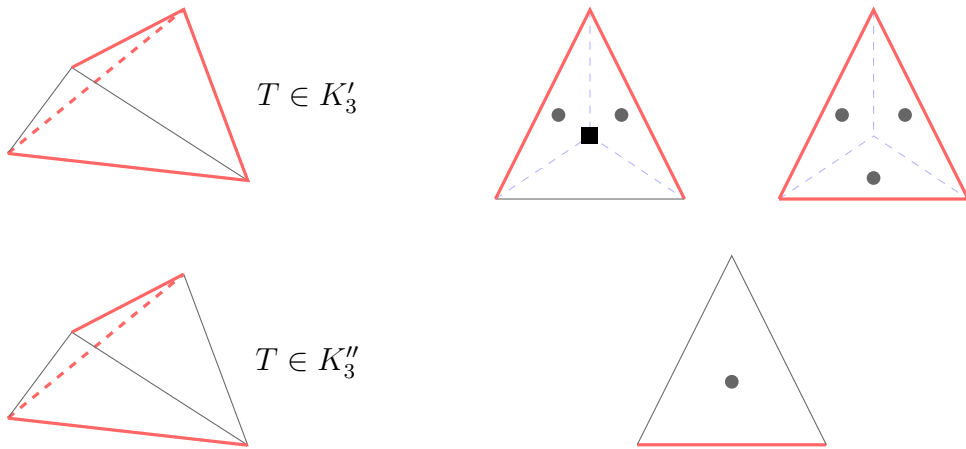


Figure 5.10: On the left, two tetrahedra representing the classes K'_3 and K''_3 are shown. The red edges are shared by tetrahedra in $K_2 \cap \Delta$. On the right, the three different situations for the faces are depicted. A face F with two red edges is split by a Clough-Tocher split, and the split point v_F is contained in the set \mathcal{X}_F constructed by algorithm 5.18. The face with three red edges is also split, but no points in its interior are contained in \mathcal{X}_F . Those faces are interior faces of Δ , while the other faces are boundary faces. The gray dots symbolize domain points whose associated B-coefficients are determined by smoothness conditions across the red edges.

Theorem 5.19. *The set $\mathcal{X} := \mathcal{X}_E \cup \mathcal{X}_F$, constructed by algorithms 5.17 and 5.18, is a minimal determining set for $\mathcal{S}_3^1(\Delta^*)$.*

Proof. Let $s \in \mathcal{S}_3^1(\Delta^*)$. Suppose that all B-coefficients of s associated with the domain points in \mathcal{X} are known. We consider the tetrahedra of the original partition Δ and show that the B-coefficients associated with the corresponding partial Worsey-Farin splits are uniquely determined. Then \mathcal{X} is consistent, and thus minimal.

We first consider the primary edges of Δ^* . Notice that for each domain point ξ associated with an edge of a tetrahedron T , there exists a unique vertex v of T with $\xi \in D_1^T(v)$. Since all domain points associated with the edges of the K_0 -tetrahedra are contained in \mathcal{X} , it suffices to consider the tetrahedra in $K_1 \cap \Delta$. Suppose $T \in K'_1$. Then by lemma 5.10, T shares three vertices with the tetrahedra in K_0 . Let v be such a vertex. Since all domain points associated with $D_1^T(v)$ sit on the edges of T , their associated B-coefficients are determined by corollary 2.60. They are uniquely determined since the balls $D_1^T(v)$ and $D_1^T(\tilde{v})$ are disjoint for two different vertices v and \tilde{v} of T . Now let v be the remaining vertex of T . Then the ball $D_1^T(v)$ is contained in \mathcal{X} , and thus all domain points associated with the edges of T are either contained in \mathcal{X} , or uniquely determined by smoothness conditions. Now suppose $T \in K_1 \cap \Delta \setminus K'_1$. Then for each vertex v of T , there exists a

tetrahedron $T_v \in (K_0 \cap \Delta) \cup K'_1$ with $D_1^{T_v}(v) \subset \mathcal{X}$. Again, all B-coefficients associated with $D_1^T(v)$ are uniquely determined by the smoothness conditions from corollary 2.60.

At this point, we have shown that all B-coefficients associated with the primary edges of Δ^* are either contained in \mathcal{X} , or uniquely determined by smoothness conditions from the known coefficients in \mathcal{X} . Now we consider the primary faces of Δ^* . Suppose $T \in K_2 \cap \Delta$ and F is a face of T . Of the ten B-coefficients of F , nine are associated with the primary edges of Δ^* . The remaining B-coefficient is contained in the set $\mathcal{M}_F(T)$ defined in algorithm 5.18. By step 2) of this algorithm, it is also contained in \mathcal{M} .

Now suppose $T \in K'_3$. Of the four faces of T , one shares three edges with tetrahedra in class K_2 . This face is an interior face has been subdivided by a Clough-Tocher split, according to definition 5.16 (ii). Let e be a shared edge, then the B-coefficients associated with $t_1^T(e)$ are uniquely determined by smoothness conditions, according to corollary 2.60. But then, by theorem 5.8, all remaining B-coefficients of this face are also uniquely determined. The two other interior faces of T have two edges that are shared with tetrahedra in class K_2 . These faces have also been split, and the split point has been added to $\mathcal{M}_F(T)$ in step 3.1) of algorithm 5.18. By corollary 5.7, all other B-coefficients associated with these faces are also uniquely determined. The last face of T is a boundary face of Δ . This face has not been split, and one of the edges is shared by a K_2 -tetrahedron. Here, the B-coefficient associated with the barycenter is determined by a C^1 smoothness condition across the shared edge. These three situations are depicted in figure 5.10

Now let $T \in K''_3$. The situation here is quite similar to the one previously discussed. Here, two of the faces are interior faces, and two edges of each face are shared by K_2 -tetrahedra. The other two edges are boundary faces whose barycenters have been added to $\mathcal{M}_F(T)$. Both situations have been discussed in the previous paragraph, and are also shown in figure 5.10.

The remaining tetrahedra in K_3 have been subdivided by a full Worsey-Farin split, and by lemma 5.12, each edge is shared by some K_2 -tetrahedron. We established in the discussion of the K'_3 -tetrahedra that all B-coefficients associated with such faces are uniquely determined.

Finally, we consider the tetrahedra in class K_4 , which belong to the octahedra $\diamondsuit(v)$. For each of these octahedra, a tetrahedron T has been singled out in step 4) of algorithm 5.18. Suppose T is a boundary tetrahedron. Then two of the faces of T are boundary faces of Δ , and the remaining two are interior faces of $\diamondsuit(v)$. Two of the edges of each of these faces are shared by tetrahedra in class K_2 , K'_3 or K''_3 , as shown in figure 5.11. In either case, the barycenter of these faces has been added to $\mathcal{M}_F(T)$ in step 4.1 b) or 4.2) of the algorithm 5.18. Again, the remaining B-coefficients are uniquely determined. If T is not a boundary tetrahedron, then one of the faces of T

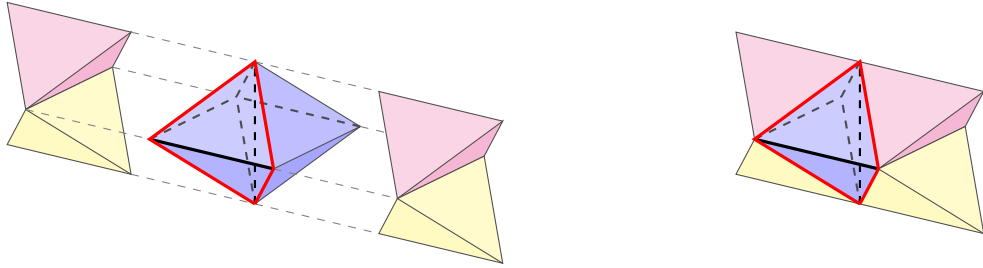


Figure 5.11: A boundary tetrahedron in class K_4 . The red edges are shared by tetrahedra in class K_2 (magenta), and K'_3 or K''_3 (yellow). The thick black edge is the boundary edge.

is shared by some tetrahedron in K_2 , according to lemma 5.13. All domain points of this face are contained in $\mathcal{M}_F(T)$. By the same lemma, one other face of T has three edges which are shared by tetrahedra in class K_2 , and all B-coefficients associated with that face are also uniquely determined. The remaining two faces are interior faces of $\diamond(v)$. Two edges of each of these faces are shared by tetrahedra in class K_2 , and their barycenters have been added to $\mathcal{M}_F(T)$ in step 4.2) of the algorithm 5.18. Hence, all B-coefficients associated with these faces are uniquely determined. Let \tilde{T} be one of the remaining three tetrahedra of $\diamond(v)$. One of the faces of \tilde{T} is shared by some tetrahedron in class K_2 . The other faces of \tilde{T} are subdivided, and their edges are shared either by T or by K_2 -tetrahedra. Thus, all their associated B-coefficients are uniquely determined.

By now all B-coefficients associated with the primary faces of Δ^* are uniquely determined. But then theorem 5.8 shows that all B-coefficients associated with the interior of the tetrahedra are also uniquely determined. The C^1 smoothness conditions across the primary faces of Δ^* are satisfied due to the choice of the split points on the faces, according to theorems 4.1 and 4.2 of [89]. This completes the proof. \square

Since \mathcal{X} is a minimal determining set for $\mathcal{S}_3^1(\Delta^*)$, we can easily define a quasi-interpolation operator for $(\mathcal{X}, \mathcal{S}_3^1(\Delta^*))$ by giving a B-coefficient computation rule for each B-coefficient associated with \mathcal{X} . The rules for the remaining B-coefficients are then defined implicitly by the smoothness conditions of the spline space. To construct a Lagrange interpolation operator, we have to show that \mathcal{X} is a Lagrange interpolation set for $\mathcal{S}_3^1(\Delta^*)$.

Theorem 5.20. *The set $\mathcal{X} := \mathcal{X}_E \cup \mathcal{X}_F$, constructed by algorithms 5.17 and 5.18, is a Lagrange interpolation set for $\mathcal{S}_3^1(\Delta^*)$.*

Proof. By theorem 5.19, \mathcal{X} is a consistent determining set for $\mathcal{S}_3^1(\Delta^*)$. Hence, by theorem 2.62, $\dim \mathcal{S}_3^1(\Delta^*) = \#\mathcal{X}$. We have to show that for all $f \in C(\Omega)$

there exists a unique spline $s \in \mathcal{S}_3^1(\Delta^*)$ satisfying $s(x) = f(x)$ for all $x \in \mathcal{X}$. Fix $f \in C(\Omega)$. We closely follow the proof of theorem 5.19. We traverse the partition Δ tetrahedron by tetrahedron in the order prescribed by the classification and construct a spline s_f from the interpolation conditions. In the first part of this proof, we show how the B-coefficients associated with the primary edges of Δ^* are uniquely determined.

Let $T \in K_0 \cap \Delta$. All B-coefficients associated with the edges of T are contained in \mathcal{M}_E . Let e be such an edge. By lemma 5.3, the conditions $s_f(x) = f(x)$, $x \in \mathcal{M}_E \cap e$ uniquely determine the B-coefficients of s_f associated with e .

Now let $T \in K'_1$. Then three of the vertices of T are shared by tetrahedra in class K_0 . The B-coefficients of s_f associated with the edges of these tetrahedra are already determined. By corollary 2.60, this also determines the B-coefficients associated with $D_1^T(v)$ for the three shared vertices. The domain points $D_1^T(\tilde{v})$ of the remaining vertex \tilde{v} are contained in \mathcal{X}_E . By lemma 5.4, the B-coefficients of s_f associated with these domain points are uniquely determined by the Lagrange interpolation conditions $s_f(x) = f(x)$, $x \in D_1^T(\tilde{v})$.

Let $T \in K_1 \cap \Delta \setminus K'_1$. Then each vertex of T is shared by some tetrahedron in $K_0 \cup K'_1$, and all B-coefficients of s_f associated with the edges of T are uniquely determined by smoothness conditions at these vertices.

At this point, the restriction of s_f to the primary edges of Δ is uniquely determined by the Lagrange interpolation conditions $s_f(x) = f(x)$, $x \in \mathcal{X}_E$. We proceed to the primary faces of Δ .

Let $T \in K_2$ and F a face of T . Then the B-coefficient associated with the barycenter x_F of F is contained in \mathcal{X}_F . Since the B-coefficients associated with the edges of F are already known, $s_{f|F}$ is uniquely determined by $s_f(x_F) = f(x_F)$, according to lemma 5.5. Notice that by now all B-coefficients associated with the K_2 -tetrahedra are uniquely determined.

Let $T \in K'_3$. One of the faces of T shares three edges with tetrahedra in K_2 , and it has been shown in the proof of the previous theorem that all B-coefficients associated with this face are uniquely determined by smoothness conditions from known coefficients. The boundary face of T shares one edge with some K_2 -tetrahedron. This face is not split, and the B-coefficient associated with the barycenter is determined by a smoothness condition across the shared edge. The B-coefficients of s_f associated with the remaining two faces are uniquely determined by the Lagrange interpolation condition $s_f(x_F) = f(x_F)$, according to lemma 5.6, where x_F is the split point of F .

Let $T \in K''_3$. Two of the faces of T share one edge each with K_2 -tetrahedra, while the other two faces share two edges each with the K_2 -tetrahedra. In the former case, the face is not split and the remaining B-coefficient is determined by a smoothness condition across the shared edge. In the latter case, 5.6 is used to determine the B-coefficients of s_f associated

with the face, since the split point is contained in \mathcal{X}_F .

The remaining tetrahedra in K_3 have been subdivided by a full Worsey-Farin split. All their primary edges are shared by K_2 -tetrahedra, and all B-coefficients associated with their faces are determined from smoothness conditions, as described in the proof of the previous theorem.

We now consider the tetrahedra in K_4 . We begin with the tetrahedra that have been singled out in step 4) of algorithm 5.18. Let T be such a tetrahedron. If T is a boundary tetrahedron, then the set \mathcal{X}_F contains the four split points x_F of these faces, and the B-coefficients of s_f associated with these faces are uniquely determined from the Lagrange interpolation conditions $s_f(x_F) = f(x_F)$ according to lemma 5.6. In the case that T is an interior tetrahedron, one of the faces of T is shared by a K_2 -tetrahedron. This face is not split, and all its B-coefficients are already determined. Another face of T has three edges that are shared by K_2 -tetrahedra. The B-coefficients of s_f associated with that face are uniquely determined by C^1 -conditions across the shared edges, as discussed in the proof of the previous theorem. The remaining two faces share two edges each with K_2 -tetrahedra, and their split points are contained in \mathcal{X}_F . Thus, the B-coefficients of s_f associated with these faces are determined by the smoothness conditions $s_f(x_F) = f(x_F)$ and lemma 5.6. The remaining tetrahedra in K_4 share one face with a K_2 -tetrahedron, two different edges with tetrahedra in K_2 , and the last edge with the tetrahedron that has been singled out in step 4) of algorithm 5.18. The B-coefficients on the shared face are already determined, and the remaining B-coefficients of s_f associated with these faces are determined by smoothness conditions.

By now, all B-coefficients of s_f associated with the primary faces of Δ^* have been uniquely determined from the values $f(x)$, $x \in \mathcal{X}$. It has already been established in proof of the previous theorem that the remaining B-coefficients of s_f are determined by smoothness conditions, using theorem 5.8. \square

Since we established that \mathcal{X} is a Lagrange interpolation set, we can now define a Lagrange interpolation operator.

Definition 5.21. *For each $f \in C(\Omega)$, let s_f be the spline constructed in the proof of theorem 5.20. Then \mathcal{L} is the Lagrange interpolation operator defined by $\mathcal{L}(f) := s_f$.*

The following theorems establish the locality and stability of the operator. The locality is measured in stars of the original partition Δ . This technique to measure the locality has also been used in [41, 42, 54, 55, 62] and allows a comparison with these methods.

Theorem 5.22. *The Lagrange interpolation operator \mathcal{L} defined in 5.21 is 2-local in the following sense. For each $T \in \Delta$, let $\Delta_{WF}^*(T)$ be the partial Worsey-Farin split of T which has been defined in 5.16, and*

$$\mathcal{X}_T^* := \bigcup_{\tilde{T} \in \Delta_{WF}^*(T)} \mathcal{X}_{\tilde{T}}.$$

Then

$$\mathcal{X}_T^* \subset \text{star}^2(T).$$

Proof. We show that for each $T \in \Delta$, the B-coefficients of $\mathcal{L}(f)|_T$ are determined only by values $f(x)$ with $x \in \text{star}^2(T)$. This proof uses the arrangement of the different classes of tetrahedra. Figures 5.3 and 5.9 depict the position of the classes relative to each other.

The classification process establishes a hierarchy of tetrahedra, such that the computation of the B-coefficients of a given K_m -tetrahedron T depends only on values that are associated with the tetrahedron itself, or with tetrahedra of a lower classes that share a common vertex, edge, or face with T . We symbolize this hierarchy with the arrow symbol, where $K_n \leftarrow K_m$ means that the computation of a K_m -tetrahedron may depend on K_n -tetrahedra. The full hierarchy then is

$$K_0 \leftarrow K'_1 \leftarrow K_1 \quad \text{and} \quad K_2 \leftarrow K'_3 \cup K''_3 \cup K_3 \leftarrow K_4.$$

Notice that the tetrahedra of $K'_3 \cup K''_3 \cup K_3$ share no edges with each other, and thus do not depend on each other. Since each tetrahedron belongs to two classes, we have to take the class combinations into account.

Let $T \in K_2 \cap K_0$. then all B-coefficients associated with T are computed from values sitting on T , and thus $\mathcal{X}_T^* \subset \text{star}^0(T)$. If $T \in K_2 \cap K'_1$, then the B-coefficients associated with the edges of T also depend on the B-coefficients of the K_0 tetrahedra surrounding T , and thus $\mathcal{X}_T^* \subset \text{star}^1(T)$. In the case that $T \in K_2 \cap K_1$, the computation also depends on the surrounding K_0 -tetrahedra. There are no surrounding K'_1 -tetrahedra for T , and hence $\mathcal{X}_T^* \subset \text{star}^1(T)$.

Let $T \in K'_3 \cup K''_3 \cup K_3$. Then the computation of the B-coefficients associated with T depends on the surrounding K_2 -tetrahedra, since some of them are determined by smoothness conditions across the shared edges (see figure 5.5). Thus, $\mathcal{X}_T^* \subset \text{star}^2(T)$.

Now let $T \in K_4$. Then T belongs to some octahedron $\diamond(v)$. If $\diamond(v)$ has no boundary faces in Δ , then the B-coefficients associated with $\diamond(v)$ are determined by the surrounding K_2 -tetrahedra, and by interpolation on $\diamond(v)$ itself. Thus, $\mathcal{X}_T^* \subset \text{star}^2(T)$. Finally, let $T \in K_4$ be a boundary tetrahedron of some octahedron $\diamond(v)$, as shown in figure 5.11. In this case, the B-coefficients of T not only depend on the surrounding K_2 -tetrahedra, but

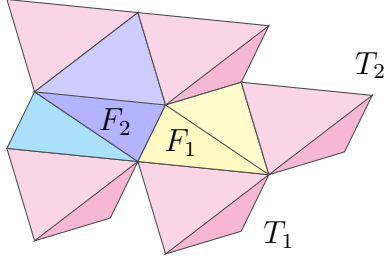


Figure 5.12: The computation of the B-coefficients associated with a blue boundary tetrahedron T in class K_4 depends not only on the surrounding K_2 -tetrahedra (top magenta), but also on the tetrahedra in $K'_3 \cup K''_3$ (yellow and cyan). These, in turn, depend on other K_2 -tetrahedra (bottom magenta), in particular on the tetrahedron $T_2 \in \text{star}^2(T)$.

also on the tetrahedra in $K'_3 \cup K''_3$, who in turn depend on their surrounding K_2 -tetrahedra. Figure 5.12 depicts this case. Notice that the tetrahedron T_2 in this figure has no direct influence on T . The only influence of the yellow K'_3 -tetrahedron on T is the smoothness condition between the faces F_1 and F_2 . But since the B-coefficients associated with F_1 depend only on T_1 and not T_2 , the computations stays 2-local. \square

Theorem 5.23. *The Lagrange interpolation operator \mathcal{L} defined in 5.21 is stable in the following sense. There exists a constant K , depending only on the shape parameter of the BCC partition, such that for each $T \in \Delta$,*

$$\mathcal{L}(f)|_T \leq K \max_{x \in \mathcal{X}_T^*} f(x)$$

for all $f \in \mathcal{F}_{\mathcal{X}}$.

Proof. By the locality of the operator, $\mathcal{L}(f)|_T$ depends only on the values $f(x)$, $x \in \mathcal{X}_T^*$. We show that each B-coefficient associated with T is bounded. The B-coefficients are calculated successively from the data values and known B-coefficients by one of the following processed.

- (i) By a C^1 smoothness conditions (2.17) between two neighboring tetrahedra T and \tilde{T} .

These smoothness conditions have the form

$$c = b_0\varphi_0 + b_1\varphi_1 + b_2\varphi_2 + b_3\varphi_3,$$

where the b_i are known coefficients associated with T and the φ_i are the barycentric coordinates of a vertex on \tilde{T} , relative to T . Since the partition is uniform, there exists an constant $K_0 \geq 0$, depending only on the shape parameter K_H of the BCC partition, such that $|c| \leq K_0 \max_{m=0}^3 |b_m|$.

- (ii) By interpolation at the domain points of a primary edge, as described in lemma 5.3.

The B-coefficients are computed as the solution of the linear system (5.1), and thus there is an absolute constant $K_1 \geq 0$ such that

$$|c_{ij}| \leq K_1 \max_{i+j=3} |f_{ij}|.$$

- (iii) By interpolation at two of the domain points of a primary edge, as described in lemma 5.4.

Here, one of the B-coefficients is equal to the data value, while the other one is directly computed as a linear combination (5.2) of known coefficients and data values. Hence, there exists an absolute constant $K_2 \geq 0$ with

$$|c_{ij}| \leq K_2 \max\{|c_{30}|, |c_{21}|, |f_{12}|, |f_{03}|\}.$$

- (iv) By interpolation at the barycenter of a face, as described in lemma 5.5.

The B-coefficient is calculated directly by (5.3) from known B-coefficients and a data value, and thus there exists an absolute constant $K_3 \geq 0$ with

$$|c_{111}| \leq K_3 c_{max},$$

where c_{max} is the maximum of the absolutes of the known B-coefficients and the data value.

- (v) By interpolation on a face that has been split using a Clough-Tocher split, as described in lemma 5.6.

In this case, the B-coefficients are computed either by C^1 smoothness conditions as in (i), or by solving the linear system (5.4). Let C be a vector containing the known B-coefficients and data values referred to in the lemma. Then there exists a constant $K_4 \geq 0$ such that for any B-coefficient c that is computed in the lemma,

$$c \leq K_4 \|C\|_\infty.$$

The constant K_4 depends on the position of the split point, which in turn depends on the shape parameter K_H of the BCC partition.

Note that $\mathcal{L}(f)|_T$ is either a polynomial or a spline defined on a partial Worsey-Farin split of T . By theorem 2.42, each polynomial piece of $\mathcal{L}(f)|_T$ is bounded by the maximum of the absolute values of its associated B-coefficients. But these B-coefficients have been computed successively from the data values of f by the processes (i)-(iv). Moreover, by the locality of \mathcal{L} established in theorem 5.22, they have been computed only from the values

$f(x)$, $x \in \mathcal{X}_T^*$. Thus there exists a constant $K \geq 0$, which is a combination of the constants K_0, \dots, K_4 , and hence depends only on the shape parameter K_H , such that

$$\mathcal{L}(f)|_T \leq K \max_{x \in \mathcal{X}_T^*} f(x).$$

□

5.2 Error bounds

In the final part of this chapter, we establish an error bound for the Lagrange interpolation operator defined in 5.21. Analogously to the error bounds in section 3.4 of chapter 3, we provide a local result, estimating the approximation error on one tetrahedron, and a global result for the error on the entire tetrahedral partition.

Theorem 5.24. *Let \mathcal{L} be the Lagrange interpolation operator defined in 5.21 and Δ the tetrahedral partition defined in 5.14. Fix $T \in \Delta$ and let*

$$\Omega_T := \bigcup_{\tilde{T} \in \text{star}^2(T)} \tilde{T}.$$

Then for every $f \in C^{m+1}(\Omega_T)$ with $0 \leq m \leq 3$,

$$\|D^\alpha(\mathcal{L}(f) - f)\|_T \leq K|T|^{m+1-|\alpha|}|f|_{m+1,\Omega_T}, \quad 0 \leq |\alpha| \leq m, \quad (5.5)$$

where K is a constant depending only on the shape parameter K_H of the BCC partition, and on the Lipschitz constant of the boundary of Ω_T .

Proof. Let p_f be the m -th degree Taylor polynomial associated with f , defined in theorem 2.29. Then there exists a constant \tilde{K}_m , depending only on m and the Lipschitz constant of the boundary of Ω_T , such that

$$\|D^\beta(f - p_f)\|_{\Omega_T} \leq \tilde{K}_m |\Omega_T|^{m+1-|\beta|} |f|_{m+1,\Omega_T}, \quad 0 \leq |\beta| \leq m.$$

Let $K_0 := \max_{m=0}^3 \tilde{K}_m$. By lemma 2.10, $|\Omega_T| \leq 6|\Delta|$. Since Δ is a subset of Δ_{BCC} , this can be further estimated using lemma 2.23 (i), and we obtain $|\Omega_T| \leq 6|T|/K_H$. $K_H \leq 1$, and thus

$$\|D^\beta(f - p_f)\|_{\Omega_T} \leq K_1 |T|^{m+1-|\beta|} |f|_{m+1,\Omega_T}, \quad 0 \leq |\beta| \leq m, \quad (5.6)$$

where $K_1 := 6^4 K_0 / K_H^4$. Using the triangle inequality and the linearity of D^α , we obtain

$$\|D^\alpha(\mathcal{L}(f) - f)\|_T \leq \|D^\alpha(\mathcal{L}(f) - p_f)\|_T + \|D^\alpha(p_f - f)\|_T. \quad (5.7)$$

Since \mathcal{L} is a Lagrange interpolation operator which gives the unique spline satisfying the interpolation conditions, it defines a projector on $\mathcal{S}_3^1(\Delta^*)$. Thus, $\mathcal{L}(s) \equiv s$ for all $s \in \mathcal{S}_3^1(\Delta^*)$. In particular, since the space of cubic polynomials is a subspace of $\mathcal{S}_3^1(\Delta^*)$, the operator \mathcal{L} reproduces polynomials up to degree 3. Combining this fact with the Markov inequality (2.1) yields

$$\|D^\alpha(\mathcal{L}(f) - p_f)\|_T \leq \frac{K_2}{\rho_T^{|\alpha|}} \|\mathcal{L}(f - p_f)\|_T,$$

where K_2 is the constant from theorem 2.28. To estimate the radius of the insphere of T , we use lemma 2.23 (ii) and the fact that $0 \leq |\alpha| \leq 4$, obtaining

$$\frac{K_2}{\rho_T^{|\alpha|}} \|\mathcal{L}(f - p_f)\|_T \leq \frac{K_2}{K_3^4 |T|^{|\alpha|}} \|\mathcal{L}(f - p_f)\|_T.$$

Here, K_3 is the constant from 2.23 (ii) which depends only on K_H . Using first the stability from theorem 5.23 and then the locality from theorem 5.22, we have

$$\|\mathcal{L}(f - p_f)\|_T \leq K_4 \max_{x \in \mathcal{X}_T^*} f(x) \leq K_4 \|f - p_f\|_{\Omega_T}.$$

Combining these results, and using (5.6) with $|\beta| = 0$, yields

$$\|D^\alpha(\mathcal{L}(f) - p_f)\|_T \leq \frac{K_1 K_2 K_4}{K_3^4} |T|^{m+1-|\alpha|} |f|_{m+1, \Omega_T}.$$

Now we can estimate (5.7) with the inequality above and with (5.6). This concludes the proof \square

We conclude with the global result.

Theorem 5.25. *Let \mathcal{L} be the Lagrange interpolation operator defined in 5.21 and Δ the tetrahedral partition defined in 5.14. Suppose $f \in C^{m+1}(\Omega)$ with $0 \leq m \leq 3$, then there exists a constant K depending only on the shape parameter K_H of the BCC partition and the Lipschitz constant of the boundary of Ω , such that*

$$\|D^\alpha(\mathcal{L}(f) - f)\|_\Omega \leq K |\Omega|^{m+1-|\alpha|} |f|_{m+1, \Omega}, \quad 0 \leq |\alpha| \leq m,$$

where

$$\Omega := \bigcup_{T \in \Delta} T.$$

Proof. We take the maximum of the error over all tetrahedra, using theorem 5.24. It follows that there exists a constant K such that

$$\|D^\alpha(\mathcal{L}(f) - f)\|_\Omega \leq \max_{T \in \Delta} \|D^\alpha(\mathcal{L}(f) - f)\|_T \leq \max_{T \in \Delta} K |T|^{m+1-|\alpha|} |f|_{m+1, \Omega_T}.$$

Since $|T| \leq |\Delta|$ for all $T \in \Delta$,

$$\begin{aligned} \max_{T \in \Delta} K|T|^{m+1-|\alpha|}|f|_{m+1,\Omega_T} &\leq \max_{T \in \Delta} K|\Delta|^{m+1-|\alpha|}|f|_{m+1,\Omega_T} \\ &= K|\Delta|^{m+1-|\alpha|} \max_{T \in \Delta} |f|_{m+1,\Omega_T}. \end{aligned}$$

This concludes the proof since $\Omega_T \subset \Omega$. □

Chapter 6

Numerical tests and visualizations

In this chapter, we present the results of our numerical tests we performed on our operators. We developed computer programs that construct trivariate splines from volume data sets, implementing the operators described in chapters 3 and 5. The programs were developed using the programming language C++.

We used these programs to generate reconstructions of well-known synthetic test functions, and calculated an estimate for the approximation error by finely sampling the reconstructions and the original functions. These results are presented in the first section of this chapter.

In the second and third sections, we show visualizations of our reconstructions. There are several ways to generate two-dimensional projections from three-dimensional data, and we provide examples using two of these techniques. To visualize the synthetic test functions used in our error tests, we extract isosurfaces from the splines by casting rays through the reconstructed volume and searching for roots along the rays. For the visualizations of real-world data, we use a volume ray casting algorithm.

6.1 Error tables

We use the well-known test function proposed by Marschner and Lobb in their 1994 article [51] to estimate the approximation error of our reconstructions.

Definition 6.1. *We call*

$$f_{ML}(x, y, z) := \frac{1 - \sin(\pi y/2) + \alpha(1 + \rho_r(\sqrt{x^2 + z^2}))}{2(1 + \alpha)},$$

where

$$\rho_r := \cos(2\pi f_M \cos(\pi r/2)),$$

the Marschner-Lobb test function. Unless stated otherwise, this function is used with parameters $f_M = 6$ and $\alpha = \frac{1}{4}$.

We now define how we measure the approximation error.

Definition 6.2. *Given a function $f \in C(\mathbb{R}^3)$ and two sets \mathcal{X}_{data} and $\mathcal{X}_{err} \in \mathbb{R}^3$ of discrete points, we define the following local norms to measure*

(i) *the maximum approximation error at the data points:*

$$err_{data} := \max_{v \in \mathcal{X}_{data}} |f(v)|,$$

(ii) *the global maximum approximation error:*

$$err_{max} := \max_{v \in \mathcal{X}_{err}} |f(v)|,$$

(iii) *the mean approximation error:*

$$err_{mean} := \frac{1}{\#\mathcal{X}_{err}} \sum_{v \in \mathcal{X}_{err}} |f(v)|,$$

(iv) *and the root-mean-square error:*

$$err_{rms} := \sqrt{\frac{1}{\#\mathcal{X}_{err}} \sum_{v \in \mathcal{X}_{err}} f^2(v)}.$$

For our tests with the quasi-interpolation operators developed in chapter 3, we used the following procedure. For various parameters N , we created sample sets \mathcal{X} (see 3.13) for the three operators Q_{conv} , Q_{opt} and Q_I , such that $(N+1)^3$ sample points are distributed equally on the unit cube. For the operators Q_{conv} and Q_{opt} , this results in partitions Δ_1 with spacing $(1, 1, 1)/N$. The partition Δ_2 used for the interpolating operator is constructed with spacing $(1, 1, 1)/(2N)$ for the same number of sample points. We reconstructed the Marschner-Lobb test function from the samples $f_{ML}(\mathcal{X})$. We calculated the error measures from 6.2, using the sets $\mathcal{X}_{data} := \mathcal{X}$ and $\mathcal{X}_{err} \subset \mathcal{D}_{13}(\Delta)$, the latter consisting of 120 points on each tetrahedron. We used the function

$$f_{err} := Q(f_{ML}) - f_{ML},$$

with $Q \in \{Q_{conv}, Q_{opt}, Q_I\}$, to calculate the error measures. To estimate the error of the gradient of our reconstructions, we used the function defined by

$$f_{err, \nabla}(v) := \|\nabla(Q(f_{ML}) - f_{ML})(v)\|_\infty,$$

where $\nabla f := (D_x f, D_y f, D_z f)$ is the gradient. We present the results in the following tables.

Error of the reconstruction by Q_{conv}

N	err_{data}	err_{max}	err_{mean}	err_{rms}
32	0.0341011	0.0442419	0.0196437	0.0230166
64	0.0106222	0.0126609	0.0057064	0.0067290
128	0.0028035	0.0032843	0.0014836	0.0017523
256	0.0007104	0.0008287	0.0003746	0.0004426

Gradient error of the reconstruction by Q_{conv}

N	err_{data}	err_{max}	err_{mean}	err_{rms}
32	2.81987	2.87701	0.95987	1.16277
64	0.80361	0.83649	0.28567	0.34358
128	0.20758	0.22020	0.07978	0.09360
256	0.05254	0.06366	0.02422	0.02750

Error of the reconstruction by Q_{opt}

N	err_{data}	err_{max}	err_{mean}	err_{rms}
32	0.0153418	0.022402	0.00749813	0.00926919
64	0.00150027	0.00193187	0.00063753	0.00079708
128	0.00010458	0.00013204	0.00004313	0.00005408
256	0.00000672	0.00000845	0.00000275	0.00000345

Gradient error of the reconstruction by Q_{opt}

N	err_{data}	err_{max}	err_{mean}	err_{rms}
32	1.51228	1.54404	0.392383	0.500773
64	0.128959	0.134256	0.034604	0.043835
128	0.008738	0.009632	0.002630	0.003232
256	0.000562	0.000845	0.000219	0.000265

Since the operator Q_I interpolates the data at the sample points, the error err_{data} is zero, and we omit this column in the following tables.

Error of the reconstruction by Q_I

N	err_{max}	err_{mean}	err_{rms}
16	0.132245	0.0385091	0.0486917
32	0.019827	0.0051867	0.0067083
64	0.001575	0.0003958	0.0005157
128	0.000105	0.0000260	0.0000340

Gradient error of the reconstruction by Q_I

N	err_{max}	err_{mean}	err_{rms}
16	6.87624	2.0717	2.52465
32	1.69128	0.394763	0.50456
64	0.277762	0.047971	0.06330
128	0.037445	0.005653	0.00774

The tests for our Lagrange interpolation operator were conducted in a similar fashion. We created various reconstructions of the Marschner-Lobb test function, based on the partitions defined in 5.14, created with parameters $N_1 = N_2 = N_3 = N$ and spacing $(1, 1, 1)/N$. The following table shows the results.

Error of the reconstruction by \mathcal{L}

N	err_{max}	err_{mean}	err_{rms}
31	4.457×10^{-3}	3.131×10^{-4}	5.135×10^{-4}
65	4.309×10^{-4}	2.194×10^{-5}	3.877×10^{-5}
127	3.008×10^{-5}	1.353×10^{-6}	2.462×10^{-6}
255	1.894×10^{-6}	8.294×10^{-8}	1.525×10^{-7}

Gradient error of the reconstruction by \mathcal{L}

N	err_{max}	err_{mean}	err_{rms}
31	0.83278	0.079310	0.105780
65	0.12823	0.010773	0.015132
127	0.01786	0.001320	0.001923
255	0.00226	0.000162	0.000239

6.2 Isosurface extraction

We use a ray casting method to create a visualization of an isosurface from our volume reconstructions. From the origin of a virtual camera, rays are cast through a virtual screen. These rays intersect the reconstructed volume, and we evaluate the spline along the rays, searching for roots. We use the root finding algorithm by Brent [16] to calculate the roots. The implementation of this algorithm is taken from [70]. Once a root is found, we calculate the gradient at the intersection and use the well-known Phong algorithm (see [67]) to generate a color.

In figure 6.1, we show the isosurface of constant value $\frac{1}{2}$ of the Marschner-Lobb test function in the upper left. We sampled this function to create a

data set of 41^3 data values on the cube $[-1, 1]^3$, as proposed in [51], which we reconstructed with our quasi-interpolation operators. The equivalent isosurfaces of the reconstructions are also shown in this figure.

The isosurfaces of the same constant value of various reconstructions by our Lagrange interpolation operator with a parameter $N \in \{31, 41, 61, 81\}$ are shown in figure 6.2. The underlying BCC partition was constructed with a spacing parameter $(1, 1, 1)/N$, while the partition Δ from definition 5.14 was constructed with parameters $N_1 = N_2 = N_3 = N$. For these reconstructions, we sampled the Marschner-Lobb test function directly at the points of the Lagrange interpolation set of theorem 5.20.

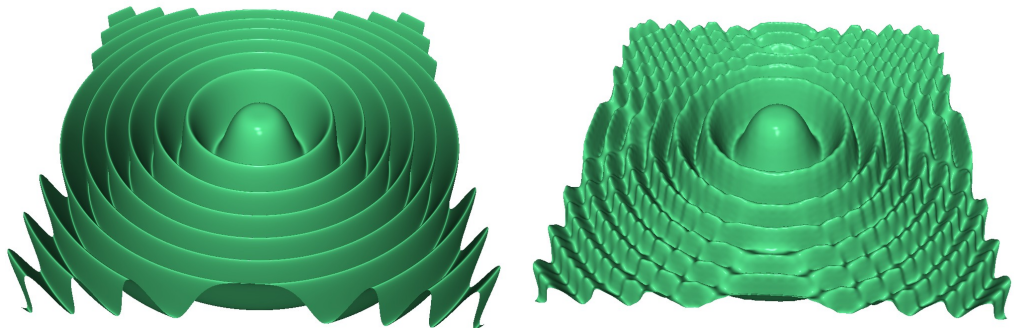
To further compare the quasi-interpolation operators, we color coded the visualizations of the isosurfaces to show the distribution of the approximation error $f_{ML} - Q(f_{ML})$. These results are shown in figure 6.3.

We show two isosurfaces in figure 6.5 which are color coded to reveal the structure of the tetrahedra classes $\mathcal{K}_1, \dots, \mathcal{K}_4$ of the interpolating quasi-interpolation operator. These classes are represented by the colors purple, green, red and teal, respectively. The darker lines on the isosurfaces represent boundaries between two neighboring tetrahedra.

The reconstructions of both the Lagrange interpolation operator and the interpolating quasi-interpolation operator produce isosurfaces that are not completely connected, resulting in holes and “bubbles”. This behavior is shown in the detail views in figure 6.4 and is attributed to the huge influence of the interpolated values. Figure 6.5 shows the same closeup of the isosurface of the interpolating quasi-interpolation operator, but is color-coded to reveal the classes of the tetrahedra. The purple regions pass through tetrahedra in class \mathcal{K}_1 . The polynomial pieces on these tetrahedra are heavily influenced by the data values, as one of their vertices coincides with a sample point. The bubbles and protruding parts of the isosurface are exclusively present in tetrahedra of this class. At the ridges of the isosurface generated by the Lagrange interpolation operator, holes can be seen. Such artifacts are common for the BCC partition, see section 4.4 in [18], and also appear in isosurfaces generated by a marching tetrahedra algorithm using this partition. The comparison of the closeups also highlights the difference between isosurfaces extracted from C^1 spline volumes and those of C^2 reconstructions. The discontinuity of the gradient of the C^1 splines causes rapid changes in the shading, especially in the highlights and shadows, and reveals the underlying BCC partition. The C^2 isosurface, on the other hand, is much smoother.

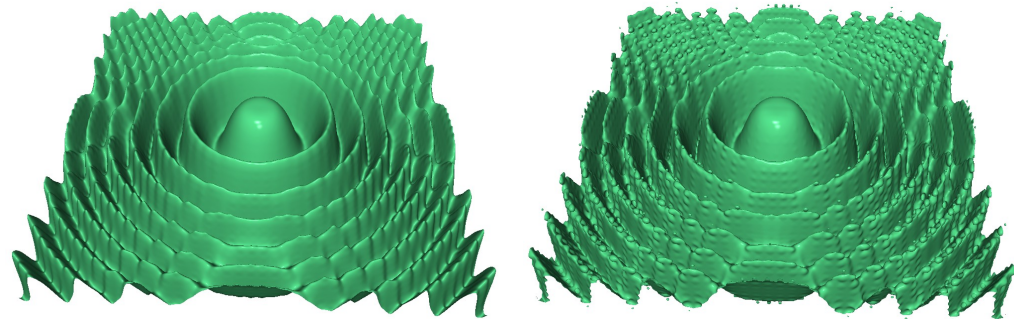
To conclude this section, figure 6.6 shows an isosurface extracted from a reconstruction by the blending operator defined in chapter 4. The blending operator uses the weights of both Q_{opt} and Q_{conv} . The parameter set θ was computed by our implementation of algorithm 4.7. The isosurface is color coded to represent the values of the blending parameters. Each blending pa-

parameter is associated with a sample point, and the color of a point v on the isosurface is the color of the blending parameter which is associated with the sample point closest to v . Parameters near zero are red, representing weights that are close to those of the optimal operator, while green colors are associated with Q_{conv} . The resulting isosurface closely resembles the one generated by Q_{opt} , while the reconstruction satisfies the convexity condition (4.2).



$$f_{ML}(v) = \frac{1}{2}$$

$$Q_{conv}(f_{ML})(v) = \frac{1}{2}$$



$$Q_{opt}(f_{ML})(v) = \frac{1}{2}$$

$$Q_I(f_{ML})(v) = \frac{1}{2}$$

Figure 6.1: The isosurface of constant value $\frac{1}{2}$ of the Marschner-Lobb test function (upper left), and the equivalent isosurfaces of various reconstructions by our quasi-interpolation operators. The reconstructions use 41^3 data values on the cube $[-1, 1]^3$.

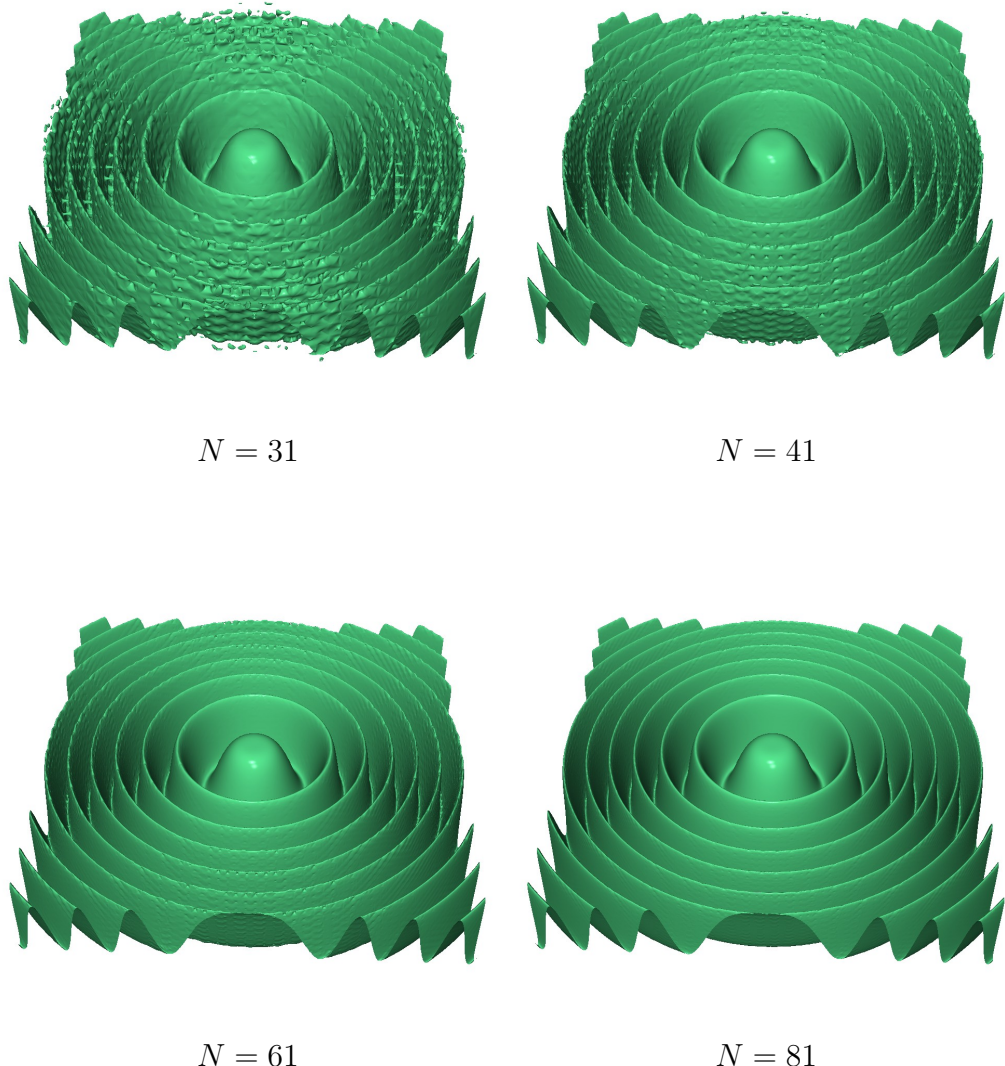


Figure 6.2: The isosurface of $\mathcal{L}(f_{ML}) = \frac{1}{2}$ of reconstructions of the Marschner-Lobb test function. The reconstructions were obtained using our Lagrange interpolation operator developed in chapter 5. The underlying BCC partitions were constructed with spacing parameters $(1, 1, 1)/(2N)$, for various values of N . The partition Δ from definition 5.14 was constructed with parameters $N_1 = N_2 = N_3 = N$.

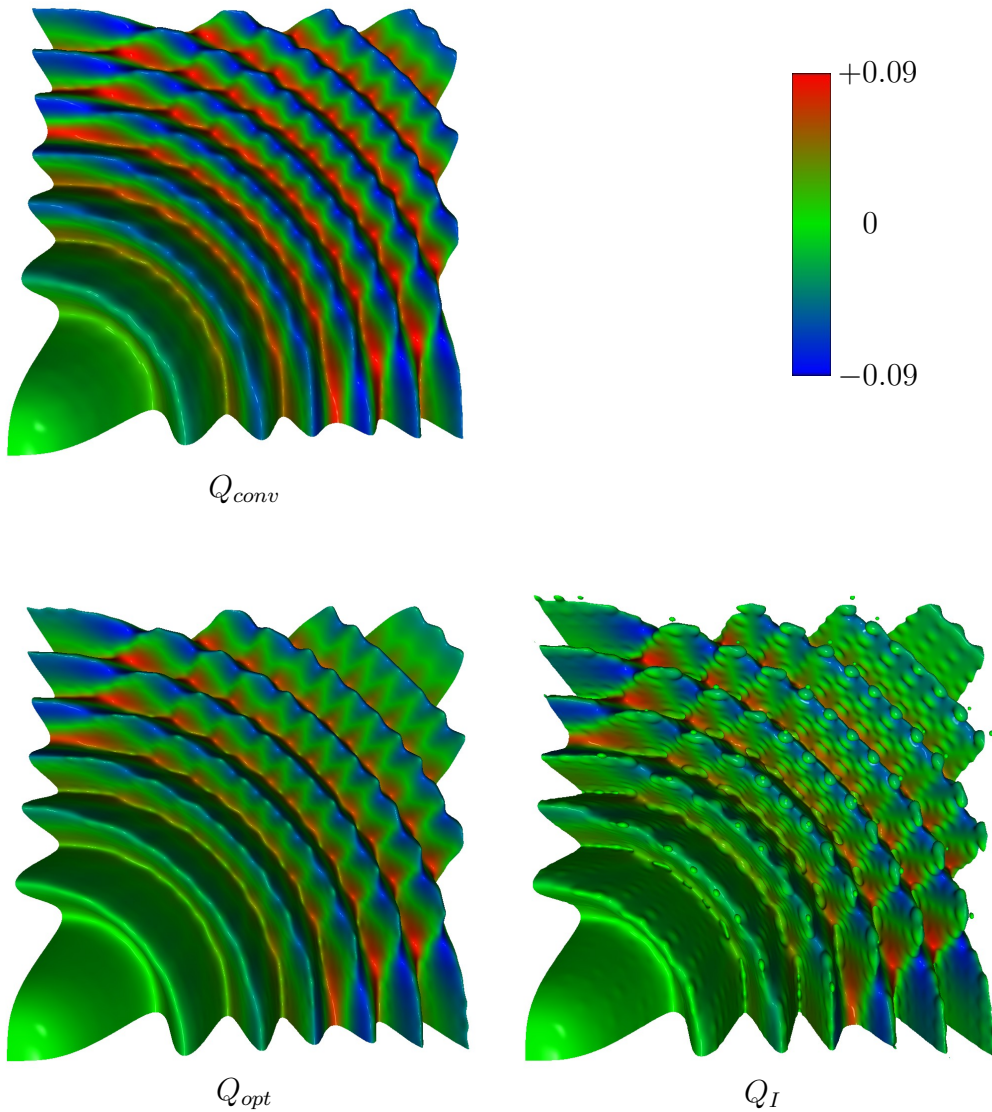


Figure 6.3: The distribution of the approximation error $f_{ML} - Q(f_{ML})$ on the isosurfaces of constant value $\frac{1}{2}$ for reconstructions of the Marschner-Lobb test function by our quasi-interpolation operators. The reconstructions used 21^3 data values on the unit cube.

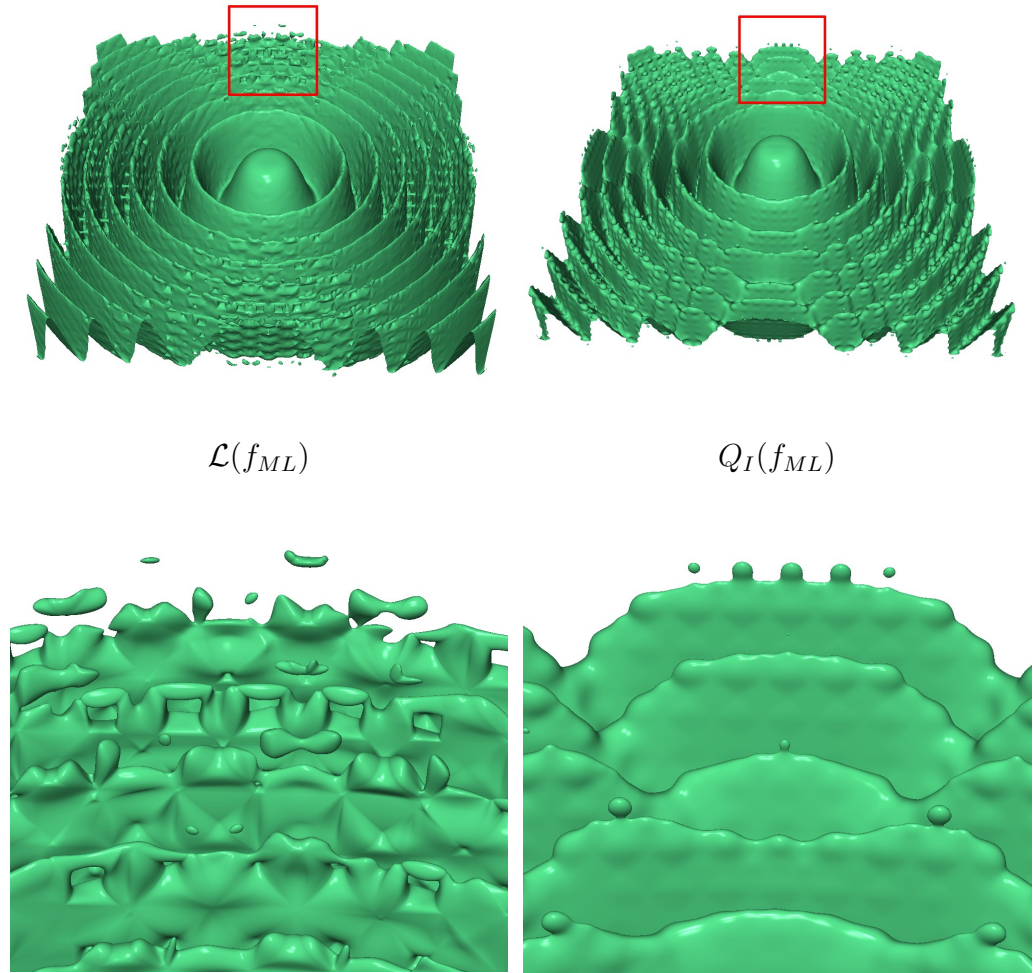


Figure 6.4: Detail views of the isosurface of constant value $\frac{1}{2}$ of reconstructions of the Marschner-Lobb test function. Left: a reconstruction by the Lagrange interpolation operator, with $N = 31$. Right: a reconstruction by the interpolating quasi-interpolation operator, using 41^3 data values on $[-1, 1]^3$.

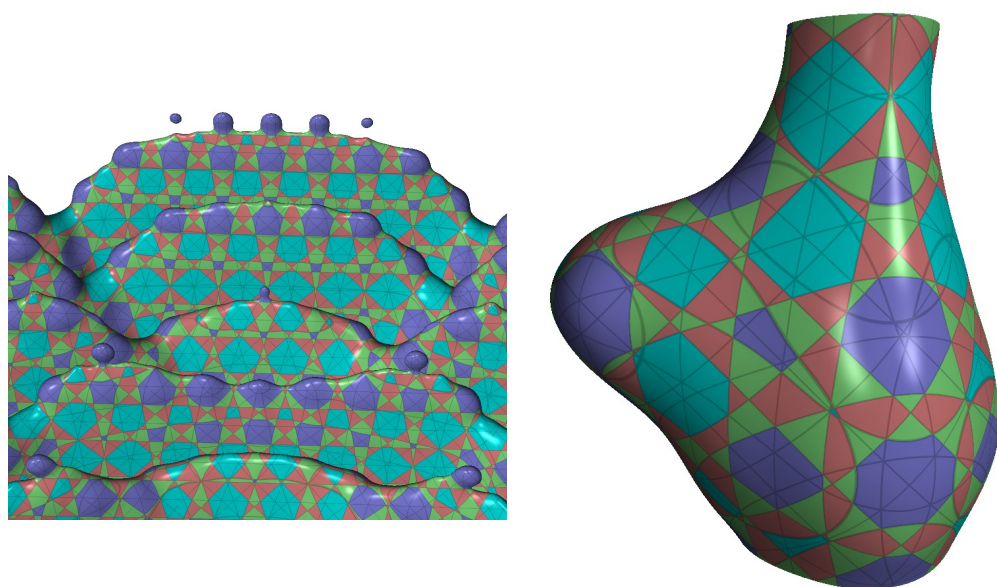


Figure 6.5: Color-coded isosurfaces extracted from reconstructions by the interpolating quasi-interpolation operator. The purple, green, red, and teal areas are located on tetrahedra in class $\mathcal{K}_1, \dots, \mathcal{K}_4$, respectively.

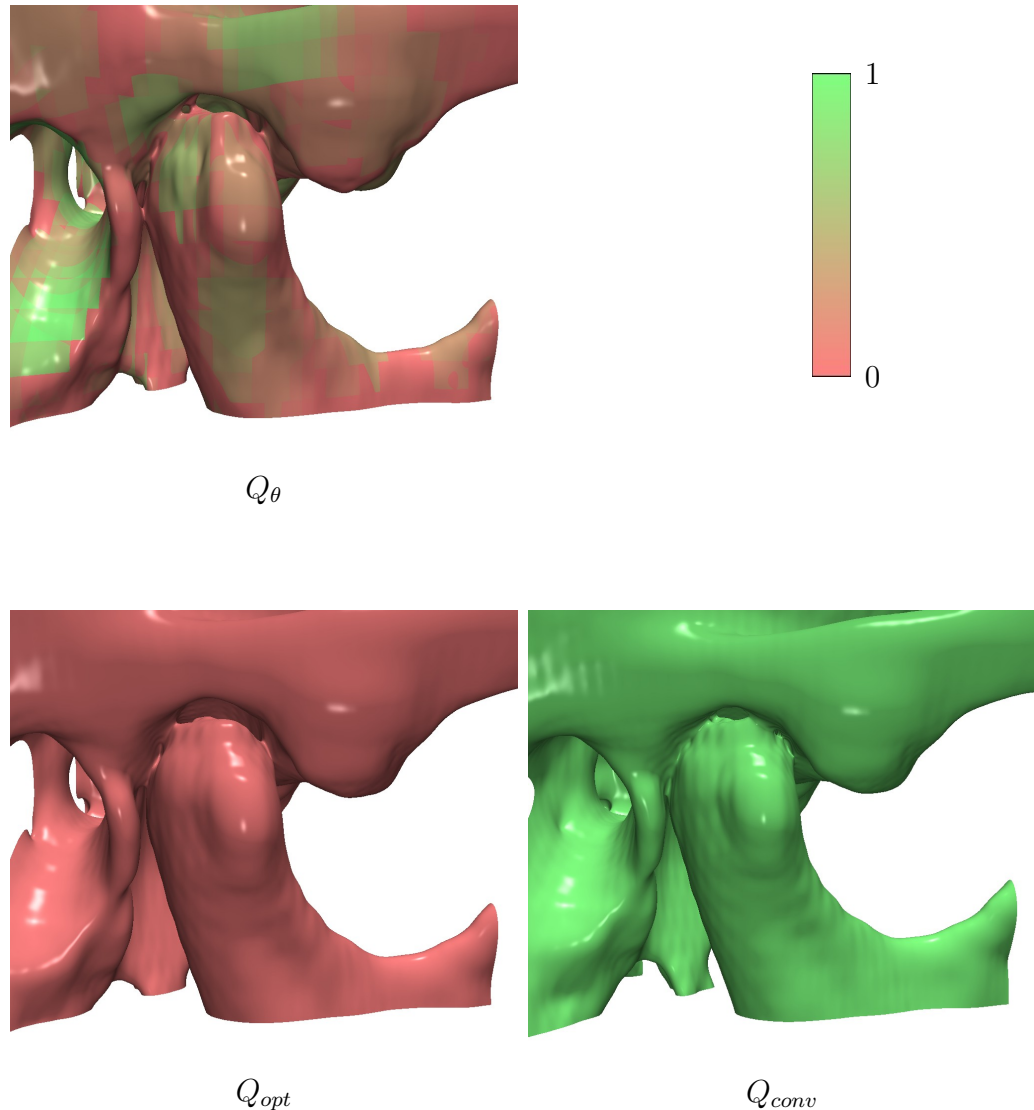


Figure 6.6: Detail view of an isosurface of reconstructions of the ‘Chapel Hill CT Head’ data set. On the bottom, the reconstructions by Q_{opt} and Q_{conv} are shown. The upper left shows a reconstruction by the blending operator Q_θ defined in chapter 4. The parameter set θ was obtained by algorithm 4.7. The colors of the isosurface indicate the value of the parameters of θ . In the red areas, the reconstruction is mainly based on Q_{opt} , while the green areas indicate a more significant influence of Q_{conv} .

6.3 Volume ray casting

In this section, we present images of real-world data sets, generated by a volume ray casting algorithm which we implemented in C++. The algorithm is based on the technique described in [48]. Using our quasi-interpolation operators from chapter 3, we create a spline from the data values. We cast rays from a virtual camera through the pixels of a virtual screen. These rays traverse the volume, and we evaluate the spline at equidistant points along the rays, generating samples. These samples are then classified using a transfer function. The transfer function uses the value and the gradient of the spline to calculate a color and an opacity for the sample. Using the color, the sample is shaded by the Phong algorithm (see [67]). Once all samples for a ray are known, a final color for the pixel is computed using back-to-front alpha compositing (see [68]). We use a two-dimensional transfer function similar to those developed in [45] to classify the samples.

We used the following real-world data sets to demonstrate the quality of our reconstructions. All data sets were obtained from “The Volume Library” online repository of the Friedrich-Alexander Universität Erlangen-Nürnberg (<http://www9.informatik.uni-erlangen.de/External/vollib/>).

- **Head** (Part of the Visible Male dataset of the National Library of Medicine, National Institutes of Health, USA).
 $128 \times 256 \times 256$ 8-bit values.
- **Chapel Hill CT Head** (Marc Levoy, Computer Graphics Laboratory, Stanford University, USA, provided courtesy of North Carolina Memorial Hospital).
 $256 \times 256 \times 113$ 16-bit values.
- **Foot** (Philips Research, Hamburg, Germany).
 $256 \times 256 \times 256$ 8-bit values.
- **Engine Block** (General Electric, USA).
 $256 \times 256 \times 256$ 8-bit values.

Due to the high amount of noise present in the ‘Foot’ data set, we applied a Gaussian filter prior to constructing the spline. The other data sets were used without any preprocessing. All reconstructions shown in figures 6.8 - 6.12 were made using the optimal quasi-interpolation operator. We show a comparison of the three quasi-interpolation operators in figure 6.13. The data used in the comparison is a subset of $48 \times 24 \times 48$ values of the ‘Chapel Hill CT Head’ data set.

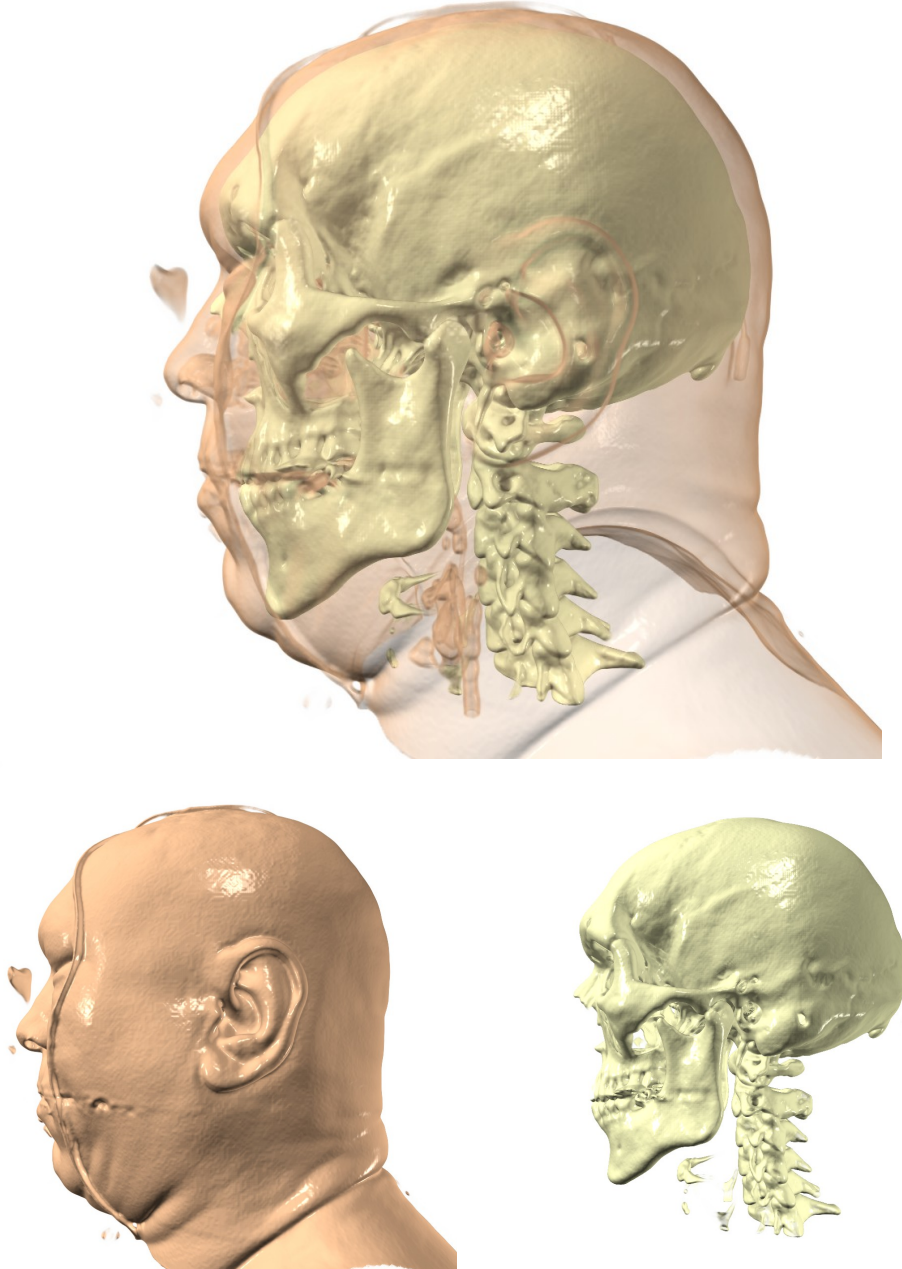


Figure 6.7: Side view of the ‘Head (Visible Male)’ dataset, reconstructed using the optimal quasi-interpolation operator. In the top image, the data corresponding to both skin and bone is rendered. The skin layer is rendered semi-transparent so the underlying bone can be seen. At the bottom left, only the data corresponding to skin is rendered, while the right shows only the data corresponding to bone.

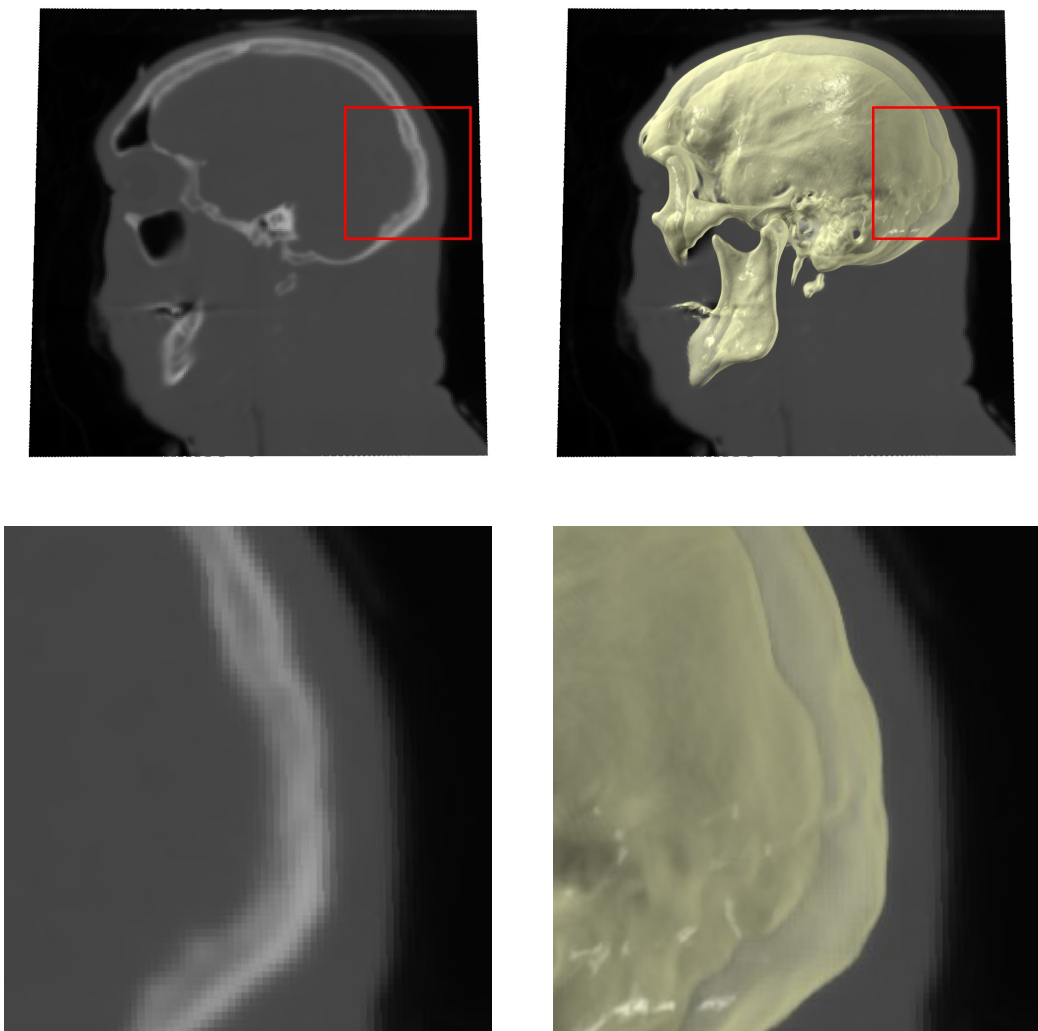


Figure 6.8: Side view of the ‘Head (Visible Male)’ dataset. The top left side shows a single 2D slice of the original data. The top right side shows a semi-transparent rendering of the data corresponding to bone, superimposed over the 2D slice. The bottom shows enlarged views of the area marked in the pictures at the top, which demonstrate that the reconstruction follows the data closely.

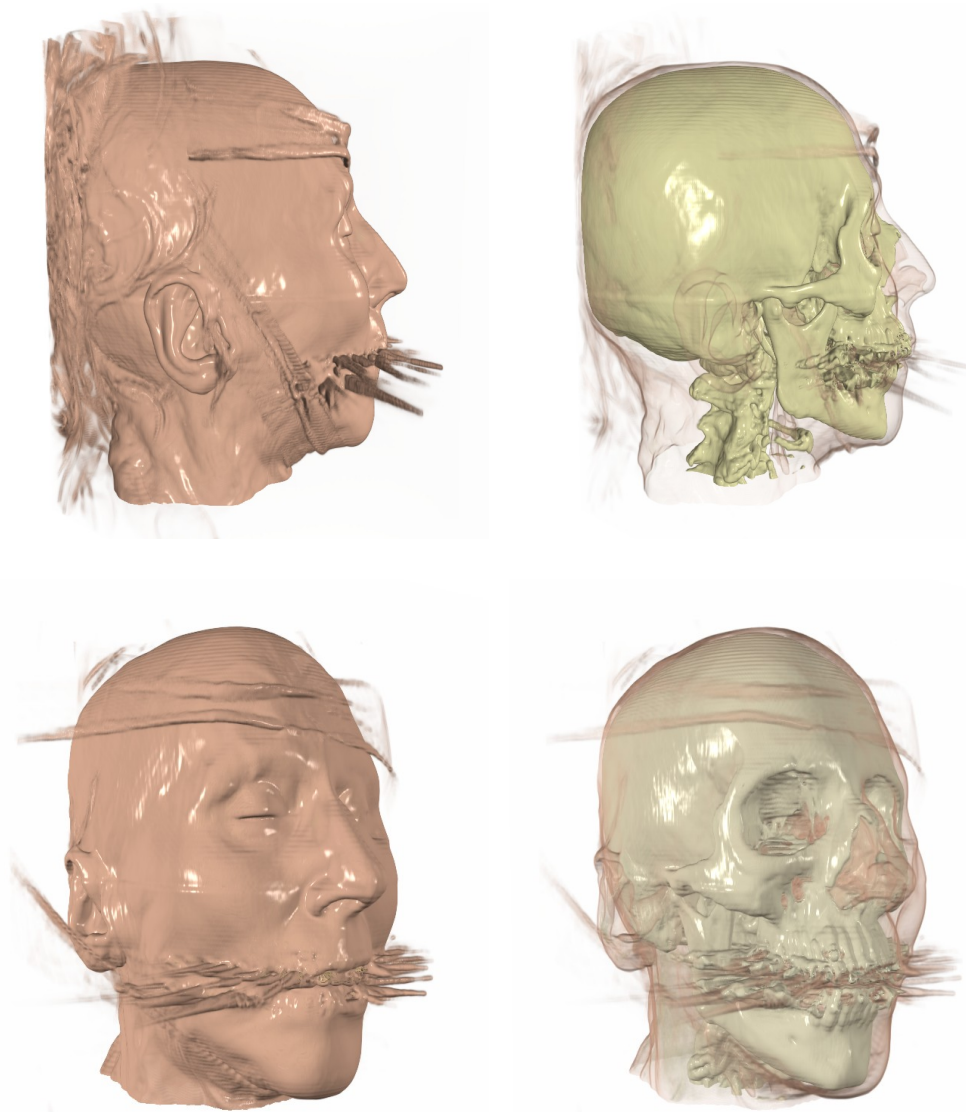


Figure 6.9: Two views of the ‘Chapel Hill CT head’ data set. Note that the artifacts around the mouth are due to scattering of X-rays from dental fillings (see [48]).

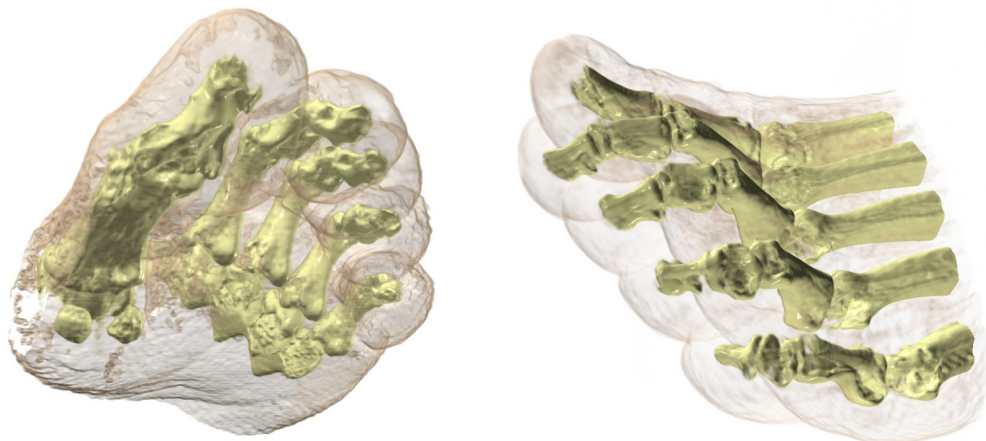


Figure 6.10: Two views of the ‘Foot’ data set.

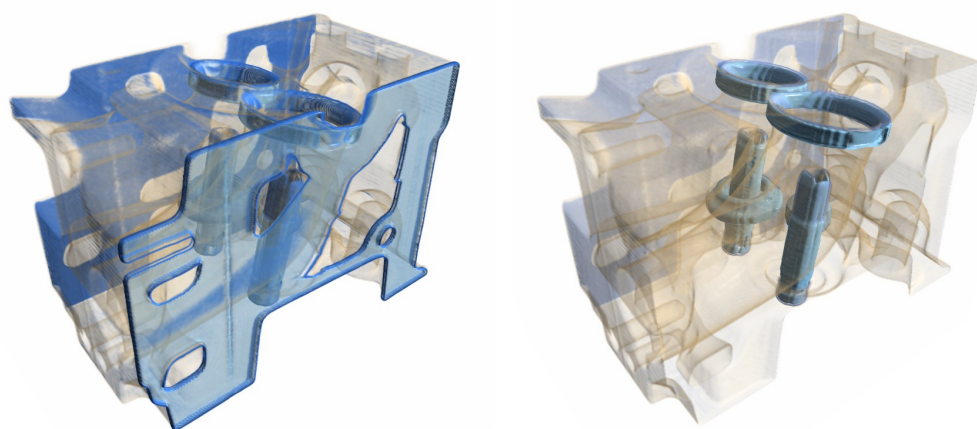


Figure 6.11: Two renderings of the ‘Engine Block’ data set.

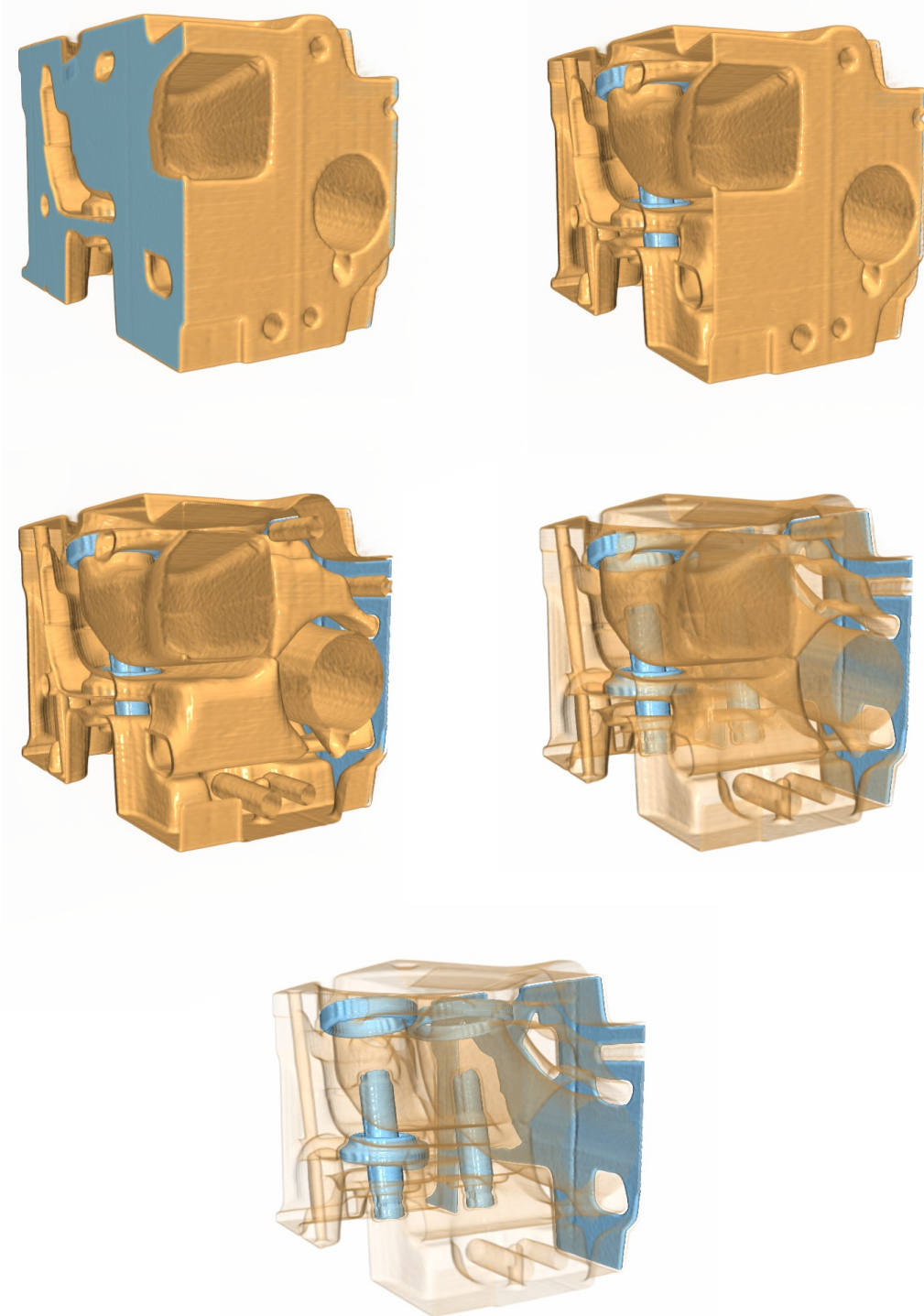


Figure 6.12: Several renderings of the ‘Engine Block’ data set, gradually revealing the interior of the engine.

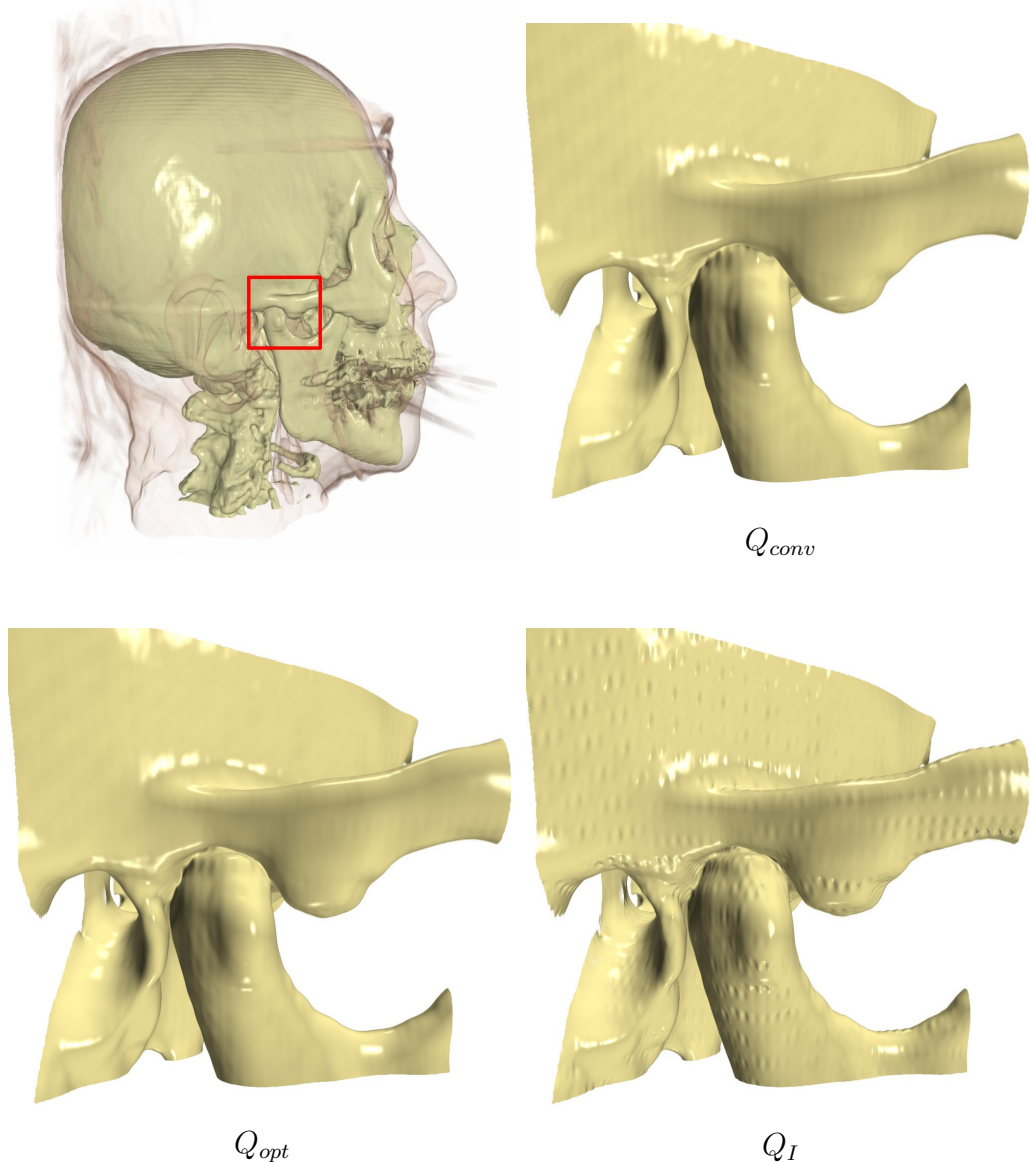


Figure 6.13: A comparison of the quasi-interpolation operators. The reconstructions were made using a $48 \times 24 \times 48$ subset of the ‘Chapel Hill’ data set, from the region marked in the upper left.

Appendix A

B-coefficient computation rules for the convex quasi-interpolation operator

This appendix contains the B-coefficient computation rules for the convex quasi-interpolation operator developed in section 3.1 of chapter 3. The sample points in these rules are given relative to a tetrahedron of the BCC partition. Each polynomial piece of the resulting spline is calculated using the same set of rules. For each rule, we also provide a weight mask which shows where the data values are located relative to the tetrahedron.

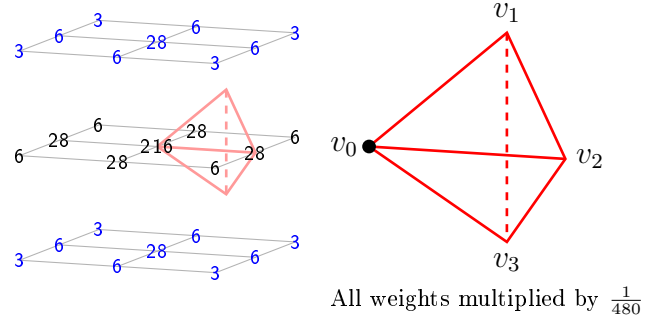


Figure A.1: Weight mask for c_{5000} . The associated domain point is shown in the teterahedron on the right.

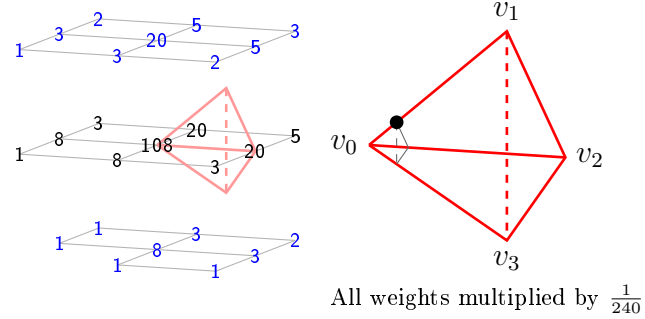


Figure A.2: Weight mask for c_{4100} . The associated domain point is shown in the teterahedron on the right. The black triangle symbolizes the ring $R_1(v_0)$.

$$\begin{aligned}
 c_{5000} := & \frac{1}{480} \left(216 f_{1,0,0,0} \right. \\
 & + 28(f_{0,1,-1,1} + f_{2,-1,1,-1} + f_{2,0,-1,0} + f_{1,-1,0,1} + f_{1,1,0,-1} + f_{0,0,1,0}) \\
 & + 6(f_{1,-1,2,-1} + f_{3,-1,0,-1} + f_{2,-2,1,0} + f_{2,1,-1,-1} + f_{2,-1,-1,1} + f_{2,0,1,-2} \\
 & \quad + f_{1,1,-2,1} + f_{-1,1,0,1} + f_{0,2,-1,0} + f_{0,1,1,-1} + f_{0,-1,1,1} + f_{0,0,-1,2}) \\
 & + 3(f_{-1,2,0,0} + f_{1,-2,2,0} + f_{1,2,-2,0} + f_{1,0,2,-2} + f_{1,0,-2,2} + f_{-1,0,0,2} \\
 & \quad \left. + f_{3,0,0,-2} + f_{3,-2,0,0} \right) \tag{A.1}
 \end{aligned}$$

The associated weight mask is shown in figure A.1.
B-coefficient c_{0050} is computed using $(0, 2)$ -symmetry.

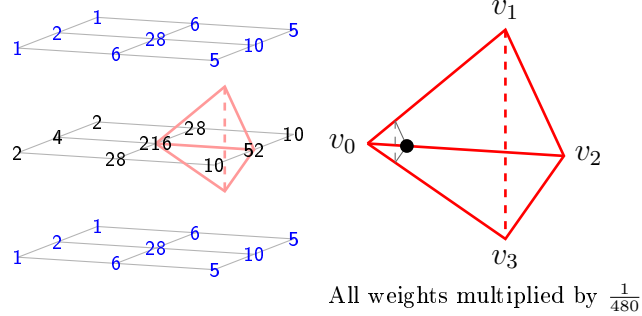


Figure A.3: Weight mask for c_{4010} . The associated domain point is shown in the teterahedron on the right. The black triangle symbolizes the ring $R_1(v_0)$.

$$\begin{aligned}
 c_{4100} := & \frac{1}{240} \left(108f_{1,0,0,0} + 20(f_{0,1,-1,1} + f_{1,1,0,-1} + f_{0,0,1,0}) \right. \\
 & + 8(f_{2,-1,1,-1} + f_{2,0,-1,0} + f_{1,-1,0,1}) + 5(f_{0,1,1,-1} + f_{0,2,-1,0} + f_{-1,1,0,1}) \\
 & + 3(f_{1,-1,2,-1} + f_{2,1,-1,-1} + f_{2,0,1,-2} + f_{-1,2,0,0} + f_{1,1,-2,1} + f_{0,-1,1,1} \\
 & \quad + f_{0,0,-1,2}) \\
 & + 2(f_{1,0,2,-2} + f_{1,2,-2,0} + f_{-1,0,0,2}) \\
 & \left. + (f_{1,-2,2,0} + f_{1,0,-2,2} + f_{2,-1,-1,1} + f_{2,-2,1,0} + f_{3,0,0,-2} + f_{3,-1,0,-1}) \right) \quad (\text{A.2})
 \end{aligned}$$

The associated weight mask is shown in figure A.2.

B-coefficient c_{0140} is computed using $(0, 2)$ -symmetry.

B-coefficient c_{4001} is computed using $(1, 3)$ -symmetry.

B-coefficient c_{0041} is computed using both $(0, 2)$ -symmetry and $(1, 3)$ -symmetry.

$$\begin{aligned}
 c_{4010} := & \frac{1}{480} \left(216f_{1,0,0,0} + 52f_{0,0,1,0} + 28(f_{2,-1,1,-1} + f_{0,1,-1,1} + f_{1,1,0,-1} + f_{1,-1,0,1}) \right. \\
 & + 10(f_{1,-1,2,-1} + f_{-1,1,0,1} + f_{0,1,1,-1} + f_{0,-1,1,1}) \\
 & + 6(f_{0,2,-1,0} + f_{2,-2,1,0} + f_{2,0,1,-2} + f_{0,0,-1,2}) \\
 & + 5(f_{1,0,2,-2} + f_{-1,0,0,2} + f_{-1,2,0,0} + f_{1,-2,2,0}) + 4f_{2,0,-1,0} \\
 & + 2(f_{3,-1,0,-1} + f_{2,1,-1,-1} + f_{2,-1,-1,1} + f_{1,1,-2,1}) \\
 & \left. + (f_{3,-2,0,0} + f_{1,2,-2,0} + f_{3,0,0,-2} + f_{1,0,-2,2}) \right) \quad (\text{A.3})
 \end{aligned}$$

The associated weight mask is shown in figure A.3.

B-coefficient c_{1040} is computed using $(0, 2)$ -symmetry.

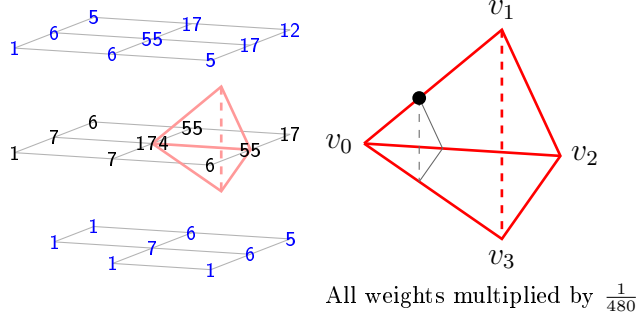


Figure A.4: Weight mask for c_{3200} . The associated domain point is shown in the tetrahedron on the right. The black triangle symbolizes the ring $R_2(v_0)$.

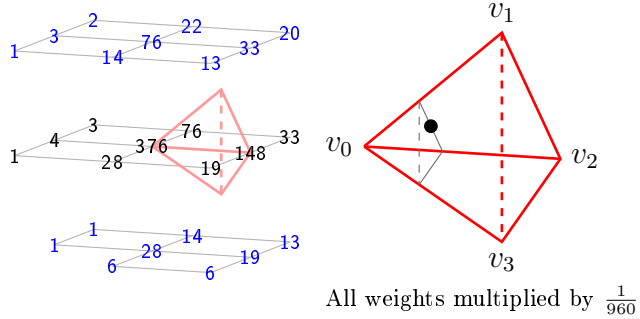


Figure A.5: Weight mask for c_{3110} . The associated domain point is shown in the tetrahedron on the right. The black triangle symbolizes the ring $R_2(v_0)$.

$$\begin{aligned}
 c_{3200} := & \frac{1}{480} \left(174f_{1,0,0,0} + 55(f_{0,1,-1,1} + f_{1,1,0,-1} + f_{0,0,1,0}) \right. \\
 & + 17(f_{0,1,1,-1} + f_{0,2,-1,0} + f_{-1,1,0,1}) + 12f_{-1,2,0,0} \\
 & + 7(f_{2,-1,1,-1} + f_{2,0,-1,0} + f_{1,-1,0,1}) \\
 & + 6(f_{1,-1,2,-1} + f_{2,1,-1,-1} + f_{2,0,1,-2} + f_{1,1,-2,1} + f_{0,-1,1,1} + f_{0,0,-1,2}) \\
 & + 5(f_{1,0,2,-2} + f_{1,2,-2,0} + f_{-1,0,0,2}) \\
 & \left. + (f_{1,-2,2,0} + f_{1,0,-2,2} + f_{2,-1,-1,1} + f_{2,-2,1,0} + f_{3,0,0,-2} + f_{3,-1,0,-1}) \right) \quad (\text{A.4})
 \end{aligned}$$

The associated weight mask is shown in figure A.4.

B-coefficient c_{0230} is computed using $(0, 2)$ -symmetry.

B-coefficient c_{3002} is computed using $(1, 3)$ -symmetry.

B-coefficient c_{0032} is computed using both $(0, 2)$ -symmetry and $(1, 3)$ -symmetry.

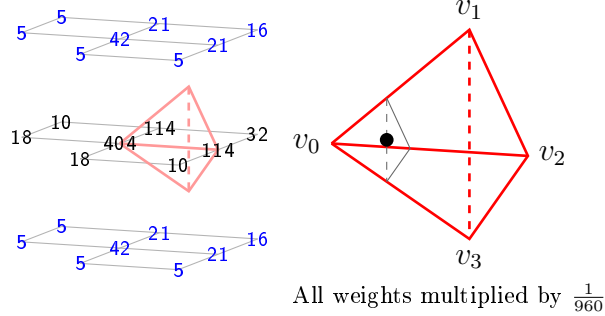


Figure A.6: Weight mask for c_{3101} . The associated domain point is shown in the tetrahedron on the right. The black triangle symbolizes the ring $R_2(v_0)$.

$$\begin{aligned}
 c_{3110} := & \frac{1}{960} \left(376f_{1,0,0,0} + 148f_{0,0,1,0} + 76(f_{0,1,-1,1} + f_{1,0,-1,1}) + 33(f_{0,1,1,-1} + f_{-1,1,0,1}) \right. \\
 & + 28(f_{2,-1,1,-1} + f_{1,-1,0,1}) + 22f_{0,2,-1,0} + 20f_{-1,2,0,0} + 19(f_{1,-1,2,-1} + f_{0,-1,1,1}) \\
 & + 14(f_{2,0,1,-2} + f_{0,0,-1,2}) + 13(f_{1,0,2,-2} + f_{-1,0,0,2}) + 6(f_{1,-2,2,0} + f_{2,-2,1,0}) \\
 & + 4f_{2,0,-1,0} + 3(f_{1,1,-2,1} + f_{2,1,-1,-1}) + 2f_{1,2,-2,0} \\
 & \left. + (f_{1,0,-2,2} + f_{2,-1,-1,1} + f_{3,0,0,-2} + f_{3,-1,0,-1}) \right) \tag{A.5}
 \end{aligned}$$

The associated weight mask is shown in figure A.5.

B-coefficient c_{1130} is computed using $(0, 2)$ -symmetry.

B-coefficient c_{3011} is computed using $(1, 3)$ -symmetry.

B-coefficient c_{1031} is computed using both $(0, 2)$ -symmetry and $(1, 3)$ -symmetry.

$$\begin{aligned}
 c_{3101} := & \frac{1}{960} \left(404f_{1,0,0,0} + 114(f_{0,0,1,0} + f_{0,1,-1,1}) + 42(f_{1,1,0,-1} + f_{1,-1,0,1}) + 32f_{-1,1,0,1} \right. \\
 & + 21(f_{0,1,1,-1} + f_{0,-1,1,1} + f_{0,0,-1,2} + f_{0,2,-1,0}) + 18(f_{2,-1,1,-1} + f_{2,0,-1,0}) \\
 & + 16(f_{-1,0,0,2} + f_{-1,2,0,0}) + 10(f_{1,1,-2,1} + f_{1,-1,2,-1}) \\
 & + 5(f_{1,-2,2,0} + f_{1,2,-2,0} + f_{1,0,2,-2} + f_{2,0,1,-2} + f_{2,-1,-1,1} + f_{1,0,-2,2} \\
 & \left. + f_{2,1,-1,-1} + f_{2,-2,1,0}) \right) \tag{A.6}
 \end{aligned}$$

The associated weight mask is shown in figure A.6.

B-coefficient c_{0131} is computed using $(0, 2)$ -symmetry.

$$\begin{aligned}
 c_{3020} := & \frac{1}{60} \left(20f_{1,0,0,0} + 12f_{0,0,1,0} + 3(f_{2,-1,1,-1} + f_{0,1,-1,1} + f_{1,1,0,-1} + f_{1,-1,0,1}) \right. \\
 & + 2(f_{-1,1,0,1} + f_{1,-1,2,-1} + f_{0,1,1,-1} + f_{0,-1,1,1}) \\
 & + (f_{1,0,2,-2} + f_{-1,0,0,2} + f_{0,2,-1,0} + f_{-1,2,0,0} + f_{1,-2,2,0} + f_{2,0,1,-2} \\
 & \left. + f_{0,0,-1,2} + f_{2,-2,1,0}) \right) \tag{A.7}
 \end{aligned}$$

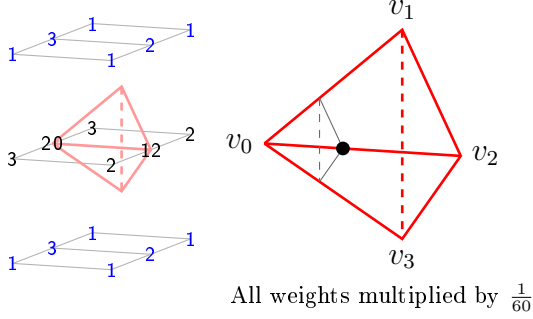


Figure A.7: Weight mask for c_{3020} . The associated domain point is shown in the teterahedron on the right. The black triangle symbolizes the ring $R_2(v_0)$.

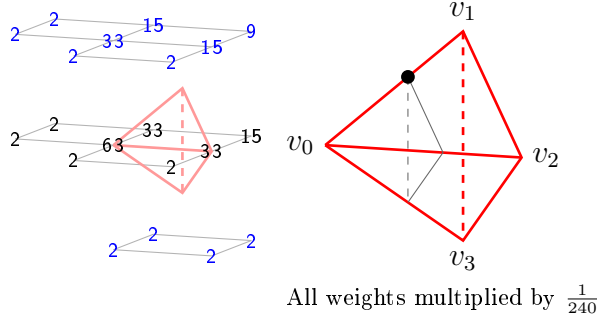


Figure A.8: Weight mask for c_{2300} . The associated domain point is shown in the teterahedron on the right. The black triangle symbolizes the ring $R_3(v_0)$.

The associated weight mask is shown in figure A.7.
B-coefficient c_{2030} is computed using $(0, 2)$ -symmetry.

$$\begin{aligned}
 c_{2300} := & \frac{1}{240} \left(63f_{1,0,0,0} + 33(f_{0,0,1,0} + f_{0,1,-1,1} + f_{1,1,0,-1}) \right. \\
 & + 15(f_{0,1,1,-1} + f_{0,2,-1,0} + f_{-1,1,0,1}) + 9f_{-1,2,0,0} \\
 & + 2(f_{2,1,-1,-1} + f_{2,-1,1,-1} + f_{2,0,1,-2} + f_{2,0,-1,0} + f_{1,2,-2,0} + f_{1,1,-2,1} \\
 & \left. + f_{1,-1,2,-1} + f_{1,-1,0,1} + f_{1,0,2,-2} + f_{-1,0,0,2} + f_{0,-1,1,1} + f_{0,0,-1,2}) \right) \quad (\text{A.8})
 \end{aligned}$$

The associated weight mask is shown in figure A.8.
B-coefficient c_{0320} is computed using $(0, 2)$ -symmetry.
B-coefficient c_{2003} is computed using $(1, 3)$ -symmetry.
B-coefficient c_{0023} is computed using both $(0, 2)$ -symmetry and $(1, 3)$ -symmetry.

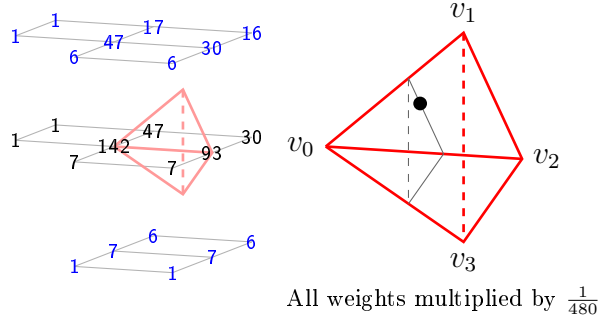


Figure A.9: Weight mask for c_{2210} . The associated domain point is shown in the teterahedron on the right. The black triangle symbolizes the ring $R_3(v_0)$.

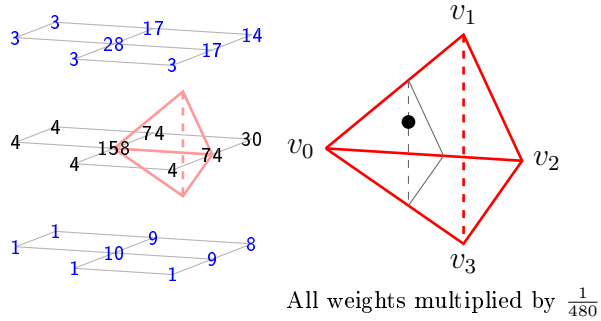


Figure A.10: Weight mask for c_{2201} . The associated domain point is shown in the teterahedron on the right. The black triangle symbolizes the ring $R_3(v_0)$.

$$\begin{aligned}
 c_{2210} := & \frac{1}{480} \left(142f_{1,0,0,0} + 93f_{0,0,1,0} + 47(f_{1,1,0,-1} + f_{0,1,-1,1}) + 30(f_{0,1,1,-1} + f_{-1,1,0,1}) \right. \\
 & + 17f_{0,2,-1,0} + 16f_{-1,2,0,0} + 7(f_{1,-1,2,-1} + f_{2,-1,1,-1} + f_{1,-1,0,1} + f_{0,-1,1,1}) \\
 & + 6(f_{0,0,-1,2} + f_{1,0,2,-2} + f_{-1,0,0,2} + f_{2,0,1,-2}) \\
 & \left. + (f_{1,1,-2,1} + f_{1,-2,2,0} + f_{1,2,-2,0} + f_{2,0,-1,0} + f_{2,1,-1,-1} + f_{2,-2,1,0}) \right) \quad (\text{A.9})
 \end{aligned}$$

The associated weight mask is shown in figure A.9.

B-coefficient c_{1220} is computed using $(0, 2)$ -symmetry.

B-coefficient c_{2012} is computed using $(1, 3)$ -symmetry.

B-coefficient c_{1022} is computed using both $(0, 2)$ -symmetry and $(1, 3)$ -symmetry.

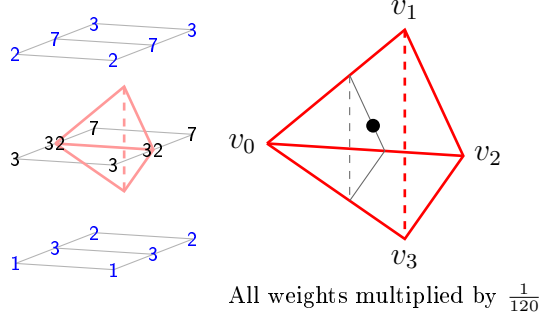


Figure A.11: Weight mask for c_{2120} . The associated domain point is shown in the teterahedron on the right. The black triangle symbolizes the ring $R_3(v_0)$.

$$\begin{aligned} c_{2201} := & \frac{1}{480} \left(158f_{1,0,0,0} + 74(f_{0,0,1,0} + f_{0,1,-1,1}) + 30f_{-1,1,0,1} + 28f_{1,1,0,-1} \right. \\ & + 17(f_{0,1,1,-1} + f_{0,2,-1,0}) + 14f_{-1,2,0,0} + 10f_{1,-1,0,1} + 9(f_{0,-1,1,1} + f_{0,0,-1,2}) \\ & + 8f_{-1,0,0,2} + 4(f_{1,1,-2,1} + f_{2,-1,1,-1} + f_{2,0,-1,0} + f_{1,-1,2,-1}) \\ & + 3(f_{1,2,-2,0} + f_{1,0,2,-2} + f_{2,0,1,-2} + f_{2,1,-1,-1}) \\ & \left. + (f_{1,-2,2,0} + f_{2,-1,-1,1} + f_{1,0,-2,2} + f_{2,-2,1,0}) \right) \end{aligned} \quad (\text{A.10})$$

The associated weight mask is shown in figure A.10.

B-coefficient c_{0221} is computed using $(0, 2)$ -symmetry.

B-coefficient c_{2102} is computed using $(1, 3)$ -symmetry.

B-coefficient c_{0122} is computed using both $(0, 2)$ -symmetry and $(1, 3)$ -symmetry.

$$\begin{aligned} c_{2120} := & \frac{1}{120} \left(32(f_{0,0,1,0} + f_{1,0,0,0}) + 7(f_{-1,1,0,1} + f_{1,1,0,-1} + f_{0,1,1,-1} + f_{0,1,-1,1}) \right. \\ & + 3(f_{0,2,-1,0} + f_{0,-1,1,1} + f_{1,-1,0,1} + f_{1,-1,2,-1} + f_{-1,2,0,0} + f_{2,-1,1,-1}) \\ & \left. + 2(f_{-1,0,0,2} + f_{1,0,2,-2} + f_{0,0,-1,2} + f_{2,0,1,-2}) + (f_{1,-2,2,0} + f_{2,-2,1,0}) \right) \end{aligned} \quad (\text{A.11})$$

The associated weight mask is shown in figure A.11.

B-coefficient c_{2021} is computed using $(1, 3)$ -symmetry.

$$\begin{aligned} c_{2111} := & \frac{1}{960} \left(316f_{1,0,0,0} + 202f_{0,0,1,0} + 94f_{0,1,-1,1} + 60f_{-1,1,0,1} + 38(f_{1,1,0,-1} + f_{1,-1,0,1}) \right. \\ & + 29(f_{0,-1,1,1} + f_{0,1,1,-1}) + 23(f_{0,2,-1,0} + f_{0,0,-1,2}) + 22(f_{-1,2,0,0} + f_{-1,0,0,2}) \\ & + 14(f_{1,-1,2,-1} + f_{2,-1,1,-1}) + 7(f_{1,0,2,-2} + f_{1,-2,2,0} + f_{2,0,1,-2} + f_{2,-2,1,0}) \\ & \left. + 2(f_{1,1,-2,1} + f_{2,0,-1,0}) + (f_{1,0,-2,2} + f_{1,2,-2,0} + f_{2,-1,-1,1} + f_{2,1,-1,-1}) \right) \end{aligned} \quad (\text{A.12})$$

The associated weight mask is shown in figure A.12.

B-coefficient c_{1121} is computed using $(0, 2)$ -symmetry.

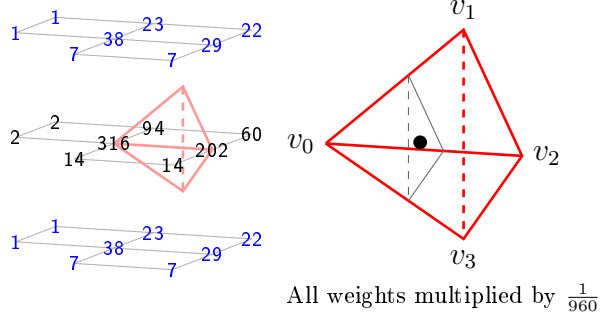


Figure A.12: Weight mask for c_{2111} . The associated domain point is shown in the tetrahedron on the right. The black triangle symbolizes the ring $R_3(v_0)$.

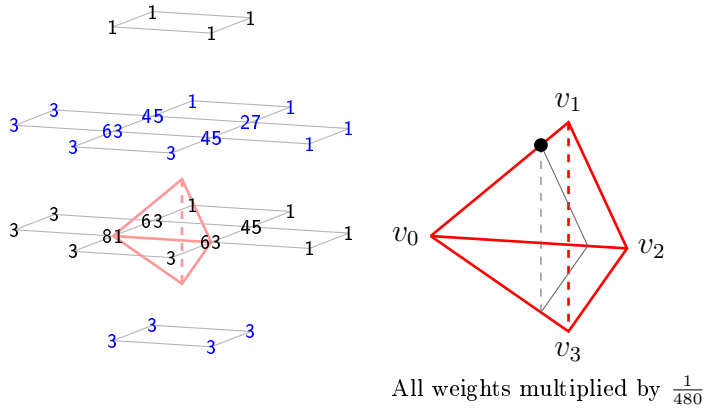


Figure A.13: Weight mask for c_{1400} . The associated domain point is shown in the tetrahedron on the right. The black triangle symbolizes the ring $R_4(v_0)$.

$$\begin{aligned}
 c_{1400} := & \frac{1}{480} \left(81f_{1,0,0,0} + 63(f_{0,1,-1,1} + f_{0,0,1,0} + f_{1,1,0,-1}) \right. \\
 & + 45(f_{0,1,1,-1} + f_{0,2,-1,0} + f_{-1,1,0,1}) + 27f_{-1,2,0,0} \\
 & + 3(f_{1,-1,2,-1} + f_{2,1,-1,-1} + f_{2,-1,1,-1} + f_{2,0,1,-2} + f_{2,0,-1,0} + f_{1,2,-2,0} \\
 & \quad + f_{1,1,-2,1} + f_{1,-1,0,1} + f_{1,0,2,-2} + f_{-1,0,0,2} + f_{0,0,-1,2} + f_{0,-1,1,1}) \\
 & + (f_{-1,3,-2,1} + f_{-2,3,-1,1} + f_{-2,2,-1,2} + f_{-2,2,1,0} + f_{-2,1,1,1} + f_{0,2,1,-2} \\
 & \quad \left. + f_{0,3,-1,-1} + f_{-1,1,2,-1} + f_{-1,3,0,-1} + f_{-1,2,-2,2} + f_{1,2,0,-2} + f_{-1,0,2,0} \right) \tag{A.13}
 \end{aligned}$$

The associated weight mask is shown in figure A.13.

B-coefficient c_{0410} is computed using $(0, 2)$ -symmetry.

B-coefficient c_{1004} is computed using $(1, 3)$ -symmetry.

B-coefficient c_{0014} is computed using both $(0, 2)$ -symmetry and $(1, 3)$ -symmetry.

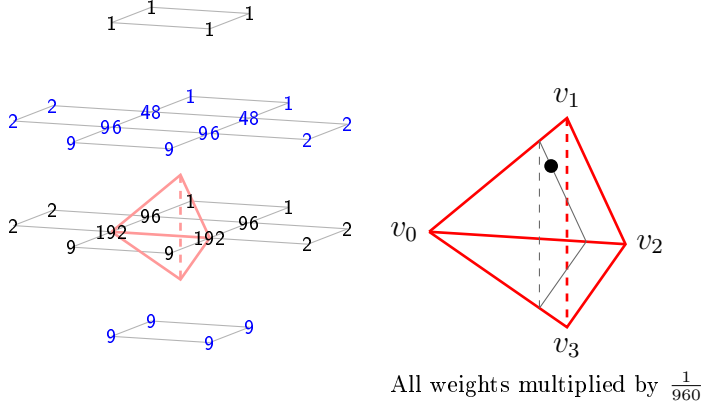


Figure A.14: Weight mask for c_{1310} . The associated domain point is shown in the teterahedron on the right. The black triangle symbolizes the ring $R_4(v_0)$.

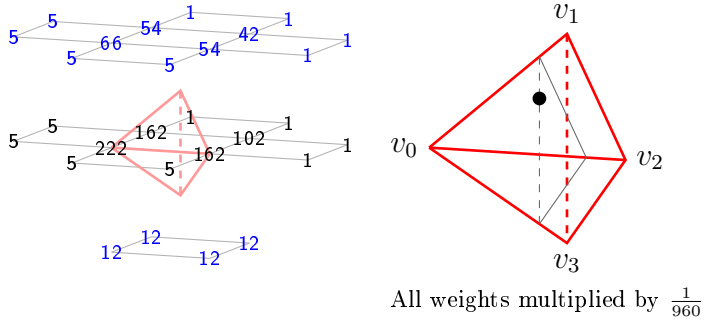


Figure A.15: Weight mask for c_{1301} . The associated domain point is shown in the teterahedron on the right. The black triangle symbolizes the ring $R_4(v_0)$.

$$\begin{aligned}
 c_{1310} := & \frac{1}{960} \left(192(f_{0,0,1,0} + f_{1,0,0,0}) + 96(f_{0,1,-1,1} + f_{0,1,1,-1} + f_{1,1,0,-1} + f_{-1,1,0,1}) \right. \\
 & + 48(f_{0,2,-1,0} + f_{-1,2,0,0}) \\
 & + 9(f_{1,-1,2,-1} + f_{2,-1,1,-1} + f_{2,0,1,-2} + f_{1,-1,0,1} + f_{-1,0,0,2} + f_{1,0,2,-2} \\
 & \quad + f_{0,0,-1,2} + f_{0,-1,1,1}) \\
 & + 2(f_{-1,0,2,0} + f_{-1,1,2,-1} + f_{1,1,-2,1} + f_{-2,2,1,0} + f_{1,2,-2,0} + f_{2,1,-1,-1} \\
 & \quad + f_{-2,1,1,1} + f_{2,0,-1,0}) \\
 & + (f_{-2,3,-1,1} + f_{-2,2,-1,2} + f_{-1,3,-2,1} + f_{-1,3,0,-1} + f_{-1,2,-2,2} + f_{1,2,0,-2} \\
 & \quad \left. + f_{0,2,1,-2} + f_{0,3,-1,-1} \right) \tag{A.14}
 \end{aligned}$$

The associated weight mask is shown in figure A.14.
B-coefficient c_{1013} is computed using (1, 3)-symmetry.

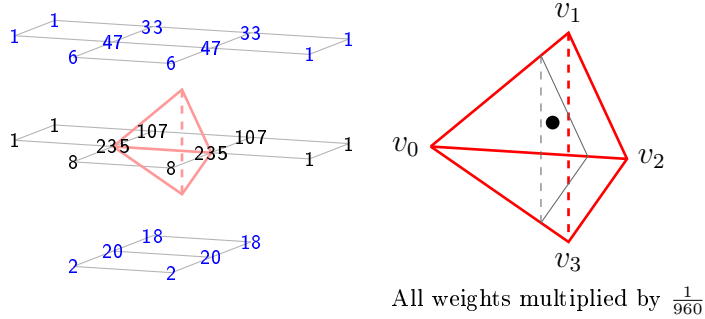


Figure A.16: Weight mask for c_{1211} . The associated domain point is shown in the teterahedron on the right. The black triangle symbolizes the ring $R_4(v_0)$.

$$\begin{aligned}
 c_{1301} := & \frac{1}{960} \left(222f_{1,0,0,0} + 162(f_{0,1,-1,1} + f_{0,0,1,0}) + 102f_{-1,1,0,1} + 66f_{1,1,0,-1} \right. \\
 & + 54(f_{0,1,1,-1} + f_{0,2,-1,0}) + 42f_{-1,2,0,0} \\
 & + 12(f_{0,0,-1,2} + f_{0,-1,1,1} + f_{-1,0,0,2} + f_{1,-1,0,1}) \\
 & + 5(f_{2,1,-1,-1} + f_{2,0,-1,0} + f_{2,0,1,-2} + f_{2,-1,1,-1} + f_{1,-1,2,-1} + f_{1,2,-2,0} \\
 & \quad + f_{1,1,-2,1} + f_{1,0,2,-2}) \\
 & + (f_{-1,2,-2,2} + f_{-1,3,-2,1} + f_{-1,1,2,-1} + f_{-2,1,1,1} + f_{-1,0,2,0} + f_{-2,2,1,0} \\
 & \quad \left. + f_{-2,2,-1,2} + f_{-2,3,-1,1} \right) \tag{A.15}
 \end{aligned}$$

The associated weight mask is shown in figure A.15.

B-coefficient c_{0311} is computed using $(0, 2)$ -symmetry.

B-coefficient c_{1103} is computed using $(1, 3)$ -symmetry.

B-coefficient c_{0113} is computed using both $(0, 2)$ -symmetry and $(1, 3)$ -symmetry.

$$\begin{aligned}
 c_{1211} := & \frac{1}{960} \left(235(f_{0,0,1,0} + f_{1,0,0,0}) + 107(f_{-1,1,0,1} + f_{0,1,-1,1}) + 47(f_{1,1,0,-1} + f_{0,1,1,-1}) \right. \\
 & + 33(f_{-1,2,0,0} + f_{0,2,-1,0}) + 20(f_{0,-1,1,1} + f_{1,-1,0,1}) + 18(f_{-1,0,0,2} + f_{0,0,-1,2}) \\
 & + 8(f_{2,-1,1,-1} + f_{1,-1,2,-1}) + 6(f_{1,0,2,-2} + f_{2,0,1,-2}) + 2(f_{2,-2,1,0} + f_{1,-2,2,0}) \\
 & + (f_{1,2,-2,0} + f_{2,0,-1,0} + f_{1,1,-2,1} + f_{-2,1,1,1} + f_{-1,1,2,-1} + f_{2,1,-1,-1} \\
 & \quad \left. + f_{-2,2,1,0} + f_{-1,0,2,0}) \right) \tag{A.16}
 \end{aligned}$$

The associated weight mask is shown in figure A.16.

B-coefficient c_{1112} is computed using $(1, 3)$ -symmetry.

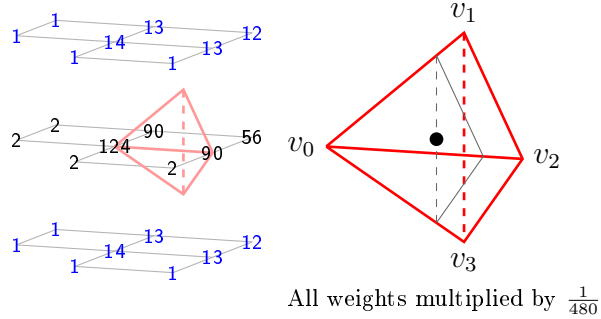


Figure A.17: Weight mask for c_{1202} . The associated domain point is shown in the teterahedron on the right. The black triangle symbolizes the ring $R_4(v_0)$.

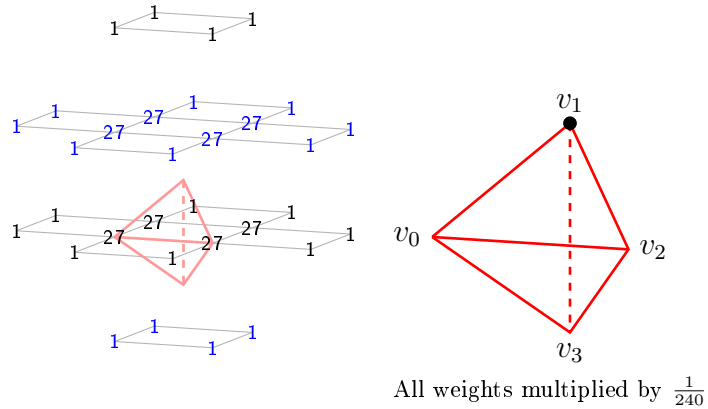


Figure A.18: Weight mask for c_{0500} . The associated domain point is shown in the teterahedron on the right.

$$\begin{aligned}
 c_{1202} := & \frac{1}{480} \left(124f_{1,0,0,0} + 90(f_{0,0,1,0} + f_{0,1,-1,1}) + 56f_{-1,1,0,1} + 14(f_{1,1,0,-1} + f_{1,-1,0,1}) \right. \\
 & + 13(f_{0,2,-1,0} + f_{0,0,-1,2} + f_{0,-1,1,1} + f_{0,1,1,-1}) + 12(f_{-1,2,0,0} + f_{-1,0,0,2}) \\
 & + 2(f_{1,-1,2,-1} + f_{1,1,-2,1} + f_{2,0,-1,0} + f_{2,-1,1,-1}) \\
 & + (f_{1,0,2,-2} + f_{1,0,-2,2} + f_{1,-2,2,0} + f_{1,2,-2,0} + f_{2,0,1,-2} + f_{2,-1,-1,1} \\
 & \left. + f_{2,1,-1,-1} + f_{2,-2,1,0}) \right) \tag{A.17}
 \end{aligned}$$

The associated weight mask is shown in figure A.17.
B-coefficient c_{0212} is computed using $(0, 2)$ -symmetry.

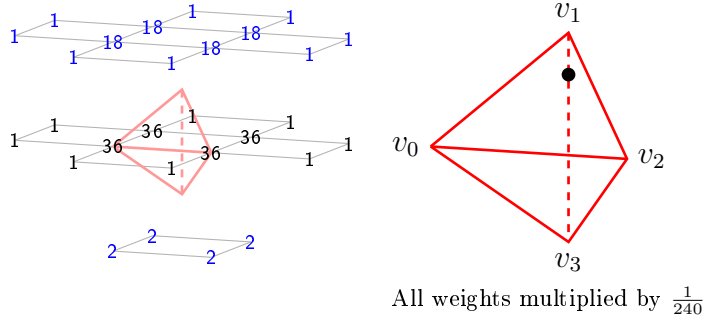


Figure A.19: Weight mask for c_{0401} . The associated domain point is shown in the teterahedron on the right.

$$\begin{aligned}
 c_{0500} := & \frac{1}{240} \left(27(f_{0,0,1,0} + f_{0,1,-1,1} + f_{0,1,1,-1} + f_{0,2,-1,0} + f_{-1,2,0,0} + f_{1,0,0,0} \right. \\
 & + f_{1,1,0,-1} + f_{-1,1,0,1}) \\
 & + (f_{-2,1,1,1} + f_{1,2,-2,0} + f_{-1,2,-2,2} + f_{-1,3,0,-1} + f_{-1,3,-2,1} + f_{2,0,-1,0} \\
 & + f_{2,0,1,-2} + f_{-2,3,-1,1} + f_{2,-1,1,-1} + f_{2,1,-1,-1} + f_{-2,2,1,0} + f_{-2,2,-1,2} \\
 & + f_{1,2,0,-2} + f_{1,1,-2,1} + f_{1,-1,2,-1} + f_{-1,1,2,-1} + f_{1,-1,0,1} + f_{1,0,2,-2} \\
 & \left. + f_{-1,0,2,0} + f_{-1,0,0,2} + f_{0,3,-1,-1} + f_{0,2,1,-2} + f_{0,-1,1,1} + f_{0,0,-1,2}) \right) \quad (\text{A.18})
 \end{aligned}$$

The associated weight mask is shown in figure A.18.
B-coefficient c_{0005} is computed using (1, 3)-symmetry.

$$\begin{aligned}
 c_{0401} := & \frac{1}{240} \left(36(f_{0,1,-1,1} + f_{1,0,0,0} + f_{0,0,1,0} + f_{-1,1,0,1}) \right. \\
 & + 18(f_{0,1,1,-1} + f_{0,2,-1,0} + f_{1,1,0,-1} + f_{-1,2,0,0}) \\
 & + 2(f_{0,0,-1,2} + f_{0,-1,1,1} + f_{-1,0,0,2} + f_{1,-1,0,1}) \\
 & + (f_{2,0,-1,0} + f_{-2,3,-1,1} + f_{2,0,1,-2} + f_{-2,1,1,1} + f_{2,-1,1,-1} + f_{2,1,-1,-1} \\
 & + f_{-2,2,1,0} + f_{-2,2,-1,2} + f_{-1,3,-2,1} + f_{-1,2,-2,2} + f_{1,2,-2,0} + f_{1,1,-2,1} \\
 & \left. + f_{1,-1,2,-1} + f_{-1,1,2,-1} + f_{1,0,2,-2} + f_{-1,0,2,0}) \right) \quad (\text{A.19})
 \end{aligned}$$

The associated weight mask is shown in figure A.19.
B-coefficient c_{0104} is computed using (1, 3)-symmetry.

$$\begin{aligned}
 c_{0302} := & \frac{1}{480} \left(90(f_{0,1,-1,1} + f_{1,0,0,0} + f_{0,0,1,0} + f_{-1,1,0,1}) \right. \\
 & + 18(f_{0,1,1,-1} + f_{0,2,-1,0} + f_{1,1,0,-1} + f_{-1,2,0,0}) \\
 & + 8(f_{0,0,-1,2} + f_{0,-1,1,1} + f_{-1,0,0,2} + f_{1,-1,0,1}) \\
 & + (f_{2,0,-1,0} + f_{-2,3,-1,1} + f_{2,0,1,-2} + f_{-2,1,1,1} + f_{2,-1,1,-1} + f_{2,1,-1,-1} \\
 & + f_{-2,2,1,0} + f_{-2,2,-1,2} + f_{-1,3,-2,1} + f_{-1,2,-2,2} + f_{1,2,-2,0} + f_{1,1,-2,1} \\
 & \left. + f_{1,-1,2,-1} + f_{-1,1,2,-1} + f_{1,0,2,-2} + f_{-1,0,2,0}) \right) \quad (\text{A.20})
 \end{aligned}$$

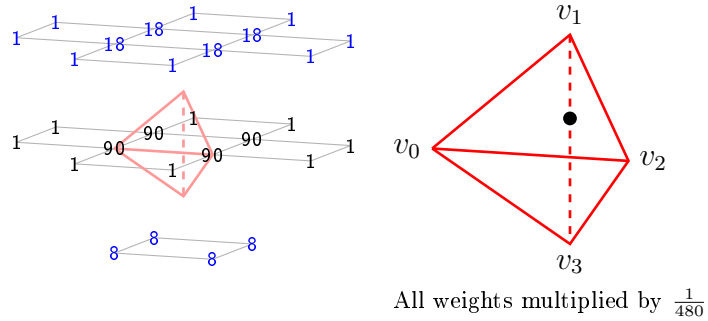


Figure A.20: Weight mask for c_{0302} . The associated domain point is shown in the teterahedron on the right.

The associated weight mask is shown in figure A.20.
 B-coefficient c_{0203} is computed using (1, 3)-symmetry.

Appendix B

B-coefficient computation rules for the optimal quasi-interpolation operator

On the following pages we give the B-coefficient computation rules that define the optimal quasi-interpolation operator developed in section 3.2 of chapter 3. We use the notation from 3.4 to specify the sample points in these rules. The rules are used to calculate the B-coefficients of $Q_{opt}(f)|_T$, where T is an arbitrary tetrahedron of the partition Δ_1 defined in 3.14. Each rule has an associated weight mask which shows the location of the samples relative to the tetrahedron.

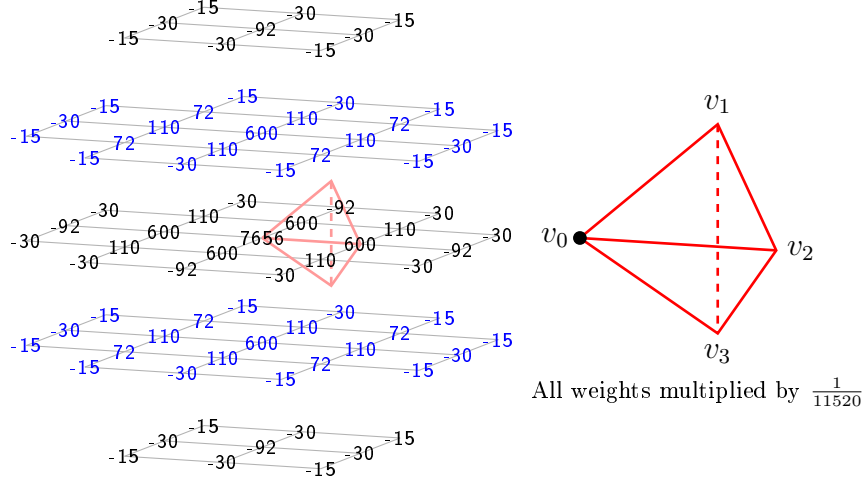


Figure B.1: Weight mask for c_{5000} . The associated domain point is shown in the teterahedron on the right.

$$\begin{aligned}
 c_{5000} := & \frac{1}{11520} \left(7656 f_{1,0,0,0} \right. \\
 & + 600(f_{2,0,-1,0} + f_{0,0,1,0} + f_{0,1,-1,1} + f_{2,-1,1,-1} + f_{1,1,0,-1} + f_{1,-1,0,1}) \\
 & + 110(f_{2,0,1,-2} + f_{2,-1,-1,1} + f_{2,1,-1,-1} + f_{1,1,-2,1} + f_{1,-1,2,-1} + f_{-1,1,0,1} \\
 & \quad + f_{3,-1,0,-1} + f_{2,-2,1,0} + f_{0,0,-1,2} + f_{0,-1,1,1} + f_{0,1,1,-1} + f_{0,2,-1,0}) \\
 & - 92(f_{3,-2,2,-2} + f_{1,-2,0,2} + f_{-1,2,-2,2} + f_{1,2,0,-2} + f_{3,0,-2,0} + f_{-1,0,2,0}) \\
 & + 72(f_{1,-2,2,0} + f_{3,-2,0,0} + f_{1,0,2,-2} + f_{3,0,0,-2} + f_{1,2,-2,0} + f_{1,0,-2,2} \\
 & \quad + f_{-1,2,0,0} + f_{-1,0,0,2}) \\
 & - 30(f_{3,1,-2,-1} + f_{-2,1,1,1} + f_{3,-3,2,-1} + f_{2,-3,1,1} + f_{2,-2,3,-2} + f_{3,-1,-2,1} \\
 & \quad + f_{2,1,1,-3} + f_{2,1,-3,1} + f_{2,2,-1,-2} + f_{2,-2,-1,2} + f_{-2,2,-1,2} + f_{3,-1,2,-3} \\
 & \quad + f_{0,-1,-1,3} + f_{0,-1,3,-1} + f_{4,-2,1,-2} + f_{0,-2,1,2} + f_{0,2,1,-2} + f_{0,2,-3,2} \\
 & \quad + f_{0,3,-1,-1} + f_{4,-1,-1,-1} + f_{-1,-1,2,1} + f_{-1,1,2,-1} + f_{-1,1,-2,3} + f_{-1,3,-2,1}) \\
 & - 15(f_{3,1,0,-3} + f_{4,-1,1,-3} + f_{4,-2,-1,0} + f_{4,0,-1,-2} + f_{4,-3,1,-1} + f_{3,-3,0,1} \\
 & \quad + f_{1,-3,2,1} + f_{0,0,3,-2} + f_{0,1,-3,3} + f_{0,-2,3,0} + f_{0,3,-3,1} + f_{-1,-1,0,3} \\
 & \quad + f_{1,-1,-2,3} + f_{1,1,2,-3} + f_{-1,3,0,-1} + f_{2,-3,3,-1} + f_{1,3,-2,-1} + f_{-2,0,1,2} \\
 & \quad \left. + f_{2,0,-3,2} + f_{-2,1,-1,3} + f_{2,-1,3,-3} + f_{-2,2,1,0} + f_{2,2,-3,0} + f_{-2,3,-1,1} \right) \tag{B.1}
 \end{aligned}$$

The associated weight mask is shown in figure B.1.
B-coefficient c_{0050} is computed using $(0, 2)$ -symmetry.

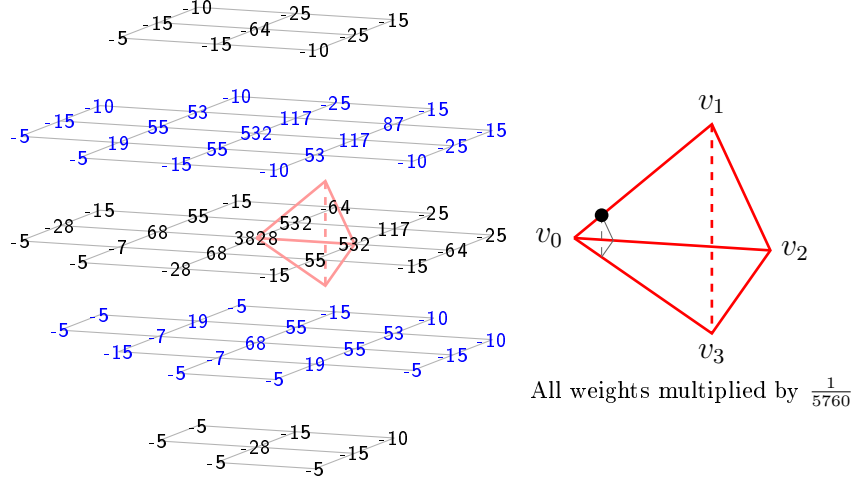


Figure B.2: Weight mask for c_{4100} . The associated domain point is shown in the teterahedron on the right. The black triangle symbolizes the ring $R_1(v_0)$.

$$\begin{aligned}
 c_{4100} := & \frac{1}{5760} \left(3828f_{1,0,0,0} + 532(f_{0,1,-1,1} + f_{1,1,0,-1} + f_{0,0,1,0}) \right. \\
 & + 117(f_{0,1,1,-1} + f_{-1,1,0,1} + f_{0,2,-1,0}) + 87f_{-1,2,0,0} \\
 & + 68(f_{1,-1,0,1} + f_{2,-1,1,-1} + f_{2,0,-1,0}) - 64(f_{1,2,0,-2} + f_{-1,0,2,0} + f_{-1,2,-2,2}) \\
 & + 55(f_{1,1,-2,1} + f_{1,-1,2,-1} + f_{2,0,1,-2} + f_{2,1,-1,-1} + f_{0,-1,1,1} + f_{0,0,-1,2}) \\
 & + 53(f_{-1,0,0,2} + f_{1,2,-2,0} + f_{1,0,2,-2}) - 28(f_{3,0,-2,0} + f_{1,-2,0,2} + f_{3,-2,2,-2}) \\
 & - 25(f_{-2,1,1,1} + f_{-2,2,-1,2} + f_{-1,3,-2,1} + f_{-1,1,2,-1} + f_{0,3,-1,-1} + f_{0,2,1,-2}) \\
 & + 19(f_{1,-2,2,0} + f_{1,0,-2,2} + f_{3,0,0,-2}) \\
 & - 15(f_{-1,1,-2,3} + f_{2,1,-3,1} + f_{2,1,1,-3} + f_{-2,2,1,0} + f_{0,-1,3,-1} + f_{0,-2,1,2} \\
 & \quad + f_{2,2,-1,-2} + f_{2,-2,3,-2} + f_{-2,3,-1,1} + f_{0,2,-3,2} + f_{0,-1,-1,3} + f_{-1,3,0,-1} \\
 & \quad + f_{3,1,-2,-1} + f_{3,-1,2,-3} + f_{-1,-1,2,1} + f_{3,-2,0,0}) \\
 & - 10(f_{2,2,-3,0} + f_{0,0,3,-2} + f_{2,-1,3,-3} + f_{1,1,2,-3} + f_{-1,-1,0,3} + f_{0,3,-3,1} \\
 & \quad + f_{-2,1,-1,3} + f_{1,3,-2,-1} + f_{-2,0,1,2}) \\
 & - 7(f_{3,-1,0,-1} + f_{2,-1,-1,1} + f_{2,-2,1,0}) \\
 & - 5(f_{2,-2,-1,2} + f_{4,-2,1,-2} + f_{4,-1,1,-3} + f_{4,-1,-1,-1} + f_{4,0,-1,-2} + f_{3,-3,2,-1} \\
 & \quad + f_{1,-1,-2,3} + f_{0,1,-3,3} + f_{0,-2,3,0} + f_{3,-1,-2,1} + f_{3,1,0,-3} + f_{1,-3,2,1} \\
 & \quad + f_{2,0,-3,2} + f_{2,-3,3,-1} + f_{2,-3,1,1}) \Big) \tag{B.2}
 \end{aligned}$$

The associated weight mask is shown in figure B.2.

B-coefficient c_{0140} is computed using $(0, 2)$ -symmetry.

B-coefficient c_{4001} is computed using $(1, 3)$ -symmetry.

B-coefficient c_{0041} is computed using both $(0, 2)$ -symmetry and $(1, 3)$ -symmetry.

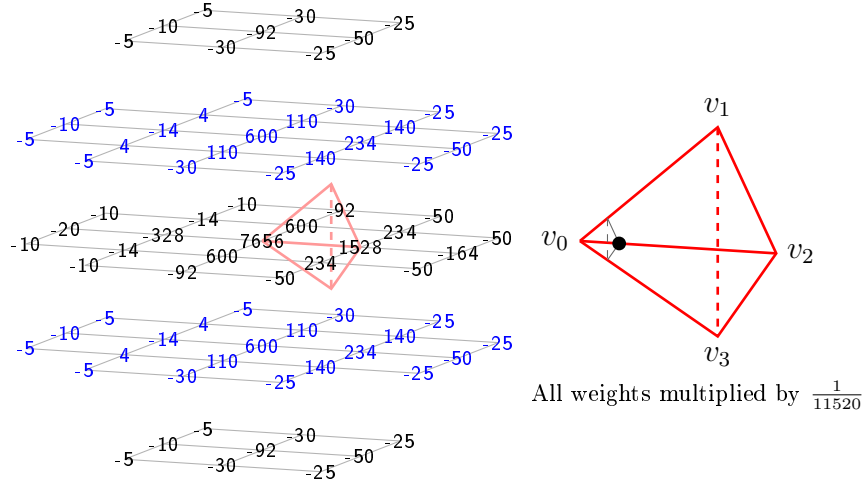


Figure B.3: Weight mask for c_{4010} . The associated domain point is shown in the tetrahedron on the right. The black triangle symbolizes the ring $R_1(v_0)$.

$$\begin{aligned}
c_{4010} := & \frac{1}{11520} \left(7656f_{1,0,0,0} + 1528f_{0,0,1,0} + 600(f_{0,1,-1,1} + f_{2,-1,1,-1} + f_{1,1,0,-1} + f_{1,-1,0,1}) \right. \\
& - 328f_{2,0,-1,0} + 234(f_{0,-1,1,1} + f_{0,1,1,-1} + f_{1,-1,2,-1} + f_{-1,1,0,1}) - 164f_{-1,0,2,0} \\
& + 140(f_{1,0,2,-2} + f_{-1,0,0,2} + f_{-1,2,0,0} + f_{1,-2,2,0}) \\
& + 110(f_{0,2,-1,0} + f_{2,0,1,-2} + f_{0,0,-1,2} + f_{2,-2,1,0}) \\
& - 92(f_{1,2,0,-2} + f_{1,-2,0,2} + f_{-1,2,-2,2} + f_{3,-2,2,-2}) \\
& - 50(f_{-2,1,1,1} + f_{-2,2,-1,2} + f_{-1,-1,2,1} + f_{2,-2,3,-2} + f_{-1,1,2,-1} + f_{0,-1,3,-1} \\
& \quad + f_{0,2,1,-2} + f_{0,-2,1,2}) \\
& - 30(f_{-1,1,-2,3} + f_{3,-3,2,-1} + f_{2,-3,1,1} + f_{0,3,-1,-1} + f_{0,-1,-1,3} + f_{3,-1,2,-3} \\
& \quad + f_{2,1,1,-3} + f_{-1,3,-2,1}) \\
& - 25(f_{1,-3,2,1} + f_{-2,1,-1,3} + f_{2,-1,3,-3} + f_{2,-3,3,-1} + f_{-2,2,1,0} + f_{-2,3,-1,1} \\
& \quad + f_{-2,0,1,2} + f_{0,0,3,-2} + f_{-1,3,0,-1} + f_{-1,-1,0,3} + f_{0,-2,3,0} + f_{1,1,2,-3}) \\
& - 20f_{3,0,-2,0} - 14(f_{1,1,-2,1} + f_{3,-1,0,-1} + f_{2,1,-1,-1} + f_{2,-1,-1,1}) \\
& - 10(f_{4,-2,1,-2} + f_{2,-2,-1,2} + f_{2,2,-1,-2} + f_{3,1,-2,-1} + f_{2,1,-3,1} + f_{4,-1,-1,-1} \\
& \quad + f_{3,-1,-2,1} + f_{0,2,-3,2}) \\
& - 5(f_{4,-1,1,-3} + f_{0,1,-3,3} + f_{3,-3,0,1} + f_{4,0,-1,-2} + f_{4,-3,1,-1} + f_{4,-2,-1,0} \\
& \quad + f_{2,0,-3,2} + f_{3,1,0,-3} + f_{0,3,-3,1} + f_{2,2,-3,0} + f_{1,-1,-2,3} + f_{1,3,-2,-1}) \\
& \left. + 4(f_{3,-2,0,0} + f_{3,0,0,-2} + f_{1,0,-2,2} + f_{1,2,-2,0}) \right) \tag{B.3}
\end{aligned}$$

The associated weight mask is shown in figure B.3. B-coefficient c_{1040} is computed using $(0, 2)$ -symmetry.

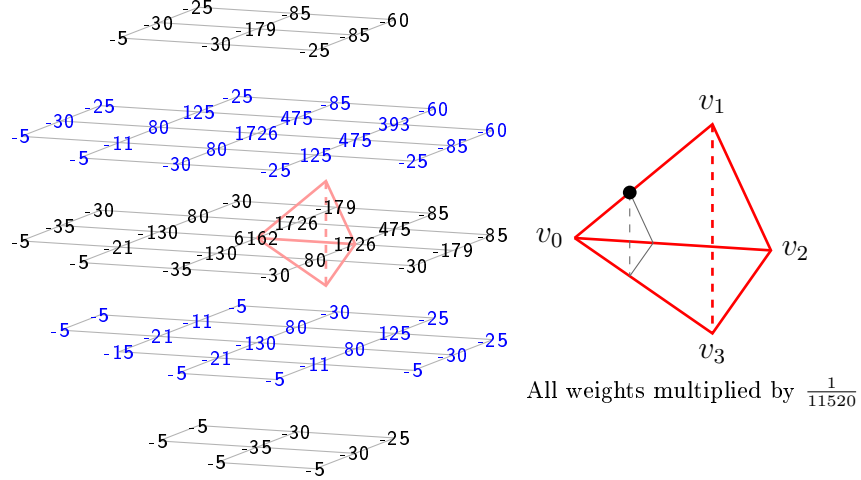


Figure B.4: Weight mask for c_{3200} . The associated domain point is shown in the teterahedron on the right. The black triangle symbolizes the ring $R_2(v_0)$.

$$\begin{aligned}
 c_{3200} := & \frac{1}{11520} \left(6162f_{1,0,0,0} + 1726(f_{1,1,0,-1} + f_{0,1,-1,1} + f_{0,0,1,0}) \right. \\
 & + 475(f_{-1,1,0,1} + f_{0,1,1,-1} + f_{0,2,-1,0}) + 393f_{-1,2,0,0} \\
 & - 179(f_{-1,2,-2,2} + f_{1,2,0,-2} + f_{-1,0,2,0}) - 130(f_{2,0,-1,0} + f_{2,-1,1,-1} + f_{1,-1,0,1}) \\
 & + 125(f_{1,2,-2,0} + f_{-1,0,0,2} + f_{1,0,2,-2}) \\
 & - 85(f_{-1,1,2,-1} + f_{-1,3,-2,1} + f_{-2,1,1,1} + f_{-2,2,-1,2} + f_{0,3,-1,-1} + f_{0,2,1,-2}) \\
 & + 80(f_{2,1,-1,-1} + f_{0,0,-1,2} + f_{1,-1,2,-1} + f_{1,1,-2,1} + f_{0,-1,1,1} + f_{2,0,1,-2}) \\
 & - 60(f_{-2,3,-1,1} + f_{-1,3,0,-1} + f_{-2,2,1,0}) - 35(f_{3,-2,2,-2} + f_{1,-2,0,2} + f_{3,0,-2,0}) \\
 & - 30(f_{0,-1,-1,3} + f_{3,-1,2,-3} + f_{2,1,-3,1} + f_{2,1,1,-3} + f_{0,-1,3,-1} + f_{3,1,-2,-1} \\
 & \quad + f_{0,-2,1,2} + f_{2,2,-1,-2} + f_{-1,1,-2,3} + f_{0,2,-3,2} + f_{-1,-1,2,1} + f_{2,-2,3,-2}) \\
 & - 25(f_{1,3,-2,-1} + f_{2,-1,3,-3} + f_{2,2,-3,0} + f_{-2,1,-1,3} + f_{0,0,3,-2} + f_{-2,0,1,2} \\
 & \quad + f_{1,1,2,-3} + f_{-1,-1,0,3} + f_{0,3,-3,1}) \\
 & - 21(f_{2,-1,-1,1} + f_{2,-2,1,0} + f_{3,-1,0,-1}) - 15f_{3,-2,0,0} \\
 & - 11(f_{1,0,-2,2} + f_{3,0,0,-2} + f_{1,-2,2,0}) \\
 & - 5(f_{2,-3,1,1} + f_{2,-3,3,-1} + f_{2,-2,-1,2} + f_{2,0,-3,2} + f_{1,-3,2,1} + f_{3,1,0,-3} \\
 & \quad + f_{3,-1,-2,1} + f_{0,1,-3,3} + f_{0,-2,3,0} + f_{1,-1,-2,3} + f_{3,-3,2,-1} + f_{4,0,-1,-2} \\
 & \quad + f_{4,-1,-1,-1} + f_{4,-1,1,-3} + f_{4,-2,1,-2}) \left. \right) \tag{B.4}
 \end{aligned}$$

The associated weight mask is shown in figure B.4.

B-coefficient c_{0230} is computed using $(0, 2)$ -symmetry.

B-coefficient c_{3002} is computed using $(1, 3)$ -symmetry.

B-coefficient c_{0032} is computed using both $(0, 2)$ -symmetry and $(1, 3)$ -symmetry.

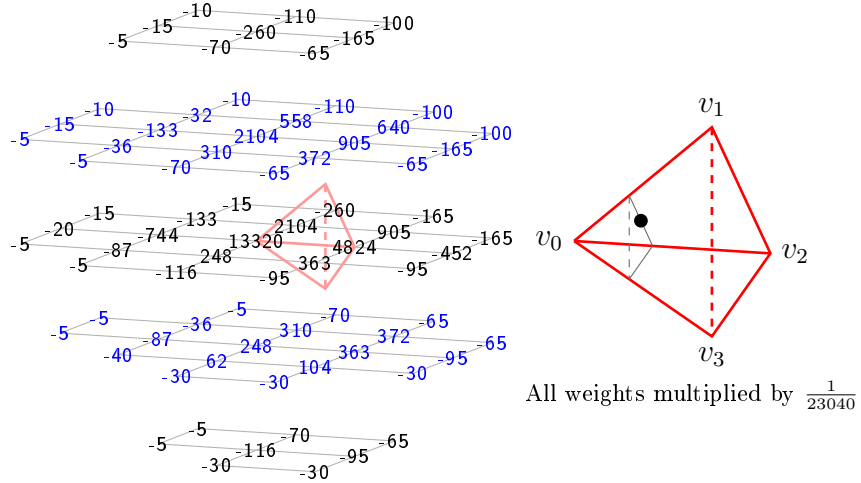


Figure B.5: Weight mask for c_{3110} . The associated domain point is shown in the tetrahedron on the right. The black triangle symbolizes the ring $R_2(v_0)$.

$$\begin{aligned}
 c_{3110} := & \frac{1}{23040} \left(13320f_{1,0,0,0} + 4824f_{0,0,1,0} + 2104(f_{0,1,-1,1} + f_{1,1,0,-1}) \right. \\
 & + 905(f_{0,1,-1,-1} + f_{-1,1,0,1}) - 744f_{2,0,-1,0} + 640f_{-1,2,0,0} + 558f_{0,2,-1,0} \\
 & - 452f_{-1,0,2,0} + 372(f_{1,0,2,-2} + f_{-1,0,0,2}) + 363(f_{1,-1,2,-1} + f_{0,-1,1,1}) \\
 & + 310(f_{2,0,1,-2} + f_{0,0,-1,2}) - 260(f_{-1,2,-2,2} + f_{1,2,0,-2}) + 248(f_{2,-1,1,-1} + f_{1,-1,0,1}) \\
 & - 165(f_{0,2,1,-2} + f_{-2,1,1,1} + f_{-1,1,2,-1} + f_{-2,2,-1,2}) - 133(f_{1,1,-2,1} + f_{2,1,-1,-1}) \\
 & - 116(f_{1,-2,0,2} + f_{3,-2,2,-2}) - 110(f_{-1,3,-2,1} + f_{0,3,-1,-1}) + 104f_{1,-2,2,0} \\
 & - 100(f_{-2,2,1,0} + f_{-1,3,0,-1} + f_{-2,3,-1,1}) \\
 & - 95(f_{0,-2,1,2} + f_{0,-1,3,-1} + f_{2,-2,3,-2} + f_{-1,-1,2,1}) - 87(f_{3,-1,0,-1} + f_{2,-1,-1,1}) \\
 & - 70(f_{0,-1,-1,3} + f_{3,-1,2,-3} + f_{-1,1,-2,3} + f_{2,1,1,-3}) \\
 & - 65(f_{-2,1,-1,3} + f_{0,0,3,-2} + f_{2,-1,3,-3} + f_{1,1,2,-3} + f_{-2,0,1,2} + f_{-1,-1,0,3}) \\
 & + 62f_{2,-2,1,0} - 40f_{3,-2,0,0} - 36(f_{3,0,0,-2} + f_{1,0,-2,2}) - 32f_{1,2,-2,0} \\
 & - 30(f_{3,-3,2,-1} + f_{2,-3,3,-1} + f_{2,-3,1,1} + f_{1,-3,2,1} + f_{0,-2,3,0}) - 20f_{3,0,-2,0} \\
 & - 15(f_{2,2,-1,-2} + f_{2,1,-3,1} + f_{0,2,-3,2} + f_{3,1,-2,-1}) \\
 & - 10(f_{2,2,-3,0} + f_{0,3,-3,1} + f_{1,3,-2,-1}) \\
 & - 5(f_{4,-1,1,-3} + f_{4,-1,-1,-1} + f_{4,0,-1,-2} + f_{2,0,-3,2} + f_{4,-2,1,-2} + f_{1,-1,-2,3} \\
 & \quad \left. + f_{3,-1,-2,1} + f_{3,1,0,-3} + f_{2,-2,-1,2} + f_{0,1,-3,3} \right) \tag{B.5}
 \end{aligned}$$

The associated weight mask is shown in figure B.5.

B-coefficient c_{1130} is computed using $(0, 2)$ -symmetry.

B-coefficient c_{3011} is computed using $(1, 3)$ -symmetry.

B-coefficient c_{1031} is computed using both $(0, 2)$ -symmetry and $(1, 3)$ -symmetry.

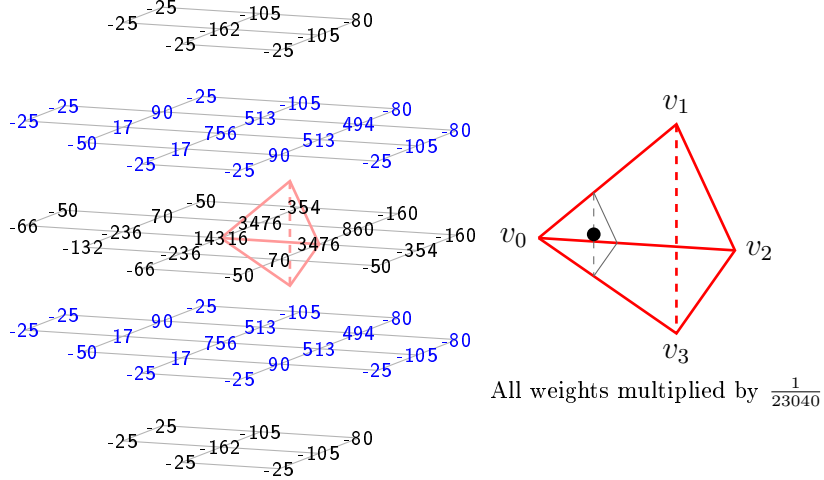


Figure B.6: Weight mask for c_{3101} . The associated domain point is shown in the teterahedron on the right. The black triangle symbolizes the ring $R_2(v_0)$.

$$\begin{aligned}
 c_{3101} := & \frac{1}{23040} \left(14316f_{1,0,0,0} + 3476(f_{0,1,-1,1} + f_{0,0,1,0}) + 860f_{-1,1,0,1} \right. \\
 & + 756(f_{1,-1,0,1} + f_{1,1,0,-1}) + 513(f_{0,0,-1,2} + f_{0,-1,1,1} + f_{0,1,1,-1} + f_{0,2,-1,0}) \\
 & + 494(f_{-1,2,0,0} + f_{-1,0,0,2}) - 354(f_{-1,2,-2,2} + f_{-1,0,2,0}) - 236(f_{2,-1,1,-1} + f_{2,0,-1,0}) \\
 & - 162(f_{1,-2,0,2} + f_{1,2,0,-2}) - 160(f_{-2,1,1,1} + f_{-2,2,-1,2}) - 132f_{3,-1,0,-1} \\
 & - 105(f_{-1,-1,2,1} + f_{-1,3,-2,1} + f_{-1,1,2,-1} + f_{-1,1,-2,3} + f_{0,3,-1,-1} + f_{0,2,1,-2} \\
 & \quad + f_{0,-2,1,2} + f_{0,-1,-1,3}) \\
 & + 90(f_{1,-2,2,0} + f_{1,2,-2,0} + f_{1,0,2,-2} + f_{1,0,-2,2}) \\
 & - 80(f_{-2,1,-1,3} + f_{-1,-1,0,3} + f_{-1,3,0,-1} + f_{-2,0,1,2} + f_{-2,3,-1,1} + f_{-2,2,1,0}) \\
 & + 70(f_{1,1,-2,1} + f_{1,-1,2,-1}) - 66(f_{3,-2,2,-2} + f_{3,0,-2,0}) \\
 & - 50(f_{0,-1,3,-1} + f_{2,1,-3,1} + f_{3,0,0,-2} + f_{2,-2,3,-2} + f_{0,2,-3,2} + f_{3,-2,0,0}) \\
 & - 25(f_{3,1,-2,-1} + f_{2,2,-3,0} + f_{2,-3,1,1} + f_{2,-3,3,-1} + f_{0,0,3,-2} + f_{3,-1,-2,1} \\
 & \quad + f_{3,-3,2,-1} + f_{3,-1,2,-3} + f_{1,1,2,-3} + f_{2,2,-1,-2} + f_{2,-2,-1,2} + f_{2,-1,3,-3} \\
 & \quad + f_{2,1,1,-3} + f_{0,1,-3,3} + f_{0,-2,3,0} + f_{2,0,-3,2} + f_{1,3,-2,-1} + f_{1,-3,2,1} \\
 & \quad + f_{0,3,-3,1} + f_{1,-1,-2,3}) \\
 & \left. + 17(f_{2,-2,1,0} + f_{2,1,-1,-1} + f_{2,-1,-1,1} + f_{2,0,1,-2}) \right) \tag{B.6}
 \end{aligned}$$

The associated weight mask is shown in figure B.6.
B-coefficient c_{0131} is computed using $(0, 2)$ -symmetry.

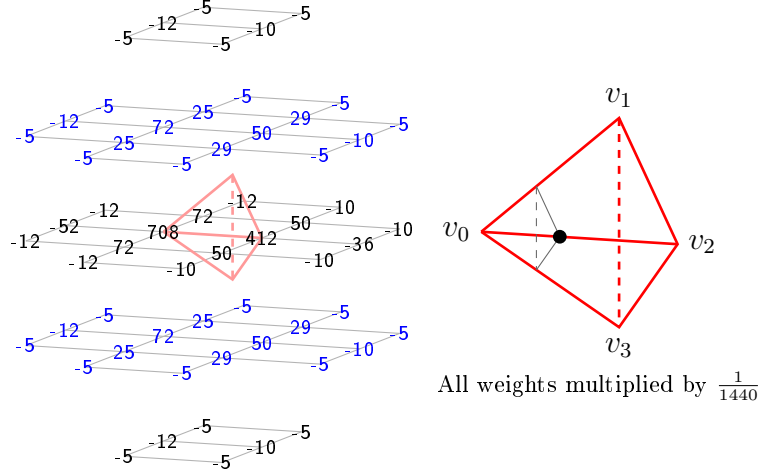


Figure B.7: Weight mask for c_{3020} . The associated domain point is shown in the teterahedron on the right. The black triangle symbolizes the ring $R_2(v_0)$.

$$\begin{aligned}
 c_{3020} := & \frac{1}{1440} \left(708f_{1,0,0,0} + 412f_{0,0,1,0} + 72(f_{0,1,-1,1} + f_{1,1,0,-1} + f_{1,-1,0,1} + f_{2,-1,1,-1}) \right. \\
 & - 52f_{2,0,-1,0} + 50(f_{1,-1,2,-1} + f_{0,-1,1,1} + f_{0,1,1,-1} + f_{-1,1,0,1}) - 36f_{-1,0,2,0} \\
 & + 29(f_{-1,2,0,0} + f_{1,-2,2,0} + f_{1,0,2,-2} + f_{-1,0,0,2}) \\
 & + 25(f_{2,0,1,-2} + f_{0,2,-1,0} + f_{2,-2,1,0} + f_{0,0,-1,2}) \\
 & - 12(f_{2,-1,-1,1} + f_{2,1,-1,-1} + f_{-1,2,-2,2} + f_{3,-1,0,-1} + f_{3,-2,2,-2} + f_{1,-2,0,2} \\
 & \quad + f_{1,2,0,-2} + f_{1,1,-2,1}) \\
 & - 10(f_{-1,1,2,-1} + f_{-1,-1,2,1} + f_{0,-1,3,-1} + f_{-2,2,-1,2} + f_{0,-2,1,2} + f_{0,2,1,-2} \\
 & \quad + f_{2,-2,3,-2} + f_{-2,1,1,1}) \\
 & - 5(f_{2,-3,3,-1} + f_{-2,2,1,0} + f_{-2,3,-1,1} + f_{2,-3,1,1} + f_{3,-3,2,-1} + f_{3,0,0,-2} \\
 & \quad + f_{0,-1,-1,3} + f_{3,-1,2,-3} + f_{3,-2,0,0} + f_{0,0,3,-2} + f_{1,1,2,-3} + f_{2,-1,3,-3} \\
 & \quad + f_{2,1,1,-3} + f_{-2,1,-1,3} + f_{0,-2,3,0} + f_{0,3,-1,-1} + f_{-2,0,1,2} + f_{1,0,-2,2} \\
 & \quad + f_{1,-3,2,1} + f_{-1,3,-2,1} + f_{-1,3,0,-1} + f_{-1,-1,0,3} + f_{1,2,-2,0} + f_{-1,1,-2,3}) \Big)
 \end{aligned} \tag{B.7}$$

The associated weight mask is shown in figure B.7.
 B -coefficient c_{2030} is computed using $(0, 2)$ -symmetry.

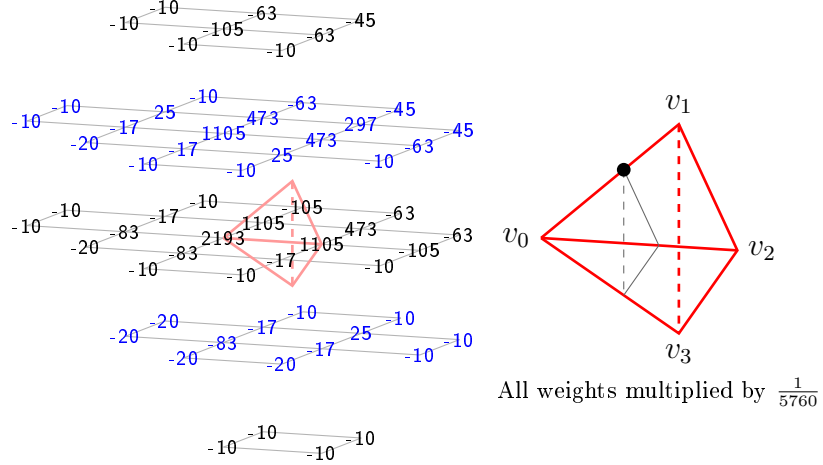


Figure B.8: Weight mask for c_{2300} . The associated domain point is shown in the teterahedron on the right. The black triangle symbolizes the ring $R_3(v_0)$.

$$\begin{aligned}
 c_{2300} := & \frac{1}{5760} \left(2193f_{1,0,0,0} + 1105(f_{0,0,1,0} + f_{0,1,-1,1} + f_{1,1,0,-1}) \right. \\
 & + 473(f_{0,1,1,-1} + f_{-1,1,0,1} + f_{0,2,-1,0}) + 297f_{-1,2,0,0} \\
 & - 105(f_{1,2,0,-2} + f_{-1,2,-2,2} + f_{-1,0,2,0}) - 83(f_{2,0,-1,0} + f_{1,-1,0,1} + f_{2,-1,1,-1}) \\
 & - 63(f_{0,3,-1,-1} + f_{-2,1,1,1} + f_{0,2,1,-2} + f_{-1,3,-2,1} + f_{-2,2,-1,2} + f_{-1,1,2,-1}) \\
 & - 45(f_{-1,3,0,-1} + f_{-2,2,1,0} + f_{-2,3,-1,1}) + 25(f_{1,2,-2,0} + f_{1,0,2,-2} + f_{-1,0,0,2}) \\
 & - 20(f_{3,0,0,-2} + f_{3,-1,0,-1} + f_{1,0,-2,2} + f_{2,-1,-1,1} + f_{2,-2,1,0} + f_{1,-2,2,0}) \\
 & - 17(f_{0,0,-1,2} + f_{1,-1,2,-1} + f_{2,0,1,-2} + f_{0,-1,1,1} + f_{1,1,-2,1} + f_{2,1,-1,-1}) \\
 & - 10(f_{2,-1,3,-3} + f_{3,-2,2,-2} + f_{2,2,-1,-2} + f_{2,2,-3,0} + f_{2,-2,3,-2} + f_{3,0,-2,0}) \\
 & + f_{3,1,-2,-1} + f_{3,-1,2,-3} + f_{0,2,-3,2} + f_{2,1,-3,1} + f_{2,1,1,-3} + f_{-2,1,-1,3} \\
 & + f_{-2,0,1,2} + f_{1,3,-2,-1} + f_{0,0,3,-2} + f_{1,-2,0,2} + f_{1,1,2,-3} + f_{-1,1,-2,3} \\
 & \left. + f_{-1,-1,2,1} + f_{-1,-1,0,3} + f_{0,-1,-1,3} + f_{0,-1,3,-1} + f_{0,-2,1,2} + f_{0,3,-3,1} \right) \tag{B.8}
 \end{aligned}$$

The associated weight mask is shown in figure B.8.

B-coefficient c_{0320} is computed using $(0, 2)$ -symmetry.

B-coefficient c_{2003} is computed using $(1, 3)$ -symmetry.

B-coefficient c_{0023} is computed using both $(0, 2)$ -symmetry and $(1, 3)$ -symmetry.

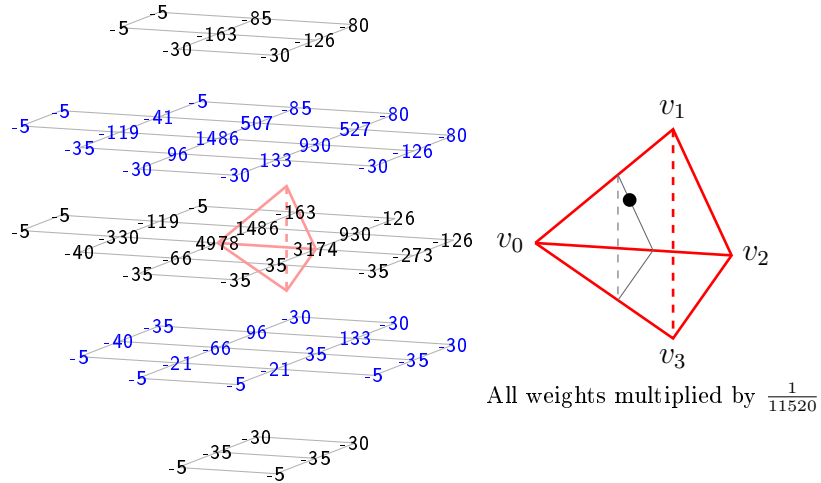


Figure B.9: Weight mask for c_{2210} . The associated domain point is shown in the teterahedron on the right. The black triangle symbolizes the ring $R_3(v_0)$.

$$\begin{aligned}
c_{2210} := & \frac{1}{11520} \left(4978f_{1,0,0,0} + 3174f_{0,0,1,0} + 1486(f_{1,1,0,-1} + f_{0,1,-1,1}) \right. \\
& + 930(f_{-1,1,0,1} + f_{0,1,1,-1}) + 527f_{-1,2,0,0} + 507f_{0,2,-1,0} - 330f_{2,0,-1,0} \\
& - 273f_{-1,0,2,0} - 163(f_{1,2,0,-2} + f_{-1,2,-2,2}) + 133(f_{-1,0,0,2} + f_{1,0,2,-2}) \\
& - 126(f_{0,2,1,-2} + f_{-2,1,1,1} + f_{-2,2,-1,2} + f_{-1,1,2,-1}) - 119(f_{1,1,-2,1} + f_{2,1,-1,-1}) \\
& + 96(f_{2,0,1,-2} + f_{0,0,-1,2}) - 85(f_{-1,3,-2,1} + f_{0,3,-1,-1}) \\
& - 80(f_{-1,3,0,-1} + f_{-2,3,-1,1} + f_{-2,2,1,0}) - 66(f_{1,-1,0,1} + f_{2,-1,1,-1}) - 41f_{1,2,-2,0} \\
& - 40(f_{3,-1,0,-1} + f_{2,-1,-1,1}) \\
& + 35(f_{1,-1,2,-1} + f_{0,-1,1,1} - f_{1,-2,0,2} - f_{3,0,0,-2} - f_{2,-2,3,-2} - f_{-1,-1,2,1} \\
& \quad - f_{1,0,-2,2} - f_{0,-1,3,-1} - f_{3,-2,2,-2} - f_{0,-2,1,2}) \\
& - 30(f_{0,-1,-1,3} + f_{-2,1,-1,3} + f_{2,1,1,-3} + f_{2,-1,3,-3} + f_{0,0,3,-2} + f_{3,-1,2,-3} \\
& \quad + f_{-2,0,1,2} + f_{1,1,2,-3} + f_{-1,-1,0,3} + f_{-1,1,-2,3}) \\
& - 21(f_{2,-2,1,0} + f_{1,-2,2,0}) \\
& - 5(f_{2,-3,3,-1} + f_{3,-3,2,-1} + f_{3,0,-2,0} + f_{3,1,-2,-1} + f_{3,-2,0,0} + f_{2,-3,1,1} \\
& \quad + f_{2,2,-3,0} + f_{2,2,-1,-2} + f_{2,1,-3,1} + f_{0,-2,3,0} + f_{0,2,-3,2} + f_{0,3,-3,1} \\
& \quad \left. + f_{1,3,-2,-1} + f_{1,-3,2,1} \right) \tag{B.9}
\end{aligned}$$

The associated weight mask is shown in figure B.9.

B-coefficient c_{1220} is computed using $(0, 2)$ -symmetry.

B-coefficient c_{2012} is computed using $(1, 3)$ -symmetry.

B-coefficient c_{1022} is computed using both $(0, 2)$ -symmetry and $(1, 3)$ -symmetry.

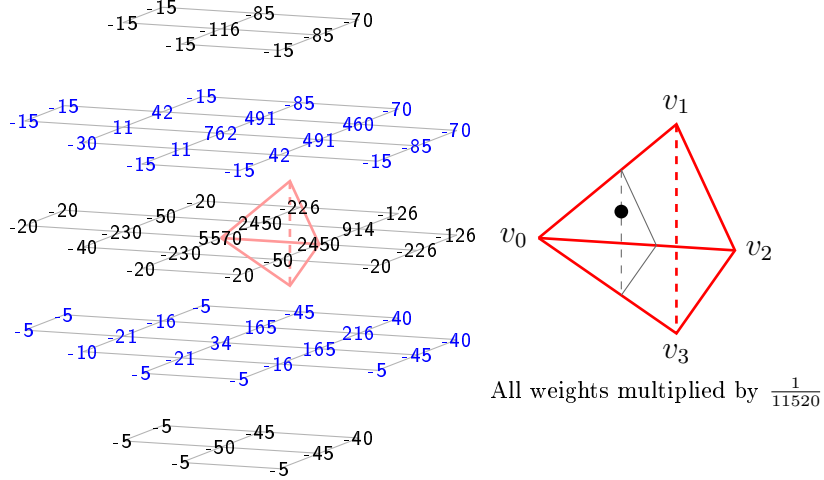


Figure B.10: Weight mask for c_{2201} . The associated domain point is shown in the teterahedron on the right. The black triangle symbolizes the ring $R_3(v_0)$.

$$\begin{aligned}
 c_{2201} := & \frac{1}{11520} \left(5570f_{1,0,0,0} + 2450(f_{0,0,1,0} + f_{0,1,-1,1}) + 914f_{-1,1,0,1} + 762f_{1,1,0,-1} \right. \\
 & + 491(f_{0,1,1,-1} + f_{0,2,-1,0}) + 460f_{-1,2,0,0} - 230(f_{2,-1,1,-1} + f_{2,0,-1,0}) \\
 & - 226(f_{-1,0,2,0} + f_{-1,2,-2,2}) + 216f_{-1,0,0,2} + 165(f_{0,0,-1,2} + f_{0,-1,1,1}) \\
 & - 126(f_{-2,2,-1,2} + f_{-2,1,1,1}) - 116f_{1,2,0,-2} \\
 & - 85(f_{0,2,1,-2} + f_{0,3,-1,-1} + f_{-1,1,2,-1} + f_{-1,3,-2,1}) \\
 & - 70(f_{-2,2,1,0} + f_{-2,3,-1,1} + f_{-1,3,0,-1}) - 50(f_{1,-1,2,-1} + f_{1,1,-2,1} + f_{1,-2,0,2}) \\
 & - 45(f_{-1,-1,2,1} + f_{0,-1,-1,3} + f_{-1,1,-2,3} + f_{0,-2,1,2}) + 42(f_{1,2,-2,0} + f_{1,0,2,-2}) \\
 & - 40(f_{-1,-1,0,3} + f_{-2,1,-1,3} + f_{3,-1,0,-1} + f_{-2,0,1,2}) + 34f_{1,-1,0,1} - 30f_{3,0,0,-2} \\
 & - 21(f_{2,-2,1,0} + f_{2,-1,-1,1}) \\
 & - 20(f_{3,0,-2,0} + f_{0,-1,3,-1} + f_{2,1,-3,1} + f_{2,-2,3,-2} + f_{0,2,-3,2} + f_{3,-2,2,-2}) \\
 & - 16(f_{1,0,-2,2} + f_{1,-2,2,0}) \\
 & - 15(f_{1,1,2,-3} + f_{0,0,3,-2} + f_{3,1,-2,-1} + f_{3,-1,2,-3} + f_{2,2,-3,0} + f_{2,2,-1,-2} \\
 & \quad + f_{2,-1,3,-3} + f_{2,1,1,-3} + f_{1,3,-2,-1} + f_{0,3,-3,1}) \\
 & + 11(f_{2,1,-1,-1} + f_{2,0,1,-2}) - 10f_{3,-2,0,0} \\
 & - 5(f_{2,0,-3,2} + f_{3,-3,2,-1} + f_{1,-1,-2,3} + f_{1,-3,2,1} + f_{3,-1,-2,1} + f_{0,1,-3,3} \\
 & \quad + f_{2,-3,3,-1} + f_{2,-3,1,1} + f_{0,-2,3,0} + f_{2,-2,-1,2}) \Big) \tag{B.10}
 \end{aligned}$$

The associated weight mask is shown in figure B.10.

B-coefficient c_{0221} is computed using $(0, 2)$ -symmetry.

B-coefficient c_{2102} is computed using $(1, 3)$ -symmetry.

B-coefficient c_{0122} is computed using both $(0, 2)$ -symmetry and $(1, 3)$ -symmetry.

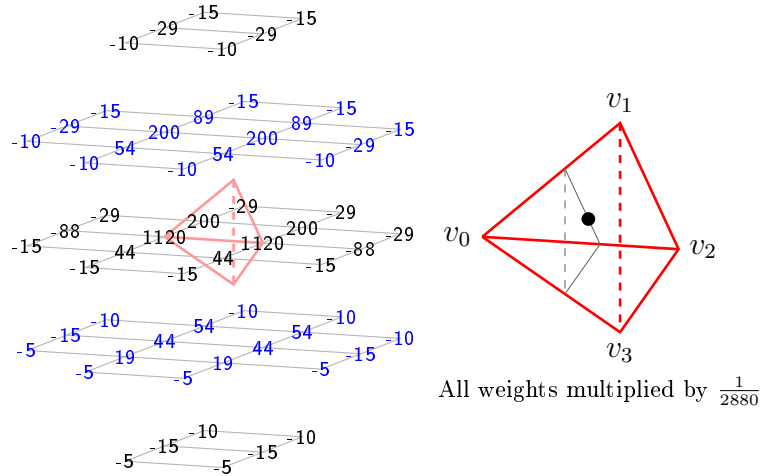


Figure B.11: Weight mask for c_{2120} . The associated domain point is shown in the tetrahedron on the right. The black triangle symbolizes the ring $R_3(v_0)$.

$$\begin{aligned}
c_{2120} := & \frac{1}{2880} \left(1120(f_{0,0,1,0} + f_{1,0,0,0}) + 200(f_{-1,1,0,1} + f_{0,1,-1,1} + f_{0,1,1,-1} + f_{1,1,0,-1}) \right. \\
& + 89(f_{0,2,-1,0} + f_{-1,2,0,0}) - 88(f_{-1,0,2,0} + f_{2,0,-1,0}) \\
& + 54(f_{0,0,-1,2} + f_{1,0,2,-2} + f_{2,0,1,-2} + f_{-1,0,0,2}) \\
& + 44(f_{1,-1,0,1} + f_{2,-1,1,-1} + f_{0,-1,1,1} + f_{1,-1,2,-1}) \\
& - 29(f_{1,1,-2,1} + f_{-1,2,-2,2} + f_{1,2,0,-2} + f_{-2,1,1,1} + f_{2,1,-1,-1} + f_{-2,2,-1,2} \\
& \quad + f_{-1,1,2,-1} + f_{0,2,1,-2}) \\
& + 19(f_{2,-2,1,0} + f_{1,-2,2,0}) \\
& - 15(f_{0,-1,3,-1} + f_{3,-2,2,-2} + f_{3,-1,0,-1} + f_{-2,3,-1,1} + f_{2,-2,3,-2} + f_{-2,2,1,0} \\
& \quad + f_{2,-1,-1,1} + f_{0,-2,1,2} + f_{-1,3,-2,1} + f_{-1,3,0,-1} + f_{0,3,-1,-1} + f_{1,2,-2,0} \\
& \quad + f_{-1,-1,2,1} + f_{1,-2,0,2}) \\
& - 10(f_{2,-1,3,-3} + f_{3,-1,2,-3} + f_{-1,1,-2,3} + f_{3,0,0,-2} + f_{1,1,2,-3} + f_{-1,-1,0,3} \\
& \quad + f_{0,0,3,-2} + f_{1,0,-2,2} + f_{2,1,1,-3} + f_{-2,1,-1,3} + f_{0,-1,-1,3} + f_{-2,0,1,2}) \\
& \left. - 5(f_{3,-3,2,-1} + f_{3,-2,0,0} + f_{1,-3,2,1} + f_{2,-3,3,-1} + f_{2,-3,1,1} + f_{0,-2,3,0}) \right) \quad (B.11)
\end{aligned}$$

The associated weight mask is shown in figure B.11. B-coefficient c_{2021} is computed using (1, 3)-symmetry.

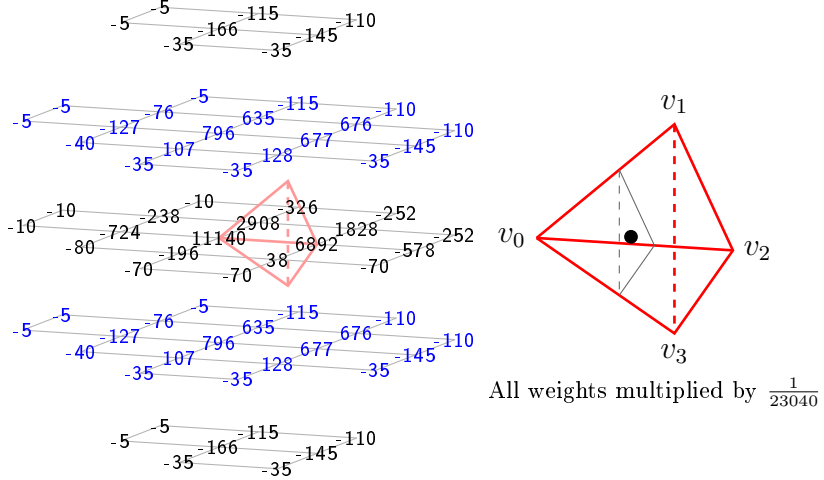


Figure B.12: Weight mask for c_{2111} . The associated domain point is shown in the teterahedron on the right. The black triangle symbolizes the ring $R_3(v_0)$.

$$\begin{aligned}
 c_{2111} := & \frac{1}{23040} \left(11140f_{1,0,0,0} + 6892f_{0,0,1,0} + 2908f_{0,1,-1,1} + 1828f_{-1,1,0,1} \right. \\
 & + 796(f_{1,1,0,-1} + f_{1,-1,0,1}) - 724f_{2,0,-1,0} + 677(f_{0,-1,1,1} + f_{0,1,1,-1}) \\
 & + 676(f_{-1,2,0,0} + f_{-1,0,0,2}) + 635(f_{0,2,-1,0} + f_{0,0,-1,2}) - 578f_{-1,0,2,0} - 326f_{-1,2,-2,2} \\
 & - 252(f_{-2,2,-1,2} + f_{-2,1,1,1}) - 238f_{1,1,-2,1} - 196f_{2,-1,1,-1} - 166(f_{1,2,0,-2} + f_{1,-2,0,2}) \\
 & - 145(f_{-1,-1,2,1} + f_{-1,1,2,-1} + f_{0,2,1,-2} + f_{0,-2,1,2}) + 128(f_{1,-2,2,0} + f_{1,0,2,-2}) \\
 & - 127(f_{2,1,-1,-1} + f_{2,-1,-1,1}) - 115(f_{0,-1,-1,3} + f_{-1,1,-2,3} + f_{0,3,-1,-1} + f_{-1,3,-2,1}) \\
 & - 110(f_{-1,3,0,-1} + f_{-2,0,1,2} + f_{-2,3,-1,1} + f_{-1,-1,0,3} + f_{-2,1,-1,3} + f_{-2,2,1,0}) \\
 & + 107(f_{2,0,1,-2} + f_{2,-2,1,0}) - 80f_{3,-1,0,-1} - 76(f_{1,2,-2,0} + f_{1,0,-2,2}) \\
 & - 70(f_{0,-1,3,-1} + f_{2,-2,3,-2} + f_{3,-2,2,-2}) - 40(f_{3,-2,0,0} + f_{3,0,0,-2}) + 38f_{1,-1,2,-1} \\
 & - 35(f_{1,1,2,-3} + f_{3,-3,2,-1} + f_{2,1,1,-3} + f_{2,-1,3,-3} + f_{0,-2,3,0} + f_{3,-1,2,-3} \\
 & \quad + f_{2,-3,3,-1} + f_{2,-3,1,1} + f_{0,0,3,-2} + f_{1,-3,2,1}) \\
 & - 10(f_{3,0,-2,0} + f_{0,2,-3,2} + f_{2,1,-3,1}) \\
 & \left. - 5(f_{3,-1,-2,1} + f_{3,1,-2,-1} + f_{2,2,-1,-2} + f_{2,2,-3,0} + f_{1,3,-2,-1} + f_{2,-2,-1,2} \right. \\
 & \quad \left. + f_{0,1,-3,3} + f_{0,3,-3,1} + f_{1,-1,-2,3} + f_{2,0,-3,2}) \right) \tag{B.12}
 \end{aligned}$$

The associated weight mask is shown in figure B.12.
B-coefficient c_{1121} is computed using $(0, 2)$ -symmetry.

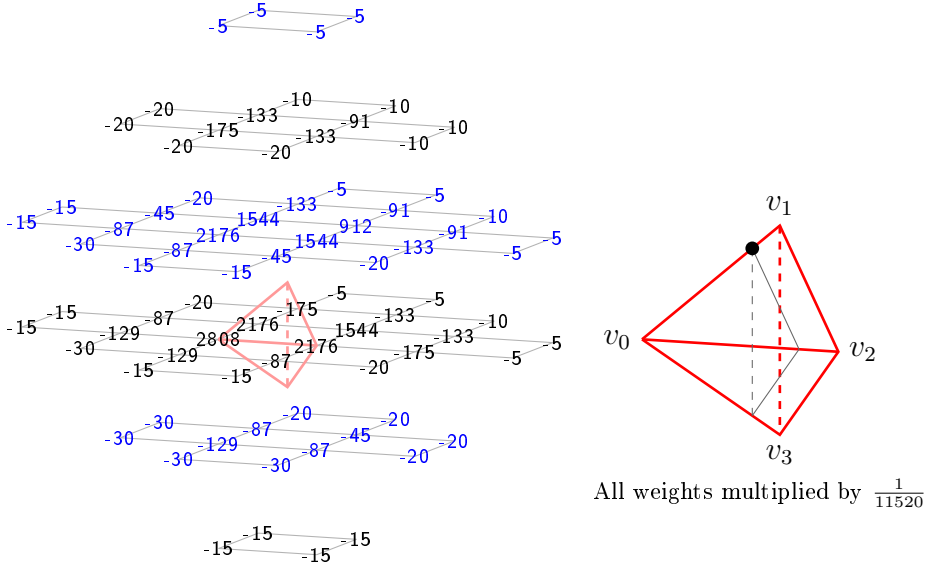


Figure B.13: Weight mask for c_{1400} . The associated domain point is shown in the teterahedron on the right. The black triangle symbolizes the ring $R_4(v_0)$.

$$\begin{aligned}
 c_{1400} := & \frac{1}{11520} \left(2808 f_{1,0,0,0} + 2176(f_{0,0,1,0} + f_{0,1,-1,1} + f_{1,1,0,-1}) \right. \\
 & + 1544(f_{0,1,1,-1} + f_{0,2,-1,0} + f_{-1,1,0,1}) + 912f_{-1,2,0,0} \\
 & - 175(f_{-1,2,-2,2} + f_{1,2,0,-2} + f_{-1,0,2,0}) \\
 & - 133(f_{-1,3,-2,1} + f_{-2,2,-1,2} + f_{-2,1,1,1} + f_{-1,1,2,-1} + f_{0,3,-1,-1} + f_{0,2,1,-2}) \\
 & - 129(f_{2,0,-1,0} + f_{1,-1,0,1} + f_{2,-1,1,-1}) - 91(f_{-2,2,1,0} + f_{-2,3,-1,1} + f_{-1,3,0,-1}) \\
 & - 87(f_{2,1,-1,-1} + f_{0,-1,1,1} + f_{0,0,-1,2} + f_{1,-1,2,-1} + f_{1,1,-2,1} + f_{2,0,1,-2}) \\
 & - 45(f_{1,2,-2,0} + f_{1,0,2,-2} + f_{-1,0,0,2}) \\
 & - 30(f_{3,-1,0,-1} + f_{2,-2,1,0} + f_{3,0,0,-2} + f_{1,-2,2,0} + f_{2,-1,-1,1} + f_{1,0,-2,2}) \\
 & - 20(f_{-2,0,1,2} + f_{-2,1,-1,3} + f_{0,0,3,-2} + f_{0,-1,3,-1} + f_{1,3,-2,-1} + f_{2,2,-1,-2} \\
 & \quad + f_{2,1,1,-3} + f_{1,1,2,-3} + f_{-1,1,-2,3} + f_{-1,-1,2,1} + f_{0,2,-3,2} + f_{0,3,-3,1}) \\
 & - 15(f_{2,1,-3,1} + f_{3,0,-2,0} + f_{2,-1,3,-3} + f_{2,2,-3,0} + f_{2,-2,3,-2} + f_{3,-2,2,-2} \\
 & \quad + f_{3,-1,2,-3} + f_{0,-1,-1,3} + f_{1,-2,0,2} + f_{0,-2,1,2} + f_{-1,-1,0,3} + f_{3,1,-2,-1}) \\
 & - 10(f_{-1,4,-2,0} + f_{-3,2,0,2} + f_{-2,4,-1,0} + f_{-2,3,1,-1} + f_{-3,3,0,1} + f_{-1,2,2,-2}) \\
 & \left. - 5(f_{-3,2,2,0} + f_{-2,0,3,0} + f_{-3,3,-2,3} + f_{-3,4,-2,2} + f_{-3,1,2,1} + f_{-2,4,-3,2} \right. \\
 & \quad \left. + f_{-2,3,-3,3} + f_{-2,1,3,-1} + f_{0,4,-1,-2} + f_{-1,4,0,-2} + f_{1,3,0,-3} + f_{0,3,1,-3}) \right) \tag{B.13}
 \end{aligned}$$

The associated weight mask is shown in figure B.13.

B-coefficient c_{0410} is computed using $(0, 2)$ -symmetry.

B-coefficient c_{1004} is computed using $(1, 3)$ -symmetry.

B-coefficient c_{0014} is computed using both $(0, 2)$ -symmetry and $(1, 3)$ -symmetry.

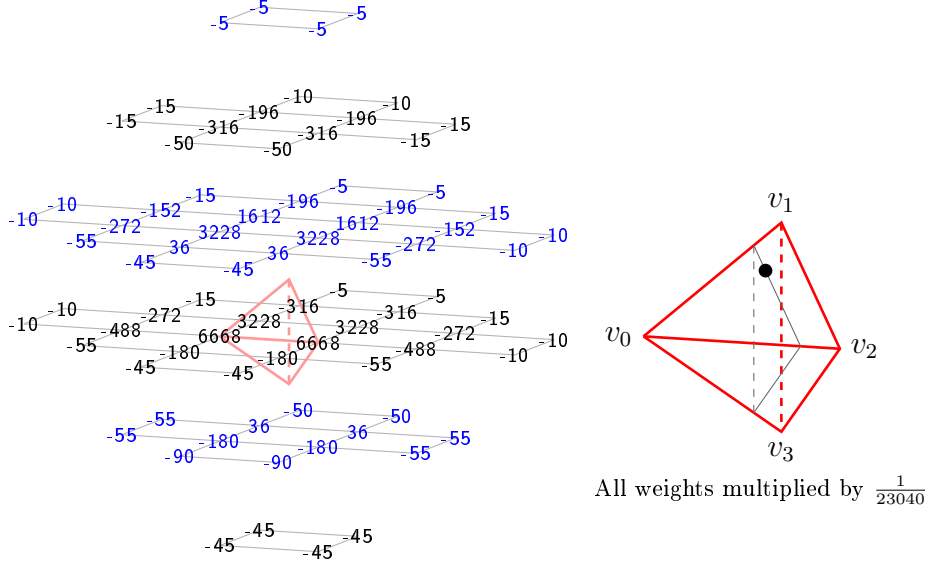


Figure B.14: Weight mask for c_{1310} . The associated domain point is shown in the teterahedron on the right. The black triangle symbolizes the ring $R_4(v_0)$.

$$\begin{aligned}
 c_{1310} := & \frac{1}{23040} \left(6668(f_{1,0,0,0} + f_{0,0,1,0}) + 3228(f_{-1,1,0,1} + f_{1,1,0,-1} + f_{0,1,-1,1} + f_{0,1,1,-1}) \right. \\
 & + 1612(f_{0,2,-1,0} + f_{-1,2,0,0}) - 488(f_{-1,0,2,0} + f_{2,0,-1,0}) \\
 & - 316(f_{0,2,1,-2} + f_{1,2,0,-2} + f_{-1,2,-2,2} + f_{-2,2,-1,2}) \\
 & - 272(f_{1,1,-2,1} + f_{-2,1,1,1} + f_{-1,1,2,-1} + f_{2,1,-1,-1}) \\
 & - 196(f_{-1,3,0,-1} + f_{-1,3,-2,1} + f_{-2,3,-1,1} + f_{0,3,-1,-1}) \\
 & - 180(f_{0,-1,1,1} + f_{2,-1,1,-1} + f_{1,-1,2,-1} + f_{1,-1,0,1}) - 152(f_{-2,2,1,0} + f_{1,2,-2,0}) \\
 & - 90(f_{2,-2,1,0} + f_{1,-2,2,0}) \\
 & - 55(f_{0,-1,3,-1} + f_{-2,0,1,2} + f_{0,0,3,-2} + f_{-1,-1,2,1} + f_{1,0,-2,2} + f_{3,0,0,-2} \\
 & + f_{3,-1,0,-1} + f_{2,-1,-1,1}) \\
 & - 50(f_{-2,1,-1,3} + f_{2,1,1,-3} + f_{1,1,2,-3} + f_{-1,1,-2,3}) \\
 & - 45(f_{0,-1,-1,3} + f_{2,-2,3,-2} + f_{2,-1,3,-3} + f_{0,-2,1,2} + f_{1,-2,0,2} + f_{3,-1,2,-3} \\
 & + f_{-1,-1,0,3} + f_{3,-2,2,-2}) \\
 & + 36(f_{0,0,-1,2} + f_{1,0,2,-2} + f_{2,0,1,-2} + f_{-1,0,0,2}) \\
 & - 15(f_{-3,3,0,1} + f_{-3,2,0,2} + f_{1,3,-2,-1} + f_{2,2,-1,-2} + f_{0,2,-3,2} + f_{-1,2,2,-2} \\
 & + f_{-2,3,1,-1} + f_{0,3,-3,1}) \\
 & - 10(f_{-2,0,3,0} + f_{-3,2,2,0} + f_{3,1,-2,-1} + f_{-3,1,2,1} + f_{3,0,-2,0} + f_{-2,4,-1,0} \\
 & + f_{2,2,-3,0} + f_{-1,4,-2,0} + f_{2,1,-3,1} + f_{-2,1,3,-1}) \\
 & - 5(f_{-2,4,-3,2} + f_{0,3,1,-3} + f_{-2,3,-3,3} + f_{1,3,0,-3} + f_{0,4,-1,-2} + f_{-1,4,0,-2} \\
 & \left. + f_{-3,3,-2,3} + f_{-3,4,-2,2} \right) \tag{B.14}
 \end{aligned}$$

The associated weight mask is shown in figure B.14.
B-coefficient c_{1013} is computed using (1, 3)-symmetry.

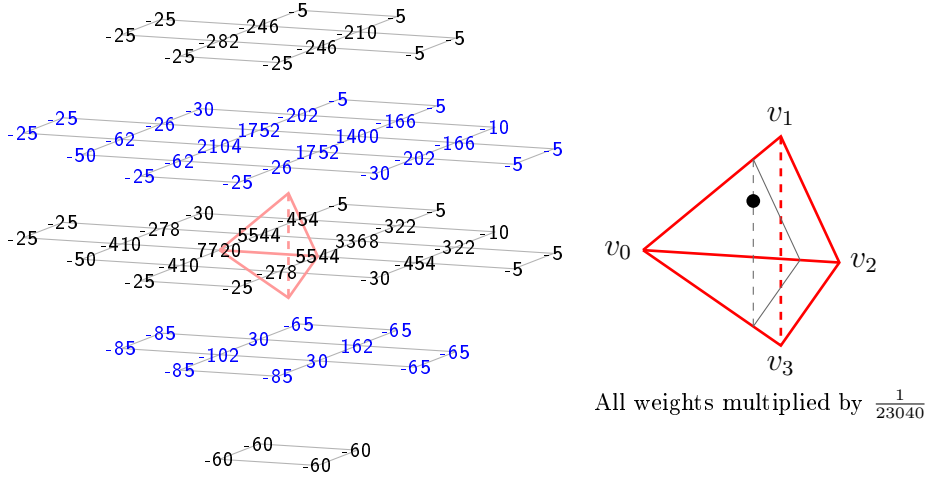


Figure B.15: Weight mask for c_{1301} . The associated domain point is shown in the teterahedron on the right. The black triangle symbolizes the ring $R_4(v_0)$.

$$\begin{aligned}
 c_{1301} := & \frac{1}{23040} \left(7720f_{1,0,0,0} + 5544(f_{0,1,-1,1} + f_{0,0,1,0}) + 3368f_{-1,1,0,1} + 2104f_{1,1,0,-1} \right. \\
 & + 1752(f_{0,1,1,-1} + f_{0,2,-1,0}) + 1400f_{-1,2,0,0} - 454(f_{-1,0,2,0} + f_{-1,2,-2,2}) \\
 & - 410(f_{2,-1,1,-1} + f_{2,0,-1,0}) - 322(f_{-2,1,1,1} + f_{-2,2,-1,2}) - 282f_{1,2,0,-2} \\
 & - 278(f_{1,1,-2,1} + f_{1,-1,2,-1}) - 246(f_{0,2,1,-2} + f_{0,3,-1,-1}) - 210f_{-1,3,0,-1} \\
 & - 202(f_{-1,1,2,-1} + f_{-1,3,-2,1}) - 166(f_{-2,2,1,0} + f_{-2,3,-1,1}) + 162f_{-1,0,0,2} - 102f_{1,-1,0,1} \\
 & - 85(f_{2,-1,-1,1} + f_{2,-2,1,0} + f_{1,0,-2,2} + f_{1,-2,2,0}) \\
 & - 65(f_{-1,1,-2,3} + f_{-2,0,1,2} + f_{-2,1,-1,3} + f_{-1,-1,2,1}) - 62(f_{2,1,-1,-1} + f_{2,0,1,-2}) \\
 & - 60(f_{0,-2,1,2} + f_{1,-2,0,2} + f_{0,-1,-1,3} + f_{-1,-1,0,3}) - 50(f_{3,0,0,-2} + f_{3,-1,0,-1}) \\
 & + 30(f_{0,0,-1,2} + f_{0,-1,1,1} - f_{0,0,3,-2} - f_{0,-1,3,-1} - f_{0,2,-3,2} - f_{0,3,-3,1}) \\
 & - 26(f_{1,2,-2,0} + f_{1,0,2,-2}) \\
 & - 25(f_{2,2,-3,0} + f_{3,-2,2,-2} + f_{2,-2,3,-2} + f_{3,0,-2,0} + f_{3,1,-2,-1} + f_{3,-1,2,-3} \\
 & \quad + f_{1,3,-2,-1} + f_{2,-1,3,-3} + f_{2,1,-3,1} + f_{2,2,-1,-2} + f_{1,1,2,-3} + f_{2,1,1,-3}) \\
 & - 10(f_{-3,3,0,1} + f_{-3,2,0,2}) \\
 & \left. - 5(f_{-3,4,-2,2} + f_{-3,3,-2,3} + f_{-3,2,2,0} + f_{-1,2,2,-2} + f_{-1,4,-2,0} + f_{-3,1,2,1} \right. \\
 & \quad \left. + f_{-2,0,3,0} + f_{-2,1,3,-1} + f_{-2,4,-3,2} + f_{-2,4,-1,0} + f_{-2,3,-3,3} + f_{-2,3,1,-1}) \right) \tag{B.15}
 \end{aligned}$$

The associated weight mask is shown in figure B.15.

B-coefficient c_{0311} is computed using $(0, 2)$ -symmetry.

B-coefficient c_{1103} is computed using $(1, 3)$ -symmetry.

B-coefficient c_{0113} is computed using both $(0, 2)$ -symmetry and $(1, 3)$ -symmetry.

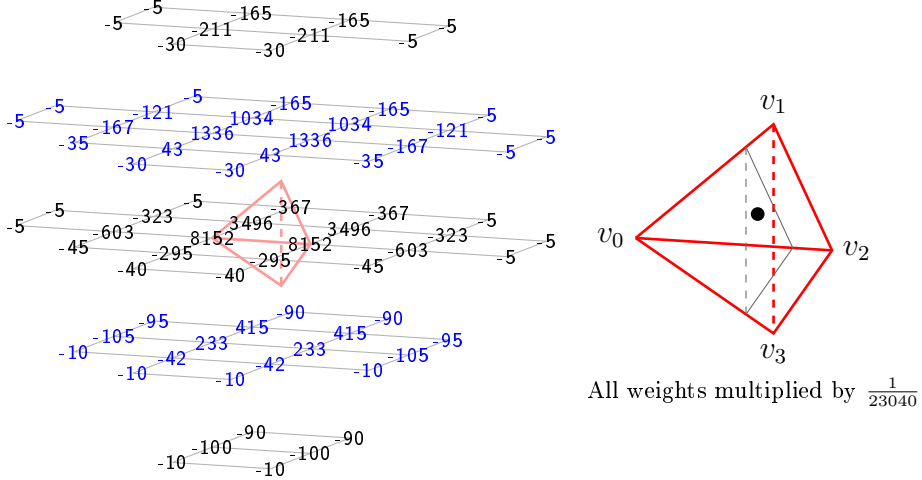


Figure B.16: Weight mask for c_{1211} . The associated domain point is shown in the teterahedron on the right. The black triangle symbolizes the ring $R_4(v_0)$.

$$\begin{aligned}
 c_{1211} := & \frac{1}{23040} \left(8152(f_{1,0,0,0} + f_{0,0,1,0}) + 3496(f_{0,1,-1,1} + f_{-1,1,0,1}) + 1336(f_{0,1,1,-1} + f_{1,1,0,-1}) \right. \\
 & + 1034(f_{-1,2,0,0} + f_{0,2,-1,0}) - 603(f_{-1,0,2,0} + f_{2,0,-1,0}) + 415(f_{-1,0,0,2} + f_{0,0,-1,2}) \\
 & - 367(f_{-1,2,-2,2} + f_{-2,2,-1,2}) - 323(f_{-2,1,1,1} + f_{1,1,-2,1}) - 295(f_{1,-1,2,-1} + f_{2,-1,1,-1}) \\
 & + 233(f_{1,-1,0,1} + f_{0,-1,1,1}) - 211(f_{0,2,1,-2} + f_{1,2,0,-2}) - 167(f_{2,1,-1,-1} + f_{-1,1,2,-1}) \\
 & - 165(f_{-1,3,0,-1} + f_{-2,3,-1,1} + f_{-1,3,-2,1} + f_{0,3,-1,-1}) - 121(f_{1,2,-2,0} + f_{-2,2,1,0}) \\
 & - 105(f_{2,-1,-1,1} + f_{-1,-1,2,1}) - 100(f_{1,-2,0,2} + f_{0,-2,1,2}) - 95(f_{-2,0,1,2} + f_{1,0,-2,2}) \\
 & - 90(f_{-1,1,-2,3} + f_{0,-1,-1,3} + f_{-1,-1,0,3} + f_{-2,1,-1,3}) - 45(f_{0,-1,3,-1} + f_{3,-1,0,-1}) \\
 & + 43(f_{1,0,2,-2} + f_{2,0,1,-2}) - 42(f_{2,-2,1,0} + f_{1,-2,2,0}) - 40(f_{2,-2,3,-2} + f_{3,-2,2,-2}) \\
 & - 35(f_{3,0,0,-2} + f_{0,0,3,-2}) - 30(f_{3,-1,2,-3} + f_{2,1,1,-3} + f_{2,-1,3,-3} + f_{1,1,2,-3}) \\
 & - 10(f_{2,-3,3,-1} + f_{2,-3,1,1} + f_{3,-2,0,0} + f_{3,-3,2,-1} + f_{0,-2,3,0} + f_{1,-3,2,1}) \\
 & - 5(f_{-3,1,2,1} + f_{-1,2,2,-2} + f_{-3,3,0,1} + f_{0,3,-3,1} + f_{-3,2,2,0} + f_{-3,2,0,2} \\
 & + f_{1,3,-2,-1} + f_{3,1,-2,-1} + f_{2,2,-3,0} + f_{0,2,-3,2} + f_{3,0,-2,0} + f_{-2,0,3,0} \\
 & \left. + f_{-2,1,3,-1} + f_{-2,3,1,-1} + f_{2,1,-3,1} + f_{2,2,-1,-2} \right) \quad (B.16)
 \end{aligned}$$

The associated weight mask is shown in figure B.16.
B-coefficient c_{1112} is computed using (1, 3)-symmetry.

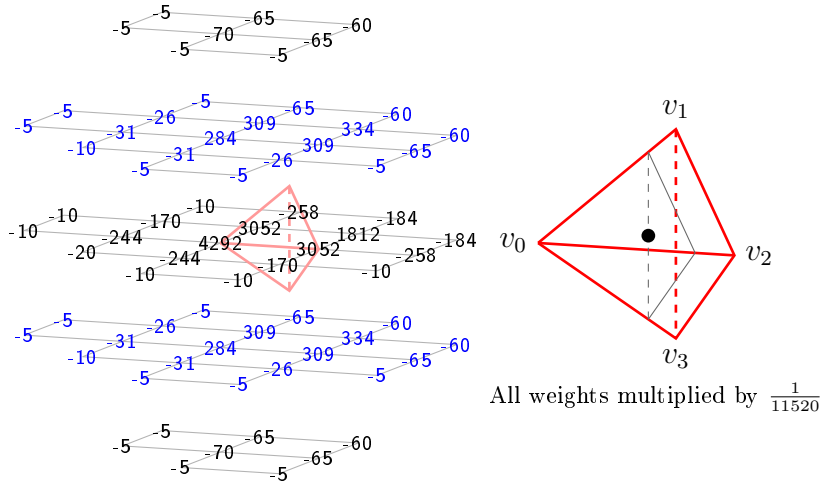


Figure B.17: Weight mask for c_{1202} . The associated domain point is shown in the tetrahedron on the right. The black triangle symbolizes the ring $R_4(v_0)$.

$$\begin{aligned}
c_{1202} := & \frac{1}{11520} \left(4292f_{1,0,0,0} + 3052(f_{0,0,1,0} + f_{0,1,-1,1}) + 1812f_{-1,1,0,1} \right. \\
& + 334(f_{-1,2,0,0} + f_{-1,0,0,2}) + 309(f_{0,0,-1,2} + f_{0,-1,1,1} + f_{0,1,1,-1} + f_{0,2,-1,0}) \\
& + 284(f_{1,1,0,-1} + f_{1,-1,0,1}) - 258(f_{-1,0,2,0} + f_{-1,2,-2,2}) - 244(f_{2,-1,1,-1} + f_{2,0,-1,0}) \\
& - 184(f_{-2,2,-1,2} + f_{-2,1,1,1}) - 170(f_{1,1,-2,1} + f_{1,-1,2,-1}) - 70(f_{1,2,0,-2} + f_{1,-2,0,2}) \\
& - 65(f_{0,3,-1,-1} + f_{0,-1,-1,3} + f_{-1,1,-2,3} + f_{-1,1,2,-1} + f_{-1,-1,2,1} + f_{0,-2,1,2} \\
& \quad + f_{0,2,1,-2} + f_{-1,3,-2,1}) \\
& - 60(f_{-1,-1,0,3} + f_{-1,3,0,-1} + f_{-2,2,1,0} + f_{-2,1,-1,3} + f_{-2,0,1,2} + f_{-2,3,-1,1}) \\
& - 31(f_{2,-1,-1,1} + f_{2,0,1,-2} + f_{2,1,-1,-1} + f_{2,-2,1,0}) \\
& - 26(f_{1,2,-2,0} + f_{1,-2,2,0} + f_{1,0,2,-2} + f_{1,0,-2,2}) - 20f_{3,-1,0,-1} \\
& - 10(f_{2,-2,3,-2} + f_{3,-2,2,-2} + f_{3,-2,0,0} + f_{0,2,-3,2} + f_{2,1,-3,1} + f_{3,0,-2,0} \\
& \quad + f_{3,0,0,-2} + f_{0,-1,3,-1}) \\
& - 5(f_{3,-1,-2,1} + f_{0,0,3,-2} + f_{2,-3,1,1} + f_{2,-3,3,-1} + f_{2,-2,-1,2} + f_{3,1,-2,-1} \\
& \quad + f_{3,-1,2,-3} + f_{3,-3,2,-1} + f_{2,2,-3,0} + f_{2,2,-1,-2} + f_{1,3,-2,-1} + f_{0,1,-3,3} \\
& \quad + f_{0,-2,3,0} + f_{2,-1,3,-3} + f_{2,1,1,-3} + f_{0,3,-3,1} + f_{1,-1,-2,3} + f_{2,0,-3,2} \\
& \quad \left. + f_{1,1,2,-3} + f_{1,-3,2,1} \right) \tag{B.17}
\end{aligned}$$

The associated weight mask is shown in figure B.17. B-coefficient c_{0212} is computed using $(0, 2)$ -symmetry.

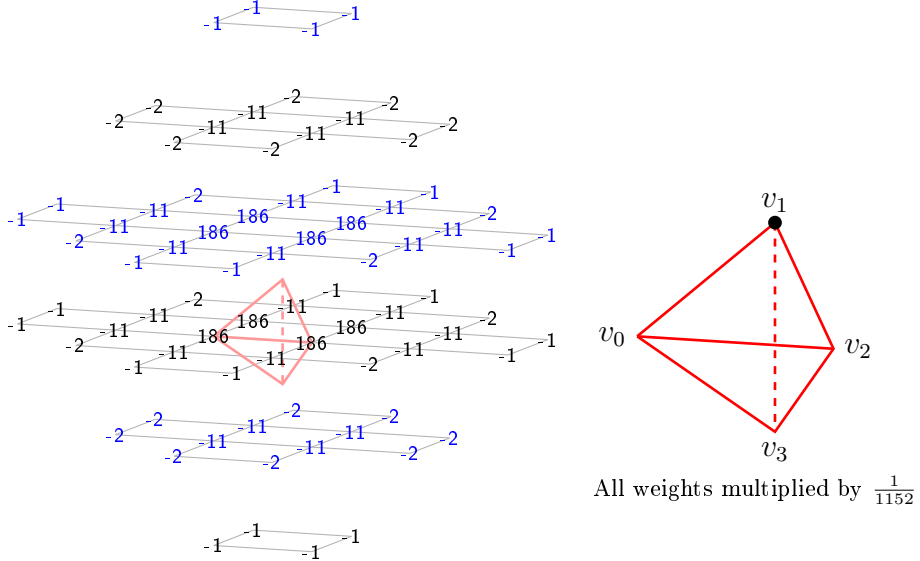


Figure B.18: Weight mask for c_{0500} . The associated domain point is shown in the tetrahedron on the right.

$$\begin{aligned}
 c_{0500} := & \frac{1}{1152} \left(186(f_{0,0,1,0} + f_{1,1,0,-1} + f_{-1,1,0,1} + f_{-1,2,0,0} + f_{1,0,0,0} + f_{0,2,-1,0} \right. \\
 & + f_{0,1,1,-1} + f_{0,1,-1,1}) \\
 & - 11(f_{1,2,-2,0} + f_{-2,3,-1,1} + f_{-1,1,2,-1} + f_{-2,2,-1,2} + f_{1,-1,2,-1} + f_{1,1,-2,1} \\
 & + f_{-2,2,1,0} + f_{1,2,0,-2} + f_{2,1,-1,-1} + f_{-1,2,-2,2} + f_{-1,3,0,-1} + f_{-1,3,-2,1} \\
 & + f_{2,0,-1,0} + f_{2,0,1,-2} + f_{-2,1,1,1} + f_{2,-1,1,-1} + f_{0,2,1,-2} + f_{1,-1,0,1} \\
 & + f_{1,0,2,-2} + f_{0,0,-1,2} + f_{-1,0,2,0} + f_{-1,0,0,2} + f_{0,3,-1,-1} + f_{0,-1,1,1}) \\
 & - 2(f_{0,0,3,-2} + f_{-3,2,0,2} + f_{2,-1,-1,1} + f_{0,-1,3,-1} + f_{-2,1,-1,3} + f_{2,1,1,-3} \\
 & + f_{3,-1,0,-1} + f_{2,-2,1,0} + f_{-2,0,1,2} + f_{2,2,-1,-2} + f_{3,0,0,-2} + f_{-2,3,1,-1} \\
 & + f_{-2,4,-1,0} + f_{-1,2,2,-2} + f_{-1,-1,2,1} + f_{1,0,-2,2} + f_{-1,1,-2,3} + f_{1,1,2,-3} \\
 & + f_{1,-2,2,0} + f_{0,3,-3,1} + f_{-3,3,0,1} + f_{1,3,-2,-1} + f_{-1,4,-2,0} + f_{0,2,-3,2}) \\
 & - (f_{3,-2,2,-2} + f_{-3,1,2,1} + f_{-3,4,-2,2} + f_{3,0,-2,0} + f_{3,1,-2,-1} + f_{-3,3,-2,3} \\
 & + f_{-1,-1,0,3} + f_{-3,2,2,0} + f_{-2,4,-3,2} + f_{3,-1,2,-3} + f_{-2,3,-3,3} + f_{2,-2,3,-2} \\
 & + f_{2,2,-3,0} + f_{2,-1,3,-3} + f_{2,1,-3,1} + f_{-2,1,3,-1} + f_{0,-1,-1,3} + f_{0,-2,1,2} \\
 & \left. + f_{-2,0,3,0} + f_{-1,4,0,-2} + f_{1,3,0,-3} + f_{0,3,1,-3} + f_{0,4,-1,-2} + f_{1,-2,0,2} \right) \tag{B.18}
 \end{aligned}$$

The associated weight mask is shown in figure B.18.
B-coefficient c_{0005} is computed using (1, 3)-symmetry.

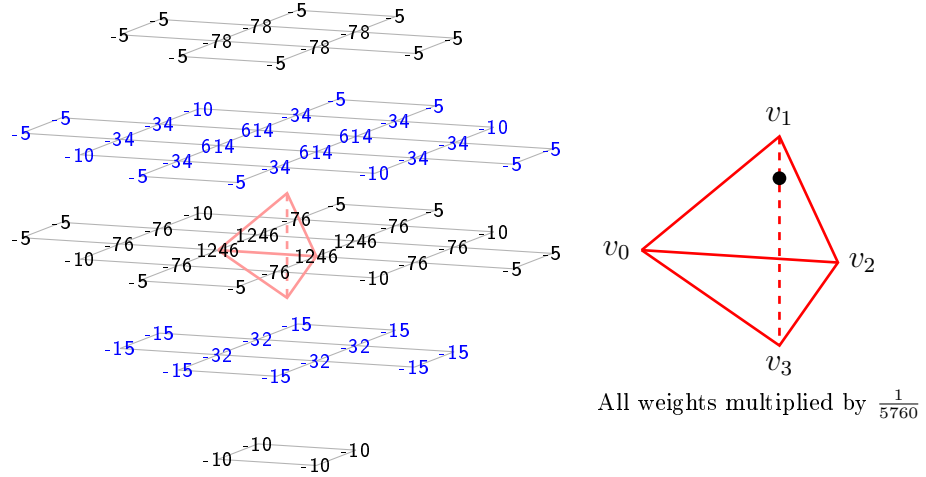


Figure B.19: Weight mask for c_{0401} . The associated domain point is shown in the teterahedron on the right.

$$\begin{aligned}
 c_{0401} := & \frac{1}{5760} \left(1246(f_{-1,1,0,1} + f_{1,0,0,0} + f_{0,1,-1,1} + f_{0,0,1,0}) \right. \\
 & + 614(f_{1,1,0,-1} + f_{0,1,1,-1} + f_{0,2,-1,0} + f_{-1,2,0,0}) \\
 & - 78(f_{1,2,0,-2} + f_{0,3,-1,-1} + f_{0,2,1,-2} + f_{-1,3,0,-1}) \\
 & - 76(f_{-2,2,-1,2} + f_{-1,2,-2,2} + f_{2,0,-1,0} + f_{1,1,-2,1} + f_{1,-1,2,-1} + f_{-2,1,1,1} \\
 & \quad + f_{2,-1,1,-1} + f_{-1,0,2,0}) \\
 & - 34(f_{1,0,2,-2} + f_{-2,2,1,0} + f_{2,1,-1,-1} + f_{-2,3,-1,1} + f_{2,0,1,-2} + f_{-1,3,-2,1} \\
 & \quad + f_{1,2,-2,0} + f_{-1,1,2,-1}) \\
 & - 32(f_{1,-1,0,1} + f_{0,0,-1,2} + f_{-1,0,0,2} + f_{0,-1,1,1}) \\
 & - 15(f_{-1,1,-2,3} + f_{2,-2,1,0} + f_{-2,1,-1,3} + f_{1,0,-2,2} + f_{2,-1,-1,1} + f_{-1,-1,2,1} \\
 & \quad + f_{-2,0,1,2} + f_{1,-2,2,0}) \\
 & - 10(f_{-3,3,0,1} + f_{0,-1,-1,3} + f_{-1,-1,0,3} + f_{0,0,3,-2} + f_{0,-1,3,-1} + f_{0,-2,1,2} \\
 & \quad + f_{1,-2,0,2} + f_{-3,2,0,2} + f_{3,0,0,-2} + f_{0,3,-3,1} + f_{3,-1,0,-1} + f_{0,2,-3,2}) \\
 & - 5(f_{-2,4,-1,0} + f_{-2,4,-3,2} + f_{3,0,-2,0} + f_{-3,4,-2,2} + f_{-3,1,2,1} + f_{3,1,-2,-1} \\
 & \quad + f_{3,-1,2,-3} + f_{-3,2,2,0} + f_{3,-2,2,-2} + f_{-3,3,-2,3} + f_{-2,3,-3,3} + f_{-2,3,1,-1} \\
 & \quad + f_{2,-2,3,-2} + f_{2,2,-3,0} + f_{2,2,-1,-2} + f_{2,-1,3,-3} + f_{2,1,-3,1} + f_{-2,1,3,-1} \\
 & \quad + f_{2,1,1,-3} + f_{-2,0,3,0} + f_{-1,4,-2,0} + f_{1,3,-2,-1} + f_{-1,2,2,-2} + f_{1,1,2,-3}) \Big) \tag{B.19}
 \end{aligned}$$

The associated weight mask is shown in figure B.19.
B-coefficient c_{0104} is computed using (1, 3)-symmetry.

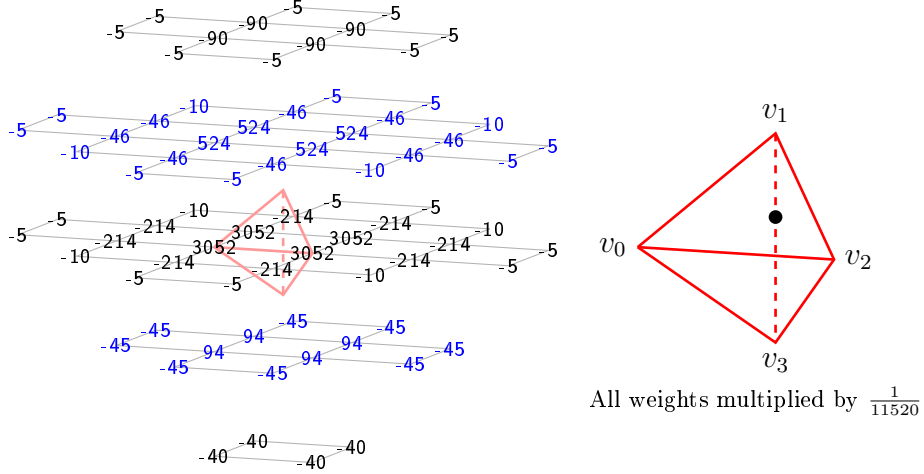


Figure B.20: Weight mask for c_{0302} . The associated domain point is shown in the teterahedron on the right.

$$\begin{aligned}
 c_{0302} := & \frac{1}{11520} \left(3052(f_{0,1,-1,1} + f_{0,0,1,0} + f_{-1,1,0,1} + f_{1,0,0,0}) \right. \\
 & + 524(f_{0,1,1,-1} + f_{-1,2,0,0} + f_{0,2,-1,0} + f_{1,1,0,-1}) \\
 & - 214(f_{-2,2,-1,2} + f_{2,-1,1,-1} + f_{-2,1,1,1} + f_{2,0,-1,0} + f_{-1,2,-2,2} + f_{1,1,-2,1} \\
 & \quad + f_{1,-1,2,-1} + f_{-1,0,2,0}) \\
 & + 94(f_{0,0,-1,2} + f_{0,-1,1,1} + f_{-1,0,0,2} + f_{1,-1,0,1}) \\
 & - 90(f_{-1,3,0,-1} + f_{1,2,0,-2} + f_{0,2,1,-2} + f_{0,3,-1,-1}) \\
 & - 46(f_{-1,1,2,-1} + f_{2,1,-1,-1} + f_{-2,2,1,0} + f_{-2,3,-1,1} + f_{2,0,1,-2} + f_{1,2,-2,0} \\
 & \quad + f_{1,0,2,-2} + f_{-1,3,-2,1}) \\
 & - 45(f_{-1,-1,2,1} + f_{1,0,-2,2} + f_{2,-1,-1,1} + f_{-2,1,-1,3} + f_{-2,0,1,2} + f_{2,-2,1,0} \\
 & \quad + f_{1,-2,2,0} + f_{-1,1,-2,3}) \\
 & - 40(f_{0,-1,-1,3} + f_{1,-2,0,2} + f_{0,-2,1,2} + f_{-1,-1,0,3}) \\
 & - 10(f_{-3,2,0,2} + f_{3,0,0,-2} + f_{-3,3,0,1} + f_{3,-1,0,-1} + f_{0,0,3,-2} + f_{0,3,-3,1} \\
 & \quad + f_{0,-1,3,-1} + f_{0,2,-3,2}) \\
 & - 5(f_{-2,4,-1,0} + f_{3,0,-2,0} + f_{-2,4,-3,2} + f_{-3,4,-2,2} + f_{-3,1,2,1} + f_{3,1,-2,-1} \\
 & \quad + f_{3,-1,2,-3} + f_{-3,2,2,0} + f_{3,-2,2,-2} + f_{-3,3,-2,3} + f_{-2,3,-3,3} + f_{-2,3,1,-1} \\
 & \quad + f_{2,-2,3,-2} + f_{2,2,-3,0} + f_{2,2,-1,-2} + f_{2,-1,3,-3} + f_{2,1,-3,1} + f_{-2,1,3,-1} \\
 & \quad + f_{2,1,1,-3} + f_{-2,0,3,0} + f_{-1,4,-2,0} + f_{1,3,-2,-1} + f_{-1,2,2,-2} + f_{1,1,2,-3}) \Big) \tag{B.20}
 \end{aligned}$$

The associated weight mask is shown in figure B.20.
 B -coefficient c_{0203} is computed using $(1, 3)$ -symmetry.

Appendix C

B-coefficient computation rules for the interpolating quasi-interpolation operator

This chapter contains the B-coefficient computation rules that define the interpolating quasi-interpolation operator from section 3.3 of chapter 3. In contrast to the two other quasi-interpolation operators developed in that chapter, this one uses four set of rules, one for each class of tetrahedra. The rules for class \mathcal{K}_1 start on page 192. From page 220 on, the rules for class \mathcal{K}_2 can be found. The rules for classes \mathcal{K}_3 and \mathcal{K}_4 begin on pages 253 and 284, respectively.

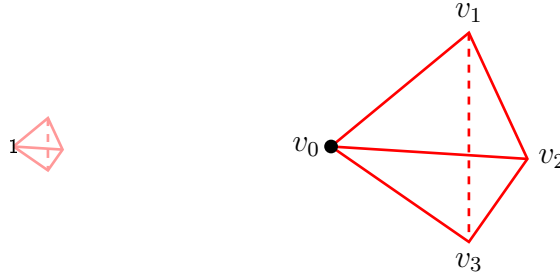


Figure C.1: Weight mask for c_{5000} . This is shown only for the sake of completeness. The associated domain point is shown in the tetrahedron on the right.

B-coefficient computation rules for the class \mathcal{K}_1

$$c_{5000} := f_{1,0,0,0} \quad (\text{C.1})$$

Due to this rule, the operator interpolates the provided data values. The associated weight mask is shown in figure C.1.

$$\begin{aligned} c_{4100} := & \frac{1}{5760} \left(5760 f_{1,0,0,0} \right. \\ & + 148(f_{-1,0,2,0} + f_{1,2,0,-2} + f_{-1,2,-2,2} - f_{1,-2,0,2} - f_{3,0,-2,0} - f_{3,-2,2,-2}) \\ & + 44(f_{-3,2,0,2} + f_{-1,2,2,-2} + f_{-1,4,-2,0} - f_{5,-2,0,-2} - f_{3,-2,-2,2} - f_{3,-4,2,0}) \\ & + 33(f_{5,-4,0,0} - f_{-3,4,0,0}) \\ & + 24(f_{5,0,-4,0} + f_{5,-4,4,-4} + f_{1,-4,0,4} - f_{-3,0,4,0} - f_{-3,4,-4,4} - f_{1,4,0,-4}) \\ & \left. + 11(f_{1,-4,4,0} + f_{5,0,0,-4} + f_{1,0,-4,4} - f_{-3,0,0,4} - f_{1,4,-4,0} - f_{1,0,4,-4}) \right) \end{aligned} \quad (\text{C.2})$$

The associated weight mask is shown in figure C.2.

B-coefficient c_{4001} is computed using (1, 3)-symmetry.

$$\begin{aligned} c_{4010} := & \frac{1}{2880} \left(2880 f_{1,0,0,0} + 148(f_{-1,0,2,0} - f_{3,0,-2,0}) + 24(f_{5,0,-4,0} - f_{-3,0,4,0}) \right. \\ & + 22(f_{-1,-2,2,2} + f_{-1,2,2,-2} + f_{1,-2,4,-2} + f_{-3,2,0,2} - f_{5,-2,0,-2} - f_{1,2,-4,2} \\ & \quad - f_{3,2,-2,-2} - f_{3,-2,-2,2}) \\ & + 11(f_{5,-4,0,0} + f_{5,0,0,-4} + f_{1,4,-4,0} + f_{1,0,-4,4} - f_{-3,0,0,4} - f_{-3,4,0,0} \\ & \quad \left. - f_{1,-4,4,0} - f_{1,0,4,-4}) \right) \end{aligned} \quad (\text{C.3})$$

The associated weight mask is shown in figure C.3.

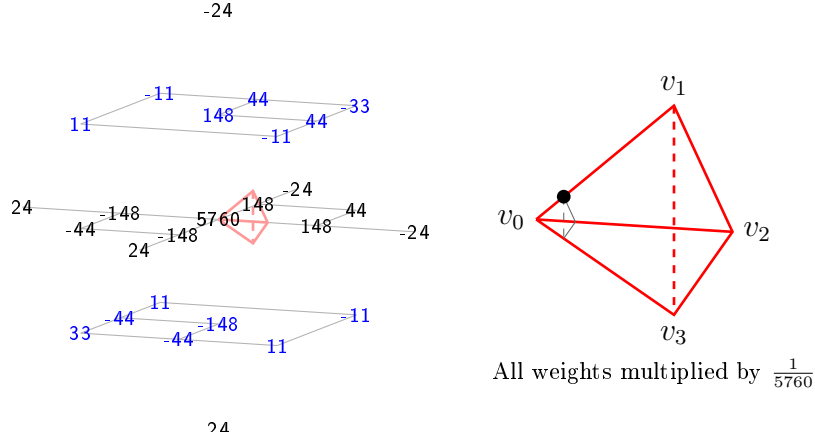


Figure C.2: Weight mask for c_{4100} . The associated domain point is shown in the teterahedron on the right. The black triangle symbolizes the ring $R_1(v_0)$.

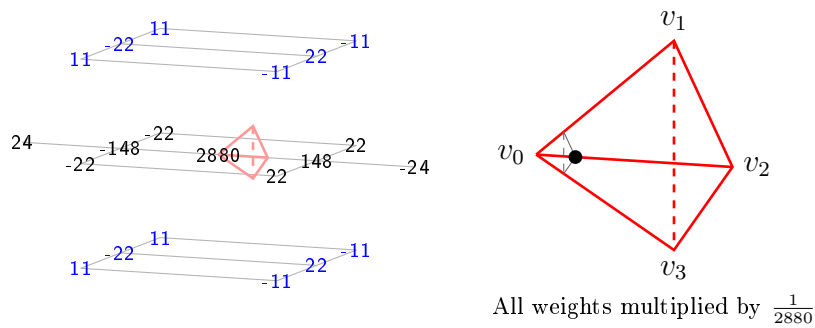


Figure C.3: Weight mask for c_{4010} . The associated domain point is shown in the teterahedron on the right. The black triangle symbolizes the ring $R_1(v_0)$.

$$\begin{aligned}
 c_{3200} := & \frac{1}{92160} \left(78960f_{1,0,0,0} + 7480(f_{-1,0,2,0} + f_{1,2,0,-2} + f_{-1,2,-2,2}) \right. \\
 & - 1992(f_{3,0,-2,0} + f_{1,-2,0,2} + f_{3,-2,2,-2}) \\
 & + 1762(f_{-1,2,2,-2} + f_{-3,2,0,2} + f_{-1,4,-2,0}) - 1431f_{-3,4,0,0} \\
 & - 1232(f_{1,4,0,-4} + f_{-3,4,-4,4} + f_{-3,0,4,0}) \\
 & - 1054(f_{3,-2,-2,2} + f_{3,-4,2,0} + f_{5,-2,0,-2}) + 681f_{5,-4,0,0} \\
 & - 667(f_{1,4,-4,0} + f_{-3,0,0,4} + f_{1,0,4,-4}) + 304(f_{1,-4,0,4} + f_{5,0,-4,0} + f_{5,-4,4,-4}) \\
 & + 37(f_{1,-4,4,0} + f_{5,0,0,-4} + f_{1,0,-4,4}) \\
 & \left. + 6(f_{3,0,2,-4} + f_{1,2,-4,2} + f_{3,2,-2,-2} + f_{1,-2,4,-2} + f_{-1,-2,2,2} + f_{-1,0,-2,4}) \right) \tag{C.4}
 \end{aligned}$$

The associated weight mask is shown in figure C.4.
B-coefficient c_{3002} is computed using (1, 3)-symmetry.

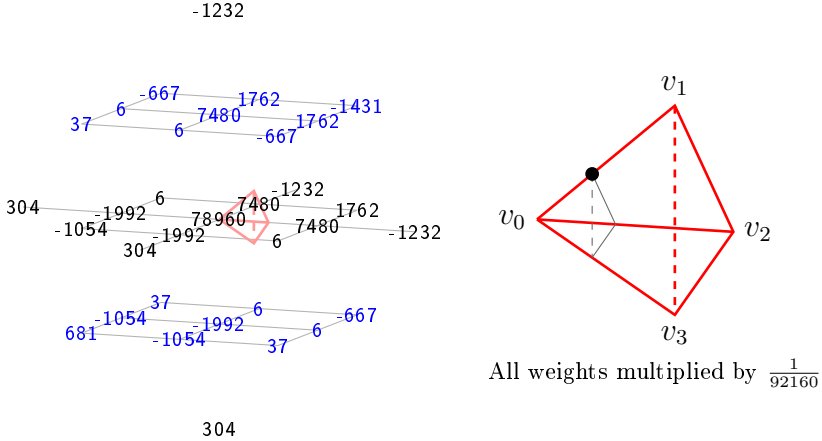


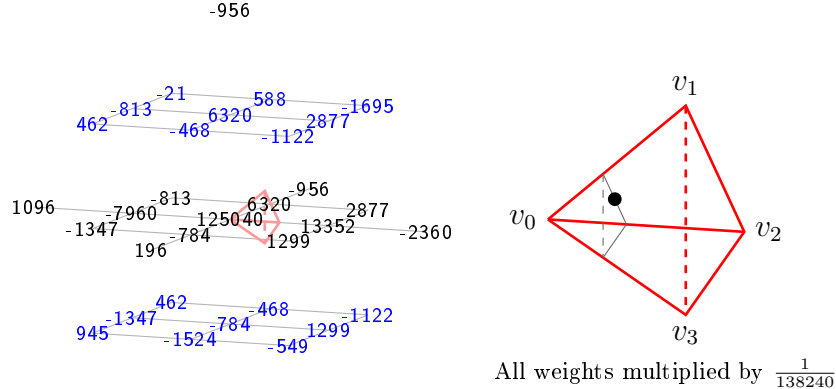
Figure C.4: Weight mask for c_{3200} . The associated domain point is shown in the teterahedron on the right. The black triangle symbolizes the ring $R_2(v_0)$.

$$\begin{aligned}
 c_{3110} := & \frac{1}{138240} \left(125040f_{1,0,0,0} + 13352f_{-1,0,2,0} - 7960f_{3,0,-2,0} \right. \\
 & + 6320(f_{1,2,0,-2} + f_{-1,2,-2,2}) + 2877(f_{-1,2,2,-2} + f_{-3,2,0,2}) - 2360f_{-3,0,4,0} \\
 & - 1695f_{-3,4,0,0} - 1524f_{3,-4,2,0} - 1347(f_{5,-2,0,-2} + f_{3,-2,-2,2}) \\
 & + 1299(f_{-1,-2,2,2} + f_{1,-2,4,-2}) - 1122(f_{-3,0,0,4} + f_{1,0,4,-4}) + 1096f_{5,0,-4,0} \\
 & - 956(f_{1,4,0,-4} + f_{-3,4,-4,4}) + 945f_{5,-4,0,0} - 813(f_{1,2,-4,2} + f_{3,2,-2,-2}) \\
 & - 784(f_{3,-2,2,-2} + f_{1,-2,0,2}) + 588f_{-1,4,-2,0} - 549f_{1,-4,4,0} \\
 & - 468(f_{3,0,2,-4} + f_{-1,0,-2,4}) + 462(f_{5,0,0,-4} + f_{1,0,-4,4}) \\
 & \left. + 196(f_{5,-4,4,-4} + f_{1,-4,0,4}) - 21f_{1,4,-4,0} \right) \tag{C.5}
 \end{aligned}$$

The associated weight mask is shown in figure C.5.
 B-coefficient c_{3011} is computed using (1, 3)-symmetry.

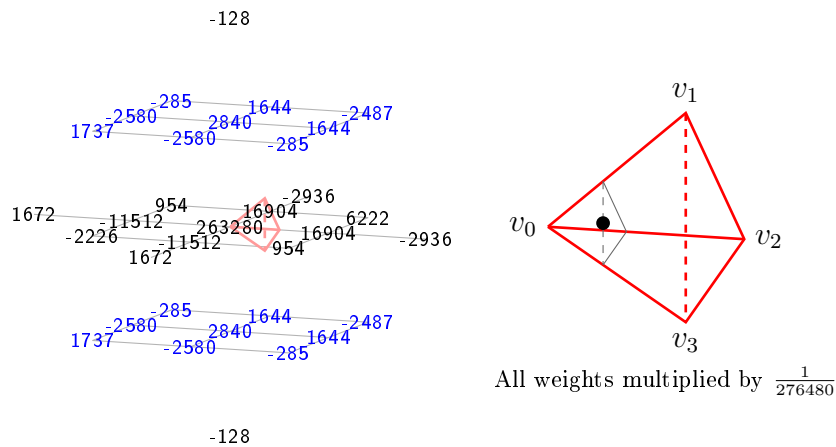
$$\begin{aligned}
 c_{3101} := & \frac{1}{276480} \left(263280f_{1,0,0,0} + 16904(f_{-1,0,2,0} + f_{-1,2,-2,2}) \right. \\
 & - 11512(f_{3,0,-2,0} + f_{3,-2,2,-2}) + 6222f_{-3,2,0,2} \\
 & - 2936(f_{-3,4,-4,4} + f_{-3,0,4,0}) + 2840(f_{1,2,0,-2} + f_{1,-2,0,2}) \\
 & - 2580(f_{3,-4,2,0} + f_{3,2,-2,-2} + f_{3,-2,-2,2} + f_{3,0,2,-4}) \\
 & - 2487(f_{-3,4,0,0} + f_{-3,0,0,4}) - 2226f_{5,-2,0,-2} + 1737(f_{5,0,0,-4} + f_{5,-4,0,0}) \\
 & + 1672(f_{5,0,-4,0} + f_{5,-4,4,-4}) \\
 & + 1644(f_{-1,4,-2,0} + f_{-1,2,2,-2} + f_{-1,-2,2,2} + f_{-1,0,-2,4}) \\
 & + 954(f_{1,2,-4,2} + f_{1,-2,4,-2}) - 285(f_{1,4,-4,0} + f_{1,-4,4,0} + f_{1,0,4,-4} + f_{1,0,-4,4}) \\
 & \left. - 128(f_{1,4,0,-4} + f_{1,-4,0,4}) \right) \tag{C.6}
 \end{aligned}$$

The associated weight mask is shown in figure C.6.



196

Figure C.5: Weight mask for c_{3110} . The associated domain point is shown in the teterahedron on the right. The black triangle symbolizes the ring $R_2(v_0)$.



-128

Figure C.6: Weight mask for c_{3101} . The associated domain point is shown in the teterahedron on the right. The black triangle symbolizes the ring $R_2(v_0)$.

$$\begin{aligned}
 c_{3020} := & \frac{1}{34560} \left(27960f_{1,0,0,0} + 4900f_{-1,0,2,0} - 2204f_{3,0,-2,0} \right. \\
 & + 1384(f_{3,-2,2,-2} + f_{1,-2,0,2} + f_{1,2,0,-2} + f_{-1,2,-2,2}) - 892f_{-3,0,4,0} \\
 & + 780(f_{-1,-2,2,2} + f_{-1,2,2,-2} + f_{1,-2,4,-2} + f_{-3,2,0,2}) \\
 & - 429(f_{-3,0,0,4} + f_{1,-4,4,0} + f_{1,0,4,-4} + f_{-3,4,0,0}) \\
 & - 276(f_{3,-2,-2,2} + f_{1,2,-4,2} + f_{3,2,-2,-2} + f_{5,-2,0,-2}) + 260f_{5,0,-4,0} \\
 & - 234(f_{3,-4,2,0} + f_{3,0,2,-4} + f_{-1,4,-2,0} + f_{-1,0,-2,4}) \\
 & - 190(f_{-3,4,-4,4} + f_{5,-4,4,-4} + f_{1,4,0,-4} + f_{1,-4,0,4}) \\
 & \left. + 99(f_{1,4,-4,0} + f_{5,0,0,-4} + f_{5,-4,0,0} + f_{1,0,-4,4}) \right) \tag{C.7}
 \end{aligned}$$

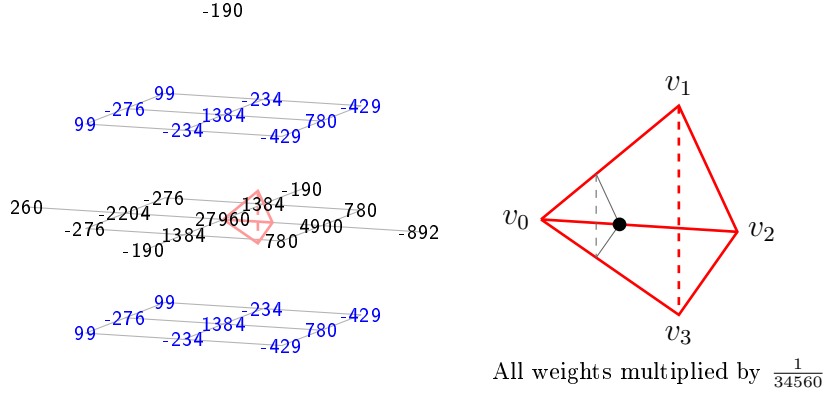


Figure C.7: Weight mask for c_{3020} . The associated domain point is shown in the teterahedron on the right. The black triangle symbolizes the ring $R_2(v_0)$.

The associated weight mask is shown in figure C.7.

$$\begin{aligned}
 c_{2300} := & \frac{1}{46080} \left(32304f_{1,0,0,0} + 6202(f_{-1,0,2,0} + f_{1,2,0,-2} + f_{-1,2,-2,2}) \right. \\
 & + 1574(f_{-3,2,0,2} + f_{-1,2,2,-2} + f_{-1,4,-2,0}) - 1113f_{-3,4,0,0} \\
 & - 960(f_{-3,4,-4,4} + f_{-3,0,4,0} + f_{1,4,0,-4}) - 726(f_{3,-2,2,-2} + f_{1,-2,0,2} + f_{3,0,-2,0}) \\
 & - 597(f_{-3,0,0,4} + f_{1,4,-4,0} + f_{1,0,4,-4}) - 506(f_{5,-2,0,-2} + f_{3,-4,2,0} + f_{3,-2,-2,2}) \\
 & + 249f_{5,-4,0,0} + 124(f_{5,-4,4,-4} + f_{1,-4,0,4} + f_{5,0,-4,0}) \\
 & - 119(f_{1,-4,4,0} + f_{5,0,0,-4} + f_{1,0,-4,4}) \\
 & - 28(f_{-3,2,4,-2} + f_{3,2,-2,-2} + f_{-1,-2,2,2} + f_{-1,0,-2,4} + f_{-3,6,-4,2} + f_{1,-2,4,-2} \\
 & \quad \left. + f_{3,0,2,-4} + f_{1,2,-4,2} + f_{-5,2,2,2} + f_{-1,6,-2,-2} + f_{-5,4,-2,4} + f_{-1,4,2,-4} \right) \tag{C.8}
 \end{aligned}$$

The associated weight mask is shown in figure C.8.

B-coefficient c_{2003} is computed using (1, 3)-symmetry.

$$\begin{aligned}
 c_{2210} := & \frac{1}{276480} \left(208176f_{1,0,0,0} + 41488f_{-1,0,2,0} + 27688(f_{1,2,0,-2} + f_{-1,2,-2,2}) \right. \\
 & - 13472f_{3,0,-2,0} + 10626(f_{-3,2,0,2} + f_{-1,2,2,-2}) - 7120f_{-3,0,4,0} \\
 & - 5883f_{-3,4,0,0} - 4230f_{3,-4,2,0} - 4048(f_{-3,4,-4,4} + f_{1,4,0,-4}) \\
 & - 3855(f_{-3,0,0,4} + f_{1,0,4,-4}) + 2922f_{-1,4,-2,0} + 2886(f_{1,-2,4,-2} + f_{-1,-2,2,2}) \\
 & - 2502(f_{3,-2,-2,2} + f_{5,-2,0,-2}) - 1863f_{1,-4,4,0} - 1698(f_{3,0,2,-4} + f_{-1,0,-2,4}) \\
 & + 1677f_{5,-4,0,0} + 1616f_{5,0,-4,0} - 1506(f_{1,2,-4,2} + f_{3,2,-2,-2}) \\
 & - 1455f_{1,4,-4,0} - 608(f_{1,-2,0,2} + f_{3,-2,2,-2}) + 392(f_{5,-4,4,-4} + f_{1,-4,0,4}) \\
 & \quad \left. + 273(f_{5,0,0,-4} + f_{1,0,-4,4}) - 168(f_{-5,2,2,2} + f_{-3,2,4,-2} + f_{-5,4,-2,4} + f_{-1,4,2,-4}) \right) \tag{C.9}
 \end{aligned}$$

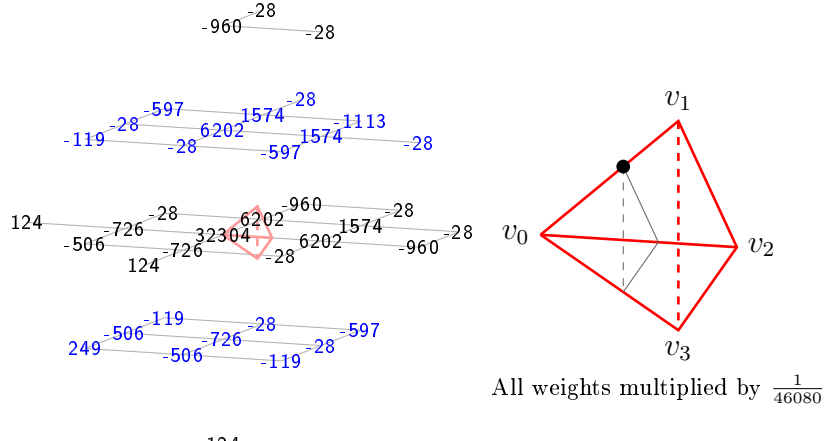


Figure C.8: Weight mask for c_{2300} . The associated domain point is shown in the teterahedron on the right. The black triangle symbolizes the ring $R_3(v_0)$.

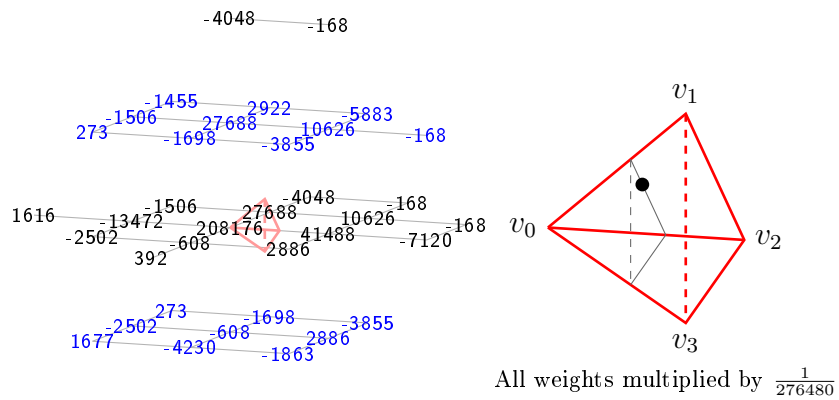
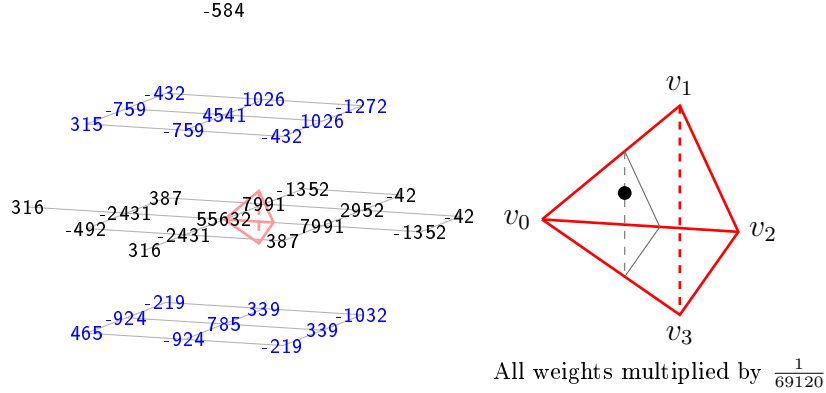


Figure C.9: Weight mask for c_{2210} . The associated domain point is shown in the teterahedron on the right. The black triangle symbolizes the ring $R_3(v_0)$.

The associated weight mask is shown in figure C.9.
 B -coefficient c_{2012} is computed using $(1, 3)$ -symmetry.



10

Figure C.10: Weight mask for c_{2201} . The associated domain point is shown in the teterahedron on the right. The black triangle symbolizes the ring $R_3(v_0)$.

$$\begin{aligned}
 c_{2201} := & \frac{1}{69120} \left(55632f_{1,0,0,0} + 7991(f_{-1,0,2,0} + f_{-1,2,-2,2}) + 4541f_{1,2,0,-2} \right. \\
 & + 2952f_{-3,2,0,2} - 2431(f_{3,-2,2,-2} + f_{3,0,-2,0}) - 1352(f_{-3,4,-4,4} + f_{-3,0,4,0}) \\
 & - 1272f_{-3,4,0,0} - 1032f_{-3,0,0,4} + 1026(f_{-1,4,-2,0} + f_{-1,2,2,-2}) \\
 & - 924(f_{3,-4,2,0} + f_{3,-2,-2,2}) + 785f_{1,-2,0,2} - 759(f_{3,0,2,-4} + f_{3,2,-2,-2}) \\
 & - 584f_{1,4,0,-4} - 492f_{5,-2,0,-2} + 465f_{5,-4,0,0} - 432(f_{1,4,-4,0} + f_{1,0,4,-4}) \\
 & + 387(f_{1,2,-4,2} + f_{1,-2,4,-2}) + 339(f_{-1,-2,2,2} + f_{-1,0,-2,4}) \\
 & + 316(f_{5,0,-4,0} + f_{5,-4,4,-4}) + 315f_{5,0,0,-4} - 219(f_{1,0,-4,4} + f_{1,-4,4,0}) \\
 & \left. - 42(f_{-5,2,2,2} + f_{-5,4,-2,4}) + 10f_{1,-4,0,4} \right) \quad (C.10)
 \end{aligned}$$

The associated weight mask is shown in figure C.10.
B-coefficient c_{2102} is computed using (1, 3)-symmetry.

$$\begin{aligned}
 c_{2120} := & \frac{1}{46080} \left(32496f_{1,0,0,0} + 8388f_{-1,0,2,0} + 3904(f_{1,2,0,-2} + f_{-1,2,-2,2}) \right. \\
 & - 2868f_{3,0,-2,0} + 1998(f_{-1,2,2,-2} + f_{-3,2,0,2}) \\
 & + 1556(f_{3,-2,2,-2} + f_{1,-2,0,2} - f_{-3,0,4,0}) + 1234(f_{-1,-2,2,2} + f_{1,-2,4,-2}) \\
 & - 971f_{-3,4,0,0} - 842f_{3,-4,2,0} - 827(f_{-3,0,0,4} + f_{1,0,4,-4}) - 683f_{1,-4,4,0} \\
 & - 598(f_{3,0,2,-4} + f_{-1,0,-2,4}) - 504(f_{1,4,0,-4} + f_{-3,4,-4,4}) - 354f_{-1,4,-2,0} \\
 & - 338(f_{1,2,-4,2} + f_{3,2,-2,-2}) - 326(f_{5,-2,0,-2} + f_{3,-2,-2,2}) + 260f_{5,0,-4,0} \\
 & + 205f_{5,-4,0,0} - 148(f_{1,-4,0,4} + f_{5,-4,4,-4}) + 105(f_{1,0,-4,4} + f_{5,0,0,-4}) \\
 & \left. - 28(f_{-5,4,-2,4} + f_{-3,2,4,-2} + f_{-5,2,2,2} + f_{-1,4,2,-4}) + 5f_{1,4,-4,0} \right) \quad (C.11)
 \end{aligned}$$

The associated weight mask is shown in figure C.11.
B-coefficient c_{2021} is computed using (1, 3)-symmetry.

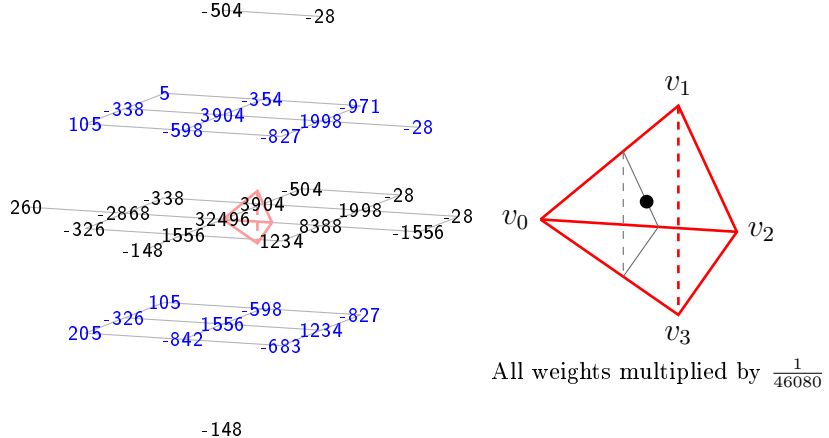


Figure C.11: Weight mask for c_{2120} . The associated domain point is shown in the teterahedron on the right. The black triangle symbolizes the ring $R_3(v_0)$.

$$\begin{aligned}
 c_{2111} := & \frac{1}{138240} \left(111264f_{1,0,0,0} + 19258f_{-1,0,2,0} + 12706f_{-1,2,-2,2} \right. \\
 & - 8282f_{3,0,-2,0} + 5904f_{-3,2,0,2} + 5326(f_{1,-2,0,2} + f_{1,2,0,-2}) \\
 & - 3514f_{-3,0,4,0} + 2967(f_{-1,-2,2,2} + f_{-1,2,2,-2}) - 2304(f_{-3,0,0,4} + f_{-3,4,0,0}) \\
 & + 2034f_{1,-2,4,-2} - 2025(f_{3,0,2,-4} + f_{3,-4,2,0}) - 1894f_{-3,4,-4,4} \\
 & - 1442f_{3,-2,2,-2} - 1341(f_{3,-2,-2,2} + f_{3,2,-2,-2}) - 1299(f_{1,-4,4,0} + f_{1,0,4,-4}) \\
 & - 984f_{5,-2,0,-2} + 938f_{5,0,-4,0} + 780(f_{5,-4,0,0} + f_{5,0,0,-4}) \\
 & - 574(f_{1,-4,0,4} + f_{1,4,0,-4}) - 486f_{1,2,-4,2} + 326f_{5,-4,4,-4} \\
 & \left. - 237(f_{-1,0,-2,4} + f_{-1,4,-2,0}) - 84(f_{-5,2,2,2} + f_{-5,4,-2,4}) - 3(f_{1,0,-4,4} + f_{1,4,-4,0}) \right) \tag{C.12}
 \end{aligned}$$

The associated weight mask is shown in figure C.12.

$$\begin{aligned}
 c_{2030} := & \frac{1}{69120} \left(41568f_{1,0,0,0} + 15364f_{-1,0,2,0} \right. \\
 & + 5422(f_{3,-2,2,-2} + f_{1,-2,0,2} + f_{1,2,0,-2} + f_{-1,2,-2,2}) - 4196f_{3,0,-2,0} \\
 & + 3288(f_{-3,2,0,2} + f_{-1,-2,2,2} + f_{-1,2,2,-2} + f_{1,-2,4,-2}) - 2884f_{-3,0,4,0} \\
 & - 1623(f_{-3,0,0,4} + f_{-3,4,0,0} + f_{1,-4,4,0} + f_{1,0,4,-4}) \\
 & - 1326(f_{-1,4,-2,0} + f_{3,-4,2,0} + f_{-1,0,-2,4} + f_{3,0,2,-4}) \\
 & - 598(f_{5,-4,4,-4} + f_{-3,4,-4,4} + f_{1,-4,0,4} + f_{1,4,0,-4}) \\
 & - 444(f_{1,2,-4,2} + f_{3,-2,-2,2} + f_{3,2,-2,-2} + f_{5,-2,0,-2}) + 260f_{5,0,-4,0} \\
 & + 117(f_{1,0,-4,4} + f_{1,4,-4,0} + f_{5,-4,0,0} + f_{5,0,0,-4}) \\
 & - 42(f_{-1,-4,2,4} + f_{-1,-2,6,-2} + f_{-5,4,-2,4} + f_{-5,2,2,2} + f_{3,-4,6,-4} + f_{-1,4,2,-4} \\
 & \left. + f_{-3,2,4,-2} + f_{-3,-2,4,2}) \right) \tag{C.13}
 \end{aligned}$$

The associated weight mask is shown in figure C.13.

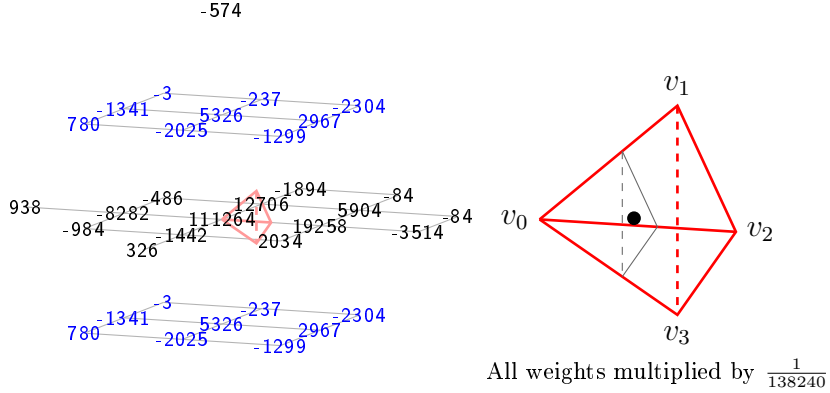


Figure C.12: Weight mask for c_{2111} . The associated domain point is shown in the teterahedron on the right. The black triangle symbolizes the ring $R_3(v_0)$.

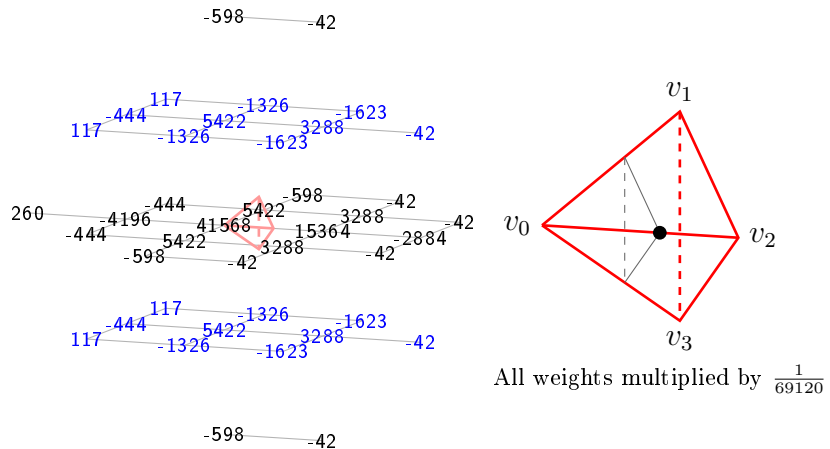


Figure C.13: Weight mask for c_{2030} . The associated domain point is shown in the teterahedron on the right. The black triangle symbolizes the ring $R_3(v_0)$.

$$\begin{aligned}
 c_{1400} := & \frac{1}{92160} \left(50562f_{1,0,0,0} + 16658(f_{-1,0,2,0} + f_{1,2,0,-2} + f_{-1,2,-2,2}) \right. \\
 & + 4636(f_{-3,2,0,2} + f_{-1,4,-2,0} + f_{-1,2,2,-2}) \\
 & - 2494(f_{-3,0,4,0} + f_{-3,4,-4,4} + f_{1,4,0,-4}) - 2133f_{-3,4,0,0} \\
 & - 1361(f_{1,4,-4,0} + f_{-3,0,0,4} + f_{1,0,4,-4}) \\
 & - 878(f_{3,0,-2,0} + f_{1,-2,0,2} + f_{3,-2,2,-2}) - 718(f_{3,-2,-2,2} + f_{3,-4,2,0} + f_{5,-2,0,-2}) \\
 & - 331(f_{1,-4,4,0} + f_{5,0,0,-4} + f_{1,0,-4,4}) \\
 & - 324(f_{3,2,-2,-2} + f_{3,0,2,-4} + f_{1,2,-4,2} + f_{1,-2,4,-2} + f_{-1,0,-2,4} + f_{-1,-2,2,2}) \\
 & + 249f_{5,-4,0,0} \\
 & - 202(f_{-1,6,-2,-2} + f_{-5,4,-2,4} + f_{-5,2,2,2} + f_{-3,6,-4,2} + f_{-3,2,4,-2} + f_{-1,4,2,-4}) \\
 & \left. + 56(f_{5,0,-4,0} + f_{1,-4,0,4} + f_{5,-4,4,-4}) - 22(f_{-3,6,0,-2} + f_{-5,4,2,0} + f_{-5,6,-2,2}) \right) \tag{C.14}
 \end{aligned}$$

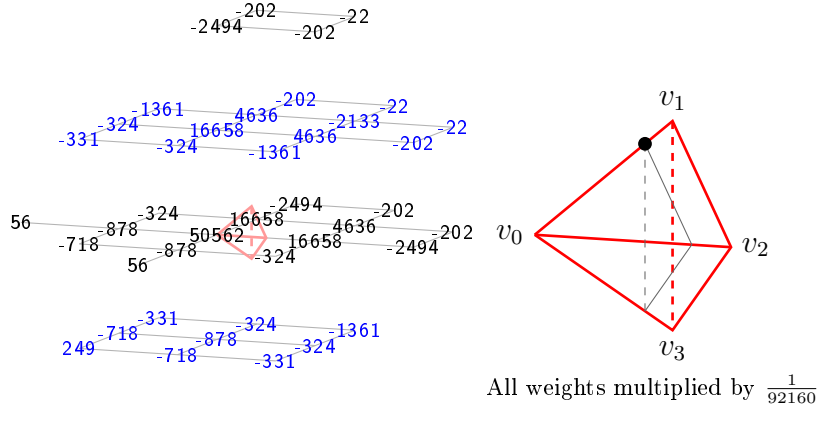


Figure C.14: Weight mask for c_{1400} . The associated domain point is shown in the teterahedron on the right. The black triangle symbolizes the ring $R_4(v_0)$.

The associated weight mask is shown in figure C.14.
B-coefficient c_{1004} is computed using (1, 3)-symmetry.

$$\begin{aligned}
 c_{1310} := & \frac{1}{276480} \left(165732f_{1,0,0,0} + 55192f_{-1,0,2,0} + 40984(f_{1,2,0,-2} + f_{-1,2,-2,2}) \right. \\
 & + 16029(f_{-3,2,0,2} + f_{-1,2,2,-2}) - 10094f_{3,0,-2,0} - 8938f_{-3,0,4,0} \\
 & - 6492f_{-3,4,0,0} - 5893(f_{-3,4,-4,4} + f_{1,4,0,-4}) + 5202f_{-1,4,-2,0} \\
 & - 4710(f_{1,0,4,-4} + f_{-3,0,0,4}) - 3834f_{3,-4,2,0} - 2415(f_{3,0,2,-4} + f_{-1,0,-2,4}) \\
 & - 2328f_{1,4,-4,0} - 2286f_{1,-4,4,0} + 2184(f_{1,-2,4,-2} + f_{-1,-2,2,2}) \\
 & - 1881(f_{1,2,-4,2} + f_{3,2,-2,-2}) - 1755(f_{3,-2,-2,2} + f_{5,-2,0,-2}) + 996f_{5,-4,0,0} \\
 & + 836f_{5,0,-4,0} - 657(f_{-5,4,-2,4} + f_{-1,4,2,-4}) - 588(f_{-3,2,4,-2} + f_{-5,2,2,2}) \\
 & + 235(f_{3,-2,2,-2} + f_{1,-2,0,2}) - 207(f_{1,0,-4,4} + f_{5,0,0,-4}) \\
 & - 135(f_{-3,6,-4,2} + f_{-1,6,-2,-2}) + 122(f_{1,-4,0,4} + f_{5,-4,4,-4}) - 66f_{-5,4,2,0} \\
 & \left. - 33(f_{-3,6,0,-2} + f_{-5,6,-2,2}) \right) \tag{C.15}
 \end{aligned}$$

The associated weight mask is shown in figure C.15.
B-coefficient c_{1013} is computed using (1, 3)-symmetry.

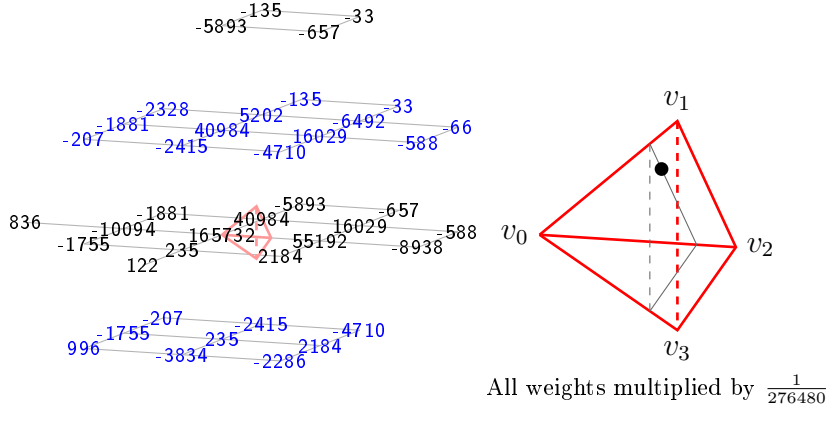


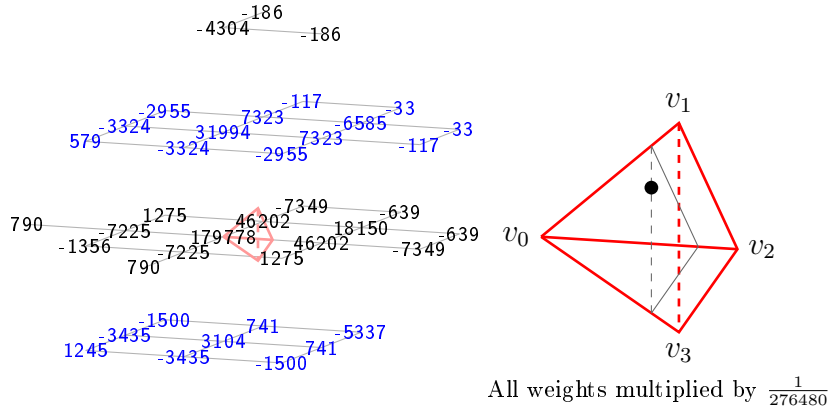
Figure C.15: Weight mask for c_{1310} . The associated domain point is shown in the teterahedron on the right. The black triangle symbolizes the ring $R_4(v_0)$.

$$\begin{aligned}
 c_{1301} := & \frac{1}{276480} \left(179778f_{1,0,0,0} + 46202(f_{-1,0,2,0} + f_{-1,2,-2,2}) + 31994f_{1,2,0,-2} \right. \\
 & + 18150f_{-3,2,0,2} - 7349(f_{-3,4,-4,4} + f_{-3,0,4,0}) \\
 & + 7323(f_{-1,2,2,-2} + f_{-1,4,-2,0}) - 7225(f_{3,0,-2,0} + f_{3,-2,2,-2}) - 6585f_{-3,4,0,0} \\
 & - 5337f_{-3,0,0,4} - 4304f_{1,4,0,-4} - 3435(f_{3,-4,2,0} + f_{3,-2,-2,2}) \\
 & - 3324(f_{3,2,-2,-2} + f_{3,0,2,-4}) + 3104f_{1,-2,0,2} - 2955(f_{1,4,-4,0} + f_{1,0,4,-4}) \\
 & - 1500(f_{1,-4,4,0} + f_{1,0,-4,4}) - 1356f_{5,-2,0,-2} + 1275(f_{1,2,-4,2} + f_{1,-2,4,-2}) \\
 & + 1245f_{5,-4,0,0} + 790(f_{5,0,-4,0} + f_{5,-4,4,-4}) + 741(f_{-1,-2,2,2} + f_{-1,0,-2,4}) \\
 & - 639(f_{-5,2,2,2} + f_{-5,4,-2,4}) + 579f_{5,0,0,-4} - 186(f_{-1,6,-2,-2} + f_{-1,4,2,-4}) \\
 & \left. - 117(f_{-3,2,4,-2} + f_{-3,6,-4,2}) + 76f_{1,-4,0,4} - 33(f_{-5,4,2,0} + f_{-5,6,-2,2}) \right) \quad (\text{C.16})
 \end{aligned}$$

The associated weight mask is shown in figure C.16.

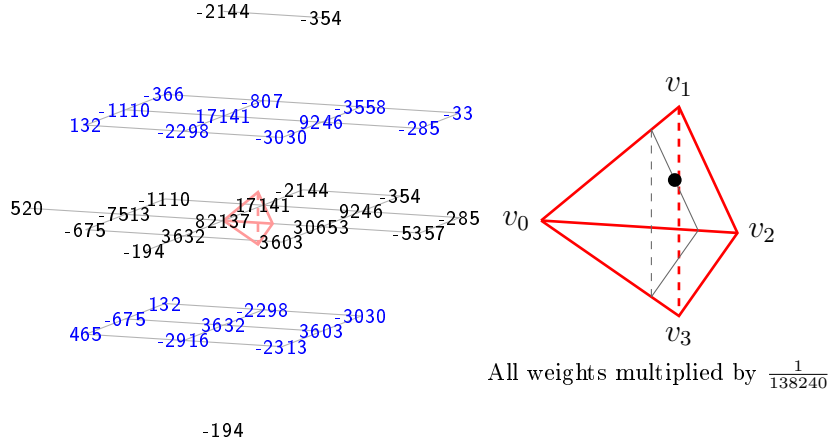
B-coefficient c_{1103} is computed using (1, 3)-symmetry.

$$\begin{aligned}
 c_{1220} := & \frac{1}{138240} \left(82137f_{1,0,0,0} + 30653f_{-1,0,2,0} + 17141(f_{-1,2,-2,2} + f_{1,2,0,-2}) \right. \\
 & + 9246(f_{-3,2,0,2} + f_{-1,2,2,-2}) - 7513f_{3,0,-2,0} - 5357f_{-3,0,4,0} \\
 & + 3632(f_{1,-2,0,2} + f_{3,-2,2,-2}) + 3603(f_{1,-2,4,-2} + f_{-1,-2,2,2}) - 3558f_{-3,4,0,0} \\
 & - 3030(f_{1,0,4,-4} + f_{-3,0,0,4}) - 2916f_{3,-4,2,0} - 2313f_{1,-4,4,0} \\
 & - 2298(f_{-1,0,-2,4} + f_{3,0,2,-4}) - 2144(f_{1,4,0,-4} + f_{-3,4,-4,4}) \\
 & - 1110(f_{3,2,-2,-2} + f_{1,2,-4,2}) - 807f_{-1,4,-2,0} - 675(f_{3,-2,-2,2} + f_{5,-2,0,-2}) \\
 & + 520f_{5,0,-4,0} + 465f_{5,-4,0,0} - 366f_{1,4,-4,0} - 354(f_{-1,4,2,-4} + f_{-5,4,-2,4}) \\
 & - 285(f_{-3,2,4,-2} + f_{-5,2,2,2}) - 194(f_{5,-4,4,-4} + f_{1,-4,0,4}) \\
 & \left. + 132(f_{5,0,0,-4} + f_{1,0,-4,4}) - 33f_{-5,4,2,0} \right) \quad (\text{C.17})
 \end{aligned}$$



76

Figure C.16: Weight mask for c_{1301} . The associated domain point is shown in the teterahedron on the right. The black triangle symbolizes the ring $R_4(v_0)$.



-194

Figure C.17: Weight mask for c_{1220} . The associated domain point is shown in the teterahedron on the right. The black triangle symbolizes the ring $R_4(v_0)$.

The associated weight mask is shown in figure C.17.
 B -coefficient c_{1022} is computed using $(1, 3)$ -symmetry.

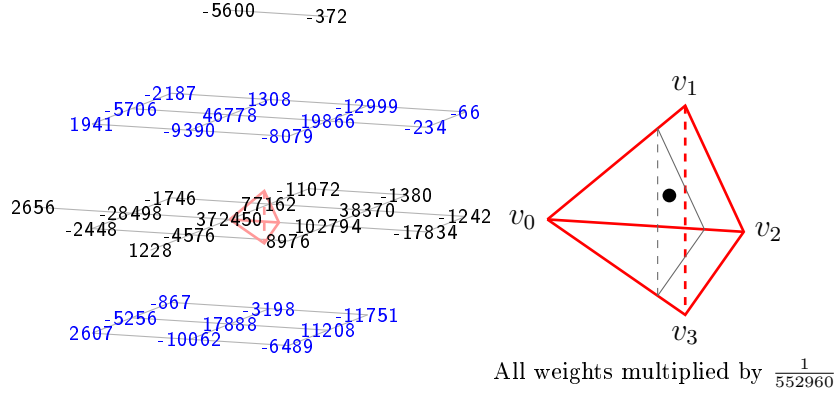


Figure C.18: Weight mask for c_{1211} . The associated domain point is shown in the teterahedron on the right. The black triangle symbolizes the ring $R_4(v_0)$.

$$\begin{aligned}
c_{1211} := & \frac{1}{552960} \left(372450 f_{1,0,0,0} + 102794 f_{-1,0,2,0} + 77162 f_{-1,2,-2,2} \right. \\
& + 46778 f_{1,2,0,-2} + 38370 f_{-3,2,0,2} - 28498 f_{3,0,-2,0} \\
& + 19866 f_{-1,2,2,-2} + 17888 f_{1,-2,0,2} - 17834 f_{-3,0,4,0} \\
& - 12999 f_{-3,4,0,0} - 11751 f_{-3,0,0,4} + 11208 f_{-1,-2,2,2} \\
& - 11072 f_{-3,4,-4,4} - 10062 f_{3,-4,2,0} - 9390 f_{3,0,2,-4} + 8976 f_{1,-2,4,-2} \\
& - 8079 f_{1,0,4,-4} - 6489 f_{1,-4,4,0} - 5706 f_{3,2,-2,-2} - 5600 f_{1,4,0,-4} \\
& - 5256 f_{3,-2,-2,2} - 4576 f_{3,-2,2,-2} - 3198 f_{-1,0,-2,4} + 2656 f_{5,0,-4,0} \\
& + 2607 f_{5,-4,0,0} - 2448 f_{5,-2,0,-2} - 2187 f_{1,4,-4,0} + 1941 f_{5,0,0,-4} \\
& - 1746 f_{1,2,-4,2} - 1380 f_{-5,4,-2,4} + 1308 f_{-1,4,-2,0} - 1242 f_{-5,2,2,2} \\
& + 1228 f_{5,-4,4,-4} - 1220 f_{1,-4,0,4} - 867 f_{1,0,-4,4} - 372 f_{-1,4,2,-4} \\
& \left. - 234 f_{-3,2,4,-2} - 66 f_{-5,4,2,0} \right) \tag{C.18}
\end{aligned}$$

The associated weight mask is shown in figure C.18.

B-coefficient c_{1112} is computed using (1, 3)-symmetry.

$$\begin{aligned}
c_{1202} := & \frac{1}{46080} \left(32112 f_{1,0,0,0} + 7296(f_{-1,0,2,0} + f_{-1,2,-2,2}) + 3370 f_{-3,2,0,2} \right. \\
& + 2464(f_{1,-2,0,2} + f_{1,2,0,-2}) - 1552(f_{3,-2,2,-2} + f_{3,0,-2,0}) \\
& - 1184(f_{-3,4,-4,4} + f_{-3,0,4,0}) - 1069(f_{-3,0,0,4} + f_{-3,4,0,0}) \\
& - 704(f_{3,0,2,-4} + f_{3,-2,-2,2} + f_{3,2,-2,-2} + f_{3,-4,2,0}) \\
& + 544(f_{-1,0,-2,4} + f_{-1,4,-2,0} + f_{-1,2,2,-2} + f_{-1,-2,2,2}) + 390(f_{1,2,-4,2} + f_{1,-2,4,-2}) \\
& - 363(f_{1,-4,4,0} + f_{1,4,-4,0} + f_{1,0,4,-4} + f_{1,0,-4,4}) + 227(f_{5,0,0,-4} + f_{5,-4,0,0}) \\
& - 216(f_{1,-4,0,4} + f_{1,4,0,-4}) + 192(f_{5,0,-4,0} + f_{5,-4,4,-4}) - 182 f_{5,-2,0,-2} \\
& \left. - 112(f_{-5,2,2,2} + f_{-5,4,-2,4}) \right) \tag{C.19}
\end{aligned}$$

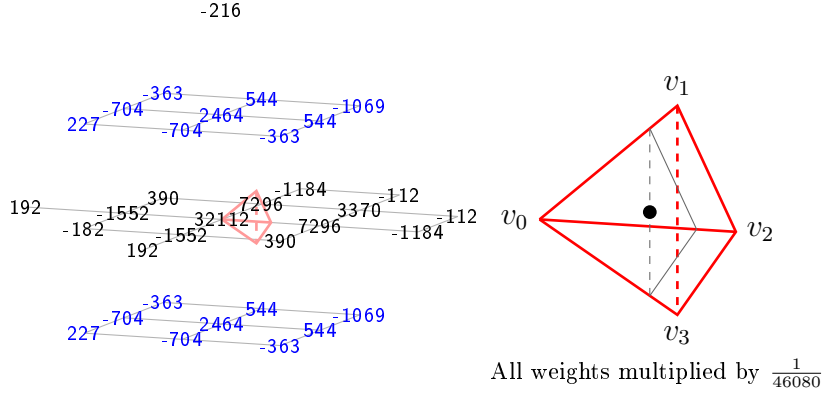


Figure C.19: Weight mask for c_{1202} . The associated domain point is shown in the teterahedron on the right. The black triangle symbolizes the ring $R_4(v_0)$.

The associated weight mask is shown in figure C.19.

$$\begin{aligned}
 c_{1130} := & \frac{1}{92160} \left(49260f_{1,0,0,0} + 23056f_{-1,0,2,0} + 9977(f_{1,2,0,-2} + f_{-1,2,-2,2}) \right. \\
 & + 6805(f_{-3,2,0,2} + f_{-1,2,2,-2}) + 5667(f_{3,-2,2,-2} + f_{1,-2,0,2}) - 5480f_{3,0,-2,0} \\
 & + 4571(f_{-1,-2,2,2} + f_{1,-2,4,-2}) - 4168f_{-3,0,4,0} - 2687f_{-3,4,0,0} \\
 & - 2560(f_{-3,0,0,4} + f_{1,0,4,-4}) - 2478f_{3,-4,2,0} - 2433f_{1,-4,4,0} \\
 & - 2263(f_{-1,0,-2,4} + f_{3,0,2,-4}) - 2048f_{-1,4,-2,0} - 1002(f_{-3,4,-4,4} + f_{1,4,0,-4}) \\
 & - 641(f_{1,2,-4,2} + f_{3,2,-2,-2}) - 414(f_{5,-4,4,-4} + f_{1,-4,0,4}) \\
 & - 375(f_{3,-2,-2,2} + f_{5,-2,0,-2}) + 260f_{5,0,-4,0} - 242(f_{-5,4,-2,4} + f_{-1,4,2,-4}) \\
 & + 183f_{5,-4,0,0} - 173(f_{-3,2,4,-2} + f_{-5,2,2,2}) + 106(f_{1,0,-4,4} + f_{5,0,0,-4}) \\
 & - 62(f_{3,-4,6,-4} + f_{-1,-4,2,4}) - 39(f_{-1,-2,6,-2} + f_{-3,-2,4,2}) + 29f_{1,4,-4,0} \\
 & \left. - 22f_{-5,4,2,0} - 11(f_{-5,0,2,4} + f_{-1,0,6,-4}) \right) \tag{C.20}
 \end{aligned}$$

The associated weight mask is shown in figure C.20.
B-coefficient c_{1031} is computed using (1, 3)-symmetry.

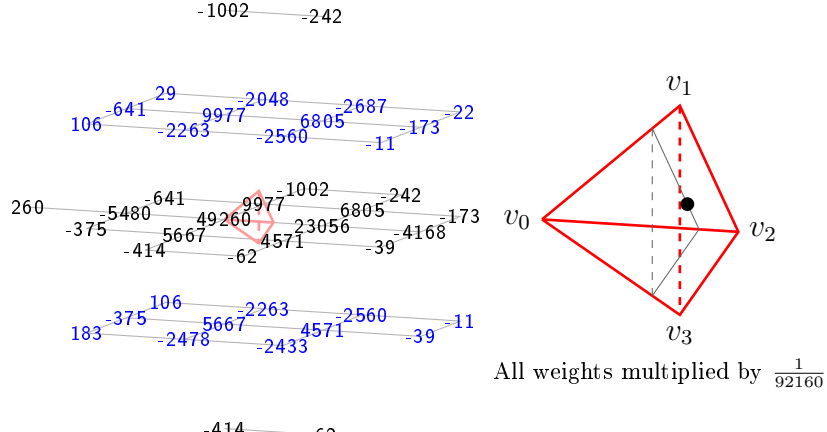


Figure C.20: Weight mask for c_{1130} . The associated domain point is shown in the teterahedron on the right. The black triangle symbolizes the ring $R_4(v_0)$.

$$\begin{aligned}
 c_{1121} := & \frac{1}{184320} \left(114252f_{1,0,0,0} + 39832f_{-1,0,2,0} + 22744f_{-1,2,-2,2} \right. \\
 & + 13370f_{-3,2,0,2} + 12826(f_{1,-2,0,2} + f_{1,2,0,-2}) - 11216f_{3,0,-2,0} \\
 & + 8232(f_{-1,2,2,-2} + f_{-1,-2,2,2}) - 7280f_{-3,0,4,0} + 5846f_{1,-2,4,-2} \\
 & + 4732f_{3,-2,2,-2} - 4629(f_{-3,4,0,0} + f_{-3,0,0,4}) - 4162(f_{3,-4,2,0} + f_{3,0,2,-4}) \\
 & - 3799(f_{1,0,4,-4} + f_{1,-4,4,0}) - 2772f_{-3,4,-4,4} - 2756(f_{-1,4,-2,0} + f_{-1,0,-2,4}) \\
 & - 1332(f_{3,-2,-2,2} + f_{3,2,-2,-2}) - 1302f_{1,2,-4,2} - 1248(f_{1,4,0,-4} + f_{1,-4,0,4}) \\
 & + 780f_{5,0,-4,0} - 722f_{5,-2,0,-2} + 593(f_{5,-4,0,0} + f_{5,0,0,-4}) - 472f_{-5,4,-2,4} \\
 & - 380f_{-5,2,2,2} - 172f_{5,-4,4,-4} - 124(f_{-1,-4,2,4} + f_{-1,4,2,-4}) \\
 & \left. - 78(f_{-3,2,4,-2} + f_{-3,-2,4,2}) + 39(f_{1,4,-4,0} + f_{1,0,-4,4}) - 22(f_{-5,0,2,4} + f_{-5,4,2,0}) \right) \\
 & \quad (C.21)
 \end{aligned}$$

The associated weight mask is shown in figure C.21.

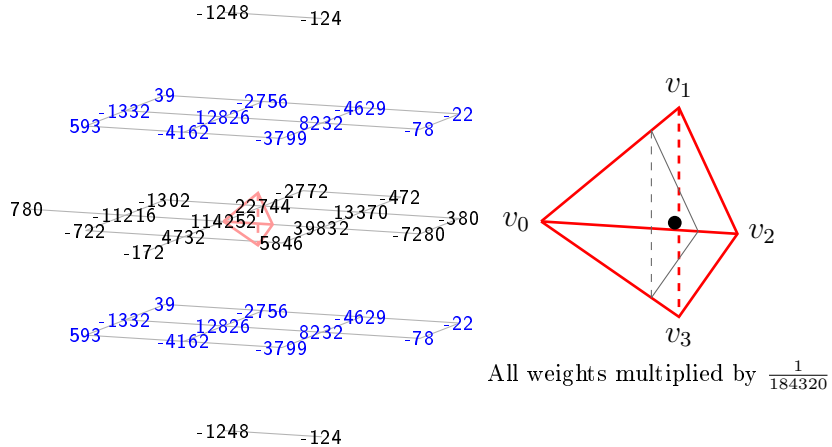


Figure C.21: Weight mask for c_{1121} . The associated domain point is shown in the teterahedron on the right. The black triangle symbolizes the ring $R_4(v_0)$.

$$\begin{aligned}
 c_{1040} := & \frac{1}{138240} \left(64644f_{1,0,0,0} + 38440f_{-1,0,2,0} \right. \\
 & + 12622(f_{3,-2,2,-2} + f_{1,-2,0,2} + f_{1,2,0,-2} + f_{-1,2,-2,2}) \\
 & + 10488(f_{-3,2,0,2} + f_{-1,-2,2,2} + f_{-1,2,2,-2} + f_{1,-2,4,-2}) - 8048f_{3,0,-2,0} \\
 & - 6736f_{-3,0,4,0} - 4434(f_{-3,0,0,4} + f_{-3,4,0,0} + f_{1,-4,4,0} + f_{1,0,4,-4}) \\
 & - 4137(f_{-1,4,-2,0} + f_{3,-4,2,0} + f_{-1,0,-2,4} + f_{3,0,2,-4}) \\
 & - 928(f_{1,4,0,-4} + f_{5,-4,4,-4} + f_{-3,4,-4,4} + f_{1,-4,0,4}) \\
 & - 636(f_{1,2,-4,2} + f_{5,-2,0,-2} + f_{3,-2,-2,2} + f_{3,2,-2,-2}) \\
 & - 372(f_{-1,-4,2,4} + f_{-5,4,-2,4} + f_{3,-4,6,-4} + f_{-1,4,2,-4}) + 260f_{5,0,-4,0} \\
 & - 234(f_{-3,2,4,-2} + f_{-3,-2,4,2} + f_{-5,2,2,2} + f_{-1,-2,6,-2}) \\
 & + 84(f_{1,4,-4,0} + f_{1,0,-4,4} + f_{5,0,0,-4} + f_{5,-4,0,0}) \\
 & \left. - 33(f_{-5,0,2,4} + f_{-1,-4,6,0} + f_{-5,4,2,0} + f_{-1,0,6,-4}) \right) \tag{C.22}
 \end{aligned}$$

The associated weight mask is shown in figure C.22.

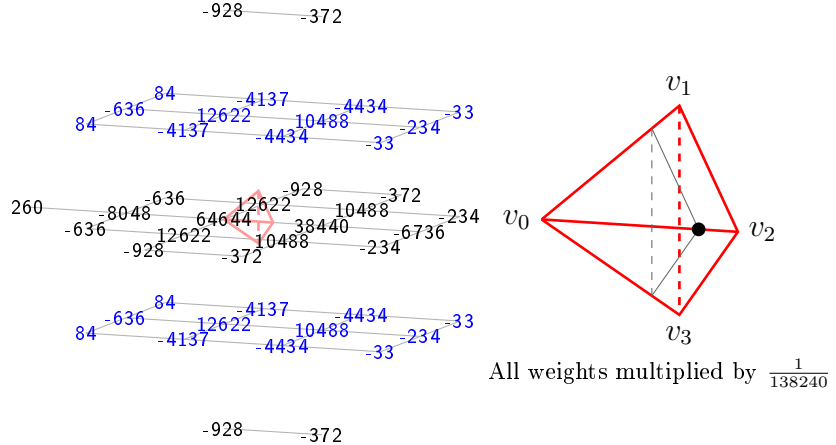


Figure C.22: Weight mask for c_{1040} . The associated domain point is shown in the teterahedron on the right. The black triangle symbolizes the ring $R_4(v_0)$.

$$\begin{aligned}
 c_{0500} := & \frac{1}{184320} \left(83712 f_{1,0,0,0} + 37028(f_{-1,0,2,0} + f_{1,2,0,-2} + f_{-1,2,-2,2}) \right. \\
 & + 12902(f_{-1,4,-2,0} + f_{-1,2,2,-2} + f_{-3,2,0,2}) \\
 & - 5228(f_{-3,4,-4,4} + f_{1,4,0,-4} + f_{-3,0,4,0}) \\
 & - 2711(f_{-3,0,0,4} + f_{1,4,-4,0} + f_{1,0,4,-4}) \\
 & - 1948(f_{3,-2,2,-2} + f_{1,-2,0,2} + f_{3,0,-2,0}) - 1671f_{-3,4,0,0} \\
 & - 1226(f_{3,2,-2,-2} + f_{3,0,2,-4} + f_{1,2,-4,2} + f_{1,-2,4,-2} + f_{-1,-2,2,2} + f_{-1,0,-2,4}) \\
 & - 986(f_{5,-2,0,-2} + f_{3,-2,-2,2} + f_{3,-4,2,0}) \\
 & - 864(f_{-1,6,-2,-2} + f_{-5,4,-2,4} + f_{-5,2,2,2} + f_{-3,6,-4,2} + f_{-3,2,4,-2} + f_{-1,4,2,-4}) \\
 & - 599(f_{1,0,-4,4} + f_{5,0,0,-4} + f_{1,-4,4,0}) - 256(f_{-3,6,0,-2} + f_{-5,4,2,0} + f_{-5,6,-2,2}) \\
 & \left. + 249f_{5,-4,0,0} - 12(f_{5,0,-4,0} + f_{1,-4,0,4} + f_{5,-4,4,-4}) \right) \quad (C.23)
 \end{aligned}$$

The associated weight mask is shown in figure C.23.
B-coefficient c_{0005} is computed using (1, 3)-symmetry.

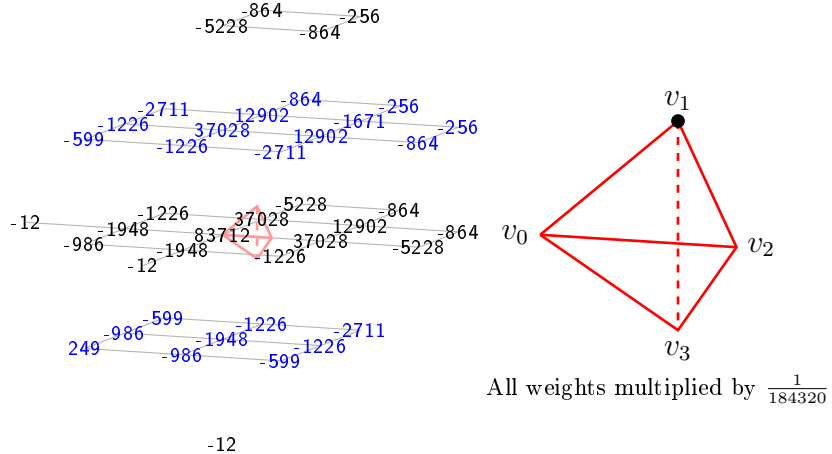


Figure C.23: Weight mask for c_{0500} . The associated domain point is shown in the teterahedron on the right.

$$\begin{aligned}
 c_{0410} := & \frac{1}{138240} \left(67137f_{1,0,0,0} + 32203f_{-1,0,2,0} + 24163(f_{1,2,0,-2} + f_{-1,2,-2,2}) \right. \\
 & + 10983(f_{-3,2,0,2} + f_{-1,2,2,-2}) - 4753f_{-3,0,4,0} + 4341f_{-1,4,-2,0} \\
 & - 3857f_{3,0,-2,0} - 3415(f_{-3,4,-4,4} + f_{1,4,0,-4}) - 2340(f_{-3,0,0,4} + f_{1,0,4,-4}) \\
 & - 1902f_{-3,4,0,0} - 1428f_{1,4,-4,0} - 1344f_{3,-4,2,0} \\
 & - 1317(f_{3,0,2,-4} + f_{-1,0,-2,4}) - 1149(f_{1,2,-4,2} + f_{3,2,-2,-2}) - 957f_{1,-4,4,0} \\
 & - 759(f_{-5,4,-2,4} + f_{-1,4,2,-4}) - 621(f_{-5,2,2,2} + f_{-3,2,4,-2}) \\
 & - 606(f_{5,-2,0,-2} + f_{3,-2,-2,2}) + 249f_{5,-4,0,0} \\
 & - 219(f_{1,0,-4,4} + f_{5,0,0,-4} + f_{-3,6,-4,2} + f_{-1,6,-2,-2}) - 191(f_{1,-2,0,2} + f_{3,-2,2,-2}) \\
 & - 183f_{-5,4,2,0} + 158f_{5,0,-4,0} + 141(f_{-1,-2,2,2} + f_{1,-2,4,-2}) \\
 & \left. - 117(f_{-3,6,0,-2} + f_{-5,6,-2,2}) - 46(f_{1,-4,0,4} + f_{5,-4,4,-4}) \right) \tag{C.24}
 \end{aligned}$$

The associated weight mask is shown in figure C.24.
B-coefficient c_{0014} is computed using (1, 3)-symmetry.

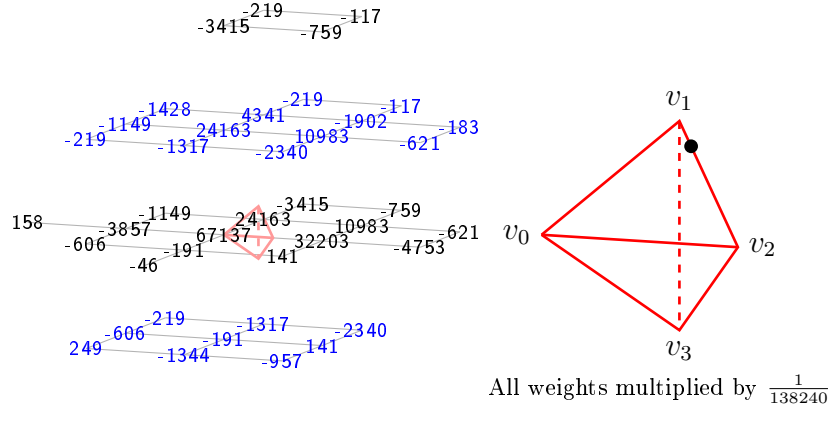


Figure C.24: Weight mask for c_{0410} . The associated domain point is shown in the teterahedron on the right.

$$\begin{aligned}
 c_{0401} := & \frac{1}{552960} \left(285960f_{1,0,0,0} + 114380(f_{-1,0,2,0} + f_{-1,2,-2,2}) + 82220f_{1,2,0,-2} \right. \\
 & + 49158f_{-3,2,0,2} + 22590(f_{-1,2,2,-2} + f_{-1,4,-2,0}) \\
 & - 16988(f_{-3,4,-4,4} + f_{-3,0,4,0}) - 11636f_{1,4,0,-4} - 10587f_{-3,0,0,4} \\
 & - 10348(f_{3,0,-2,0} + f_{3,-2,2,-2}) - 10203f_{-3,4,0,0} \\
 & - 6939(f_{1,4,-4,0} + f_{1,0,4,-4}) - 6186(f_{3,2,-2,-2} + f_{3,0,2,-4}) \\
 & - 4842(f_{3,-2,-2,2} + f_{3,-4,2,0}) + 4316f_{1,-2,0,2} - 2928(f_{-5,4,-2,4} + f_{-5,2,2,2}) \\
 & - 2907(f_{1,-4,4,0} + f_{1,0,-4,4}) - 1890f_{5,-2,0,-2} - 1320(f_{-1,4,2,-4} + f_{-1,6,-2,-2}) \\
 & + 1245f_{5,-4,0,0} - 1026(f_{-1,0,-2,4} + f_{-1,-2,2,2}) - 768(f_{-3,2,4,-2} + f_{-3,6,-4,2}) \\
 & + 484(f_{5,0,-4,0} + f_{5,-4,4,-4}) - 432(f_{-5,4,2,0} + f_{-5,6,-2,2}) \\
 & \left. - 354(f_{1,-2,4,-2} + f_{1,2,-4,2}) - 332f_{1,-4,0,4} - 168f_{-3,6,0,-2} + 45f_{5,0,0,-4} \right) \tag{C.25}
 \end{aligned}$$

The associated weight mask is shown in figure C.25.
B-coefficient c_{0104} is computed using (1, 3)-symmetry.

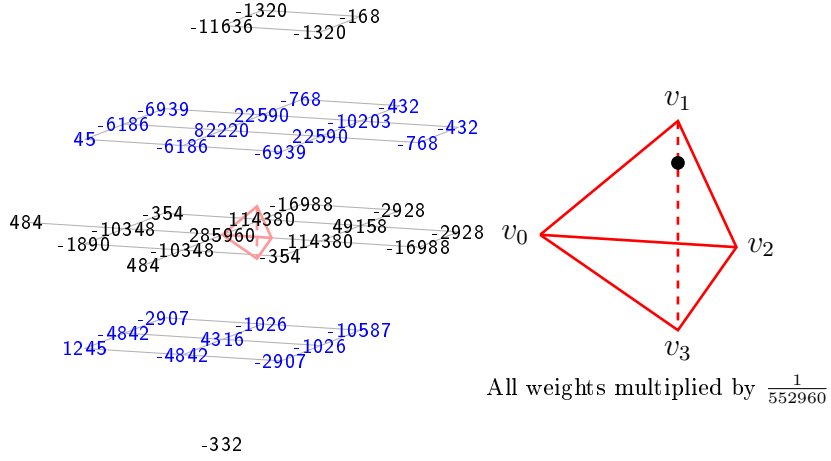


Figure C.25: Weight mask for c_{0401} . The associated domain point is shown in the teterahedron on the right.

$$\begin{aligned}
 c_{0320} := & \frac{1}{552960} \left(279048f_{1,0,0,0} + 140996f_{-1,0,2,0} + 80852(f_{1,2,0,-2} + f_{-1,2,-2,2}) \right. \\
 & + 50166(f_{-3,2,0,2} + f_{-1,2,2,-2}) - 25660f_{3,0,-2,0} - 21908f_{-3,0,4,0} \\
 & - 11811(f_{-3,0,0,4} + f_{1,0,4,-4}) - 10851f_{-3,4,0,0} \\
 & - 10196(f_{1,4,0,-4} + f_{-3,4,-4,4}) - 9810f_{3,-4,2,0} \\
 & + 9342(f_{-1,-2,2,2} + f_{1,-2,4,-2}) - 9090(f_{3,0,2,-4} + f_{-1,0,-2,4}) \\
 & + 8564(f_{3,-2,2,-2} + f_{1,-2,0,2}) - 7875f_{1,-4,4,0} - 4866(f_{1,2,-4,2} + f_{3,2,-2,-2}) \\
 & - 3480(f_{-1,4,2,-4} + f_{-5,4,-2,4}) - 2643f_{1,4,-4,0} - 2376(f_{-3,2,4,-2} + f_{-5,2,2,2}) \\
 & - 1890(f_{3,-2,-2,2} + f_{5,-2,0,-2}) + 1300f_{5,0,-4,0} + 1245f_{5,-4,0,0} \\
 & - 696f_{-5,4,2,0} + 630f_{-1,4,-2,0} - 332(f_{5,-4,4,-4} + f_{1,-4,0,4}) \\
 & \left. - 168(f_{-5,6,-2,2} + f_{-3,6,-4,2} + f_{-3,6,0,-2} + f_{-1,6,-2,-2}) + 45(f_{5,0,0,-4} + f_{1,0,-4,4}) \right) \tag{C.26}
 \end{aligned}$$

The associated weight mask is shown in figure C.26.
B-coefficient c_{0023} is computed using (1, 3)-symmetry.

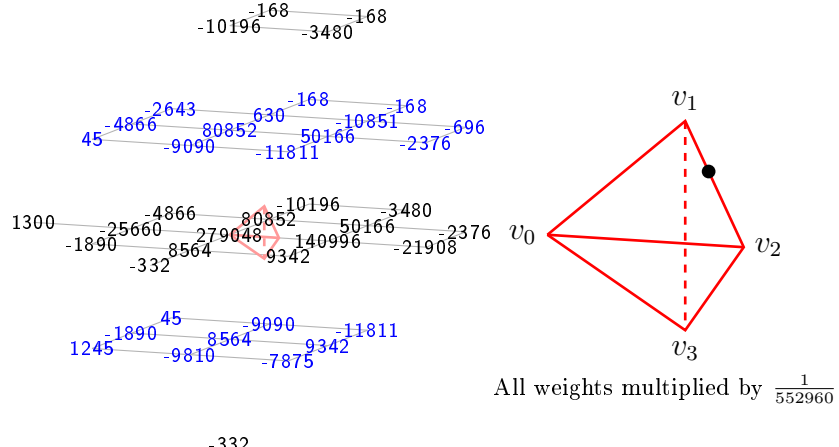


Figure C.26: Weight mask for c_{0320} . The associated domain point is shown in the teterahedron on the right.

$$\begin{aligned}
 c_{0311} := & \frac{1}{1105920} \left(610512f_{1,0,0,0} + 251380f_{-1,0,2,0} + 195412f_{-1,2,-2,2} \right. \\
 & + 130228f_{1,2,0,-2} + 107478f_{-3,2,0,2} + 56970f_{-1,2,2,-2} \\
 & - 45848f_{3,0,-2,0} - 39784f_{-3,0,4,0} - 27064f_{-3,4,-4,4} \\
 & + 24796f_{1,-2,0,2} - 24123f_{-3,0,0,4} - 23835f_{-3,4,0,0} \\
 & - 18339f_{1,0,4,-4} - 18162f_{3,0,2,-4} - 17478f_{3,-4,2,0} \\
 & - 16900f_{1,4,0,-4} + 15522f_{-1,-2,2,2} - 12447f_{1,-4,4,0} \\
 & + 11898f_{1,-2,4,-2} - 11058f_{3,2,-2,-2} + 11034f_{-1,4,-2,0} \\
 & - 9678f_{-1,0,-2,4} - 7542f_{3,-2,-2,2} - 7299f_{1,4,-4,0} - 6728f_{3,-2,2,-2} \\
 & - 6708f_{-5,4,-2,4} - 6198f_{1,2,-4,2} - 5604f_{-5,2,2,2} - 3258f_{5,-2,0,-2} \\
 & + 3237f_{5,-4,0,0} + 2972f_{5,0,-4,0} - 2880f_{-1,4,2,-4} - 2511f_{1,0,-4,4} \\
 & + 1773f_{5,0,0,-4} - 1516f_{1,-4,0,4} - 1500f_{-3,2,4,-2} + 1340f_{5,-4,4,-4} \\
 & \left. - 828f_{-5,4,2,0} - 576f_{-1,6,-2,-2} - 300(f_{-3,6,-4,2} + f_{-5,6,-2,2}) - 168f_{-3,6,0,-2} \right) \tag{C.27}
 \end{aligned}$$

The associated weight mask is shown in figure C.27.
B-coefficient c_{0113} is computed using (1, 3)-symmetry.

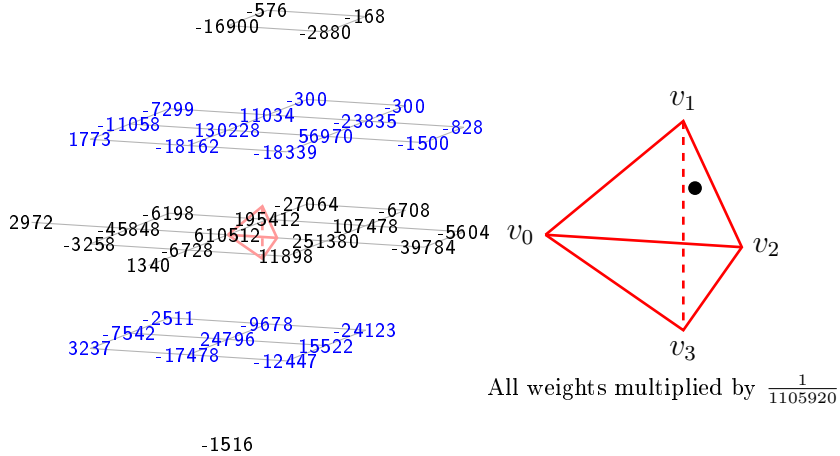


Figure C.27: Weight mask for c_{0311} . The associated domain point is shown in the teterahedron on the right.

$$\begin{aligned}
 c_{0302} := & \frac{1}{138240} \left(81138f_{1,0,0,0} + 27254(f_{-1,0,2,0} + f_{-1,2,-2,2}) + 14580f_{-3,2,0,2} \right. \\
 & + 12002f_{1,2,0,-2} + 5120f_{1,-2,0,2} - 4109(f_{-3,4,-4,4} + f_{-3,0,4,0}) \\
 & - 3985(f_{3,0,-2,0} + f_{3,-2,2,-2}) - 3408f_{-3,4,0,0} - 3384f_{-3,0,0,4} \\
 & + 2853(f_{-1,4,-2,0} + f_{-1,2,2,-2}) - 2106(f_{3,0,2,-4} + f_{3,2,-2,-2}) \\
 & - 1917(f_{3,-4,2,0} + f_{3,-2,-2,2}) - 1470(f_{1,4,-4,0} + f_{1,0,4,-4}) - 1316f_{1,4,0,-4} \\
 & - 1143(f_{1,-4,4,0} + f_{1,0,-4,4}) + 987(f_{-1,0,-2,4} + f_{-1,-2,2,2}) \\
 & - 807(f_{-5,2,2,2} + f_{-5,4,-2,4}) + 801(f_{1,-2,4,-2} + f_{1,2,-4,2}) + 498f_{5,-4,0,0} \\
 & + 432f_{5,0,0,-4} + 418(f_{5,0,-4,0} + f_{5,-4,4,-4}) - 342f_{5,-2,0,-2} - 296f_{1,-4,0,4} \\
 & \left. - 102(f_{-1,6,-2,-2} + f_{-1,4,2,-4}) - 33(f_{-3,2,4,-2} + f_{-3,6,-4,2} + f_{-5,4,2,0} + f_{-5,6,-2,2}) \right) \\
 & \quad (C.28)
 \end{aligned}$$

The associated weight mask is shown in figure C.28.
B-coefficient c_{0203} is computed using (1, 3)-symmetry.

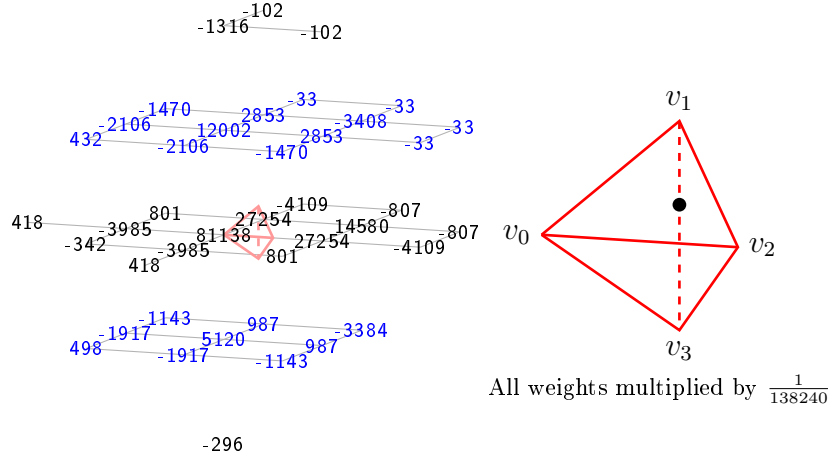


Figure C.28: Weight mask for c_{0302} . The associated domain point is shown in the teterahedron on the right.

$$\begin{aligned}
 c_{0230} := & \frac{1}{138240} \left(65103f_{1,0,0,0} + 38899f_{-1,0,2,0} + 17350(f_{-1,2,-2,2} + f_{1,2,0,-2}) \right. \\
 & + 13659(f_{-3,2,0,2} + f_{-1,2,2,-2}) - 7535f_{3,0,-2,0} - 6223f_{-3,0,4,0} \\
 & + 5977(f_{3,-2,2,-2} + f_{1,-2,0,2}) + 5400(f_{-1,-2,2,2} + f_{1,-2,4,-2}) \\
 & - 3624(f_{1,0,4,-4} + f_{-3,0,0,4}) - 3483f_{-3,4,0,0} - 3450f_{3,-4,2,0} \\
 & - 3327(f_{-1,0,-2,4} + f_{3,0,2,-4}) - 3234f_{1,-4,4,0} - 2673f_{-1,4,-2,0} \\
 & - 1810(f_{-3,4,-4,4} + f_{1,4,0,-4}) - 1035(f_{1,2,-4,2} + f_{3,2,-2,-2}) \\
 & - 948(f_{-1,4,2,-4} + f_{-5,4,-2,4}) - 534(f_{-5,2,2,2} + f_{-3,2,4,-2}) \\
 & - 352(f_{5,-4,4,-4} + f_{1,-4,0,4}) - 336(f_{3,-2,-2,2} + f_{5,-2,0,-2}) + 260f_{5,0,-4,0} \\
 & + 216f_{5,-4,0,0} - 165f_{-5,4,2,0} - 147f_{1,4,-4,0} - 102(f_{-1,-4,2,4} + f_{3,-4,6,-4}) \\
 & \left. + 84(f_{5,0,0,-4} + f_{1,0,-4,4}) - 33(f_{-1,0,6,-4} + f_{-5,0,2,4} + f_{-3,-2,4,2} + f_{-1,-2,6,-2}) \right) \tag{C.29}
 \end{aligned}$$

The associated weight mask is shown in figure C.29.
B-coefficient c_{0032} is computed using (1, 3)-symmetry.

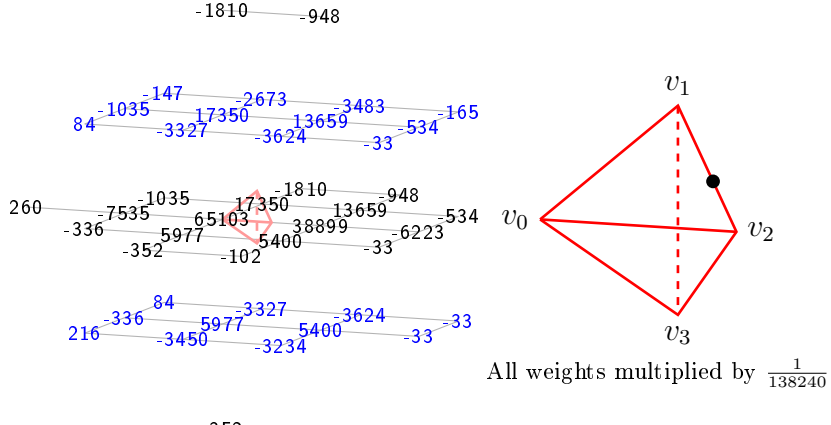


Figure C.29: Weight mask for c_{0230} . The associated domain point is shown in the teterahedron on the right.

$$\begin{aligned}
 c_{0221} := & \frac{1}{92160} \left(49080f_{1,0,0,0} + 23184f_{-1,0,2,0} + 14088f_{-1,2,-2,2} \right. \\
 & + 9550f_{-3,2,0,2} + 8906f_{1,2,0,-2} + 5720f_{-1,2,2,-2} - 5016f_{3,0,-2,0} \\
 & + 4630f_{1,-2,0,2} - 3860f_{-3,0,4,0} + 3520f_{-1,-2,2,2} + 2482f_{1,-2,4,-2} \\
 & - 2363f_{-3,0,0,4} - 2347f_{-3,4,0,0} - 2122f_{3,-4,2,0} - 2118f_{3,0,2,-4} \\
 & - 2073f_{1,0,4,-4} - 1849f_{1,-4,4,0} + 1776f_{3,-2,2,-2} - 1684f_{-3,4,-4,4} \\
 & - 1632f_{-1,0,-2,4} - 1160f_{-1,4,-2,0} - 952f_{1,4,0,-4} - 750f_{1,2,-4,2} \\
 & - 680f_{3,2,-2,-2} - 608f_{-5,4,-2,4} - 448f_{3,-2,-2,2} - 424f_{-5,2,2,2} \\
 & - 352f_{1,-4,0,4} + 260(f_{5,0,-4,0} - f_{-1,4,2,-4}) + 227f_{5,-4,0,0} - 226f_{5,-2,0,-2} \\
 & + 183f_{5,0,0,-4} - 171f_{1,4,-4,0} - 122f_{-3,2,4,-2} - 68f_{-1,-4,2,4} \\
 & \left. - 66f_{-5,4,2,0} - 39f_{1,0,-4,4} - 22(f_{-3,-2,4,2} + f_{-5,0,2,4}) - 12f_{5,-4,4,-4} \right) \quad (C.30)
 \end{aligned}$$

The associated weight mask is shown in figure C.30.
B-coefficient c_{0122} is computed using (1, 3)-symmetry.

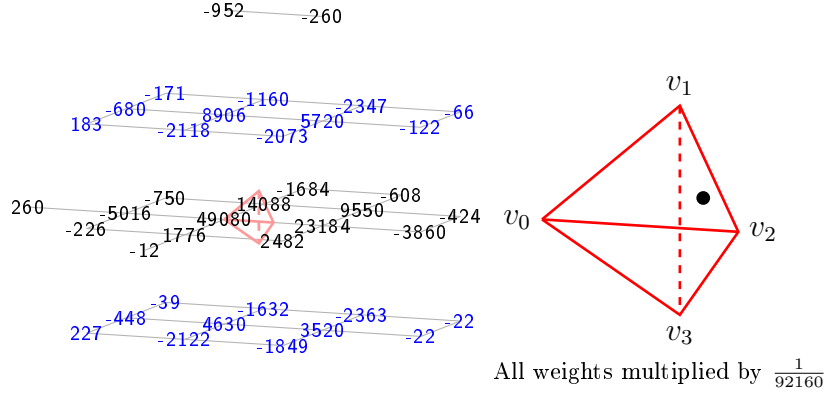


Figure C.30: Weight mask for c_{0221} . The associated domain point is shown in the teterahedron on the right.

$$\begin{aligned}
 c_{0212} := & \frac{1}{138240} \left(81138f_{1,0,0,0} + 30578f_{-1,0,2,0} + 23930f_{-1,2,-2,2} \right. \\
 & + 14580f_{-3,2,0,2} + 8561(f_{1,-2,0,2} + f_{1,2,0,-2}) - 6634f_{3,0,-2,0} \\
 & - 4946f_{-3,0,4,0} + 4209(f_{-1,2,2,-2} + f_{-1,-2,2,2}) - 3396(f_{-3,4,0,0} + f_{-3,0,0,4}) \\
 & - 3272f_{-3,4,-4,4} - 2646(f_{3,-4,2,0} + f_{3,0,2,-4}) + 2094f_{1,-2,4,-2} \\
 & - 2043(f_{1,0,4,-4} + f_{1,-4,4,0}) - 1377(f_{3,-2,-2,2} + f_{3,2,-2,-2}) - 1336f_{3,-2,2,-2} \\
 & - 876f_{-5,4,-2,4} - 806(f_{1,-4,0,4} + f_{1,4,0,-4}) - 738f_{-5,2,2,2} \\
 & - 570(f_{1,0,-4,4} + f_{1,4,-4,0}) + 520f_{5,0,-4,0} - 492f_{1,2,-4,2} \\
 & + 465(f_{5,0,0,-4} + f_{5,-4,0,0}) - 369(f_{-1,4,-2,0} + f_{-1,0,-2,4}) - 342f_{5,-2,0,-2} \\
 & + 316f_{5,-4,4,-4} - 102(f_{-1,-4,2,4} + f_{-1,4,2,-4}) \\
 & \left. - 33(f_{-3,-2,4,2} + f_{-3,2,4,-2} + f_{-5,0,2,4} + f_{-5,4,2,0}) \right) \tag{C.31}
 \end{aligned}$$

The associated weight mask is shown in figure C.31.

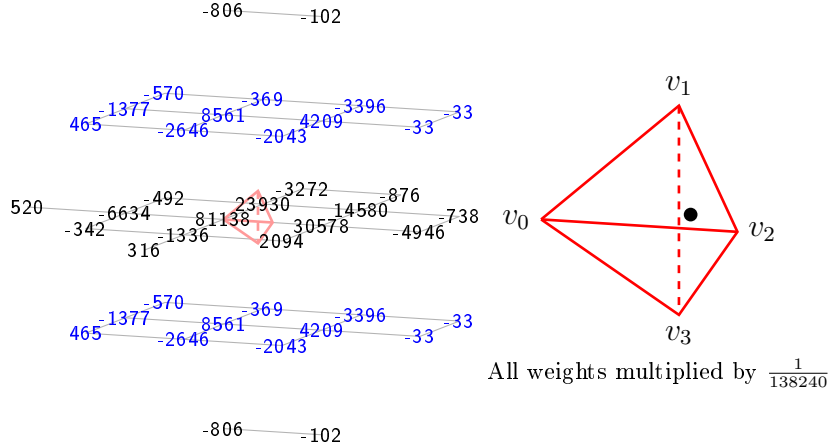


Figure C.31: Weight mask for c_{0212} . The associated domain point is shown in the teterahedron on the right.

$$\begin{aligned}
 c_{0140} := & \frac{1}{552960} \left(232372f_{1,0,0,0} + 179964f_{-1,0,2,0} + 58170(f_{1,2,0,-2} + f_{-1,2,-2,2}) \right. \\
 & + 53902(f_{-3,2,0,2} + f_{-1,2,2,-2}) + 38538(f_{3,-2,2,-2} + f_{1,-2,0,2}) \\
 & + 34270(f_{1,-2,4,-2} + f_{-1,-2,2,2}) - 30880f_{3,0,-2,0} - 28256f_{-3,0,4,0} \\
 & - 17703f_{1,-4,4,0} - 17439(f_{-3,0,0,4} + f_{1,0,4,-4}) - 17175f_{-3,4,0,0} \\
 & - 17109f_{3,-4,2,0} - 16845(f_{3,0,2,-4} + f_{-1,0,-2,4}) - 16581f_{-1,4,-2,0} \\
 & - 4308(f_{-3,4,-4,4} + f_{1,4,0,-4}) - 3196(f_{-5,4,-2,4} + f_{-1,4,2,-4}) \\
 & - 2742(f_{1,2,-4,2} + f_{3,2,-2,-2}) - 2004(f_{5,-4,4,-4} + f_{1,-4,0,4}) \\
 & - 1938(f_{-3,2,4,-2} + f_{-5,2,2,2}) - 1542(f_{3,-2,-2,2} + f_{5,-2,0,-2}) \\
 & - 892(f_{-1,-4,2,4} + f_{3,-4,6,-4}) + 780f_{5,0,-4,0} - 738(f_{-1,-2,6,-2} + f_{-3,-2,4,2}) \\
 & + 483f_{5,-4,0,0} - 279f_{-5,4,2,0} + 260f_{-5,0,6,0} + 249f_{-1,-4,6,0} \\
 & \left. + 219(f_{5,0,0,-4} + f_{1,0,-4,4}) - 45f_{1,4,-4,0} - 15(f_{-5,0,2,4} + f_{-1,0,6,-4}) \right) \quad (C.32)
 \end{aligned}$$

The associated weight mask is shown in figure C.32.
B-coefficient c_{0041} is computed using (1, 3)-symmetry.

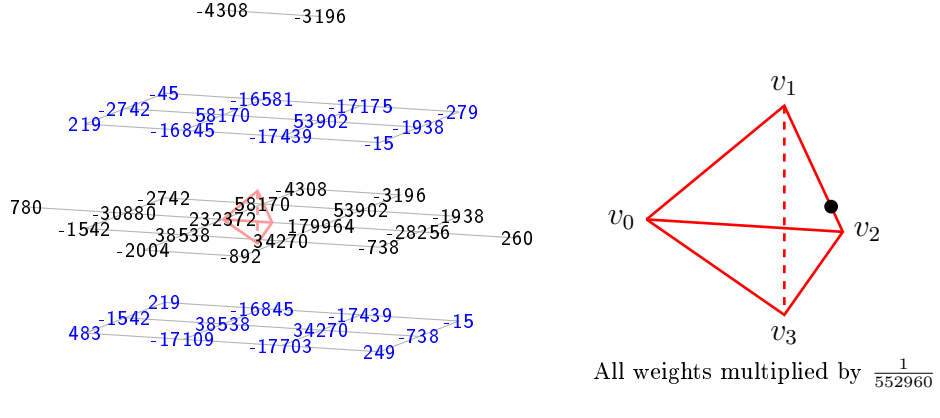


Figure C.32: Weight mask for c_{0140} . The associated domain point is shown in the teterahedron on the right.

$$\begin{aligned}
 c_{0131} := & \frac{1}{1105920} \left(527932f_{1,0,0,0} + 318300f_{-1,0,2,0} + 145026f_{-1,2,-2,2} \right. \\
 & + 115498f_{-3,2,0,2} + 91038(f_{1,-2,0,2} + f_{1,2,0,-2}) \\
 & + 73966(f_{-1,2,2,-2} + f_{-1,-2,2,2}) - 63760f_{3,0,-2,0} + 54042f_{3,-2,2,-2} \\
 & - 53264f_{-3,0,4,0} + 49426f_{1,-2,4,-2} - 33297(f_{-3,0,0,4} + f_{-3,4,0,0}) \\
 & - 32301(f_{1,-4,4,0} + f_{1,0,4,-4}) - 31977(f_{3,-4,2,0} + f_{3,0,2,-4}) \\
 & - 28869(f_{-1,4,-2,0} + f_{-1,0,-2,4}) - 13740f_{-3,4,-4,4} - 8490f_{1,2,-4,2} \\
 & - 6900(f_{1,4,0,-4} + f_{1,-4,0,4}) - 6844f_{-5,4,-2,4} - 4686(f_{3,2,-2,-2} + f_{3,-2,-2,2}) \\
 & - 4482f_{-5,2,2,2} - 2898f_{5,-2,0,-2} - 2452(f_{-1,4,2,-4} + f_{-1,-4,2,4}) \\
 & + 2340f_{5,0,-4,0} - 2076f_{5,-4,4,-4} + 1581(f_{5,0,0,-4} + f_{5,-4,0,0}) \\
 & - 1470(f_{-3,2,4,-2} + f_{-3,-2,4,2}) - 474f_{-1,-2,6,-2} - 411(f_{-5,0,2,4} + f_{-5,4,2,0}) \\
 & + 260f_{-5,0,6,0} + 249(f_{-1,-4,6,0} + f_{-1,0,6,-4}) + 129(f_{1,0,-4,4} + f_{1,4,-4,0}) \\
 & \left. - 76f_{3,-4,6,-4} \right) \quad (C.33)
 \end{aligned}$$

The associated weight mask is shown in figure C.33.

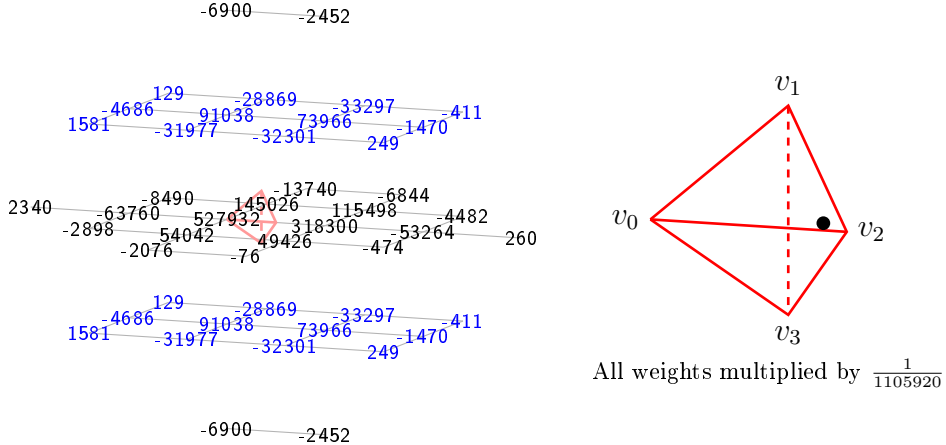


Figure C.33: Weight mask for c_{0131} . The associated domain point is shown in the teterahedron on the right.

$$\begin{aligned}
 c_{0050} := & \frac{1}{276480} \left(103084(f_{-1,0,2,0} + f_{1,0,0,0}) \right. \\
 & + 23110(f_{3,-2,2,-2} + f_{-3,2,0,2} + f_{1,-2,0,2} + f_{1,2,0,-2} + f_{-1,-2,2,2} + f_{-1,2,-2,2} \\
 & \quad + f_{-1,2,2,-2} + f_{1,-2,4,-2}) \\
 & - 14784(f_{3,0,-2,0} + f_{-3,0,4,0}) \\
 & - 8571(f_{-1,0,-2,4} + f_{-1,4,-2,0} + f_{1,0,4,-4} + f_{3,0,2,-4} + f_{1,-4,4,0} + f_{3,-4,2,0} \\
 & \quad + f_{-3,4,0,0} + f_{-3,0,0,4}) \\
 & - 1300(f_{-5,4,-2,4} + f_{-3,4,-4,4} + f_{3,-4,6,-4} + f_{-1,4,2,-4} + f_{-1,-4,2,4} + f_{1,4,0,-4} \\
 & \quad + f_{1,-4,0,4} + f_{5,-4,4,-4}) \\
 & - 870(f_{-5,2,2,2} + f_{5,-2,0,-2} + f_{3,2,-2,-2} + f_{-3,2,4,-2} + f_{-3,-2,4,2} + f_{1,2,-4,2} \\
 & \quad + f_{3,-2,-2,2} + f_{-1,-2,6,-2}) \\
 & + 260(f_{5,0,-4,0} + f_{-5,0,6,0}) \\
 & + 51(f_{1,0,-4,4} + f_{5,0,0,-4} + f_{-5,0,2,4} + f_{-1,0,6,-4} + f_{-1,-4,6,0} + f_{5,-4,0,0} \\
 & \quad \left. + f_{-5,4,2,0} + f_{1,4,-4,0} \right) \tag{C.34}
 \end{aligned}$$

The associated weight mask is shown in figure C.34.

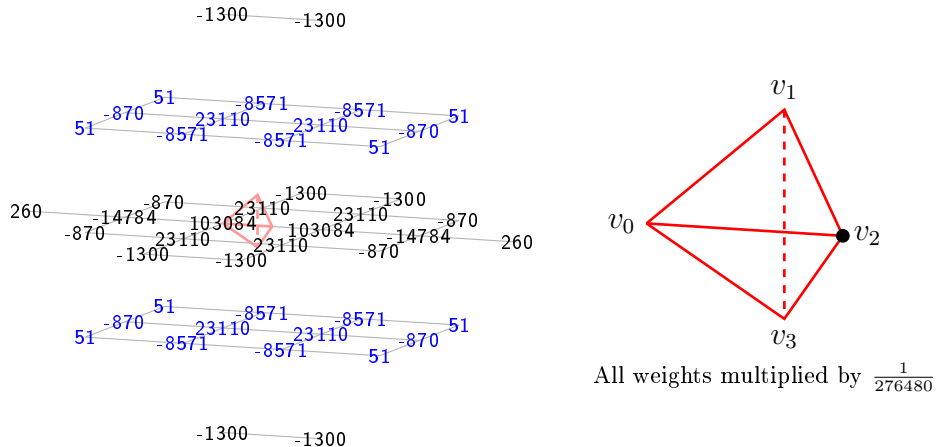


Figure C.34: Weight mask for c_{0050} . The associated domain point is shown in the teterahedron on the right.

B-coefficient computation rules for the class \mathcal{K}_2

$$\begin{aligned}
c_{5000} := & \frac{1}{276480} \left(103084(f_{0,1,-1,1} + f_{2,-1,1,-1}) \right. \\
& + 23110(f_{0,-1,-1,3} + f_{0,-1,3,-1} + f_{0,3,-1,-1} + f_{4,-1,-1,-1} + f_{2,-3,1,1} + f_{-2,1,1,1} \\
& \quad + f_{2,1,1,-3} + f_{2,1,-3,1}) \\
& - 14784(f_{4,-3,3,-3} + f_{-2,3,-3,3}) \\
& - 8571(f_{2,3,-3,-1} + f_{4,-3,-1,1} + f_{4,1,-1,-3} + f_{-2,3,1,-1} + f_{0,1,3,-3} + f_{2,-1,-3,3} \\
& \quad + f_{-2,-1,1,3} + f_{0,-3,3,1}) \\
& - 1300(f_{-2,-1,5,-1} + f_{2,3,1,-5} + f_{0,5,-1,-3} + f_{4,1,-5,1} + f_{2,-5,1,3} + f_{6,-1,-3,-1} \\
& \quad + f_{0,-3,-1,5} + f_{-4,1,3,1}) \\
& - 870(f_{-2,5,-3,1} + f_{-4,3,-1,3} + f_{4,-5,3,-1} + f_{4,-1,3,-5} + f_{2,-3,5,-3} + f_{0,3,-5,3} \\
& \quad + f_{6,-3,1,-3} + f_{-2,1,-3,5}) \\
& + 260(f_{-4,5,-5,5} + f_{6,-5,5,-5}) \\
& + 51(f_{-4,5,-1,1} + f_{0,1,-5,5} + f_{-4,1,-1,5} + f_{6,-1,1,-5} + f_{2,-5,5,-1} + f_{0,5,-5,1} \\
& \quad \left. + f_{6,-5,1,-1} + f_{2,-1,5,-5} \right) \tag{C.35}
\end{aligned}$$

The associated weight mask is shown in figure C.35.

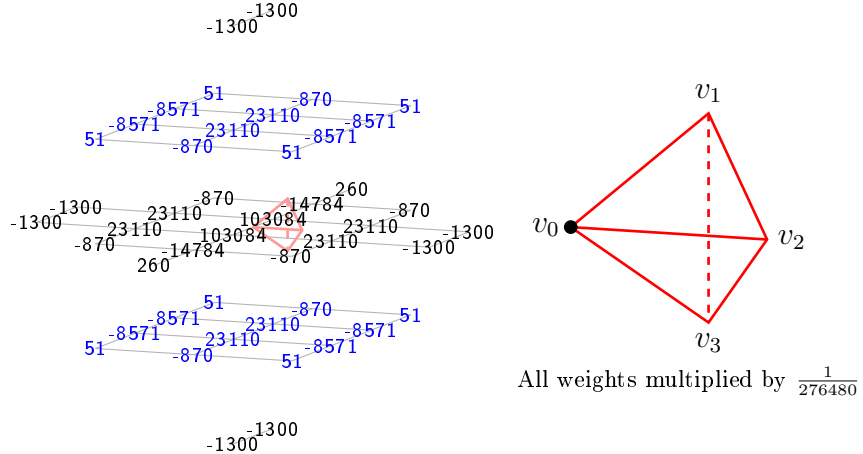


Figure C.35: Weight mask for c_{5000} . The associated domain point is shown in the teterahedron on the right.

$$\begin{aligned}
 c_{4100} := & \frac{1}{552960} \left(232372f_{0,1,-1,1} + 179964f_{2,-1,1,-1} + 58170(f_{0,3,-1,-1} + f_{-2,1,1,1}) \right. \\
 & + 53902(f_{0,-1,3,-1} + f_{2,1,1,-3}) + 38538(f_{0,-1,-1,3} + f_{2,1,-3,1}) \\
 & + 34270(f_{4,-1,-1,-1} + f_{2,-3,1,1}) - 30880f_{-2,3,-3,3} - 28256f_{4,-3,3,-3} \\
 & - 17703f_{4,-3,-1,1} - 17439(f_{4,1,-1,-3} + f_{0,-3,3,1}) - 17175f_{0,1,3,-3} \\
 & - 17109f_{2,-1,-3,3} - 16845(f_{2,3,-3,-1} + f_{-2,-1,1,3}) - 16581f_{-2,3,1,-1} \\
 & - 4308(f_{-4,1,3,1} + f_{0,5,-1,-3}) - 3196(f_{-2,-1,5,-1} + f_{2,3,1,-5}) \\
 & - 2742(f_{-4,3,-1,3} + f_{-2,5,-3,1}) - 2004(f_{4,1,-5,1} + f_{0,-3,-1,5}) \\
 & - 1938(f_{4,-1,3,-5} + f_{2,-3,5,-3}) - 1542(f_{-2,1,-3,5} + f_{0,3,-5,3}) \\
 & - 892(f_{2,-5,1,3} + f_{6,-1,-3,-1}) + 780f_{-4,5,-5,5} - 738(f_{6,-3,1,-3} + f_{4,-5,3,-1}) \\
 & + 483f_{0,1,-5,5} - 279f_{2,-1,5,-5} + 260f_{6,-5,5,-5} + 249f_{6,-5,1,-1} \\
 & \left. + 219(f_{0,5,-5,1} + f_{-4,1,-1,5}) - 45f_{-4,5,-1,1} - 15(f_{6,-1,1,-5} + f_{2,-5,5,-1}) \right) \tag{C.36}
 \end{aligned}$$

The associated weight mask is shown in figure C.36.
B-coefficient c_{4001} is computed using (1, 3)-symmetry.

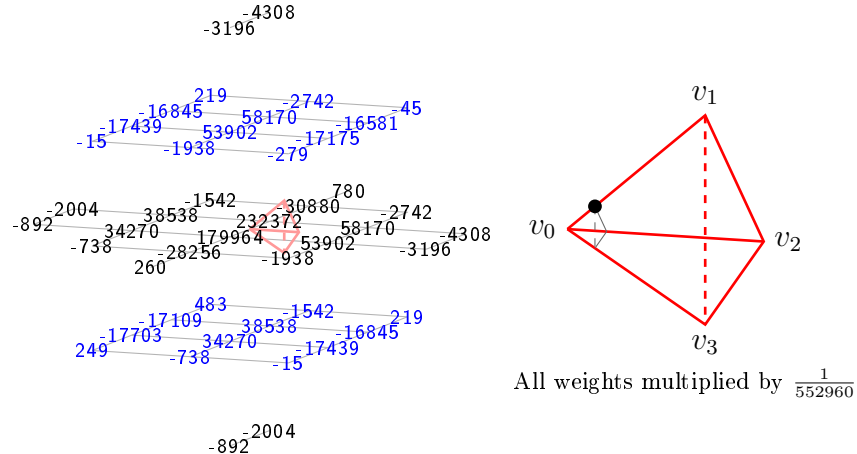


Figure C.36: Weight mask for c_{4100} . The associated domain point is shown in the teterahedron on the right. The black triangle symbolizes the ring $R_1(v_0)$.

$$\begin{aligned}
 c_{4010} := & \frac{1}{276480} \left(103084(f_{0,1,-1,1} + f_{2,-1,1,-1}) + 32926(f_{0,-1,3,-1} + f_{-2,1,1,1}) \right. \\
 & + 23110(f_{0,-1,-1,3} + f_{0,3,-1,-1} + f_{2,-3,1,1} + f_{2,1,1,-3}) \\
 & - 14784(f_{4,-3,3,-3} + f_{-2,3,-3,3}) + 13294(f_{4,-1,-1,-1} + f_{2,1,-3,1}) \\
 & - 8703(f_{2,3,-3,-1} + f_{4,-3,-1,1} + f_{4,1,-1,-3} + f_{2,-1,-3,3}) \\
 & - 8439(f_{-2,-1,1,3} + f_{-2,3,1,-1} + f_{0,1,3,-3} + f_{0,-3,3,1}) \\
 & - 2452(f_{-2,-1,5,-1} + f_{-4,1,3,1}) - 1470(f_{-4,3,-1,3} + f_{2,-3,5,-3}) \\
 & - 1300(f_{2,-5,1,3} + f_{0,-3,-1,5} + f_{0,5,-1,-3} + f_{2,3,1,-5}) \\
 & - 870(f_{-2,5,-3,1} + f_{4,-5,3,-1} + f_{4,-1,3,-5} + f_{-2,1,-3,5}) - 270(f_{0,3,-5,3} + f_{6,-3,1,-3}) \\
 & + 260(f_{6,-5,5,-5} + f_{-4,5,-5,5}) + 183(f_{0,1,-5,5} + f_{6,-1,1,-5} + f_{0,5,-5,1} + f_{6,-5,1,-1}) \\
 & \left. - 148(f_{4,1,-5,1} + f_{6,-1,-3,-1}) - 81(f_{-4,5,-1,1} + f_{-4,1,-1,5} + f_{2,-5,5,-1} + f_{2,-1,5,-5}) \right) \tag{C.37}
 \end{aligned}$$

The associated weight mask is shown in figure C.37.

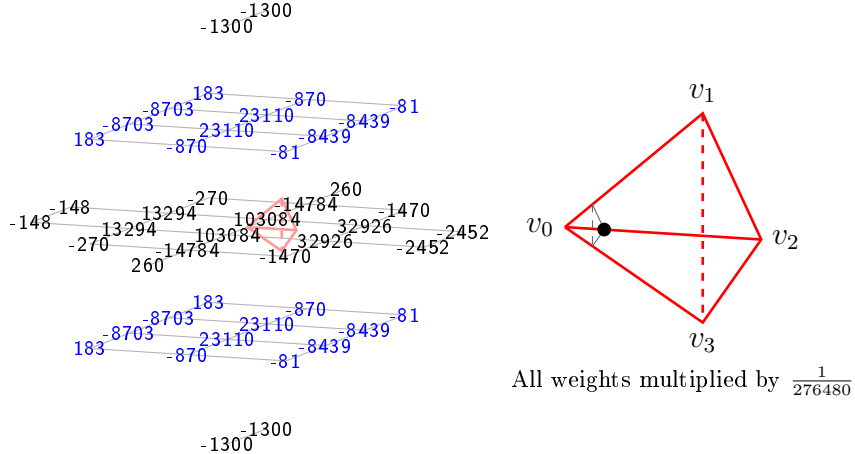


Figure C.37: Weight mask for c_{4010} . The associated domain point is shown in the teterahedron on the right. The black triangle symbolizes the ring $R_1(v_0)$.

$$\begin{aligned}
 c_{3200} := & \frac{1}{138240} \left(65103f_{0,1,-1,1} + 38899f_{2,-1,1,-1} + 17350(f_{0,3,-1,-1} + f_{-2,1,1,1}) \right. \\
 & + 13659(f_{0,-1,3,-1} + f_{2,1,1,-3}) - 7535f_{-2,3,-3,3} - 6223f_{4,-3,3,-3} \\
 & + 5977(f_{0,-1,-1,3} + f_{2,1,-3,1}) + 5400(f_{2,-3,1,1} + f_{4,-1,-1,-1}) \\
 & - 3624(f_{4,1,-1,-3} + f_{0,-3,3,1}) - 3483f_{0,1,3,-3} - 3450f_{2,-1,-3,3} \\
 & - 3327(f_{-2,-1,1,3} + f_{2,3,-3,-1}) - 3234f_{4,-3,-1,1} - 2673f_{-2,3,1,-1} \\
 & - 1810(f_{-4,1,3,1} + f_{0,5,-1,-3}) - 1035(f_{-4,3,-1,3} + f_{-2,5,-3,1}) \\
 & - 948(f_{2,3,1,-5} + f_{-2,-1,5,-1}) - 534(f_{2,-3,5,-3} + f_{4,-1,3,-5}) \\
 & - 352(f_{4,1,-5,1} + f_{0,-3,-1,5}) - 336(f_{-2,1,-3,5} + f_{0,3,-5,3}) + 260f_{-4,5,-5,5} \\
 & + 216f_{0,1,-5,5} - 165f_{2,-1,5,-5} - 147f_{-4,5,-1,1} - 102(f_{2,-5,1,3} + f_{6,-1,-3,-1}) \\
 & \left. + 84(f_{-4,1,-1,5} + f_{0,5,-5,1}) - 33(f_{2,-5,5,-1} + f_{4,-5,3,-1} + f_{6,-1,1,-5} + f_{6,-3,1,-3}) \right) \tag{C.38}
 \end{aligned}$$

The associated weight mask is shown in figure C.38.
B-coefficient c_{3002} is computed using (1, 3)-symmetry.

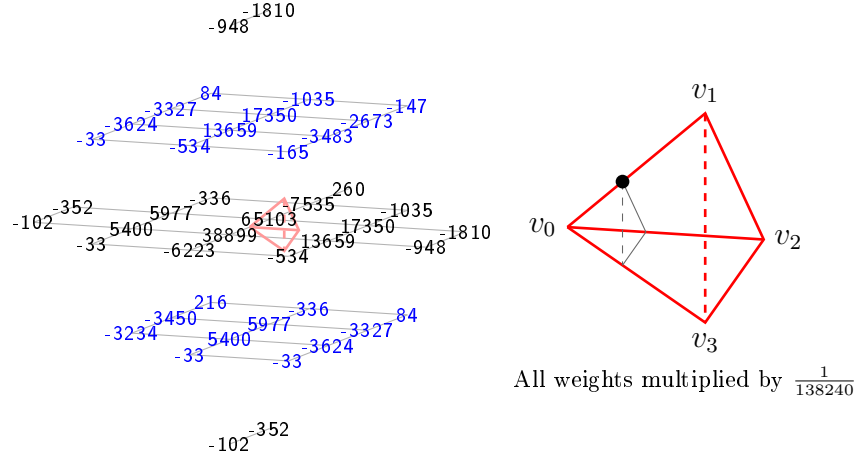


Figure C.38: Weight mask for c_{3200} . The associated domain point is shown in the teterahedron on the right. The black triangle symbolizes the ring $R_2(v_0)$.

$$\begin{aligned}
 c_{3110} := & \frac{1}{1105920} \left(457636 f_{0,1,-1,1} + 352820 f_{2,-1,1,-1} + 164102 f_{-2,1,1,1} \right. \\
 & + 143110 f_{0,-1,3,-1} + 110114 f_{0,3,-1,-1} + 101578 f_{2,1,1,-3} \\
 & + 70850 f_{0,-1,-1,3} + 62314 f_{2,-3,1,1} - 58280 f_{-2,3,-3,3} \\
 & - 53032 f_{4,-3,3,-3} + 37774 f_{4,-1,-1,-1} + 33854 f_{2,1,-3,1} \\
 & - 31569 f_{0,-3,3,1} - 31437 f_{2,3,-3,-1} - 30573 f_{4,1,-1,-3} \\
 & - 29841 f_{2,-1,-3,3} - 28977 f_{4,-3,-1,1} - 28917 f_{0,1,3,-3} \\
 & - 28329 f_{-2,-1,1,3} - 25677 f_{-2,3,1,-1} - 16196 f_{-4,1,3,1} \\
 & - 11524 f_{-2,-1,5,-1} - 9356 f_{0,5,-1,-3} - 9078 f_{-4,3,-1,3} - 7132 f_{2,3,1,-5} \\
 & - 6678 f_{2,-3,5,-3} - 5274 f_{-2,5,-3,1} - 4748 f_{0,-3,-1,5} - 3666 f_{4,-1,3,-5} \\
 & - 2874 f_{-2,1,-3,5} - 2524 f_{2,-5,1,3} - 1467 f_{2,-1,5,-5} - 1395 f_{-4,5,-1,1} \\
 & + 1300 f_{-4,5,-5,5} - 1266 f_{4,-5,3,-1} + 1113 f_{0,1,-5,5} - 1086 f_{0,3,-5,3} \\
 & + 981 f_{0,5,-5,1} - 543 f_{2,-5,5,-1} - 471 f_{-4,1,-1,5} - 270 f_{6,-3,1,-3} \\
 & + 260 f_{6,-5,5,-5} + 249 f_{6,-5,1,-1} - 148 f_{6,-1,-3,-1} + 117 f_{6,-1,1,-5} \\
 & \left. + 76 f_{4,1,-5,1} \right) \quad (C.39)
 \end{aligned}$$

The associated weight mask is shown in figure C.39.
B-coefficient c_{3011} is computed using (1, 3)-symmetry.

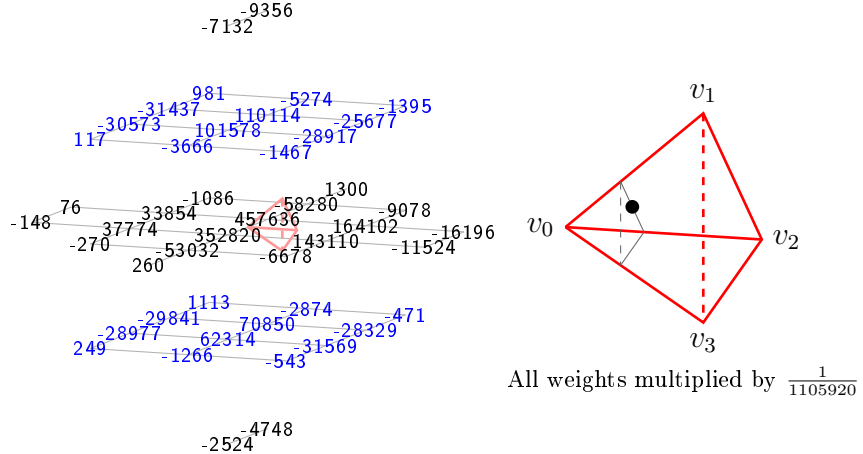


Figure C.39: Weight mask for c_{3110} . The associated domain point is shown in the teterahedron on the right. The black triangle symbolizes the ring $R_2(v_0)$.

$$\begin{aligned}
 c_{3101} := & \frac{1}{1105920} \left(527932f_{0,1,-1,1} + 318300f_{2,-1,1,-1} + 145026f_{-2,1,1,1} \right. \\
 & + 115498f_{0,-1,3,-1} + 91038(f_{0,-1,-1,3} + f_{0,3,-1,-1}) \\
 & + 73966(f_{2,-3,1,1} + f_{2,1,1,-3}) - 63760f_{-2,3,-3,3} + 54042f_{2,1,-3,1} \\
 & - 53264f_{4,-3,3,-3} + 49426f_{4,-1,-1,-1} - 33297(f_{0,1,3,-3} + f_{0,-3,3,1}) \\
 & - 32301(f_{4,1,-1,-3} + f_{4,-3,-1,1}) - 31977(f_{2,3,-3,-1} + f_{2,-1,-3,3}) \\
 & - 28869(f_{-2,3,1,-1} + f_{-2,-1,1,3}) - 13740f_{-4,1,3,1} - 8490f_{-4,3,-1,3} \\
 & - 6900(f_{0,-3,-1,5} + f_{0,5,-1,-3}) - 6844f_{-2,-1,5,-1} - 4686(f_{-2,5,-3,1} + f_{-2,1,-3,5}) \\
 & - 4482f_{2,-3,5,-3} - 2898f_{0,3,-5,3} - 2452(f_{2,3,1,-5} + f_{2,-5,1,3}) \\
 & + 2340f_{-4,5,-5,5} - 2076f_{4,1,-5,1} + 1581(f_{0,5,-5,1} + f_{0,1,-5,5}) \\
 & - 1470(f_{4,-1,3,-5} + f_{4,-5,3,-1}) - 474f_{6,-3,1,-3} - 411(f_{2,-5,5,-1} + f_{2,-1,5,-5}) \\
 & + 260f_{6,-5,5,-5} + 249(f_{6,-1,1,-5} + f_{6,-5,1,-1}) + 129(f_{-4,5,-1,1} + f_{-4,1,-1,5}) \\
 & \left. - 76f_{6,-1,-3,-1} \right) \tag{C.40}
 \end{aligned}$$

The associated weight mask is shown in figure C.40.

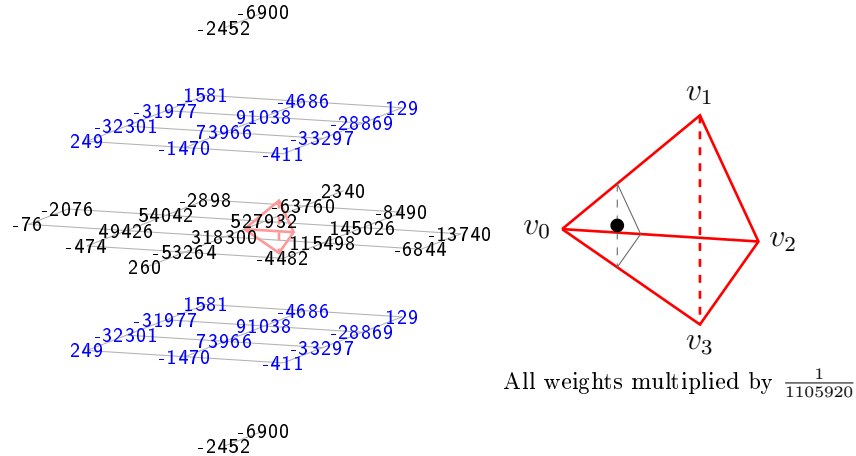


Figure C.40: Weight mask for c_{3101} . The associated domain point is shown in the teterahedron on the right. The black triangle symbolizes the ring $R_2(v_0)$.

$$\begin{aligned}
 c_{3020} := & \frac{1}{552960} \left(199060(f_{0,1,-1,1} + f_{2,-1,1,-1}) + 87754(f_{0,-1,3,-1} + f_{-2,1,1,1}) \right. \\
 & + 39994(f_{0,-1,-1,3} + f_{0,3,-1,-1} + f_{2,-3,1,1} + f_{2,1,1,-3}) \\
 & - 26088(f_{4,-3,3,-3} + f_{-2,3,-3,3}) \\
 & - 12801(f_{2,3,-3,-1} + f_{4,-3,-1,1} + f_{4,1,-1,-3} + f_{2,-1,-3,3}) \\
 & - 11745(f_{0,1,3,-3} + f_{-2,3,1,-1} + f_{-2,-1,1,3} + f_{0,-3,3,1}) \\
 & + 9226(f_{2,1,-3,1} + f_{4,-1,-1,-1}) - 8956(f_{-2,-1,5,-1} + f_{-4,1,3,1}) \\
 & - 4938(f_{-4,3,-1,3} + f_{2,-3,5,-3}) \\
 & - 3340(f_{0,-3,-1,5} + f_{2,-5,1,3} + f_{2,3,1,-5} + f_{0,5,-1,-3}) \\
 & - 1530(f_{-2,5,-3,1} + f_{4,-1,3,-5} + f_{-2,1,-3,5} + f_{4,-5,3,-1}) \\
 & - 807(f_{2,-5,5,-1} + f_{-4,1,-1,5} + f_{2,-1,5,-5} + f_{-4,5,-1,1}) \\
 & + 260(f_{6,-5,5,-5} + f_{6,-1,-3,-1} + f_{-4,5,-5,5} + f_{4,1,-5,1}) \\
 & \left. + 249(f_{0,5,-5,1} + f_{0,1,-5,5} + f_{6,-1,1,-5} + f_{6,-5,1,-1}) - 138(f_{6,-3,1,-3} + f_{0,3,-5,3}) \right) \\
 & \quad (C.41)
 \end{aligned}$$

The associated weight mask is shown in figure C.41.

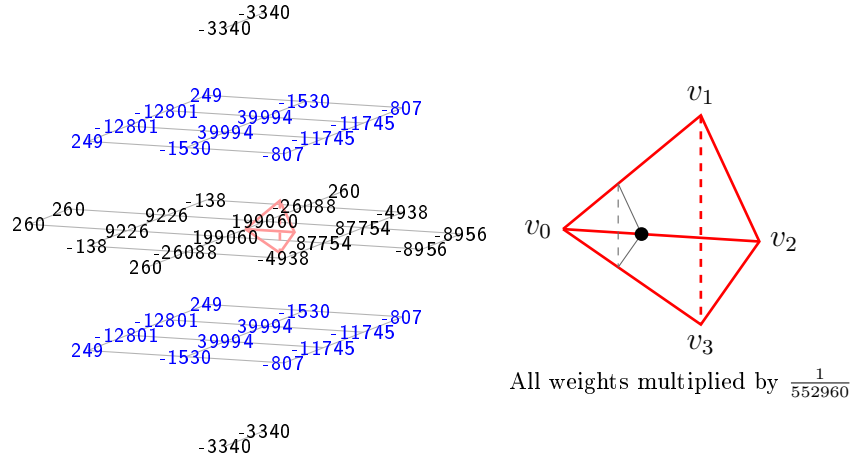


Figure C.41: Weight mask for c_{3020} . The associated domain point is shown in the teterahedron on the right. The black triangle symbolizes the ring $R_2(v_0)$.

$$\begin{aligned}
 c_{2300} := & \frac{1}{552960} \left(279048f_{0,1,-1,1} + 140996f_{2,-1,1,-1} + 80852(f_{0,3,-1,-1} + f_{-2,1,1,1}) \right. \\
 & + 50166(f_{0,-1,3,-1} + f_{2,1,1,-3}) - 25660f_{-2,3,-3,3} - 21908f_{4,-3,3,-3} \\
 & - 11811(f_{4,1,-1,-3} + f_{0,-3,3,1}) - 10851f_{0,1,3,-3} \\
 & - 10196(f_{0,5,-1,-3} + f_{-4,1,3,1}) - 9810f_{2,-1,-3,3} \\
 & + 9342(f_{4,-1,-1,-1} + f_{2,-3,1,1}) - 9090(f_{-2,-1,1,3} + f_{2,3,-3,-1}) \\
 & + 8564(f_{2,1,-3,1} + f_{0,-1,-1,3}) - 7875f_{4,-3,-1,1} - 4866(f_{-4,3,-1,3} + f_{-2,5,-3,1}) \\
 & - 3480(f_{-2,-1,5,-1} + f_{2,3,1,-5}) - 2643f_{-4,5,-1,1} - 2376(f_{4,-1,3,-5} + f_{2,-3,5,-3}) \\
 & - 1890(f_{-2,1,-3,5} + f_{0,3,-5,3}) + 1300f_{-4,5,-5,5} + 1245f_{0,1,-5,5} \\
 & - 696f_{2,-1,5,-5} + 630f_{-2,3,1,-1} - 332(f_{4,1,-5,1} + f_{0,-3,-1,5}) \\
 & \left. - 168(f_{-2,5,1,-3} + f_{-2,1,5,-3} + f_{-4,3,3,-1} + f_{0,3,3,-5}) + 45(f_{-4,1,-1,5} + f_{0,5,-5,1}) \right) \tag{C.42}
 \end{aligned}$$

The associated weight mask is shown in figure C.42.
B-coefficient c_{2003} is computed using (1, 3)-symmetry.

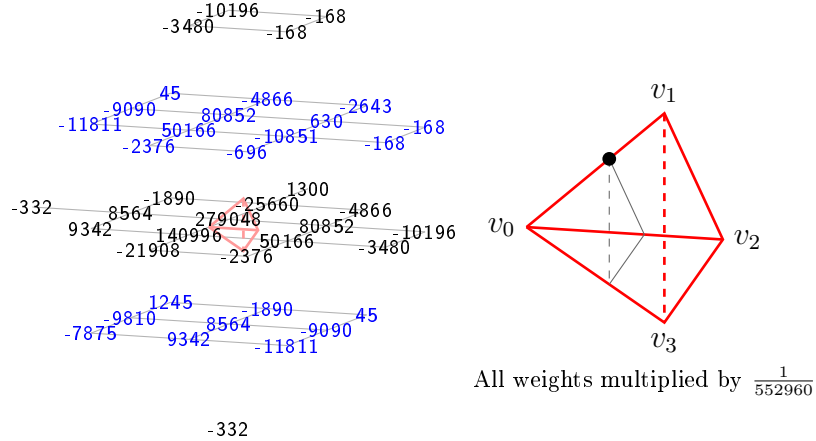


Figure C.42: Weight mask for c_{2300} . The associated domain point is shown in the teterahedron on the right. The black triangle symbolizes the ring $R_3(v_0)$.

$$\begin{aligned}
 c_{2210} := & \frac{1}{184320} \left(81660f_{0,1,-1,1} + 52496f_{2,-1,1,-1} + 32272f_{-2,1,1,1} \right. \\
 & + 23494f_{0,-1,3,-1} + 21908f_{0,3,-1,-1} + 15834f_{2,1,1,-3} \\
 & - 8568f_{-2,3,-3,3} - 7880f_{4,-3,3,-3} + 7272f_{0,-1,-1,3} + 5350f_{2,-3,1,1} \\
 & - 4623f_{0,-3,3,1} - 4202f_{2,3,-3,-1} - 4043f_{4,1,-1,-3} - 3908f_{-4,1,3,1} \\
 & - 3626f_{2,-1,-3,3} - 3567f_{0,1,3,-3} + 3274f_{4,-1,-1,-1} - 3239f_{4,-3,-1,1} \\
 & - 3230f_{-2,-1,1,3} - 2444f_{0,5,-1,-3} - 1904f_{-2,-1,5,-1} - 1642f_{-4,3,-1,3} \\
 & + 1564f_{2,1,-3,1} - 1502f_{-2,5,-3,1} - 1260f_{2,-3,5,-3} - 1208f_{2,3,1,-5} \\
 & - 1034f_{-2,3,1,-1} - 735f_{-4,5,-1,1} - 656f_{4,-1,3,-5} - 626f_{-2,1,-3,5} \\
 & - 556f_{0,-3,-1,5} - 320f_{2,-1,5,-5} + 260f_{-4,5,-5,5} + 249f_{0,1,-5,5} \\
 & - 239f_{-4,1,-1,5} + 205f_{0,5,-5,1} - 182f_{0,3,-5,3} - 136f_{2,-5,1,3} \\
 & + 124f_{4,1,-5,1} - 56(f_{-2,1,5,-3} + f_{0,3,3,-5} + f_{-4,3,3,-1} + f_{-2,5,1,-3}) \\
 & \left. - 44(f_{2,-5,5,-1} + f_{4,-5,3,-1}) \right) \tag{C.43}
 \end{aligned}$$

The associated weight mask is shown in figure C.43.
B-coefficient c_{2012} is computed using (1, 3)-symmetry.

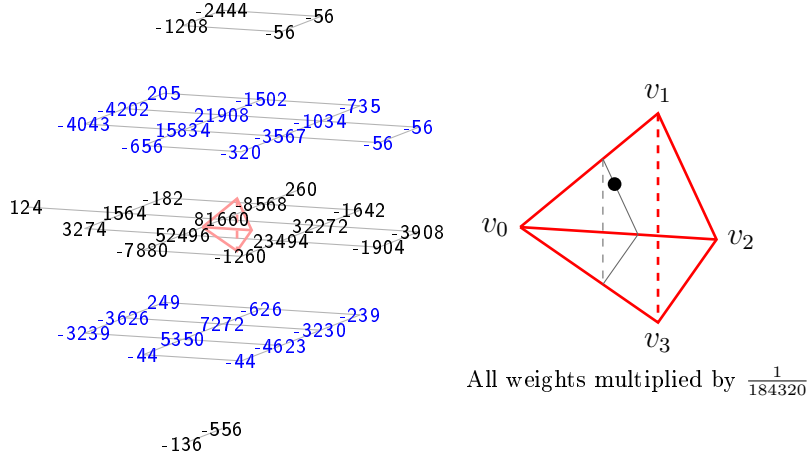


Figure C.43: Weight mask for c_{2210} . The associated domain point is shown in the teterahedron on the right. The black triangle symbolizes the ring $R_3(v_0)$.

$$\begin{aligned}
 c_{2201} := & \frac{1}{92160} \left(49080f_{0,1,-1,1} + 23184f_{2,-1,1,-1} + 14088f_{-2,1,1,1} \right. \\
 & + 9550f_{0,-1,3,-1} + 8906f_{0,3,-1,-1} + 5720f_{2,1,1,-3} - 5016f_{-2,3,-3,3} \\
 & + 4630f_{0,-1,-1,3} - 3860f_{4,-3,3,-3} + 3520f_{2,-3,1,1} + 2482f_{4,-1,-1,-1} \\
 & - 2363f_{0,-3,3,1} - 2347f_{0,1,3,-3} - 2122f_{2,-1,-3,3} - 2118f_{2,3,-3,-1} \\
 & - 2073f_{4,1,-1,-3} - 1849f_{4,-3,-1,1} + 1776f_{2,1,-3,1} - 1684f_{-4,1,3,1} \\
 & - 1632f_{-2,-1,1,3} - 1160f_{-2,3,1,-1} - 952f_{0,5,-1,-3} - 750f_{-4,3,-1,3} \\
 & - 680f_{-2,5,-3,1} - 608f_{-2,-1,5,-1} - 448f_{-2,1,-3,5} - 424f_{2,-3,5,-3} \\
 & - 352f_{0,-3,-1,5} + 260(f_{-4,5,-5,5} - f_{2,3,1,-5}) + 227f_{0,1,-5,5} - 226f_{0,3,-5,3} \\
 & + 183f_{0,5,-5,1} - 171f_{-4,5,-1,1} - 122f_{4,-1,3,-5} - 68f_{2,-5,1,3} \\
 & \left. - 66f_{2,-1,5,-5} - 39f_{-4,1,-1,5} - 22(f_{4,-5,3,-1} + f_{2,-5,5,-1}) - 12f_{4,1,-5,1} \right) \tag{C.44}
 \end{aligned}$$

The associated weight mask is shown in figure C.44.
B-coefficient c_{2102} is computed using (1, 3)-symmetry.

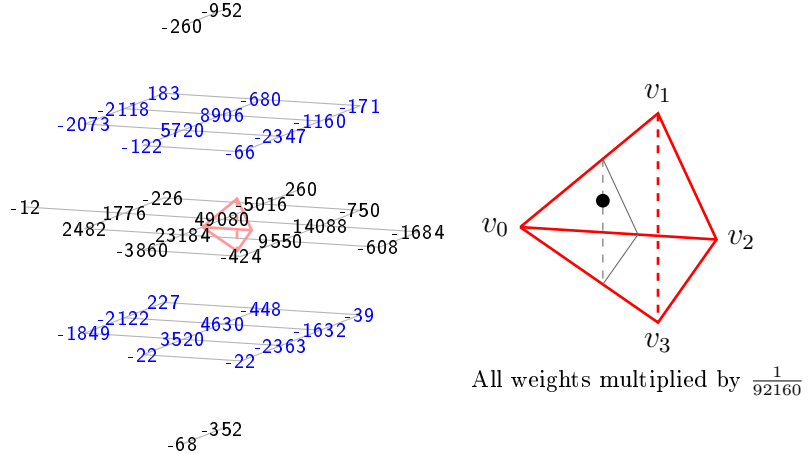


Figure C.44: Weight mask for c_{2201} . The associated domain point is shown in the teterahedron on the right. The black triangle symbolizes the ring $R_3(v_0)$.

$$\begin{aligned}
 c_{2120} := & \frac{1}{552960} \left(209832f_{0,1,-1,1} + 174748f_{2,-1,1,-1} + 107692f_{-2,1,1,1} \right. \\
 & + 91854f_{0,-1,3,-1} + 48268f_{0,3,-1,-1} + 40542f_{2,1,1,-3} \\
 & + 30220f_{0,-1,-1,3} - 23524f_{4,-3,3,-3} - 22964f_{-2,3,-3,3} \\
 & + 22494f_{2,-3,1,1} - 12772f_{-4,1,3,1} - 12159f_{0,-3,3,1} \\
 & - 11058f_{2,3,-3,-1} - 10671f_{4,1,-1,-3} - 9786f_{2,-1,-3,3} - 9399f_{4,-3,-1,1} \\
 & - 9096f_{-2,-1,5,-1} - 8607f_{0,1,3,-3} - 7890f_{-2,-1,1,3} - 5784f_{2,-3,5,-3} \\
 & - 5730f_{-4,3,-1,3} - 5140f_{0,5,-1,-3} + 4926f_{4,-1,-1,-1} - 4338f_{-2,3,1,-1} \\
 & - 3768f_{2,3,1,-5} - 3004f_{0,-3,-1,5} - 2898f_{-2,5,-3,1} - 2175f_{-4,5,-1,1} \\
 & - 1866f_{-2,1,-3,5} + 1756f_{2,1,-3,1} - 1632f_{2,-5,1,3} - 1560f_{4,-1,3,-5} \\
 & - 1479f_{-4,1,-1,5} - 1224f_{2,-1,5,-5} - 528(f_{2,-5,5,-1} + f_{4,-5,3,-1}) \\
 & + 260(f_{4,1,-5,1} + f_{-4,5,-5,5}) + 249(f_{0,5,-5,1} + f_{0,1,-5,5}) \\
 & \left. - 168(f_{-2,5,1,-3} + f_{0,3,3,-5} + f_{-2,1,5,-3} + f_{-4,3,3,-1}) - 138f_{0,3,-5,3} \right) \quad (C.45)
 \end{aligned}$$

The associated weight mask is shown in figure C.45.
B-coefficient c_{2021} is computed using (1, 3)-symmetry.

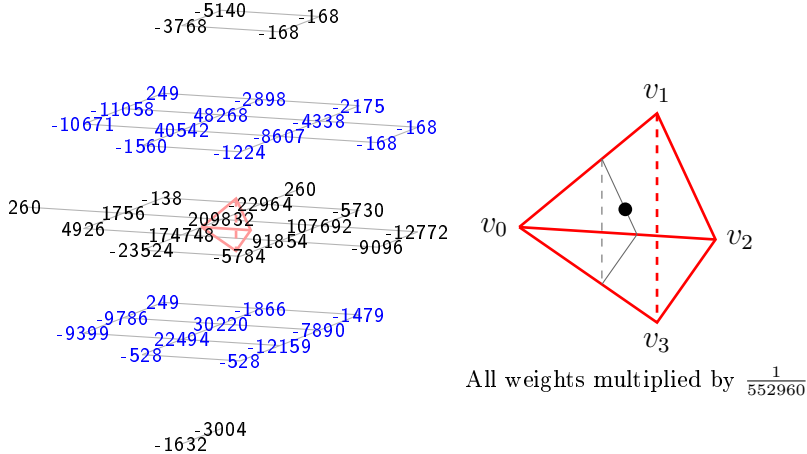


Figure C.45: Weight mask for c_{2120} . The associated domain point is shown in the teterahedron on the right. The black triangle symbolizes the ring $R_3(v_0)$.

$$\begin{aligned}
 c_{2111} := & \frac{1}{184320} \left(82068f_{0,1,-1,1} + 52904f_{2,-1,1,-1} + 33608f_{-2,1,1,1} \right. \\
 & + 24830f_{0,-1,3,-1} + 14246(f_{0,-1,-1,3} + f_{0,3,-1,-1}) \\
 & + 10248(f_{2,-3,1,1} + f_{2,1,1,-3}) - 8848f_{-2,3,-3,3} - 8160f_{4,-3,3,-3} \\
 & - 4791(f_{0,1,3,-3} + f_{0,-3,3,1}) - 4318(f_{2,-1,-3,3} + f_{2,3,-3,-1}) + 4082f_{4,-1,-1,-1} \\
 & - 4045(f_{4,1,-1,-3} + f_{4,-3,-1,1}) - 3964f_{-4,1,3,1} - 2828(f_{-2,3,1,-1} + f_{-2,-1,1,3}) \\
 & + 2372f_{2,1,-3,1} - 1960f_{-2,-1,5,-1} - 1698f_{-4,3,-1,3} \\
 & - 1360(f_{0,5,-1,-3} + f_{0,-3,-1,5}) - 1316f_{2,-3,5,-3} - 924(f_{-2,1,-3,5} + f_{-2,5,-3,1}) \\
 & - 532(f_{2,3,1,-5} + f_{2,-5,1,3}) - 459(f_{-4,5,-1,1} + f_{-4,1,-1,5}) + 260f_{-4,5,-5,5} \\
 & + 227(f_{0,5,-5,1} + f_{0,1,-5,5}) - 210(f_{4,-1,3,-5} + f_{4,-5,3,-1}) - 182f_{0,3,-5,3} \\
 & \left. - 154(f_{2,-5,5,-1} + f_{2,-1,5,-5}) + 124f_{4,1,-5,1} \right) \tag{C.46}
 \end{aligned}$$

The associated weight mask is shown in figure C.46.

$$\begin{aligned}
 c_{2030} := & \frac{1}{23040} \left(7730(f_{0,1,-1,1} + f_{2,-1,1,-1}) + 4658(f_{0,-1,3,-1} + f_{-2,1,1,1}) \right. \\
 & + 1282(f_{0,-1,-1,3} + f_{0,3,-1,-1} + f_{2,-3,1,1} + f_{2,1,1,-3}) \\
 & - 850(f_{-2,3,-3,3} + f_{4,-3,3,-3}) - 538(f_{-4,1,3,1} + f_{-2,-1,5,-1}) \\
 & - 319(f_{4,1,-1,-3} + f_{2,-1,-3,3} + f_{4,-3,-1,1} + f_{2,3,-3,-1}) - 274(f_{-4,3,-1,3} + f_{2,-3,5,-3}) \\
 & - 198(f_{-2,-1,1,3} + f_{0,-3,3,1} + f_{-2,3,1,-1} + f_{0,1,3,-3}) \\
 & - 143(f_{2,-5,1,3} + f_{0,5,-1,-3} + f_{0,-3,-1,5} + f_{2,3,1,-5}) - 106(f_{4,-1,-1,-1} + f_{2,1,-3,1}) \\
 & - 79(f_{4,-1,3,-5} + f_{-4,1,-1,5} + f_{-4,5,-1,1} + f_{4,-5,3,-1} + f_{2,-5,5,-1} + f_{-2,5,-3,1} \\
 & \quad + f_{2,-1,5,-5} + f_{-2,1,-3,5}) \\
 & - 7(f_{-2,5,1,-3} + f_{-2,-3,5,1} + f_{-4,-1,3,3} + f_{-2,-3,1,5} + f_{-2,1,5,-3} + f_{-4,3,3,-1} \\
 & \quad + f_{0,-5,3,3} + f_{0,3,3,-5}) \left. \right) \tag{C.47}
 \end{aligned}$$

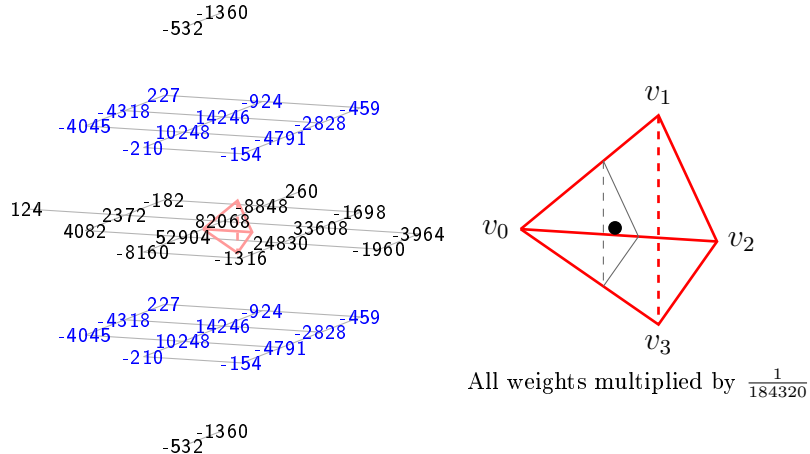


Figure C.46: Weight mask for c_{2111} . The associated domain point is shown in the teterahedron on the right. The black triangle symbolizes the ring $R_3(v_0)$.

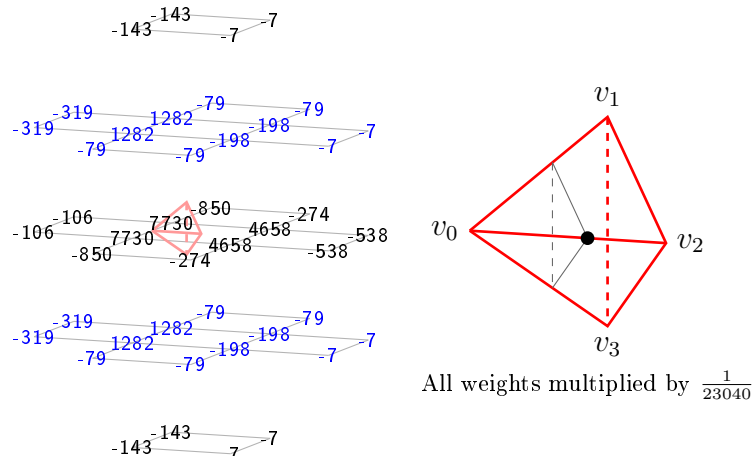


Figure C.47: Weight mask for c_{2030} . The associated domain point is shown in the teterahedron on the right. The black triangle symbolizes the ring $R_3(v_0)$.

The associated weight mask is shown in figure C.47.

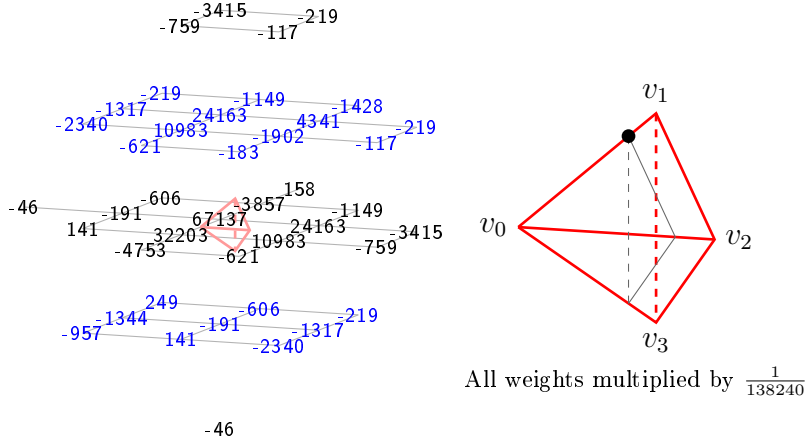


Figure C.48: Weight mask for c_{1400} . The associated domain point is shown in the teterahedron on the right. The black triangle symbolizes the ring $R_4(v_0)$.

$$\begin{aligned}
 c_{1400} := & \frac{1}{138240} \left(67137f_{0,1,-1,1} + 32203f_{2,-1,1,-1} + 24163(f_{0,3,-1,-1} + f_{-2,1,1,1}) \right. \\
 & + 10983(f_{0,-1,3,-1} + f_{2,1,1,-3}) - 4753f_{4,-3,3,-3} + 4341f_{-2,3,1,-1} \\
 & - 3857f_{-2,3,-3,3} - 3415(f_{0,5,-1,-3} + f_{-4,1,3,1}) - 2340(f_{0,-3,3,1} + f_{4,1,-1,-3}) \\
 & - 1902f_{0,1,3,-3} - 1428f_{-4,5,-1,1} - 1344f_{2,-1,-3,3} \\
 & - 1317(f_{2,3,-3,-1} + f_{-2,-1,1,3}) - 1149(f_{-2,5,-3,1} + f_{-4,3,-1,3}) - 957f_{4,-3,-1,1} \\
 & - 759(f_{2,3,1,-5} + f_{-2,-1,5,-1}) - 621(f_{2,-3,5,-3} + f_{4,-1,3,-5}) \\
 & - 606(f_{-2,1,-3,5} + f_{0,3,-5,3}) + 249f_{0,1,-5,5} \\
 & - 219(f_{-4,3,3,-1} + f_{-2,5,1,-3} + f_{0,5,-5,1} + f_{-4,1,-1,5}) - 191(f_{2,1,-3,1} + f_{0,-1,-1,3}) \\
 & - 183f_{2,-1,5,-5} + 158f_{-4,5,-5,5} + 141(f_{4,-1,-1,-1} + f_{2,-3,1,1}) \\
 & \left. - 117(f_{-2,1,5,-3} + f_{0,3,3,-5}) - 46(f_{4,1,-5,1} + f_{0,-3,-1,5}) \right) \quad (C.48)
 \end{aligned}$$

The associated weight mask is shown in figure C.48.
B-coefficient c_{1004} is computed using (1, 3)-symmetry.

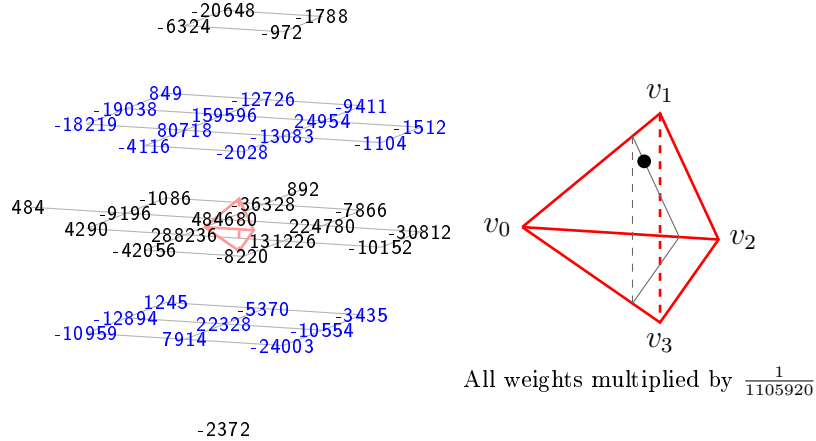


Figure C.49: Weight mask for c_{1310} . The associated domain point is shown in the teterahedron on the right. The black triangle symbolizes the ring $R_4(v_0)$.

$$\begin{aligned}
 c_{1310} := & \frac{1}{1105920} \left(484680f_{0,1,-1,1} + 288236f_{2,-1,1,-1} + 224780f_{-2,1,1,1} \right. \\
 & + 159596f_{0,3,-1,-1} + 131226f_{0,-1,3,-1} + 80718f_{2,1,1,-3} \\
 & - 42056f_{4,-3,3,-3} - 36328f_{-2,3,-3,3} - 30812f_{-4,1,3,1} \\
 & + 24954f_{-2,3,1,-1} - 24003f_{0,-3,3,1} + 22328f_{0,-1,-1,3} \\
 & - 20648f_{0,5,-1,-3} - 19038f_{2,3,-3,-1} - 18219f_{4,1,-1,-3} \\
 & - 13083f_{0,1,3,-3} - 12894f_{2,-1,-3,3} - 12726f_{-2,5,-3,1} \\
 & - 10959f_{4,-3,-1,1} - 10554f_{-2,-1,1,3} - 10152f_{-2,-1,5,-1} \\
 & - 9411f_{-4,5,-1,1} - 9196f_{2,1,-3,1} - 8220f_{2,-3,5,-3} + 7914f_{2,-3,1,1} \\
 & - 7866f_{-4,3,-1,3} - 6324f_{2,3,1,-5} - 5370f_{-2,1,-3,5} + 4290f_{4,-1,-1,-1} \\
 & - 4116f_{4,-1,3,-5} - 3435f_{-4,1,-1,5} - 2372f_{0,-3,-1,5} - 2028f_{2,-1,5,-5} \\
 & - 1788f_{-2,5,1,-3} - 1512f_{-4,3,3,-1} + 1245f_{0,1,-5,5} - 1104f_{-2,1,5,-3} \\
 & - 1086f_{0,3,-5,3} - 972f_{0,3,3,-5} + 892f_{-4,5,-5,5} + 849f_{0,5,-5,1} \\
 & \left. + 484f_{4,1,-5,1} \right) \quad (C.49)
 \end{aligned}$$

The associated weight mask is shown in figure C.49.
B-coefficient c_{1013} is computed using (1, 3)-symmetry.

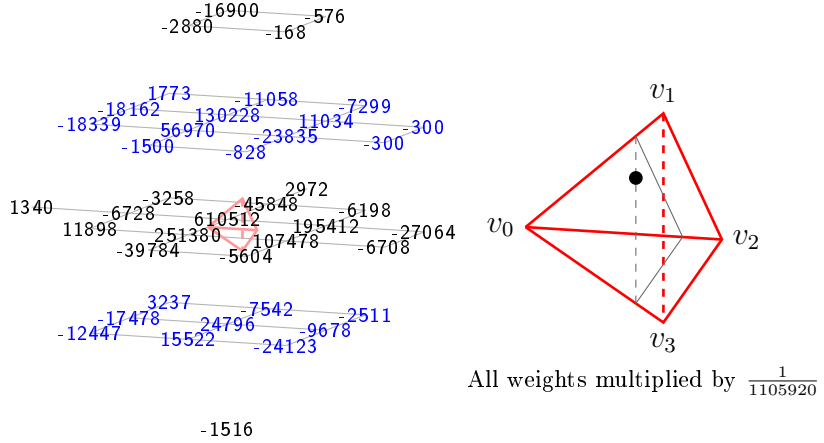


Figure C.50: Weight mask for c_{1301} . The associated domain point is shown in the teterahedron on the right. The black triangle symbolizes the ring $R_4(v_0)$.

$$\begin{aligned}
 c_{1301} := & \frac{1}{1105920} \left(610512f_{0,1,-1,1} + 251380f_{2,-1,1,-1} + 195412f_{-2,1,1,1} \right. \\
 & + 130228f_{0,3,-1,-1} + 107478f_{0,-1,3,-1} + 56970f_{2,1,1,-3} \\
 & - 45848f_{-2,3,-3,3} - 39784f_{4,-3,3,-3} - 27064f_{-4,1,3,1} \\
 & + 24796f_{0,-1,-1,3} - 24123f_{0,-3,3,1} - 23835f_{0,1,3,-3} \\
 & - 18339f_{4,1,-1,-3} - 18162f_{2,3,-3,-1} - 17478f_{2,-1,-3,3} \\
 & - 16900f_{0,5,-1,-3} + 15522f_{2,-3,1,1} - 12447f_{4,-3,-1,1} \\
 & + 11898f_{4,-1,-1,-1} - 11058f_{-2,5,-3,1} + 11034f_{-2,3,1,-1} \\
 & - 9678f_{-2,-1,1,3} - 7542f_{-2,1,-3,5} - 7299f_{-4,5,-1,1} - 6728f_{2,1,-3,1} \\
 & - 6708f_{-2,-1,5,-1} - 6198f_{-4,3,-1,3} - 5604f_{2,-3,5,-3} - 3258f_{0,3,-5,3} \\
 & + 3237f_{0,1,-5,5} + 2972f_{-4,5,-5,5} - 2880f_{2,3,1,-5} - 2511f_{-4,1,-1,5} \\
 & + 1773f_{0,5,-5,1} - 1516f_{0,-3,-1,5} - 1500f_{4,-1,3,-5} + 1340f_{4,1,-5,1} \\
 & \left. - 828f_{2,-1,5,-5} - 576f_{-2,5,1,-3} - 300(f_{-2,1,5,-3} + f_{-4,3,3,-1}) - 168f_{0,3,3,-5} \right) \\
 & \quad (C.50)
 \end{aligned}$$

The associated weight mask is shown in figure C.50.
B-coefficient c_{1103} is computed using (1, 3)-symmetry.

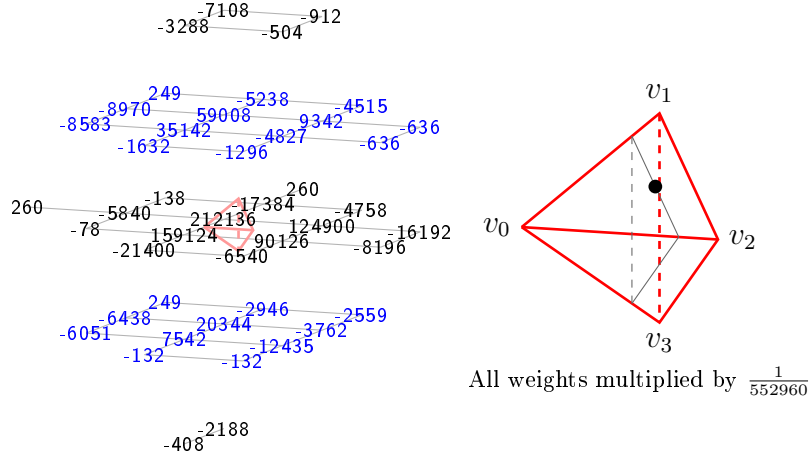


Figure C.51: Weight mask for c_{1220} . The associated domain point is shown in the teterahedron on the right. The black triangle symbolizes the ring $R_4(v_0)$.

$$\begin{aligned}
 c_{1220} := & \frac{1}{552960} \left(212136f_{0,1,-1,1} + 159124f_{2,-1,1,-1} + 124900f_{-2,1,1,1} \right. \\
 & + 90126f_{0,-1,3,-1} + 59008f_{0,3,-1,-1} + 35142f_{2,1,1,-3} \\
 & - 21400f_{4,-3,3,-3} + 20344f_{0,-1,-1,3} - 17384f_{-2,3,-3,3} \\
 & - 16192f_{-4,1,3,1} - 12435f_{0,-3,3,1} + 9342f_{-2,3,1,-1} - 8970f_{2,3,-3,-1} \\
 & - 8583f_{4,1,-1,-3} - 8196f_{-2,-1,5,-1} + 7542f_{2,-3,1,1} - 7108f_{0,5,-1,-3} \\
 & - 6540f_{2,-3,5,-3} - 6438f_{2,-1,-3,3} - 6051f_{4,-3,-1,1} - 5840f_{2,1,-3,1} \\
 & - 5238f_{-2,5,-3,1} - 4827f_{0,1,3,-3} - 4758f_{-4,3,-1,3} - 4515f_{-4,5,-1,1} \\
 & - 3762f_{-2,-1,1,3} - 3288f_{2,3,1,-5} - 2946f_{-2,1,-3,5} - 2559f_{-4,1,-1,5} \\
 & - 2188f_{0,-3,-1,5} - 1632f_{4,-1,3,-5} - 1296f_{2,-1,5,-5} - 912f_{-2,5,1,-3} \\
 & - 636(f_{-4,3,3,-1} + f_{-2,1,5,-3}) - 504f_{0,3,3,-5} - 408f_{2,-5,1,3} \\
 & + 260(f_{-4,5,-5,5} + f_{4,1,-5,1}) + 249(f_{0,1,-5,5} + f_{0,5,-5,1}) - 138f_{0,3,-5,3} \\
 & \left. - 132(f_{2,-5,5,-1} + f_{4,-5,3,-1}) - 78f_{4,-1,-1,-1} \right) \tag{C.51}
 \end{aligned}$$

The associated weight mask is shown in figure C.51.
B-coefficient c_{1022} is computed using (1, 3)-symmetry.

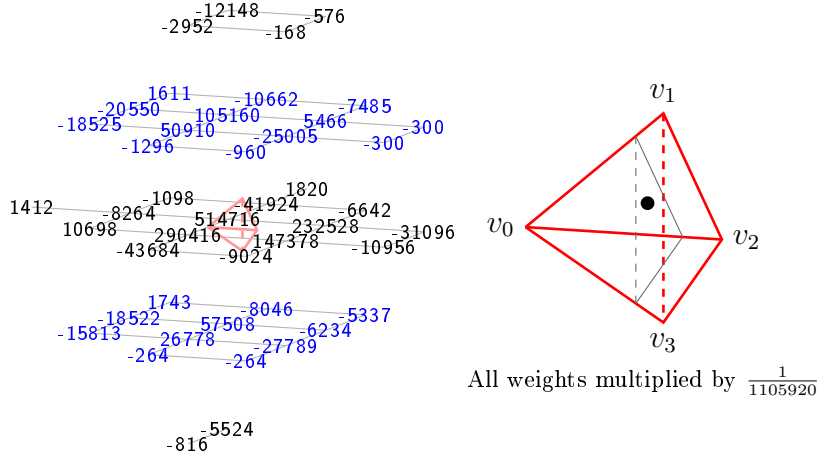


Figure C.52: Weight mask for c_{1211} . The associated domain point is shown in the teterahedron on the right. The black triangle symbolizes the ring $R_4(v_0)$.

$$\begin{aligned}
 c_{1211} := & \frac{1}{1105920} \left(514716f_{0,1,-1,1} + 290416f_{2,-1,1,-1} + 232528f_{-2,1,1,1} \right. \\
 & + 147378f_{0,-1,3,-1} + 105160f_{0,3,-1,-1} + 57508f_{0,-1,-1,3} \\
 & + 50910f_{2,1,1,-3} - 43684f_{4,-3,3,-3} - 41924f_{-2,3,-3,3} \\
 & - 31096f_{-4,1,3,1} - 27789f_{0,-3,3,1} + 26778f_{2,-3,1,1} \\
 & - 25005f_{0,1,3,-3} - 20550f_{2,3,-3,-1} - 18525f_{4,1,-1,-3} \\
 & - 18522f_{2,-1,-3,3} - 15813f_{4,-3,-1,1} - 12148f_{0,5,-1,-3} \\
 & - 10956f_{-2,-1,5,-1} + 10698f_{4,-1,-1,-1} - 10662f_{-2,5,-3,1} \\
 & - 9024f_{2,-3,5,-3} - 8264f_{2,1,-3,1} - 8046f_{-2,1,-3,5} - 7485f_{-4,5,-1,1} \\
 & - 6642f_{-4,3,-1,3} - 6234f_{-2,-1,1,3} - 5524f_{0,-3,-1,5} + 5466f_{-2,3,1,-1} \\
 & - 5337f_{-4,1,-1,5} - 2952f_{2,3,1,-5} + 1820f_{-4,5,-5,5} + 1743f_{0,1,-5,5} \\
 & + 1611f_{0,5,-5,1} + 1412f_{4,1,-5,1} - 1296f_{4,-1,3,-5} - 1098f_{0,3,-5,3} \\
 & - 960f_{2,-1,5,-5} - 816f_{2,-5,1,3} - 576f_{-2,5,1,-3} - 300(f_{-2,1,5,-3} + f_{-4,3,3,-1}) \\
 & \left. - 264(f_{2,-5,5,-1} + f_{4,-5,3,-1}) - 168f_{0,3,3,-5} \right) \tag{C.52}
 \end{aligned}$$

The associated weight mask is shown in figure C.52.
B-coefficient c_{1112} is computed using (1, 3)-symmetry.

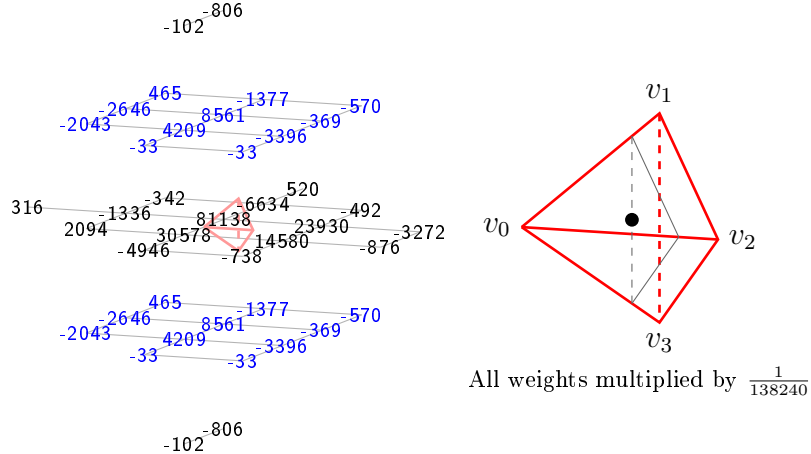


Figure C.53: Weight mask for c_{1202} . The associated domain point is shown in the teterahedron on the right. The black triangle symbolizes the ring $R_4(v_0)$.

$$\begin{aligned}
 c_{1202} := & \frac{1}{138240} \left(81138f_{0,1,-1,1} + 30578f_{2,-1,1,-1} + 23930f_{-2,1,1,1} \right. \\
 & + 14580f_{0,-1,3,-1} + 8561(f_{0,-1,-1,3} + f_{0,3,-1,-1}) - 6634f_{-2,3,-3,3} \\
 & - 4946f_{4,-3,3,-3} + 4209(f_{2,-3,1,1} + f_{2,1,1,-3}) - 3396(f_{0,1,3,-3} + f_{0,-3,3,1}) \\
 & - 3272f_{-4,1,3,1} - 2646(f_{2,3,-3,-1} + f_{2,-1,-3,3}) + 2094f_{4,-1,-1,-1} \\
 & - 2043(f_{4,1,-1,-3} + f_{4,-3,-1,1}) - 1377(f_{-2,5,-3,1} + f_{-2,1,-3,5}) - 1336f_{2,1,-3,1} \\
 & - 876f_{-2,-1,5,-1} - 806(f_{0,5,-1,-3} + f_{0,-3,-1,5}) - 738f_{2,-3,5,-3} \\
 & - 570(f_{-4,1,-1,5} + f_{-4,5,-1,1}) + 520f_{-4,5,-5,5} - 492f_{-4,3,-1,3} \\
 & + 465(f_{0,5,-5,1} + f_{0,1,-5,5}) - 369(f_{-2,3,1,-1} + f_{-2,-1,1,3}) - 342f_{0,3,-5,3} \\
 & + 316f_{4,1,-5,1} - 102(f_{2,-5,1,3} + f_{2,3,1,-5}) \\
 & \left. - 33(f_{2,-5,5,-1} + f_{2,-1,5,-5} + f_{4,-1,3,-5} + f_{4,-5,3,-1}) \right) \quad (C.53)
 \end{aligned}$$

The associated weight mask is shown in figure C.53.

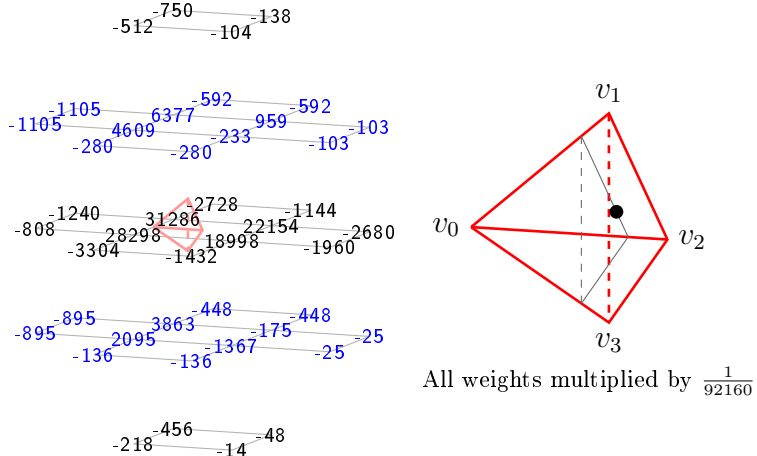


Figure C.54: Weight mask for c_{1130} . The associated domain point is shown in the teterahedron on the right. The black triangle symbolizes the ring $R_4(v_0)$.

$$\begin{aligned}
 c_{1130} := & \frac{1}{92160} \left(31286f_{0,1,-1,1} + 28298f_{2,-1,1,-1} + 22154f_{-2,1,1,1} \right. \\
 & + 18998f_{0,-1,3,-1} + 6377f_{0,3,-1,-1} + 4609f_{2,1,1,-3} + 3863f_{0,-1,-1,3} \\
 & - 3304f_{4,-3,3,-3} - 2728f_{-2,3,-3,3} - 2680f_{-4,1,3,1} + 2095f_{2,-3,1,1} \\
 & - 1960f_{-2,-1,5,-1} - 1432f_{2,-3,5,-3} - 1367f_{0,-3,3,1} - 1240f_{2,1,-3,1} \\
 & - 1144f_{-4,3,-1,3} - 1105(f_{4,1,-1,-3} + f_{2,3,-3,-1}) + 959f_{-2,3,1,-1} \\
 & - 895(f_{2,-1,-3,3} + f_{4,-3,-1,1}) - 808f_{4,-1,-1,-1} - 750f_{0,5,-1,-3} \\
 & - 592(f_{-2,5,-3,1} + f_{-4,5,-1,1}) - 512f_{2,3,1,-5} - 456f_{0,-3,-1,5} \\
 & - 448(f_{-2,1,-3,5} + f_{-4,1,-1,5}) - 280(f_{2,-1,5,-5} + f_{4,-1,3,-5}) - 233f_{0,1,3,-3} \\
 & - 218f_{2,-5,1,3} - 175f_{-2,-1,1,3} - 138f_{-2,5,1,-3} - 136(f_{4,-5,3,-1} + f_{2,-5,5,-1}) \\
 & - 104f_{0,3,3,-5} - 103(f_{-4,3,3,-1} + f_{-2,1,5,-3}) - 48f_{-2,-3,1,5} \\
 & \left. - 25(f_{-4,-1,3,3} + f_{-2,-3,5,1}) - 14f_{0,-5,3,3} \right) \quad (C.54)
 \end{aligned}$$

The associated weight mask is shown in figure C.54.
B-coefficient c_{1031} is computed using (1, 3)-symmetry.

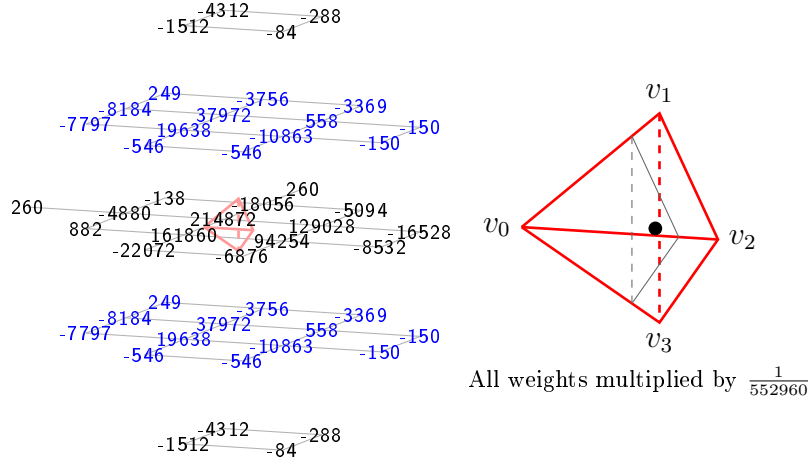


Figure C.55: Weight mask for c_{1121} . The associated domain point is shown in the teterahedron on the right. The black triangle symbolizes the ring $R_4(v_0)$.

$$\begin{aligned}
 c_{1121} := & \frac{1}{552960} \left(214872f_{0,1,-1,1} + 161860f_{2,-1,1,-1} + 129028f_{-2,1,1,1} \right. \\
 & + 94254f_{0,-1,3,-1} + 37972(f_{0,-1,-1,3} + f_{0,3,-1,-1}) - 22072f_{4,-3,3,-3} \\
 & + 19638(f_{2,-3,1,1} + f_{2,1,1,-3}) - 18056f_{-2,3,-3,3} - 16528f_{-4,1,3,1} \\
 & - 10863(f_{0,-3,3,1} + f_{0,1,3,-3}) - 8532f_{-2,-1,5,-1} \\
 & - 8184(f_{2,-1,-3,3} + f_{2,3,-3,-1}) - 7797(f_{4,-3,-1,1} + f_{4,1,-1,-3}) - 6876f_{2,-3,5,-3} \\
 & - 5094f_{-4,3,-1,3} - 4880f_{2,1,-3,1} - 4312(f_{0,5,-1,-3} + f_{0,-3,-1,5}) \\
 & - 3756(f_{-2,1,-3,5} + f_{-2,5,-3,1}) - 3369(f_{-4,5,-1,1} + f_{-4,1,-1,5}) \\
 & - 1512(f_{2,-5,1,3} + f_{2,3,1,-5}) + 882f_{4,-1,-1,-1} + 558(f_{-2,3,1,-1} + f_{-2,-1,1,3}) \\
 & - 546(f_{2,-5,5,-1} + f_{2,-1,5,-5} + f_{4,-5,3,-1} + f_{4,-1,3,-5}) - 288(f_{-2,-3,1,5} + f_{-2,5,1,-3}) \\
 & + 260(f_{4,1,-5,1} + f_{-4,5,-5,5}) + 249(f_{0,1,-5,5} + f_{0,5,-5,1}) \\
 & - 150(f_{-2,-3,5,1} + f_{-4,3,3,-1} + f_{-4,-1,3,3} + f_{-2,1,5,-3}) - 138f_{0,3,-5,3} \\
 & \left. - 84(f_{0,3,3,-5} + f_{0,-5,3,3}) \right) \quad (C.55)
 \end{aligned}$$

The associated weight mask is shown in figure C.55.

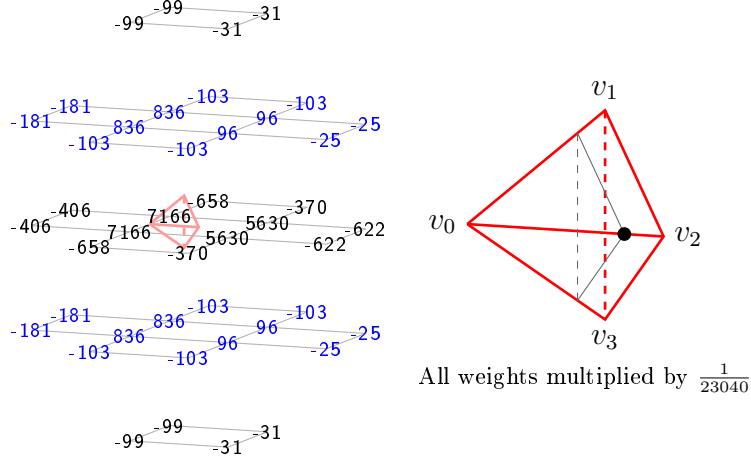


Figure C.56: Weight mask for c_{1040} . The associated domain point is shown in the teterahedron on the right. The black triangle symbolizes the ring $R_4(v_0)$.

$$\begin{aligned}
 c_{1040} := & \frac{1}{23040} \left(7166(f_{0,1,-1,1} + f_{2,-1,1,-1}) + 5630(f_{0,-1,3,-1} + f_{-2,1,1,1}) \right. \\
 & + 836(f_{0,-1,-1,3} + f_{0,3,-1,-1} + f_{2,-3,1,1} + f_{2,1,1,-3}) - 658(f_{-2,3,-3,3} + f_{4,-3,3,-3}) \\
 & - 622(f_{-4,1,3,1} + f_{-2,-1,5,-1}) - 406(f_{2,1,-3,1} + f_{4,-1,-1,-1}) \\
 & - 370(f_{-4,3,-1,3} + f_{2,-3,5,-3}) - 181(f_{4,-3,-1,1} + f_{2,-1,-3,3} + f_{4,1,-1,-3} + f_{2,3,-3,-1}) \\
 & - 103(f_{4,-5,3,-1} + f_{4,-1,3,-5} + f_{-2,5,-3,1} + f_{-4,5,-1,1} + f_{2,-5,5,-1} + f_{-4,1,-1,5} \\
 & \quad + f_{2,-1,5,-5} + f_{-2,1,-3,5}) \\
 & - 99(f_{2,3,1,-5} + f_{2,-5,1,3} + f_{0,-3,-1,5} + f_{0,5,-1,-3}) \\
 & + 96(f_{-2,-1,1,3} + f_{0,1,3,-3} + f_{0,-3,3,1} + f_{-2,3,1,-1}) \\
 & - 31(f_{0,-5,3,3} + f_{0,3,3,-5} + f_{-2,-3,1,5} + f_{-2,5,1,-3}) \\
 & \left. - 25(f_{-2,-3,5,1} + f_{-4,-1,3,3} + f_{-2,1,5,-3} + f_{-4,3,3,-1}) \right) \tag{C.56}
 \end{aligned}$$

The associated weight mask is shown in figure C.56.

$$\begin{aligned}
 c_{0500} := & \frac{1}{184320} \left(83712f_{0,1,-1,1} + 37028(f_{0,3,-1,-1} + f_{-2,1,1,1} + f_{2,-1,1,-1}) \right. \\
 & + 12902(f_{0,-1,3,-1} + f_{-2,3,1,-1} + f_{2,1,1,-3}) \\
 & - 5228(f_{-4,1,3,1} + f_{4,-3,3,-3} + f_{0,5,-1,-3}) \\
 & - 2711(f_{4,1,-1,-3} + f_{-4,5,-1,1} + f_{0,-3,3,1}) \\
 & - 1948(f_{2,1,-3,1} + f_{-2,3,-3,3} + f_{0,-1,-1,3}) - 1671f_{0,1,3,-3} \\
 & - 1226(f_{-2,-1,1,3} + f_{4,-1,-1,-1} + f_{-2,5,-3,1} + f_{2,3,-3,-1} + f_{2,-3,1,1} + f_{-4,3,-1,3}) \\
 & - 986(f_{0,3,-5,3} + f_{-2,1,-3,5} + f_{2,-1,-3,3}) \\
 & - 864(f_{4,-1,3,-5} + f_{2,3,1,-5} + f_{-4,3,3,-1} + f_{2,-3,5,-3} + f_{-2,5,1,-3} + f_{-2,-1,5,-1}) \\
 & - 599(f_{4,-3,-1,1} + f_{-4,1,-1,5} + f_{0,5,-5,1}) - 256(f_{2,-1,5,-5} + f_{-2,1,5,-3} + f_{0,3,3,-5}) \\
 & \left. + 249f_{0,1,-5,5} - 12(f_{4,1,-5,1} + f_{0,-3,-1,5} + f_{-4,5,-5,5}) \right) \tag{C.57}
 \end{aligned}$$

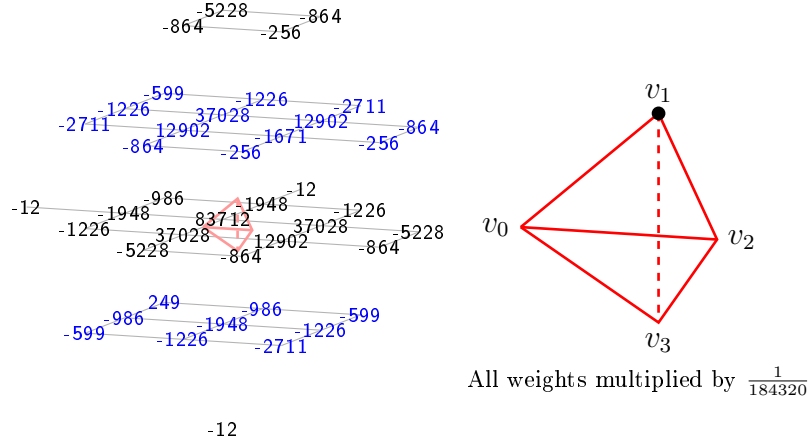


Figure C.57: Weight mask for c_{0500} . The associated domain point is shown in the teterahedron on the right.

The associated weight mask is shown in figure C.57.

B-coefficient c_{0005} is computed using (1, 3)-symmetry.

$$\begin{aligned}
 c_{0410} := & \frac{1}{276480} \left(116862f_{0,1,-1,1} + 62758(f_{2,-1,1,-1} + f_{-2,1,1,1}) + 46678f_{0,3,-1,-1} \right. \\
 & + 30024f_{0,-1,3,-1} + 16740(f_{-2,3,1,-1} + f_{2,1,1,-3}) \\
 & - 8854(f_{-4,1,3,1} + f_{4,-3,3,-3}) - 6178f_{0,5,-1,-3} - 5462(f_{-2,3,-3,3} + f_{2,1,-3,1}) \\
 & - 5277f_{0,-3,3,1} - 3960(f_{-2,5,-3,1} + f_{2,3,-3,-1}) - 3453(f_{4,1,-1,-3} + f_{-4,5,-1,1}) \\
 & - 2154(f_{2,-3,5,-3} + f_{-2,-1,5,-1}) + 1870f_{0,-1,-1,3} - 1746(f_{2,-1,-3,3} + f_{-2,1,-3,5}) \\
 & - 1380(f_{2,-3,1,1} + f_{-2,-1,1,3}) - 1359(f_{4,-3,-1,1} + f_{-4,1,-1,5}) \\
 & - 1350(f_{2,3,1,-5} + f_{-2,5,1,-3}) - 1209f_{0,1,3,-3} - 1074(f_{4,-1,3,-5} + f_{-4,3,3,-1}) \\
 & - 1044(f_{-4,3,-1,3} + f_{4,-1,-1,-1}) - 534(f_{2,-1,5,-5} + f_{-2,1,5,-3}) - 402f_{0,3,3,-5} \\
 & - 352f_{0,-3,-1,5} - 270f_{0,3,-5,3} + 249f_{0,1,-5,5} + 117f_{0,5,-5,1} \\
 & \left. + 56(f_{4,1,-5,1} + f_{-4,5,-5,5}) \right) \tag{C.58}
 \end{aligned}$$

The associated weight mask is shown in figure C.58.

B-coefficient c_{0014} is computed using (1, 3)-symmetry.

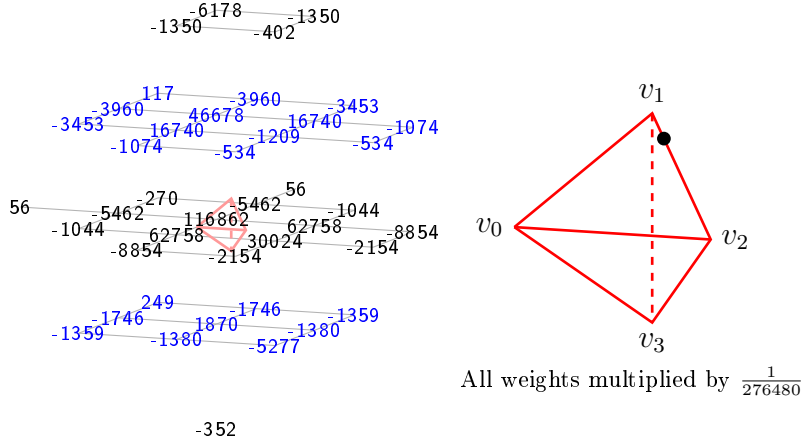


Figure C.58: Weight mask for c_{0410} . The associated domain point is shown in the teterahedron on the right.

$$\begin{aligned}
 c_{0410} := & \frac{1}{552960} \left(285960f_{0,1,-1,1} + 114380(f_{-2,1,1,1} + f_{2,-1,1,-1}) + 82220f_{0,3,-1,-1} \right. \\
 & + 49158f_{0,-1,3,-1} + 22590(f_{-2,3,1,-1} + f_{2,1,1,-3}) \\
 & - 16988(f_{-4,1,3,1} + f_{4,-3,3,-3}) - 11636f_{0,5,-1,-3} - 10587f_{0,-3,3,1} \\
 & - 10348(f_{-2,3,-3,3} + f_{2,1,-3,1}) - 10203f_{0,1,3,-3} \\
 & - 6939(f_{4,1,-1,-3} + f_{-4,5,-1,1}) - 6186(f_{2,3,-3,-1} + f_{-2,5,-3,1}) \\
 & - 4842(f_{2,-1,-3,3} + f_{-2,1,-3,5}) + 4316f_{0,-1,-1,3} - 2928(f_{-2,-1,5,-1} + f_{2,-3,5,-3}) \\
 & - 2907(f_{4,-3,-1,1} + f_{-4,1,-1,5}) - 1890f_{0,3,-5,3} - 1320(f_{2,3,1,-5} + f_{-2,5,1,-3}) \\
 & + 1245f_{0,1,-5,5} - 1026(f_{-2,-1,1,3} + f_{2,-3,1,1}) - 768(f_{4,-1,3,-5} + f_{-4,3,3,-1}) \\
 & + 484(f_{4,1,-5,1} + f_{-4,5,-5,5}) - 432(f_{2,-1,5,-5} + f_{-2,1,5,-3}) \\
 & \left. - 354(f_{4,-1,-1,-1} + f_{-4,3,-1,3}) - 332f_{0,-3,-1,5} - 168f_{0,3,3,-5} + 45f_{0,5,-5,1} \right) \tag{C.59}
 \end{aligned}$$

The associated weight mask is shown in figure C.59.
B-coefficient c_{0104} is computed using (1, 3)-symmetry.

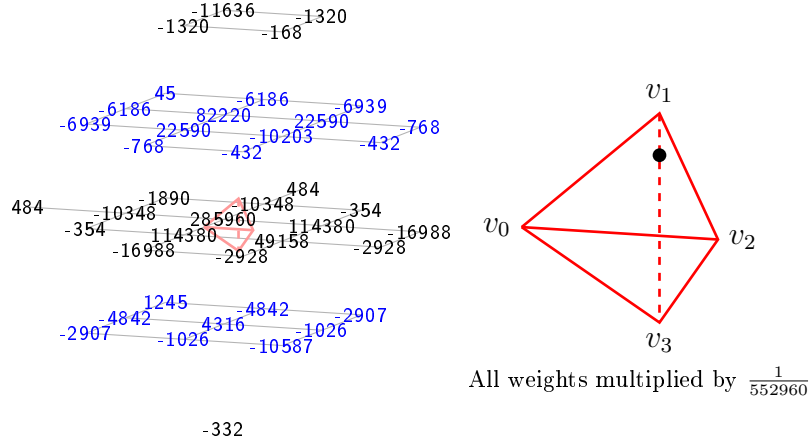


Figure C.59: Weight mask for c_{0401} . The associated domain point is shown in the teterahedron on the right.

$$\begin{aligned}
 c_{0320} := & \frac{1}{552960} \left(209400f_{0,1,-1,1} + 138580(f_{2,-1,1,-1} + f_{-2,1,1,1}) + 85998f_{0,-1,3,-1} \right. \\
 & + 70084f_{0,3,-1,-1} + 29262(f_{2,1,1,-3} + f_{-2,3,1,-1}) \\
 & - 18292(f_{4,-3,3,-3} + f_{-4,1,3,1}) + 12676f_{0,-1,-1,3} - 12327f_{0,-3,3,1} \\
 & - 11756(f_{-2,3,-3,3} + f_{2,1,-3,1}) - 8596f_{0,5,-1,-3} \\
 & - 7626(f_{2,3,-3,-1} + f_{-2,5,-3,1}) - 7032(f_{-2,-1,5,-1} + f_{2,-3,5,-3}) \\
 & - 6903(f_{4,1,-1,-3} + f_{-4,5,-1,1}) - 4026(f_{-2,1,-3,5} + f_{2,-1,-3,3}) \\
 & - 3639(f_{4,-3,-1,1} + f_{-4,1,-1,5}) - 2808(f_{2,3,1,-5} + f_{-2,5,1,-3}) \\
 & - 2730(f_{-4,3,-1,3} + f_{4,-1,-1,-1}) - 1704(f_{4,-1,3,-5} + f_{-4,3,3,-1}) - 1372f_{0,-3,-1,5} \\
 & - 1368(f_{2,-1,5,-5} + f_{-2,1,5,-3}) - 1194(f_{2,-3,1,1} + f_{-2,-1,1,3}) - 840f_{0,3,3,-5} \\
 & - 471f_{0,1,3,-3} + 260(f_{4,1,-5,1} + f_{-4,5,-5,5}) + 249(f_{0,5,-5,1} + f_{0,1,-5,5}) \\
 & \left. - 138f_{0,3,-5,3} \right) \tag{C.60}
 \end{aligned}$$

The associated weight mask is shown in figure C.60.
B-coefficient c_{0023} is computed using (1, 3)-symmetry.

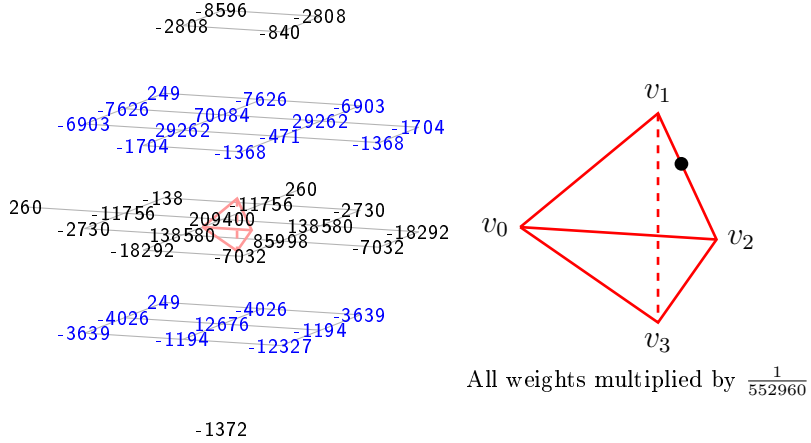


Figure C.60: Weight mask for c_{0320} . The associated domain point is shown in the teterahedron on the right.

$$\begin{aligned}
 c_{0311} := & \frac{1}{184320} \left(83652f_{0,1,-1,1} + 43664(f_{-2,1,1,1} + f_{2,-1,1,-1}) + 23726f_{0,-1,3,-1} \right. \\
 & + 22080f_{0,3,-1,-1} + 6452(f_{-2,3,1,-1} + f_{2,1,1,-3}) \\
 & - 6242(f_{4,-3,3,-3} + f_{-4,1,3,1}) + 6196f_{0,-1,-1,3} - 4483f_{0,-3,3,1} \\
 & - 3946(f_{-2,3,-3,3} + f_{2,1,-3,1}) - 3555f_{0,1,3,-3} - 2764f_{0,5,-1,-3} \\
 & - 2654(f_{2,3,-3,-1} + f_{-2,5,-3,1}) - 2303(f_{4,1,-1,-3} + f_{-4,5,-1,1}) \\
 & - 1880(f_{-2,1,-3,5} + f_{2,-1,-3,3}) - 1626(f_{-2,-1,5,-1} + f_{2,-3,5,-3}) \\
 & - 1493(f_{-4,1,-1,5} + f_{4,-3,-1,1}) - 556f_{0,-3,-1,5} + 480(f_{-2,-1,1,3} + f_{2,-3,1,1}) \\
 & - 452(f_{2,3,1,-5} + f_{-2,5,1,-3}) + 249f_{0,1,-5,5} - 222(f_{4,-1,3,-5} + f_{-4,3,3,-1}) \\
 & + 205f_{0,5,-5,1} + 192(f_{-4,5,-5,5} + f_{4,1,-5,1}) - 182f_{0,3,-5,3} \\
 & \left. - 166(f_{2,-1,5,-5} + f_{-2,1,5,-3}) + 100(f_{4,-1,-1,-1} + f_{-4,3,-1,3}) - 56f_{0,3,3,-5} \right) \tag{C.61}
 \end{aligned}$$

The associated weight mask is shown in figure C.61.
B-coefficient c_{0113} is computed using (1, 3)-symmetry.

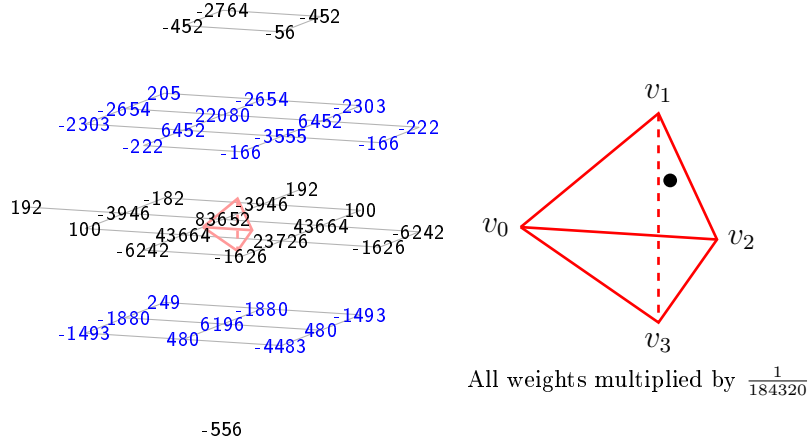


Figure C.61: Weight mask for c_{0311} . The associated domain point is shown in the teterahedron on the right.

$$\begin{aligned}
 c_{0302} := & \frac{1}{138240} \left(81138f_{0,1,-1,1} + 27254(f_{-2,1,1,1} + f_{2,-1,1,-1}) + 14580f_{0,-1,3,-1} \right. \\
 & + 12002f_{0,3,-1,-1} + 5120f_{0,-1,-1,3} - 4109(f_{-4,1,3,1} + f_{4,-3,3,-3}) \\
 & - 3985(f_{-2,3,-3,3} + f_{2,1,-3,1}) - 3408f_{0,1,3,-3} - 3384f_{0,-3,3,1} \\
 & + 2853(f_{-2,3,1,-1} + f_{2,1,1,-3}) - 2106(f_{-2,5,-3,1} + f_{2,3,-3,-1}) \\
 & - 1917(f_{2,-1,-3,3} + f_{-2,1,-3,5}) - 1470(f_{-4,5,-1,1} + f_{4,1,-1,-3}) - 1316f_{0,5,-1,-3} \\
 & - 1143(f_{4,-3,-1,1} + f_{-4,1,-1,5}) + 987(f_{-2,-1,1,3} + f_{2,-3,1,1}) \\
 & - 807(f_{-2,-1,5,-1} + f_{2,-3,5,-3}) + 801(f_{-4,3,-1,3} + f_{4,-1,-1,-1}) + 498f_{0,1,-5,5} \\
 & + 432f_{0,5,-5,1} + 418(f_{-4,5,-5,5} + f_{4,1,-5,1}) - 342f_{0,3,-5,3} - 296f_{0,-3,-1,5} \\
 & \left. - 102(f_{-2,5,1,-3} + f_{2,3,1,-5}) - 33(f_{4,-1,3,-5} + f_{2,-1,5,-5} + f_{-4,3,3,-1} + f_{-2,1,5,-3}) \right) \tag{C.62}
 \end{aligned}$$

The associated weight mask is shown in figure C.62.
B-coefficient c_{0203} is computed using (1, 3)-symmetry.

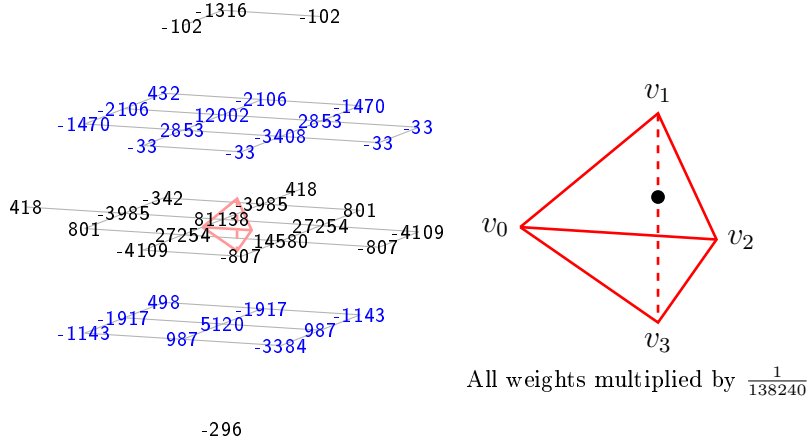


Figure C.62: Weight mask for c_{0302} . The associated domain point is shown in the teterahedron on the right.

$$\begin{aligned}
 c_{0230} := & \frac{1}{46080} \left(15484f_{0,1,-1,1} + 12454(f_{-2,1,1,1} + f_{2,-1,1,-1}) + 9340f_{0,-1,3,-1} \right. \\
 & + 3912f_{0,3,-1,-1} + 1943(f_{2,1,1,-3} + f_{-2,3,1,-1}) - 1499(f_{4,-3,3,-3} + f_{-4,1,3,1}) \\
 & + 1398f_{0,-1,-1,3} - 995(f_{-2,3,-3,3} + f_{2,1,-3,1}) - 872f_{0,-3,3,1} \\
 & - 851(f_{2,-3,5,-3} + f_{-2,-1,5,-1}) - 491(f_{4,-1,-1,-1} + f_{-4,3,-1,3}) \\
 & - 467(f_{-4,5,-1,1} + f_{2,3,-3,-1} + f_{-2,5,-3,1} + f_{4,1,-1,-3}) - 464f_{0,5,-1,-3} \\
 & - 290(f_{-4,1,-1,5} + f_{4,-3,-1,1} + f_{-2,1,-3,5} + f_{2,-1,-3,3}) + 262f_{0,1,3,-3} \\
 & - 226(f_{2,3,1,-5} + f_{-2,5,1,-3}) - 170f_{0,-3,-1,5} \\
 & - 122(f_{2,-1,5,-5} + f_{-2,1,5,-3} + f_{-4,3,3,-1} + f_{4,-1,3,-5}) + 119(f_{2,-3,1,1} + f_{-2,-1,1,3}) \\
 & \left. - 90f_{0,3,3,-5} - 34(f_{-2,-3,1,5} + f_{2,-5,1,3}) - 11(f_{-4,-1,3,3} + f_{2,-5,5,-1} + f_{-2,-3,5,1} + f_{4,-5,3,-1}) \right) \quad (C.63)
 \end{aligned}$$

The associated weight mask is shown in figure C.63.
B-coefficient c_{0032} is computed using (1, 3)-symmetry.

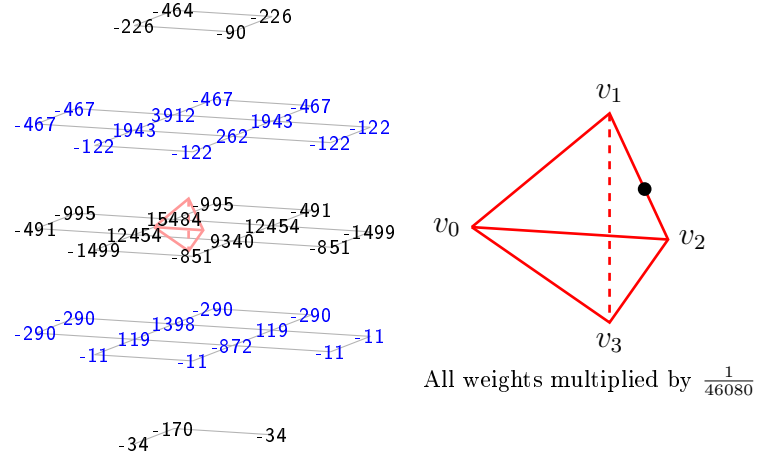


Figure C.63: Weight mask for c_{0230} . The associated domain point is shown in the teterahedron on the right.

$$\begin{aligned}
 c_{0221} := & \frac{1}{552960} \left(214872f_{0,1,-1,1} + 145444(f_{2,-1,1,-1} + f_{-2,1,1,1}) + 94254f_{0,-1,3,-1} \right. \\
 & + 47932f_{0,3,-1,-1} + 28012f_{0,-1,-1,3} - 19300(f_{4,-3,3,-3} + f_{-4,1,3,1}) \\
 & + 15222(f_{2,1,1,-3} + f_{-2,3,1,-1}) - 12543f_{0,-3,3,1} \\
 & - 11468(f_{2,1,-3,1} + f_{-2,3,-3,3}) - 9183f_{0,1,3,-3} \\
 & - 7704(f_{2,-3,5,-3} + f_{-2,-1,5,-1}) - 6582(f_{2,3,-3,-1} + f_{-2,5,-3,1}) \\
 & - 6195(f_{4,1,-1,-3} + f_{-4,5,-1,1}) - 5620f_{0,5,-1,-3} - 5358(f_{2,-1,-3,3} + f_{-2,1,-3,5}) \\
 & + 4974(f_{-2,-1,1,3} + f_{2,-3,1,1}) - 4971(f_{4,-3,-1,1} + f_{-4,1,-1,5}) - 3004f_{0,-3,-1,5} \\
 & - 2106(f_{-4,3,-1,3} + f_{4,-1,-1,-1}) - 1392(f_{2,3,1,-5} + f_{-2,5,1,-3}) \\
 & - 564(f_{2,-1,5,-5} + f_{-2,1,5,-3} + f_{4,-1,3,-5} + f_{-4,3,3,-1}) - 408(f_{-2,-3,1,5} + f_{2,-5,1,3}) \\
 & + 260(f_{4,1,-5,1} + f_{-4,5,-5,5}) + 249(f_{0,5,-5,1} + f_{0,1,-5,5}) - 168f_{0,3,3,-5} \\
 & \left. - 138f_{0,3,-5,3} - 132(f_{2,-5,5,-1} + f_{-4,-1,3,3} + f_{-2,-3,5,1} + f_{4,-5,3,-1}) \right) \quad (C.64)
 \end{aligned}$$

The associated weight mask is shown in figure C.64.
B-coefficient c_{0122} is computed using (1, 3)-symmetry.

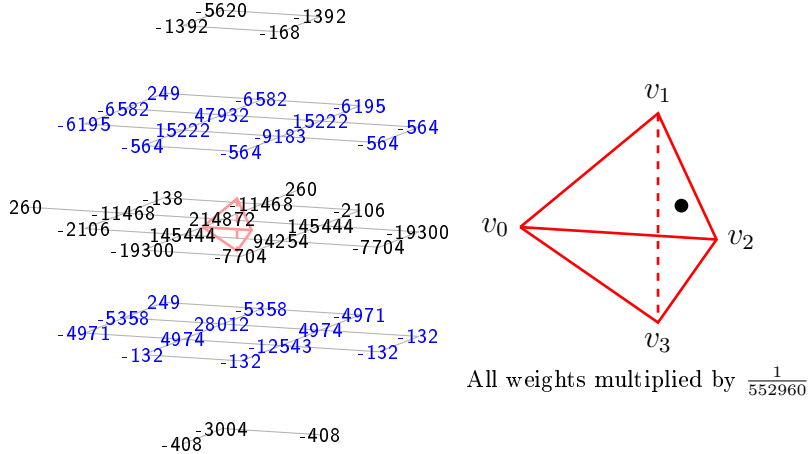


Figure C.64: Weight mask for c_{0221} . The associated domain point is shown in the tetrahedron on the right.

$$\begin{aligned}
 c_{0212} := & \frac{1}{138240} \left(65940f_{0,1,-1,1} + 32620(f_{2,-1,1,-1} + f_{-2,1,1,1}) + 19050f_{0,-1,3,-1} \right. \\
 & + 9730(f_{0,-1,-1,3} + f_{0,3,-1,-1}) - 4666(f_{-4,1,3,1} + f_{4,-3,3,-3}) \\
 & - 3585(f_{0,1,3,-3} + f_{0,-3,3,1}) - 3314(f_{-2,3,-3,3} + f_{2,1,-3,1}) \\
 & + 2208(f_{2,-3,1,1} + f_{-2,-1,1,3} + f_{2,1,1,-3} + f_{-2,3,1,-1}) \\
 & - 1911(f_{2,3,-3,-1} + f_{2,-1,-3,3} + f_{-2,5,-3,1} + f_{-2,1,-3,5}) \\
 & - 1524(f_{4,-3,-1,1} + f_{-4,5,-1,1} + f_{-4,1,-1,5} + f_{4,1,-1,-3}) \\
 & - 1278(f_{-2,-1,5,-1} + f_{2,-3,5,-3}) - 964(f_{0,5,-1,-3} + f_{0,-3,-1,5}) \\
 & + 432(f_{-4,3,-1,3} + f_{4,-1,-1,-1}) + 260(f_{4,1,-5,1} + f_{-4,5,-5,5}) \\
 & + 249(f_{0,5,-5,1} + f_{0,1,-5,5}) - 138f_{0,3,-5,3} \\
 & - 102(f_{2,-5,1,3} + f_{-2,5,1,-3} + f_{2,3,1,-5} + f_{-2,-3,1,5}) \\
 & - 33(f_{2,-5,5,-1} + f_{-2,-3,5,1} + f_{-4,-1,3,3} + f_{4,-1,3,-5} + f_{2,-1,5,-5} + f_{-2,1,5,-3} \\
 & \quad \left. + f_{-4,3,3,-1} + f_{4,-5,3,-1} \right) \tag{C.65}
 \end{aligned}$$

The associated weight mask is shown in figure C.65.

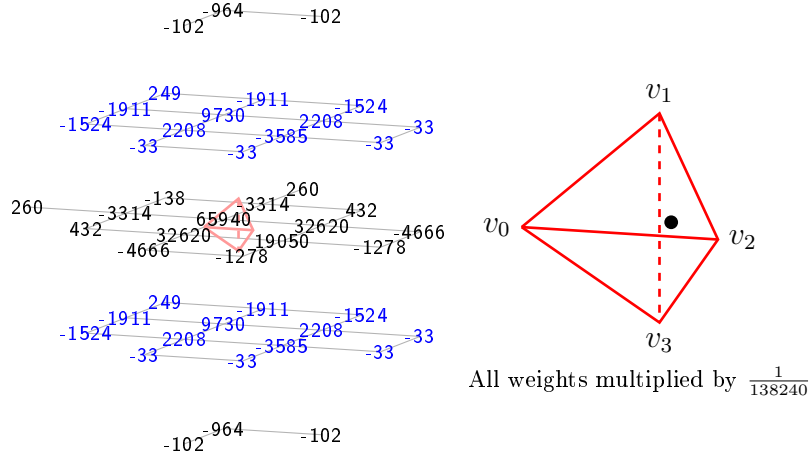


Figure C.65: Weight mask for c_{0212} . The associated domain point is shown in the teterahedron on the right.

$$\begin{aligned}
 c_{0140} := & \frac{1}{23040} \left(7166f_{0,1,-1,1} + 6398(f_{2,-1,1,-1} + f_{-2,1,1,1}) + 5630f_{0,-1,3,-1} \right. \\
 & + 1064f_{0,3,-1,-1} + 694(f_{-2,3,1,-1} + f_{2,1,1,-3}) - 640(f_{-4,1,3,1} + f_{4,-3,3,-3}) \\
 & + 608f_{0,-1,-1,3} - 532(f_{-2,3,-3,3} + f_{2,1,-3,1}) - 496(f_{2,-3,5,-3} + f_{-2,-1,5,-1}) \\
 & - 388(f_{-4,3,-1,3} + f_{4,-1,-1,-1}) + 324f_{0,1,3,-3} + 238(f_{-2,-1,1,3} + f_{2,-3,1,1}) \\
 & - 160(f_{-4,5,-1,1} + f_{2,3,-3,-1} + f_{4,1,-1,-3} + f_{-2,5,-3,1}) - 132f_{0,-3,3,1} \\
 & - 124(f_{-2,1,-3,5} + f_{-4,1,-1,5} + f_{2,-1,-3,3} + f_{4,-3,-1,1}) - 123f_{0,5,-1,-3} \\
 & - 89(f_{2,3,1,-5} + f_{-2,5,1,-3}) - 82(f_{2,-1,5,-5} + f_{4,-1,3,-5} + f_{-4,3,3,-1} + f_{-2,1,5,-3}) \\
 & - 75f_{0,-3,-1,5} - 55f_{0,3,3,-5} - 46(f_{4,-5,3,-1} + f_{-4,-1,3,3} + f_{2,-5,5,-1} + f_{-2,-3,5,1}) \\
 & \left. - 41(f_{2,-5,1,3} + f_{-2,-3,1,5}) - 7f_{0,-5,3,3} \right) \tag{C.66}
 \end{aligned}$$

The associated weight mask is shown in figure C.66.
B-coefficient c_{0041} is computed using (1, 3)-symmetry.

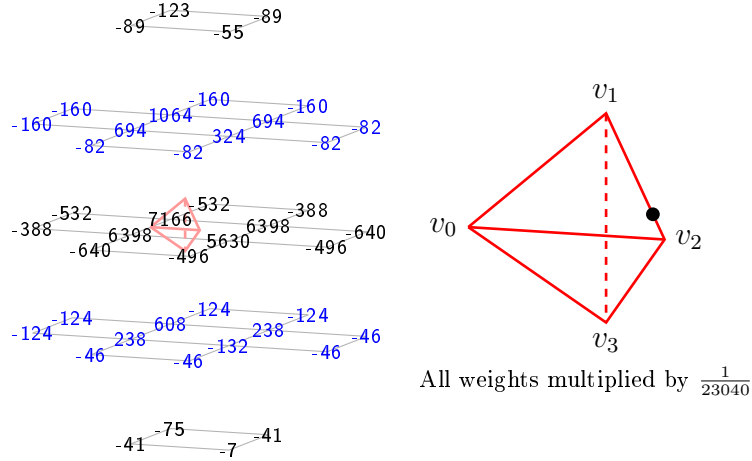


Figure C.66: Weight mask for c_{0140} . The associated domain point is shown in the teterahedron on the right.

$$\begin{aligned}
 c_{0131} := & \frac{1}{92160} \left(31604 f_{0,1,-1,1} + 25544(f_{-2,1,1,1} + f_{2,-1,1,-1}) + 19316 f_{0,-1,3,-1} \right. \\
 & + 4930(f_{0,-1,-1,3} + f_{0,3,-1,-1}) - 2986(f_{-4,1,3,1} + f_{4,-3,3,-3}) \\
 & - 1978(f_{-2,3,-3,3} + f_{2,1,-3,1}) - 1690(f_{-2,-1,5,-1} + f_{2,-3,5,-3}) \\
 & + 1682(f_{-2,-1,1,3} + f_{2,-3,1,1} + f_{-2,3,1,-1} + f_{2,1,1,-3}) \\
 & - 990(f_{0,-3,3,1} + f_{0,1,3,-3}) - 970(f_{-4,3,-1,3} + f_{4,-1,-1,-1}) \\
 & - 763(f_{-4,1,-1,5} + f_{2,-1,-3,3} + f_{4,1,-1,-3} + f_{-2,5,-3,1} + f_{2,3,-3,-1} + f_{4,-3,-1,1} \\
 & \quad + f_{-2,1,-3,5} + f_{-4,5,-1,1}) \\
 & - 572(f_{0,5,-1,-3} + f_{0,-3,-1,5}) - 198(f_{-2,-3,1,5} + f_{2,-5,1,3} + f_{-2,5,1,-3} + f_{2,3,1,-5}) \\
 & - 139(f_{2,-5,5,-1} + f_{-2,-3,5,1} + f_{-4,-1,3,3} + f_{4,-1,3,-5} + f_{2,-1,5,-5} + f_{-2,1,5,-3} \\
 & \quad + f_{-4,3,3,-1} + f_{4,-5,3,-1}) \\
 & \left. - 28(f_{0,-5,3,3} + f_{0,3,3,-5}) \right) \tag{C.67}
 \end{aligned}$$

The associated weight mask is shown in figure C.67.

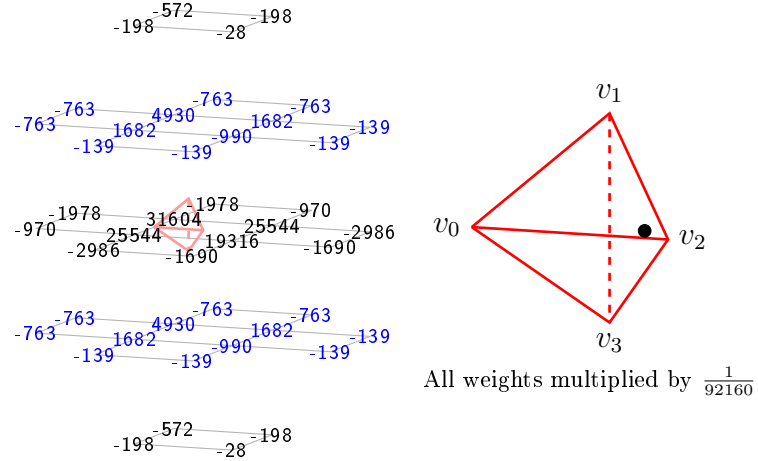


Figure C.67: Weight mask for c_{0131} . The associated domain point is shown in the teterahedron on the right.

$$\begin{aligned}
 c_{0050} := & \frac{1}{23040} \left(6398(f_{0,-1,3,-1} + f_{0,1,-1,1} + f_{-2,1,1,1} + f_{2,-1,1,-1}) \right. \\
 & - 514(f_{-2,3,-3,3} + f_{4,-1,-1,-1} + f_{-2,-1,5,-1} + f_{2,-3,5,-3} + f_{4,-3,3,-3} + f_{-4,1,3,1} \\
 & + f_{-4,3,-1,3} + f_{2,1,-3,1}) \\
 & + 466(f_{2,-3,1,1} + f_{-2,3,1,-1} + f_{2,1,1,-3} + f_{-2,-1,1,3} + f_{0,-3,3,1} + f_{0,3,-1,-1} \\
 & + f_{0,1,3,-3} + f_{0,-1,-1,3}) \\
 & - 103(f_{-2,5,-3,1} + f_{4,1,-1,-3} + f_{2,-5,5,-1} + f_{4,-5,3,-1} + f_{-4,1,-1,5} + f_{-4,-1,3,3} \\
 & + f_{4,-1,3,-5} + f_{4,-3,-1,1} + f_{-4,3,3,-1} + f_{-4,5,-1,1} + f_{-2,-3,5,1} + f_{2,3,-3,-1} \\
 & + f_{2,-1,5,-5} + f_{-2,1,5,-3} + f_{-2,1,-3,5} + f_{2,-1,-3,3}) \\
 & \left. - 65(f_{2,-5,1,3} + f_{-2,5,1,-3} + f_{2,3,1,-5} + f_{-2,-3,1,5} + f_{0,-5,3,3} + f_{0,5,-1,-3} \right. \\
 & \left. + f_{0,3,3,-5} + f_{0,-3,-1,5}) \right) \quad (C.68)
 \end{aligned}$$

The associated weight mask is shown in figure C.68.

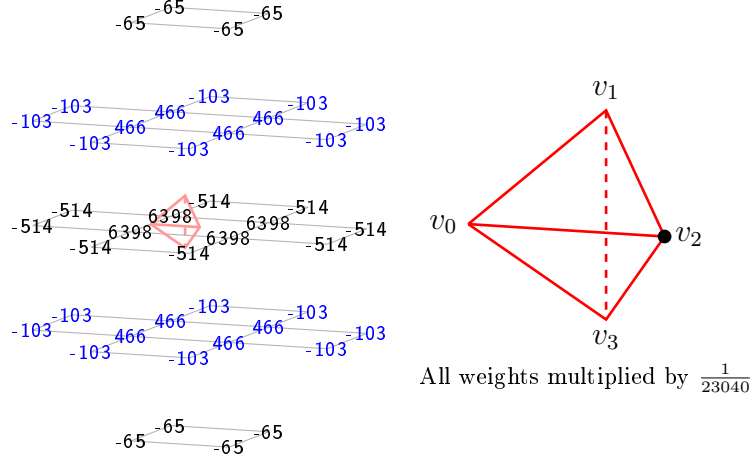


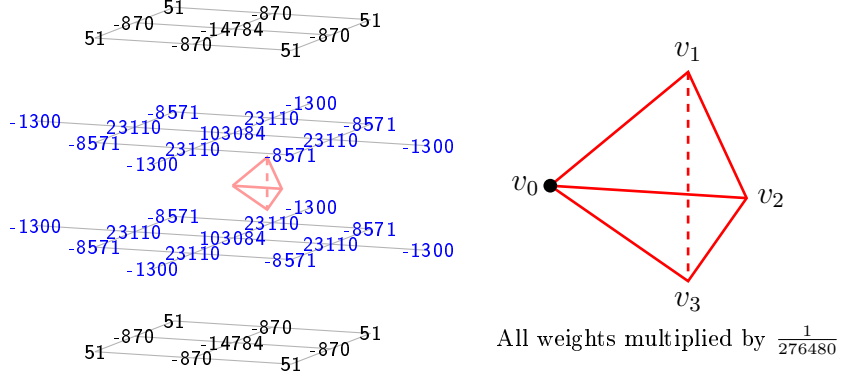
Figure C.68: Weight mask for c_{0050} . The associated domain point is shown in the teterahedron on the right.

B-coefficient computation rules for the class \mathcal{K}_3

$$\begin{aligned}
 c_{5000} := & \frac{1}{276480} \left(103084(f_{1,1,0,-1} + f_{1,-1,0,1}) \right. \\
 & + 23110(f_{-1,-1,2,1} + f_{-1,1,2,-1} + f_{-1,1,-2,3} + f_{3,-3,2,-1} + f_{3,-1,-2,1} + f_{-1,3,-2,1} \\
 & \quad + f_{3,-1,2,-3} + f_{3,1,-2,-1}) \\
 & - 14784(f_{1,-3,0,3} + f_{1,3,0,-3}) \\
 & - 8571(f_{-3,1,0,3} + f_{-3,3,0,1} + f_{5,-1,0,-3} + f_{1,3,-4,1} + f_{1,-3,4,-1} + f_{5,-3,0,-1} \\
 & \quad + f_{1,1,-4,3} + f_{1,-1,4,-3}) \\
 & - 1300(f_{-3,-1,4,1} + f_{-3,1,4,-1} + f_{5,-1,-4,1} + f_{-3,3,-4,5} + f_{-3,5,-4,3} + f_{5,-5,4,-3} \\
 & \quad + f_{5,1,-4,-1} + f_{5,-3,4,-5}) \\
 & - 870(f_{3,1,2,-5} + f_{-1,-1,-2,5} + f_{-1,-3,2,3} + f_{-1,3,2,-3} + f_{3,-5,2,1} + f_{-1,5,-2,-1} \\
 & \quad + f_{3,3,-2,-3} + f_{3,-3,-2,3}) \\
 & + 260(f_{1,5,0,-5} + f_{1,-5,0,5}) \\
 & + 51(f_{-3,5,0,-1} + f_{5,1,0,-5} + f_{1,-5,4,1} + f_{1,5,-4,-1} + f_{1,1,4,-5} + f_{1,-1,-4,5} \\
 & \quad \left. + f_{5,-5,0,1} + f_{-3,-1,0,5} \right) \tag{C.69}
 \end{aligned}$$

The associated weight mask is shown in figure C.69.

260

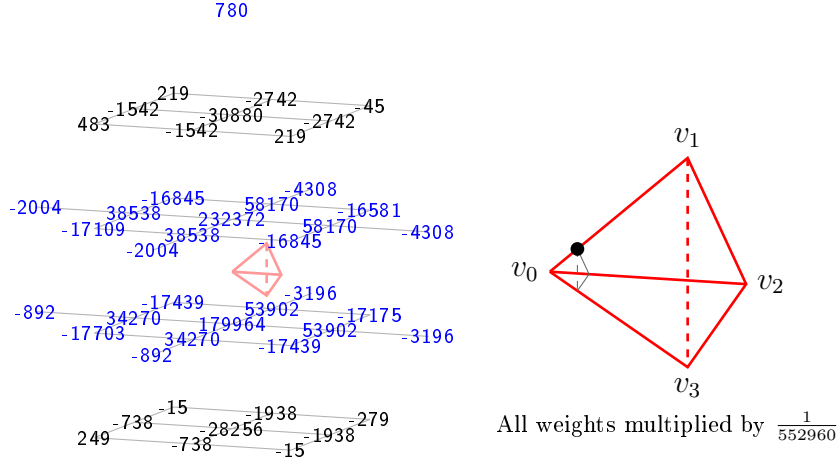


260

Figure C.69: Weight mask for c_{5000} . The associated domain point is shown in the teterahedron on the right.

$$\begin{aligned}
 c_{4100} := & \frac{1}{552960} \left(232372f_{1,1,0,-1} + 179964f_{1,-1,0,1} + 58170(f_{-1,1,2,-1} + f_{-1,3,-2,1}) \right. \\
 & + 53902(f_{-1,-1,2,1} + f_{-1,1,-2,3}) + 38538(f_{3,1,-2,-1} + f_{3,-1,2,-3}) \\
 & + 34270(f_{3,-3,2,-1} + f_{3,-1,-2,1}) - 30880f_{1,3,0,-3} - 28256f_{1,-3,0,3} \\
 & - 17703f_{5,-3,0,-1} - 17439(f_{1,1,-4,3} + f_{1,-3,4,-1}) - 17175f_{-3,1,0,3} \\
 & - 17109f_{5,-1,0,-3} - 16845(f_{1,3,-4,1} + f_{1,-1,4,-3}) - 16581f_{-3,3,0,1} \\
 & - 4308(f_{-3,5,-4,3} + f_{-3,1,4,-1}) - 3196(f_{-3,3,-4,5} + f_{-3,-1,4,1}) \\
 & - 2742(f_{-1,5,-2,-1} + f_{-1,3,2,-3}) - 2004(f_{5,1,-4,-1} + f_{5,-3,4,-5}) \\
 & - 1938(f_{-1,-3,2,3} + f_{-1,-1,-2,5}) - 1542(f_{3,3,-2,-3} + f_{3,1,2,-5}) \\
 & - 892(f_{5,-1,-4,1} + f_{5,-5,4,-3}) + 780f_{1,5,0,-5} - 738(f_{3,-3,-2,3} + f_{3,-5,2,1}) \\
 & + 483f_{5,1,0,-5} - 279f_{-3,-1,0,5} + 260f_{1,-5,0,5} + 249f_{5,-5,0,1} \\
 & \left. + 219(f_{1,5,-4,-1} + f_{1,1,4,-5}) - 45f_{-3,5,0,-1} - 15(f_{1,-5,4,1} + f_{1,-1,-4,5}) \right) \quad (C.70)
 \end{aligned}$$

The associated weight mask is shown in figure C.70.
B-coefficient c_{4001} is computed using (1, 3)-symmetry.



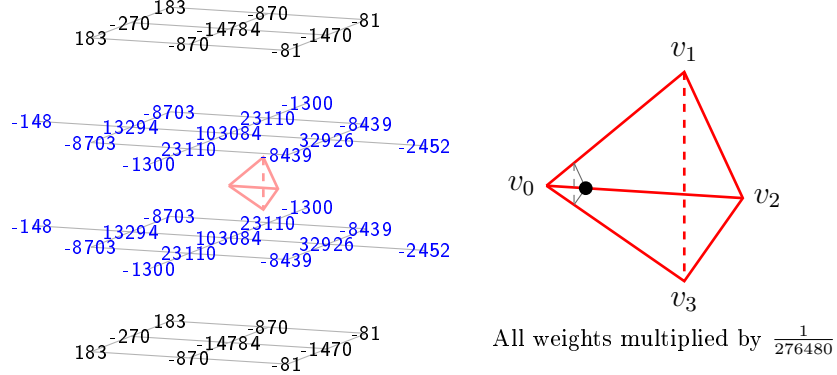
260

Figure C.70: Weight mask for c_{4100} . The associated domain point is shown in the tetrahedron on the right. The black triangle symbolizes the ring $R_1(v_0)$.

$$\begin{aligned}
 c_{4010} := & \frac{1}{276480} \left(103084(f_{1,1,0,-1} + f_{1,-1,0,1}) + 32926(f_{-1,-1,2,1} + f_{-1,1,2,-1}) \right. \\
 & + 23110(f_{-1,1,-2,3} + f_{3,-3,2,-1} + f_{-1,3,-2,1} + f_{3,-1,2,-3}) \\
 & - 14784(f_{1,-3,0,3} + f_{1,3,0,-3}) + 13294(f_{3,-1,-2,1} + f_{3,1,-2,-1}) \\
 & - 8703(f_{5,-3,0,-1} + f_{5,-1,0,-3} + f_{1,3,-4,1} + f_{1,1,-4,3}) \\
 & - 8439(f_{-3,1,0,3} + f_{-3,3,0,1} + f_{1,-3,4,-1} + f_{1,-1,4,-3}) \\
 & - 2452(f_{-3,1,4,-1} + f_{-3,-1,4,1}) - 1470(f_{-1,3,2,-3} + f_{-1,-3,2,3}) \\
 & - 1300(f_{-3,3,-4,5} + f_{-3,5,-4,3} + f_{5,-5,4,-3} + f_{5,-3,4,-5}) \\
 & - 870(f_{3,1,2,-5} + f_{-1,-1,-2,5} + f_{3,-5,2,1} + f_{-1,5,-2,-1}) - 270(f_{3,-3,-2,3} + f_{3,3,-2,-3}) \\
 & + 260(f_{1,5,0,-5} + f_{1,-5,0,5}) + 183(f_{1,5,-4,-1} + f_{5,1,0,-5} + f_{1,-1,-4,5} + f_{5,-5,0,1}) \\
 & \left. - 148(f_{5,-1,-4,1} + f_{5,1,-4,-1}) - 81(f_{1,-5,4,1} + f_{-3,5,0,-1} + f_{1,1,4,-5} + f_{-3,-1,0,5}) \right) \tag{C.71}
 \end{aligned}$$

The associated weight mask is shown in figure C.71.

260



260

Figure C.71: Weight mask for c_{4010} . The associated domain point is shown in the teterahedron on the right. The black triangle symbolizes the ring $R_1(v_0)$.

$$\begin{aligned}
 c_{3200} := & \frac{1}{138240} \left(65103 f_{1,1,0,-1} + 38899 f_{1,-1,0,1} + 17350 (f_{-1,1,2,-1} + f_{-1,3,-2,1}) \right. \\
 & + 13659 (f_{-1,-1,2,1} + f_{-1,1,-2,3}) - 7535 f_{1,3,0,-3} - 6223 f_{1,-3,0,3} \\
 & + 5977 (f_{3,-1,2,-3} + f_{3,1,-2,-1}) + 5400 (f_{3,-3,2,-1} + f_{3,-1,-2,1}) \\
 & - 3624 (f_{1,-3,4,-1} + f_{1,1,-4,3}) - 3483 f_{-3,1,0,3} - 3450 f_{5,-1,0,-3} \\
 & - 3327 (f_{1,3,-4,1} + f_{1,-1,4,-3}) - 3234 f_{5,-3,0,-1} - 2673 f_{-3,3,0,1} \\
 & - 1810 (f_{-3,5,-4,3} + f_{-3,1,4,-1}) - 1035 (f_{-1,3,2,-3} + f_{-1,5,-2,-1}) \\
 & - 948 (f_{-3,3,-4,5} + f_{-3,-1,4,1}) - 534 (f_{-1,-1,-2,5} + f_{-1,-3,2,3}) \\
 & - 352 (f_{5,-3,4,-5} + f_{5,1,-4,-1}) - 336 (f_{3,3,-2,-3} + f_{3,1,2,-5}) + 260 f_{1,5,0,-5} \\
 & + 216 f_{5,1,0,-5} - 165 f_{-3,-1,0,5} - 147 f_{-3,5,0,-1} - 102 (f_{5,-1,-4,1} + f_{5,-5,4,-3}) \\
 & \left. + 84 (f_{1,5,-4,-1} + f_{1,1,4,-5}) - 33 (f_{3,-5,2,1} + f_{3,-3,-2,3} + f_{1,-5,4,1} + f_{1,-1,-4,5}) \right) \quad (C.72)
 \end{aligned}$$

The associated weight mask is shown in figure C.72.
B-coefficient c_{3002} is computed using (1, 3)-symmetry.

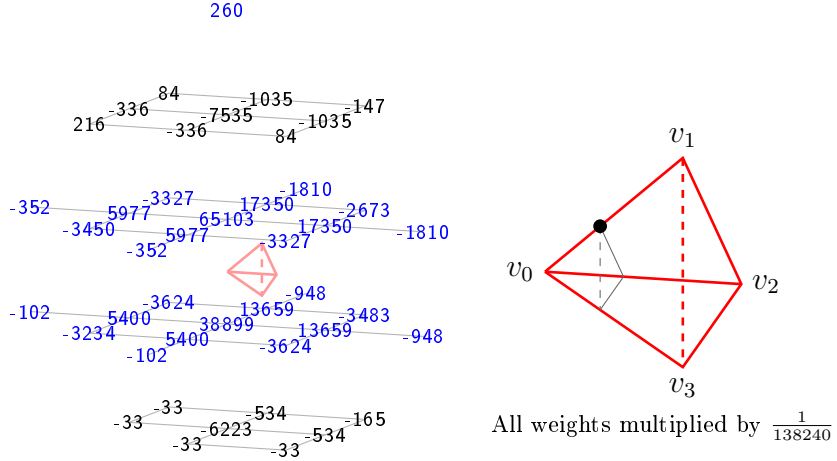


Figure C.72: Weight mask for c_{3200} . The associated domain point is shown in the teterahedron on the right. The black triangle symbolizes the ring $R_2(v_0)$.

$$\begin{aligned}
 c_{3110} := & \frac{1}{1105920} \left(457636 f_{1,1,0,-1} + 352820 f_{1,-1,0,1} + 164102 f_{-1,1,2,-1} \right. \\
 & + 143110 f_{-1,-1,2,1} + 110114 f_{-1,3,-2,1} + 101578 f_{-1,1,-2,3} \\
 & + 70850 f_{3,-1,2,-3} + 62314 f_{3,-3,2,-1} - 58280 f_{1,3,0,-3} \\
 & - 53032 f_{1,-3,0,3} + 37774 f_{3,-1,-2,1} + 33854 f_{3,1,-2,-1} \\
 & - 31569 f_{1,-3,4,-1} - 31437 f_{1,3,-4,1} - 30573 f_{1,1,-4,3} \\
 & - 29841 f_{5,-1,0,-3} - 28977 f_{5,-3,0,-1} - 28917 f_{-3,1,0,3} \\
 & - 28329 f_{1,-1,4,-3} - 25677 f_{-3,3,0,1} - 16196 f_{-3,1,4,-1} \\
 & - 11524 f_{-3,-1,4,1} - 9356 f_{-3,5,-4,3} - 9078 f_{-1,3,2,-3} - 7132 f_{-3,3,-4,5} \\
 & - 6678 f_{-1,-3,2,3} - 5274 f_{-1,5,-2,-1} - 4748 f_{5,-3,4,-5} - 3666 f_{-1,-1,-2,5} \\
 & - 2874 f_{3,1,2,-5} - 2524 f_{5,-5,4,-3} - 1467 f_{-3,-1,0,5} - 1395 f_{-3,5,0,-1} \\
 & + 1300 f_{1,5,0,-5} - 1266 f_{3,-5,2,1} + 1113 f_{5,1,0,-5} - 1086 f_{3,3,-2,-3} \\
 & + 981 f_{1,5,-4,-1} - 543 f_{1,-5,4,1} - 471 f_{1,1,4,-5} - 270 f_{3,-3,-2,3} \\
 & + 260 f_{1,-5,0,5} + 249 f_{5,-5,0,1} - 148 f_{5,-1,-4,1} + 117 f_{1,-1,-4,5} \\
 & \left. + 76 f_{5,1,-4,-1} \right) \tag{C.73}
 \end{aligned}$$

The associated weight mask is shown in figure C.73.
B-coefficient c_{3011} is computed using (1, 3)-symmetry.

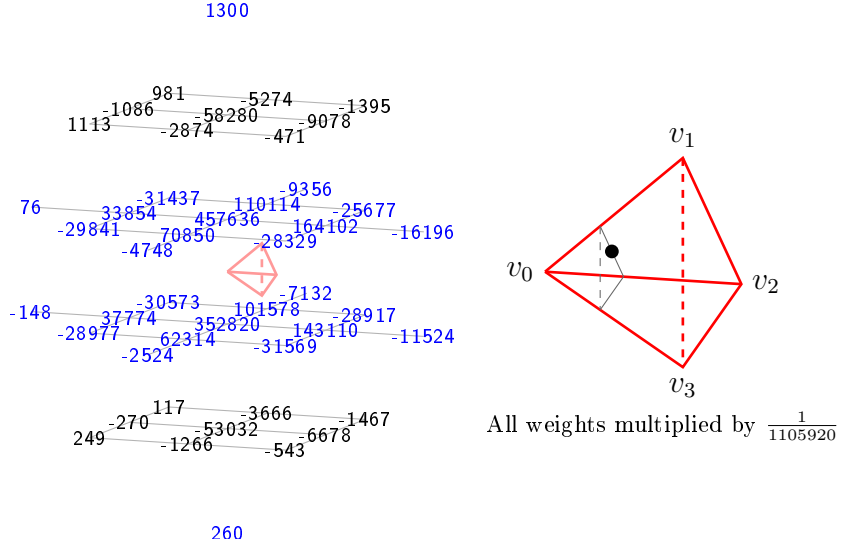
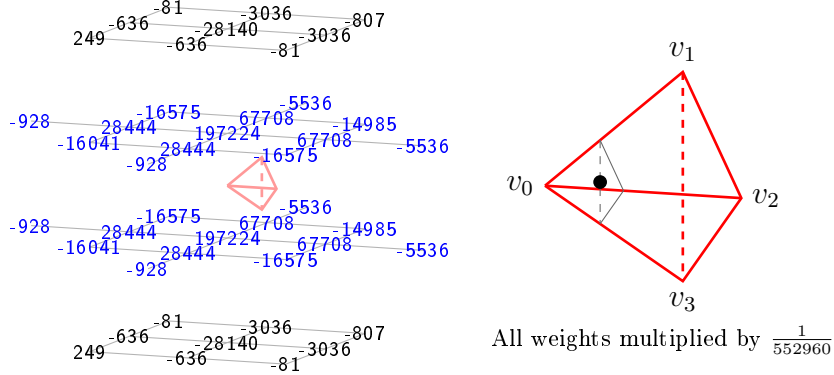


Figure C.73: Weight mask for c_{3101} . The associated domain point is shown in the teterahedron on the right. The black triangle symbolizes the ring $R_2(v_0)$.

$$\begin{aligned}
 c_{3101} := & \frac{1}{552960} \left(197224(f_{1,1,0,-1} + f_{1,-1,0,1}) \right. \\
 & + 67708(f_{-1,-1,2,1} + f_{-1,1,2,-1} + f_{-1,1,-2,3} + f_{-1,3,-2,1}) \\
 & + 28444(f_{3,-3,2,-1} + f_{3,-1,2,-3} + f_{3,1,-2,-1} + f_{3,-1,-2,1}) \\
 & - 28140(f_{1,-3,0,3} + f_{1,3,0,-3}) \\
 & - 16575(f_{1,3,-4,1} + f_{1,-3,4,-1} + f_{1,-1,4,-3} + f_{1,1,-4,3}) \\
 & - 16041(f_{5,-3,0,-1} + f_{5,-1,0,-3}) - 14985(f_{-3,3,0,1} + f_{-3,1,0,3}) \\
 & - 5536(f_{-3,1,4,-1} + f_{-3,-1,4,1} + f_{-3,3,-4,5} + f_{-3,5,-4,3}) \\
 & - 3036(f_{-1,-1,-2,5} + f_{-1,3,2,-3} + f_{-1,5,-2,-1} + f_{-1,-3,2,3}) \\
 & - 928(f_{5,-3,4,-5} + f_{5,-1,-4,1} + f_{5,1,-4,-1} + f_{5,-5,4,-3}) - 807(f_{-3,5,0,-1} + f_{-3,-1,0,5}) \\
 & - 636(f_{3,-3,-2,3} + f_{3,3,-2,-3} + f_{3,1,2,-5} + f_{3,-5,2,1}) + 260(f_{1,5,0,-5} + f_{1,-5,0,5}) \\
 & \left. + 249(f_{5,1,0,-5} + f_{5,-5,0,1}) - 81(f_{1,5,-4,-1} + f_{1,-5,4,1} + f_{1,1,4,-5} + f_{1,-1,-4,5}) \right) \\
 & \quad (C.74)
 \end{aligned}$$

The associated weight mask is shown in figure C.74.

260



260

Figure C.74: Weight mask for c_{3101} . The associated domain point is shown in the teterahedron on the right. The black triangle symbolizes the ring $R_2(v_0)$.

$$\begin{aligned}
 c_{3020} := & \frac{1}{552960} \left(199060(f_{1,1,0,-1} + f_{1,-1,0,1}) + 87754(f_{-1,-1,2,1} + f_{-1,1,2,-1}) \right. \\
 & + 39994(f_{-1,1,-2,3} + f_{3,-3,2,-1} + f_{-1,3,-2,1} + f_{3,-1,2,-3}) \\
 & - 26088(f_{1,-3,0,3} + f_{1,3,0,-3}) \\
 & - 12801(f_{1,1,-4,3} + f_{5,-3,0,-1} + f_{5,-1,0,-3} + f_{1,3,-4,1}) \\
 & - 11745(f_{-3,1,0,3} + f_{-3,3,0,1} + f_{1,-3,4,-1} + f_{1,-1,4,-3}) \\
 & + 9226(f_{3,1,-2,-1} + f_{3,-1,-2,1}) - 8956(f_{-3,1,4,-1} + f_{-3,-1,4,1}) \\
 & - 4938(f_{-1,3,2,-3} + f_{-1,-3,2,3}) \\
 & - 3340(f_{-3,3,-4,5} + f_{-3,5,-4,3} + f_{5,-5,4,-3} + f_{5,-3,4,-5}) \\
 & - 1530(f_{3,1,2,-5} + f_{-1,-1,-2,5} + f_{3,-5,2,1} + f_{-1,5,-2,-1}) \\
 & - 807(f_{1,-5,4,1} + f_{-3,5,0,-1} + f_{1,1,4,-5} + f_{-3,-1,0,5}) \\
 & + 260(f_{1,5,0,-5} + f_{1,-5,0,5} + f_{5,-1,-4,1} + f_{5,1,-4,-1}) \\
 & \left. + 249(f_{1,5,-4,-1} + f_{5,1,0,-5} + f_{1,-1,-4,5} + f_{5,-5,0,1}) - 138(f_{3,-3,-2,3} + f_{3,3,-2,-3}) \right) \tag{C.75}
 \end{aligned}$$

The associated weight mask is shown in figure C.75.

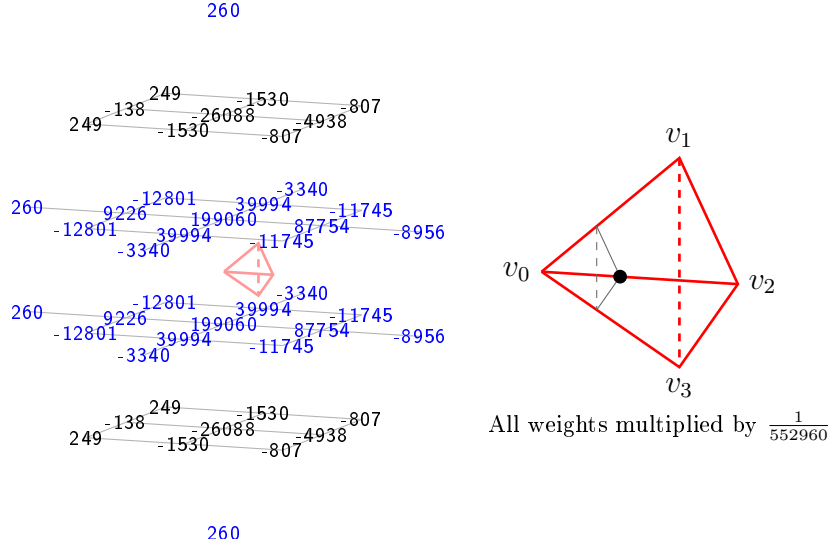


Figure C.75: Weight mask for c_{3020} . The associated domain point is shown in the teterahedron on the right. The black triangle symbolizes the ring $R_2(v_0)$.

$$\begin{aligned}
 c_{2300} := & \frac{1}{552960} \left(279048 f_{1,1,0,-1} + 140996 f_{1,-1,0,1} + 80852 (f_{-1,1,2,-1} + f_{-1,3,-2,1}) \right. \\
 & + 50166 (f_{-1,-1,2,1} + f_{-1,1,-2,3}) - 25660 f_{1,3,0,-3} - 21908 f_{1,-3,0,3} \\
 & - 11811 (f_{1,1,-4,3} + f_{1,-3,4,-1}) - 10851 f_{-3,1,0,3} \\
 & - 10196 (f_{-3,5,-4,3} + f_{-3,1,4,-1}) - 9810 f_{5,-1,0,-3} \\
 & + 9342 (f_{3,-1,-2,1} + f_{3,-3,2,-1}) - 9090 (f_{1,3,-4,1} + f_{1,-1,4,-3}) \\
 & + 8564 (f_{3,1,-2,-1} + f_{3,-1,2,-3}) - 7875 f_{5,-3,0,-1} - 4866 (f_{-1,5,-2,-1} + f_{-1,3,2,-3}) \\
 & - 3480 (f_{-3,-1,4,1} + f_{-3,3,-4,5}) - 2643 f_{-3,5,0,-1} - 2376 (f_{-1,-1,-2,5} + f_{-1,-3,2,3}) \\
 & - 1890 (f_{3,1,2,-5} + f_{3,3,-2,-3}) + 1300 f_{1,5,0,-5} + 1245 f_{5,1,0,-5} \\
 & - 696 f_{-3,-1,0,5} + 630 f_{-3,3,0,1} - 332 (f_{5,1,-4,-1} + f_{5,-3,4,-5}) \\
 & \left. - 168 (f_{-5,1,2,3} + f_{-5,3,2,1} + f_{-5,3,-2,5} + f_{-5,5,-2,3}) + 45 (f_{1,1,4,-5} + f_{1,5,-4,-1}) \right) \tag{C.76}
 \end{aligned}$$

The associated weight mask is shown in figure C.76.
B-coefficient c_{2003} is computed using (1, 3)-symmetry.

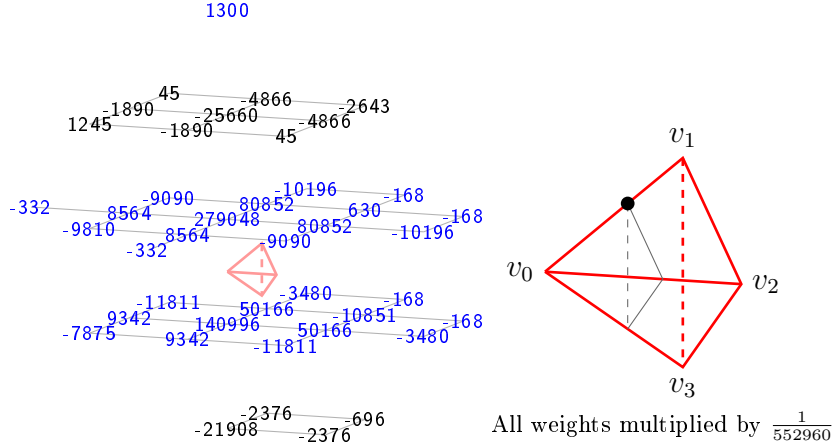


Figure C.76: Weight mask for c_{2300} . The associated domain point is shown in the teterahedron on the right. The black triangle symbolizes the ring $R_3(v_0)$.

$$\begin{aligned}
 c_{2210} := & \frac{1}{184320} \left(81660f_{1,1,0,-1} + 52496f_{1,-1,0,1} + 32272f_{-1,1,2,-1} \right. \\
 & + 23494f_{-1,-1,2,1} + 21908f_{-1,3,-2,1} + 15834f_{-1,1,-2,3} \\
 & - 8568f_{1,3,0,-3} - 7880f_{1,-3,0,3} + 7272f_{3,-1,2,-3} + 5350f_{3,-3,2,-1} \\
 & - 4623f_{1,-3,4,-1} - 4202f_{1,3,-4,1} - 4043f_{1,1,-4,3} - 3908f_{-3,1,4,-1} \\
 & - 3626f_{5,-1,0,-3} - 3567f_{-3,1,0,3} + 3274f_{3,-1,-2,1} - 3239f_{5,-3,0,-1} \\
 & - 3230f_{1,-1,4,-3} - 2444f_{-3,5,-4,3} - 1904f_{-3,-1,4,1} - 1642f_{-1,3,2,-3} \\
 & + 1564f_{3,1,-2,-1} - 1502f_{-1,5,-2,-1} - 1260f_{-1,-3,2,3} - 1208f_{-3,3,-4,5} \\
 & - 1034f_{-3,3,0,1} - 735f_{-3,5,0,-1} - 656f_{-1,-1,-2,5} - 626f_{3,1,2,-5} \\
 & - 556f_{5,-3,4,-5} - 320f_{-3,-1,0,5} + 260f_{1,5,0,-5} + 249f_{5,1,0,-5} \\
 & - 239f_{1,1,4,-5} + 205f_{1,5,-4,-1} - 182f_{3,3,-2,-3} - 136f_{5,-5,4,-3} \\
 & + 124f_{5,1,-4,-1} - 56(f_{-5,1,2,3} + f_{-5,3,2,1} + f_{-5,3,-2,5} + f_{-5,5,-2,3}) \\
 & \left. - 44(f_{3,-5,2,1} + f_{1,-5,4,1}) \right) \tag{C.77}
 \end{aligned}$$

The associated weight mask is shown in figure C.77.
B-coefficient c_{2012} is computed using (1, 3)-symmetry.

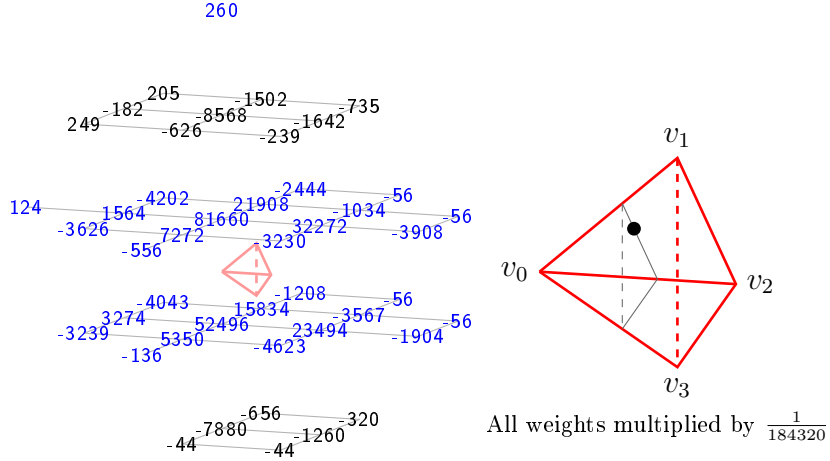


Figure C.77: Weight mask for c_{2210} . The associated domain point is shown in the tetrahedron on the right. The black triangle symbolizes the ring $R_3(v_0)$.

$$\begin{aligned}
 c_{2201} := & \frac{1}{552960} \left(210912f_{1,1,0,-1} + 173980f_{1,-1,0,1} + 81688(f_{-1,1,2,-1} + f_{-1,3,-2,1}) \right. \\
 & + 67818(f_{-1,-1,2,1} + f_{-1,1,-2,3}) - 25748f_{1,3,0,-3} - 25372f_{1,-3,0,3} \\
 & + 17944(f_{3,1,-2,-1} + f_{3,-1,2,-3}) + 16530(f_{3,-3,2,-1} + f_{3,-1,-2,1}) \\
 & - 14187(f_{1,1,-4,3} + f_{1,-3,4,-1}) - 13206(f_{1,3,-4,1} + f_{1,-1,4,-3}) \\
 & - 11946f_{5,-1,0,-3} - 11559f_{5,-3,0,-1} - 10551f_{-3,1,0,3} \\
 & - 8860(f_{-3,5,-4,3} + f_{-3,1,4,-1}) - 6834f_{-3,3,0,1} - 5856(f_{-3,-1,4,1} + f_{-3,3,-4,5}) \\
 & - 4566(f_{-1,5,-2,-1} + f_{-1,3,2,-3}) - 3372(f_{-1,-1,-2,5} + f_{-1,-3,2,3}) - 1767f_{-3,5,0,-1} \\
 & - 1224f_{-3,-1,0,5} - 964(f_{5,1,-4,-1} + f_{5,-3,4,-5}) - 534(f_{3,1,2,-5} + f_{3,3,-2,-3}) \\
 & - 408(f_{5,-1,-4,1} + f_{5,-5,4,-3}) + 260f_{1,5,0,-5} + 249f_{5,1,0,-5} \\
 & - 168(f_{-5,1,2,3} + f_{-5,3,2,1} + f_{-5,3,-2,5} + f_{-5,5,-2,3}) - 147(f_{1,5,-4,-1} + f_{1,1,4,-5}) \\
 & \left. - 132(f_{3,-5,2,1} + f_{3,-3,-2,3} + f_{1,-5,4,1} + f_{1,-1,-4,5}) \right) \quad (C.78)
 \end{aligned}$$

The associated weight mask is shown in figure C.78.
B-coefficient c_{2102} is computed using (1, 3)-symmetry.

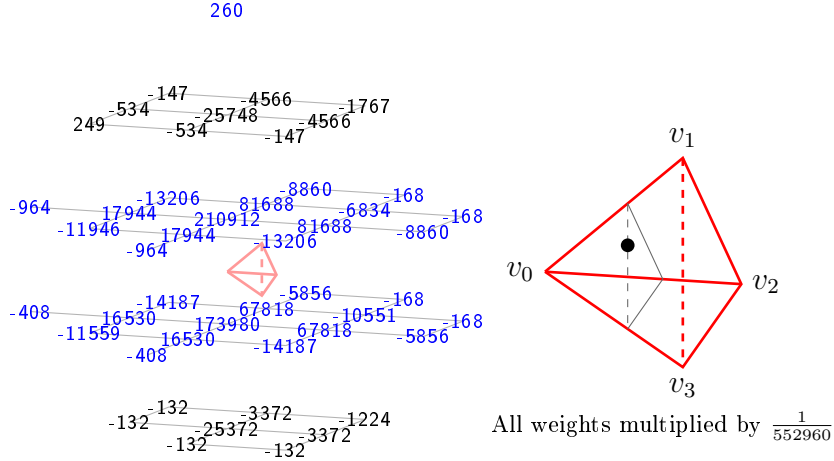


Figure C.78: Weight mask for c_{2201} . The associated domain point is shown in the teterahedron on the right. The black triangle symbolizes the ring $R_3(v_0)$.

$$\begin{aligned}
 c_{2120} := & \frac{1}{552960} \left(209832f_{1,1,0,-1} + 174748f_{1,-1,0,1} + 107692f_{-1,1,2,-1} \right. \\
 & + 91854f_{-1,-1,2,1} + 48268f_{-1,3,-2,1} + 40542f_{-1,1,-2,3} \\
 & + 30220f_{3,-1,2,-3} - 23524f_{1,-3,0,3} - 22964f_{1,3,0,-3} \\
 & + 22494f_{3,-3,2,-1} - 12772f_{-3,1,4,-1} - 12159f_{1,-3,4,-1} \\
 & - 11058f_{1,3,-4,1} - 10671f_{1,1,-4,3} - 9786f_{5,-1,0,-3} - 9399f_{5,-3,0,-1} \\
 & - 9096f_{-3,-1,4,1} - 8607f_{-3,1,0,3} - 7890f_{1,-1,4,-3} - 5784f_{-1,-3,2,3} \\
 & - 5730f_{-1,3,2,-3} - 5140f_{-3,5,-4,3} + 4926f_{3,-1,-2,1} - 4338f_{-3,3,0,1} \\
 & - 3768f_{-3,3,-4,5} - 3004f_{5,-3,4,-5} - 2898f_{-1,5,-2,-1} - 2175f_{-3,5,0,-1} \\
 & - 1866f_{3,1,2,-5} + 1756f_{3,1,-2,-1} - 1632f_{5,-5,4,-3} - 1560f_{-1,-1,-2,5} \\
 & - 1479f_{1,1,4,-5} - 1224f_{-3,-1,0,5} - 528(f_{1,-5,4,1} + f_{3,-5,2,1}) \\
 & + 260(f_{1,5,0,-5} + f_{5,1,-4,-1}) + 249(f_{5,1,0,-5} + f_{1,5,-4,-1}) \\
 & \left. - 168(f_{-5,1,2,3} + f_{-5,3,2,1} + f_{-5,3,-2,5} + f_{-5,5,-2,3}) - 138f_{3,3,-2,-3} \right) \quad (C.79)
 \end{aligned}$$

The associated weight mask is shown in figure C.79.
B-coefficient c_{2021} is computed using (1, 3)-symmetry.

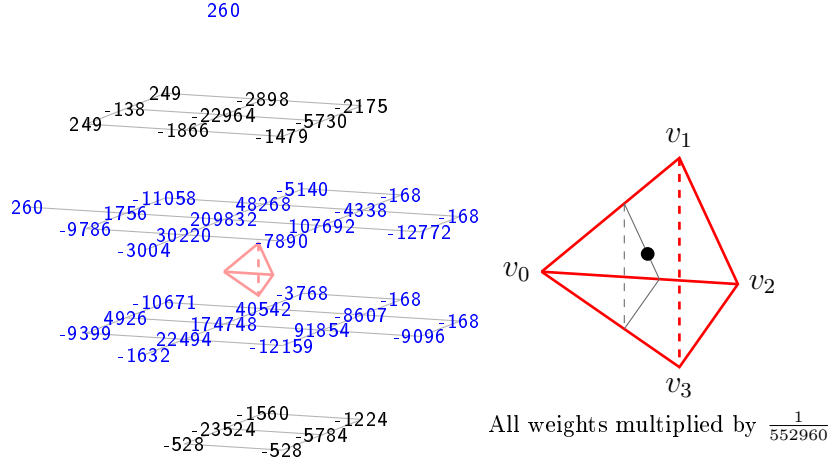
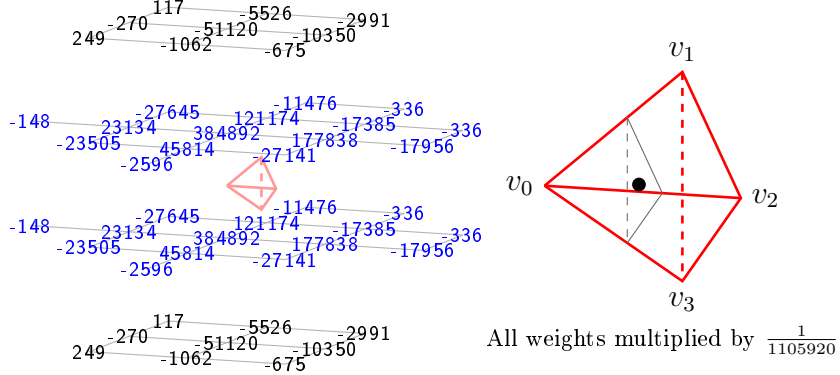


Figure C.79: Weight mask for c_{2120} . The associated domain point is shown in the tetrahedron on the right. The black triangle symbolizes the ring $R_3(v_0)$.

$$\begin{aligned}
 c_{2111} := & \frac{1}{1105920} \left(384892(f_{1,1,0,-1} + f_{1,-1,0,1}) + 177838(f_{-1,-1,2,1} + f_{-1,1,2,-1}) \right. \\
 & + 121174(f_{-1,1,-2,3} + f_{-1,3,-2,1}) - 51120(f_{1,-3,0,3} + f_{1,3,0,-3}) \\
 & + 45814(f_{3,-3,2,-1} + f_{3,-1,2,-3}) - 27645(f_{1,3,-4,1} + f_{1,1,-4,3}) \\
 & - 27141(f_{1,-1,4,-3} + f_{1,-3,4,-1}) - 23505(f_{5,-1,0,-3} + f_{5,-3,0,-1}) \\
 & + 23134(f_{3,-1,-2,1} + f_{3,1,-2,-1}) - 17956(f_{-3,-1,4,1} + f_{-3,1,4,-1}) \\
 & - 17385(f_{-3,1,0,3} + f_{-3,3,0,1}) - 11476(f_{-3,5,-4,3} + f_{-3,3,-4,5}) \\
 & - 10350(f_{-1,3,2,-3} + f_{-1,-3,2,3}) - 5526(f_{-1,5,-2,-1} + f_{-1,-1,-2,5}) \\
 & - 2991(f_{-3,-1,0,5} + f_{-3,5,0,-1}) - 2596(f_{5,-5,4,-3} + f_{5,-3,4,-5}) \\
 & - 1062(f_{3,1,2,-5} + f_{3,-5,2,1}) - 675(f_{1,1,4,-5} + f_{1,-5,4,1}) \\
 & - 336(f_{-5,5,-2,3} + f_{-5,1,2,3} + f_{-5,3,-2,5} + f_{-5,3,2,1}) - 270(f_{3,3,-2,-3} + f_{3,-3,-2,3}) \\
 & + 260(f_{1,5,0,-5} + f_{1,-5,0,5}) + 249(f_{5,1,0,-5} + f_{5,-5,0,1}) \\
 & \left. - 148(f_{5,1,-4,-1} + f_{5,-1,-4,1}) + 117(f_{1,5,-4,-1} + f_{1,-1,-4,5}) \right) \quad (C.80)
 \end{aligned}$$

The associated weight mask is shown in figure C.80.

260



260

Figure C.80: Weight mask for c_{2111} . The associated domain point is shown in the teterahedron on the right. The black triangle symbolizes the ring $R_3(v_0)$.

$$\begin{aligned}
 c_{2030} := & \frac{1}{23040} \left(7730(f_{1,1,0,-1} + f_{1,-1,0,1}) + 4658(f_{-1,-1,2,1} + f_{-1,1,2,-1}) \right. \\
 & + 1282(f_{-1,1,-2,3} + f_{3,-1,2,-3} + f_{3,-3,2,-1} + f_{-1,3,-2,1}) \\
 & - 850(f_{1,-3,0,3} + f_{1,3,0,-3}) - 538(f_{-3,-1,4,1} + f_{-3,1,4,-1}) \\
 & - 319(f_{1,3,-4,1} + f_{5,-1,0,-3} + f_{5,-3,0,-1} + f_{1,1,-4,3}) - 274(f_{-1,-3,2,3} + f_{-1,3,2,-3}) \\
 & - 198(f_{1,-3,4,-1} + f_{-3,1,0,3} + f_{-3,3,0,1} + f_{1,-1,4,-3}) \\
 & - 143(f_{-3,5,-4,3} + f_{-3,3,-4,5} + f_{5,-5,4,-3} + f_{5,-3,4,-5}) - 106(f_{3,1,-2,-1} + f_{3,-1,-2,1}) \\
 & - 79(f_{3,1,2,-5} + f_{-1,-1,-2,5} + f_{1,1,4,-5} + f_{-1,5,-2,-1} + f_{3,-5,2,1} + f_{-3,5,0,-1} \\
 & \quad + f_{1,-5,4,1} + f_{-3,-1,0,5}) \\
 & \left. - 7(f_{3,-3,6,-5} + f_{3,-5,6,-3} + f_{-1,-3,6,-1} + f_{-5,1,2,3} + f_{-1,-1,6,-3} + f_{-5,3,2,1} \right. \\
 & \quad \left. + f_{-5,3,-2,5} + f_{-5,5,-2,3}) \right) \tag{C.81}
 \end{aligned}$$

The associated weight mask is shown in figure C.81.

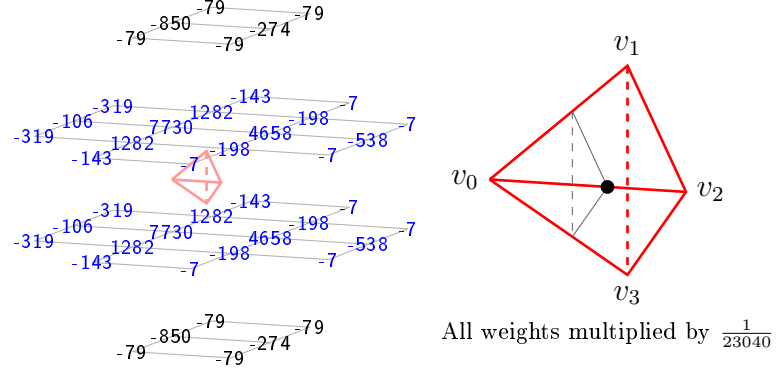


Figure C.81: Weight mask for c_{2030} . The associated domain point is shown in the tetrahedron on the right. The black triangle symbolizes the ring $R_3(v_0)$.

$$\begin{aligned}
 c_{1400} := & \frac{1}{138240} \left(67137f_{1,1,0,-1} + 32203f_{1,-1,0,1} + 24163(f_{-1,1,2,-1} + f_{-1,3,-2,1}) \right. \\
 & + 10983(f_{-1,-1,2,1} + f_{-1,1,-2,3}) - 4753f_{1,-3,0,3} + 4341f_{-3,3,0,1} \\
 & - 3857f_{1,3,0,-3} - 3415(f_{-3,1,4,-1} + f_{-3,5,-4,3}) - 2340(f_{1,1,-4,3} + f_{1,-3,4,-1}) \\
 & - 1902f_{-3,1,0,3} - 1428f_{-3,5,0,-1} - 1344f_{5,-1,0,-3} \\
 & - 1317(f_{1,3,-4,1} + f_{1,-1,4,-3}) - 1149(f_{-1,5,-2,-1} + f_{-1,3,2,-3}) - 957f_{5,-3,0,-1} \\
 & - 759(f_{-3,-1,4,1} + f_{-3,3,-4,5}) - 621(f_{-1,-3,2,3} + f_{-1,-1,-2,5}) \\
 & - 606(f_{3,3,-2,-3} + f_{3,1,2,-5}) + 249f_{5,1,0,-5} \\
 & - 219(f_{-5,3,2,1} + f_{-5,5,-2,3} + f_{1,5,-4,-1} + f_{1,1,4,-5}) - 191(f_{3,-1,2,-3} + f_{3,1,-2,-1}) \\
 & - 183f_{-3,-1,0,5} + 158f_{1,5,0,-5} + 141(f_{3,-3,2,-1} + f_{3,-1,-2,1}) \\
 & \left. - 117(f_{-5,1,2,3} + f_{-5,3,-2,5}) - 46(f_{5,1,-4,-1} + f_{5,-3,4,-5}) \right) \quad (C.82)
 \end{aligned}$$

The associated weight mask is shown in figure C.82.
B-coefficient c_{1004} is computed using (1, 3)-symmetry.

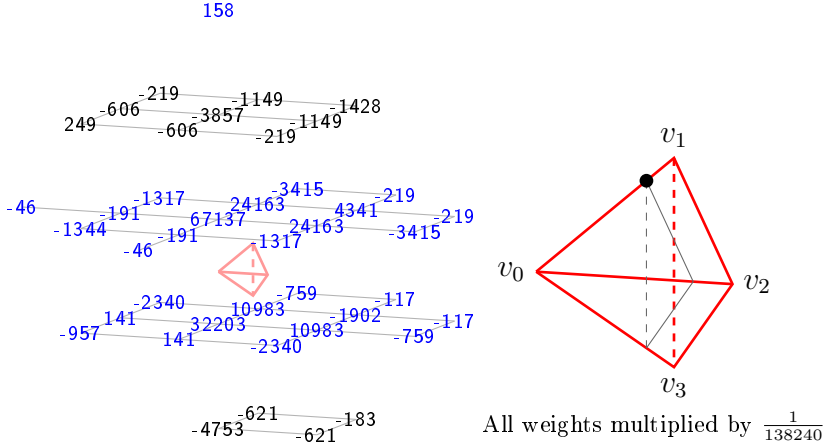


Figure C.82: Weight mask for c_{1400} . The associated domain point is shown in the teterahedron on the right. The black triangle symbolizes the ring $R_4(v_0)$.

$$\begin{aligned}
 c_{1310} := & \frac{1}{1105920} \left(484680f_{1,1,0,-1} + 288236f_{1,-1,0,1} + 224780f_{-1,1,2,-1} \right. \\
 & + 159596f_{-1,3,-2,1} + 131226f_{-1,-1,2,1} + 80718f_{-1,1,-2,3} \\
 & - 42056f_{1,-3,0,3} - 36328f_{1,3,0,-3} - 30812f_{-3,1,4,-1} \\
 & + 24954f_{-3,3,0,1} - 24003f_{1,-3,4,-1} + 22328f_{3,-1,2,-3} \\
 & - 20648f_{-3,5,-4,3} - 19038f_{1,3,-4,1} - 18219f_{1,1,-4,3} \\
 & - 13083f_{-3,1,0,3} - 12894f_{5,-1,0,-3} - 12726f_{-1,5,-2,-1} \\
 & - 10959f_{5,-3,0,-1} - 10554f_{1,-1,4,-3} - 10152f_{-3,-1,4,1} \\
 & - 9411f_{-3,5,0,-1} - 9196f_{3,1,-2,-1} - 8220f_{-1,-3,2,3} + 7914f_{3,-3,2,-1} \\
 & - 7866f_{-1,3,2,-3} - 6324f_{-3,3,-4,5} - 5370f_{3,1,2,-5} + 4290f_{3,-1,-2,1} \\
 & - 4116f_{-1,-1,-2,5} - 3435f_{1,1,4,-5} - 2372f_{5,-3,4,-5} - 2028f_{-3,-1,0,5} \\
 & - 1788f_{-5,5,-2,3} - 1512f_{-5,3,2,1} + 1245f_{5,1,0,-5} - 1104f_{-5,1,2,3} \\
 & - 1086f_{3,3,-2,-3} - 972f_{-5,3,-2,5} + 892f_{1,5,0,-5} + 849f_{1,5,-4,-1} \\
 & \left. + 484f_{5,1,-4,-1} \right) \tag{C.83}
 \end{aligned}$$

The associated weight mask is shown in figure C.83.
B-coefficient c_{1013} is computed using (1, 3)-symmetry.

892

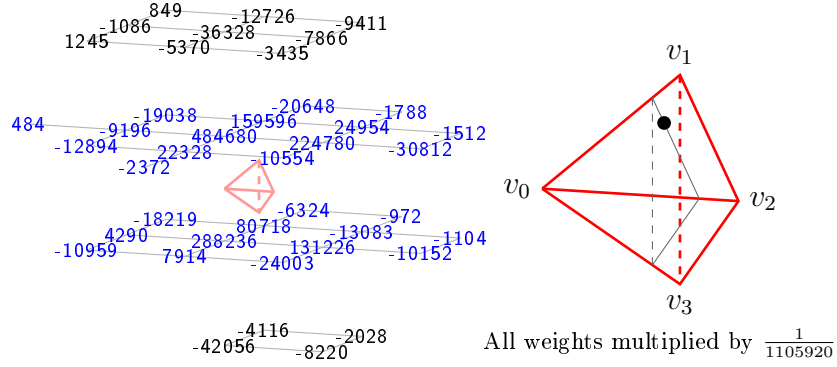


Figure C.83: Weight mask for c_{1310} . The associated domain point is shown in the teterahedron on the right. The black triangle symbolizes the ring $R_4(v_0)$.

$$\begin{aligned}
 c_{1310} := & \frac{1}{552960} \left(216132f_{1,1,0,-1} + 159424f_{1,-1,0,1} + 95536(f_{-1,1,2,-1} + f_{-1,3,-2,1}) \right. \\
 & + 62040(f_{-1,-1,2,1} + f_{-1,1,-2,3}) - 23044f_{1,-3,0,3} - 20900f_{1,3,0,-3} \\
 & - 12070(f_{-3,1,4,-1} + f_{-3,5,-4,3}) - 11751(f_{1,1,-4,3} + f_{1,-3,4,-1}) \\
 & - 9528(f_{1,-1,4,-3} + f_{1,3,-4,1}) + 7590f_{-3,3,0,1} - 7518f_{5,-1,0,-3} \\
 & + 7330(f_{3,-1,2,-3} + f_{3,1,-2,-1}) - 7131f_{5,-3,0,-1} - 5700(f_{-1,5,-2,-1} + f_{-1,3,2,-3}) \\
 & + 5538(f_{3,-3,2,-1} + f_{3,-1,-2,1}) - 5475f_{-3,1,0,3} - 5202(f_{-3,-1,4,1} + f_{-3,3,-4,5}) \\
 & - 3699f_{-3,5,0,-1} - 3684(f_{-1,-1,-2,5} + f_{-1,-3,2,3}) - 1296f_{-3,-1,0,5} \\
 & - 804(f_{3,3,-2,-3} + f_{3,1,2,-5}) - 774(f_{-5,3,2,1} + f_{-5,5,-2,3}) \\
 & - 760(f_{5,1,-4,-1} + f_{5,-3,4,-5}) - 570(f_{-5,1,2,3} + f_{-5,3,-2,5}) \\
 & \left. - 417(f_{1,5,-4,-1} + f_{1,1,4,-5}) + 260f_{1,5,0,-5} + 249f_{5,1,0,-5} \right) \quad (C.84)
 \end{aligned}$$

The associated weight mask is shown in figure C.84.
B-coefficient c_{1103} is computed using (1, 3)-symmetry.

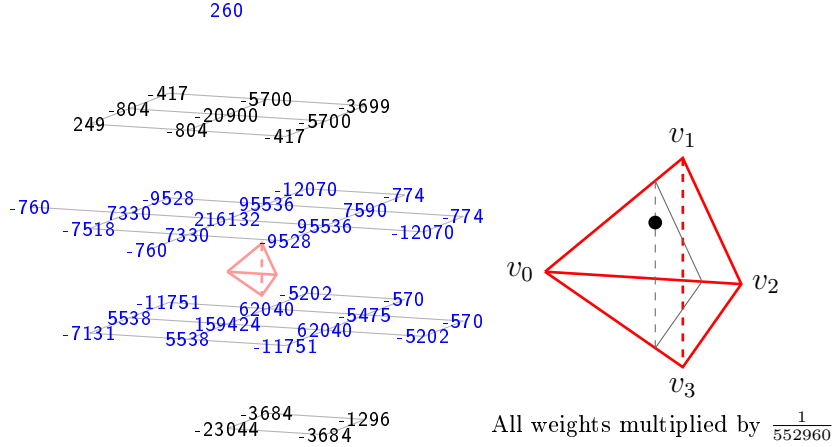


Figure C.84: Weight mask for c_{1301} . The associated domain point is shown in the teterahedron on the right. The black triangle symbolizes the ring $R_4(v_0)$.

$$\begin{aligned}
 c_{1220} := & \frac{1}{552960} \left(212136f_{1,1,0,-1} + 159124f_{1,-1,0,1} + 124900f_{-1,1,2,-1} \right. \\
 & + 90126f_{-1,-1,2,1} + 59008f_{-1,3,-2,1} + 35142f_{-1,1,-2,3} \\
 & - 21400f_{1,-3,0,3} + 20344f_{3,-1,2,-3} - 17384f_{1,3,0,-3} \\
 & - 16192f_{-3,1,4,-1} - 12435f_{1,-3,4,-1} + 9342f_{-3,3,0,1} - 8970f_{1,3,-4,1} \\
 & - 8583f_{1,1,-4,3} - 8196f_{-3,-1,4,1} + 7542f_{3,-3,2,-1} - 7108f_{-3,5,-4,3} \\
 & - 6540f_{-1,-3,2,3} - 6438f_{5,-1,0,-3} - 6051f_{5,-3,0,-1} - 5840f_{3,1,-2,-1} \\
 & - 5238f_{-1,5,-2,-1} - 4827f_{-3,1,0,3} - 4758f_{-1,3,2,-3} - 4515f_{-3,5,0,-1} \\
 & - 3762f_{1,-1,4,-3} - 3288f_{-3,3,-4,5} - 2946f_{3,1,2,-5} - 2559f_{1,1,4,-5} \\
 & - 2188f_{5,-3,4,-5} - 1632f_{-1,-1,-2,5} - 1296f_{-3,-1,0,5} - 912f_{-5,5,-2,3} \\
 & - 636(f_{-5,1,2,3} + f_{-5,3,2,1}) - 504f_{-5,3,-2,5} - 408f_{5,-5,4,-3} \\
 & + 260(f_{5,1,-4,-1} + f_{1,5,0,-5}) + 249(f_{5,1,0,-5} + f_{1,5,-4,-1}) - 138f_{3,3,-2,-3} \\
 & \left. - 132(f_{3,-5,2,1} + f_{1,-5,4,1}) - 78f_{3,-1,-2,1} \right) \tag{C.85}
 \end{aligned}$$

The associated weight mask is shown in figure C.85.
B-coefficient c_{1022} is computed using (1, 3)-symmetry.

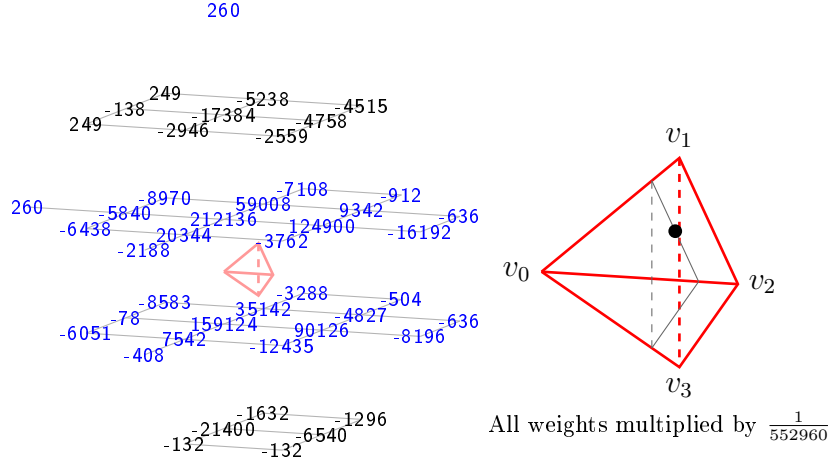


Figure C.85: Weight mask for c_{1220} . The associated domain point is shown in the tetrahedron on the right. The black triangle symbolizes the ring $R_4(v_0)$.

$$\begin{aligned}
 c_{1211} := & \frac{1}{1105920} \left(399516f_{1,1,0,-1} + 342808f_{1,-1,0,1} + 210904f_{-1,1,2,-1} \right. \\
 & + 173838f_{-1,-1,2,1} + 144304f_{-1,3,-2,1} + 114378f_{-1,1,-2,3} \\
 & - 46396f_{1,-3,0,3} - 44252f_{1,3,0,-3} + 26812f_{3,-1,2,-3} \\
 & - 24819f_{1,-3,4,-1} - 24736f_{-3,1,4,-1} - 22899f_{1,1,-4,3} \\
 & - 22602f_{1,3,-4,1} - 20670f_{1,-1,4,-3} + 20406f_{3,-3,2,-1} \\
 & - 16860f_{-3,-1,4,1} - 16732f_{-3,5,-4,3} - 16110f_{5,-1,0,-3} \\
 & - 15723f_{5,-3,0,-1} - 12726f_{-1,3,2,-3} - 11616f_{-1,-3,2,3} \\
 & - 10872f_{-3,3,-4,5} - 8826f_{-1,5,-2,-1} + 8790f_{3,-1,-2,1} + 7014f_{-3,3,0,1} \\
 & - 6051f_{-3,1,0,3} + 5968f_{3,1,-2,-1} - 5955f_{-3,5,0,-1} - 5904f_{-1,-1,-2,5} \\
 & - 3552f_{-3,-1,0,5} - 2188f_{5,-3,4,-5} - 1602f_{3,1,2,-5} - 1584f_{-5,5,-2,3} \\
 & - 1308(f_{-5,3,2,1} + f_{-5,1,2,3}) - 1215f_{1,1,4,-5} - 1176f_{-5,3,-2,5} \\
 & - 816f_{5,-5,4,-3} - 270f_{3,3,-2,-3} - 264(f_{3,-5,2,1} + f_{1,-5,4,1}) + 260f_{1,5,0,-5} \\
 & \left. + 249f_{5,1,0,-5} - 148f_{5,1,-4,-1} + 117f_{1,5,-4,-1} \right) \quad (C.86)
 \end{aligned}$$

The associated weight mask is shown in figure C.86.
B-coefficient c_{1112} is computed using (1, 3)-symmetry.

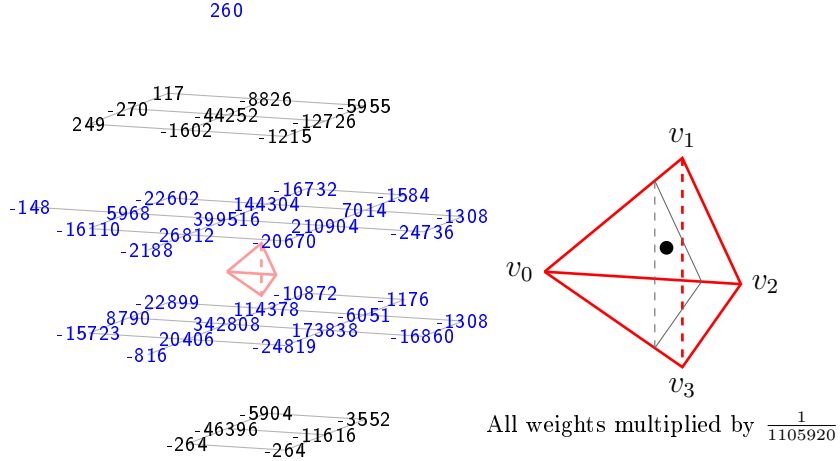


Figure C.86: Weight mask for c_{1211} . The associated domain point is shown in the teterahedron on the right. The black triangle symbolizes the ring $R_4(v_0)$.

$$\begin{aligned}
 c_{1202} := & \frac{1}{46080} \left(15282(f_{1,1,0,-1} + f_{1,-1,0,1}) \right. \\
 & + 6839(f_{-1,-1,2,1} + f_{-1,1,2,-1} + f_{-1,1,-2,3} + f_{-1,3,-2,1}) \\
 & - 1946(f_{1,-3,0,3} + f_{1,3,0,-3}) \\
 & - 1009(f_{1,-1,4,-3} + f_{1,1,-4,3} + f_{1,3,-4,1} + f_{1,-3,4,-1}) \\
 & + 755(f_{3,1,-2,-1} + f_{3,-3,2,-1} + f_{3,-1,2,-3} + f_{3,-1,-2,1}) \\
 & - 722(f_{-3,5,-4,3} + f_{-3,3,-4,5} + f_{-3,-1,4,1} + f_{-3,1,4,-1}) - 716(f_{5,-1,0,-3} + f_{5,-3,0,-1}) \\
 & - 423(f_{-1,5,-2,-1} + f_{-1,3,2,-3} + f_{-1,-3,2,3} + f_{-1,-1,-2,5}) - 188(f_{-3,-1,0,5} + f_{-3,5,0,-1}) \\
 & - 56(f_{-5,1,2,3} + f_{-5,3,2,1} + f_{-5,3,-2,5} + f_{-5,5,-2,3}) - 48(f_{-3,3,0,1} + f_{-3,1,0,3}) \\
 & - 34(f_{5,1,-4,-1} + f_{5,-3,4,-5} + f_{5,-1,-4,1} + f_{5,-5,4,-3}) \\
 & - 11(f_{3,-5,2,1} + f_{3,3,-2,-3} + f_{3,-3,-2,3} + f_{3,1,2,-5} + f_{1,-1,-4,5} + f_{1,1,4,-5} \\
 & \quad \left. + f_{1,5,-4,-1} + f_{1,-5,4,1} \right) \tag{C.87}
 \end{aligned}$$

The associated weight mask is shown in figure C.87.

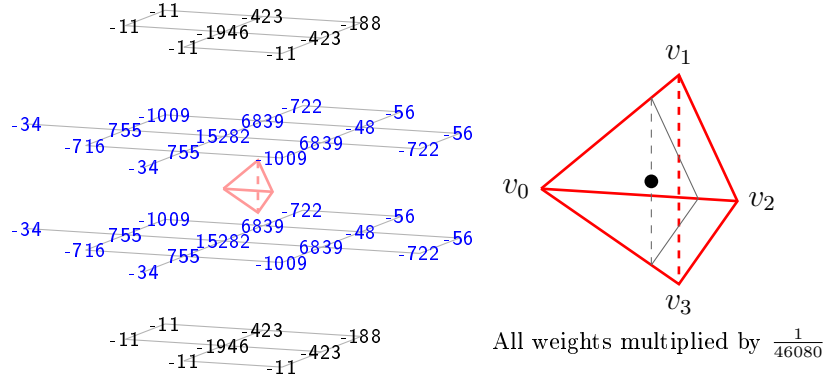


Figure C.87: Weight mask for c_{1202} . The associated domain point is shown in the teterahedron on the right. The black triangle symbolizes the ring $R_4(v_0)$.

$$\begin{aligned}
 c_{1130} := & \frac{1}{92160} \left(31286f_{1,1,0,-1} + 28298f_{1,-1,0,1} + 22154f_{-1,1,2,-1} \right. \\
 & + 18998f_{-1,-1,2,1} + 6377f_{-1,3,-2,1} + 4609f_{-1,1,-2,3} + 3863f_{3,-1,2,-3} \\
 & - 3304f_{1,-3,0,3} - 2728f_{1,3,0,-3} - 2680f_{-3,1,4,-1} + 2095f_{3,-3,2,-1} \\
 & - 1960f_{-3,-1,4,1} - 1432f_{-1,-3,2,3} - 1367f_{1,-3,4,-1} - 1240f_{3,1,-2,-1} \\
 & - 1144f_{-1,3,2,-3} - 1105(f_{1,1,-4,3} + f_{1,3,-4,1}) + 959f_{-3,3,0,1} \\
 & - 895(f_{5,-1,0,-3} + f_{5,-3,0,-1}) - 808f_{3,-1,-2,1} - 750f_{-3,5,-4,3} \\
 & - 592(f_{-1,5,-2,-1} + f_{-3,5,0,-1}) - 512f_{-3,3,-4,5} - 456f_{5,-3,4,-5} \\
 & - 448(f_{3,1,2,-5} + f_{1,1,4,-5}) - 280(f_{-3,-1,0,5} + f_{-1,-1,-2,5}) - 233f_{-3,1,0,3} \\
 & - 218f_{5,-5,4,-3} - 175f_{1,-1,4,-3} - 138f_{-5,5,-2,3} - 136(f_{3,-5,2,1} + f_{1,-5,4,1}) \\
 & - 104f_{-5,3,-2,5} - 103(f_{-5,1,2,3} + f_{-5,3,2,1}) - 48f_{3,-3,6,-5} \\
 & \left. - 25(f_{-1,-1,6,-3} + f_{-1,-3,6,-1}) - 14f_{3,-5,6,-3} \right) \quad (C.88)
 \end{aligned}$$

The associated weight mask is shown in figure C.88.
B-coefficient c_{1031} is computed using (1, 3)-symmetry.

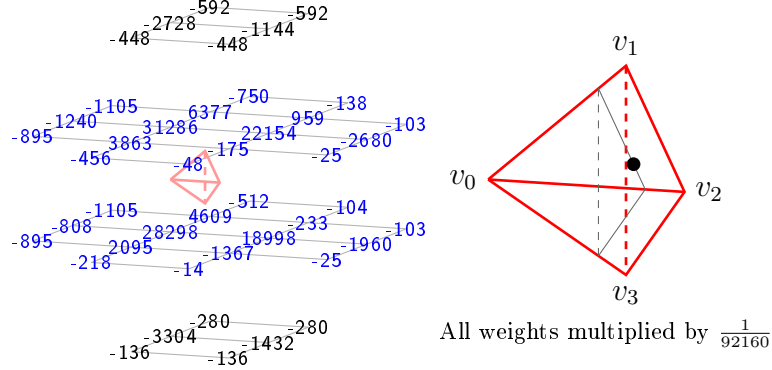


Figure C.88: Weight mask for c_{1130} . The associated domain point is shown in the teterahedron on the right. The black triangle symbolizes the ring $R_4(v_0)$.

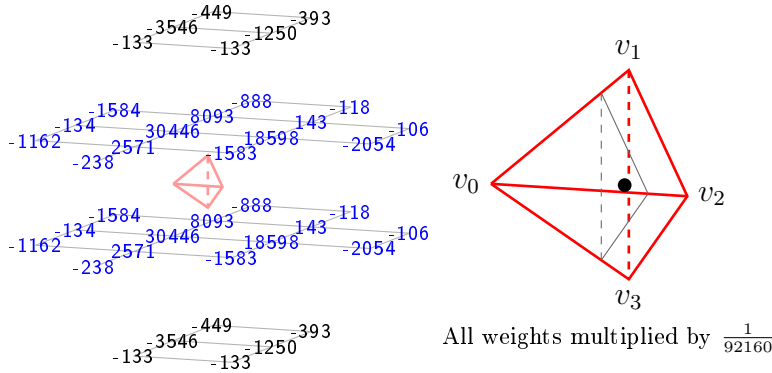


Figure C.89: Weight mask for c_{1121} . The associated domain point is shown in the teterahedron on the right. The black triangle symbolizes the ring $R_4(v_0)$.

$$\begin{aligned}
 c_{1121} := & \frac{1}{92160} \left(30446(f_{1,1,0,-1} + f_{1,-1,0,1}) + 18598(f_{-1,-1,2,1} + f_{-1,1,2,-1}) \right. \\
 & + 8093(f_{-1,1,-2,3} + f_{-1,3,-2,1}) - 3546(f_{1,-3,0,3} + f_{1,3,0,-3}) \\
 & + 2571(f_{3,-3,2,-1} + f_{3,-1,2,-3}) - 2054(f_{-3,1,4,-1} + f_{-3,-1,4,1}) \\
 & - 1584(f_{1,1,-4,3} + f_{1,3,-4,1}) - 1583(f_{1,-3,4,-1} + f_{1,-1,4,-3}) \\
 & - 1250(f_{-1,3,2,-3} + f_{-1,-3,2,3}) - 1162(f_{5,-3,0,-1} + f_{5,-1,0,-3}) \\
 & - 888(f_{-3,5,-4,3} + f_{-3,3,-4,5}) - 449(f_{-1,5,-2,-1} + f_{-1,-1,-2,5}) \\
 & - 393(f_{-3,-1,0,5} + f_{-3,5,0,-1}) - 238(f_{5,-5,4,-3} + f_{5,-3,4,-5}) \\
 & + 143(f_{-3,3,0,1} + f_{-3,1,0,3}) - 134(f_{3,1,-2,-1} + f_{3,-1,-2,1}) \\
 & - 133(f_{3,1,2,-5} + f_{3,-5,2,1} + f_{1,-5,4,1} + f_{1,1,4,-5}) - 118(f_{-5,3,-2,5} + f_{-5,5,-2,3}) \\
 & \left. - 106(f_{-5,1,2,3} + f_{-5,3,2,1}) \right) \tag{C.89}
 \end{aligned}$$

The associated weight mask is shown in figure C.89.

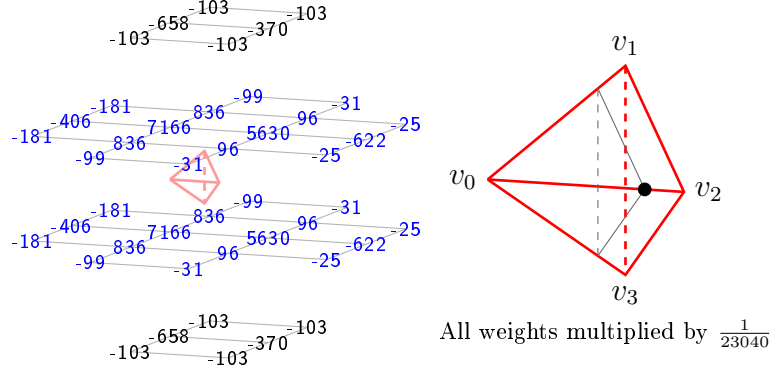


Figure C.90: Weight mask for c_{1040} . The associated domain point is shown in the tetrahedron on the right. The black triangle symbolizes the ring $R_4(v_0)$.

$$\begin{aligned}
 c_{1040} := & \frac{1}{23040} \left(7166(f_{1,1,0,-1} + f_{1,-1,0,1}) + 5630(f_{-1,-1,2,1} + f_{-1,1,2,-1}) \right. \\
 & + 836(f_{-1,1,-2,3} + f_{3,-3,2,-1} + f_{3,-1,2,-3} + f_{-1,3,-2,1}) - 658(f_{1,-3,0,3} + f_{1,3,0,-3}) \\
 & - 622(f_{-3,1,4,-1} + f_{-3,-1,4,1}) - 406(f_{3,-1,-2,1} + f_{3,1,-2,-1}) \\
 & - 370(f_{-1,3,2,-3} + f_{-1,-3,2,3}) - 181(f_{5,-3,0,-1} + f_{1,3,-4,1} + f_{5,-1,0,-3} + f_{1,1,-4,3}) \\
 & - 103(f_{-1,-1,-2,5} + f_{3,-5,2,1} + f_{-3,5,0,-1} + f_{3,1,2,-5} + f_{1,1,4,-5} + f_{-3,-1,0,5} \\
 & \quad + f_{-1,5,-2,-1} + f_{1,-5,4,1}) \\
 & - 99(f_{5,-5,4,-3} + f_{5,-3,4,-5} + f_{-3,5,-4,3} + f_{-3,3,-4,5}) \\
 & + 96(f_{-3,1,0,3} + f_{-3,3,0,1} + f_{1,-3,4,-1} + f_{1,-1,4,-3}) \\
 & - 31(f_{3,-3,6,-5} + f_{3,-5,6,-3} + f_{-5,3,-2,5} + f_{-5,5,-2,3}) \\
 & \left. - 25(f_{-1,-3,6,-1} + f_{-5,1,2,3} + f_{-5,3,2,1} + f_{-1,-1,6,-3}) \right) \tag{C.90}
 \end{aligned}$$

The associated weight mask is shown in figure C.90.

$$\begin{aligned}
 c_{0500} := & \frac{1}{184320} \left(83712f_{1,1,0,-1} + 37028(f_{-1,1,2,-1} + f_{1,-1,0,1} + f_{-1,3,-2,1}) \right. \\
 & + 12902(f_{-1,-1,2,1} + f_{-1,1,-2,3} + f_{-3,3,0,1}) \\
 & - 5228(f_{-3,5,-4,3} + f_{1,-3,0,3} + f_{-3,1,4,-1}) \\
 & - 2711(f_{-3,5,0,-1} + f_{1,1,-4,3} + f_{1,-3,4,-1}) \\
 & - 1948(f_{3,1,-2,-1} + f_{3,-1,2,-3} + f_{1,3,0,-3}) - 1671f_{-3,1,0,3} \\
 & - 1226(f_{3,-3,2,-1} + f_{3,-1,-2,1} + f_{-1,5,-2,-1} + f_{1,3,-4,1} + f_{-1,3,2,-3} + f_{1,-1,4,-3}) \\
 & - 986(f_{3,1,2,-5} + f_{5,-1,0,-3} + f_{3,3,-2,-3}) \\
 & - 864(f_{-3,3,-4,5} + f_{-5,5,-2,3} + f_{-5,3,2,1} + f_{-1,-1,-2,5} + f_{-1,-3,2,3} + f_{-3,-1,4,1}) \\
 & - 599(f_{1,5,-4,-1} + f_{1,1,4,-5} + f_{5,-3,0,-1}) - 256(f_{-5,1,2,3} + f_{-5,3,-2,5} + f_{-3,-1,0,5}) \\
 & \left. + 249f_{5,1,0,-5} - 12(f_{5,1,-4,-1} + f_{1,5,0,-5} + f_{5,-3,4,-5}) \right) \tag{C.91}
 \end{aligned}$$

The associated weight mask is shown in figure C.91.

B-coefficient c_{0005} is computed using (1, 3)-symmetry.

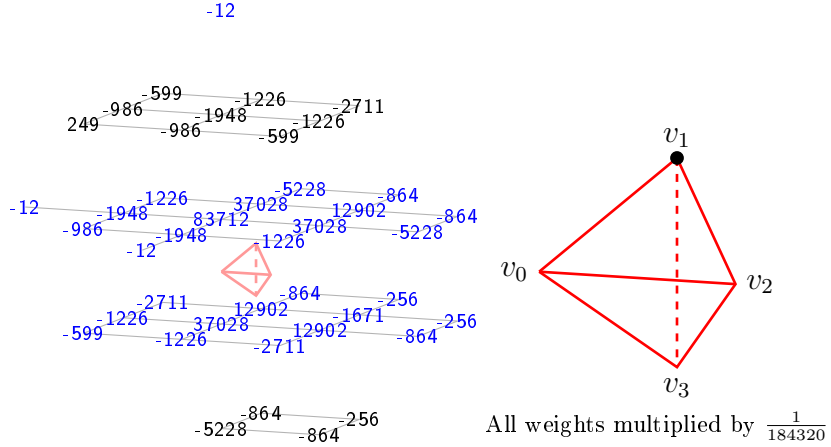


Figure C.91: Weight mask for c_{0500} . The associated domain point is shown in the teterahedron on the right.

$$\begin{aligned}
 c_{0410} := & \frac{1}{276480} \left(116862f_{1,1,0,-1} + 62758(f_{-1,1,2,-1} + f_{1,-1,0,1}) + 46678f_{-1,3,-2,1} \right. \\
 & + 30024f_{-1,-1,2,1} + 16740(f_{-1,1,-2,3} + f_{-3,3,0,1}) \\
 & - 8854(f_{-3,1,4,-1} + f_{1,-3,0,3}) - 6178f_{-3,5,-4,3} - 5462(f_{3,1,-2,-1} + f_{1,3,0,-3}) \\
 & - 5277f_{1,-3,4,-1} - 3960(f_{1,3,-4,1} + f_{-1,5,-2,-1}) - 3453(f_{-3,5,0,-1} + f_{1,1,-4,3}) \\
 & - 2154(f_{-1,-3,2,3} + f_{-3,-1,4,1}) + 1870f_{3,-1,2,-3} - 1746(f_{5,-1,0,-3} + f_{3,1,2,-5}) \\
 & - 1380(f_{3,-3,2,-1} + f_{1,-1,4,-3}) - 1359(f_{5,-3,0,-1} + f_{1,1,4,-5}) \\
 & - 1350(f_{-5,5,-2,3} + f_{-3,3,-4,5}) - 1209f_{-3,1,0,3} - 1074(f_{-5,3,2,1} + f_{-1,-1,-2,5}) \\
 & - 1044(f_{3,-1,-2,1} + f_{-1,3,2,-3}) - 534(f_{-3,-1,0,5} + f_{-5,1,2,3}) - 402f_{-5,3,-2,5} \\
 & - 352f_{5,-3,4,-5} - 270f_{3,3,-2,-3} + 249f_{5,1,0,-5} + 117f_{1,5,-4,-1} \\
 & \left. + 56(f_{1,5,0,-5} + f_{5,1,-4,-1}) \right) \tag{C.92}
 \end{aligned}$$

The associated weight mask is shown in figure C.92.
B-coefficient c_{0014} is computed using (1, 3)-symmetry.

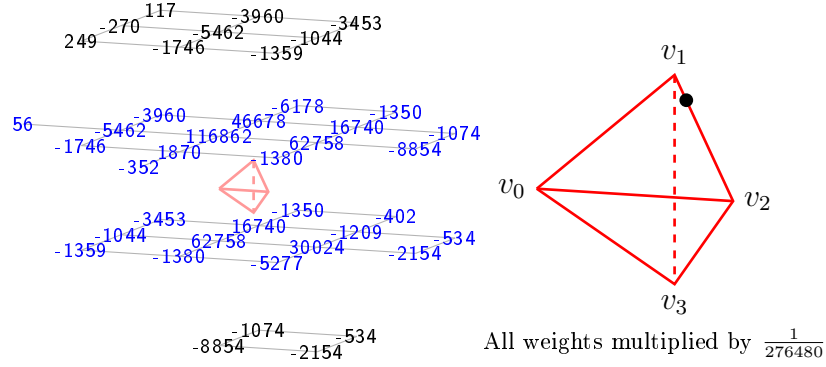


Figure C.92: Weight mask for c_{0410} . The associated domain point is shown in the teterahedron on the right.

$$\begin{aligned}
 c_{0401} := & \frac{1}{552960} \left(216312f_{1,1,0,-1} + 139948f_{1,-1,0,1} + 107788(f_{-1,1,2,-1} + f_{-1,3,-2,1}) \right. \\
 & + 54822(f_{-1,-1,2,1} + f_{-1,1,-2,3}) + 28254f_{-3,3,0,1} - 19732f_{1,-3,0,3} \\
 & - 16004f_{1,3,0,-3} - 14380(f_{-3,5,-4,3} + f_{-3,1,4,-1}) \\
 & - 9327(f_{1,1,-4,3} + f_{1,-3,4,-1}) - 7002(f_{1,-1,4,-3} + f_{1,3,-4,1}) \\
 & - 6330(f_{-1,3,2,-3} + f_{-1,5,-2,-1}) - 5679f_{-3,5,0,-1} - 4416(f_{-3,3,-4,5} + f_{-3,-1,4,1}) \\
 & - 4026f_{5,-1,0,-3} - 3864(f_{-1,-3,2,3} + f_{-1,-1,-2,5}) - 3639f_{5,-3,0,-1} \\
 & - 2256(f_{-5,3,2,1} + f_{-5,5,-2,3}) - 1368f_{-3,-1,0,5} - 1340(f_{3,-1,2,-3} + f_{3,1,-2,-1}) \\
 & - 1170(f_{3,-3,2,-1} + f_{3,-1,-2,1}) - 1104(f_{-5,1,2,3} + f_{-5,3,-2,5}) \\
 & - 1074(f_{3,1,2,-5} + f_{3,3,-2,-3}) - 687(f_{1,5,-4,-1} + f_{1,1,4,-5}) \\
 & \left. - 556(f_{5,1,-4,-1} + f_{5,-3,4,-5}) + 260f_{1,5,0,-5} + 249f_{5,1,0,-5} + 177f_{-3,1,0,3} \right) \tag{C.93}
 \end{aligned}$$

The associated weight mask is shown in figure C.93.
B-coefficient c_{0104} is computed using (1, 3)-symmetry.

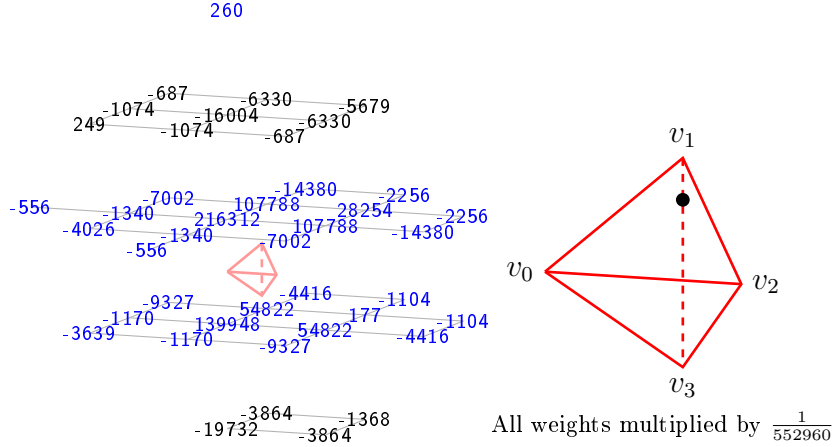


Figure C.93: Weight mask for c_{0401} . The associated domain point is shown in the teterahedron on the right.

$$\begin{aligned}
 c_{0320} := & \frac{1}{552960} \left(209400f_{1,1,0,-1} + 138580(f_{-1,1,2,-1} + f_{1,-1,0,1}) + 85998f_{-1,-1,2,1} \right. \\
 & + 70084f_{-1,3,-2,1} + 29262(f_{-1,1,-2,3} + f_{-3,3,0,1}) \\
 & - 18292(f_{-3,1,4,-1} + f_{1,-3,0,3}) + 12676f_{3,-1,2,-3} - 12327f_{1,-3,4,-1} \\
 & - 11756(f_{1,3,0,-3} + f_{3,1,-2,-1}) - 8596f_{-3,5,-4,3} \\
 & - 7626(f_{1,3,-4,1} + f_{-1,5,-2,-1}) - 7032(f_{-1,-3,2,3} + f_{-3,-1,4,1}) \\
 & - 6903(f_{1,1,-4,3} + f_{-3,5,0,-1}) - 4026(f_{3,1,2,-5} + f_{5,-1,0,-3}) \\
 & - 3639(f_{1,1,4,-5} + f_{5,-3,0,-1}) - 2808(f_{-3,3,-4,5} + f_{-5,5,-2,3}) \\
 & - 2730(f_{3,-1,-2,1} + f_{-1,3,2,-3}) - 1704(f_{-5,3,2,1} + f_{-1,-1,-2,5}) - 1372f_{5,-3,4,-5} \\
 & - 1368(f_{-3,-1,0,5} + f_{-5,1,2,3}) - 1194(f_{3,-3,2,-1} + f_{1,-1,4,-3}) - 840f_{-5,3,-2,5} \\
 & - 471f_{-3,1,0,3} + 260(f_{1,5,0,-5} + f_{5,1,-4,-1}) + 249(f_{1,5,-4,-1} + f_{5,1,0,-5}) \\
 & \left. - 138f_{3,3,-2,-3} \right) \tag{C.94}
 \end{aligned}$$

The associated weight mask is shown in figure C.94.
B-coefficient c_{0023} is computed using (1, 3)-symmetry.

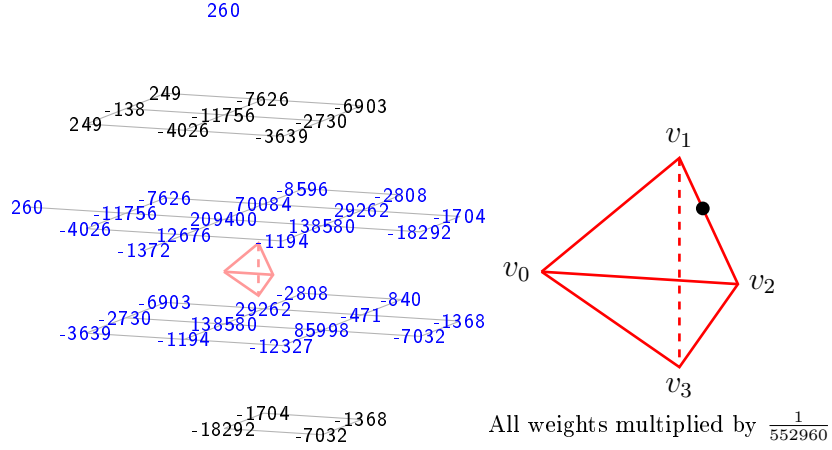


Figure C.94: Weight mask for c_{0320} . The associated domain point is shown in the teterahedron on the right.

$$\begin{aligned}
 c_{0311} := & \frac{1}{1105920} \left(401568f_{1,1,0,-1} + 303412f_{1,-1,0,1} + 239956f_{-1,1,2,-1} \right. \\
 & + 167284f_{-1,3,-2,1} + 160866f_{-1,-1,2,1} + 100530f_{-1,1,-2,3} \\
 & + 44766f_{-3,3,0,1} - 41188f_{1,-3,0,3} - 36164f_{1,3,0,-3} \\
 & - 29944f_{-3,1,4,-1} - 21759f_{1,-3,4,-1} - 21256f_{-3,5,-4,3} \\
 & - 18366f_{1,3,-4,1} - 18207f_{1,1,-4,3} - 15822f_{1,-1,4,-3} \\
 & - 14460f_{-3,-1,4,1} - 13926f_{-1,3,2,-3} - 12528f_{-1,-3,2,3} \\
 & - 12054f_{-1,5,-2,-1} + 10504f_{3,-1,2,-3} - 9666f_{5,-1,0,-3} - 9399f_{-3,5,0,-1} \\
 & - 9279f_{5,-3,0,-1} - 9228f_{-3,3,-4,5} - 9032f_{3,1,-2,-1} + 7305f_{-3,1,0,3} \\
 & - 6192f_{-1,-1,-2,5} - 4692f_{-5,5,-2,3} - 3768f_{-3,-1,0,5} - 3588f_{-5,3,2,1} \\
 & - 2844f_{-5,1,2,3} + 2646f_{3,-3,2,-1} - 2316f_{-5,3,-2,5} - 2142f_{3,1,2,-5} \\
 & - 1780f_{5,-3,4,-5} - 1770f_{3,-1,-2,1} - 1755f_{1,1,4,-5} - 270f_{3,3,-2,-3} \\
 & \left. + 260f_{1,5,0,-5} + 249f_{5,1,0,-5} - 148f_{5,1,-4,-1} + 117f_{1,5,-4,-1} \right) \quad (C.95)
 \end{aligned}$$

The associated weight mask is shown in figure C.95.
B-coefficient c_{0113} is computed using (1, 3)-symmetry.

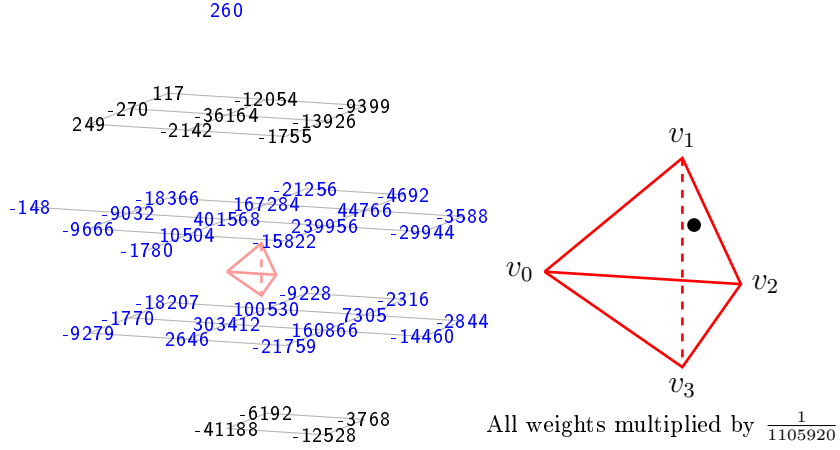


Figure C.95: Weight mask for c_{0311} . The associated domain point is shown in the teterahedron on the right.

$$\begin{aligned}
 c_{0302} := & \frac{1}{46080} \left(15438f_{1,1,0,-1} + 13622f_{1,-1,0,1} + 7986(f_{-1,1,2,-1} + f_{-1,3,-2,1}) \right. \\
 & + 6323(f_{-1,-1,2,1} + f_{-1,1,-2,3}) - 1788f_{1,-3,0,3} - 1680f_{1,3,0,-3} \\
 & + 1376f_{-3,3,0,1} - 935(f_{-3,5,-4,3} + f_{-3,1,4,-1}) - 888(f_{1,1,-4,3} + f_{1,-3,4,-1}) \\
 & - 841(f_{1,-1,4,-3} + f_{1,3,-4,1}) - 619(f_{-3,-1,4,1} + f_{-3,3,-4,5}) + 594f_{-3,1,0,3} \\
 & - 555(f_{-1,5,-2,-1} + f_{-1,3,2,-3}) - 470(f_{5,-3,0,-1} + f_{5,-1,0,-3}) \\
 & - 458(f_{-1,-3,2,3} + f_{-1,-1,-2,5}) - 310f_{-3,5,0,-1} - 200f_{-3,-1,0,5} \\
 & + 173(f_{3,1,-2,-1} + f_{3,-1,2,-3}) - 157(f_{-5,3,2,1} + f_{-5,5,-2,3}) \\
 & + 134(f_{3,-3,2,-1} + f_{3,-1,-2,1}) - 123(f_{-5,1,2,3} + f_{-5,3,-2,5}) \\
 & \left. - 34(f_{5,1,-4,-1} + f_{5,-3,4,-5}) - 11(f_{3,3,-2,-3} + f_{3,1,2,-5} + f_{1,5,-4,-1} + f_{1,1,4,-5}) \right) \\
 & \quad (C.96)
 \end{aligned}$$

The associated weight mask is shown in figure C.96.
B-coefficient c_{0203} is computed using (1, 3)-symmetry.

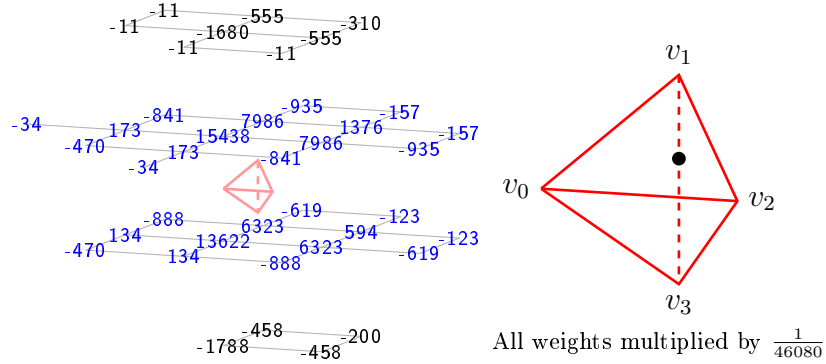


Figure C.96: Weight mask for c_{0302} . The associated domain point is shown in the tetrahedron on the right.

$$\begin{aligned}
 c_{0230} := & \frac{1}{46080} \left(15484f_{1,1,0,-1} + 12454(f_{-1,1,2,-1} + f_{1,-1,0,1}) + 9340f_{-1,-1,2,1} \right. \\
 & + 3912f_{-1,3,-2,1} + 1943(f_{-1,1,-2,3} + f_{-3,3,0,1}) - 1499(f_{-3,1,4,-1} + f_{1,-3,0,3}) \\
 & + 1398f_{3,-1,2,-3} - 995(f_{1,3,0,-3} + f_{3,1,-2,-1}) - 872f_{1,-3,4,-1} \\
 & - 851(f_{-3,-1,4,1} + f_{-1,-3,2,3}) - 491(f_{-1,3,2,-3} + f_{3,-1,-2,1}) \\
 & - 467(f_{1,3,-4,1} + f_{-3,5,0,-1} + f_{-1,5,-2,-1} + f_{1,1,-4,3}) - 464f_{-3,5,-4,3} \\
 & - 290(f_{5,-3,0,-1} + f_{3,1,2,-5} + f_{1,1,4,-5} + f_{5,-1,0,-3}) + 262f_{-3,1,0,3} \\
 & - 226(f_{-3,3,-4,5} + f_{-5,5,-2,3}) - 170f_{5,-3,4,-5} \\
 & - 122(f_{-5,1,2,3} + f_{-3,-1,0,5} + f_{-5,3,2,1} + f_{-1,-1,-2,5}) + 119(f_{3,-3,2,-1} + f_{1,-1,4,-3}) \\
 & - 90f_{-5,3,-2,5} - 34(f_{3,-3,6,-5} + f_{5,-5,4,-3}) \\
 & \left. - 11(f_{3,-5,2,1} + f_{1,-5,4,1} + f_{-1,-3,6,-1} + f_{-1,-1,6,-3}) \right) \quad (C.97)
 \end{aligned}$$

The associated weight mask is shown in figure C.97.

B-coefficient c_{0032} is computed using (1, 3)-symmetry.

$$\begin{aligned}
 c_{0221} := & \frac{1}{46080} \left(15256f_{1,1,0,-1} + 13594f_{1,-1,0,1} + 10742f_{-1,1,2,-1} \right. \\
 & + 8996f_{-1,-1,2,1} + 4835f_{-1,3,-2,1} + 3603f_{-1,1,-2,3} - 1674f_{1,-3,0,3} \\
 & - 1488f_{1,3,0,-3} + 1453f_{-3,3,0,1} - 1240f_{-3,1,4,-1} - 892f_{-3,-1,4,1} \\
 & - 863f_{1,-3,4,-1} + 759f_{3,-1,2,-3} - 754f_{-1,-3,2,3} - 712f_{-1,3,2,-3} \\
 & - 666(f_{1,3,-4,1} + f_{1,1,-4,3}) + 625f_{-3,1,0,3} - 609f_{1,-1,4,-3} - 588f_{-3,5,-4,3} \\
 & - 526f_{3,1,-2,-1} - 384f_{-3,3,-4,5} - 380(f_{5,-1,0,-3} + f_{5,-3,0,-1}) - 355f_{-1,5,-2,-1} \\
 & + 333f_{3,-3,2,-1} - 327f_{-3,5,0,-1} - 322f_{3,-1,-2,1} - 211f_{-1,-1,-2,5} \\
 & - 186f_{-5,5,-2,3} - 183f_{-3,-1,0,5} - 128(f_{-5,1,2,3} + f_{-5,3,2,1}) - 118f_{-5,3,-2,5} \\
 & - 102f_{5,-3,4,-5} - 89(f_{3,1,2,-5} + f_{1,1,4,-5}) - 34f_{5,-5,4,-3} \\
 & \left. - 11(f_{3,-5,2,1} + f_{1,-5,4,1}) \right) \quad (C.98)
 \end{aligned}$$

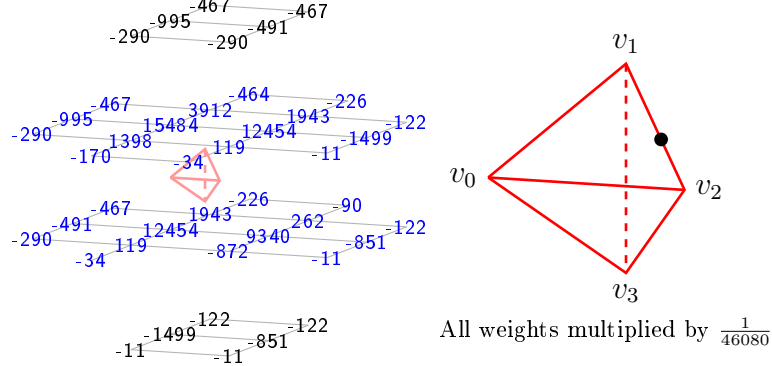


Figure C.97: Weight mask for c_{0230} . The associated domain point is shown in the teterahedron on the right.

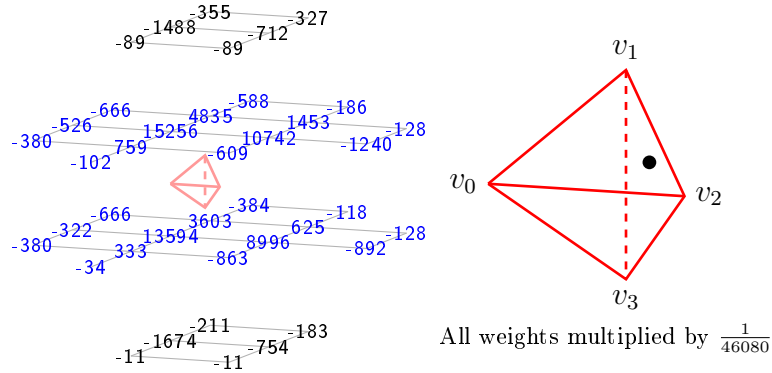


Figure C.98: Weight mask for c_{0221} . The associated domain point is shown in the teterahedron on the right.

The associated weight mask is shown in figure C.98.
 B -coefficient c_{0122} is computed using $(1, 3)$ -symmetry.

$$\begin{aligned}
 c_{0212} := & \frac{1}{46080} \left(14530(f_{1,1,0,-1} + f_{1,-1,0,1}) + 8594(f_{-1,-1,2,1} + f_{-1,1,2,-1}) \right. \\
 & + 5715(f_{-1,1,-2,3} + f_{-1,3,-2,1}) - 1734(f_{1,-3,0,3} + f_{1,3,0,-3}) \\
 & + 985(f_{-3,1,0,3} + f_{-3,3,0,1}) - 922(f_{-3,1,4,-1} + f_{-3,-1,4,1}) \\
 & - 889(f_{1,-1,4,-3} + f_{1,-3,4,-1}) - 840(f_{1,1,-4,3} + f_{1,3,-4,1}) \\
 & - 646(f_{-1,-3,2,3} + f_{-1,3,2,-3}) - 632(f_{-3,3,-4,5} + f_{-3,5,-4,3}) \\
 & - 470(f_{5,-3,0,-1} + f_{5,-1,0,-3}) + 389(f_{3,-3,2,-1} + f_{3,-1,2,-3}) \\
 & - 367(f_{-1,5,-2,-1} + f_{-1,-1,-2,5}) - 255(f_{-3,-1,0,5} + f_{-3,5,0,-1}) \\
 & - 146(f_{-5,3,-2,5} + f_{-5,5,-2,3}) - 134(f_{-5,3,2,1} + f_{-5,1,2,3}) \\
 & - 82(f_{3,-1,-2,1} + f_{3,1,-2,-1}) - 34(f_{5,-3,4,-5} + f_{5,-5,4,-3}) \\
 & \left. - 11(f_{3,-5,2,1} + f_{3,1,2,-5} + f_{1,-5,4,1} + f_{1,1,4,-5}) \right) \tag{C.99}
 \end{aligned}$$

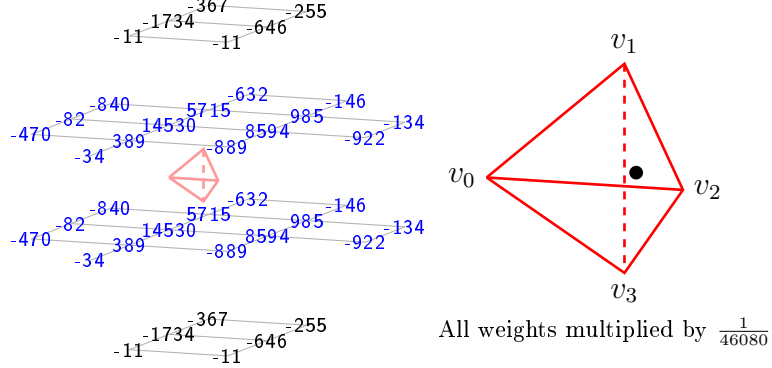


Figure C.99: Weight mask for c_{0212} . The associated domain point is shown in the teterahedron on the right.

The associated weight mask is shown in figure C.99.

$$\begin{aligned}
 c_{0140} := & \frac{1}{23040} \left(7166f_{1,1,0,-1} + 6398(f_{-1,1,2,-1} + f_{1,-1,0,1}) + 5630f_{-1,-1,2,1} \right. \\
 & + 1064f_{-1,3,-2,1} + 694(f_{-1,1,-2,3} + f_{-3,3,0,1}) - 640(f_{-3,1,4,-1} + f_{1,-3,0,3}) \\
 & + 608f_{3,-1,2,-3} - 532(f_{3,1,-2,-1} + f_{1,3,0,-3}) - 496(f_{-3,-1,4,1} + f_{-1,-3,2,3}) \\
 & - 388(f_{3,-1,-2,1} + f_{-1,3,2,-3}) + 324f_{-3,1,0,3} + 238(f_{3,-3,2,-1} + f_{1,-1,4,-3}) \\
 & - 160(f_{1,3,-4,1} + f_{-3,5,0,-1} + f_{-1,5,-2,-1} + f_{1,1,-4,3}) - 132f_{1,-3,4,-1} \\
 & - 124(f_{3,1,2,-5} + f_{5,-3,0,-1} + f_{5,-1,0,-3} + f_{1,1,4,-5}) - 123f_{-3,5,-4,3} \\
 & - 89(f_{-3,3,-4,5} + f_{-5,5,-2,3}) - 82(f_{-1,-1,-2,5} + f_{-3,-1,0,5} + f_{-5,1,2,3} + f_{-5,3,2,1}) \\
 & - 75f_{5,-3,4,-5} - 55f_{-5,3,-2,5} - 46(f_{1,-5,4,1} + f_{-1,-3,6,-1} + f_{3,-5,2,1} + f_{-1,-1,6,-3}) \\
 & \left. - 41(f_{3,-3,6,-5} + f_{5,-5,4,-3}) - 7f_{3,-5,6,-3} \right) \tag{C.100}
 \end{aligned}$$

The associated weight mask is shown in figure C.100.

B-coefficient c_{0041} is computed using (1, 3)-symmetry.

$$\begin{aligned}
 c_{0131} := & \frac{1}{92160} \left(28346(f_{1,1,0,-1} + f_{1,-1,0,1}) + 22202(f_{-1,-1,2,1} + f_{-1,1,2,-1}) \right. \\
 & + 5703(f_{-1,1,-2,3} + f_{-1,3,-2,1}) - 2878(f_{1,-3,0,3} + f_{1,3,0,-3}) \\
 & - 2254(f_{-3,1,4,-1} + f_{-3,-1,4,1}) + 2053(f_{-3,3,0,1} + f_{-3,1,0,3}) \\
 & - 1726(f_{-1,-3,2,3} + f_{-1,3,2,-3}) - 1390(f_{3,-1,-2,1} + f_{3,1,-2,-1}) \\
 & + 1365(f_{3,-3,2,-1} + f_{3,-1,2,-3}) - 982(f_{1,3,-4,1} + f_{1,1,-4,3}) \\
 & - 905(f_{1,-3,4,-1} + f_{1,-1,4,-3}) - 670(f_{-3,3,-4,5} + f_{-3,5,-4,3}) \\
 & - 628(f_{5,-3,0,-1} + f_{5,-1,0,-3}) - 469(f_{-3,-1,0,5} + f_{-1,-1,-2,5} + f_{-1,5,-2,-1} + f_{-3,5,0,-1}) \\
 & - 296(f_{-5,5,-2,3} + f_{-5,3,-2,5}) - 292(f_{-5,3,2,1} + f_{-5,1,2,3}) \\
 & - 184(f_{5,-5,4,-3} + f_{5,-3,4,-5}) - 181(f_{1,1,4,-5} + f_{3,-5,2,1} + f_{1,-5,4,1} + f_{3,1,2,-5}) \\
 & \left. - 70(f_{-1,-3,6,-1} + f_{-1,-1,6,-3}) - 14(f_{3,-5,6,-3} + f_{3,-3,6,-5}) \right) \tag{C.101}
 \end{aligned}$$

The associated weight mask is shown in figure C.101.

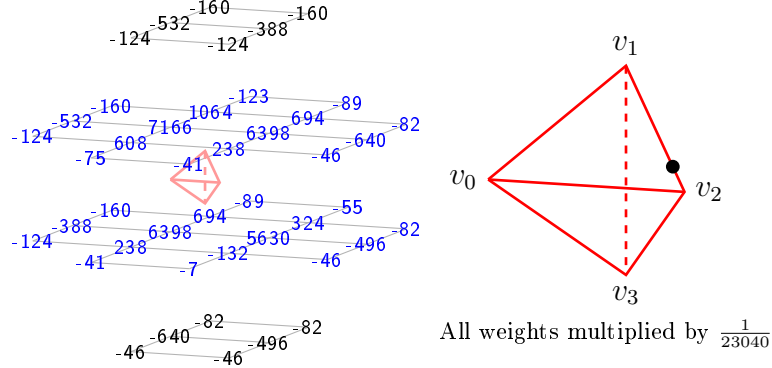


Figure C.100: Weight mask for c_{0140} . The associated domain point is shown in the teterahedron on the right.

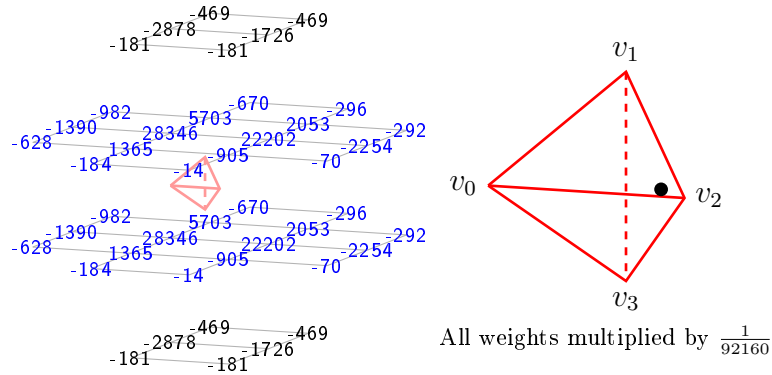


Figure C.101: Weight mask for c_{0131} . The associated domain point is shown in the teterahedron on the right.

$$\begin{aligned}
 c_{0050} := & \frac{1}{23040} \left(6398(f_{1,1,0,-1} + f_{-1,-1,2,1} + f_{-1,1,2,-1} + f_{1,-1,0,1}) \right. \\
 & - 514(f_{3,-1,-2,1} + f_{-3,1,4,-1} + f_{-3,-1,4,1} + f_{3,1,-2,-1} + f_{-1,3,2,-3} + f_{-1,-3,2,3} \\
 & \quad + f_{1,3,0,-3} + f_{1,-3,0,3}) \\
 & + 466(f_{-1,1,-2,3} + f_{3,-3,2,-1} + f_{-3,3,0,1} + f_{3,-1,2,-3} + f_{1,-1,4,-3} + f_{-3,1,0,3} \\
 & \quad + f_{1,-3,4,-1} + f_{-1,3,-2,1}) \\
 & - 103(f_{-5,3,2,1} + f_{5,-3,0,-1} + f_{-5,1,2,3} + f_{5,-1,0,-3} + f_{3,-5,2,1} + f_{-3,5,0,-1} \\
 & \quad + f_{-1,5,-2,-1} + f_{-1,-1,6,-3} + f_{1,1,4,-5} + f_{-1,-1,-2,5} + f_{3,1,2,-5} + f_{1,3,-4,1} \\
 & \quad + f_{1,1,-4,3} + f_{-3,-1,0,5} + f_{-1,-3,6,-1} + f_{1,-5,4,1}) \\
 & \left. - 65(f_{-5,5,-2,3} + f_{5,-3,4,-5} + f_{-5,3,-2,5} + f_{5,-5,4,-3} + f_{3,-5,6,-3} + f_{-3,5,-4,3} \right. \\
 & \quad \left. + f_{3,-3,6,-5} + f_{-3,3,-4,5}) \right) \tag{C.102}
 \end{aligned}$$

The associated weight mask is shown in figure C.102.

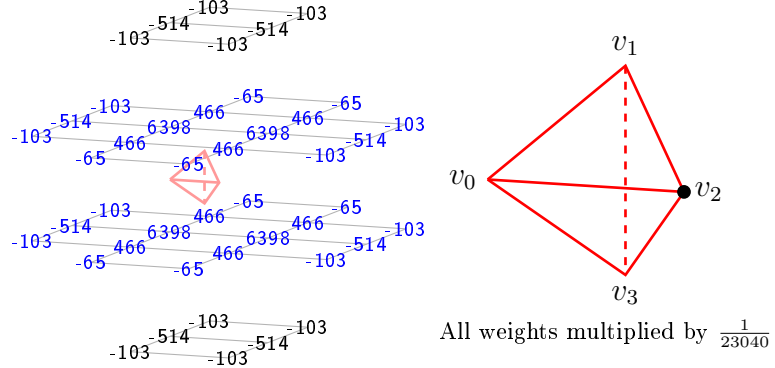


Figure C.102: Weight mask for c_{0050} . The associated domain point is shown in the teterahedron on the right.

B-coefficient computation rules for the class \mathcal{K}_4

$$\begin{aligned}
 c_{5000} := & \frac{1}{23040} \left(6398(f_{0,2,-1,0} + f_{0,0,-1,2} + f_{2,0,1,-2} + f_{2,-2,1,0}) \right. \\
 & - 514(f_{0,-2,-1,4} + f_{-2,2,-3,4} + f_{0,4,-1,-2} + f_{4,-4,3,-2} + f_{-2,4,-3,2} + f_{2,2,1,-4} \\
 & + f_{4,-2,3,-4} + f_{2,-4,1,2}) \\
 & + 466(f_{4,-2,-1,0} + f_{4,0,-1,-2} + f_{2,2,-3,0} + f_{-2,2,1,0} + f_{2,0,-3,2} + f_{-2,0,1,2} \\
 & + f_{0,-2,3,0} + f_{0,0,3,-2}) \\
 & - 103(f_{2,-4,5,-2} + f_{-4,4,-1,2} + f_{-4,2,-1,4} + f_{4,2,-1,-4} + f_{6,-4,1,-2} + f_{4,-4,-1,2} \\
 & + f_{6,-2,1,-4} + f_{-2,-2,1,4} + f_{0,2,3,-4} + f_{0,2,-5,4} + f_{0,-4,3,2} + f_{0,4,-5,2} \\
 & + f_{2,4,-3,-2} + f_{2,-2,-3,4} + f_{2,-2,5,-4} + f_{-2,4,1,-2}) \\
 & - 65(f_{-4,2,3,0} + f_{-2,-2,5,0} + f_{4,2,-5,0} + f_{-2,0,5,-2} + f_{4,0,-5,2} + f_{6,0,-3,-2} \\
 & \left. + f_{-4,0,3,2} + f_{6,-2,-3,0} \right) \tag{C.103}
 \end{aligned}$$

The associated weight mask is shown in figure C.103.

$$\begin{aligned}
 c_{4100} := & \frac{1}{23040} \left(7166f_{0,2,-1,0} + 6398(f_{0,0,-1,2} + f_{2,0,1,-2}) + 5630f_{2,-2,1,0} \right. \\
 & + 1064f_{-2,2,1,0} + 694(f_{0,0,3,-2} + f_{-2,0,1,2}) - 640(f_{0,-2,-1,4} + f_{4,-2,3,-4}) \\
 & + 608f_{2,2,-3,0} - 532(f_{0,4,-1,-2} + f_{-2,4,-3,2}) - 496(f_{2,-4,1,2} + f_{4,-4,3,-2}) \\
 & - 388(f_{-2,2,-3,4} + f_{2,2,1,-4}) + 324f_{0,-2,3,0} + 238(f_{2,0,-3,2} + f_{4,0,-1,-2}) \\
 & - 160(f_{-2,4,1,-2} + f_{-4,4,-1,2} + f_{-4,2,-1,4} + f_{0,2,3,-4}) - 132f_{4,-2,-1,0} \\
 & - 124(f_{2,4,-3,-2} + f_{4,2,-1,-4} + f_{0,4,-5,2} + f_{0,2,-5,4}) - 123f_{-4,2,3,0} \\
 & - 89(f_{-2,0,5,-2} + f_{-4,0,3,2}) - 82(f_{2,-2,5,-4} + f_{2,-4,5,-2} + f_{-2,-2,1,4} + f_{0,-4,3,2}) \\
 & - 75f_{4,2,-5,0} - 55f_{-2,-2,5,0} - 46(f_{2,-2,-3,4} + f_{4,-4,-1,2} + f_{6,-2,1,-4} + f_{6,-4,1,-2}) \\
 & \left. - 41(f_{4,0,-5,2} + f_{6,0,-3,-2}) - 7f_{6,-2,-3,0} \right) \tag{C.104}
 \end{aligned}$$

The associated weight mask is shown in figure C.104.

B-coefficient c_{4001} is computed using (1, 3)-symmetry.

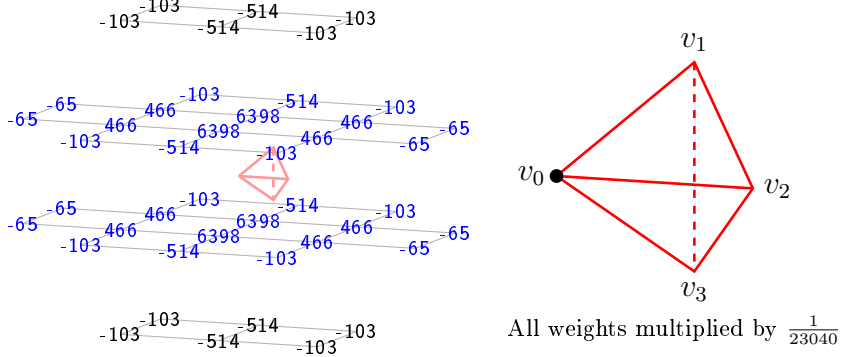


Figure C.103: Weight mask for c_{5000} . The associated domain point is shown in the teterahedron on the right.

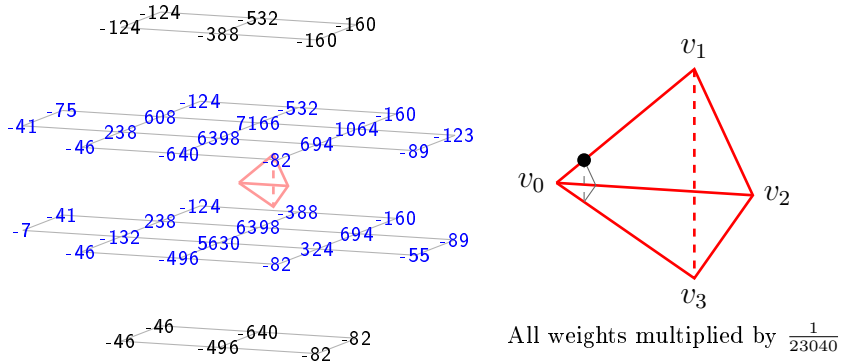


Figure C.104: Weight mask for c_{4100} . The associated domain point is shown in the teterahedron on the right. The black triangle symbolizes the ring $R_1(v_0)$.

$$\begin{aligned}
 c_{4010} := & \frac{1}{23040} \left(6398(f_{0,0,-1,2} + f_{0,2,-1,0} + f_{2,-2,1,0} + f_{2,0,1,-2}) \right. \\
 & + 922(f_{-2,0,1,2} + f_{-2,2,1,0} + f_{0,-2,3,0} + f_{0,0,3,-2}) \\
 & - 514(f_{0,4,-1,-2} + f_{4,-2,3,-4} + f_{4,-4,3,-2} + f_{-2,4,-3,2} + f_{0,-2,-1,4} + f_{2,-4,1,2} \\
 & \quad + f_{2,2,1,-4} + f_{-2,2,-3,4}) \\
 & - 139(f_{-4,4,-1,2} + f_{-4,2,-1,4} + f_{2,-2,5,-4} + f_{2,-4,5,-2} + f_{-2,4,1,-2} + f_{-2,-2,1,4} \\
 & \quad + f_{0,2,3,-4} + f_{0,-4,3,2}) \\
 & - 113(f_{-2,-2,5,0} + f_{-2,0,5,-2} + f_{-4,0,3,2} + f_{-4,2,3,0}) \\
 & - 67(f_{6,-4,1,-2} + f_{6,-2,1,-4} + f_{4,-4,-1,2} + f_{0,2,-5,4} + f_{4,2,-1,-4} + f_{0,4,-5,2} \\
 & \quad + f_{2,4,-3,-2} + f_{2,-2,-3,4}) \\
 & - 17(f_{4,0,-5,2} + f_{4,2,-5,0} + f_{6,0,-3,-2} + f_{6,-2,-3,0}) \\
 & \left. + 10(f_{4,-2,-1,0} + f_{4,0,-1,-2} + f_{2,0,-3,2} + f_{2,2,-3,0}) \right) \tag{C.105}
 \end{aligned}$$

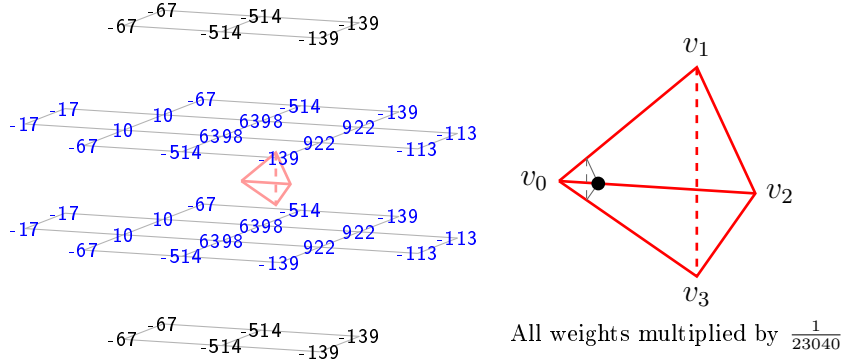


Figure C.105: Weight mask for c_{4010} . The associated domain point is shown in the tetrahedron on the right. The black triangle symbolizes the ring $R_1(v_0)$.

The associated weight mask is shown in figure C.105.

$$\begin{aligned}
 c_{3200} := & \frac{1}{46080} \left(15484 f_{0,2,-1,0} + 12454(f_{0,0,-1,2} + f_{2,0,1,-2}) + 9340 f_{2,-2,1,0} \right. \\
 & + 3912 f_{-2,2,1,0} + 1943(f_{0,0,3,-2} + f_{-2,0,1,2}) - 1499(f_{0,-2,-1,4} + f_{4,-2,3,-4}) \\
 & + 1398 f_{2,2,-3,0} - 995(f_{-2,4,-3,2} + f_{0,4,-1,-2}) - 872 f_{4,-2,-1,0} \\
 & - 851(f_{4,-4,3,-2} + f_{2,-4,1,2}) - 491(f_{2,2,1,-4} + f_{-2,2,-3,4}) \\
 & - 467(f_{-4,4,-1,2} + f_{0,2,3,-4} + f_{-4,2,-1,4} + f_{-2,4,1,-2}) - 464 f_{-4,2,3,0} \\
 & - 290(f_{0,4,-5,2} + f_{4,2,-1,-4} + f_{0,2,-5,4} + f_{2,4,-3,-2}) + 262 f_{0,-2,3,0} \\
 & - 226(f_{-4,0,3,2} + f_{-2,0,5,-2}) - 170 f_{4,2,-5,0} \\
 & - 122(f_{2,-4,5,-2} + f_{2,-2,5,-4} + f_{-2,-2,1,4} + f_{0,-4,3,2}) + 119(f_{4,0,-1,-2} + f_{2,0,-3,2}) \\
 & - 90 f_{-2,-2,5,0} - 34(f_{4,0,-5,2} + f_{6,0,-3,-2}) \\
 & \left. - 11(f_{4,-4,-1,2} + f_{2,-2,-3,4} + f_{6,-2,1,-4} + f_{6,-4,1,-2}) \right) \tag{C.106}
 \end{aligned}$$

The associated weight mask is shown in figure C.106.
B-coefficient c_{3002} is computed using (1, 3)-symmetry.

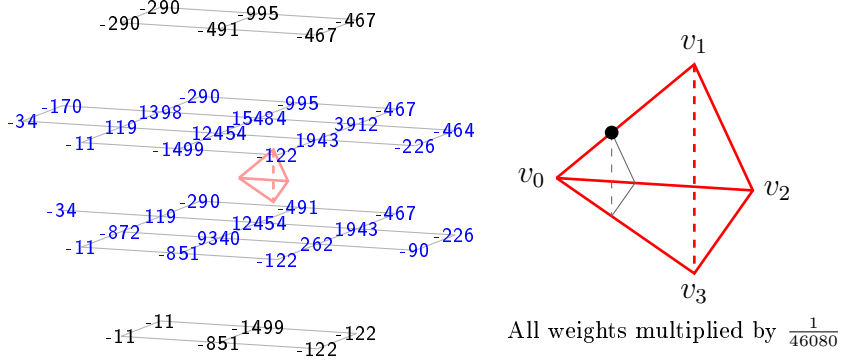


Figure C.106: Weight mask for c_{3200} . The associated domain point is shown in the teterahedron on the right. The black triangle symbolizes the ring $R_2(v_0)$.

$$\begin{aligned}
 c_{3110} := & \frac{1}{92160} \left(28028f_{0,2,-1,0} + 24956(f_{0,0,-1,2} + f_{2,0,1,-2}) + 21884f_{2,-2,1,0} \right. \\
 & + 7150f_{-2,2,1,0} + 4980(f_{0,0,3,-2} + f_{-2,0,1,2}) + 2810f_{0,-2,3,0} \\
 & - 2572(f_{0,-2,-1,4} + f_{4,-2,3,-4}) - 2140(f_{-2,4,-3,2} + f_{0,4,-1,-2}) \\
 & - 1996(f_{4,-4,3,-2} + f_{2,-4,1,2}) - 1564(f_{2,2,1,-4} + f_{-2,2,-3,4}) - 1282f_{4,-2,-1,0} \\
 & - 848f_{-4,2,3,0} - 811(f_{-4,4,-1,2} + f_{-2,4,1,-2} + f_{0,2,3,-4} + f_{-4,2,-1,4}) \\
 & - 610(f_{-2,0,5,-2} + f_{-4,0,3,2}) - 492(f_{2,0,-3,2} + f_{4,0,-1,-2}) \\
 & - 433(f_{-2,-2,1,4} + f_{2,-2,5,-4} + f_{0,-4,3,2} + f_{2,-4,5,-2}) - 372f_{-2,-2,5,0} \\
 & - 313(f_{2,4,-3,-2} + f_{4,2,-1,-4} + f_{0,4,-5,2} + f_{0,2,-5,4}) + 298f_{2,2,-3,0} \\
 & - 68f_{4,2,-5,0} - 67(f_{2,-2,-3,4} + f_{4,-4,-1,2} + f_{6,-2,1,-4} + f_{6,-4,1,-2}) \\
 & \left. - 34(f_{4,0,-5,2} + f_{6,0,-3,-2}) \right) \tag{C.107}
 \end{aligned}$$

The associated weight mask is shown in figure C.107.

B-coefficient c_{3011} is computed using (1, 3)-symmetry.

$$\begin{aligned}
 c_{3101} := & \frac{1}{92160} \left(28346(f_{0,0,-1,2} + f_{0,2,-1,0}) + 22202(f_{2,0,1,-2} + f_{2,-2,1,0}) \right. \\
 & + 5703(f_{-2,0,1,2} + f_{-2,2,1,0}) - 2878(f_{0,4,-1,-2} + f_{0,-2,-1,4}) \\
 & - 2254(f_{4,-4,3,-2} + f_{4,-2,3,-4}) + 2053(f_{0,-2,3,0} + f_{0,0,3,-2}) \\
 & - 1726(f_{2,-4,1,2} + f_{2,2,1,-4}) - 1390(f_{-2,4,-3,2} + f_{-2,2,-3,4}) \\
 & + 1365(f_{2,0,-3,2} + f_{2,2,-3,0}) - 982(f_{-4,4,-1,2} + f_{-4,2,-1,4}) \\
 & - 905(f_{4,-2,-1,0} + f_{4,0,-1,-2}) - 670(f_{-4,2,3,0} + f_{-4,0,3,2}) \\
 & - 628(f_{0,4,-5,2} + f_{0,2,-5,4}) - 469(f_{-2,-2,1,4} + f_{-2,4,1,-2} + f_{0,-4,3,2} + f_{0,2,3,-4}) \\
 & - 296(f_{-2,-2,5,0} + f_{-2,0,5,-2}) - 292(f_{2,-2,5,-4} + f_{2,-4,5,-2}) \\
 & - 184(f_{4,0,-5,2} + f_{4,2,-5,0}) - 181(f_{4,2,-1,-4} + f_{2,4,-3,-2} + f_{4,-4,-1,2} + f_{2,-2,-3,4}) \\
 & \left. - 70(f_{6,-2,1,-4} + f_{6,-4,1,-2}) - 14(f_{6,0,-3,-2} + f_{6,-2,-3,0}) \right) \tag{C.108}
 \end{aligned}$$

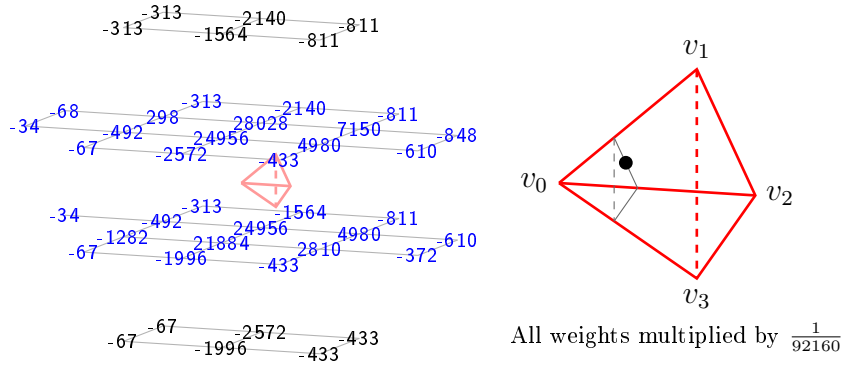


Figure C.107: Weight mask for c_{3110} . The associated domain point is shown in the teterahedron on the right. The black triangle symbolizes the ring $R_2(v_0)$.

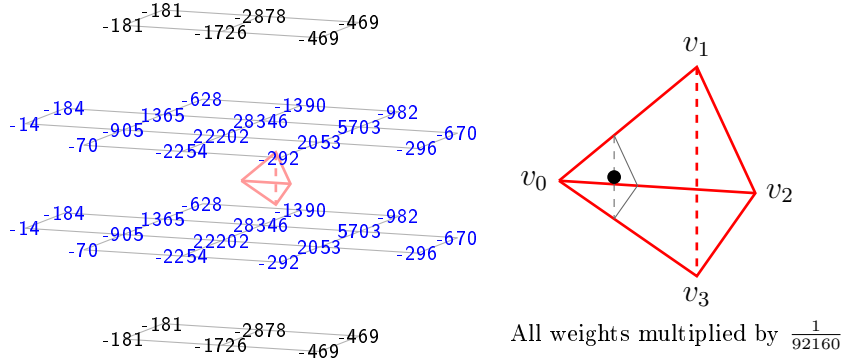


Figure C.108: Weight mask for c_{3101} . The associated domain point is shown in the teterahedron on the right. The black triangle symbolizes the ring $R_2(v_0)$.

The associated weight mask is shown in figure C.108.

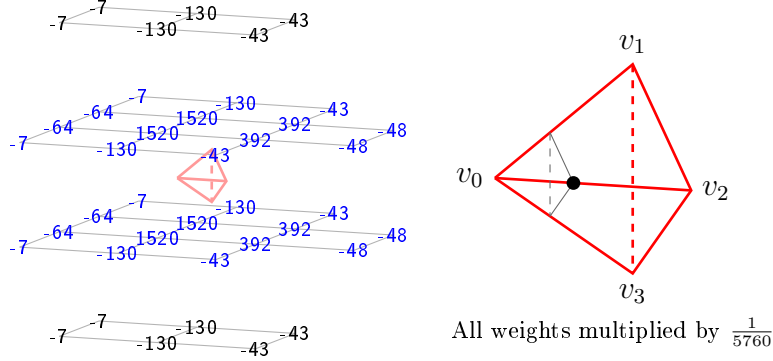


Figure C.109: Weight mask for c_{3020} . The associated domain point is shown in the teterahedron on the right. The black triangle symbolizes the ring $R_2(v_0)$.

$$\begin{aligned}
 c_{3020} := & \frac{1}{5760} \left(1520(f_{0,2,-1,0} + f_{0,0,-1,2} + f_{2,0,1,-2} + f_{2,-2,1,0}) \right. \\
 & + 392(f_{0,0,3,-2} + f_{0,-2,3,0} + f_{-2,0,1,2} + f_{-2,2,1,0}) \\
 & - 130(f_{2,2,1,-4} + f_{4,-2,3,-4} + f_{-2,4,-3,2} + f_{2,-4,1,2} + f_{4,-4,3,-2} + f_{-2,2,-3,4} \\
 & \quad + f_{0,4,-1,-2} + f_{0,-2,-1,4}) \\
 & - 64(f_{2,0,-3,2} + f_{2,2,-3,0} + f_{4,-2,-1,0} + f_{4,0,-1,-2}) \\
 & - 48(f_{-4,2,3,0} + f_{-2,-2,5,0} + f_{-2,0,5,-2} + f_{-4,0,3,2}) \\
 & - 43(f_{0,2,3,-4} + f_{-4,4,-1,2} + f_{-4,2,-1,4} + f_{2,-4,5,-2} + f_{-2,-2,1,4} + f_{-2,4,1,-2} \\
 & \quad + f_{2,-2,5,-4} + f_{0,-4,3,2}) \\
 & - 7(f_{4,-4,-1,2} + f_{6,-2,1,-4} + f_{6,-4,1,-2} + f_{4,2,-1,-4} + f_{2,4,-3,-2} + f_{2,-2,-3,4} \\
 & \quad + f_{0,4,-5,2} + f_{0,2,-5,4}) \left. \right) \tag{C.109}
 \end{aligned}$$

The associated weight mask is shown in figure C.109.

$$\begin{aligned}
 c_{2300} := & \frac{1}{552960} \left(209400f_{0,2,-1,0} + 138580(f_{0,0,-1,2} + f_{2,0,1,-2}) + 85998f_{2,-2,1,0} \right. \\
 & + 70084f_{-2,2,1,0} + 29262(f_{0,0,3,-2} + f_{-2,0,1,2}) \\
 & - 18292(f_{0,-2,-1,4} + f_{4,-2,3,-4}) + 12676f_{2,2,-3,0} - 12327f_{4,-2,-1,0} \\
 & - 11756(f_{-2,4,-3,2} + f_{0,4,-1,-2}) - 8596f_{-4,2,3,0} \\
 & - 7626(f_{-4,4,-1,2} + f_{-2,4,1,-2}) - 7032(f_{4,-4,3,-2} + f_{2,-4,1,2}) \\
 & - 6903(f_{-4,2,-1,4} + f_{0,2,3,-4}) - 4026(f_{0,4,-5,2} + f_{2,4,-3,-2}) \\
 & - 3639(f_{4,2,-1,-4} + f_{0,2,-5,4}) - 2808(f_{-2,0,5,-2} + f_{-4,0,3,2}) \\
 & - 2730(f_{-2,2,-3,4} + f_{2,2,1,-4}) - 1704(f_{2,-2,5,-4} + f_{-2,-2,1,4}) - 1372f_{4,2,-5,0} \\
 & - 1368(f_{2,-4,5,-2} + f_{0,-4,3,2}) - 1194(f_{4,0,-1,-2} + f_{2,0,-3,2}) - 840f_{-2,-2,5,0} \\
 & - 471f_{0,-2,3,0} + 260(f_{0,6,-1,-4} + f_{-4,6,-5,4}) + 249(f_{0,6,-5,0} + f_{-4,6,-1,0}) \\
 & \left. - 138f_{-2,6,-3,0} \right) \tag{C.110}
 \end{aligned}$$

260

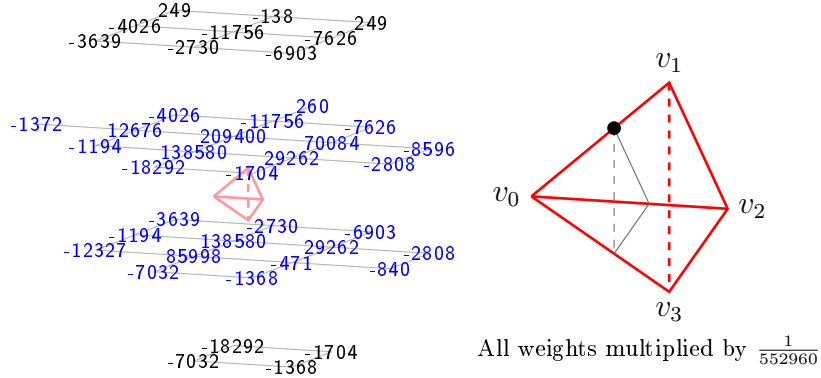


Figure C.110: Weight mask for c_{2300} . The associated domain point is shown in the teterahedron on the right. The black triangle symbolizes the ring $R_3(v_0)$.

The associated weight mask is shown in figure C.110.
B-coefficient c_{2003} is computed using (1, 3)-symmetry.

$$\begin{aligned}
 c_{2210} := & \frac{1}{46080} \left(15028f_{0,2,-1,0} + 11882(f_{0,0,-1,2} + f_{2,0,1,-2}) + 8652f_{2,-2,1,0} \right. \\
 & + 5758f_{-2,2,1,0} + 3113(f_{0,0,3,-2} + f_{-2,0,1,2}) - 1415(f_{0,-2,-1,4} + f_{4,-2,3,-4}) \\
 & - 1019(f_{0,4,-1,-2} + f_{-2,4,-3,2}) + 988f_{0,-2,3,0} - 854f_{4,-2,-1,0} \\
 & - 795(f_{4,-4,3,-2} + f_{2,-4,1,2}) - 712f_{-4,2,3,0} - 554(f_{-4,4,-1,2} + f_{-2,4,1,-2}) \\
 & - 543(f_{2,2,1,-4} + f_{-2,2,-3,4}) - 526(f_{0,2,3,-4} + f_{-4,2,-1,4}) \\
 & - 395(f_{2,0,-3,2} + f_{4,0,-1,-2}) - 344(f_{-2,0,5,-2} + f_{-4,0,3,2}) \\
 & - 217(f_{2,-2,5,-4} + f_{-2,-2,1,4}) - 189(f_{2,-4,5,-2} + f_{0,-4,3,2}) \\
 & - 179(f_{2,4,-3,-2} + f_{0,4,-5,2} + f_{4,2,-1,-4} + f_{0,2,-5,4}) - 146f_{-2,-2,5,0} \\
 & \left. + 120f_{2,2,-3,0} - 34f_{4,2,-5,0} \right) \tag{C.111}
 \end{aligned}$$

The associated weight mask is shown in figure C.111.
B-coefficient c_{2012} is computed using (1, 3)-symmetry.

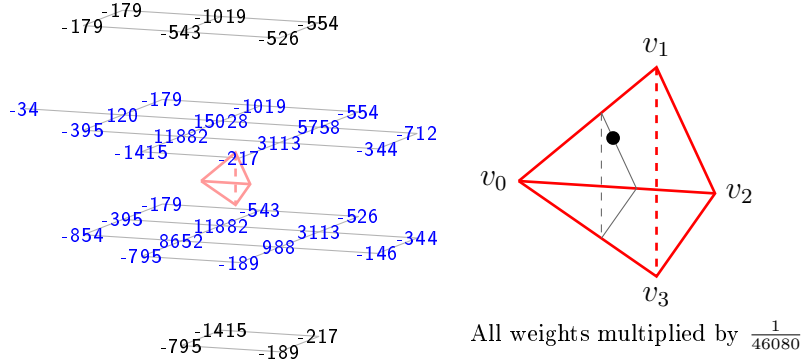


Figure C.111: Weight mask for c_{2210} . The associated domain point is shown in the tetrahedron on the right. The black triangle symbolizes the ring $R_3(v_0)$.

$$\begin{aligned}
 c_{2201} := & \frac{1}{46080} \left(15256f_{0,2,-1,0} + 13594f_{0,0,-1,2} + 10742f_{2,0,1,-2} \right. \\
 & + 8996f_{2,-2,1,0} + 4835f_{-2,2,1,0} + 3603f_{-2,0,1,2} - 1674f_{0,-2,-1,4} \\
 & - 1488f_{0,4,-1,-2} + 1453f_{0,0,3,-2} - 1240f_{4,-2,3,-4} - 892f_{4,-4,3,-2} \\
 & - 863f_{4,-2,-1,0} + 759f_{2,2,-3,0} - 754f_{2,-4,1,2} - 712f_{2,2,1,-4} \\
 & - 666(f_{-4,4,-1,2} + f_{-4,2,-1,4}) + 625f_{0,-2,3,0} - 609f_{4,0,-1,-2} - 588f_{-4,2,3,0} \\
 & - 526f_{-2,4,-3,2} - 384f_{-4,0,3,2} - 380(f_{0,4,-5,2} + f_{0,2,-5,4}) - 355f_{-2,4,1,-2} \\
 & + 333f_{2,0,-3,2} - 327f_{0,2,3,-4} - 322f_{-2,2,-3,4} - 211f_{-2,-2,1,4} \\
 & - 186f_{-2,0,5,-2} - 183f_{0,-4,3,2} - 128(f_{2,-2,5,-4} + f_{2,-4,5,-2}) - 118f_{-2,-2,5,0} \\
 & - 102f_{4,2,-5,0} - 89(f_{4,2,-1,-4} + f_{2,4,-3,-2}) - 34f_{4,0,-5,2} \\
 & \left. - 11(f_{4,-4,-1,2} + f_{2,-2,-3,4}) \right) \tag{C.112}
 \end{aligned}$$

The associated weight mask is shown in figure C.112.

B-coefficient c_{2102} is computed using (1, 3)-symmetry.

$$\begin{aligned}
 c_{2120} := & \frac{1}{11520} \left(3310f_{0,2,-1,0} + 2897(f_{0,0,-1,2} + f_{2,0,1,-2}) + 2484f_{2,-2,1,0} \right. \\
 & + 1302f_{-2,2,1,0} + 977(f_{0,0,3,-2} + f_{-2,0,1,2}) + 652f_{0,-2,3,0} \\
 & - 302(f_{0,-2,-1,4} + f_{4,-2,3,-4}) - 275(f_{0,4,-1,-2} + f_{-2,4,-3,2}) \\
 & - 237(f_{4,-4,3,-2} + f_{2,-4,1,2}) - 210(f_{2,2,1,-4} + f_{-2,2,-3,4}) - 180f_{4,-2,-1,0} \\
 & - 158f_{-4,2,3,0} - 157(f_{2,0,-3,2} + f_{4,0,-1,-2}) - 134f_{2,2,-3,0} \\
 & - 119(f_{-4,4,-1,2} + f_{-2,4,1,-2}) - 117(f_{-2,0,5,-2} + f_{-4,0,3,2}) \\
 & - 112(f_{0,2,3,-4} + f_{-4,2,-1,4}) - 82(f_{2,-2,5,-4} + f_{-2,-2,1,4}) - 76f_{-2,-2,5,0} \\
 & \left. - 75(f_{2,-4,5,-2} + f_{0,-4,3,2}) - 14(f_{2,4,-3,-2} + f_{0,4,-5,2} + f_{4,2,-1,-4} + f_{0,2,-5,4}) \right) \tag{C.113}
 \end{aligned}$$

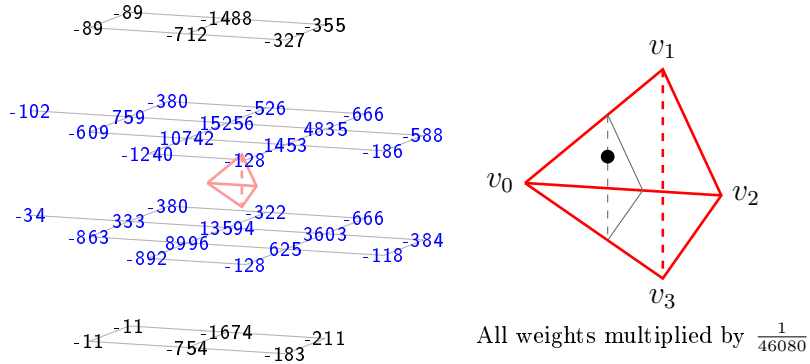


Figure C.112: Weight mask for c_{2201} . The associated domain point is shown in the teterahedron on the right. The black triangle symbolizes the ring $R_3(v_0)$.

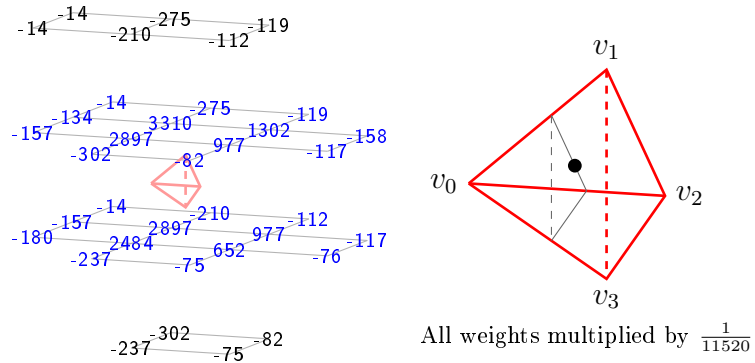


Figure C.113: Weight mask for c_{2120} . The associated domain point is shown in the teterahedron on the right. The black triangle symbolizes the ring $R_3(v_0)$.

The associated weight mask is shown in figure C.113.
B-coefficient c_{2021} is computed using (1, 3)-symmetry.

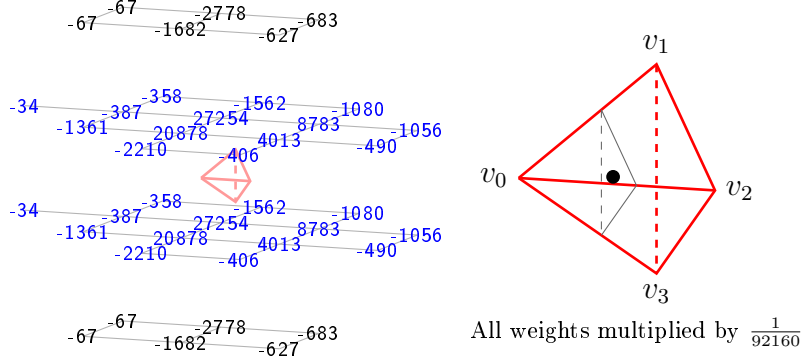


Figure C.114: Weight mask for c_{2111} . The associated domain point is shown in the teterahedron on the right. The black triangle symbolizes the ring $R_3(v_0)$.

$$\begin{aligned}
 c_{2111} := & \frac{1}{92160} \left(27254(f_{0,2,-1,0} + f_{0,0,-1,2}) + 20878(f_{2,-2,1,0} + f_{2,0,1,-2}) \right. \\
 & + 8783(f_{-2,2,1,0} + f_{-2,0,1,2}) + 4013(f_{0,0,3,-2} + f_{0,-2,3,0}) \\
 & - 2778(f_{0,-2,-1,4} + f_{0,4,-1,-2}) - 2210(f_{4,-4,3,-2} + f_{4,-2,3,-4}) \\
 & - 1682(f_{2,2,1,-4} + f_{2,-4,1,2}) - 1562(f_{-2,2,-3,4} + f_{-2,4,-3,2}) \\
 & - 1361(f_{4,-2,-1,0} + f_{4,0,-1,-2}) - 1080(f_{-4,4,-1,2} + f_{-4,2,-1,4}) \\
 & - 1056(f_{-4,2,3,0} + f_{-4,0,3,2}) - 683(f_{-2,-2,1,4} + f_{-2,4,1,-2}) \\
 & - 627(f_{0,2,3,-4} + f_{0,-4,3,2}) - 490(f_{-2,-2,5,0} + f_{-2,0,5,-2}) \\
 & - 406(f_{2,-4,5,-2} + f_{2,-2,5,-4}) - 387(f_{2,0,-3,2} + f_{2,2,-3,0}) \\
 & - 358(f_{0,2,-5,4} + f_{0,4,-5,2}) - 67(f_{2,4,-3,-2} + f_{4,2,-1,-4} + f_{2,-2,-3,4} + f_{4,-4,-1,2}) \\
 & \left. - 34(f_{4,0,-5,2} + f_{4,2,-5,0}) \right) \tag{C.114}
 \end{aligned}$$

The associated weight mask is shown in figure C.114.

$$\begin{aligned}
 c_{2030} := & \frac{1}{1920} \left(459(f_{0,2,-1,0} + f_{0,0,-1,2} + f_{2,0,1,-2} + f_{2,-2,1,0}) \right. \\
 & + 195(f_{0,0,3,-2} + f_{0,-2,3,0} + f_{-2,0,1,2} + f_{-2,2,1,0}) \\
 & - 42(f_{4,-4,3,-2} + f_{4,-2,3,-4} + f_{-2,4,-3,2} + f_{2,-4,1,2} + f_{-2,2,-3,4} + f_{2,2,1,-4}) \\
 & + f_{0,-2,-1,4} + f_{0,4,-1,-2}) \\
 & - 31(f_{2,2,-3,0} + f_{2,0,-3,2} + f_{4,0,-1,-2} + f_{4,-2,-1,0}) \\
 & - 23(f_{-2,0,5,-2} + f_{-2,-2,5,0} + f_{-4,2,3,0} + f_{-4,0,3,2}) \\
 & - 18(f_{2,-4,5,-2} + f_{-4,4,-1,2} + f_{0,2,3,-4} + f_{-4,2,-1,4} + f_{-2,-2,1,4} + f_{0,-4,3,2}) \\
 & \left. + f_{-2,4,1,-2} + f_{2,-2,5,-4}) \right) \tag{C.115}
 \end{aligned}$$

The associated weight mask is shown in figure C.115.

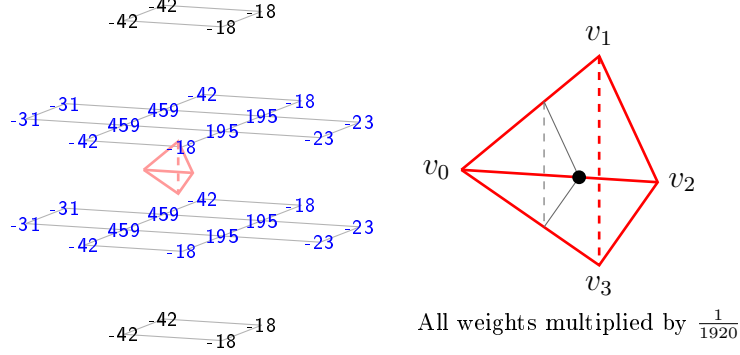


Figure C.115: Weight mask for c_{2030} . The associated domain point is shown in the teterahedron on the right. The black triangle symbolizes the ring $R_3(v_0)$.

$$\begin{aligned}
 c_{1400} := & \frac{1}{276480} \left(116862f_{0,2,-1,0} + 62758(f_{0,0,-1,2} + f_{2,0,1,-2}) + 46678f_{-2,2,1,0} \right. \\
 & + 30024f_{2,-2,1,0} + 16740(f_{0,0,3,-2} + f_{-2,0,1,2}) \\
 & - 8854(f_{0,-2,-1,4} + f_{4,-2,3,-4}) - 6178f_{-4,2,3,0} - 5462(f_{-2,4,-3,2} + f_{0,4,-1,-2}) \\
 & - 5277f_{4,-2,-1,0} - 3960(f_{-4,4,-1,2} + f_{-2,4,1,-2}) - 3453(f_{-4,2,-1,4} + f_{0,2,3,-4}) \\
 & - 2154(f_{4,-4,3,-2} + f_{2,-4,1,2}) + 1870f_{2,2,-3,0} - 1746(f_{0,4,-5,2} + f_{2,4,-3,-2}) \\
 & - 1380(f_{2,0,-3,2} + f_{4,0,-1,-2}) - 1359(f_{0,2,-5,4} + f_{4,2,-1,-4}) \\
 & - 1350(f_{-4,0,3,2} + f_{-2,0,5,-2}) - 1209f_{0,-2,3,0} - 1074(f_{2,-2,5,-4} + f_{-2,-2,1,4}) \\
 & - 1044(f_{-2,2,-3,4} + f_{2,2,1,-4}) - 534(f_{2,-4,5,-2} + f_{0,-4,3,2}) - 402f_{-2,-2,5,0} \\
 & - 352f_{4,2,-5,0} - 270f_{-2,6,-3,0} + 249f_{0,6,-5,0} + 117f_{-4,6,-1,0} \\
 & \left. + 56(f_{0,6,-1,-4} + f_{-4,6,-5,4}) \right) \tag{C.116}
 \end{aligned}$$

The associated weight mask is shown in figure C.116.

B-coefficient c_{1004} is computed using (1, 3)-symmetry.

$$\begin{aligned}
 c_{1310} := & \frac{1}{92160} \left(32028f_{0,2,-1,0} + 22184(f_{0,0,-1,2} + f_{2,0,1,-2}) + 16200f_{-2,2,1,0} \right. \\
 & + 12478f_{2,-2,1,0} + 7231(f_{0,0,3,-2} + f_{-2,0,1,2}) \\
 & - 2879(f_{0,-2,-1,4} + f_{4,-2,3,-4}) - 2110f_{-4,2,3,0} - 1807(f_{-2,4,-3,2} + f_{0,4,-1,-2}) \\
 & - 1572f_{4,-2,-1,0} + 1296f_{0,-2,3,0} - 1264(f_{-2,4,1,-2} + f_{-4,4,-1,2}) \\
 & - 1150(f_{-4,2,-1,4} + f_{0,2,3,-4}) - 1077(f_{4,-4,3,-2} + f_{2,-4,1,2}) \\
 & - 899(f_{2,0,-3,2} + f_{4,0,-1,-2}) - 853(f_{-2,2,-3,4} + f_{2,2,1,-4}) \\
 & - 692(f_{-2,0,5,-2} + f_{-4,0,3,2}) - 531(f_{2,-2,5,-4} + f_{-2,-2,1,4}) - 362f_{2,2,-3,0} \\
 & - 323(f_{2,-4,5,-2} + f_{0,-4,3,2}) - 313(f_{2,4,-3,-2} + f_{4,2,-1,-4} + f_{0,4,-5,2} + f_{0,2,-5,4}) \\
 & - 246f_{-2,-2,5,0} - 68f_{4,2,-5,0} - 34(f_{0,6,-1,-4} + f_{-4,6,-5,4}) \\
 & \left. - 22(f_{-2,6,-3,0} + f_{-4,6,-1,0}) \right) \tag{C.117}
 \end{aligned}$$

56

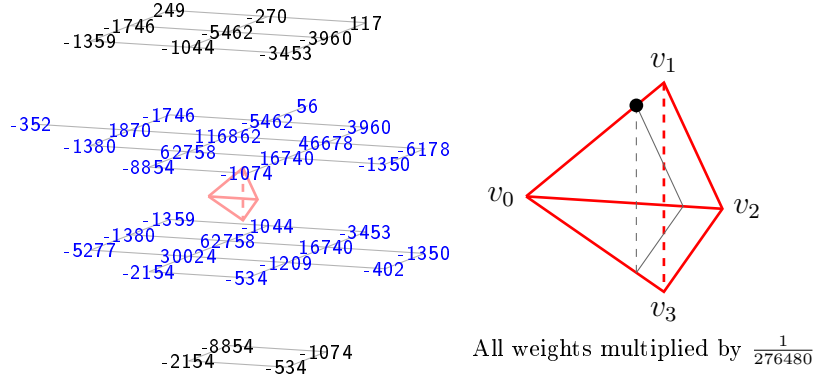


Figure C.116: Weight mask for c_{1400} . The associated domain point is shown in the teterahedron on the right. The black triangle symbolizes the ring $R_4(v_0)$.

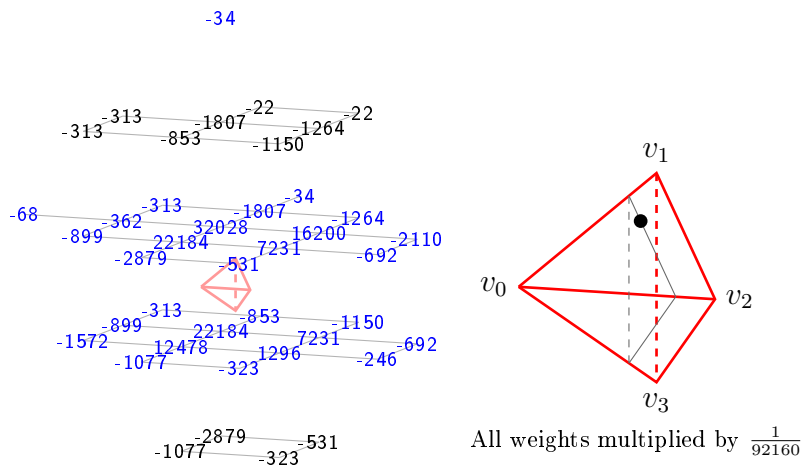


Figure C.117: Weight mask for c_{1310} . The associated domain point is shown in the teterahedron on the right. The black triangle symbolizes the ring $R_4(v_0)$.

The associated weight mask is shown in figure C.117.
B-coefficient c_{1013} is computed using (1, 3)-symmetry.

260

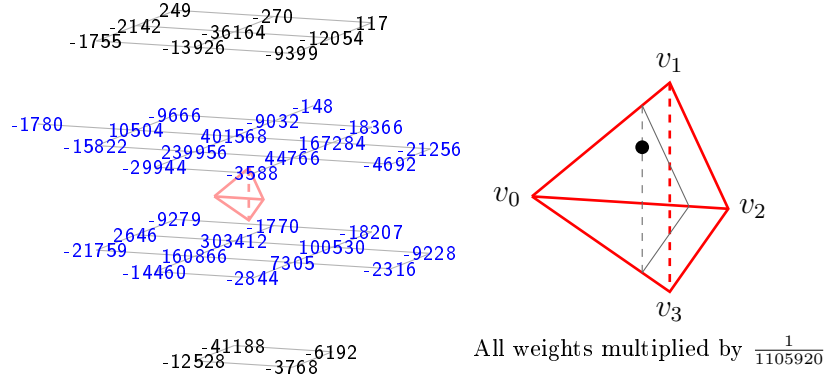


Figure C.118: Weight mask for c_{1301} . The associated domain point is shown in the teterahedron on the right. The black triangle symbolizes the ring $R_4(v_0)$.

$$\begin{aligned}
 c_{1301} := & \frac{1}{1105920} \left(401568f_{0,2,-1,0} + 303412f_{0,0,-1,2} + 239956f_{2,0,1,-2} \right. \\
 & + 167284f_{-2,2,1,0} + 160866f_{2,-2,1,0} + 100530f_{-2,0,1,2} \\
 & + 44766f_{0,0,3,-2} - 41188f_{0,-2,-1,4} - 36164f_{0,4,-1,-2} \\
 & - 29944f_{4,-2,3,-4} - 21759f_{4,-2,-1,0} - 21256f_{-4,2,3,0} \\
 & - 18366f_{-4,4,-1,2} - 18207f_{-4,2,-1,4} - 15822f_{4,0,-1,-2} \\
 & - 14460f_{4,-4,3,-2} - 13926f_{2,2,1,-4} - 12528f_{2,-4,1,2} \\
 & - 12054f_{-2,4,1,-2} + 10504f_{2,2,-3,0} - 9666f_{0,4,-5,2} - 9399f_{0,2,3,-4} \\
 & - 9279f_{0,2,-5,4} - 9228f_{-4,0,3,2} - 9032f_{-2,4,-3,2} + 7305f_{0,-2,3,0} \\
 & - 6192f_{-2,-2,1,4} - 4692f_{-2,0,5,-2} - 3768f_{0,-4,3,2} - 3588f_{2,-2,5,-4} \\
 & - 2844f_{2,-4,5,-2} + 2646f_{2,0,-3,2} - 2316f_{-2,-2,5,0} - 2142f_{2,4,-3,-2} \\
 & - 1780f_{4,2,-5,0} - 1770f_{-2,2,-3,4} - 1755f_{4,2,-1,-4} - 270f_{-2,6,-3,0} \\
 & \left. + 260f_{0,6,-1,-4} + 249f_{0,6,-5,0} - 148f_{-4,6,-5,4} + 117f_{-4,6,-1,0} \right) \quad (C.118)
 \end{aligned}$$

The associated weight mask is shown in figure C.118.
B-coefficient c_{1103} is computed using (1, 3)-symmetry.

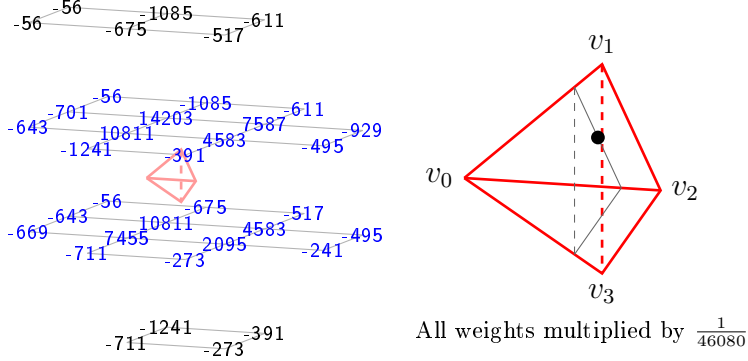


Figure C.119: Weight mask for c_{1220} . The associated domain point is shown in the tetrahedron on the right. The black triangle symbolizes the ring $R_4(v_0)$.

$$\begin{aligned}
 c_{1220} := & \frac{1}{46080} \left(14203 f_{0,2,-1,0} + 10811(f_{0,0,-1,2} + f_{2,0,1,-2}) + 7587 f_{-2,2,1,0} \right. \\
 & + 7455 f_{2,-2,1,0} + 4583(f_{0,0,3,-2} + f_{-2,0,1,2}) + 2095 f_{0,-2,3,0} \\
 & - 1241(f_{0,-2,-1,4} + f_{4,-2,3,-4}) - 1085(f_{0,4,-1,-2} + f_{-2,4,-3,2}) - 929 f_{-4,2,3,0} \\
 & - 711(f_{4,-4,3,-2} + f_{2,-4,1,2}) - 701 f_{2,2,-3,0} - 675(f_{2,2,1,-4} + f_{-2,2,-3,4}) \\
 & - 669 f_{4,-2,-1,0} - 643(f_{2,0,-3,2} + f_{4,0,-1,-2}) - 611(f_{-4,4,-1,2} + f_{-2,4,1,-2}) \\
 & - 517(f_{0,2,3,-4} + f_{-4,2,-1,4}) - 495(f_{-2,0,5,-2} + f_{-4,0,3,2}) \\
 & - 391(f_{2,-2,5,-4} + f_{-2,-2,1,4}) - 273(f_{2,-4,5,-2} + f_{0,-4,3,2}) - 241 f_{-2,-2,5,0} \\
 & \left. - 56(f_{2,4,-3,-2} + f_{0,4,-5,2} + f_{4,2,-1,-4} + f_{0,2,-5,4}) \right) \quad (C.119)
 \end{aligned}$$

The associated weight mask is shown in figure C.119.

B-coefficient c_{1022} is computed using (1, 3)-symmetry.

$$\begin{aligned}
 c_{1211} := & \frac{1}{92160} \left(29231 f_{0,2,-1,0} + 25777 f_{0,0,-1,2} + 19609 f_{2,0,1,-2} \right. \\
 & + 16107 f_{2,-2,1,0} + 13345 f_{-2,2,1,0} + 10276 f_{-2,0,1,2} \\
 & + 5116 f_{0,0,3,-2} + 3083 f_{0,-2,3,0} - 3034 f_{0,-2,-1,4} - 2794 f_{0,4,-1,-2} \\
 & - 2278 f_{4,-2,3,-4} - 1644 f_{4,-4,3,-2} - 1641 f_{-4,2,3,0} - 1523 f_{4,-2,-1,0} \\
 & - 1414 f_{-2,4,-3,2} - 1392 f_{2,2,1,-4} - 1374 f_{4,0,-1,-2} - 1368 f_{2,-4,1,2} \\
 & - 1327 f_{-4,4,-1,2} - 1289 f_{-4,2,-1,4} - 1127 f_{-4,0,3,2} - 1044 f_{-2,2,-3,4} \\
 & - 1003 f_{-2,4,1,-2} - 797 f_{0,2,3,-4} - 758 f_{-2,-2,1,4} - 702 f_{2,0,-3,2} \\
 & - 581 f_{2,2,-3,0} - 551 f_{-2,0,5,-2} - 528 f_{0,-4,3,2} - 458 f_{2,-2,5,-4} \\
 & - 403(f_{0,4,-5,2} + f_{0,2,-5,4}) - 396 f_{2,-4,5,-2} - 387 f_{-2,-2,5,0} \\
 & \left. - 67(f_{2,4,-3,-2} + f_{4,2,-1,-4}) - 34 f_{4,2,-5,0} \right) \quad (C.120)
 \end{aligned}$$

The associated weight mask is shown in figure C.120.

B-coefficient c_{1112} is computed using (1, 3)-symmetry.

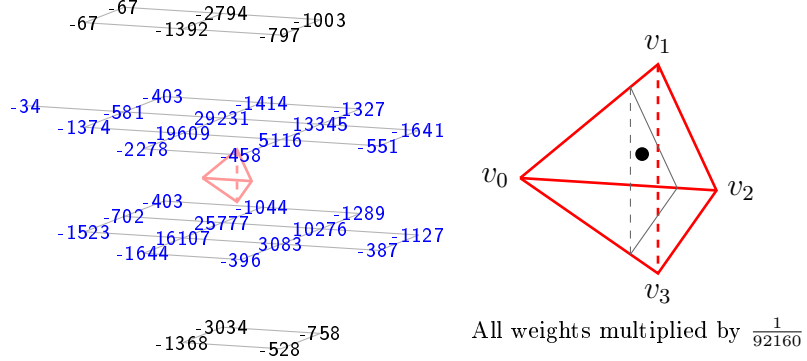


Figure C.120: Weight mask for c_{1211} . The associated domain point is shown in the teterahedron on the right. The black triangle symbolizes the ring $R_4(v_0)$.

$$\begin{aligned}
 c_{1202} := & \frac{1}{46080} \left(14530(f_{0,2,-1,0} + f_{0,0,-1,2}) + 8594(f_{2,-2,1,0} + f_{2,0,1,-2}) \right. \\
 & + 5715(f_{-2,2,1,0} + f_{-2,0,1,2}) - 1734(f_{0,-2,-1,4} + f_{0,4,-1,-2}) \\
 & + 985(f_{0,0,3,-2} + f_{0,-2,3,0}) - 922(f_{4,-4,3,-2} + f_{4,-2,3,-4}) \\
 & - 889(f_{4,-2,-1,0} + f_{4,0,-1,-2}) - 840(f_{-4,4,-1,2} + f_{-4,2,-1,4}) \\
 & - 646(f_{2,2,1,-4} + f_{2,-4,1,2}) - 632(f_{-4,2,3,0} + f_{-4,0,3,2}) \\
 & - 470(f_{0,4,-5,2} + f_{0,2,-5,4}) + 389(f_{2,0,-3,2} + f_{2,2,-3,0}) \\
 & - 367(f_{-2,-2,1,4} + f_{-2,4,1,-2}) - 255(f_{0,2,3,-4} + f_{0,-4,3,2}) \\
 & - 146(f_{-2,-2,5,0} + f_{-2,0,5,-2}) - 134(f_{2,-4,5,-2} + f_{2,-2,5,-4}) \\
 & - 82(f_{-2,4,-3,2} + f_{-2,2,-3,4}) - 34(f_{4,0,-5,2} + f_{4,2,-5,0}) \\
 & \left. - 11(f_{2,4,-3,-2} + f_{4,2,-1,-4} + f_{2,-2,-3,4} + f_{4,-4,-1,2}) \right) \quad (C.121)
 \end{aligned}$$

The associated weight mask is shown in figure C.121.

$$\begin{aligned}
 c_{1130} := & \frac{1}{15360} \left(3994f_{0,2,-1,0} + 3420(f_{2,0,1,-2} + f_{0,0,-1,2}) + 2846f_{2,-2,1,0} \right. \\
 & + 2318f_{-2,2,1,0} + 1836(f_{0,0,3,-2} + f_{-2,0,1,2}) + 1354f_{0,-2,3,0} \\
 & - 349(f_{0,4,-1,-2} + f_{-2,4,-3,2}) - 345(f_{0,-2,-1,4} + f_{4,-2,3,-4}) - 288f_{2,2,-3,0} \\
 & - 279(f_{2,2,1,-4} + f_{-2,2,-3,4}) - 275(f_{4,-4,3,-2} + f_{2,-4,1,2}) - 264f_{-4,2,3,0} \\
 & - 252(f_{2,0,-3,2} + f_{4,0,-1,-2}) - 216f_{4,-2,-1,0} - 204(f_{-2,0,5,-2} + f_{-4,0,3,2}) \\
 & - 195(f_{-2,4,1,-2} + f_{-4,4,-1,2}) - 169(f_{-4,2,-1,4} + f_{0,2,3,-4}) \\
 & \left. - 167(f_{2,-2,5,-4} + f_{-2,-2,1,4}) - 144f_{-2,-2,5,0} - 141(f_{2,-4,5,-2} + f_{0,-4,3,2}) \right) \quad (C.122)
 \end{aligned}$$

The associated weight mask is shown in figure C.122.
B-coefficient c_{1031} is computed using (1, 3)-symmetry.

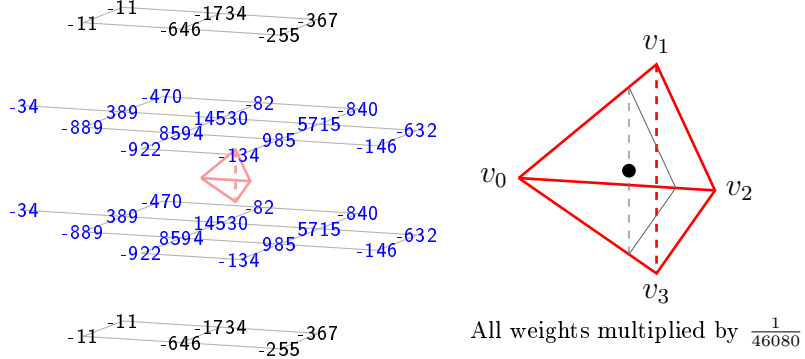


Figure C.121: Weight mask for c_{1202} . The associated domain point is shown in the teterahedron on the right. The black triangle symbolizes the ring $R_4(v_0)$.

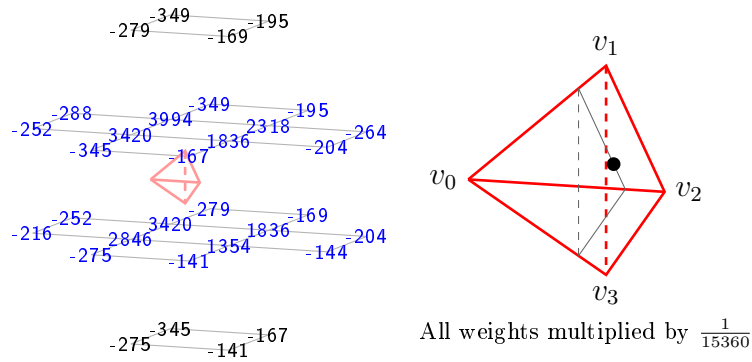


Figure C.122: Weight mask for c_{1130} . The associated domain point is shown in the teterahedron on the right. The black triangle symbolizes the ring $R_4(v_0)$.

$$\begin{aligned}
 c_{1121} := & \frac{1}{46080} \left(12611(f_{0,2,-1,0} + f_{0,0,-1,2}) + 9237(f_{2,-2,1,0} + f_{2,0,1,-2}) \right. \\
 & + 6081(f_{-2,2,1,0} + f_{-2,0,1,2}) + 3335(f_{0,0,3,-2} + f_{0,-2,3,0}) \\
 & - 1267(f_{0,-2,-1,4} + f_{0,4,-1,-2}) - 976(f_{4,-4,3,-2} + f_{4,-2,3,-4}) \\
 & - 880(f_{-2,4,-3,2} + f_{-2,2,-3,4}) - 797(f_{2,-4,1,2} + f_{2,2,1,-4}) \\
 & - 712(f_{-4,2,3,0} + f_{-4,0,3,2}) - 700(f_{2,0,-3,2} + f_{2,2,-3,0}) \\
 & - 684(f_{4,0,-1,-2} + f_{4,-2,-1,0}) - 564(f_{-4,2,-1,4} + f_{-4,4,-1,2}) \\
 & - 497(f_{-2,4,1,-2} + f_{-2,-2,1,4}) - 391(f_{0,-4,3,2} + f_{0,2,3,-4}) \\
 & - 368(f_{-2,-2,5,0} + f_{-2,0,5,-2}) - 332(f_{2,-2,5,-4} + f_{2,-4,5,-2}) \\
 & \left. - 56(f_{0,4,-5,2} + f_{0,2,-5,4}) \right) \tag{C.123}
 \end{aligned}$$

The associated weight mask is shown in figure C.123.

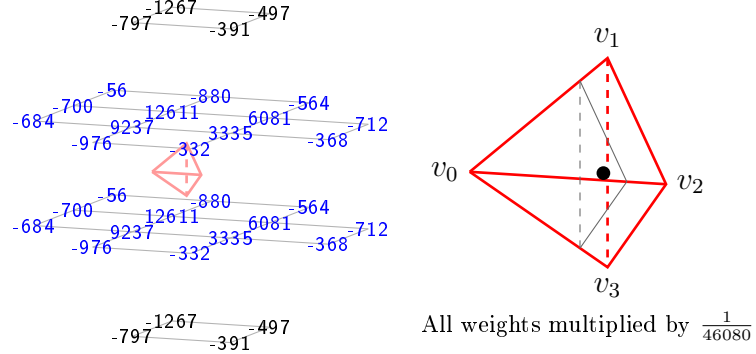


Figure C.123: Weight mask for c_{1121} . The associated domain point is shown in the teterahedron on the right. The black triangle symbolizes the ring $R_4(v_0)$.

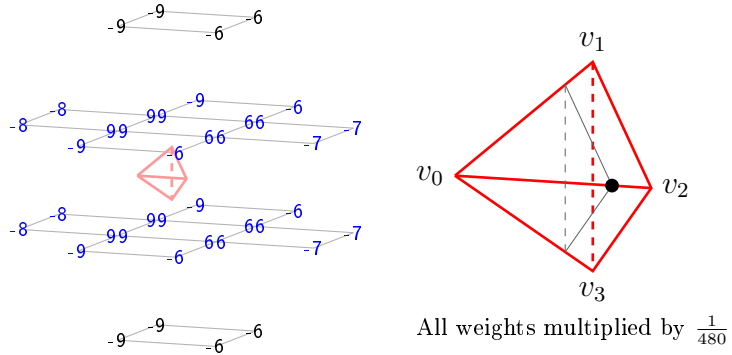


Figure C.124: Weight mask for c_{1040} . The associated domain point is shown in the teterahedron on the right. The black triangle symbolizes the ring $R_4(v_0)$.

$$\begin{aligned}
 c_{1040} := & \frac{1}{480} \left(99(f_{0,2,-1,0} + f_{0,0,-1,2} + f_{2,0,1,-2} + f_{2,-2,1,0}) \right. \\
 & + 66(f_{0,0,3,-2} + f_{0,-2,3,0} + f_{-2,0,1,2} + f_{-2,2,1,0}) \\
 & - 9(f_{4,-4,3,-2} + f_{4,-2,3,-4} + f_{-2,4,-3,2} + f_{2,-4,1,2} + f_{-2,2,-3,4} + f_{2,2,1,-4} \\
 & + f_{0,-2,-1,4} + f_{0,4,-1,-2}) \\
 & - 8(f_{2,2,-3,0} + f_{2,0,-3,2} + f_{4,0,-1,-2} + f_{4,-2,-1,0}) \\
 & - 7(f_{-2,0,5,-2} + f_{-2,-2,5,0} + f_{-4,2,3,0} + f_{-4,0,3,2}) \\
 & - 6(f_{2,-4,5,-2} + f_{-4,4,-1,2} + f_{0,2,3,-4} + f_{-4,2,-1,4} + f_{-2,-2,1,4} + f_{0,-4,3,2} \\
 & \left. + f_{-2,4,1,-2} + f_{2,-2,5,-4}) \right) \tag{C.124}
 \end{aligned}$$

The associated weight mask is shown in figure C.124.

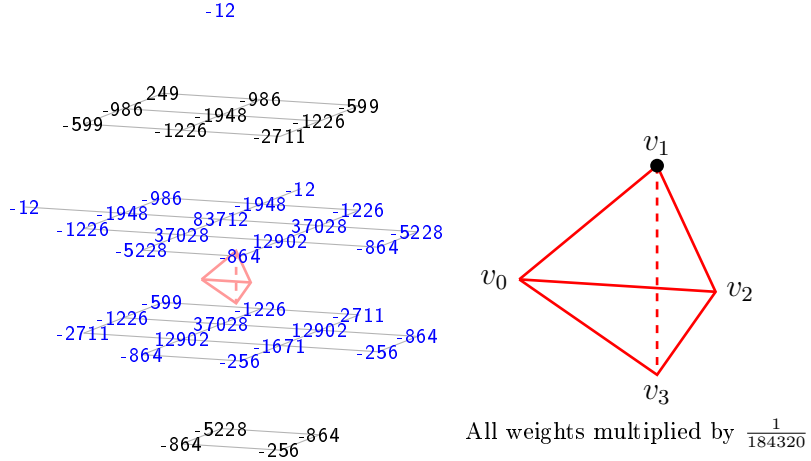


Figure C.125: Weight mask for c_{0500} . The associated domain point is shown in the teterahedron on the right.

$$\begin{aligned}
 c_{0500} := & \frac{1}{184320} \left(83712 f_{0,2,-1,0} + 37028(f_{0,0,-1,2} + f_{-2,2,1,0} + f_{2,0,1,-2}) \right. \\
 & + 12902(f_{0,0,3,-2} + f_{2,-2,1,0} + f_{-2,0,1,2}) \\
 & - 5228(f_{0,-2,-1,4} + f_{4,-2,3,-4} + f_{-4,2,3,0}) \\
 & - 2711(f_{0,2,3,-4} + f_{-4,2,-1,4} + f_{4,-2,-1,0}) \\
 & - 1948(f_{2,2,-3,0} + f_{-2,4,-3,2} + f_{0,4,-1,-2}) - 1671f_{0,-2,3,0} \\
 & - 1226(f_{4,0,-1,-2} + f_{-4,4,-1,2} + f_{-2,4,1,-2} + f_{-2,2,-3,4} + f_{2,2,1,-4} + f_{2,0,-3,2}) \\
 & - 986(f_{0,4,-5,2} + f_{-2,6,-3,0} + f_{2,4,-3,-2}) \\
 & - 864(f_{-4,0,3,2} + f_{4,-4,3,-2} + f_{-2,0,5,-2} + f_{2,-4,1,2} + f_{-2,-2,1,4} + f_{2,-2,5,-4}) \\
 & - 599(f_{4,2,-1,-4} + f_{0,2,-5,4} + f_{-4,6,-1,0}) - 256(f_{2,-4,5,-2} + f_{0,-4,3,2} + f_{-2,-2,5,0}) \\
 & \left. + 249f_{0,6,-5,0} - 12(f_{0,6,-1,-4} + f_{4,2,-5,0} + f_{-4,6,-5,4}) \right) \quad (C.125)
 \end{aligned}$$

The associated weight mask is shown in figure C.125.
B-coefficient c_{0005} is computed using (1, 3)-symmetry.

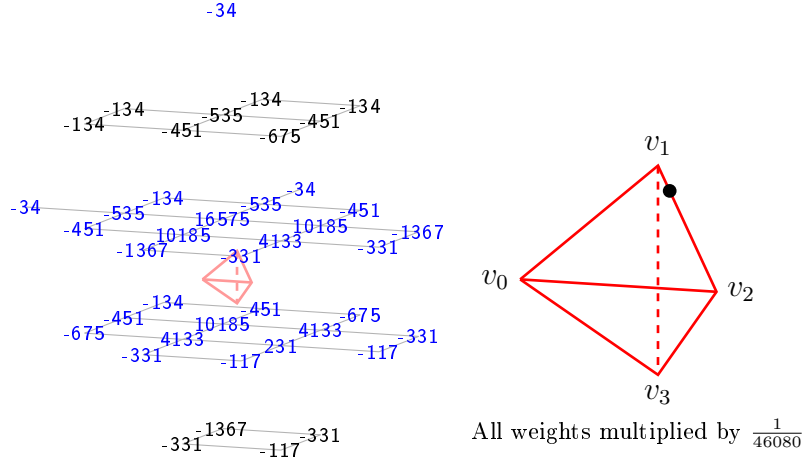


Figure C.126: Weight mask for c_{0410} . The associated domain point is shown in the teterahedron on the right.

$$\begin{aligned}
 c_{0410} := & \frac{1}{46080} \left(16575 f_{0,2,-1,0} + 10185(f_{0,0,-1,2} + f_{2,0,1,-2} + f_{-2,2,1,0}) \right. \\
 & + 4133(f_{0,0,3,-2} + f_{2,-2,1,0} + f_{-2,0,1,2}) \\
 & - 1367(f_{0,-2,-1,4} + f_{4,-2,3,-4} + f_{-4,2,3,0}) \\
 & - 675(f_{0,2,3,-4} + f_{-4,2,-1,4} + f_{4,-2,-1,0}) - 535(f_{2,2,-3,0} + f_{-2,4,-3,2} + f_{0,4,-1,-2}) \\
 & - 451(f_{4,0,-1,-2} + f_{-2,4,1,-2} + f_{-4,4,-1,2} + f_{-2,2,-3,4} + f_{2,2,1,-4} + f_{2,0,-3,2}) \\
 & - 331(f_{-4,0,3,2} + f_{4,-4,3,-2} + f_{-2,0,5,-2} + f_{2,-4,1,2} + f_{-2,-2,1,4} + f_{2,-2,5,-4}) \\
 & + 231f_{0,-2,3,0} \\
 & - 134(f_{2,4,-3,-2} + f_{-2,6,-3,0} + f_{0,4,-5,2} + f_{4,2,-1,-4} + f_{0,2,-5,4} + f_{-4,6,-1,0}) \\
 & \left. - 117(f_{2,-4,5,-2} + f_{0,-4,3,2} + f_{-2,-2,5,0}) - 34(f_{0,6,-1,-4} + f_{4,2,-5,0} + f_{-4,6,-5,4}) \right) \\
 & \quad (C.126)
 \end{aligned}$$

The associated weight mask is shown in figure C.126.
B-coefficient c_{0014} is computed using (1, 3)-symmetry.

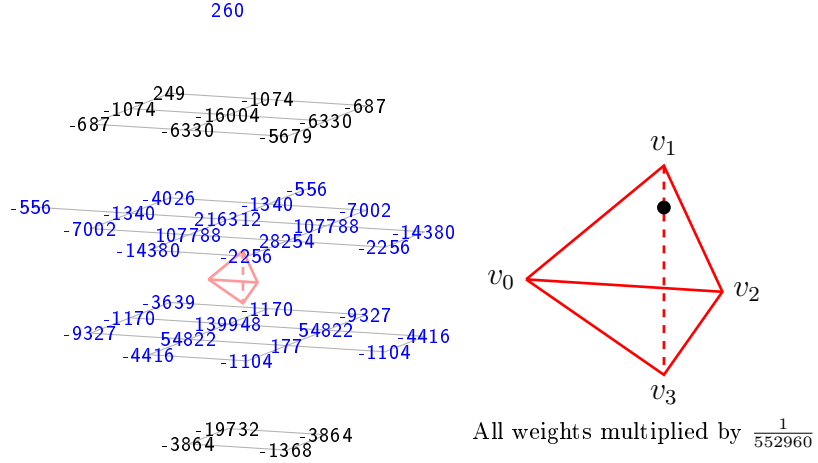


Figure C.127: Weight mask for c_{0401} . The associated domain point is shown in the teterahedron on the right.

$$\begin{aligned}
 c_{0401} := & \frac{1}{552960} \left(216312f_{0,2,-1,0} + 139948f_{0,0,-1,2} + 107788(f_{-2,2,1,0} + f_{2,0,1,-2}) \right. \\
 & + 54822(f_{2,-2,1,0} + f_{-2,0,1,2}) + 28254f_{0,0,3,-2} - 19732f_{0,-2,-1,4} \\
 & - 16004f_{0,4,-1,-2} - 14380(f_{-4,2,3,0} + f_{4,-2,3,-4}) \\
 & - 9327(f_{-4,2,-1,4} + f_{4,-2,-1,0}) - 7002(f_{4,0,-1,-2} + f_{-4,4,-1,2}) \\
 & - 6330(f_{2,2,1,-4} + f_{-2,4,1,-2}) - 5679f_{0,2,3,-4} - 4416(f_{-4,0,3,2} + f_{4,-4,3,-2}) \\
 & - 4026f_{0,4,-5,2} - 3864(f_{-2,-2,1,4} + f_{2,-4,1,2}) - 3639f_{0,2,-5,4} \\
 & - 2256(f_{-2,0,5,-2} + f_{2,-2,5,-4}) - 1368f_{0,-4,3,2} - 1340(f_{-2,4,-3,2} + f_{2,2,-3,0}) \\
 & - 1170(f_{-2,2,-3,4} + f_{2,0,-3,2}) - 1104(f_{2,-4,5,-2} + f_{-2,-2,5,0}) \\
 & - 1074(f_{-2,6,-3,0} + f_{2,4,-3,-2}) - 687(f_{4,2,-1,-4} + f_{-4,6,-1,0}) \\
 & \left. - 556(f_{4,2,-5,0} + f_{-4,6,-5,4}) + 260f_{0,6,-1,-4} + 249f_{0,6,-5,0} + 177f_{0,-2,3,0} \right) \tag{C.127}
 \end{aligned}$$

The associated weight mask is shown in figure C.127.
B-coefficient c_{0104} is computed using (1, 3)-symmetry.

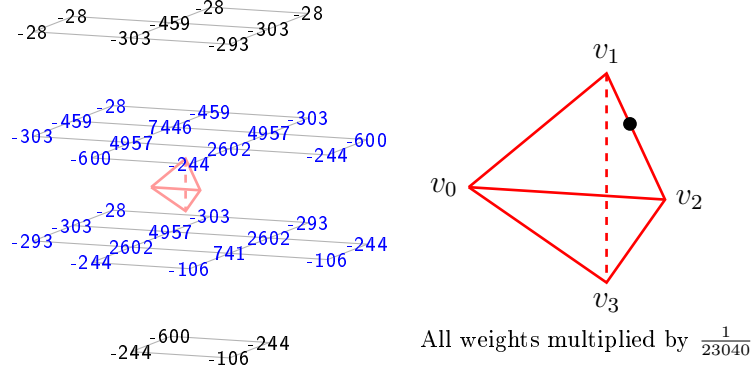


Figure C.128: Weight mask for c_{0320} . The associated domain point is shown in the teterahedron on the right.

$$\begin{aligned}
 c_{0320} := & \frac{1}{23040} \left(7446 f_{0,2,-1,0} + 4957(f_{0,0,-1,2} + f_{2,0,1,-2} + f_{-2,2,1,0}) \right. \\
 & + 2602(f_{0,0,3,-2} + f_{-2,0,1,2} + f_{2,-2,1,0}) + 741 f_{0,-2,3,0} \\
 & - 600(f_{0,-2,-1,4} + f_{4,-2,3,-4} + f_{-4,2,3,0}) - 459(f_{2,2,-3,0} + f_{0,4,-1,-2} + f_{-2,4,-3,2}) \\
 & - 303(f_{4,0,-1,-2} + f_{-2,4,1,-2} + f_{-2,2,-3,4} + f_{-4,4,-1,2} + f_{2,0,-3,2} + f_{2,2,1,-4}) \\
 & - 293(f_{0,2,3,-4} + f_{4,-2,-1,0} + f_{-4,2,-1,4}) \\
 & - 244(f_{-2,-2,1,4} + f_{2,-2,5,-4} + f_{-2,0,5,-2} + f_{2,-4,1,2} + f_{4,-4,3,-2} + f_{-4,0,3,2}) \\
 & - 106(f_{-2,-2,5,0} + f_{2,-4,5,-2} + f_{0,-4,3,2}) \\
 & \left. - 28(f_{-4,6,-1,0} + f_{0,2,-5,4} + f_{4,2,-1,-4} + f_{0,4,-5,2} + f_{-2,6,-3,0} + f_{2,4,-3,-2}) \right) \\
 & \quad (C.128)
 \end{aligned}$$

The associated weight mask is shown in figure C.128.

B-coefficient c_{0023} is computed using (1, 3)-symmetry.

$$\begin{aligned}
 c_{0311} := & \frac{1}{92160} \left(30906 f_{0,2,-1,0} + 23998 f_{0,0,-1,2} + 18014(f_{-2,2,1,0} + f_{2,0,1,-2}) \right. \\
 & + 11443(f_{-2,0,1,2} + f_{2,-2,1,0}) + 6196 f_{0,0,3,-2} - 3024 f_{0,-2,-1,4} \\
 & - 2544 f_{0,4,-1,-2} - 2255(f_{-4,2,3,0} + f_{4,-2,3,-4}) + 2130 f_{0,-2,3,0} \\
 & - 1372(f_{-4,2,-1,4} + f_{4,-2,-1,0}) - 1261(f_{4,0,-1,-2} + f_{-4,4,-1,2}) \\
 & - 1215(f_{-2,4,1,-2} + f_{2,2,1,-4}) - 1107(f_{-4,0,3,2} + f_{4,-4,3,-2}) \\
 & - 1099(f_{-2,4,-3,2} + f_{2,2,-3,0}) - 950 f_{0,2,3,-4} - 946(f_{-2,-2,1,4} + f_{2,-4,1,2}) \\
 & - 850(f_{-2,2,-3,4} + f_{2,0,-3,2}) - 561(f_{2,-2,5,-4} + f_{-2,0,5,-2}) - 412 f_{0,-4,3,2} \\
 & - 358(f_{0,4,-5,2} + f_{0,2,-5,4}) - 335(f_{-2,-2,5,0} + f_{2,-4,5,-2}) \\
 & \left. - 67(f_{4,2,-1,-4} + f_{-2,6,-3,0} + f_{2,4,-3,-2} + f_{-4,6,-1,0}) - 34(f_{4,2,-5,0} + f_{-4,6,-5,4}) \right) \\
 & \quad (C.129)
 \end{aligned}$$

The associated weight mask is shown in figure C.129.

B-coefficient c_{0113} is computed using (1, 3)-symmetry.

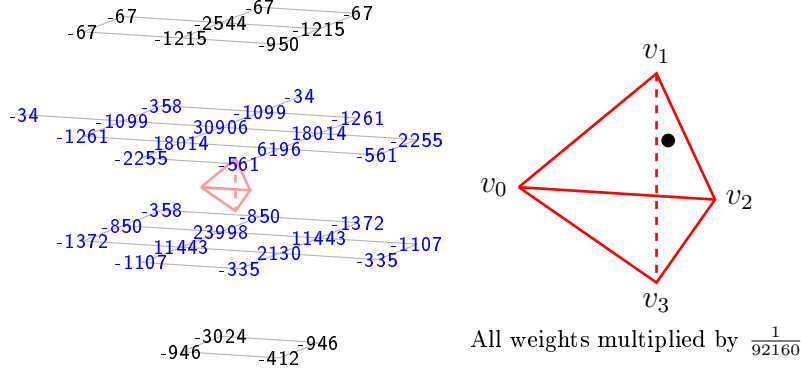


Figure C.129: Weight mask for c_{0311} . The associated domain point is shown in the tetrahedron on the right.

$$\begin{aligned}
 c_{0302} := & \frac{1}{46080} \left(15438f_{0,2,-1,0} + 13622f_{0,0,-1,2} + 7986(f_{-2,2,1,0} + f_{2,0,1,-2}) \right. \\
 & + 6323(f_{2,-2,1,0} + f_{-2,0,1,2}) - 1788f_{0,-2,-1,4} - 1680f_{0,4,-1,-2} \\
 & + 1376f_{0,0,3,-2} - 935(f_{4,-2,3,-4} + f_{-4,2,3,0}) - 888(f_{-4,2,-1,4} + f_{4,-2,-1,0}) \\
 & - 841(f_{4,0,-1,-2} + f_{-4,4,-1,2}) - 619(f_{4,-4,3,-2} + f_{-4,0,3,2}) + 594f_{0,-2,3,0} \\
 & - 555(f_{-2,4,1,-2} + f_{2,2,1,-4}) - 470(f_{0,4,-5,2} + f_{0,2,-5,4}) \\
 & - 458(f_{-2,-2,1,4} + f_{2,-4,1,2}) - 310f_{0,2,3,-4} - 200f_{0,-4,3,2} \\
 & + 173(f_{-2,4,-3,2} + f_{2,2,-3,0}) - 157(f_{2,-2,5,-4} + f_{-2,0,5,-2}) \\
 & + 134(f_{-2,2,-3,4} + f_{2,0,-3,2}) - 123(f_{-2,-2,5,0} + f_{2,-4,5,-2}) \\
 & \left. - 34(f_{4,2,-5,0} + f_{-4,6,-5,4}) - 11(f_{4,2,-1,-4} + f_{-2,6,-3,0} + f_{2,4,-3,-2} + f_{-4,6,-1,0}) \right) \\
 & \quad (C.130)
 \end{aligned}$$

The associated weight mask is shown in figure C.130.

B-coefficient c_{0203} is computed using (1, 3)-symmetry.

$$\begin{aligned}
 c_{0230} := & \frac{1}{15360} \left(4275f_{0,2,-1,0} + 3127(f_{0,0,-1,2} + f_{-2,2,1,0} + f_{2,0,1,-2}) \right. \\
 & + 2071(f_{0,0,3,-2} + f_{2,-2,1,0} + f_{-2,0,1,2}) + 1107f_{0,-2,3,0} \\
 & - 345(f_{2,2,-3,0} + f_{-2,4,-3,2} + f_{0,4,-1,-2}) - 337(f_{4,-2,3,-4} + f_{-4,2,3,0} + f_{0,-2,-1,4}) \\
 & - 239(f_{2,0,-3,2} + f_{-4,4,-1,2} + f_{2,2,1,-4} + f_{-2,2,-3,4} + f_{4,0,-1,-2} + f_{-2,4,1,-2}) \\
 & - 207(f_{4,-4,3,-2} + f_{-4,0,3,2} + f_{2,-4,1,2} + f_{2,-2,5,-4} + f_{-2,-2,1,4} + f_{-2,0,5,-2}) \\
 & \left. - 177(f_{4,-2,-1,0} + f_{-4,2,-1,4} + f_{0,2,3,-4}) - 121(f_{2,-4,5,-2} + f_{-2,-2,5,0} + f_{0,-4,3,2}) \right) \\
 & \quad (C.131)
 \end{aligned}$$

The associated weight mask is shown in figure C.131.

B-coefficient c_{0032} is computed using (1, 3)-symmetry.

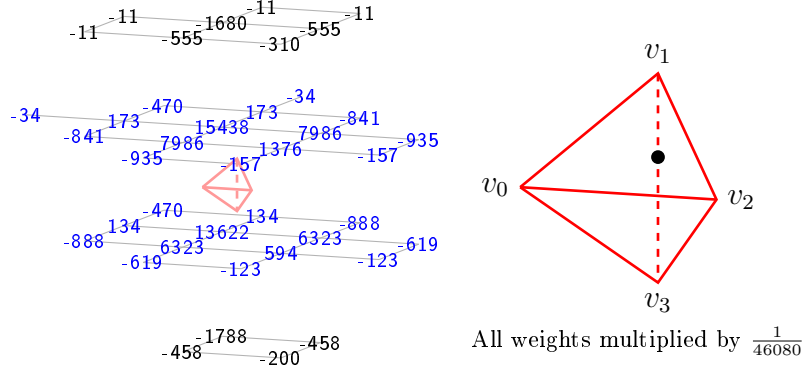


Figure C.130: Weight mask for c_{0302} . The associated domain point is shown in the teterahedron on the right.

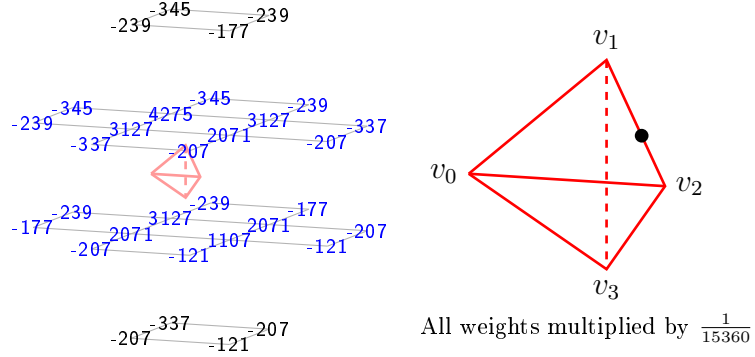


Figure C.131: Weight mask for c_{0230} . The associated domain point is shown in the teterahedron on the right.

$$\begin{aligned}
 c_{0221} := & \frac{1}{23040} \left(6757f_{0,2,-1,0} + 5854f_{0,0,-1,2} + 4242(f_{2,0,1,-2} + f_{-2,2,1,0}) \right. \\
 & + 3417(f_{-2,0,1,2} + f_{2,-2,1,0}) + 1981f_{0,0,3,-2} + 1354f_{0,-2,3,0} \\
 & - 641f_{0,-2,-1,4} - 626f_{0,4,-1,-2} - 485(f_{4,-2,3,-4} + f_{-4,2,3,0}) \\
 & - 434(f_{-2,4,-3,2} + f_{2,2,-3,0}) - 359(f_{4,-4,3,-2} + f_{-4,0,3,2}) \\
 & - 356(f_{-2,2,-3,4} + f_{2,0,-3,2}) - 340(f_{2,2,1,-4} + f_{-2,4,1,-2}) \\
 & - 324(f_{-4,4,-1,2} + f_{4,0,-1,-2}) - 307(f_{-2,-2,1,4} + f_{2,-4,1,2}) \\
 & - 300(f_{-4,2,-1,4} + f_{4,-2,-1,0}) - 224f_{0,2,3,-4} - 199(f_{2,-2,5,-4} + f_{-2,0,5,-2}) \\
 & \left. - 167f_{0,-4,3,2} - 151(f_{2,-4,5,-2} + f_{-2,-2,5,0}) - 28(f_{0,4,-5,2} + f_{0,2,-5,4}) \right) \tag{C.132}
 \end{aligned}$$

The associated weight mask is shown in figure C.132.
B-coefficient c_{0122} is computed using (1, 3)-symmetry.

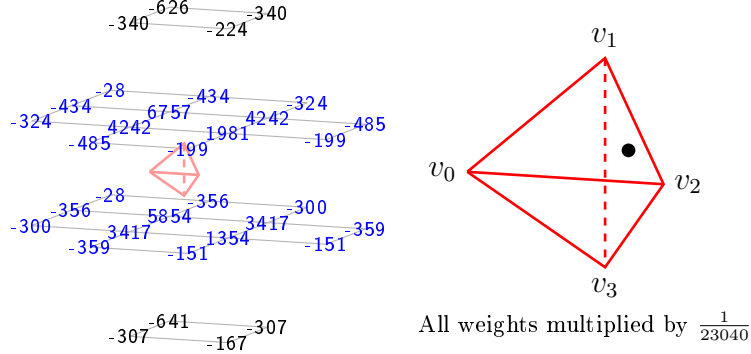


Figure C.132: Weight mask for c_{0221} . The associated domain point is shown in the teterahedron on the right.

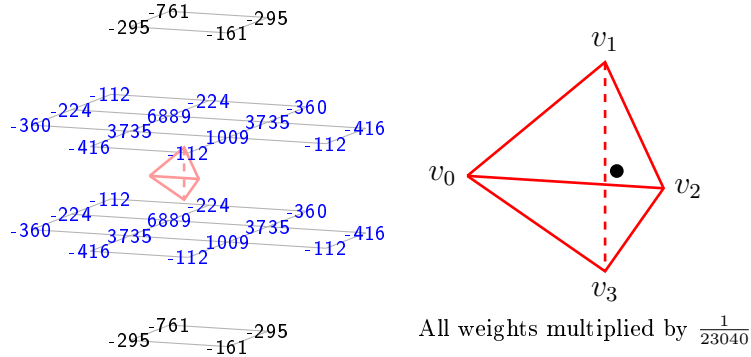


Figure C.133: Weight mask for c_{0212} . The associated domain point is shown in the teterahedron on the right.

$$\begin{aligned}
 c_{0212} := & \frac{1}{23040} \left(6889(f_{0,2,-1,0} + f_{0,0,-1,2}) \right. \\
 & + 3735(f_{-2,0,1,2} + f_{2,0,1,-2} + f_{2,-2,1,0} + f_{-2,2,1,0}) \\
 & + 1009(f_{0,0,3,-2} + f_{0,-2,3,0}) - 761(f_{0,-2,-1,4} + f_{0,4,-1,-2}) \\
 & - 416(f_{4,-4,3,-2} + f_{4,-2,3,-4} + f_{-4,2,3,0} + f_{-4,0,3,2}) \\
 & - 360(f_{-4,4,-1,2} + f_{-4,2,-1,4} + f_{4,0,-1,-2} + f_{4,-2,-1,0}) \\
 & - 295(f_{-2,-2,1,4} + f_{2,2,1,-4} + f_{-2,4,1,-2} + f_{2,-4,1,2}) \\
 & - 224(f_{2,0,-3,2} + f_{2,2,-3,0} + f_{-2,2,-3,4} + f_{-2,4,-3,2}) - 161(f_{0,2,3,-4} + f_{0,-4,3,2}) \\
 & \left. - 112(f_{0,4,-5,2} + f_{2,-4,5,-2} + f_{2,-2,5,-4} + f_{0,2,-5,4} + f_{-2,-2,5,0} + f_{-2,0,5,-2}) \right) \\
 & \quad (C.133)
 \end{aligned}$$

The associated weight mask is shown in figure C.133.

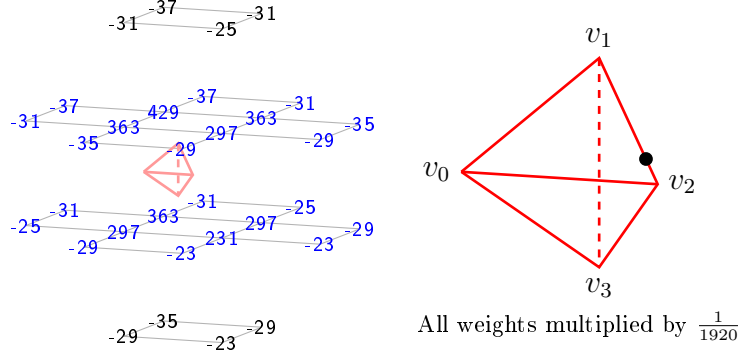


Figure C.134: Weight mask for c_{0140} . The associated domain point is shown in the tetrahedron on the right.

$$\begin{aligned}
 c_{0140} := & \frac{1}{1920} \left(429f_{0,2,-1,0} + 363(f_{0,0,-1,2} + f_{-2,2,1,0} + f_{2,0,1,-2}) \right. \\
 & + 297(f_{0,0,3,-2} + f_{2,-2,1,0} + f_{-2,0,1,2}) + 231f_{0,-2,3,0} \\
 & - 37(f_{2,2,-3,0} + f_{-2,4,-3,2} + f_{0,4,-1,-2}) - 35(f_{4,-2,3,-4} + f_{-4,2,3,0} + f_{0,-2,-1,4}) \\
 & - 31(f_{2,0,-3,2} + f_{-4,4,-1,2} + f_{2,2,1,-4} + f_{-2,2,-3,4} + f_{4,0,-1,-2} + f_{-2,4,1,-2}) \\
 & - 29(f_{4,-4,3,-2} + f_{-4,0,3,2} + f_{2,-4,1,2} + f_{2,-2,5,-4} + f_{-2,-2,1,4} + f_{-2,0,5,-2}) \\
 & \left. - 25(f_{4,-2,-1,0} + f_{-4,2,-1,4} + f_{0,2,3,-4}) - 23(f_{2,-4,5,-2} + f_{-2,-2,5,0} + f_{0,-4,3,2}) \right) \\
 & \quad (C.134)
 \end{aligned}$$

The associated weight mask is shown in figure C.134.
B-coefficient c_{0041} is computed using (1, 3)-symmetry.

$$\begin{aligned}
 c_{0131} := & \frac{1}{15360} \left(3713(f_{0,2,-1,0} + f_{0,0,-1,2}) \right. \\
 & + 2611(f_{-2,0,1,2} + f_{2,0,1,-2} + f_{2,-2,1,0} + f_{-2,2,1,0}) \\
 & + 1601(f_{0,0,3,-2} + f_{0,-2,3,0}) - 353(f_{0,-2,-1,4} + f_{0,4,-1,-2}) \\
 & - 292(f_{2,2,-3,0} + f_{-2,4,-3,2} + f_{-2,2,-3,4} + f_{2,0,-3,2}) \\
 & - 272(f_{4,-4,3,-2} + f_{4,-2,3,-4} + f_{-4,2,3,0} + f_{-4,0,3,2}) \\
 & - 235(f_{-2,-2,1,4} + f_{2,2,1,-4} + f_{-2,4,1,-2} + f_{2,-4,1,2}) \\
 & - 208(f_{-4,4,-1,2} + f_{-4,2,-1,4} + f_{4,0,-1,-2} + f_{4,-2,-1,0}) \\
 & \left. - 164(f_{-2,0,5,-2} + f_{2,-4,5,-2} + f_{2,-2,5,-4} + f_{-2,-2,5,0}) - 161(f_{0,2,3,-4} + f_{0,-4,3,2}) \right) \\
 & \quad (C.135)
 \end{aligned}$$

The associated weight mask is shown in figure C.135.

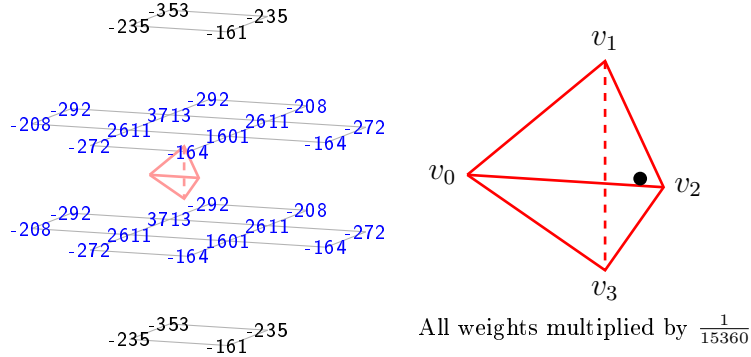


Figure C.135: Weight mask for c_{0131} . The associated domain point is shown in the teterahedron on the right.

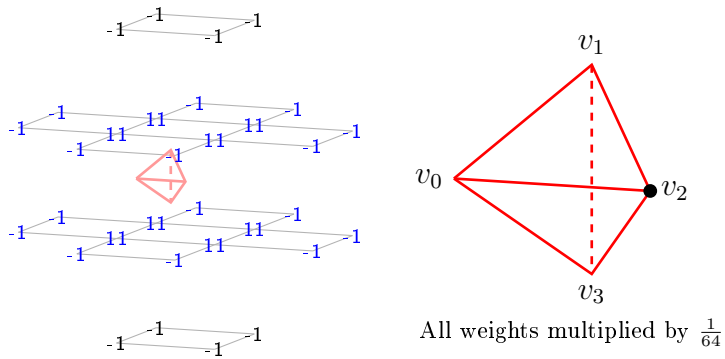


Figure C.136: Weight mask for c_{0050} . The associated domain point is shown in the teterahedron on the right.

$$\begin{aligned}
 c_{0050} := & \frac{1}{64} \left(11(f_{0,0,3,-2} + f_{0,2,-1,0} + f_{0,0,-1,2} + f_{0,-2,3,0} + f_{-2,0,1,2} + f_{2,0,1,-2} \right. \\
 & + f_{-2,2,1,0} + f_{2,-2,1,0}) \\
 & - (f_{-4,2,-1,4} + f_{-2,4,1,-2} + f_{2,-4,1,2} + f_{-2,4,-3,2} + f_{2,-4,5,-2} + f_{4,0,-1,-2} \\
 & + f_{-4,0,3,2} + f_{4,-2,-1,0} + f_{4,-4,3,-2} + f_{-4,2,3,0} + f_{4,-2,3,-4} + f_{-4,4,-1,2} \\
 & + f_{2,-2,5,-4} + f_{-2,-2,5,0} + f_{-2,2,-3,4} + f_{2,2,-3,0} + f_{2,2,1,-4} + f_{-2,-2,1,4} \\
 & \left. + f_{-2,0,5,-2} + f_{2,0,-3,2} + f_{0,-4,3,2} + f_{0,4,-1,-2} + f_{0,2,3,-4} + f_{0,-2,-1,4} \right) \tag{C.136}
 \end{aligned}$$

The associated weight mask is shown in figure C.136.

Appendix D

A program used in the proofs of several theorems for the quasi-interpolation operators

We used the computer algebra system Mathematica[®] by Wolfram Research (<http://www.wolfram.com/mathematica>) to write a computer program which performs certain calculations involving the B-coefficient computation rules of our quasi-interpolation operators. The program verifies that all smoothness conditions referred to in the proofs of theorems 3.18, 3.23 and 3.34, are satisfied. It further verifies the reproduction properties of the operators by performing the calculations described in the proofs of theorems 3.21, 3.26 and 3.38. In this appendix, we provide a complete listing of the source code of our program, as well as a detailed description of all functions. For the documentation of Mathematica[®], which contains the documentation of its syntax, we refer to [88]. All functions used in the following source code that are not explicitly discussed in this appendix, like `Flatten` or `Table`, are part of the Mathematica[®] software package. These functions are also documented in [88].

The calculations in our program involve only rational numbers, which are represented in Mathematica[®] by a ratio of two integer values. The integer values, in turn, are exact and can be of arbitrary length. Thus, no rounding occurs during the calculations, and the results produced by the program are exact.

Basic functions for Bernstein-Bézier techniques

The functions in this section are the basic tools needed to perform the calculations. They provide a way to generate indices of the form $i + j + k + l = d$, an implementation of the Bernstein basis polynomials, and the degree raising

technique described in lemma 2.41.

bivIndices

This function generates a list of all 3-tuples of the form (i, j, k) with $i + j + k = d$.

1. `bivIndices[d_]:=Flatten[`
2. `Table[{i, j, d-i-j}, {i, d, 0, -1}, {j, d-i, 0, -1}], 1]`

triIndices

Analogously to the function `bivIndices`, this function generates a list of all 4-tuples of the form (i, j, k, l) with $i + j + k + l = d$.

1. `triIndices[d_] := Flatten[`
2. `Table[{i, j, k, d-i-j-k}, {i, d, 0, -1}, {j, d-i, 0, -1},`
3. `{k, d-i-j, 0, -1}], 2]`

mypow

The expression 0^0 is undefined in Mathematica®. In the context of definition 2.33, we defined $0^0 := 1$. This function takes two numbers m, e as input, and returns 1 if $m = 0$ and $e = 0$, and m^e otherwise.

1. `mypow[m_, e_] := If[m == 0 && e == 0, 1, m^e]`

BPoly

This implements the Bernstein basis polynomials defined in 2.33. The function takes two parameters, `ind` and `bary`, which are both 4-tuples. The first parameter represents indices i, j, k, l . The second parameter is a tuple $(\varphi_0(v), \varphi_1(v), \varphi_2(v), \varphi_3(v))$ of barycentric coordinates. The function returns $B_{ijkl}(v)$.

1. `BPoly[ind_, bary_] :=`
2. `Total[ind]!*Product[`
3. `mypow[bary[[i]], ind[[i]]]/(ind[[i]]!), {i, 4}]`
4. `]`

raiseDegree

This function takes two parameters, a positive integer d and a coefficient vector `coeffs`. The coefficient vector is interpreted as the vector of B-coefficients of a trivariate polynomial p of degree d in B-form. It is assumed that the order of the B-coefficients corresponds to the order of the indices generated by `triIndices[d]`. The function generates and returns a coefficient vector `res` which represents the B-coefficients of p written as a polynomial of degree $d+1$. These coefficients are calculated in the loop in lines 7-32, according to the formula of lemma 2.41.

In lines 3 and 4, the local variables `indices1` and `indices2` are initialized as trivariate index lists of degrees d and $d+1$, respectively, such that `coeffs[pos]` is the B-coefficient with indices `indices1[pos]`, and `res[m]` is the B-coefficient with indices `indices2[m]`. The coefficient vector `res` is initialized as the zero vector in line 6. In the first step of the main loop (line 8), an index tuple `ind2` is taken from the index list `indices2`. This tuple corresponds to the indices i, j, k, l of the sum in lemma 2.41. The four *if*-statements correspond to the four terms in the lemma. We look in detail at the first of these statements. The value `ind2[[1]]` represents the value i in the lemma. If this is zero, then $i-1$ is negative and the first term of the lemma does not contribute to c_{ijkl} . In line 11, the index tuple `ind1` is initialized and represents the indices $i-1, j, k, l$. The contribution of the term $ic_{i-1,j,k,l}$ to c_{ijkl} is calculated in line 13. The contribution of the other terms is calculated in the remaining three *if*-statements.

```

1.  raiseDegree[d_, coeffs_] := Module[
2.    {indices1, indices2, ind1, ind2, pos, res},
3.    indices1 = triIndices[d];
4.    indices2 = triIndices[d + 1];
5.    res = Table[0, {Dimensions[indices2][[1]]}];
6.    Do[
7.      Do[
8.        ind2 = indices2[[m]];
9.        If[ind2[[1]] > 0,
10.          ind1 = ind2 - {1, 0, 0, 0};
11.          pos = Position[indices1, ind1][[1, 1]];
12.          res[[m]] += ind2[[1]]*coeffs[[pos]]
13.        ];
14.        ];
15.        If[ind2[[2]] > 0,
16.          ind1 = ind2 - {0, 1, 0, 0};
17.          pos = Position[indices1, ind1][[1, 1]];
18.          res[[m]] += ind2[[2]]*coeffs[[pos]]
19.        ];
20.        If[ind2[[3]] > 0,

```

```

21.      ind1 = ind2 - {0, 0, 1, 0};
22.      pos = Position[indices1, ind1][[1, 1]];
23.      res[[m]] += ind2[[3]]*coeffs[[pos]]
24.    ];
25.    If[ind2[[4]] > 0,
26.      ind1 = ind2 - {0, 0, 0, 1};
27.      pos = Position[indices1, ind1][[1, 1]];
28.      res[[m]] += ind2[[4]]*coeffs[[pos]]
29.    ];
30.    res[[m]] /= (d + 1),
31.    {m, Dimensions[indices2][[1]]}
32.  ];
33.  res
34. ]

```

raiseToDegree

This function calls `raiseDegree` repeatedly. to generate the B-form of a polynomial p of degree `startd`, written as a polynomial of degree `endd`. The initial B-coefficients of p are supplied as the parameter `coeffs`.

```

1.  raiseToDegree[startd_, endd_, coeffs_] := Module[{res},
2.    res = coeffs;
3.    For[d = startd, d < endd, ++d, res = raiseDegree[d, res]];
4.    res
5.  ]

```

B-Coefficient computation rule manipulation functions

The functions in this section are related to the B-coefficient computation rules defined in 3.2. Each rule is represented in Mathematica® by a list containing four entries. The first entry is a 4-tuple representing the indices i, j, k, l of the B-coefficient which is calculated by the rule. The second entry is a factor by which all weights are multiplied. This is usually the least common multiple of the denominators of the weights. The third entry is a list of the weights, divided by the common factor. The final entry is a list of the barycentric coordinates of the sample points, as defined in 3.4.

findRule

This function takes two parameters, a list `rulelist` of B-coefficient computation rules, which are assumed to be in the format described above, and an index tuple `ind`. If the list contains a rule associated with the specified index, this rule is returned. Otherwise, an the value `False` is returned.

In line 2, the first entry of all rules in the list is compared to the index. If one or more entries match the index, `rind` is not empty, and the local variable `res` is set to the first rule in the list that matches the specified index in line 6. Otherwise, `res` is set to `False` in line 4.

```

1.  findRule[rulelist_, ind_] := Module[{res, rind},
2.    rind = Position[rulelist[[All, 1]], ind_];
3.    If[rind == {}, 
4.      res = False,
5.      (* else *)
6.      res = rulelist[[ rind[[1, 1]] ]]
7.    ];
8.    res
9.  ]

```

addRules

This function takes two B-coefficient computation rules, `r1` and `r2`, as input and generates a *pseudo-rule* representing the sum of the rules. The output is in the format described in the beginning of this section, but the first entry of the output, which usually defines the B-coefficient which is calculated by the rule, is meaningless.

In lines 4 and 5, the weights of the rules are multiplied by the common factors, and the results are stored in `w1` and `w2`.

In the main loop (lines 8-17), the sum of the rules is calculated. The resulting weights are stored in `w1`, while the associated sample points are stored in `sp1`. Each sample point of `r2` is examined. If this sample point is also a sample point of `s1`, then the weights are added in line 11 and stored in `w1`. Otherwise, The sample point and associated weight are appended to the sum in lines 14 and 13, respectively.

At the end of the loop, `w1` holds the weights of the sum of `r1` and `r2`, but some of these weights may be zero. The weights and sample points of the final result are initialized as empty lists in lines 18 and 19, respectively. In the loop in lines 20-26, each weight in `w1` is examined, and if it is non-zero, the weight and associated sample point are appended to the final result in lines 22 and 23, respectively.

In line 27, the least common multiple of the denominators of the weights of the sum is calculated. Line 28 defines the output.

```

1. addRules[r1_, r2_] := Module[
2.   {w1, w2, wres, sp1, sp2, spres, j, denom},
3.
4.   w1 = r1[[2, 1]]*r1[[3]];
5.   w2 = r2[[2, 1]]*r2[[3]];
6.   sp1 = r1[[4]];
7.   sp2 = r2[[4]];
8.   Do[
9.     If[MemberQ[sp1, sp2[[i]]],
10.      j = Position[sp1, sp2[[i]]][[1, 1]];
11.      w1[[j]] = w1[[j]] + w2[[i]],
12.      (* else *)
13.      AppendTo[w1, w2[[i]]];
14.      AppendTo[sp1, sp2[[i]]]
15.    ],
16.    {i, Dimensions[sp2][[1]]}
17.  ];
18.  wres = {};
19.  spres = {};
20.  Do[
21.    If[w1[[i]] != 0,
22.      AppendTo[wres, w1[[i]]];
23.      AppendTo[spres, sp1[[i]]]
24.    ],
25.    {i, Dimensions[w1][[1]]}
26.  ];
27.  denom = LCM @@ Denominator[wres];
28.  {r1[[1]] + r2[[1]], {1/denom}, wres*denom, spres}
29. ]

```

rewriteRule

This function rewrites the B-coefficient computation rule in the parameter **rule** by multiplying each sample point of the rule with the transpose of the matrix **M**. We use this process to compare two B-coefficient computation rules defined relative to two neighboring tetrahedra, as first described in case 1 of the proof of theorem 3.18. In that case, the row vector $(\varphi_0, \varphi_1, \varphi_2, \varphi_3)$ is

multiplied by the transpose of the matrix

$$M := \begin{pmatrix} 1 & 0 & 0 & 1 \\ 0 & 1 & 0 & 0 \\ 0 & 0 & 1 & 1 \\ 0 & 0 & 0 & -1 \end{pmatrix},$$

resulting in $(\varphi_0 + \varphi_3, \varphi_1, \varphi_2 + \varphi_3, -\varphi_3)$.

```

1. rewriteRule[rule_, M_] := Module[{spres},
2.   spres = rule[[4]].Transpose[M];
3.   {rule[[1]], rule[[2]], rule[[3]], spres}
4. ]

```

rulesEqual

This function compares two rules or pseudo-rules, **r1** and **r2**. It return **True** if the rules are equal, which means that they use the same set of sample points and the same weights, and **False** otherwise. The local variables **w1**, **w2**, **sp1** and **sp2** are initialized exactly as in the function **addRules**. The local variable **res** is set to **True**. The first test in line 7 makes sure that the number of sample points of both rules is equal. Otherwise, the rules are not equal and **res** is set to **False**. In the main loop (lines 9-16), each sample point in **sp2** is examined. If it is not a member of **sp1**, then the rules are not equal and **res** is set to **False**. Otherwise, the weights associated with these sample points are compared, and again, **res** is set to **False** if they are not equal. Finally, **res** is returned.

```

1. rulesEqual[r1_, r2_] := Module[{w1, w2, sp1, sp2, res, j},
2.   w1 = r1[[2, 1]]*r1[[3]];
3.   w2 = r2[[2, 1]]*r2[[3]];
4.   sp1 = r1[[4]];
5.   sp2 = r2[[4]];
6.   res = True;
7.   If[Dimensions[sp1] != Dimensions[sp2],
8.     res = False,
9.     Do[
10.       If[MemberQ[sp1, sp2[[i]]],
11.         j = Position[sp1, sp2[[i]]][[1, 1]];
12.         If[w1[[j]] != w2[[i]], res = False],
13.         res = False
14.       ],
15.       {i, Dimensions[sp2][[1]]}]

```

```

16.      ];
17.      ];
18.      res
19.  ]

```

applyRuleToBPolynomial

This function is an implementation of (3.1). It calculates the B-coefficient specified in first entry of the parameter `rule`. The sample values f_ϕ^T are hereby the values of the Bernstein basis polynomial B_{ijkl}^T with the index specified by the parameter `ind`.

```

1.  applyRuleToBPolynomial[rule_, ind_] := Module[{res, w, sp, indices},
2.    w = rule[[3]];
3.    sp = rule[[4]];
4.    res = rule[[2, 1]] * Sum[
5.      w[[i]]*BPolynomial[ind, sp[[i]]], {i, Dimensions[w][[1]]}]
6.    ];
7.    res
8.  ]

```

Functions to test smoothness conditions and reproduction of Bernstein basis polynomials

In this section we discuss the two main functions of this program. The first function tests if all smoothness conditions (3.4)-(3.6) between two neighboring tetrahedra of the BCC partition are satisfied. The second function tests if Bernstein basis polynomials are reproduced by a quasi-interpolation operator defined by a set of B-coefficient computation rules. We use the first functions to proof some of our claims in theorems 3.18, 3.23 and 3.34, and the second function to proof theorems 3.21, 3.26 and 3.38.

smoothnessTest

This function performs all calculations necessary to verify that all smoothness conditions (3.4)-(3.6) between two neighboring tetrahedra T and \tilde{T} of the BCC partition are satisfied. These calculations are described in detail in the proof of theorem 3.18. The function takes four parameters. The parameters `rules1` and `rules2` are two sets of B-coefficient computation rules which define a quasi-interpolation operator on T and \tilde{T} , respectively. The

parameters `ind1` and `ind2` are 4-tuples that define two permutations σ_1, σ_2 that are used in conjunction with lemma 2.40 to align the vertices of T and \tilde{T} to reflect the situation described in theorem 2.53

In lines 5 and 6, permutation matrices are generated to reflect the permutations σ_1 and σ_2 . Line 7 defines a matrix `M` that is used to rewrite the sample points of `rules2` relative to T , using the function `rewriteRule`. This matrix, applied to a vector of barycentric coordinates, implements (3.7). The index rearrangement of the vertices of T and \tilde{T} , defined by σ_1 and σ_2 , together with the sample point transformation defined by `M`, results in the matrix defined in line 8. The output generated in lines 9-19 prints information about the vertex alignment and index transformation which confirms that the tests are performed correctly.

In lines 23-44, the C^0 conditions (3.4) are verified. In line 23, the indices $i + j + k = 5$ are generated. These indices are transformed in lines 27 and 29, using the permutations σ_1 and σ_2 . The associated rules are obtained in lines 28 and 30. The test in line 32 ascertains that both rules are present in the rule sets `rules1` and `rules2`. If one of the rules is not found, the test fails. Otherwise, `rule2` is rewritten in line 38, and line 39 tests if the rules are equal.

The same technique is used in lines 48-76 to verify the C^1 conditions (3.5). Lines 69 and 70 calculate the sums $c_{ijk1}^T + c_{ijk1}^T$ and $c_{i+1,j,k,0}^T + c_{i,j,k+1,0}^T$ in these conditions, respectively, using the function `addRules` introduced in the previous section. The C^2 conditions (3.6) are verified in lines 80-119.

The output of this function, generated in lines 43,44,75,76,117 and 118, is a list of values `True` or `False` which represent that a test passes or fails, respectively.

```

1.  smoothnessTest[rules1_, ind1_, rules2_, ind2_] := Module[
2.    {P1, P2, M, rule1, rule2, rule3, rule4, rule5, rule6, ind,
3.     rind, indices, res, phi, tphi},
4.
5.    P1 = IdentityMatrix[4][[ind1]];
6.    P2 = IdentityMatrix[4][[ind2]];
7.    M = {{1, 0, 0, 1}, {0, 1, 0, 0}, {0, 0, 1, 1}, {0, 0, 0, -1}};
8.    M = P1.M.Transpose[P2];
9.    phi = (Transpose[P1].{"v0", "v1", "v2", "v3"})[[1 ;; 3]];
10.   tphi = (Transpose[P2].{"v0", "v1", "v2", "v3"})[[1 ;; 3]];
11.   Print["Vertices ", phi, " of T correspond to vertices ",
12.     tphi, " of T"];
13.   phi = {"phi0", "phi1", "phi2", "phi3"};
14.   tphi = M.phi;
15.   Print["Rewrite sample points: f^ T", phi, "=f^T", tphi];
16.   tphi = P1.{ "i", "j", "k", "l"};
```

```

17. Print["Rearrange indices for T:", tphi];
18. tphi = P2.{ "i", "j", "k", "l" };
19. Print["Rearrange indices for T:", tphi];
20.
21. (* C^0 tests *)
22.
23. indices = bivIndices[5];
24. res = {};
25. Do[
26.   ind = indices[[i]];
27.   rind = P1.{ind[[1]], ind[[2]], ind[[3]], 0};
28.   rule1 = findRule[rules1, rind];
29.   rind = P2.{ind[[1]], ind[[2]], ind[[3]], 0};
30.   rule2 = findRule[rules2, rind];
31.
32.   If[Dimensions[rule1] == {} || Dimensions[rule2] == {},
33.
34.     AppendTo[res, False],
35.
36.   (* else *)
37.
38.   rule2 = rewriteRule[rule2, M];
39.   AppendTo[res, rulesEqual[rule1, rule2] ]
40. ],
41. {i, Dimensions[indices][[1]]}
42. ];
43. Print["results of the C^0 tests:"];
44. Print[" ", res];
45.
46. (* C^1 tests *)
47.
48. indices = bivIndices[4];
49. res = {};
50. Do[
51.   ind = indices[[i]];
52.   rind = P1.{ind[[1]], ind[[2]], ind[[3]], 1};
53.   rule1 = findRule[rules1, rind];
54.   rind = P1.{ind[[1]] + 1, ind[[2]], ind[[3]], 0};
55.   rule2 = findRule[rules1, rind];
56.   rind = P1.{ind[[1]], ind[[2]], ind[[3]] + 1, 0};
57.   rule3 = findRule[rules1, rind];
58.   rind = P2.{ind[[1]], ind[[2]], ind[[3]], 1};

```

```

59.     rule4 = findRule[rules2, rind];
60.
61.     If[Dimensions[rule1] == {} || Dimensions[rule2] == {} ||
62.         Dimensions[rule3] == {} || Dimensions[rule4] == {}, 
63.
64.         AppendTo[res, False],
65.
66.         (* else *)
67.
68.         rule4 = rewriteRule[rule4, M];
69.         rule1 = addRules[rule1, rule4];
70.         rule2 = addRules[rule2, rule3];
71.         AppendTo[res, rulesEqual[rule1, rule2] ]
72.     ],
73.     {i, Dimensions[indices][[1]]}
74. ];
75. Print["results of the C^1 tests:"];
76. Print[" ", res];
77.
78. (* C^2 tests *)
79.
80. indices = bivIndices[3];
81. res = {};
82. Do[
83.     ind = indices[[i]];
84.     rind = P1.{ind[[1]], ind[[2]], ind[[3]], 2};
85.     rule1 = findRule[rules1, rind];
86.     rind = P1.{ind[[1]] + 1, ind[[2]], ind[[3]], 1};
87.     rule2 = findRule[rules1, rind];
88.     rind = P1.{ind[[1]], ind[[2]], ind[[3]] + 1, 1};
89.     rule3 = findRule[rules1, rind];
90.     rind = P2.{ind[[1]], ind[[2]], ind[[3]], 2};
91.     rule4 = findRule[rules2, rind];
92.     rind = P2.{ind[[1]] + 1, ind[[2]], ind[[3]], 1};
93.     rule5 = findRule[rules2, rind];
94.     rind = P2.{ind[[1]], ind[[2]], ind[[3]] + 1, 1};
95.     rule6 = findRule[rules2, rind];
96.
97.     If[Dimensions[rule1] == {} || Dimensions[rule2] == {} ||
98.         Dimensions[rule3] == {} || Dimensions[rule4] == {} ||
99.         Dimensions[rule5] == {} || Dimensions[rule6] == {}, 
100.
101.

```

```

102.      AppendTo[res, False],
103.
104.      (* else *)
105.
106.      rule4 = rewriteRule[rule4, M];
107.      rule5 = rewriteRule[rule5, M];
108.      rule6 = rewriteRule[rule6, M];
109.      rule1 = addRules[rule1, rule5];
110.      rule1 = addRules[rule1, rule6];
111.      rule2 = addRules[rule2, rule3];
112.      rule2 = addRules[rule2, rule4];
113.      AppendTo[res, rulesEqual[rule1, rule2] ]
114.      ],
115.      {i, Dimensions[indices][[1]]}
116.      ];
117.      Print["results of the C^2 tests:"];
118.      Print[" ", res];
119.  ]

```

reproductionTest

This function performs the calculations that are necessary to verify that Bernstein basis polynomials of a certain degree are reproduced by a quasi-interpolation operator. It takes two parameters, **rules**, which is a set of B-coefficient computation rules that represent a quasi-interpolation operator Q , and **degree**, which is the degree of the Bernstein basis polynomials that are tested.

In line 4, the function generates a list of indices $i + j + k + l = \text{degree}$. In the main loop of the function (lines 7-18), the B-form of each Bernstein basis polynomial B_{ijkl} is generated in lines 8 and 9. Note that the B-coefficients of this B-form are all zero except for the B-coefficient c_{ijkl} which is 1. The B-coefficients are stored in the local variable **Pcoeffs**. Then the degree of the polynomial is raised to 5 in line 10, using the function **raiseToDegree**, which is discussed earlier in this appendix. In lines 11 and 12, the B-coefficients of $Q(B_{ijkl})$ are calculated using the B-coefficient computation rules specified in **rules**. Lines 13-16 perform the test by comparing the B-coefficients of the polynomial to the B-coefficients calculated by the operator. If they match, the value **True** is appended to the result, otherwise the value **False** is appended.

1. reproductionTest[rules_, degree_] := Module[
2. {indices, numPolys, Qcoeffs, Pcoeffs, res},

```

3.
4.   indices = triIndices[degree];
5.   numPolys = Dimensions[indices][[1]];
6.   res = {};
7.   Do[
8.     Pcoeffs = Table[0, {numPolys}];
9.     Pcoeffs[[m]] = 1;
10.    Pcoeffs = raiseToDegree[degree, 5, Pcoeffs];
11.    Qcoeffs = Table[
12.      applyRuleToBPoly[ rules[[i]], indices[[m]] ], {i, 56}];
13.    If[Pcoeffs == Qcoeffs,
14.      AppendTo[res, True],
15.      AppendTo[res, False]
16.    ],
17.    {m, numPolys}
18.  ];
19.  res
20. ]

```

Tests and results

The final section of this appendix contains the commands we used to perform the tests, as well as the output of our functions. Preceding these tests, we created the following sets of B-coefficient computation rules in Mathematica®.

- **rulesconv**, containing the rules (A.1)-(A.20).
- **rulesopt**, containing the rules (B.1)-(B.20).
- **rulesinter1**, containing the rules (C.1)-(C.34).
- **rulesinter2**, containing the rules (C.35)-(C.68).
- **rulesinter3**, containing the rules (C.69)-(C.102).
- **rulesinter4**, containing the rules (C.103)-(C.136).

All rules were created using the format described in the second section of this appendix.

Throughout this section, the bold statements in the listings below are the commands we invoked in Mathematica®, while the lines following these commands are the output that the functions produced.

Tests for the convex quasi-interpolation operator

The tests described here verify that all smoothness conditions (3.4)-(3.6) are satisfied by the convex quasi-interpolation operator developed in section 3.1 of chapter 3. The tests in lines 1 and 16 perform the calculations referred to in cases 1 and 2, respectively, of the proof of theorem 3.18. The text in line 31 performs the calculations which are described in the proof of theorem 3.21.

The output of lines 2-6, and in particular of line 4, shows that the situation described in case 1 of the proof of theorem 3.18 is recreated during the test. Likewise, the output of lines 17-21 mirrors the situation described in case 2 of that proof.

The output shows that all tests passed, which completes the proofs of theorems 3.18 and 3.21.

1. **smoothnessTest[rulesconv, {1, 2, 3, 4}, rulesconv, {1, 2, 3, 4}]**
2. Vertices {v0,v1,v2} of T correspond to vertices {v0,v1,v2} of $\sim T$
3. Rewrite sample points:
4. $f^{\sim T}\{\phi_0, \phi_1, \phi_2, \phi_3\} = f^T\{\phi_0 + \phi_3, \phi_1, \phi_2 + \phi_3, -\phi_3\}$
5. Rearrange indices for $T:\{i, j, k, l\}$
6. Rearrange indices for $\sim T:\{i, j, k, l\}$
7. results of the C^0 tests:
 8. {True, True, True, True, True, True, True, True, True, True,
 9. True, True, True, True, True, True, True, True, True}
10. results of the C^1 tests:
 11. {True, True, True, True, True, True, True, True, True, True,
 12. True, True, True, True}
13. results of the C^2 tests:
 14. {True, True, True, True, True, True, True, True, True}
- 15.
16. **smoothnessTest[rulesconv, {4, 1, 2, 3}, rulesconv, {4, 1, 2, 3}]**
17. Vertices {v1,v2,v3} of T correspond to vertices {v1,v2,v3} of $\sim T$
18. Rewrite sample points:
19. $f^{\sim T}\{\phi_0, \phi_1, \phi_2, \phi_3\} = f^T\{-\phi_0, \phi_0 + \phi_1, \phi_2, \phi_0 + \phi_3\}$
20. Rearrange indices for $T:\{l, i, j, k\}$
21. Rearrange indices for $\sim T:\{l, i, j, k\}$
22. results of the C^0 tests:
 23. {True, True, True, True, True, True, True, True, True, True,
 24. True, True, True, True, True, True, True, True, True}
25. results of the C^1 tests:
 26. {True, True, True, True, True, True, True, True, True, True,
 27. True, True, True, True}
28. results of the C^2 tests:

```
29. {True, True, True, True, True, True, True, True, True, True}
30.
31. reproductionTest[rulesconv, 1]
32. {True, True, True, True}
```

Tests for the optimal quasi-interpolation operator

The tests performed in lines 1 and 16 of the following listing verify that all smoothness conditions (3.4)-(3.6) are satisfied by the optimal quasi-interpolation operator developed in section 3.2 of chapter 3. These tests complete the proof of theorem 3.23. The tests are the same as in the listing above, but use a different set of rules.

The test in line 31 verifies that the operator reproduces cubic polynomials, and thus completes the proof of theorem 3.26.

```

28. results of the C^2 tests:
29. {True,True,True,True,True,True,True,True,True}
30.
31. reproductionTest[rulesopt, 3]
32. {True, True, True, True, True, True, True, True, True, True,
33. True, True, True, True, True, True, True, True, True}

```

Tests for the interpolating quasi-interpolation operator

The interpolating quasi-interpolation operator developed in section 3.3 of chapter 3 is far more complex than the other two operators, because it uses four different sets of B-coefficient computation rules instead of just one. The complexity is reflected in the number of tests that need to be performed in order to verify that all smoothness conditions are satisfied.

In case 1 of the proof of theorem 3.34, three situations are discussed. These situations are reflected by the tests performed in lines 1, 16, and 31. The output of these tests contains the arrangement of the vertices of the neighboring tetrahedra, as well as the formula by which the sample points are rewritten. This makes it easy to match each test to the associated situation in the proof. The following two tests in lines 46 and 61 reflect the situations described in case 2 of the proof. The tests in lines 76 and 91 are related to the situations described in case 3, while the tests in lines 106 and 121 verify the situations of case 4.

For each set of rules, a test is performed to verify the reproduction of cubic polynomials claimed in theorem 3.38. These tests can be found in lines 136, 140, 144 and 148.

The output shows that all tests pass, completing the proofs of theorems 3.34 and 3.38.

1. **smoothnessTest[rulesinter1, {4,1,2,3}, rulesinter2, {2,1,4,3}]**
2. Vertices {v1,v2,v3} of T correspond to vertices {v1,v0,v3} of $\sim T$
3. Rewrite sample points:
4. $f^{\sim T}\{\phi_0, \phi_1, \phi_2, \phi_3\} = f^T\{-\phi_2, \phi_1+\phi_2, \phi_0, \phi_2+\phi_3\}$
5. Rearrange indices for $T:\{l,i,j,k\}$
6. Rearrange indices for $\sim T:\{j,i,l,k\}$
7. results of the C^0 tests:
8. {True,True,True,True,True,True,True,True,True,
9. True,True,True,True,True,True,True,True}
10. results of the C^1 tests:
11. {True,True,True,True,True,True,True,True,True,
12. True,True,True,True}
13. results of the C^2 tests:

```

14. {True,True,True,True,True,True,True,True}
15.
16. smoothnessTest[rulesinter1, {2,1,4,3}, rulesinter1, {2,1,4,3}]
17. Vertices {v1,v0,v3} of T correspond to vertices {v1,v0,v3} of ~T
18. Rewrite sample points:
19.    $f^{\sim}T\{\phi_0, \phi_1, \phi_2, \phi_3\} = f^T\{\phi_0, \phi_1 + \phi_2, -\phi_2, \phi_2 + \phi_3\}$ 
20. Rearrange indices for T:{j,i,l,k}
21. Rearrange indices for ~T:{j,i,l,k}
22. results of the C^0 tests:
23.   {True,True,True,True,True,True,True,True, True,
24.     True,True,True,True,True,True,True,True}
25. results of the C^1 tests:
26.   {True,True,True,True,True,True,True,True, True,
27.     True,True,True,True}
28. results of the C^2 tests:
29.   {True,True,True,True,True,True,True,True,True}
30.
31. smoothnessTest[rulesinter1, {1,2,3,4}, rulesinter1, {1,2,3,4}]
32. Vertices {v0,v1,v2} of T correspond to vertices {v0,v1,v2} of ~T
33. Rewrite sample points:
34.    $f^{\sim}T\{\phi_0, \phi_1, \phi_2, \phi_3\} = f^T\{\phi_0 + \phi_3, \phi_1, \phi_2 + \phi_3, -\phi_3\}$ 
35. Rearrange indices for T:{i,j,k,l}
36. Rearrange indices for ~T:{i,j,k,l}
37. results of the C^0 tests:
38.   {True,True,True,True,True,True,True,True, True,
39.     True,True,True,True,True,True,True,True}
40. results of the C^1 tests:
41.   {True,True,True,True,True,True,True,True, True,
42.     True,True,True,True}
43. results of the C^2 tests:
44.   {True,True,True,True,True,True,True,True,True}
45.
46. smoothnessTest[rulesinter2, {4,1,2,3}, rulesinter2, {4,1,2,3}]
47. Vertices {v1,v2,v3} of T correspond to vertices {v1,v2,v3} of ~T
48. Rewrite sample points:
49.    $f^{\sim}T\{\phi_0, \phi_1, \phi_2, \phi_3\} = f^T\{-\phi_0, \phi_0 + \phi_1, \phi_2, \phi_0 + \phi_3\}$ 
50. Rearrange indices for T:{l,i,j,k}
51. Rearrange indices for ~T:{l,i,j,k}
52. results of the C^0 tests:
53.   {True,True,True,True,True,True,True,True, True,
54.     True,True,True,True,True,True,True,True}
55. results of the C^1 tests:

```

```

56.      {True,True,True,True,True,True,True,True,True,True,
57.           True,True,True,True}
58. results of the C^2 tests:
59.      {True,True,True,True,True,True,True,True}
60.
61. smoothnessTest[rulesinter2, {1,2,3,4}, rulesinter3, {1,2,3,4}]
62. Vertices {v0,v1,v2} of T correspond to vertices {v0,v1,v2} of ~T
63. Rewrite sample points:
64.      f^^T{phi0,phi1,phi2,phi3}=f^T{phi0+phi3,phi1,phi2+phi3,-phi3}
65. Rearrange indices for T:{i,j,k,l}
66. Rearrange indices for ~T:{i,j,k,l}
67. results of the C^0 tests:
68.      {True,True,True,True,True,True,True,True,True,True,
69.           True,True,True,True,True,True,True,True}
70. results of the C^1 tests:
71.      {True,True,True,True,True,True,True,True,True,True,
72.           True,True,True,True}
73. results of the C^2 tests:
74.      {True,True,True,True,True,True,True,True,True}
75.
76. smoothnessTest[rulesinter3, {4,1,2,3}, rulesinter4, {2,1,4,3}]
77. Vertices {v1,v2,v3} of T correspond to vertices {v1,v0,v3} of ~T
78. Rewrite sample points:
79.      f^^T{phi0,phi1,phi2,phi3}=f^T{-phi2,phi1+phi2,phi0,phi2+phi3}
80. Rearrange indices for T:{l,i,j,k}
81. Rearrange indices for ~T:{j,i,l,k}
82. results of the C^0 tests:
83.      {True,True,True,True,True,True,True,True,True,True,
84.           True,True,True,True,True,True,True,True}
85. results of the C^1 tests:
86.      {True,True,True,True,True,True,True,True,True,True,
87.           True,True,True,True}
88. results of the C^2 tests:
89.      {True,True,True,True,True,True,True,True,True}
90.
91. smoothnessTest[rulesinter3, {2,1,4,3}, rulesinter3, {2,1,4,3}]
92. Vertices {v1,v0,v3} of T correspond to vertices {v1,v0,v3} of ~T
93. Rewrite sample points:
94.      f^^T{phi0,phi1,phi2,phi3}=f^T{phi0,phi1+phi2,-phi2,phi2+phi3}
95. Rearrange indices for T:{j,i,l,k}
96. Rearrange indices for ~T:{j,i,l,k}
97. results of the C^0 tests:

```

```

98.      {True,True,True,True,True,True,True,True,True,True,
99.          True,True,True,True,True,True,True,True,True}
100. results of the C^1 tests:
101.      {True,True,True,True,True,True,True,True,True,True,
102.          True,True,True,True}
103. results of the C^2 tests:
104.      {True,True,True,True,True,True,True,True,True}
105.
106. smoothnessTest[rulesinter4, {4,1,2,3}, rulesinter4, {4,1,2,3}]
107. Vertices {v1,v2,v3} of T correspond to vertices {v1,v2,v3} of ~T
108. Rewrite sample points:
109.      f^~T{phi0,phi1,phi2,phi3}=f^T{-phi0,phi0+phi1,phi2,phi0+phi3}
110. Rearrange indices for T:{l,i,j,k}
111. Rearrange indices for ~T:{l,i,j,k}
112. results of the C^0 tests:
113.      {True,True,True,True,True,True,True,True,True,True,
114.          True,True,True,True,True,True,True,True}
115. results of the C^1 tests:
116.      {True,True,True,True,True,True,True,True,True,True,
117.          True,True,True,True}
118. results of the C^2 tests:
119.      {True,True,True,True,True,True,True,True,True}
120.
121. smoothnessTest[rulesinter4, {1,2,3,4}, rulesinter4, {1,2,3,4}]
122. Vertices {v0,v1,v2} of T correspond to vertices {v0,v1,v2} of ~T
123. Rewrite sample points:
124.      f^~T{phi0,phi1,phi2,phi3}=f^T{phi0+phi3,phi1,phi2+phi3,-phi3}
125. Rearrange indices for T:{i,j,k,l}
126. Rearrange indices for ~T:{i,j,k,l}
127. results of the C^0 tests:
128.      {True,True,True,True,True,True,True,True,True,True,
129.          True,True,True,True,True,True,True,True}
130. results of the C^1 tests:
131.      {True,True,True,True,True,True,True,True,True,True,
132.          True,True,True,True}
133. results of the C^2 tests:
134.      {True,True,True,True,True,True,True,True,True}
135.
136. reproductionTest[rulesinter1, 3]
137. {True, True, True, True, True, True, True, True, True, True,
138.     True, True, True, True, True, True, True, True, True, True}
139.

```

330 APPENDIX D. PROGRAM FOR COMPUTER-ASSISTED PROOFS

```
140. reproductionTest[rulesinter2, 3]
141. {True, True, True, True, True, True, True, True, True, True,
142.   True, True, True, True, True, True, True, True, True, True}
143.
144. reproductionTest[rulesinter3, 3]
145. {True, True, True, True, True, True, True, True, True, True,
146.   True, True, True, True, True, True, True, True, True, True}
147.
148. reproductionTest[rulesinter4, 3]
149. {True, True, True, True, True, True, True, True, True, True,
150.   True, True, True, True, True, True, True, True, True, True}
```

Bibliography

- [1] Alfeld, P.: A discrete C^1 interpolant for tetrahedral data. *Rocky Mountain J. Math.* **14**, 5–16 (1984)
- [2] Alfeld, P.: A trivariate Clough-Tocher scheme for tetrahedral data. *Comput. Aided Geom. Design* **1**, 169–181 (1984)
- [3] Alfeld, P., Schumaker, L., Whiteley, W.: The Generic Dimension of the Space of C^1 Splines of Degree $d \geq 8$ on Tetrahedral Decompositions. *SIAM J. Numer. Anal.* **30**, 889–920 (1993)
- [4] Alfeld, P., Schumaker, L.L.: Bounds on the dimensions of trivariate spline spaces. *Advances in Computational Mathematics* **29**(4), 315–335 (2008)
- [5] Alfeld, P., Schumaker, L.L., Sirvent, M.: On dimension and existence of local bases for multivariate spline spaces. *Journal of Approximation Theory* **70**(2), 243 – 264 (1992)
- [6] Alfeld, P., Sirvent, M.: A Recursion Formula for the Dimension of Super Spline Spaces of Smoothness r and Degree $d > r2^k$. In: *Multivariate Approximation Theory IV*, pp. 1–8. Birkhäuser Verlag (1989)
- [7] Alfeld, P., Sirvent, M.: The Structure of Multivariate Superspline Spaces of High Degree. *Math. Comp.* **57**, 299–308 (1991)
- [8] Bernstein, S.N.: Démonstration du Théorème de Weierstrass fondée sur le calcul des Probabilités. *Comm. Soc. Math. Kharkov* **2**(Series XIII No.1), 1–2 (1912)
- [9] Bézier, P.: Numerical control; mathematics and applications. Wiley series in computing. J. Wiley (1972)
- [10] Böhm, W., Farin, G., Kahmann, J.: A survey of curve and surface methods in CAGD. *Comput. Aided Geom. Des.* **1**(1), 1–60 (1984)
- [11] de Boor, C.: On Calculating with B-Splines. *J. Approx. Theory* **6**, 50–62 (1972)

- [12] de Boor, C.: A Practical Guide to Splines. Springer (1978)
- [13] de Boor, C.: B-form basics. In: G.E. Farin (ed.) Geometric Modeling: Algorithms and New Trends, pp. 131–148. SIAM (1987)
- [14] de Boor, C., Höllig, K., Riemenschneider, S.: Box Splines. Applied Mathematical Sciences. Springer (1993)
- [15] Brenner, S.C., Scott, L.R.: The Mathematical Theory of Finite Element Methods. Texts in Applied Mathematics. Springer–Verlag, New York (1994)
- [16] Brent, R.: Algorithms for minimization without derivatives. Dover books on mathematics. Dover Publications, Incorporated (1973)
- [17] Burns, G., Glazer, A.: Space groups for solid state scientists. Academic Press (1990)
- [18] Carr, H., Möller, T., Snoeyink, J.: Simplicial subdivisions and sampling artifacts. In: Proceedings of the conference on Visualization '01, VIS '01, pp. 99–106. IEEE Computer Society, Washington, DC, USA (2001)
- [19] de Casteljau, P.: Outilage méthodes calcul. Tech. rep., André Citroën Automobiles (1959)
- [20] de Casteljau, P.: Courbes et Surfaces à Pôles. Tech. rep., André Citroën Automobiles (1963)
- [21] Chui, C.: Multivariate Splines. No. Bd. 2 in CBMS-NSF Regional Conference Series in Applied Mathematics. Society for Industrial and Applied Mathematics (1988)
- [22] Chui, C.K., Hecklin, G., Nürnberger, G., Zeilfelder, F.: Optimal Lagrange interpolation by quartic C^1 splines on triangulations. Journal of Computational and Applied Mathematics **216**, 344–363 (2008)
- [23] Chui, C.K., Lai, M.J.: Vandermonde determinants and Lagrange interpolations in R^s . In: B. Lin, S. Simons (eds.) Nonlinear and Convex Analysis, pp. 23–35. Marcel Dekker, N.Y. (1987)
- [24] Chung, K.C., Yao, T.H.: On Lattices Admitting Unique Lagrange Interpolations. SIAM J. Numer. Anal. **14**(4), 735–743 (1977)
- [25] Clough, R., Tocher, J.: Finite element stiffness matrices for analysis of plates in bending. In: Matrix Methods in Structural Analysis. Wright-Patterson Air Force Base, Ohio (1965)

- [26] Coatmelec, C.: Approximation et interpolation des fonctions différentes de plusieurs variables (1966)
- [27] Cox, M.G.: The numerical evaluation of B-splines. *J. Inst. Math. Appl.* **10**, 134–149 (1972)
- [28] Curtis, P.C.: n -parameter families and best approximation. *Pacific J. Math.* **9**(4), 1013–1027 (1959)
- [29] Davydov, O., Schumaker, L.L.: On Stable Local Bases for Bivariate Polynomial Spline Spaces. *Constr. Approx.* **18**, 87–116 (1999)
- [30] Entezari, A., Dyer, R., Möller, T.: Linear and Cubic Box Splines for the Body Centered Cubic Lattice. In: Proceedings of the conference on Visualization '04, VIS '04, pp. 11–18. IEEE Computer Society, Washington, DC, USA (2004)
- [31] Entezari, A., Van De Ville, D., Möller, T.: Practical Box Splines for Reconstruction on the Body Centered Cubic Lattice. *IEEE Trans. Vis. Comput. Graph.* **14**(2), 313–328 (2008)
- [32] Ewing, D.J.F., Fawkes, A.J., Griffiths, J.R.: Rules governing the numbers of nodes and elements in a finite element mesh. *International Journal for Numerical Methods in Engineering* **2**(4), 597–600 (1970)
- [33] Farin, G.: Konstruktion und Eigenschaften von Bézier-Kurven und -Flächen. Master's thesis, Technical University Braunschweig (1977)
- [34] Farin, G.: Subsplines über Dreiecken. Ph.D. thesis, Technical University Braunschweig (1979)
- [35] Farin, G.: Bézier Polynomials over Triangles and the Construction of Piecewise C^r Polynomials. Tech. Rep. TR/91, Brunel University (1980)
- [36] Farin, G.: Triangular Bernstein-Bézier patches. *Comput. Aided Geom. Design* **3**, 83–127 (1986)
- [37] Farin, G.: Curves and Surfaces for Computer Aided Geometric Design. Academic Press (1988)
- [38] Finkbeiner, B., Entezari, A., Van De Ville, D., Möller, T.: Technical Section: Efficient volume rendering on the body centered cubic lattice using box splines. *Comput. Graph.* **34**(4), 409–423 (2010)
- [39] Goldman, R.N.: Using degenerate Bézier triangles and tetrahedra to subdivide Bézier curves. *Computer-Aided Design* **14**(6), 307–311 (1982)

- [40] Goldman, R.N.: Subdivision algorithms for Bézier triangles. Computer-Aided Design **15**(3), 159–166 (1983)
- [41] Hecklin, G., Nürnberger, G., Schumaker, L.L., Zeilfelder, F.: A local lagrange interpolation method based on C^1 cubic splines on Freudenthal partitions. Math. Comp. **77**(1-2), 1017–1036 (2008)
- [42] Hecklin, G., Nürnberger, G., Schumaker, L.L., Zeilfelder, F.: Local lagrange interpolation with cubic C^1 splines on tetrahedral partitions. J. Approx. Theory **160**(1-2), 89–102 (2009)
- [43] Hecklin, G., Nürnberger, G., Zeilfelder, F.: Local Lagrange interpolation by classical bivariate C^1 -spline spaces. In: Proc. Conf. Interaction between wavelets and splines. Nashboro Press (2006)
- [44] Hecklin, G., Nürnberger, G., Zeilfelder, F.: Local data interpolation by quintic C^1 splines on tetrahedral partitions. In: P. Chenin, T. Lyche, L.L. Schumaker (eds.) Curve and surface design : Avignon 2006, pp. 163–172 (2007)
- [45] Kniss, J., Kindlmann, G., Hansen, C.: Multidimensional Transfer Functions for Interactive Volume Rendering. IEEE Transactions on Visualization and Computer Graphics **8**(3), 270–285 (2002)
- [46] Lai, M.J., Schumaker, L.: Spline Functions on Triangulations. Cambridge University Press (2007)
- [47] Lasser, D.: Bernstein-Bézier-Darstellung trivariater Splines. Ph.D. thesis, University of Darmstadt (1987)
- [48] Levoy, M.: Display of surfaces from volume data. Computer Graphics and Applications, IEEE **8**(3), 29–37 (1988)
- [49] Lorentz, G.: Bernstein polynomials. University of Toronto Press (1953)
- [50] Mairhuber, J.C.: On Haar's theorem concerning Chebychev approximation problems having unique solutions. In: Proc. Amer. Math. Soc., vol. 7, pp. 609–615 (1956)
- [51] Marschner, S.R., Lobb, R.J.: An evaluation of reconstruction filters for volume rendering. In: Proceedings of the conference on Visualization '94, VIS '94, pp. 100–107. IEEE Computer Society Press, Los Alamitos, CA, USA (1994)
- [52] Matt, M.: A C^r trivariate macro-element based on the Worsey-Farin split of a tetrahedron. Numerische Mathematik **123**(1), 121–144 (2013)

- [53] Matt, M.A.: Trivariate Local Lagrange Interpolation and Macro-Elements of Arbitrary Smoothness. Ph.D. thesis, University of Mannheim, Germany (2012)
- [54] Matt, M.A.: Trivariate Local Lagrange Interpolation and Macro-Elements of Arbitrary Smoothness, chap. Local Lagrange Interpolation with $\mathcal{S}_9^2(\Delta^*)$, pp. 161–199. Springer Spektrum (2012)
- [55] Matt, M.A., Nürnberger, G.: Local Lagrange interpolation using cubic C^1 splines on type-4 cube partitions. *J. Approx. Theory* **162**(3), 494–511 (2010)
- [56] Möbius, A.F.: Über eine neue Behandlungsweise der analytischen Sphärik. In: Abhandlungen bei Begründung der Königl. Sächs. Gesellschaft der Wissenschaften, pp. 45–86. Jablonowski Gesellschaft, Leipzig (1886)
- [57] Nürnberger, G.: Approximation by spline functions. Springer (1989)
- [58] Nürnberger, G., Rayevskaya, V., Schumaker, L.L., Zeilfelder, F.: Local Lagrange Interpolation with Bivariate Splines of Arbitrary Smoothness. *Cons* **23**(1), 33–59 (2005)
- [59] Nürnberger, G., Rhein, M., Schneider, G.: Local Lagrange interpolation by quintic C^1 splines on type-6 tetrahedral partitions. *J. Comput. Appl. Math.* **236**(4), 529–542 (2011)
- [60] Nürnberger, G., Rössl, C., Seidel, H.P., Zeilfelder, F.: Quasi-interpolation by quadratic piecewise polynomials in three variables. *Comput. Aided Geom. Des.* **22**(3), 221–249 (2005)
- [61] Nürnberger, G., Schneider, G.: A Lagrange interpolation method by trivariate cubic C^1 splines of low locality., pp. 231–248. New York, NY: Springer (2012)
- [62] Nürnberger, G., Schumaker, L., Zeilfelder, F.: Two Lagrange interpolation methods based on C^1 splines on tetrahedral partitions. In: C. Chui, M. Neamtu, L.L. Schumaker (eds.) *Approximation Theory XI: Gatlinburg 2004*, pp. 327–344 (2005)
- [63] Nürnberger, G., Schumaker, L.L., Zeilfelder, F.: Local Lagrange interpolation by bivariate C^1 cubic splines. In: T. Lyche, L.L. Schumaker (eds.) *Mathematical Methods for Curves and Surfaces*, pp. 393–404. Vanderbilt University, Nashville, TN, USA (2001)

- [64] Nürnberger, G., Schumaker, L.L., Zeilfelder, F.: Lagrange Interpolation by C^1 Cubic Splines on Triangulated Quadrangulations. *Adv. Comput. Math* **21**, 357–380 (2004)
- [65] Nürnberger, G., Zeilfelder, F.: Developments in bivariate spline interpolation. *Journal of Computational and Applied Mathematics* **121**(1-2), 125 – 152 (2000)
- [66] Nürnberger, G., Zeilfelder, F.: Lagrange Interpolation by Bivariate C^1 -Splines with Optimal Approximation Order. *Adv. Comput. Math* **21**(3-4), 381–419 (2004)
- [67] Phong, B.T.: Illumination for computer generated pictures. *Commun. ACM* **18**(6), 311–317 (1975)
- [68] Porter, T., Duff, T.: Compositing digital images. *SIGGRAPH Comput. Graph.* **18**(3), 253–259 (1984)
- [69] Prautzsch, H., Boehm, W., Paluszny, M.: Bezier and B-Spline Techniques. *Mathematics and Visualization*. Springer (2002)
- [70] Press, W., Teukolsky, S., Vetterling, W., Flannery, B.: Numerical recipes in C++: the art of scientific computing. Cambridge : Cambridge University Press (2002)
- [71] Rhein, M.: Trivariate C^1 -Splines auf gleichmäßigen Partitionen. Ph.D. thesis, University of Mannheim, Germany (2009)
- [72] Rhein, M., Kalbe, T.: Quasi-interpolation by quadratic C1-splines on truncated octahedral partitions. *Comput. Aided Geom. Des.* **26**(8), 825–841 (2009)
- [73] Sabin, M.A.: The use of piecewise forms for the numerical representation of shape. Ph.D. thesis, MTA Budapest (1977)
- [74] Sbibih, D., Serghini, A., Tijini, A.: Bivariate Simplex Spline Quasi-Interpolants. *Numer. Math. Theor. Meth. Appl.* **3**, 97–118 (2009)
- [75] Schoenberg, I.J.: Contributions to the problem of approximation of equidistant data by analytic functions, Part A: On the problem of smoothing of graduation, a first class of analytic approximation. *Quarterly of Applied Mathematics* **4**, 45–88 (1946)
- [76] Schoenberg, I.J., Whitney, A.: On Polya Frequency Function. III. The Positivity of Translation Determinants With an Application to the Interpolation Problem by Spline Curves. *Trans. Amer. Math. Soc.* **74**(2), 246–259 (1953)

- [77] Schumaker, L.: Spline functions: basic theory. Pure and applied mathematics. Wiley (1981)
- [78] Schumaker, L.L., Sorokina, T.: C^1 Quintic Splines on Type-4 Tetrahedral Partitions. In: Advances in Comp. Math., pp. 421–444 (2004)
- [79] Sommer, M., Strauss, H.: A condition of Schoenberg-Whitney type for multivariate spline interpolation. Adv. Comput. Math. **5**(1), 381–397 (1996)
- [80] Sorokina, T., Zeilfelder, F.: Optimal quasi-interpolation by quadratic C^1 splines on type-2 triangulations. In: Approximation Theory XI: Gatlinburg 2004 (2004)
- [81] Sorokina, T., Zeilfelder, F.: Local quasi-interpolation by cubic C^1 splines on type-6 tetrahedral partitions. IMA Journal of Numerical Analysis **27**(1), 74–101 (2007)
- [82] Sorokina, T., Zeilfelder, F.: An explicit quasi-interpolation scheme based on C^1 quartic splines on type-1 triangulations. Comput. Aided Geom. Des. **25**(1), 1–13 (2008)
- [83] Stancu, D.D.: De l'approximation par des polynômes du type Bernstein, des fonctions de deux variables. Comm. Akad. R. P. Romaine **9**, 773–777 (1959)
- [84] Stein, E.: Singular integrals and differentiability properties of functions. Monographs in harmonic analysis. Princeton University Press (1970)
- [85] Strang, G., Fix, G.J.: Constructive Aspects of Functional Analysis, chap. A Fourier Analysis of the Finite Element Variational Method, pp. 796–830. Springer (1971)
- [86] Ženíšek, A.: Polynomial approximation on tetrahedrons in the finite element method. J. Approx. Theory **7**, 334–351 (1973)
- [87] Wilhelmsen, D.R.: A Markov inequality in several dimensions. J. Approx. Theory **11**, 216–220 (1974)
- [88] Wolfram, S.: The Mathematica® Book. Wolfram Media (2003)
- [89] Worsey, A., Farin, G.: An n-dimensional Clough-Tocher interpolant. Constr. Approx. **3**, 99–110 (1987)
- [90] Worsey, A., Piper, B.: A trivariate Powell-Sabin interpolant. Computer Aided Geometric Design **5**(3), 177 – 186 (1988)